DEPARTMENT OF BIOMEDICAL ENGINEERING

University of Strathclyde Engineering

Design of ophthalmic equipment for low-income countries: a workflow perspective

A submission to the University of Strathclyde for the award of

Doctorate of Philosophy

by Nigel M Bolster

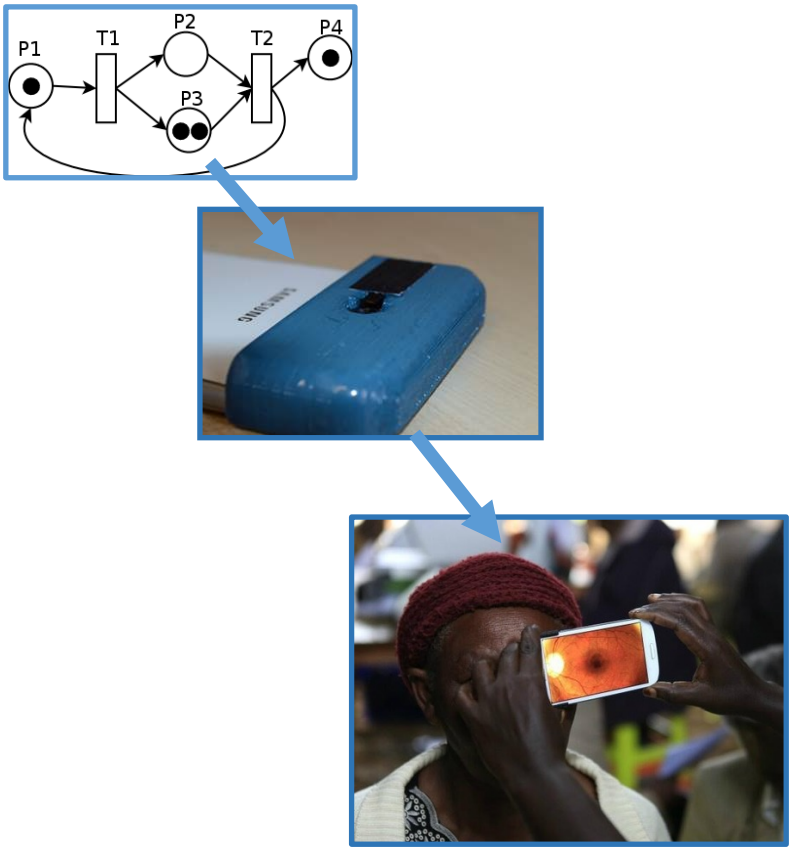

Declaration of Authenticity and Author's Rights

Signed: _____

Date: _____

Abstract

Global proliferation of mobile technology presents huge opportunities for healthcare, specifically regards improving operational efficiency, lowering costs, extending health systems' reach and improving adherence and acceptance. Foremost of reasons cited as prohibiting advancement of mHealth technologies from pilot to widespread adoption is paucity of data concerning the full impact on the health system's workflow. The aim of this thesis is to investigate whether workflow modelling techniques, established in other fields, might be applied to the field of mHealth to address the lack of knowledge concerning its full health-system impact. Thus, it seeks to provide information that will help reduce the number of mHealth designs that fail to produce results in clinical pilots that lead to adoption at scale.

Data on the operation of proposed mHealth designs for use in community eye screening and retinopathy of prematurity screening were sourced from the scientific literature, technical datasheets and lab-based testing in the first instance and then pilot studies embedded in a community eye health study in Nakuru, Kenya. This included the design and prototyping of a novel smartphone-based ophthalmoscope appropriate for community settings in low-income countries.

The data acquired were analysed using standard statistical techniques. These analyses were then used to build stochastic timed coloured Petri-nets.

Classical statistical simulations based on these models generated data concerning the optimal design, workflow placement and usage of the mHealth devices. The data relating to retinopathy of prematurity screening specifically was used to design a tablet-computer operated, portable fundus camera for screening of preterm infants.

The results suggest that several mHealth design parameters have optimal values at odds with many of the piloted technologies that have failed to achieve adoption within the respective scenarios. It is recommended that further research, extending the techniques discussed and validating their effectiveness at producing designs appropriate for scale, be undertaken.

Keywords

mHealth, clinical workflow modelling, health systems, coloured Petri Nets, eye care, fundoscopy, ophthalmoscopy, retinal camera, community eye screening, retinopathy of prematurity, smartphones.

Author Details

NIGEL M BOLSTER
Biomedical Engineering
University of Strathclyde
Correspondence email: nigel.m.bolster@gmail.com

Copyright and Citation Information

Acknowledgements

Firstly, I would like to offer my sincere thanks to my PhD supervisor, Dr. Mario E. Giardini, for his guidance and tutorship throughout this programme. In addition, I wish to thank him for the knowledge he has imparted to me and the many new skills he has taught me throughout which I am certain will have a lasting impact on my research career. Finally, I would like to thank him for the many hours he has dedicated to my supervision and the review of my work.

Besides my programme supervisor, I also wish to warmly thank Prof. Patricia Connolly, Prof. Bernard Conway, Prof. Philip Rowe, Prof. Terry Gourlay, Dr. Andy Ward and Prof. Matthew Burton for their insightful appraisals of my work over the course of the programme. I would further like to thank Prof. Helen Grant for the help she offered in her role as course co-ordinator.

I extend my heartfelt appreciation to The Queen Elizabeth Diamond Jubilee Trust including its vice patron Her Royal Highness The Countess of Wessex, its trustees and chief executive Dr. Astrid Bonfield, for providing funding support over the course of the PhD programme. I also wish to thank The Commonwealth Eye Health Consortium, in particular the International Centre for Eye Health at the London School of Hygiene and Tropical Medicine and Glasgow Centre of Ophthalmic Research, NHS Greater Glasgow and Clyde, for collaborating with me on this research programme.

I gratefully acknowledge the work and many hours spent by Dr. Iain Livingstone in supporting lab-based testing of the prototypes described in this thesis and for his clinical oversight.

For their work in collecting the field data required for the workflow model of a community eye health clinic described in this thesis I would like to acknowledge Dr. Andrew Bastawrous and the Nakuru Community Eye Cohort Study team. I would also like to thank Dr. Bastawrous alongside Dr. Hillary Rono for their insights into the practicalities of eye care in a low-income setting. I would also like to thank the team for hosting me at the beginning of my PhD programme.

Further to this, I would like to acknowledge the following people for their work in support of my PhD programme:

Miss Kirsty Jordan for her support with 3D printing and maintenance, the manufacture of multiple copies of the third iteration of the smartphone-based direct ophthalmoscope and for support the re-design of the smartphone-based direct ophthalmoscope's housing for placement on newer phone models.
Prof. Clare Gilbert for her support in testing the portable preterm fundus camera described in this thesis as well as her advice on the practicalities of screening preterm eyes.
Dr. Muhammed Aman Ullah for his support in testing the preterm eye phantom
Dr. Hekio Philippin and Mr. Patrick Massae for their assistance in field testing the second and third iterations of the smartphone-based ophthalmoscope design.
Mrs. Tara Mtuy for her help in organising my field visit to Moshi, Tanzania.
Dr. Claire Tarbert for providing access to Glasgow Centre of Ophthalmic Research's spectrometer.
Mr. Stephen Murray for his support with the 3D printing of the preterm eye phantom and selection of tools and materials.
Mr. Harry Kinsman for his support with the vacuum forming of the preterm corneal phantom and Mr. William MacKinnon with the 3D scanning of the neonatal manikin.
Mrs. Ashley MacIntyre for her assistance in ordering the equipment and consumables required throughout the PhD programme.
Mr. Stewart Jordan, Mr. Brian Cartlidge, Mrs Catherine Henderson, Mr John Wilson, Mr John MacLean, Ms Sarah O'Regan the Biomedical Engineering office staff and the department cleaners.
I would also like to express my gratitude for colleagues at Peek Vision Ltd. for accommodating the time and energy spent on the writing of this thesis.
Finally, I would like to thank my friends, family, the leadership and congregations of Sandyford Henderson Memorial Church and St. Peter's Bethnal Green, my Wednesday 'Life Group', my mother Daphne and especially my wife, Charlotte, for their unfailing prayers, love, support and patience throughout this programme.

Table of Contents

FRONT MATTER

DECLARATION OF AUTHENTICITY AND AUTHOR'S RIGHTS iii

ABSTRACT v

KEYWORDS vii

AUTHOR DETAILS vii

COPYRIGHT AND CITATION INFORMATION vii

ACKNOWLEDGEMENTS ix

ACRONYMS AND ABBREVIATIONS xxv

1 THESIS OVERVIEW 1

1.1 INTRODUCTION 2

1.2 AIMS 3

1.3 OBJECTIVES 3

1.4 THESIS ORGANISATION 4

SECTION 1

2 REVIEW OF GLOBAL MHEALTH ADOPTION LITERATURE 7

2.1 BACKGROUND 8

2.1.1 Technological Context: The Ascent of Mobile Devices 8

2.1.2 mHealth: Mobile Devices in a Healthcare Setting 10

2.2 LITERATURE REVIEW METHODS 11

2.2.1 Inclusion Criteria 12

2.2.2 Exclusion Criteria 12

2.2.3 Information Sources 13

2.2.4 Search Criteria 13

2.2.5 Article Selection 13

2.2.6 Data Collection and Synthesis 13

2.3 RESULTS 14

2.3.1 Article Selection 14

2.3.2 Article Characteristics 14

2.3.3 Results of Individual Articles 15

2.3.4 Synthesis of Results 15

2.4 DISCUSSION 20

2.4.1 Goals of mHealth Systems and Perceived Opportunities 20

2.4.2 Barriers to Adoption at Scale and Proposed Solutions 22

2.4.3 Limitations 27

2.5 CONCLUSIONS 27

3 mHEALTH SOLUTIONS FOR EYE CARE DELIVERY IN LOW INCOME SETTINGS 28

3.1 INTRODUCTION 29

3.2 BRIEF OVERVIEW OF THE MAJOR CHALLENGES IN GLOBAL EYE CARE 30

3.2.1 Measuring Visual Impairment and Blindness 30

3.2.2 Major Causes of Visual Impairment and their Assessment 31

3.2.3 Access to Eye Care: The global inverse care law *39*
3.2.4 Summary *39*
3.3 mHEALTH IN EYE CARE DELIVERY 40
3.3.1 Visual Acuity *41*
3.3.2 Smartphone Ophthalmoscopy *46*
3.3.3 Visual Fields *52*
3.3.4 Anterior Segment Imaging *56*
3.3.5 Discussion *58*
4 AN INTRODUCTION TO CLINICAL WORKFLOW MODELLING 60
4.1 INTRODUCTION 61
4.2 REVIEW OF CLINICAL WORKFLOW MODELLING OF mHEALTH IN LOW- AND MIDDLE-INCOME SETTINGS 62
4.2.1 Aim *62*
4.2.2 Methods *62*
4.2.3 Results *64*
4.2.4 Discussion *66*
4.3 AN OVERVIEW OF INFORMATION SYSTEMS DEVELOPMENT AND MODELLING 66
4.3.1 The Development Cycle *66*
4.3.2 System Modelling *71*
4.4 TIMED COLOURED PETRI NETS 75
4.5 CONCLUSION 77
SECTION 2
5 DESIGN OF A SMARTPHONE OPHTHALMOSCOPE 79
5.1 INTRODUCTION 80
5.2 BACKGROUND 81
5.2.1 The direct ophthalmoscope *81*
5.2.2 Prior design of a smartphone ophthalmoscope *82*
5.3 REQUIREMENTS 83
5.3.1 Functional Requirements *83*
5.3.2 Material Requirements *84*
5.3.3 Operating Environment *84*
5.3.4 Maintenance *85*
5.3.5 Safety Standards *85*
5.3.6 Ergonomics and Aesthetics *85*
5.4 DESIGN ITERATION 1: FIRST SAMSUNG GALAXY S3-BASED UNIT 86
5.4.1 Design *86*
5.4.2 Prototyping *93*
5.4.3 Performance Testing *94*
5.4.4 Discussion *100*
5.5 DESIGN ITERATION 2: SECOND SAMSUNG GALAXY S3-BASED UNIT 101
5.5.1 Design *101*
5.5.2 Prototyping *103*
5.5.3 Performance Testing *104*
5.5.4 Discussion *108*
5.6 DESIGN ITERATION 3: SONY XPERIA Z3 / Z3 COMPACT-BASED UNIT 109
5.6.1 Introduction *109*
5.6.2 Design *109*

5.6.3 Prototyping 111
5.6.4 Performance Testing 114
5.6.5 Results 115
5.6.6 Discussion 117
5.7 Discussion 117

SECTION 3

6 RETROSPECTIVE ANALYSIS OF THE MHEALTH DEVICES IN THE NAKURU EYE DISEASE STUDY ... 122

6.1 Introduction 123

6.1.1 Rationale 123
6.1.2 Background 123
6.1.3 Chosen Study's Design and Implementation 124
6.1.4 Embedded mHealth Devices 125
6.2 Methods 125

6.2.1 Modelling of Participants 125
6.2.2 Modelling of Devices 129
6.2.3 Modelling of Clinic's Workflow 130
6.2.4 Simulation and Statistical Analysis of Model 132
6.3 Results 133

6.3.1 Modelling of Participants 133
6.3.2 Modelling of the Clinic's Workflow 134
6.3.3 Simulation Results 137
6.4 Discussion 140

6.4.1 Implications for an mHealth equipped advance team 140
6.4.2 Referral adherence and pathway 141
6.4.3 Limitations and future work 143
6.5 Licensing Information 145

SECTION 4

7 MODELLING OF AN ROP SCREENING PROGRAMME 147

7.1 Introduction 148

7.1.1 Aim 148
7.1.2 Model Basis 149
7.2 Methods 149

7.2.1 Modelling of the Logistic Workflow 150
7.2.2 Modelling the Screening Workflow 151
7.2.3 Modelling of the Report Review and Management Decisions 153
7.2.4 Modelling of the Treatment Outreach Workflow 154
7.2.5 Simulation and Statistical Analysis 154
7.2.6 Estimation of Ongoing Programme Costs 155
7.3 Results 156

7.3.1 Simulations Summary 156
7.3.2 Screening Coverage and Efficacy 157
7.3.3 Treatment Coverage 158
7.3.4 Task Distribution 158
7.3.5 Ongoing Costs 159
7.3.6 Setup Costs and Estimation of Camera Production Cost 160
7.4 Discussion 160

7.4.1 Design implications 160

7.4.2 Limitations *162*
7.5 Licensing Information 162

SECTION 5

8 POSTMENSTRUAL AGE-DEPENDENT STATISTICAL AND OPTICAL MODELS OF THE PRETERM EYE 164

8.1 Introduction 165
8.2 Methods 165
8.2.1 Protocol and registration *165*
8.2.1 Inclusion criteria *166*
8.2.2 Exclusion criteria *166*
8.2.3 Information Sources *166*
8.2.4 Literature Search *166*
8.2.5 Article Selection *167*
8.2.6 Data Collection and Synthesis *167*
8.2.7 Data items and Summary Measures *167*
8.2.8 Risk of bias in individual studies *168*
8.2.9 Synthesis of results *168*
8.2.10 Risk of bias across studies *169*
8.2.11 Optical modelling *169*
8.3 Results 171
8.3.1 Study selection *171*
8.3.2 Study Characteristics and Findings *172*
8.3.3 Risk of Bias within Studies *175*
8.3.4 Meta-analysis *177*
8.3.5 Risk of Bias Across Studies *178*
8.3.6 Optical Model *179*
8.4 Discussion 179
8.4.1 Limitations *181*
8.5 Conclusion 182

9 DESIGN AND PROTOTYPING OF A PRETERM INFANT RETINAL IMAGING PHANTOM 183

9.1 Introduction 184
9.2 Methods 184
9.2.1 Simulation of a Stock Lens Model *184*
9.2.2 Construction of Preterm Infant Phantom, Eye and Enclosure *186*
9.2.3 Validation of Eye Phantom *191*
9.3 Results 192
9.4 Discussion 194

10 LMIC ROP CAMERA TECHNOLOGY DEMONSTRATOR 196

10.1 Introduction 197
10.2 Methods 198
10.2.1 Optical Design *198*
10.2.2 System Design *199*
10.2.3 Graphical User Interface *205*
10.2.4 Performance Testing *206*
10.3 Results 208
10.4 Discussion 211

10.5 Licensing Information 214

SECTION 6

11 DISCUSSION AND CONCLUSIONS 216

11.1 Contributions of this Thesis 217

11.2 Limitations 220

11.3 Conclusion 222

12 PROPOSALS FOR FUTURE WORK 225

12.1 Smartphone Retinal Image Mosaicking 226

12.2 Diabetic Retinopathy Time and Motion Study 227

12.3 ROP Camera Design for Manufacture 228

12.4 Enhanced Clinical Workflow Modelling 229

BACK MATTER

LIST OF PUBLICATIONS 231

REFERENCES 235

APPENDICES 273

Appendix 2.1 .....

PRISMA Checklist for Review of Reviews and Critical Analyses of Global mHealth Adoption ... 273

Appendix 2.2 .....

PICOS Worksheet and Search Strategy document for Review of Reviews and Critical Analyses of Global mHealth Adoption 275A

Appendix 5.1 .....

Code for non-sequential polygon object for Zemax OpticStudio modelling first design-iteration of the smartphone ophthalmoscope 275

Appendix 5.2 .....

Bill of materials for prototyping the first design iteration of the smartphone-based ophthalmoscope 276A

Appendix 5.3 .....

Code for non-sequential polygon object for Zemax OpticStudio modelling second design-iteration of the smartphone ophthalmoscope 276A

Appendix 5.4 .....

Bill of materials for prototyping the second design iteration of the smartphone-based ophthalmoscope 276

Appendix 5.5 .....

Bill of materials for prototyping the third design iteration of the smartphone-based ophthalmoscope 277A

Appendix 5.6 .....

Spectral weighting functions for light hazard protection calculations 277

Appendix 6.1 .....

R-script for fitting curves to Nakuru Cohort Study Patient Data 279A

Appendix 6.2 .....

R-script for generating participants for Nakuru community eye health workflow model 280

APPENDIX 7.1 .....
PowerShell 2.0 Script for Extracting Events by Clinic 283A
APPENDIX 7.2 .....
PowerShell 2.0 Script for Extracting Event Timings 285
APPENDIX 8.1 .....
PRISMA 2009 Checklist 289A
APPENDIX 8.2 .....
PICOS Worksheet and Search Strategy document for review of preterm eye biometry literature ...290
APPENDIX 8.3 .....
Full Preterm Biometry Meta-analysis Search Code 291A
APPENDIX 8.4 .....
Preterm Optical CAD Model 291A
APPENDIX 9.1 .....
Bill of materials for prototyping preterm retinal eye phantom 291
APPENDIX 10.1 .....
Bill of materials for prototyping the low-cost portable widefield fundus camera 292A

Acronyms and Abbreviations

app – application
ANOVA – analysis of variance
AMOLED - Active matrix organic light emitting diode
API – application programming interface
CBA – controlled before and after study
CDF – Cumulative Distribution Function
CEHW – Community eye health worker
CHW – community health worker
CI – confidence interval
COR – cortical cataract
CPN – coloured Petri net
DM – diabetes mellitus
DMO - diabetic macular oedema
DR – diabetic retinopathy
ETDRS – Early Treatment Diabetic Retinopathy Study
ECDF – Empirical cumulative distribution function
e-health – electronic health
EPO - erythropoietin
EU – European Union
FDA – Food and Drugs Administration
FoV – field of view
GA – gestational age
GUI – graphical user interface
HIC – High-income country
HFA - Humphrey field analyser
ITS – interrupted time series
KIDROP - Karnataka Internet Assisted Diagnosis of Retinopathy of Prematurity
KS test – Kolmogorov-Smirnov test
LICs – Low-income countries
LMIC – Low and Middle Income Country
logMAR – Logarithm of the minimum angle of resolution
mERA – mHealth Evidence Reporting and Assessment
mHealth – mobile health
MRF – Melbourne rapid fields
mServices – mobile services
NCD – Non-communicable disease
NICU – neonatal intensive care unit
NPDR - non-proliferative diabetic retinopathy
NUC – nuclear cataract
OCT - Optical coherence tomography
PC – personal computer
PDA – personal digital assistant
PDR – proliferative diabetic retinopathy
pixel – picture element
PLA – polylactic acid
PMA – postmenstrual age

PMMA - Polymethylmethacrylate
PSC - posterior subcapsular cataract
QRCT – quasi-randomised controlled trial
RCT – Randomised
ROP – Retinopathy of prematurity
SITA - Swedish Interactive Thresholding Algorithm
SSA – Sub-Saharan Africa
T&M – time and motion
TRV – test-retest variability
TFT LCD - thin film transistor liquid crystal display
UI – uncertainty interval
WfMS – workflow management system
YAWL – yet another workflow language
VCDR – Vertical cup-to-disc ratio
VEGF - vascular endothelium growth factor
VTDR- vision-threatening diabetic retinopathy
WHO – World Health Organisation
WIPO – World Intellectual Property Organization.
UN – United Nations
USB – universal serial bus
USB OTG – universal serial bus on-the-go

1 Thesis Overview

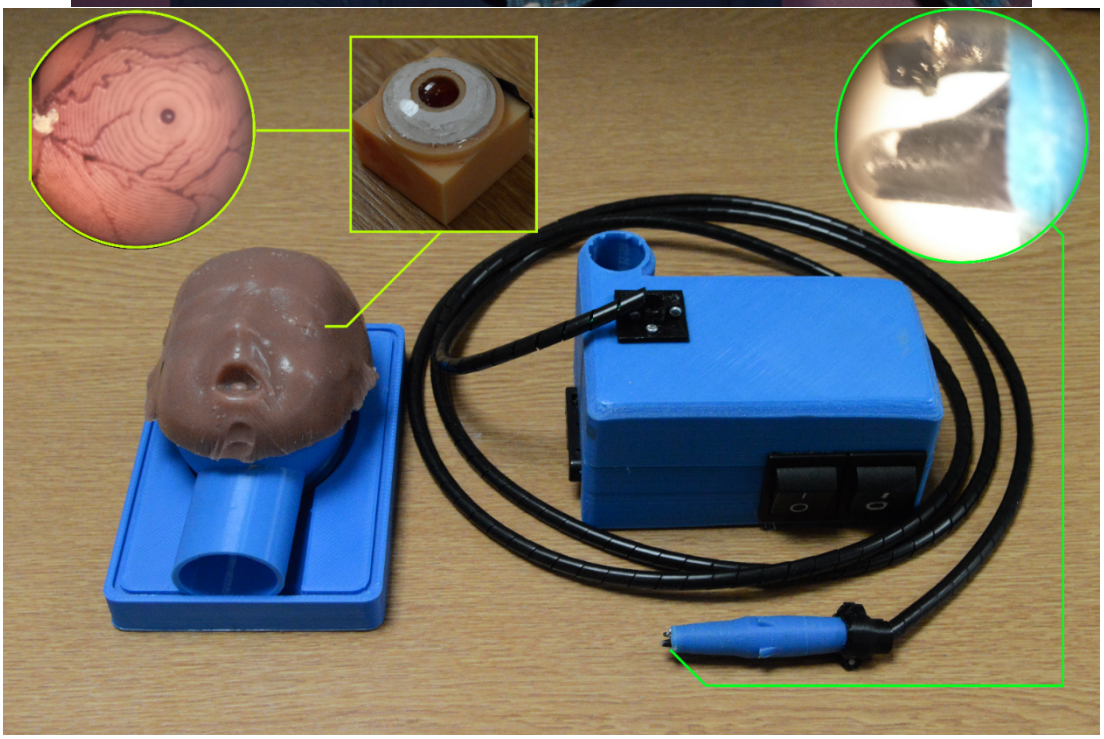

1.1 Introduction

Mobile phone technology has revolutionised the way the world's population communicates. The relatively low cost of both handsets and provision of wireless network services has allowed the technology to spread across the globe, including to remote and highly deprived areas, and it is now estimated that there are in excess of 7 billion active mobile phone subscriptions worldwide (1). Furthermore, an increasing share of these are smartphones, mobile devices combining the simple communication capabilities of their predecessors, alongside more advanced capabilities such as operating systems allowing application (app) installation and upgrade, more powerful computer processing, high-resolution digital cameras and global positioning systems, as well as accelerometers and other sensors (2). The widespread availability of such a technology-rich resource provides the potential for a host of applications within medicine, particularly in those areas with poor health service provision, and consequently the field of mobile health, normally referred to as mHealth, has emerged (3-8).

However, full adoption of mHealth interventions into healthcare systems has been slow, in-spite of a large number of mHealth pilot studies reporting success (9, 10). It has been proposed in the scientific literature that one cause of this discrepancy is a mismatch between the technological requirements tested in these pilot studies and the requirements for integration and adoption into the clinical workflow (10, 11). There has therefore been a call for more analysis of the clinical workflows which are expected to adopt mHealth technology (12).

Eye care in low- and middle-income countries (LMICs) represents an appropriate sub-field for the testing of this hypothesis, given the current disparity in care provision between high- and low-income settings (13) and the significant potential of mHealth in addressing this (14). Coloured Petri nets (CPNs) have long been used in the analysis of a particular workflow's sensitivity to the variation of the parameters of its component processes in assembly line analysis and information technology infrastructure design (15). The applicability of CPNs to clinical workflows has also been widely reported and thus represents a promising means for accessing the sensitivity of the clinical workflows involved in eye care in low-income

settings to the variation of design parameters relating to relevant mHealth interventions (16).

This doctoral thesis examines the link between the technical design parameters of a suite of prototype mHealth devices for the delivery of eye care in LMICs and the clinical workflows they are expected to interact with, through a combination of workflow modelling, optical modelling, prototyping and field testing.

Two settings are considered. The first of these is a temporary community eye clinic based in a low-income country. This clinic screens those over 50 years' of age, a population in which 77% of the visual impaired reside (17). The second is a screening programme for retinopathy of prematurity, a leading cause of childhood blindness (18).

1.2 Aims

The aim of this thesis is to investigate whether workflow modelling techniques, established in other fields, might be applied to the field of mHealth in order to reduce the number mHealth device designs that fail to produce results in clinical pilots that lead to subsequent adoption at scale. Eye care is used as a template example of mHealth.

1.3 Objectives

The above aim was pursued through the following objectives.

1. Identify the main goals, applications and barriers to adoption at scale of mHealth, as currently understood, from the scientific literature.
2. Establish the state-of-the-art in mHealth interventions for eye care in LMICs by reviewing the scientific literature.
3. Design a smartphone-based digital ophthalmoscope appropriate for use in community settings in low-income countries.
4. Model the workflow of the community eye clinics of the Nakuru Eye Disease Cohort Study in Kenya, deploy the aforementioned smartphone-based ophthalmoscope and study the interaction between the ophthalmoscope and the clinical workflow.

5. Model the workflow of the KIDROP retinopathy of prematurity screening programme in Karnataka, India. Then use the aforementioned model to estimate the screening coverage, treatment coverage, task distribution and programme costs achieved by deploying a dedicated, tablet computer operated, portable fundus camera for the screening of preterm infants.
6. Develop a simulation model of the preterm eye to aid the design of a device for imaging preterm ocular fundi.
7. Design a dedicated portable fundus camera operated by a tablet computer for the screening of preterm infants.
8. Summarise and qualitatively generalise the findings from the studies above to workflow analysis of mHealth devices in eye care in LMICs.

1.4 Thesis Organisation

This thesis is divided into 12 chapters which themselves fall into six over-arching sections.

The first section, Chapters 2 to 4, addresses Objectives 1 and 2 as well as justifying the relevance of the stated aims and objectives. Thus, it includes literature reviews of the global adoption of mHealth and the state-of-the-art in mHealth solutions for eye care as well as an introduction to the modelling techniques used in this study.

The second section, consisting of Chapter 5, addresses Objective 3. It describes three iterations of a design for a smartphone-based direct ophthalmoscope suitable for use within a community setting in low-income countries.

The third section, consisting of Chapter 6, addresses Objective 4. The clinical workflow of the Nakuru Eye Disease Cohort Study, in which prototypes of the aforementioned smartphone-based ophthalmoscope design was deployed, is modelled and the interaction between the clinical workflow and the ophthalmoscope studied.

The fourth section, consisting of Chapter 7, addresses Objective 5. In this chapter, the workflow of the KIDROP retinopathy of prematurity screening programme in Karnataka, India is modelled. Workflow simulations based on this model are then used to estimate the screening coverage, treatment coverage, task distribution and

programme costs that would be achieved by deploying a dedicated, tablet computer operated, portable fundus camera for the screening of preterm infants.

The fifth section, including Chapters 8 to 10, addresses Objectives 6 and 7. Chapter 8 concerns the optical modelling of the preterm eye during its early postnatal development based on a meta-analysis of the scientific literature. Chapter 9 then describes the development of a preterm ocular fundus imaging phantom for conducting lab-tests with a prototype of the subsequent portable fundus camera design. Next, Chapter 10 details the design and prototyping of a tablet computer-based portable retinal camera suitable for retinopathy of prematurity screening in middle-income settings.

The Sixth and final section, consisting of Chapters 11 and 12 and addressing Objective 8, then discusses the implications of the results of the above with respect to the aim of the thesis and suggests topics for further research.

SECTION 1

Chapter 2 -Review of Global mHealth Adoption Literature

Chapter 3 - mHealth Solutions for Eye Care Delivery in Low Income Settings

Chapter 4 – An Introduction to Clinical Workflow Modelling

2 Review of Global mHealth Adoption Literature

"There's 5.6 billion people using wireless today in the world. To put that in a health care context, that's more people using cell phones than toothbrushes."

Paul Jacobs, Ph.D., CEO, Qualcomm (mHealth Summit, Washington, D.C., December 2011)

2.1 Background

2.1.1 Technological Context: The Ascent of Mobile Devices

Before reviewing the recent progress of mHealth it is first necessary to understand the wider context in which mHealth has arisen. The proliferation of portable, consumer-level wireless technology has been one of the major technology events of recent decades (19). The expansion in the use of mobile technology has been made possible by the availability of affordable mobile devices, including mobile phones, smartphones, tablet computers and personal digital assistants (PDAs), coupled with the rapid and extensive expansion of mobile network coverage (20). In conjunction with this phenomenon a vast ecosystem of mobile services has arisen granting mobile devices' users access to services (mServices) in areas as diverse as banking to livestock management (21, 22).

By far the most common mobile device is the mobile phone (23). These portable handsets initially combined voice calls with short-messaging and multimedia services (SMS and MMS), simple applications and basic internet browsing. The widespread adoption of the smartphone has greatly enhanced the features available to mobile phone users. In addition to the simple communication abilities of their predecessors, today's smartphone handsets incorporate more powerful computer processing, allowing more sophisticated application (app) installation and upgrade, as well as touch-screen interfaces, global positioning systems (GPS), high-resolution cameras and a number of other sensors including accelerometers and fingerprint scanners.

Having started the 21st century on rough parity with (landline) fixed-telephones, the number of mobile phone subscriptions globally is steadily increasing, as shown in Figure 1, with recent data published by the International Telecommunications Union suggesting that the number of active subscriptions worldwide is approaching that of the global population (24). Notably, this phenomenon is a universal one, with it being estimated that 66% of people globally have a mobile phone subscription, including 67% of those in the Latin America and Asia Pacific regions and as many as 44% of people in Sub-Saharan Africa (SSA) (20).

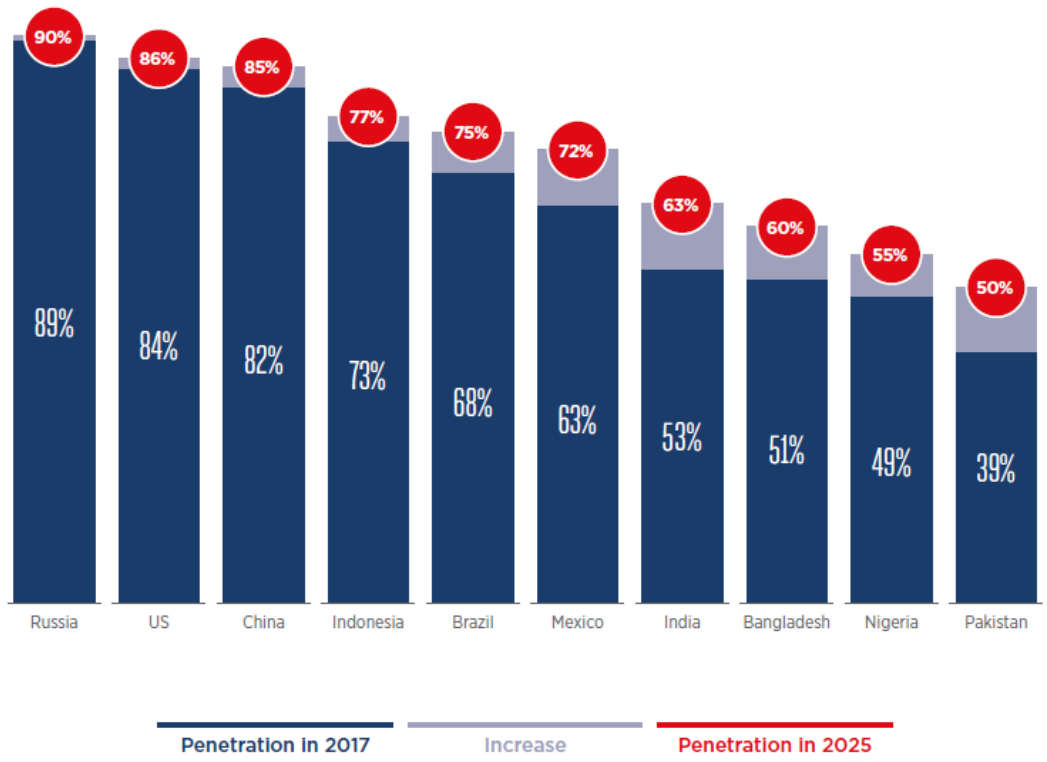

Figure 1 – Proportion of persons in 2017 with a mobile phone subscriptions in the ten most populous countries and the projected increase by 2025. Reproduced from (25)

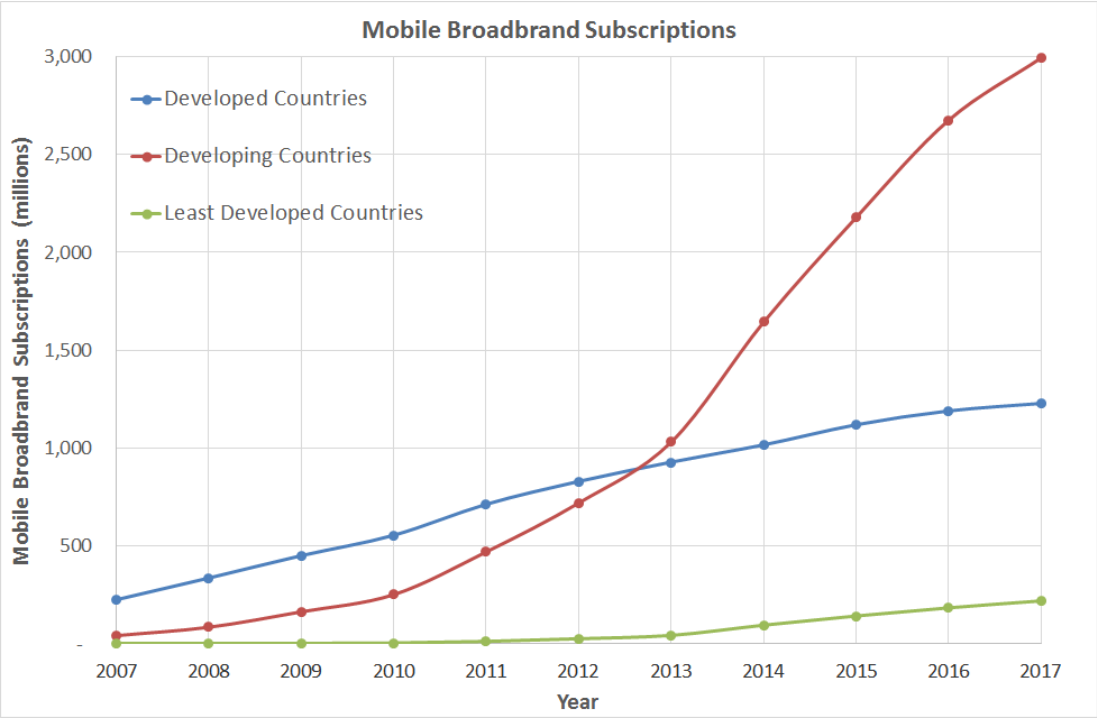

Figure 2 - Active mobile broadband subscriptions per 100 people, 2007-2017

Similarly, with their powerful computer processing, access to mobile broadband, host of sensors, low cost and lightweight form, tablet PCs offer affordable access to more powerful mobile computing. Indeed, it is estimated that global sales of tablet computers in 2015 exceeded that of laptop and desktop computers combined and that by 2017 there were 1.14 billion users of tablet computers, accounting for 32.9% of all internet users (26, 27). Furthermore, a large proportion of these sales have been in low- and middle-income countries (LMICs) with four of the top five countries by tablet ownership being classified as middle-income (28).

The spread of such mobile devices has been facilitated by the rapid expansion of mobile networks, which can be built quicker and at a much lower cost than wired fixed-telephone networks (29). It is this fact that has allowed LMICs to "leapfrog" the older technologies which preceded mobile technology's introduction in high-income countries (HICs) and rapidly bridge the global inequality in access to portable communications technology (29, 30).

Indeed, access to broadband internet is steadily rising in LMICs on the back of mobile technology with the International Telecommunications Union (ITU) estimating that in 2017 there were 2,993 million mobile broadband subscriptions in nations classified as developing, as shown in Figure 2. This has also been estimated to constitute over 80% of all broadband subscriptions in such countries (1).

The sudden arrival of so many new internet users onto the market has posed a significant opportunity for innovators throughout the world. Today, a vast number of both SMS and application-based services (mServices) are available to the mobile device user. To give a sense of the scale of this industry, the two main sellers of mobile device applications, the Apple (Cupertino, CA, USA) 'App Store' and Google (Mountain View, CA, USA) 'Play Store', have upwards of two million apps each (31). This, of course, does not include SMS-based services or applications for operating systems other that iOS and Android. Whilst in HICs many of the services offered represent a convenient means of accessing existing services, in LMICs mServices are opening access to particular services to millions of users for the very first time. For example, in East Africa the mFinance service 'M-PESA' (SafariCom, Nairobi, Kenya) has seen phenomenal growth, subscribing over six million customers in Kenya alone in its first two years of operation (32), and is now seen as

an integral part of the national economy (33). Such has been the success of the service that it has fostered its own ecosystem of innovations including, for example, 'BusinessOS' (Kopo Kopo, Morningside Office Park, Ngong Rd, Nairobi, Kenya), which provides small and medium enterprises (SMEs) with automated book-keeping, financial analytics, forecasting and targeted marketing capabilities. Similar mServices have not achieved widespread adoption in HICs, where the vast majority of the population have access to such services by other means. Consequently, it has been suggested that, increasingly, innovation and scaling of mServices will occur in LMICs, where the demand and potential for rapid growth is greatest.

It is into this fertile but rapidly changing environment that mHealth, the provision of healthcare via mobile technology, has come. The remainder of this chapter focusses on how mHealth has fared during the swift ascent of mobile technology and what challenges are to be overcome if mobile technology is to extend the access to healthcare in the way it has to other services.

2.1.2 mHealth: Mobile Devices in a Healthcare Setting

The term 'mHealth' was coined by Robert Istepanian in 2000 who later defined this as "mobile computing, medical sensor and communications technology for healthcare" (34). Whilst perhaps fit-for-purpose ten years ago, this definition is very broad. For example, in 2014 it was reported that more than 100,000 apps fell into the health, fitness, or medical categories in the various app stores. These range from dieting and fitness aids to medical devices requiring regulatory approval. Nevertheless, the widely varying applications of mHealth software and hardware can be largely allocated into a number of discrete categories, as has been noted by numerous reviews of the subject (35).

Lifestyle apps constitute a sizeable proportion of the total available apps in the respective app stores. These range from those developed and/or sanctioned by healthcare providers to sports companies to dieting organisations and other third-party organisations.

Whilst lifestyle apps may have a significant impact on public health and health monitoring, they do not directly impact health systems. Hence, these applications were considered outside the scope of the present study, given its focus on mHealth interventions directly impacting health system clinical workflows.

There has been huge excitement surrounding the potential for mHealth. For example, in 2011 the U.S. Secretary of Health and Human Services, Kathleen Sebelius, described mHealth as being "the biggest technology breakthrough of our time" (36). However, it has also been noted that there has been a significant proliferation of pilot studies of mHealth technology
whilst the rate of these technologies being adopted into clinical practice at any meaningful scale has lagged well behind (37).

If mHealth's significant potential is to be realised it is therefore of the upmost importance that a proper understanding of the reasons why the pilots of so many mHealth interventions are reporting success and not attaining successful adoption into clinical practice. Such an understanding would not only allow for better identification of which piloted interventions to progress but would also inform the future design of mHealth pilots and even the underlying technology being studied.

2.2 Literature Review Methods

In order to develop an understanding of why pilots of mHealth technologies fail to progress from the pilot stage, the remainder of this chapter describes a systematic review of the reviews and expert opinion published in the scientific literature in the past five years, as well as selected widely cited texts from the grey literature, that is texts that are not themselves formally peer-reviewed but are referenced by peer-reviewed sources.
The review was conducted and is presented in this thesis in accordance with the Preferred Reporting Items for Systematic Reviews and Meta-Analyses (PRISMA) guidelines for reporting systematic reviews (38).[1] Owing to the heterogeneity of the included literature, a quantitative analysis was not considered appropriate and thus only a qualitative synthesis was conducted.

[1] See Appendix 2.1 for the completed PRISMA 2009 Checklist for this review.

2.2.1 Inclusion Criteria

The aim of the review was to synthesise current perceptions of the barriers to mHealth's integration into healthcare systems a topic regarding which a large number of reviews have already been published. It was therefore decided that the most appropriate route to achieving this aim would be to survey the secondary research relating to the topic as opposed to sifting through the large volume of primary research studying mHealth. Therefore, the inclusion criteria for the review were any publication of type meta-analysis, systematic review, thematic review, editorial, essay, letter or opinion that discusses the barriers to mHealth adoption at scale or proposed solutions to such barriers, rather than those reporting the results from a single study conducted by the authors.

Given the rapid development of the sector in question, it was decided that only articles written in the past five years (publication date between 1st January 2011 and 15th September 2016) were eligible for inclusion in the review. Finally, only those articles available in English were considered eligible as this is the only language in which the author is fluent.[2]

2.2.2 Exclusion Criteria

Eligibility was restricted to articles discussing mHealth as a tool for disease management, treatment or rehabilitation within the community or for use within the healthcare system itself. Articles solely discussing consumer health and wellbeing apps, for example, were therefore out of the scope of this review. Internet or video-based interventions not specifically designed for mobile technologies were considered out of scope, as was the use of mobile devices' core functionality without any particular modification for use in healthcare (e.g. discussion of doctors' use of personal mobile phones versus landline telephones). Articles only discussing applications involving raising awareness of a particular disease in the general population, whether for the purpose of fundraising or otherwise, or those providing training relating to first aid were also considered out of scope.

[2] See Appendix 2.2 for the completed PICOS Worksheet and Search Strategy document for this review.

	AND				
	Title Contains one of	**Subjects Includes**	**Subjects do not Include**	**Document Type**	**Publication Year**
OR	smartphone smart phone smartphones smart phones mobile phone mobile phones cell phone cell phones cellular phone cellular phones cellular network tablet pc tablet computer tablet computers m-health mHealth mobile health mobile device mobile devices mobile telephone mobile telephones mobile telephony cellphone cellphones	Medicine Health Biomedical	Public Environmental Occupational Health	Discussion Editorial Material Letter Review	2011-2016

Table 1 - Search criteria for the review of reviews of mHealth in the scientific literature.

2.2.3 Information Sources

MIMAS Web of Knowledge. Grey literature was selected from those recommended by The World Health Organisation (WHO), World Bank and United Nations (UN) or a department thereof.

2.2.4 Search Criteria

The Web of Knowledge search terms are shown in Table 1. Included indices were SCI-EXPANDED, SSCI, A&HCI, CPCI-S, CPCI-SSH, BKCI-S, BKCI-SSH, ESCI, CCR-EXPANDED.

2.2.5 Article Selection

Eligibility assessment was conducted in an unblinded manner by the author only. Articles were screened and reviewed according to the process represented graphically in Figure 3. Duplicates were removed using EndNote X7 (Thomson Reuters Corp., New York City, NY, USA) leaving only unique articles whose titles were then screened for relevance. The articles that were considered eligible had their abstracts screened and those that were deemed to qualify underwent full-text assessment.

2.2.6 Data Collection and Synthesis

The reported goals, application types, barriers to scale of mHealth were recorded for each of the reviewed articles as well as general observations. Categories for each of the data types were developed by taking those listed by Qiang and colleagues (35) and then adding to these lists when an article contained data which was deemed outside of these categories.

Limitations of each article were noted, although no article was deemed ineligible for inclusion in the analysis. A formal assessment of risk of bias was not conducted, except for noting the specific sub-field of medicine, application, host technology or end-users each article sought to address in its analysis.

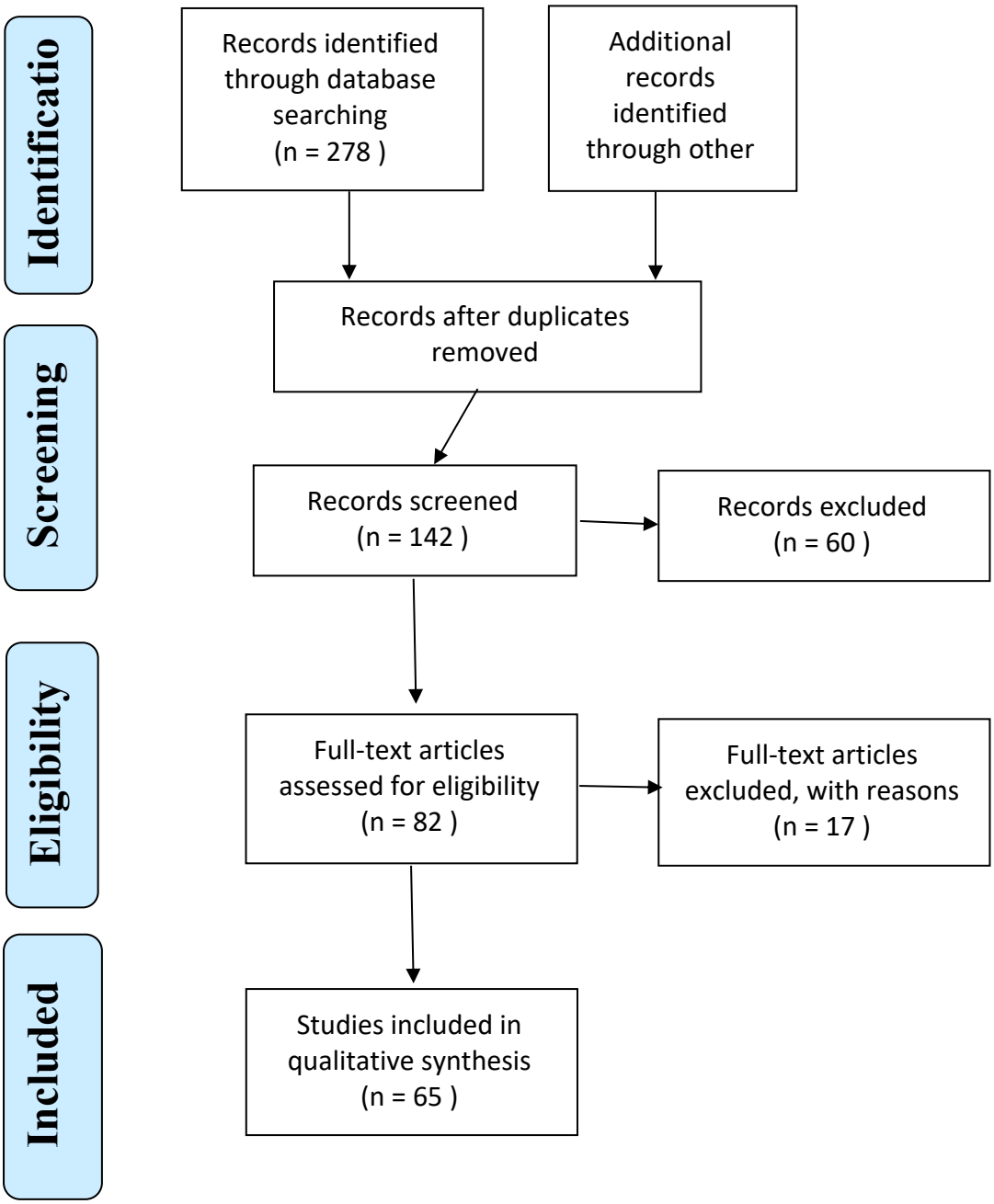

Figure 3 - PRISMA 2009 Flow Diagram for the review of mHealth reviews. Adapted from (38) with permissions.

2.3 Results

2.3.1 Article Selection

278 records were returned from the database search detailed above to which 9 reports from the grey literature were added. Duplicates were removed using EndNote X7 leaving 281 unique articles whose titles were then screened for relevance. 142 of these articles were then considered eligible for having their abstract screened of which 82 were deemed to qualify for full text assessment of eligibility. The full texts of seven of these articles were not available and a further ten articles were deemed to not meet the eligibility criteria. Therefore, a total of 65 articles were included in the qualitative synthesis.

2.3.2 Article Characteristics

Of the 65 articles selected for review, twenty-one were systematic reviews (3-6, 37, 39-54), four thematic reviews (7, 55-57), thirty-one letters or editorials (8, 11, 58-86) and nine non-peer reviewed reports taken from the grey literature (9, 10, 35, 87-92). Two of the selected articles involved a meta-analysis of the reviewed studies. Three of the articles were published in 2011 (9, 58, 62), eight in 2012 (3, 35, 41-44, 63, 64), eighteen in 2013 (4, 7, 11, 45-50, 59, 65-71, 89), eighteen in 2014 (5, 6, 57, 72-83, 88, 90, 91), twelve in 2015 (8, 39, 40, 51-53, 55, 56, 60, 84, 85, 87), and six in 2016 (10, 37, 54, 61, 86, 92).

Six of the systematic reviews (44, 45, 47, 48, 50, 54) and six of the letters and editorials (11, 56, 70, 76, 81, 83) reviewed discussed the field of mHealth in general as did five of the grey literature sources selected (9, 35, 87, 88, 910). The rest of articles had a broad range of foci. These included the use of mHealth in medical education (58, 66, 67, 75, 79), by healthcare professionals (37, 86), by community health workers (7), in LMICs (3-8, 91), for a specific disease or within a particular speciality (5, 46, 59, 69, 82, 85), for a specific application type (3, 41-43, 49, 53), within a certain age-group (40) and within a particular country or geographic region (4). In addition, one systematic review and eight letters and editorials primarily discussed standards or study design relating to mHealth (19, 62, 71-74, 77, 80) and one thematic review quantitatively analysed barriers to adoption (57). Finally, one

systematic review reviewed cost-utility and cost-benefit analyses of mHealth (51).

2.3.3 Results of Individual Articles

The goals, application types, barriers and suggested solutions to barriers to mHealth identified in the articles selected for review are shown in Table 2 and Table 3.

2.3.4 Synthesis of Results

Next to the primary outcome of any health intervention, improving or at least maintaining health outcomes, twenty-six secondary goals of mHealth technology and programmes were identified from the articles included in the review as can be seen in Figure 4.

There were eighteen separate applications of mHealth identified from the reviewed literature, namely:

- Self-management of treatments (3-9, 11, 35, 39-42, 46, 47, 50, 52-54, 57, 63, 69, 70, 82, 85, 90)
- Patient tracking and monitoring (4, 6, 9, 11, 35, 37, 40, 48, 50, 54, 55, 58, 59, 81, 88, 91)
- Supply chain management (5, 6, 10, 35, 90, 91)
- Health financing (8, 35, 63, 90, 91)
- Clinical decision support (5, 9, 35, 37, 39, 40, 43, 45, 48, 54, 55, 61, 63, 74, 86, 90, 91)
- Electronic health records (EHRs) (4, 5, 7-9, 35, 43, 54, 55, 58, 59, 63, 81, 83, 86, 88, 90)
- Population surveys (4, 9, 90)
- Capture of real-time health information (4, 7-9, 35, 63, 90)
- Disaster management (35, 90)
- Health system social and financial accountability and anti-counterfeiting (35, 90)
- Research (44, 45, 54, 56, 58, 62, 69, 83)
- Clinical training and reference material (39, 70)
- Human resource management (6, 7, 9, 11, 37, 39, 44, 45, 47, 54, 63, 64, 66, 67, 75, 79, 81, 84, 88, 90, 91)
- Screening and direct provision of care (90, 91)
- Patient / clinician / peer communication (4, 5, 9, 11, 37, 40, 42, 44-50, 53-56, 62, 63, 69-71, 76, 81, 82, 84, 86, 88, 90, 91)
- Workflow monitoring (91)

Forty-six barriers to mHealth adoption at scale were identified from the included articles. Of these, the twenty-seven that were identified by more than one of the included sources are shown in Figure 5.

Author and publication year	Type of article; number of studies (K)	Article focus	Mobile devices discussed	Type of research design included	Comments
Subhi et al. (2015) (39)	Systematic review K = 52	Clinical validity of mHealth apps	Smartphone	Assessments of expert involvement in app development	6520 apps assessed across the included studies. 17 studies found no apps with expert involvement, 17 found none fully adhered to the compared evidence and 13 studies found 10-87% fully adhered.
Majeed-Ariss et al. (2015) (40)	Systematic review K = 4	Apps for 10-24 year-olds with chronic illness	Smartphones and tablets	RCTs	
De Jongh et al. (2012) (41)	Systematic review K = 4	Chronic illness self-management via SMS	Mobile phones	RCTs, QRCTs, CBAs and ITSs	Found very limited indications that SMS interventions may provide benefit in self-management of long-term illnesses
Deglise et al. (2012) (3)	Systematic review K = 31	Disease control in LMICs via SMS	Mobile phones	Peer-reviewed and grey literature	
Gurol-Uraganci et al. (2012) (42)	Systematic review K = 1	Communicating results via SMS	Mobile phones	RCTs, QRCTs, CBAs and ITSs	The included study involved pre-natal screening for Down's syndrome. Noted that this decreased anxiety for those with serum-negative results but increased it for those with serum-positive results.
Kharrazi et al. (2012) (43)	Systematic review K = 19	Mobile personal health records	Smartphones only	Publically available apps	

Author and publication year	Type of article; number of studies (K)	Article focus	Mobile devices discussed	Type of research design included	Comments
Ozdalga et al. (2012) (44)	Systematic review K = 60	General mHealth	Smartphones only	Peer-reviewed literature	
Bastawrous and Armstrong (2013) (45)	Systematic review (K not reported)	General mHealth	Mobile phones	RCTs	
Bender et al. (2013) (46)	Systematic review K = 295	Cancer	Smartphones only	Publically available apps	
Fiordelli et al. (2013) (47)	Systematic review K = 117	General mHealth	Mobile phones	Peer-reviewed literature	Identified that more recently the development of mHealth has become more accurately described and grounded in evidence and theory.
Free et al. (2013) (48)	Systematic review K = 42 and meta-analysis K = 29	General mHealth	All mobile devices		
Gurol-Urganci et al. (2013) (49)	Systematic review K = 8	SMS appointment reminders	Mobile phones	RCTs, QRCTs, CBAs and ITSs	
Iwaya et al. (2013) (4)	Systematic review; K = 42	Brazil	All mobile devices	Peer-reviewed and grey literature	Comprehensive survey of mHealth programmes in Brazil.
Martinez-Perez et al. (2013) (50)	Systematic review K = 247 papers; 3673 apps	Eight most prevalent health conditions	All mobile devices	Peer-reviewed literature and publically available apps	

Author and publication year	Type of article; number of studies (K)	Article focus	Mobile devices discussed	Type of research design included	Comments
de la Torre-Diez (2015) (51)	Systematic review K = 35	Cost benefit analyses of mHealth and eHealth	All mobile devices	Peer-reviewed literature	
Mourcou et al. (2015) (52)	Thematic review K = 28	Joint angle measurement	Smartphones only	Peer-reviewed studies	
Gagnon et al. (2016) (37)	Systematic review K = 33	Use by healthcare professionals	All mobile devices	Empirical studies including healthcare professionals perceptions of mHealth	Identifies 179 barriers and facilitators of mHealth.
Anglada-Martinez (2015) (53)	Systematic review K = 20	Adherence to medication for chronic illnesses	Mobile phones	RCTs, QRCTs, cross-sectional, case-control, pre- and post-intervention, literature reviews	Found 65% of studies had positive outcomes but suggest more high-quality studies are required to demonstrate cost-effectiveness. High level of patient satisfaction found throughout the included studies.
Aranda-Jan et al. (2014) (6)	Systematic review K = 44	Africa		All peer reviewed literature	Conducted SWOT analysis of included studies.
Bloomfield et al. (2014) (5)	Systematic review K = 5	NCDs in SSA	All mobile devices	Peer reviewed and grey literature	Also includes an ‘mHealth Framework for NCDs in SSA’ based on the authors’ analysis of the reviewed studies.
Ali et al. (2016) (54)	Systematic review K = 515	General mHealth	All mobile devices	All peer reviewed literature	

Author and publication year	Type of article; number of studies (K)	Article focus	Mobile devices discussed	Type of research design included	Comments
Kallander et al. (2013) (7)	Thematic review (K not reported)	Use by CHWs in LMICs	All mobile devices	Peer-reviewed and grey literature	Extracts six themes of mHealth.
Al Dandah et al. (2015) (55)	Thematic review (K not reported)	LMICs	All mobile devices	Not reported	
Steinhubl et al. (2015) (56)	Thematic review (K not reported)	General	All mobile devices plus wearables	Not reported	
Dehzad et al. (2014) (57)	Meta-analysis K = 10	Barriers to mHealth	All mobile devices	Peer reviewed and grey literature	Also included an original study of the views of key opinion leaders within the Dutch healthcare system (86 participants by online questionnaire of which 9 were selected for semi-structured interview)

Table 2 - Summary of the reviews, both systematic and thematic, qualifying for review.

Author and publication year	Publishing Organisation	Report focus	Mobile devices discussed	Comments
Qiang et al. (2013) (35)	World Bank	General	All mobile devices	Comprehensive overview of global progress in mHealth. Contains a review of the mHealth ecosystem, a model for new mHealth interventions and a review of the business models found in three LMICs.
WHO (2015) (87)	WHO	Strategy for mHealth at scale	All mobile devices	'The MAPS Toolkit' is a comprehensive planning and strategy tool for mHealth at scale drawn from a variety of sources.
Economist Intelligence Unit (2014) (88)	PriceWaterhouseCooper	General	All mobile devices	Survey of doctors and executives from healthcare payer organisations.
Agarwal et al. (2016) (10)	BMJ	mHealth study reporting guide	Mobile phones	Contains the 'Mobile Health Evidence Reporting and Assessment (mERA) Checklist'

Author and publication year	Publishing Organisation	Report focus	Mobile devices discussed	Comments
Kay (2011) (9)	WHO Global Observatory for eHealth	General	All mobile devices	Review of mHealth initiatives globally and assessment of the barriers to mHealth implementation.
Smith and Patty (2013) (89)	Vital Wave Consulting	Sustainable finance for mHealth	All mobile devices	Presentation of techniques for ensuring sustainable financing of mHealth.
Keisling (2014) (90)	N/A	General	All mobile devices	Guide for programme managers seeking to integrate mHealth solutions into their health systems.
K4Health (2014) (91)	K4Health`	LMICs	All mobile devices	Planning guide for integrating mHealth in to health programmes at scale.
Philippot (2016) (92)	Dimagi	Sustainable finance for mHealth	All mobile devices	Total Cost of Ownership model for mHealth.

Table 3 - Summary of the grey literature including in the review

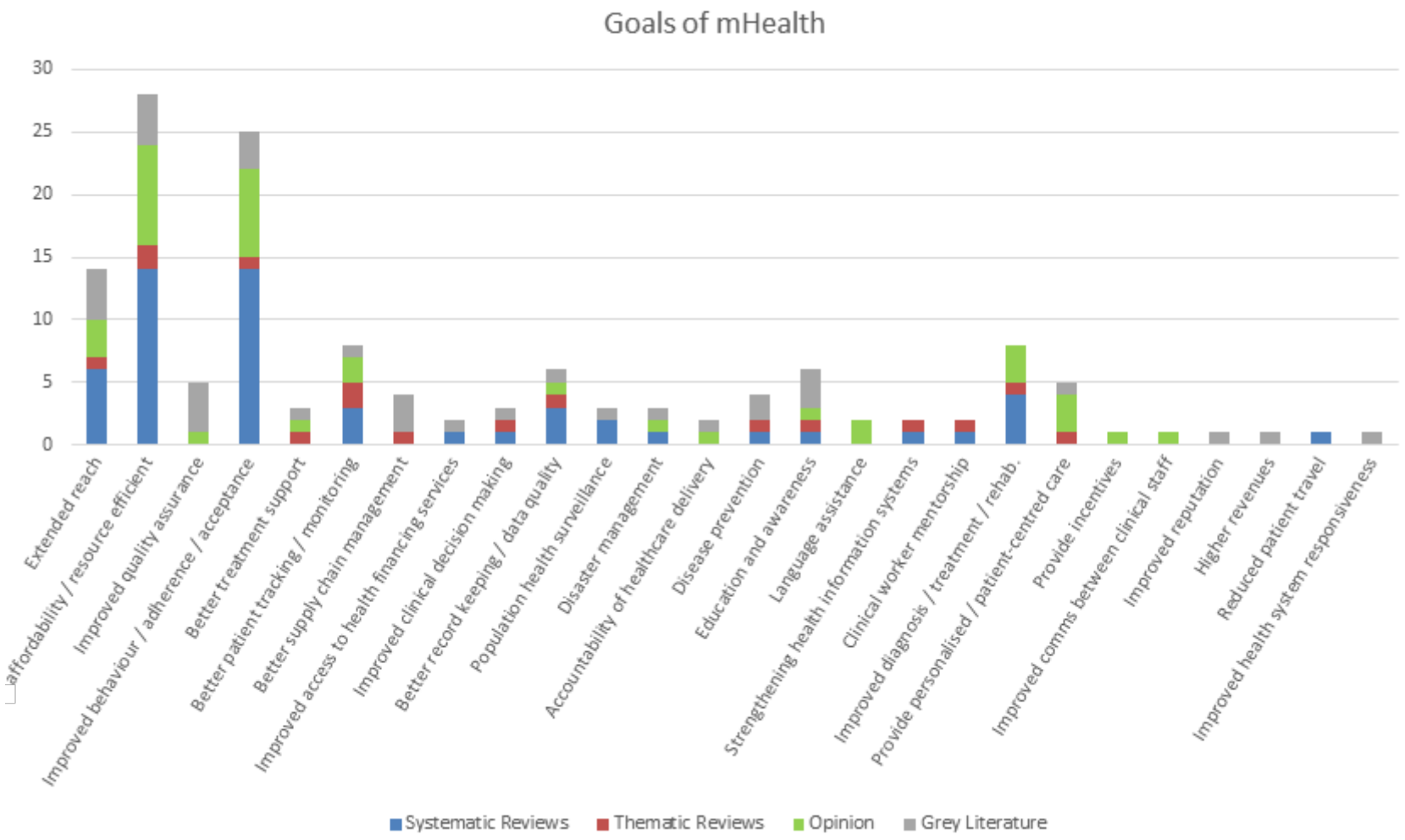

Figure 4 - Goals of mHealth technology and programmes identified from the articles included in the qualitative synthesis.

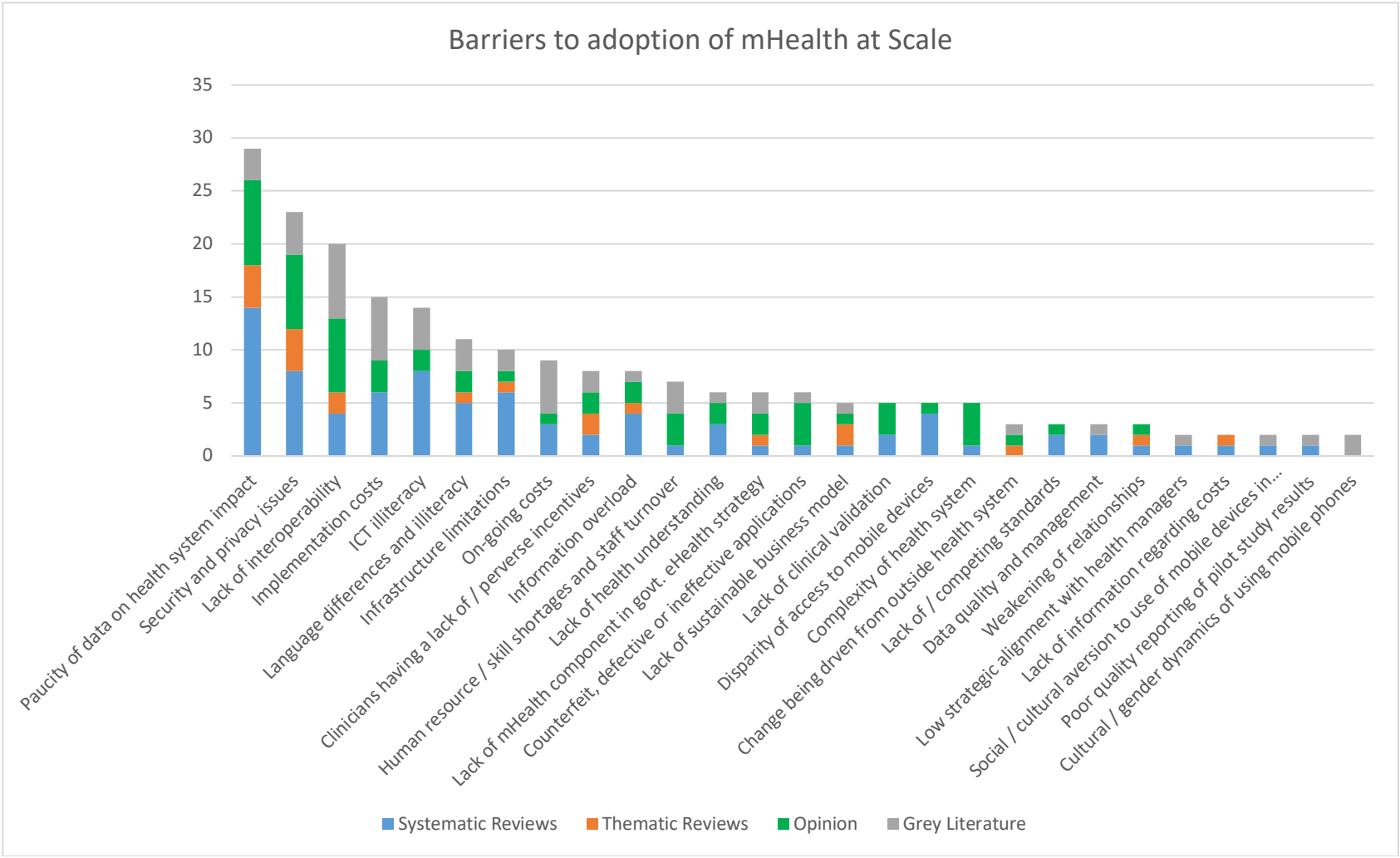

Figure 5 - The barriers to adoption of mHealth at scale with health systems identified from the included literature.

2.4 Discussion

From the breadth of the applications of mHealth listed above, it is clear that mHealth can involve an exceptionally wide range of functions, end-users, settings and complexity. These range from simple informational SMS-based services equivalent to an electronic patient information pamphlet to complicated diagnostic equipment qualifying as class-II medical devices or higher. Consequently, due to this significant clinical and methodological heterogeneity in the reviewed literature, it was not possible to perform a formal meta-analysis. Nevertheless, the reviewed literature does highlight several points applicable to the majority, if not all, mHealth technologies.

2.4.1 Goals of mHealth Systems and Perceived Opportunities

2.4.1.1 Increasing Affordability

Throughout the reviewed literature, mHealth is seen as a means of increasing affordability and resource efficiency of healthcare provision. Such improvements come in a variety of different forms. Shifting tasks from clinically skilled personnel to those with less clinical skill, or even patients themselves, allows doctors and nurses to spend more time on more specialist tasks. mHealth's ease-of-use and ability to make use of software that guides the user through diagnostic and treatment workflows offers a means of shifting many tasks that currently require a health professional's involvement. Patient management tools also offer a means of increasing efficiency. For example, it was found by Gurol-Urganci and colleagues that patients who sent SMS appointment reminders had a 14% higher attendance rate than those sent no reminder at all (49). Given that missed appointments cost NHS England £794 million alone, the financial savings could be profound. Reducing patient contact time with clinicians through better self-management and disease information, resulting in fewer unnecessary appointments, also has the potential to reduce the burden on healthcare professionals.

2.4.1.2 Improving Patient Adherence

mHealth is also seen as having the potential to improve patients' adherence to treatment regimes. There are numerous methods by which mHealth programmes have attempted to achieve this. These range from simple education and awareness campaigns conducted via SMS to personalised treatment programmes that train algorithms on patients' health data to provide a care plan that is unique for each patient. The use of diagnostic supports also helps ensure that healthcare professionals adhere to approved protocols, ensuring that care remains based on up-to-date evidence-based medicine.

2.4.1.3 Extending Health System Reach

The third most frequently cited goal for mHealth was extending the reach of health systems. It is within this goal that this thesis seeks to operate given that a lack of data concerning health system impact is also the most commonly cited barrier to mHealth adoption. Furthermore, extending health system reach being a key goal of LMIC sustainable development in general (93). It can therefore be argued that this goal is the most pressing priority for further research, particularly when concerned with healthcare in LMICs.

mHealth's portability, sophistication and its ability to be operated by non-clinical workers all combine to provide even relatively complex healthcare services to even the remotest settings. For example, Bloomfield and colleagues cite the example community health workers (CHWs) in Zambia using a combination of mobile phone integrated biosensors and cameras to gather patient data relating to dermatopathology and then remotely connect with trained providers (5). Furthermore, the use of mobile electronic health records (mEHRs) allows such clinical data to be drawn together for easier analysis and tracking over the long-term. In addition, the ability for CHWs to be trained and mentored using mobile technology means that they can stay longer in the field, if not indefinitely, enhancing the level of service that can be provided in their area operation.

2.4.1.4 Goals of mHealth in LMICs

Moreover, articles discussing mHealth in LMICs specifically yielded broadly similar goals as those found in the body of literature at large. The proportion of the literature in which each goal arose was also approximately the same. An exception to this

were three goals identified exclusively in articles focusing on LMICs. These were: strengthening health information systems (5, 7), reduction in patient travel times (54) and improved health system responsiveness (91). Each of these relate to the generally poorer quality of infrastructure found in LMICs when compared to HICs. As such this lends more credence to the notion that, like other mServices, there may be higher returns to be reaped in deploying mHealth to LMICs where infrastructure improvements previously seen as prerequisites to improved healthcare are by-passed entirely (88). Thus, LMICs have been quickest to adopt mHealth and this is providing many patients with access to certain health services for the first time, rather than simply making existing services more efficient, cost effective or convenient (88). Hence, whilst mHealth programmes initially were more concentrated in HICs (76), there is now growing consensus that LMICs are the most important 'test-bed' for mHealth.

2.4.2 Barriers to Adoption at Scale and Proposed Solutions

Common to almost all varieties of mHealth is the apparent difficulty of moving the technology from pilot stage to integration into the health system at scale. This follows from the fact that hosting a medical device on a mobile platform presents some intrinsic challenges as well as opportunities.

2.4.2.1 Lack of Data Concerning Health System Impact

The most frequently cited reason for lack of clinical adoption was the paucity of data on the comprehensive impact of mHealth services. This includes the state of so-called 'Pilotitis', the proliferation of small-scale pilot studies of relatively poor methodological quality. Whilst some high-quality studies begin to appear (94, 95), there is a call throughout the reviewed literature for large sample, multi-site trials of mHealth so to allow better assessment of the technologies' impact. However, quality of methodology is not the only issue in this regard, there is also a lack of reported data on the impact on other aspects of the health system into which mHealth is introduced (35). Indeed, Oreskovic and colleagues posit that "it is not sufficient to marshal mHealth resources to [automate] complex health problems" and suggest that combining engineering solutions with systems science may present a means of determining how to deploy mHealth technologies so to have the greatest impact on

efficiency and effectiveness of healthcare delivery (60).

In business, highly disruptive technology, which violently upends established conventions and operational practices, can often be seen as desirable (96). Whilst the failure of individual businesses who fail to adapt to a changing technological environment has little or even a positive impact on the wider economy and society as a whole, health systems or elements therein cannot simply be allowed to fail in such a way without causing damage to patient care. Therefore, as summarised by Labrique and colleagues, "Identifying the least disruptive 'fit' within existing health systems may make mHealth strategies more palatable for systems that normally eschew changes to status quo." (68) Hence understanding the workflow impact of mHealth before it is deployed at scale is of high importance.

2.4.2.2 Lack of Interoperability

Another highly cited barrier to mHealth at scale that is a consequence of research largely conducted through pilot studies is the lack of interoperability between applications of mHealth. The authors of the WHO's 'MAPS Toolkit' agree that interoperability is a critical element of large-scale deployments of mHealth, stating that developers ought to determine which data standards must be adhered to and demonstrate that the solution can interoperate with those systems which it will be deployed alongside (87). The development of, and adherence to, design and data standards for mHealth development may and has been an important means of fostering interoperability. Keeping these standards open, so that not only well-funded and institutional developers can access these, may also prove to be a multiplier of interoperability (57, 97). Open source code may also improve interoperability by allowing developers to learn from each other, be more accountable, re-use each other's code and even embed entire solutions within larger frameworks and applications (57, 59, 62, 91).

2.4.2.3 Poor Clinical Validation

Potentially of even more concern than the quality of mHealth research, is the relatively high quantity of mHealth applications that are available to the end-user that have not reported any validation whatsoever. It is important that all applications that make a clinical claim are compliant with the medical device regulations in which

they are made available, whether it be the Medical Device Regulation in the European Union (EU), Food and Drugs Administration (FDA) in the United States or other national regulations. However, the Apple App Store and Google Play Store only test that an app runs before it can be deployed and any such app can be classified as a "health and fitness" app. mHealth apps with no clinical validation whatsoever can therefore be deployed into the mass-market relatively easily. Similarly, counterfeit apps, which are purposefully designed to be confused with genuine, clinically validated apps, also pose a threat. To counteract both these issues some healthcare providers have developed their own app store containing only a small set of approved apps. Further to this, the cooperation of the companies operating the largest app stores in helping to reduce the number of counterfeit, defective and ineffective mHealth apps would be of great benefit to healthcare providers and patients alike.

2.4.2.4 The Need for Local Adaption

mHealth solutions must also be adaptable to local systems and circumstances. This includes the ability to adapt the technology to different users and health domains, the content to different sociocultural settings and into different languages and the ability of the technology to function across the wide range of available mobile devices and operating systems (87). Bloomsfield and colleagues in their review of mHealth for non-communicable diseases in sub-Saharan Africa (SSA) highlight that there is also considerable benefit in designing systems for integration with other mServices such as mFinance. Doing so opens up an alternative method of financing healthcare, particularly for those in LMICs who are currently least able to afford healthcare costs.

2.4.2.5 Lack of Quantitative Cost-benefit Analyses

Whilst mHealth has huge potential for providing cost savings to healthcare systems, the reviewed literature highlighted a lack of quantitative analysis relating to the cost benefits as well as requisite implementation and ongoing costs of the mHealth systems themselves. As such, a lack of sustainable business models was frequently cited as a barrier to mHealth at scale. Both implementation and ongoing costs are particularly critical in resource-constrained settings where such costs can prevent an mHealth programme getting off the ground regardless of the medium or long term

cost benefits. A trope found throughout the mHealth literature is that the intervention in question is faster, cheaper and easier to use than standard practice and is therefore appropriate for use in LMICs. However, how fast, how cheap and how easy to use such a device needs to be in order to be applicable to such settings is rarely quantified making it difficult to access the basis for such claims. Indeed, in their review of cost-utility and cost-effectiveness studies of telemedical, eHealth and mHealth systems, de la Torre-Diez and colleagues suggested that not enough publications concerning the cost-effectiveness of mHealth and that the vast majority of investigations are pragmatic assessments that add poorly to the knowledge concerning the cost and benefits of integrating such systems into clinical practice (51).

2.4.2.6 Users' ICT Proficiency

The requirements of users of mHealth can vary widely depending on a variety of factors. These include ICT skills, level of education, literacy and language which are each related to age, wealth and location (98) and also determine the level of training and support required to implement and maintain a sustainable mHealth programme. The adoption of user-centred design is therefore highly recommended (4, 40, 90, 91) as is providing tailored training and support. Specifically, providing general mobile device training, particularly to those user groups who are likely to have low exposure to such. Qiang and colleagues also highlighted that in scenarios where tasks are shifted from personnel with a high level of clinical skill to those who are less skilled, it may also be necessary to provide additional training with respect to the more advanced responsibilities that they would then be expected to undertake (35).

2.4.2.7 Health Policy

There are also a number of policy challenges posed by mHealth, ranging from the local to the international. On the national level, the lack of a specific mHealth component within government and national health systems' eHealth strategy was noted as a barrier by several of the reviewed publications (6-9, 35, 69, 90). Conversely, a lack of attention to local and national health priorities by mHealth device and programme designers was also cited as limitation on its adoption (7, 35, 87, 90, 91). Consequently, several of the guides to implement mHealth at scale identified the critical nature of achieving "buy-in" from local and national health

authorities by establishing a clear link between the mHealth system and the relevant health priorities (35, 87, 90, 91). On the international level, lack or inappropriateness of international standards was often cited as being a significant barrier in the earlier publications included in this review (4, 37, 41, 42, 46, 49, 84). However, later publications often suggest appropriate standards that mHealth designers ought to adhere to suggesting that lack of appropriate standards has become less of an issue more recently (87).

2.4.2.8 Security and Privacy

Challenges concerning security and privacy were frequently cited barriers amongst the reviewed literature. These include issues applicable to e-health in general such as encryption, access (both to the data and the servers hosting the data) and the physical location of the hardware hosting the data, with many countries' legislation requiring that this not be held in foreign countries. There are also issues more specific to mHealth such as the higher likelihood of device theft due to their size and the ease such consumer devices can be re-sold compared to standard medical equipment. Another trade-off that mHealth programmes often have to weigh up is whether to deploy mHealth solutions on the personal devices of its users or to provide dedicated units to each user. The latter has clear cost implications whilst the former brings a host of privacy and security concerns with personal and clinical data residing on the same device and limited control over what other software is installed alongside that belonging to the programme.

2.4.2.9 Additional Challenges in LMICs

As well as those challenges mentioned, designing and deploying mHealth solutions for LMICs present their own unique set of challenges. One such challenge is the severe limitations of infrastructure found in many lower income countries. Although mHealth is likely to be less restrained by this than standard equipment, poor transportation links, for example, can still limit health worker and patient access. Several of the reviewed publications also raised the issue of skills shortages amongst the health workers to which the technology is deployed along with a higher rate of staff turnover, particularly amongst highly skilled staff, compared to their counterparts in high-income countries (HICs).

2.4.3 Limitations

The authors of various articles categorised each of the goals, application types, barriers and proposed solutions in differing ways and there are therefore likely to be several ways to categorise each of these in the synthesis of the review's results.

Recording the count of the goals, applications and barriers to scale of each gave a good indication of what the key benefits, implementation types and issues encountered in taking mHealth technologies to scale. However, it is important to note that a particular issue being frequently cited as such does not necessarily mean that it is any more or less of barrier than an issue which is cited by fewer sources, especially when the reviews in question are concentrating on different contexts.

Finally, only one indexing service, Web of Science, was used in searching the scientific literature. Whilst this service has considerable coverage of the literature, the use of additional indexing services, such as Scopus and IEEE Xplore, would have allowed for a more robust search of the literature, even though these indices have considerable overlap (99).

2.5 Conclusions

The global proliferation of mobile technology presents huge opportunities for healthcare, specifically with regard to improving operational efficiency, lower costs, extending health systems' reach and improving adherence and acceptance. The opportunities are of particular consequence in LMICs where less developed health systems exist and greater degrees of improvement can be leveraged. However, the quality of research into mHealth has thus far been relatively poor with most studies taking the form of pilots with low participant numbers and little regard for the wider health system or how such technologies interact with one-another. As such, few mHealth products have launched with business models that are sustainable at scale.

Foremost of the reasons cited as prohibiting the advancement of mHealth technologies from pilot phase to widespread adoption is a paucity of data concerning the full impact on the full health system's workflow. Thus, those concerned by the lack of progression in the field of mHealth should look to filling this particular gap in their pursuit of empowering health systems in low-resource settings. This thesis intends to provide a contribution in this direction.

3 mHealth Solutions for Eye Care Delivery in Low Income Settings

3.1 Introduction

In 1995 it was estimated that by 2020 the number of blind people worldwide would have grown to 76 million, from the 38 million estimated to be blind in 1990 (100). These projections were based on existing service level as well as projected population growth and age distribution. Furthermore, it was also estimated that 80% of this blindness was avoidable and that 90% of the blind and visual impaired lived in LMICs (101).

By 2002, global eye data estimated that the number of blind people had indeed increased to 45 million, broadly in line with the 1995 projections (102). This reinforced the need for urgent action in tackling avoidable blindness. In response to this, VISION 2020, a global initiative aiming to eliminate avoidable blindness by 2020, was launched in February 1999 (103). Huge strides have been made in tackling avoidable blindness since, with over 100 national plans aiming at eliminating avoidable blindness being implemented, notable progress on infectious eye diseases being made and evidence of a reduction in the prevalence of global blindness (103). However, in 2017 it was reported by Flaxman and colleagues that there remains as many as 36 million blind people, 77% of whom are blind due avoidable causes (18).

There are a combination of reasons as to why eye care is a good candidate for being one of the first sectors to make a major breakthrough in the adoption of mHealth at scale. Namely, these are the high proportion of avoidable blindness, the high prevalence in LMICs compared to HICs and the relatively straightforward means of screening and treatment. Indeed, if realised in eye care, the goals discussed in the previous chapter would allow considerable progress to be made concerning the major challenges in global eye care. This chapter will summarise these challenges and then go on to review the progress made in developing mHealth technology for use within LMIC eye care.

3.2 Brief Overview of the Major Challenges in Global Eye Care

The two main causes of visual impairment are uncorrected refractive errors and cataract, accounting for 42% and 33% of visual impairment according to estimates made in 2011 (101). For both of these conditions cost-effective interventions to reduce their burden exist in all countries (104). This highlights that, for the majority of avoidable blindness, the issue is not treatment availability but rather reaching patients and having those in need arriving at the appropriate healthcare provider for treatment (105).

A set of focal diseases, which are diseases that can be prevented but not reversed in their end state, including trachoma, onchocerciasis and xerophthalmia, were found to account for approximately 15% of avoidable blindness in a 2011 estimate of the causes of global blindness. Great strides have been made in reducing blindness due to these conditions with sufferers having dropped from 7.2 million in 1990 to less than 5.7 million in 2010 despite the increase in global population (100, 101).

A number of chronic disease cause blindness of which the most prevalent are diabetic retinopathy and glaucoma. Having demonstrated effective models for service delivery in many locations and achieved a demonstrable reduction in global blindness despite population growth and aging, the success of VISION 2020 in its first decade is hugely encouraging. The challenge for global eye health improvement is now to tackle low vision in taxing locations and vision loss due to chronic diseases such as diabetes and glaucoma, both of which are increasing concerns.

Retinopathy of prematurity (ROP), a potentially blinding condition affecting preterm infants and which is preventable but not reversible, is similarly a growing cause of concern as survival rates among preterm infants improves in LMICs at a rate that outstrips that of eye care provision for this population.

3.2.1 Measuring Visual Impairment and Blindness

Visual acuity is an objective, quantitative measure of visual function (106). There are a number of standardised charts for measuring visual acuity based on distance vision including the Snellen, Landholt's C, E and Early Treatment Diabetic Retinopathy Study (ETDRS) charts (106-108). In each case, visual acuity is tested in

WHO Category		Presenting distance vision			
		worse than	equal to or better than		
0	Mild or no visual impairment		6/18		
1	Moderate visual impairment	6/18	6/60	**Low vision**	**Visual Impairment**
2	Severe visual impairment	6/60	3/60		
3	Blindness	3/60	1/60		
4	Blindness	No light perception	Light perception		
5	Blindness		No light perception		

Table 4 – Categorisation of visual impairment according to Section H54 of the ICD-10, of WHO disability standards (109).

each eye individually at six metres. The WHO classifies visual function into either mild or no visual impairment, moderate visual impairment, severe visual impairment or blindness (109). Blindness is also further sub-categorised into those who can count fingers at 1m (approximately 1/60), those who can only perceive light and those with no perception of light. Low vision refers to either moderate or severe visual impairment and visual impairment refers to either low vision or blindness, as shown in Table 4.

3.2.2 Major Causes of Visual Impairment and their Assessment

3.2.2.1 Refractive error

Uncorrected refractive errors are the biggest contributor to visual impairment worldwide accounting for 43% of the total according to estimates made in 2011 (101). Myopia, the main refractive error affecting distance vision, was estimated by Holden and colleagues in to affect over 28% of the global population in 2016 (110). However, the distribution is highly asymmetric, with Holden and colleagues also concluding that high-income Asia-Pacific countries having a combined prevalence of 48% in the same 2016 estimate of global myopia prevalence (110).

Refractive errors encompass a number of conditions, each of which involve the introduction of some form of aberration into the eye's optical system. Secondary order aberrations, namely defocus, oblique astigmatism and vertical astigmatism, are those which most commonly affect vision. In ophthalmology and optometry, owing to the type of lenses used to correct the errors, defocus is referred to as a 'spherical error' and astigmatisms as 'cylindrical errors'. The four most prevalent refractive errors are described in more detail below.

Myopia is caused by the axial length of the eye being larger than the focal length of the eye's optics, resulting in a spherical error being introduced into the visual system. Its onset generally occurs during childhood or the teenage years (111). As well as significantly impairing vision itself, those with high-myopia (-5D or worse), are at higher risk of sight-treating conditions such as cataract, glaucoma, retinal detachment and myopic macular degeneration (112).

Astigmatism is a refractive error generally caused by one meridian of the cornea having a steeper curve than the other, resulting in a cylindrical error being introduced

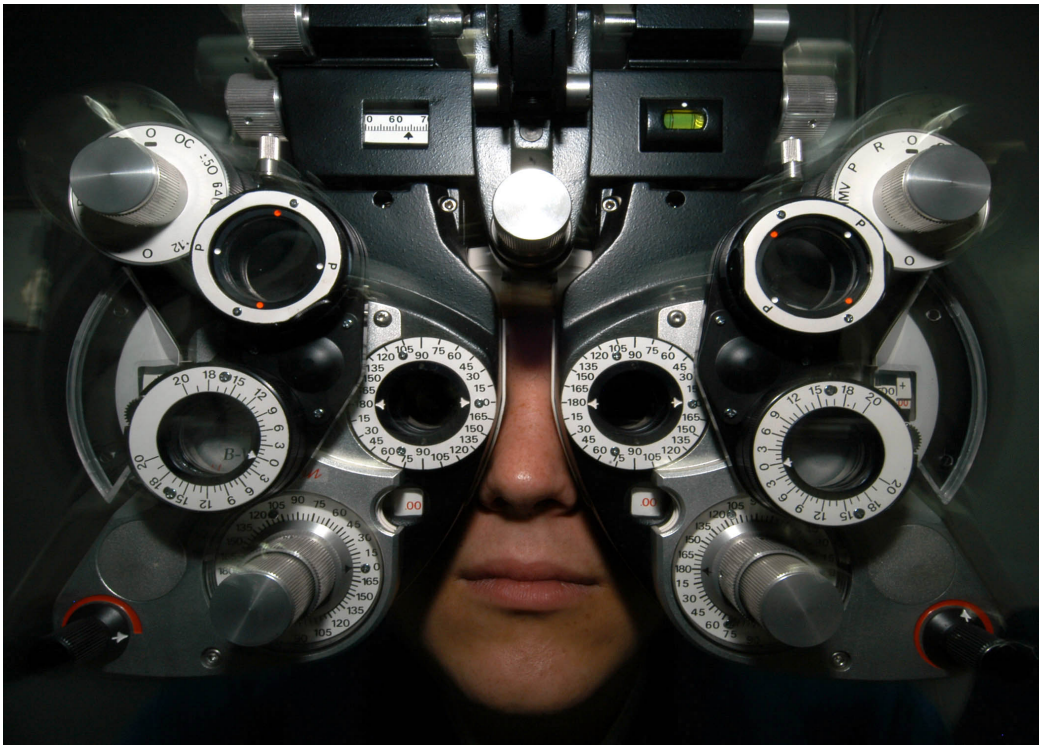

Figure 6 - A phoropter in use during subjective refraction. The instrument allows an eye care professional to quickly and easily insert and remove lenses from in front of a patient's eyes while they attempt to read a vision chart placed at 6 metres. Subjective feedback from the patient throughout the examination allows the eye care professional to determine which spectacle lenses ought to improve the patient's vision. Image is in the public domain. Reproduced from www.navy.mil[3].

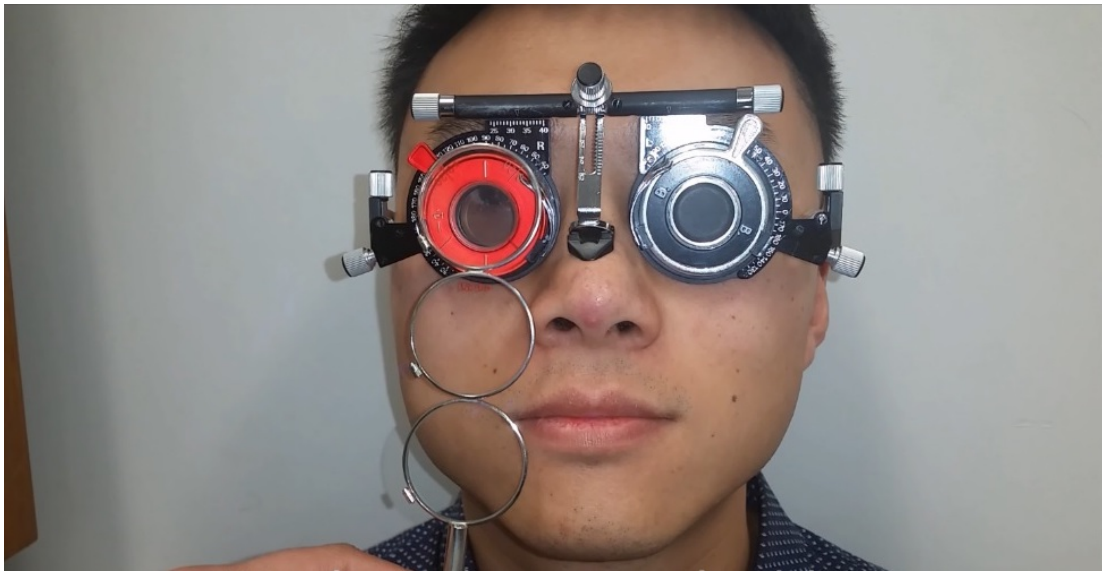

Figure 7 - A patient undergoing subjective refraction whilst wearing a pair of trial frames. These allow an eye care professional to manually insert and remove lenses from in front of a patient's eyes while they attempt to read a vision chart placed at 6 metres. Original image by 'ORT5CLA_Team_H'. Reproduced under Creative Commons BY-SA 4.0 license[4].

[3] Image number: 040305-N-4190W-001; URL: https://www.navy.mil/view_image.asp?id=12477
[4] License available at: https://creativecommons.org/licenses/by-sa/4.0/legalcode

into the visual system (113). Astigmatism tends to be present at birth but can also occur due to injury or as a result of other conditions such as keratoconus (113, 114).

Hyperopia is a common refractive condition affecting near vision normally resulting from non-pathological eye structure, such as a shorter axial length or flatter cornea compared to a normal eye (115). It is more prevalent in children and the condition's prevalence varies significantly across geographical location (115). Hyperopia is associated with poor school performance and can also lead to other visual impairments including strabismus and amblyopia (116, 117).

Presbyopia is a condition affecting near vision caused by the gradually thickening and loss of elasticity of the crystalline lens with age. As such, accommodation becomes more difficult making it more difficult to achieve near focus. Presbyopia tends to present at around age 40 and its severity increases with age beyond this.

Dispensing corrective lenses, in the form of spectacles or contact lenses, via subjective refraction is the gold standard for correcting refractive errors (118). Subjective refraction makes use of a phoropter, Figure 6, or trial lenses frames, Figure 7. Both these instruments are placed on the face of a patient and allow different powered lenses to be quickly introduced or removed from the patient's line of sight. When a new lens is introduced the patient is asked if a vision chart appears clearer or not compared to the previous lens until it is possible to determine the lenses required to best correct for his or her refractive error. The three elements of the lens prescription are refined in the following sequence: initial check of the spherical corrective power, refinement of the cylinder correction axis, refinement of the cylindrical corrective power and a final check of the spherical corrective power (119). The phoropter will usually be started from the patient's existing prescription or from that determined by objective refraction where available. The refractionist will then dial the spherical power in 0.5D increments before further refining at 0.25D increments until the patient achieves the clearest view of an acuity chart. A Jackson cross cylinder (JCC) is then used to determine the cylindrical axis (119).

Objective refraction, using either a retinoscope or an autorefractor, determines a starting point for subjective refraction, reducing the total time of the procedure. However, it is generally considered that objective techniques are less effective in

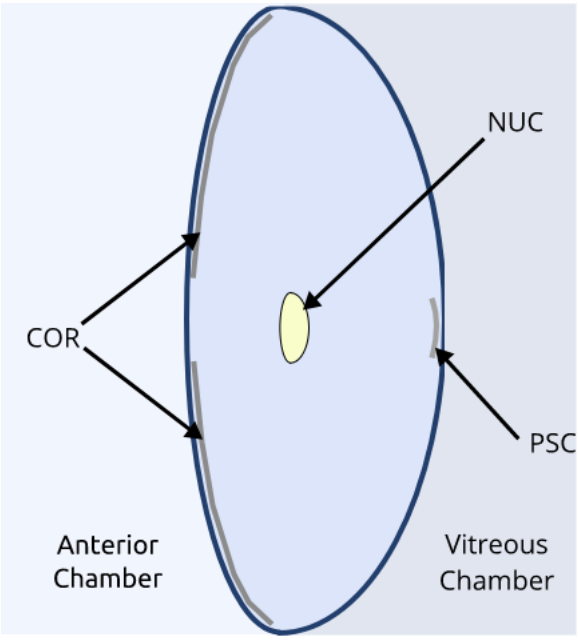

Figure 8 - The three forms of cataract: cortical (COR) which begins at the periphery of the lens cortex and grows inwards, nuclear (NUC) which is a yellowing of the lens nucleus and posterior subcapsular which is opacification in or near the centre of the posterior lens capsule.

ascertaining the most comfortable prescription, particularly when not conducted under cycloplegia (118).

3.2.2.2 Cataract

Cataract is the leading cause of blindness worldwide (120). At present it is not preventable but sight can be restored by relatively simple surgical intervention irrespective of the severity of the disease (120). The vast majority of cataract is age related although a small number of infants are born with congenital cataract (121).

There are three common forms of cataract, as shown in Figure 8, namely:

- Nuclear cataract (NUC) – a gradual opacification of the nucleus (centre) of the lens.
- Cortical cataract (COR) – opacification that begins at the periphery of the lens cortex and moves inwards.
- Posterior subcapsular cataract (PSC) – opacification in or near the centre of the posterior lens capsule.

The WHO/PBD simplified cataract grading system is designed for use by appropriately trained staff who examine the lens using a slit lamp with 10x magnification and the ability to adjust the width, height and angulation of the slit beam (120). Consenting patients are to be pharmacologically dilated twenty minutes before the examination, in order to achieve a pupil diameter of at least 6.5mm. The severity of each type of cataract is graded on a scale of zero to three. The severity of NUC is graded by comparing the degree of opacification observed with a set of standard photographs. The severity of COR is graded according to the aggregated fraction of the total lens circumference opacification and the severity of PSC is graded according to the size of the vertical dimension of the opacification. In the case of COR, it is also noted if the cataract involves the 3mm diameter zone in the centre of the lens.

As well as facilitating epidemiological studies and national blindness prevalence surveys, the WHO/PBD simplified cataract grading system also provides an estimate of cases that are likely to be in need of surgery, as is shown in Table 5. However, in reality the decision of whether or not to refer for surgical intervention is influenced by a number of factors, including availability of necessary services, willingness of

	NUC	COR	PSC	Clinical Significance
0	Less than the NUC-1 STD	Less than one eight of total circumference	<1mm	Clinically insignificant
1	Equal to or greater than the NUC-STD 1 but less than the NUC-STD 2	More than one eight of total circumference but less than a quarter	>1mm and <2mm	Clinically significant
2	Equal to or greater than the NUC-STD 2 but less than the NUC STD 3	More than a quarter but less than half of total circumference	>2mm and <3mm	Moderately advanced progression, consider surgery for PSC.
3	Equal to or greater than the NUC-STD 3	More than half of total circumference	>3mm	Severity sufficient to consider surgery for NUC and/or PSC.
9	Cannot grade	Cannot grade	Cannot grade	Unknown

Table 5 – Grading criteria for the three classifications of cataract according to the WHO/PBD simplified cataract grading system (120). NUC denote nuclear cataract, COR cortical cataract and PSC posterior subcapsular cataract.

patient, presence of other severe co-morbidity and health of the patient's other eye (122). To highlight two common scenarios: surgery will generally not be undertaken if another eye pathology is known to exist and therefore removal of the cataract is unlikely to improve visual performance. In regions where eye care resources are relatively scarce then a patient with good vision in one of their eyes may not be referred for surgery in order to a patient with poor vision in both eyes to receive sight in at least one eye (with surgery typically performed on the eye with the most severe cataract if there is a choice).

3.2.2.3 Glaucoma

Glaucomas are a group of pathologies in which progressive optic nerve damage causes a gradual reduction of the sufferer's field of view (123). It was estimated in 2008 that 64 million people suffer from glaucoma with approximately half of these being undiagnosed and the vast majority of whom are over the age of sixty (122, 124).

Glaucomas are most commonly caused by an increase in intraocular pressure resulting from a blockage of the trabecular meshwork which is responsible for draining aqueous humour from the anterior chamber (125). The condition is subdivided into closed-angle glaucomas, involving a clear blockage of the aqueous humours outflow by a reduction in the angle between the cornea and the iris, and open-angle glaucomas, where the angle between the cornea and the iris is not reduced but outflow is nevertheless inhibited, usually by gradual degeneration of the trabecular meshwork (125). These are then further classified into primary glaucomas, those that develop in the absence of another eye condition, and secondary glaucomas that result from trauma, certain medications or an underlying condition, such as pigment dispersion (125). Open-angle glaucoma accounts for approximately 90% of the total prevalence with the most common being primary chronic glaucoma where gradual degeneration of the trabecular network causes a gradual increase in IOP (125). In contrast, closed-angle glaucoma can be either chronic or acute with, for example, part of the iris being displaced causing a blockage of Schlemm's canal (126).

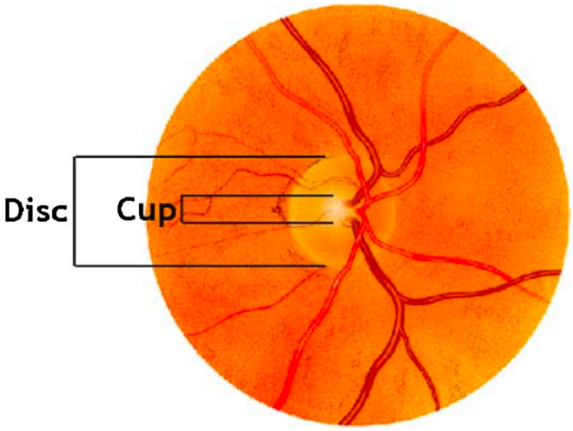

Figure 9 – The optic nerve as seen when viewing the ocular fundus during ophthalmoscopy. The optic nerve consists of an outer 'disc' of retinal nerve fibre layers and a central depression referred to as the 'cup'. When viewed monoscopically the cup appears as a paler region in the centre of the slightly duller disc. Reproduced with permissions from (127)[5]

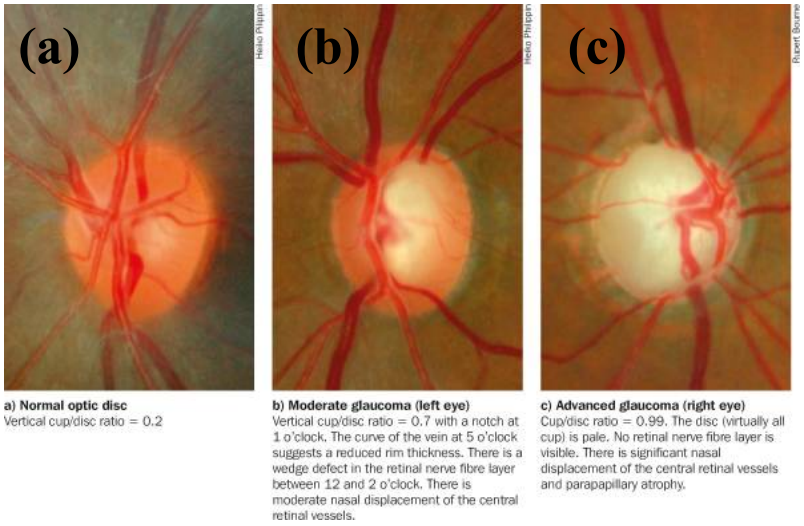

Figure 10 – Images of three optic nerve heads, obtained via fundus photography, with increasing vertical cup-to-disc (VCDR) ratios. (a) represents a normal optic nerve with a VCDR of 0.2. (b) shows an optic nerve within a moderately glaucomatous eye, there is substantial retinal fibre loss resulting in a VCDR of 0.7. (c) is an image of an optic nerve in a case of advanced glaucoma. The VCDR is 0.99, with barely any retinal nerve fibre layer being visible, and there is significant central retinal vessel displacement. © Heiko Philippin ((a) and (b)), Rupert Bourne (c). Reproduced from (128) under Creative Commons Attribution Non-Commercial License[6]

[5] Reprinted from Computerized Medical Imaging and Graphics, Vol 37, MS Haleem, L Han, J v. Hermet, B Li, Automatic extraction of retinal features from colour images of glaucoma diagnosis: A review, Pages 581-596, Copyright (2013), with permission from Elsevier.
[6] License available at: https://creativecommons.org/licenses/by-nc/4.0/legalcode

All glaucomas result in progressive damage to the axons of retinal ganglion cells responsible for carrying visual information through the optic nerve to the brain. The death of the retinal ganglion cells results in optic nerve atrophy and thus vision loss (125, 129).

Diagnosis of glaucomas relies upon a battery of tests (130). Measurement of IOP with a tonometer is an important such test, however it is not enough by itself as the pressure measured externally will varies with corneal thickness as well as IOP. As such, approximately one third of those diagnosed with glaucoma do not have a measured IOP greater than 21 mm Hg, the diagnostic threshold for the disease (131). It is therefore necessary to image the optic nerve, a diagram of which is shown in Figure 9, in order to directly detect damage. Imaging can be conducted either by fundoscopy or optical coherence tomography (OCT) (132, 133). In fundoscopy, 'optical nerve cupping', where the optic nerve's cup appears larger due to retinal nerve fibre loss, is a key characteristic of glaucoma. This is measured by vertically measuring the cup and dividing this by the vertical diameter of the full disc (the vertical cup-to-disc ratio, VCDR) with a ratio of 0.3 or less usually being considered normal (134). Examples of healthy, moderately glaucomatous and severely glaucomatous optic nerves are shown in Figure 10. However, it is important to note that the relative size of the optic cup varies across healthy eyes and it is therefore a change in cup size or an abnormally large cup that is a cause for concern. Retinal nerve fibre loss can also be observed via OCT. Finally, peripheral vision loss is detected using a visual fields test, normally using either a Humphrey or Goldmann visual field analyser (135).

Glaucoma cannot be reversed but the damage to the optic nerve can be limited by reducing the IOP to a healthy level by using drugs, laser surgery or incisional surgery to modify the aqueous secretion and drainage systems (129).

3.2.2.4 Diabetic Retinopathy

Diabetic retinopathy (DR) is the leading cause of blindness amongst working-age people (136). It has been estimated that in 2015 there were 415 million people between the ages of 20 and 79 suffering from diabetes mellitus (DM) with three quarters of these living in LMICs (137). It is also estimated that approximately

Disease Severity Level	Findings Observable via Dilated Ophthalmoscopy
No apparent retinopathy	No observable retinal abnormalities
Mild NPDR	Retinal microaneurysms only
Moderate NPDR	Not just retinal microaneurysms but not yet satisfying the criteria for sever NPDR
Severe NPDR	Any of the following when no signs of PDR: • More than 20 intraretinal haemorrhages in each retinal quadrant • Venous bleeding in more than two retinal quadrants • Prominent intraretinal microvascular abnormalities in more than one retinal quadrant
PDR	One or more of the following: • Neovascularisation • Vitreous or preretinal haemorrhages
DMO	Any apparent retinal thickening or hard exudates within the posterior pole

Table 6 - Grading criteria for diabetic retinopathy as categorised by Wilkinson and colleagues (138). NPDR refers to non-proliferative diabetic retinopathy and PDR to proliferative diabetic retinopathy.

46.5% of all DM sufferers are undiagnosed (137). Moreover, the number on DM sufferers is projected to rise to 642 million by 2040 (137). As such, the prevalence of diabetic eye disease is expected to rise in the coming decades. The growth is adoption of the Western diet (137, 139). In addition, a number of ethnicities present in LMICs are genetically predisposed to developing diabetes compared to those of White European origin (137).

Non-proliferative diabetic retinopathy (NPDR) occurs when blood sugar levels are elevated for extended periods, causing damage to retinal capillaries. This damage causes microaneurysms, and proteins and lipids to leak out into the retinal tissue, forming hard exudates (140, 141).

Both of these retinal changes result in retinal ischemia causing vascular endothelium growth factor (VEGF) to be released and neovascularisation to occur (142). This is known as proliferative diabetic retinopathy (PDR). The new vessels produced cause bleeding into the eye, increasing intraocular pressure and thus the risk of glaucoma, and scar tissue to form resulting in retinal detachments (143).

Diabetic macular oedema (DMO) can also develop at all stages of retinopathy (143). This involves the macular swelling due to the release of fluids into the retina, or macular ischemia due to vessel damage disrupting the supply of blood to the macular (143, 144).

Of the above classifications of DR, DMO and PDR are considered vision-threatening diabetic retinopathy (VTDR). Precise criteria for the grading, as defined by Wilkinson and colleagues, of each classification of DR are shown in Table 6.

As the early stages of NPDR are often asymptomatic, it is important to image the retinas of those suffering from diabetes frequently. Slit lamp biomicroscopy and retinal photography can be used to detect microaneurysms, intraretinal haemorrhages and neovascularisation, the absence or presence of which can then be used to determine the stage and severity of retinopathy (145). Retinal imaging can also detect the presence of DMO through the

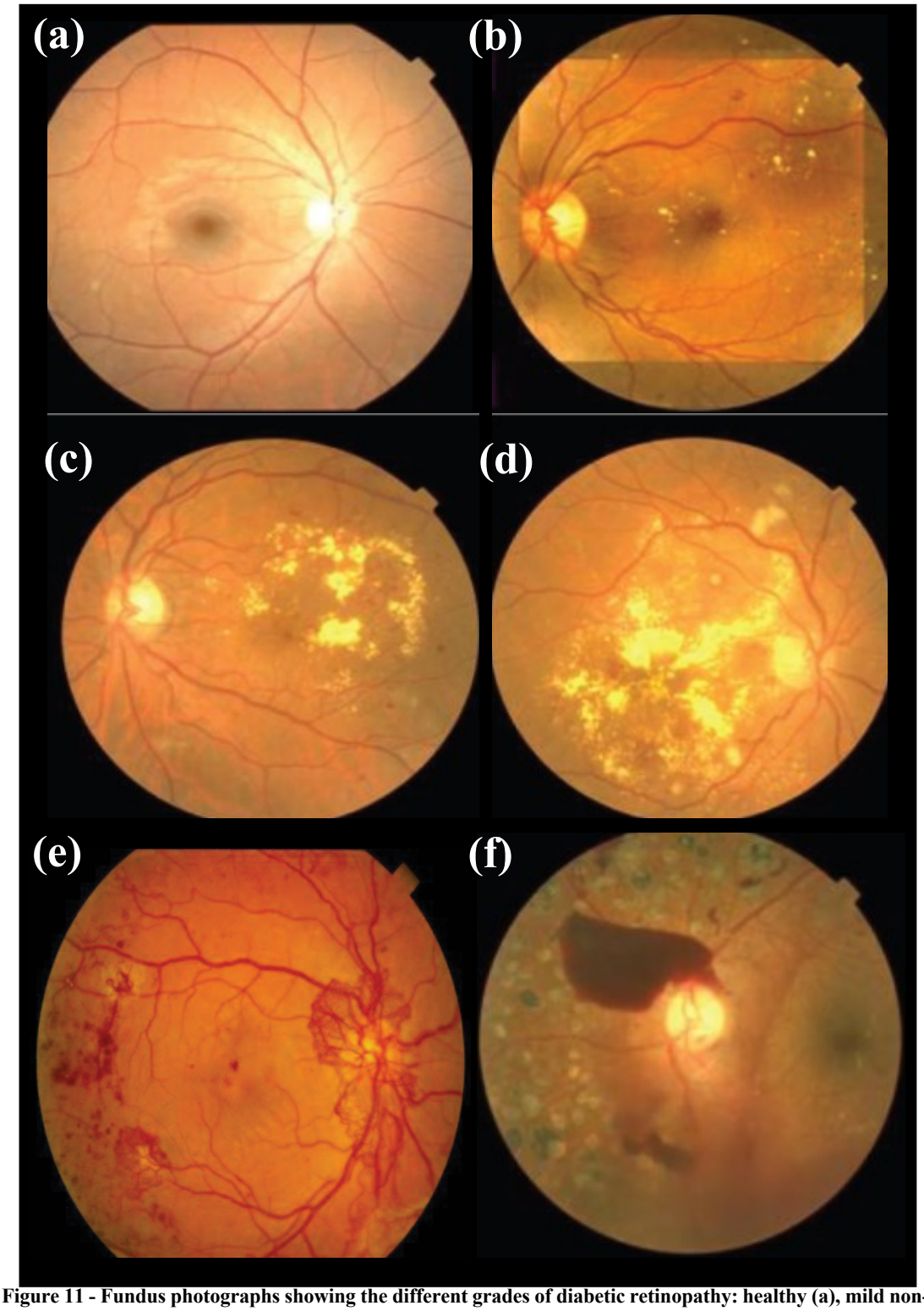

Figure 11 - Fundus photographs showing the different grades of diabetic retinopathy: healthy (a), mild non-proliferative diabetic retinopathy (NPDR) (b), moderate NPDR (c), severe NPDR (d), proliferative diabetic retinopathy (PDR) (e). Additionally, (f) shows a fundus with PDR that has caused vitreous haemorrhaging and also has marks from laser photocoagulation. (e) reprinted, with permission, from (146) © 2016 IEEE. All other panes reproduced from (147) with permissions.

observation of hard exudates and retinal thickening involving the macula (145). OCT can also be used to accurately measure the thickness of the retina (148).

Risk of developing DR can be reduced by blood glucose regulation (149). Once NPDR develops and symptoms begin to appear patients are placed on anti-VEGF medication in order to prevent progression to PDR (150). If a patient's retinopathy does subsequently advance to PDR, laser photocoagulation is used to stop neovascularisation and more serious complications occurring (151).

3.2.2.5 Retinopathy of Prematurity

ROP is a leading cause of avoidable childhood blindness worldwide, with it being estimated that some 184,700 preterm infants developed the disease in 2010, of which 20,000 were left severely visually impaired for the rest of their lives. Of those visually impaired by ROP 65% are born in middle-income regions (152).

Premature infants born before 32 weeks' postmenstrual age (PMA) are delivered at a stage where considerable retinal neuronal and vascular development is still yet to occur (153). ROP is the arrest of this retinal development that would ordinarily occur in utero. This results in pathological compensatory mechanisms that leads to abnormal vascularisation of the retina. The arrest of retinal development occurs due to the retina's exposure to harmful factors, such as higher oxygen concentrations, which would not otherwise be experienced in utero (154,155). After approximately 30 weeks' PMA the hypoxic retina then begins to produce oxygen-regulated factors including erythropoietin (EPO) and VEGF, causing neovascularisation (154, 155). If the aberrant growth of the retinal vasculature is left unchecked, it may cause retinal fibrosis and retinal detachment leading to permanent blindness in the infant (153).

Such an outcome can be avoided by preventing neovascularisation by limiting oxygen exposure and increasing insulin like growth factor 1 (IGF-1) to in-utero levels, in order to suppress the production of VEGF (156). The level of oxygenation whereby survival chances and risk of blindness are optimally balanced is still a matter of debate. Where neovascularisation does occur further vessel proliferation can be avoided by laser therapy (157).

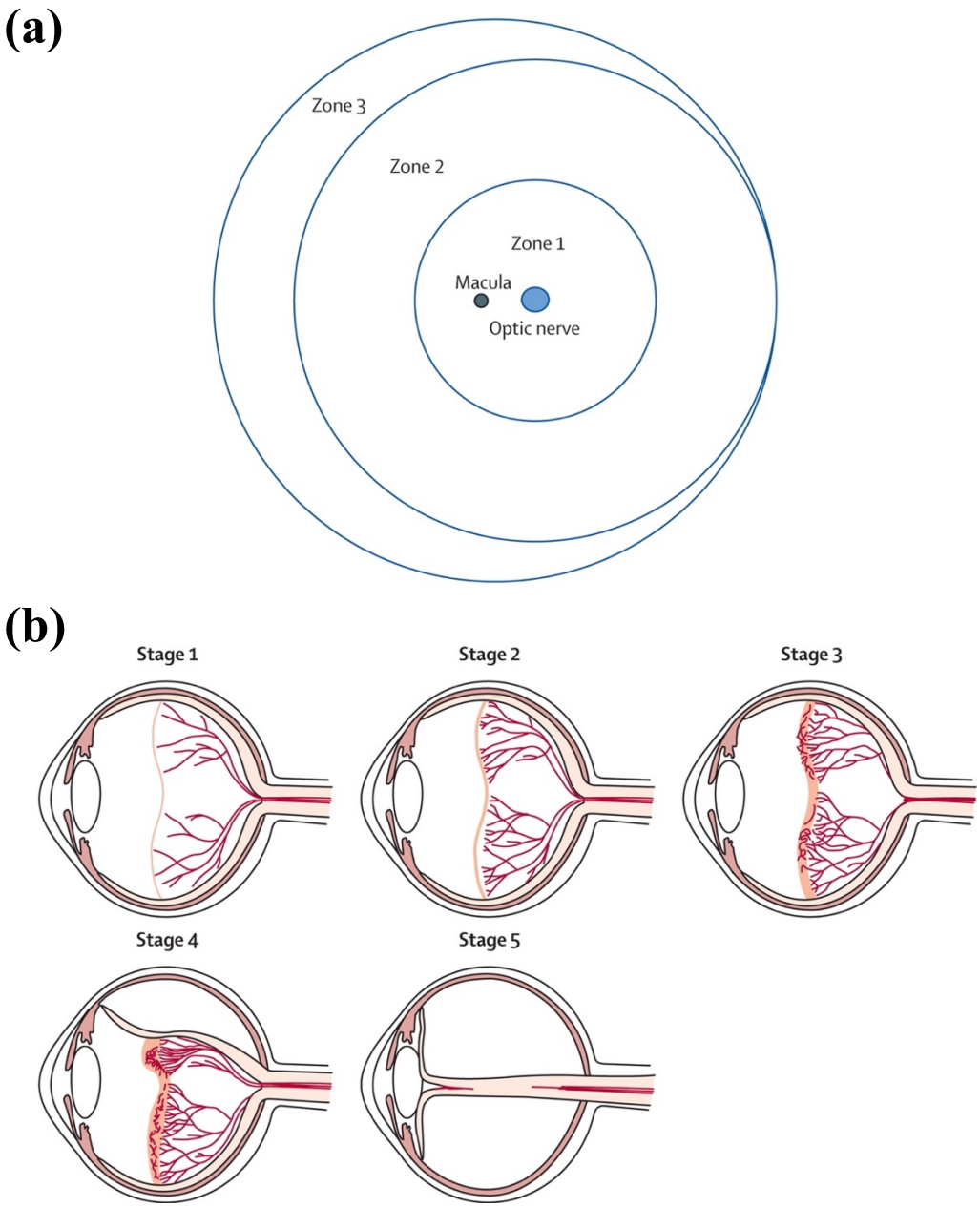

Figure 12 -For the purposes of ROP screening, the retina is divided into three zones as shown for the right eye in (a). The severity of retinopathy classified into the five stages shown in (b). In stage 1 a thin line appears between the vascularised retina and, as of yet, non-vascularised area. By stage 2, this line has begun to form a ridge. At stage 3 neovascularisation begins to occur. If the disease is allowed to advance beyond stage 3, this can result in either partial or total retinal detachment (stages 4 and 5 respectively) both of which are likely to leave the sufferer permanently and irreversibly blind (158).

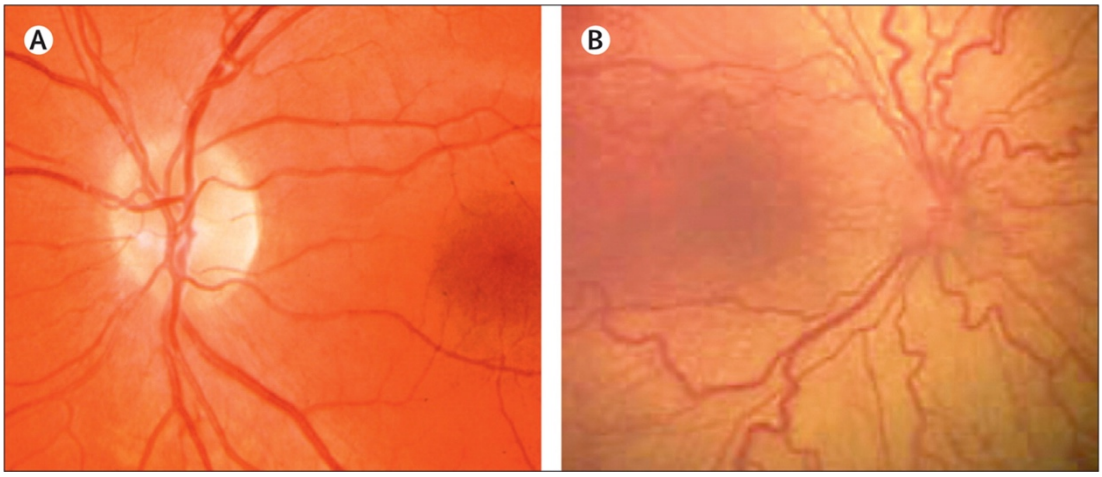

Figure 13 – An image of a normal retina (A) alongside that of a retina exhibiting venous dilation and increased arterial tortuosity, collectively referred to as 'plus disease' (B). The presence of plus disease is a key criterion for deciding to treat ROP with laser photocoagulation (158).

The threshold for treatment of the disease is considered to be met if five contiguous or eight total clock hours of extraretinal fibrovascular proliferation occur within the posterior pole alongside 'plus disease' (159). Plus disease consists of marked vascular changes, comprising dilated venules and tortuous arterioles such as that shown in Figure 13B, in at least two quadrants of the posterior pole in the presence of ROP. Vascular changes that are not normal but are insufficient for the diagnosis of plus disease are clinically defined as pre-plus changes of ROP (160)

Infants are usually considered to be at risk of developing ROP if they are born at less than 32 weeks' gestational age (GA), have a birthweight of less than 1500g and have required additional oxygen.

In many high-income countries, blinding ROP has been brought under control through effective screening programmes (18). These involve frequent widefield imaging of the retina by a sub-specialist ophthalmologist in order to detect and monitor the progression of any disease, as outlined in Figure 12, and thus establish those who are in need of treatment, allowing for timely intervention (165). However, in middle-income countries, where improvements in maternal health have resulted in many more infants surviving prematurity, access to such specialist care is limited (156). Whilst wide-field retinal digital imaging solutions that can be operated by the non-specialist exist, these are expensive and are well beyond the budget of the vast

majority of middle-income health systems (161, 162). As a result, some 65% of those visually impaired by ROP are born in middle-income countries (152).

3.2.3 Access to Eye Care: The global inverse care law

It has recently been reported that globally there are approximately 200,000 ophthalmologists and over 200,000 optometrists (163, 164). However, the distribution of these eye specialists is highly uneven, with a mean of just nine ophthalmologists per million population in low-income countries compared to 79 per million population in high income countries (163). Given that 90% of blindness occurs in LMICs, the provision of eye services is therefore the inverse of what is required to address global avoidable blindness. It was reported that in 2010 SSA had the lowest concentration of ophthalmologists with 2.7 per million population, with certain Francophone and Lusophone countries having less than one per million population (165). This is well below VISION 2020's target for the region of four per million population (165). Furthermore, the geographical distribution of eye specialists tends to be concentrated in capital cities and some specialists serve private practices only (165). Therefore, with the proportion of ophthalmologists only increasing slightly in low-income countries (LICs) and the population over sixty years of age increasing at twice the rate of that in HICs, it is vital to find both technical and process innovations that allow tasks within eye care to be shifted to less skilled workers within eye service provision (166). Additionally, if such innovations are to achieve universal eye care, they must also enable those not resident in major urban centres in LICs to access eye care without placing a workload well beyond the capacity of specialist eye care provision found in such countries.

3.2.4 Summary

The main causes of blindness can either be cured or prevented through early intervention. Despite this, some 80% of those who are blind are blind due to such avoidable blindness. Furthermore, blind people are disproportionally concentrated in low-income countries whilst eye care resources are disproportionally concentrated in high-income countries (101, 163). Common to each of the interventions necessary in

avoiding the causes of blindness discussed in this chapter is the requirement that they be delivered by an eye care specialist, namely an optometrist in the case of dispensing lenses correcting refractive error and an ophthalmologist when performing the surgical interventions typically required in tackling cataract, glaucoma, sight-threatening DR and threshold ROP. Moreover, the longer glaucoma, DR and threshold ROP remain untreated, the more irreversible damage to sight is caused. Timely treatment is therefore essential.

The need to increase the number of specialists in LMICs is therefore clear, as is the need to increase the time specialists spend on delivering interventions compared to other tasks, such as identifying those in need of treatment, which are nevertheless crucial to effective eye care. It has proved difficult to train and retain eye specialists in LICs, in particular, at a rate which counters factors posing challenges to blindness reduction such as aging populations, more infants surviving prematurity and an increasing prevalence of diabetes (47, 167). Providing means by which tasks within eye care can be effectively performed by lower skilled eye health workers is therefore essential if global blindness is to be reduced.

3.3 mHealth in Eye Care Delivery

This section aims to give an overview of the phone apps and hardware adapters that have been developed in recent years specifically for eye care in LMICs. mHealth interventions that are designed to identify low prevalence or low impact conditions, such as poor stereopsis, were excluded from the review (168). Such interventions clearly have a place within high-income settings, where other, higher-prevalence conditions are under control and where the conditions that they identify can be treated or where aid can be provided to those diagnosed with the conditions. However, this is not the case in LMICs where the current focus is the establishment of more basic eye care systems capable of tackling the major causes of avoidable blindness.

The interventions are sorted by application type.

3.3.1 Visual Acuity

3.3.1.1 Overview of mobile device display technologies

The potential benefits of hosting a visual acuity test on a smartphone or tablet PC are portability, reduction of cost compared to standard back-illuminated charts and the ability to re-configure the test for different sequences or test distances on the fly. However, before such benefits can be realised it is first necessary to consider whether the display screens of mobile devices are an appropriate technology for displaying a visual acuity chart.

Two display technologies are commonly used in mobile device displays. Thin film transistor liquid crystal displays (TFT LCD), a display technology that is particularly common in low cost smartphones, consists of a twisted nematic liquid crystal layer sandwiched between two crossed linear polarising filters. Under normal conditions, these liquid crystals are twisted and cause the polarisation of incident light to change by 90° and therefore pass through the second polariser unimpeded. However, if electrically charged the liquid crystal begins to straighten and when fully charged will allow light to pass through without any shift in the polarisation angle. Thus, the second polariser blocks the perpendicularly polarised light originating from the LED backlight causing the display to appear black.

In TFT LCD displays each picture element (pixel) consists of a layer of insulating liquid crystal placed between two layers of the transparent conductor indium tin oxide (ITO). Each pixel is controlled by a transistor switch contained within the pixel. The pixels are arranged in an active matrix where each pixel can be individually activated by addressing its row and delivering a charge down the appropriate column. The charge delivered is sufficient to maintain the pixel's state until the next cycle. Furthermore, by controlling the voltage supplied to the crystal it is common to be able to achieve a grayscale of 256 brightness levels per pixel. Therefore, by adding a red, green or blue colour filter to each pixel a total of 16.78 million colours can be produced.

Whilst LCDs can operate without an internal light source by placing a mirror behind, those designed for mobile devices are almost exclusive lit by a white backlight. No polarising filter is 100% efficient and thus some light is transmitted through each

pixel even when fully discharged, with the intensity of light transmitted being proportional to the backlight's intensity. Another drawback of LCDs is their limited viewing angle. This results from the increased distance light rays at wider angles travel through the liquid crystal causing it to arrive at the second polariser with a different polarisation compared to those light rays perpendicular to the polariser. Thus, each pixel has a different illuminance when viewed from different angles.

Active matrix organic light emitting diode (AMOLED) displays similarly uses a matrix of thin-film transistors to activate individual pixels. Light is generated in each pixel by a layer of a semiconducting emissive electroluminescent organic compound situated between two electrodes. Usually the anode is made of ITO allowing light to be transmitted. Typical two transistors are used per a pixel, one to charge a storage capacitor and another to provide the voltage required to deliver a constant current to the pixel. As AMOLED displays turn off pixels completely they tend to have a better contrast ratio than LCDs. However, unlike LCDs they are prone to 'screen burn-in' where a permanent artefact is left when a particular image is overused.

3.3.1.2 Comparison of mobile device displays to vision charts

As both contrast and screen luminance are known to vary according to display technology and to affect acuity measurements, it is important to assess the performance of mobile devices with respect to these parameters (169, 170). Such an assessment was conducted by Livingstone and colleagues who measured performance with respect to both of the aforementioned parameters on the iPad 3, iPad 4 and iPad Air 2s (Apple Inc.) tablet PCs (171). The authors benchmarked against the ETDRS specifications, the design of which is shown in Figure 14b, which are based on the International Council of Ophthalmology (ICO) recommendations, and the British specifications for visual acuity charts, BS 4274-1:2003 (172). The former specifies that acuity charts have a luminance of not less than 80 cd/m2 with the black optotypes having a luminance of less than 15% of the surrounding field whilst the latter specifies that the Weber contrast should be 90% or greater with any variance in luminance across the chart being 20% or less.

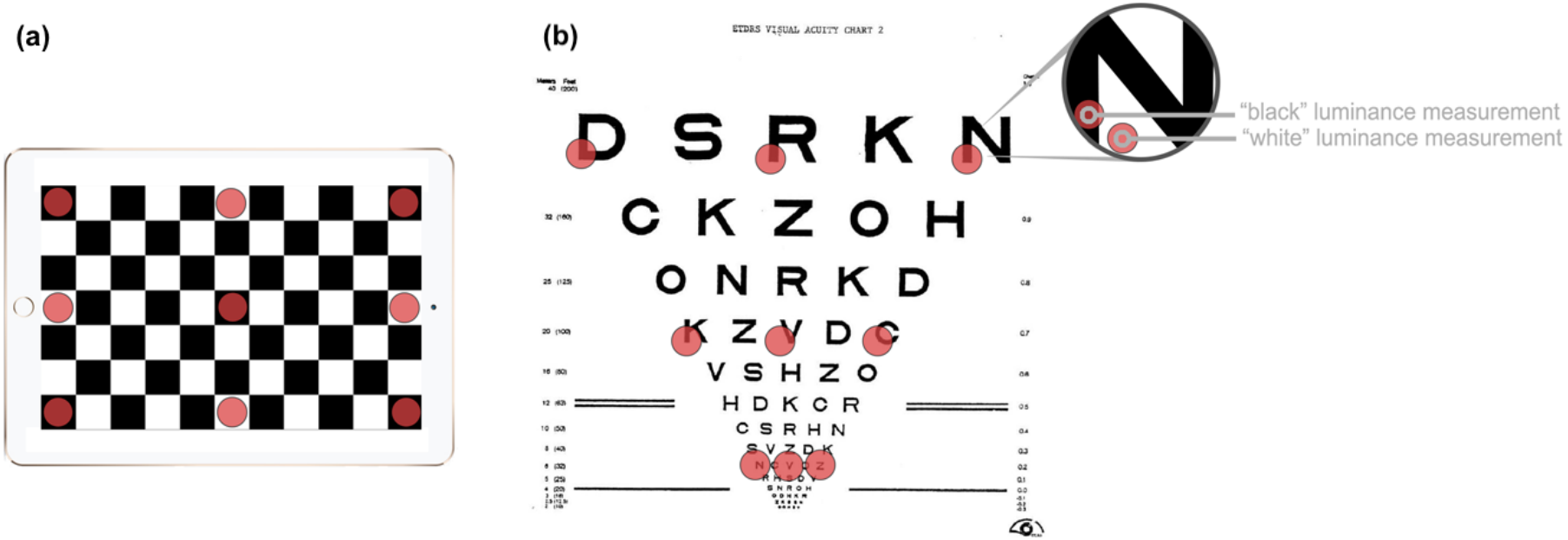

Figure 14 - Livingstone and colleagues conducted an assessment of contrast and screen luminance of a tablet computer (a) compared to equivalent parameters on the reference standard ETDRS vision chart (b) (164). Red circles represent where luminance measurements were taken using a photometer. Adapter from (171) under Creative Commons Attribution License 4.0[7]..

[7] License available from: https://creativecommons.org/licenses/by/4.0/deed.ast

Webber contrast is calculated as specified as**Error! Reference source not found.**,

$$C_W = \frac{L_{background}[cd/m^2] + L_{optotype}[cd/m^2]}{L_{background}[cd/m^2]} \quad \textbf{(1)}$$

where $L_{background}$ is the background luminance and $L_{optotype}$ is the optotype luminance. A luminance meter was used to measure the luminance at various points on each tablet's display and at various screen brightness levels whilst displaying a black and white checkerboard pattern whose colour inverted at regular intervals, as shown in Figure 14a. A similar method was used to ascertain the luminance and contrast of three EDTRS charts, as shown in Figure 14. It was found that all of the tablets met the aforementioned contrast requirements and met the luminance requirements providing that the brightness level was set to 50% or greater. Luminance uniformity was found to be either close to or exceeding the requirements of BS 4274-1:2003. By comparison, the EDTRS charts were found to have lower contrast and poorer uniformity with two of the three charts falling below that which is deemed acceptable. Finally, turning on room lights was found to have little effect on the luminance and contrast of the tablets and marginally improved the luminance uniformity.

Aslam and colleagues also sought to determine the suitability of iPad 3 (Apple Inc.) tablet PCs for visual assessment by investigating the consistency of a screens performance with respect to different areas of the screen and at different viewing angle (173). It was found that, although absolute illuminance was up to 23% less in the corners of the tablet compared to centre for the same pixel intensity, contrast between background and foreground was remarkably stable, varying by under 1.2%. The authors found similar results with respect to viewing angle.

3.3.1.3 Overview of selected mobile device visual acuity applications

There are more than 100 vision test apps on the Google Play Store alone with a similar number of such apps on the Apple App Store (171, 174). Few of these provide information pertaining to clinical validation (174).

Perera and colleagues found that of the eleven visual acuity apps identified in the Australian Apple App Store, none were capable of consistently predicting visual acuity within one line of that measured by a six metre Snellen visual acuity chart (175). Furthermore, the authors found that only three of the applications had

optotypes within 10% of the required dimensions and even the acuity recorded by the most accurate of these was significantly different to those regarded by a 6m Snellen visual acuity chart (p=0.293; n=83) and was especially underestimated at lower acuities.

3.3.1.3.1 EyeHandBook

A similar study by Tofigh and colleagues examined a near visual acuity app, EyeHandBook, on an iPhone 5 running iOS7 (Apple Inc.) in a study similar to that of Perera and colleagues (177). Their comparison of the corrected monocular near acuity recorded for one hundred subjects with that recorded by an LPO Rosenbaum card found that the application consistently overestimated the near acuity by a statistically significant average of 0.11 logMAR ($p<0.0001$), with those with lower vision having a particularly overestimated acuity.

3.3.1.3.2 EyeSnellen

In contrast to the aboveaforementioned studies, Gounder and colleagues found good agreement with a Snellen light box chart in their investigation of the EyeSnellen application (version 1.6; Steve Colley, Perth, Australia) (176). Using a wall mounted first-generation iPad Mini with an iPhone 5s acting as a controller (Apple Inc.), the authors reported a mean difference of 0.001 in the logarithm of the minimum angle of resolution (logMAR) between the two tests (95% confidence interval (CI): -0.169 to 0.171). Whilst the accuracy reported represented an important improvement compared to previously studied applications, the need to mount the tablet and conduct the test at six metres reduces the potential for the test to be used in scenarios where the use of traditional Snellen charts may be difficult, such as conducting vision tests in patients' homes.

3.3.1.3.3 Peek Acuity Pro

Given the large number of deficient applications that are available for public download on the most popular application stores, it is vital that clinicians assess the available results of peer-reviewed clinical validation before using such applications in clinical practice. Furthermore, it can be strongly argued that such software ought to be classified as a medical device and therefore should attain regulatory approval from the relevant authorities in the regions where it is distributed.

To the author's best knowledge, only one application, 'Peek Acuity Pro' (Peek Vision Ltd., London, United Kingdom) has been granted such regulatory approval for visual acuity, having attained approval as a class-1 medical device in the European Union. The application also differs from the above applications in its use of an iterative test procedure . This involves the size of the optotype being displayed based on the patient's performance within the test as opposed to manual selection by the operator. This allows visual acuity to be measured without the operator needing to determine which size of optotype the patient needs to be asked to read at every stage of the test. Indeed, the operator does not even need to look at the smartphone's display during the test which has the additional advantage of removing the possibility of observer bias, which is known to be an issue in many healthcare observations (178).

Peek Acuity has been validated for measurement of monocular visual acuity by comparing its test-retest variability (TRV) and measurement time against the Snellen chart and the ETDRS-based tumbling E logMAR chart (95). The study was nested within a follow-up of a community eye disease cohort study in central Kenya with comparisons being made both in patients' homes and within a temporary eye clinics (179). In total, 272 participants underwent all three tests in the clinic with 233 (86%) of these having undergone tests with Peek Acuity and a portable Snellen chart in their home the previous day. In each case, the tests were conducted by non-healthcare workers who had been trained to deliver the test.

Bland-Altman and Pearson correlation analysis of pairwise comparisons of the various tests showed that Peek Acuity was comparable in accuracy to the reference standard ETDRS chart (0.055 logMAR difference of average with 95% CI of 0.023 to 0.088 logMAR; 95% limits of agreement being -0.438 to 0.549 logMAR; κ=0.917 with 95% CI of 0.893 to 0.935). Furthermore, the smartphone-based test was found to be no slower than the Snellen test with the mean testing time for both eyes being measured as 77 seconds (95% CI: 71-84 seconds) compared to 82 seconds (95% CI: 73-91 seconds) respectively. Finally, Peek Acuity was shown to be repeatable and consistent when tested in the community and in the clinic (-0.054 logMAR difference of average with 95% CI of -0.083 to -0.025 logMAR; 95% limits of agreement being -0.498 to 0.390 logMAR; κ=0.933 with 95% CI of 0.914 to 0.948).

3.3.2 Smartphone Ophthalmoscopy

3.3.2.1 Conventional Digital Fundus Photography

Ophthalmoscopy has long been established as an important procedure in the detection of eye diseases, such as glaucoma, diabetic retinopathy and macular degeneration as well as other systemic issues such as hypertension, malaria and neurological conditions. For this reason, every medical doctor is expected to be competent in the use of a direct ophthalmoscope. However, it should be noted that often this competency is lacking, with it being reported that as many as 47% of medical students in their final year reporting that they are "not at all" or only "a little" confident in performing direct ophthalmoscopy (180). The ocular fundus has been photographed using film cameras since the 19th century (181). With digital camera sensors having exceeded the spatial resolution typically possible with 35-mm film[8] these have how superseded their film counterparts in modern retinal cameras. However, it is important to note that the resolution of a camera is not solely determined by the number of pixels found on the sensor despite many manufacturers and even some peer-reviewed literature quoting this as a proxy for camera performance. Factors affecting image spatial resolution include aberrations with the camera's optics, distortion, field curvature and ultimately the resolution is limited by diffraction. An accurate and objective measure of an imaging system's resolving power can be obtained using specially designed test targets such as the USAF 1951 resolution test chart (183). The resolving power is found by finding the minimum resolvable separation of a set of 3 parallel black lines, with a width equal to their separation, on a white background (183). The current international standards covering image quality for fundus cameras specifies a minimum resolving power of 80lp/mm (line pairs per millimetre) in the centre of the image to 40lp/mm at the periphery for a field of view (FoV) of 30° or less. Cameras with a wider FoV are not required to have such a high resolving power, with a minimum of 60lp/mm at the centre to 25lp/mm at the periphery being specified (184).

[8] The spatial resolution of photographic film is limited by the size and density of the light sensitive silver halide crystals it contains. This will vary depending on a film's light sensitivity (ISO) with less sensitive films having smaller, more tightly packed crystals than more sensitive films. Langford estimated a 36mm x 24mm frame of ISO 100-speed film to contain the equivalent of 20MP (182).

Mobile phones have begun to integrate digital cameras since 2000. There are a number of engineering challenges associated with designing a camera that is viable for smartphone integration and capable of general photography. Plastic lenses and apertures of fixed sizes are generally used to keep costs low and allow for a wide range of scenes. The full camera system also needs to be thin, limiting the space available between optical components. As with any digital camera, image encoding and compression can also degrade the quality, and the associated algorithms need to be able to run within the computing and storage constraints of the host mobile device.

The introduction of digital imaging technologies allows electronic storage and transmission of fundus photographs. As such, it is now standard practice in the United Kingdom for retinal images to be captured by a retinal photographer and sent electronically for grading by a trained retinal grader at a separate grading centre (145).

Furthermore, the fact that digital images are machine readable opens up the possibility of automated screening algorithms with algorithms for diabetic retinopathy having already been demonstrated (185, 186).

However, standard fundus cameras are expensive, require technical skills, bulky and are difficult to transport. Modern smartphones by contrast are inexpensive, mobile and almost universally contain integrated digital cameras for operation by those with little skill in photography. The prospect of a smartphone-based ophthalmoscope is therefore a very attractive one.

3.3.2.2 Indirect Smartphone Ophthalmoscopy

3.3.2.2.1 Smartphone Adapters for Standard Indirect Ophthalmoscopes

The simplest way to use a smartphone in fundus photography is simply to insert its camera into an indirect biomicroscope in place of the operator's eye. A wide selection of attachments are available which allow the phone to be held steady at the slit lamp's eyepiece. These range from commercial products costing up to hundreds of U.S. dollars to DIY kits costing less than 10 USD (187). Such adapters allow images of both the anterior and posterior segments to be quickly captured, stored and

shared with colleagues without needing to send the patient for another examination on a separate instrument. This is particularly beneficial in clinical environments that have tight time or resource constraints and separate devices for retinal image documentation are not available.

Whilst the ability to add an inexpensive digital photography capability to a slit lamp has a number of advantages, the full potential of smartphone ophthalmoscopy can only truly be realised if it is able to operate in the absence of bulky and expensive equipment designed for hospital use.

Blackenberg and Sheffer made an early attempt to rely upon inexpensive and portable equipment by attaching a digital camera to a 'Panoptic' monocular indirect ophthalmoscope (Welch-Allyn Inc., Skaneateles Falls, NY, USA) (188). Following this work Welch Allyn released the 'iExaminer' attachment that allowed an iPhone 4 or 4s (Apple Inc.) to replace the eyepiece and capture ocular fundus images using the iExaminer app (189). This way quality fundus images can be captured, emailed, printed and stored without the need for large hospital-based equipment. The iExaminer was also the first smartphone ophthalmoscope adapter to achieve regulatory approval having achieved US FDA approval. Nevertheless, the full system, excluding phone, costs the end user in the region of 800 USD (www.medicaldevicedepot.com) which, although cheaper than standard fundus photography equipment, is in the price range of premium hand-held ophthalmoscopes. Furthermore, updates to the iExaminer's compatibility tends to lag significantly behind new iPhone releases and at time of writing is only compatible with iPhone 6, 6s and 6 Plus series, 7 months after the release of the iPhone 8 (Apple) (190). This highlights one of the major difficulties encountered by smartphone ophthalmoscope designers, namely the speed at which the mobile phone market develops.

3.3.2.2.2 Smartphone Ophthalmoscopy with Hand-held Lens

Lord and colleagues demonstrated a simpler system for capturing fundus images when they used a 20 dioptre lens (Volk Optical Inc., Mentor, OH, USA), iPhone (Apple Inc.) and pen torch. Their method involved positioning the lens close to the eye, as per standard indirect ophthalmoscopy, and holding the phone and torch at

an appropriate distance from the lens in order to provide imaging and illumination respectively. The need for complex imaging optics, ordinarily worn on the operator's head, is removed with the phone's autofocus bringing the image of the fundus into focus on the imaging sensor. However, the technique requires a high level of skill and capturing high quality images was found to be difficult (191). As with standard indirect ophthalmoscopy, producing an image is sensitive to the distance between the cornea and the 20D lens, which varies according to the patient's refractive error, and the distance between the lens and the phone's optics. The need to hold all three items at once also contributes to the method's difficulty. Fortunately, integrated LED flashes soon became standard with smartphones. By capturing a video stream with the flash enabled in the phone's stock camera application, the need for a pen torch to be held alongside was therefore eliminated (191). The ease-of-use and image quality of the technique can be further improved by using any one of a number of specialist photography apps allowing control over settings such as focus, exposure, white balance and flash light intensity. For example, Haddock and colleagues found that they were able to produce consistently higher-quality images of animals, comatose and awake adults by using the camera app 'Filmic Pro' (Cinegenix LLC, Seattle, WA, USA) (192). As well as allowing independent control over the aforementioned settings, the app also allowed the extraction of individual frames after recording a period of video. Thus, even if only a fleeting glimpse of a feature of interest is achieved, a still image can still be extracted without requiring the operator to react and press a button within the short time the feature is visible. Furthermore, extracting frames in this manner also does not require large video files, only a few seconds of which may have clinically relevant information, to be stored or transferred. This is particularly useful when considering patients who are less likely to comply with the operators instructions, such as children.

Indirect smartphone ophthalmoscopy's potential with challenging patients was demonstrated by Lin and colleagues when they applied the technique to screening neonatal patients for retinopathy of prematurity (193). As screening for this condition requires a wide field of view, the combination of a smartphone with a 30D

lens was not sufficient. However, with scleral indentation a full view of the retina could be achieved. It is typical in ROP screening for an ophthalmologist to perform conventional widefield indirect ophthalmoscopy and then to draw from memory what they observed concerning the infant's retinal development. Lin and colleagues' method therefore offers an alternative, objective means of recording such details without needing to rely upon an expensive wide-field retinal camera.

3.3.2.2.3 EyeGo / Paxos Scope

The precise alignment needed between eye, lens and phone is a limiting factor in making indirect smartphone fundus photography feasible for the non-specialist. To improve the usability of the method, Myung and colleagues developed a lightweight arm that holds the lens at the correct distance from the camera optics (194). The authors produced both 3D printed and machined arms, which held a 20D lens at an adjustable fixed distance from an iPhone 5 running Filmic Pro. Using the native LED flash, the authors were able to produce a selection of good quality images from both normal and abnormal dilated eyes. Clinical validation of Myung and colleagues' prototype, which they named 'EyeGo', was undertaken on 144 patients presenting at an eye hospital in Hyderabad, India. Each of the patients included in the study were dilated to pupil diameters of 6mm or more. Either an ophthalmic technician (with two years optometric training), medical student, optometrist or ophthalmologist imaged the study participants using EyeGo. Images were then graded by a single grader on a desktop display who was able to adjust the colour and brightness of images as deemed necessary.

The image quality of 86.7% of the videos acquired with EyeGo was sufficient to exclude the presence of optic disc oedema, optic disc pallor, retinal vascular occlusion, intraocular haemorrhages, and grade III/IV hypertensive retinopathy. By comparison, the images taken with a desktop fundus camera were of sufficient quality to exclude the presence of the same features in 97.7% of eyes.

Following the EyeGo's clinical evaluation, an FDA approved commercial version named 'Paxos Scope' (Digisight, San Francisco, CA, USA) was released alongside image capture, cloud storage and encryption software and is available for 79 USD per month[9].

[9] As of July 2018 Paxos Scope is no longer available for purchase.

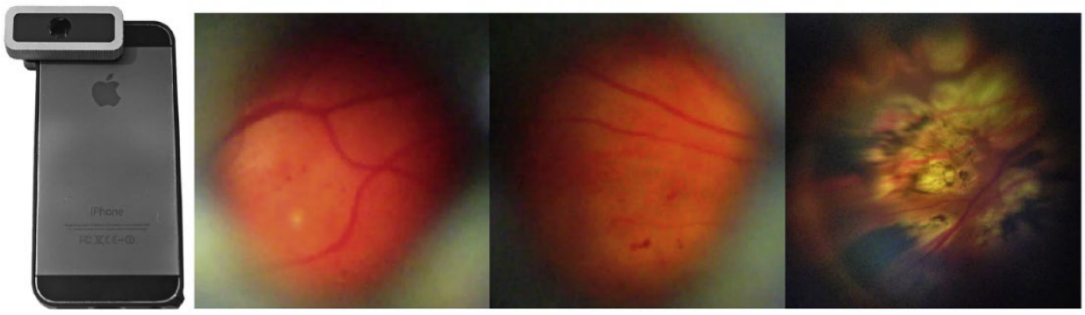

Figure 15 - Example of mydriatic retinal images taken with the D-Eye on iPhone 6 (far left) by a retinal specialist. Conditions that have reportedly been identified include mild nonproliferative diabetic retinopathy (second from left), moderate nonproliferative diabetic retinopathy (second from right), and panretinal photocoagulation scars on a retina with proliferative diabetic retinopathy (far right) (195)[10].

[10] Reprinted from American Journal of Ophthalmology, 159, Russo A; Morescalchi, F; Costagliola, C; Delcassi, L; Semeraro, F, Comparison of smartphone ophthalmoscopy with slit-lamp biomicroscopy for grading diabetic retinopathy, 360-364. e1, Copyright (2005), with permission from Elsevier

3.3.2.2.4 Ocular Cellscope

One drawback of smartphone ophthalmoscopy compared to standard retinal photographs is the reduced field-of-view. Maamari and colleagues demonstrated how a software method called image mosaicking can increase the field presented by a single image (196). Images captured using the 'Ocular Cellscope', which consists of a system of independent LEDs, lenses and polarisers, were inputted into the image mosaicking software installed on a desktop computer. Although the software was originally developed for use with desktop retinal cameras, the authors reported mosaics that both encompassed a large field and were of good clarity. Having demonstrated the viability of the technique with smartphone ophthalmoscopes, the next step is to develop such software capable of being deployed on the phone itself and even building a mosaic in real-time during the examination itself.

3.3.2.3 Direct Smartphone Ophthalmoscopy

Whilst smartphone ophthalmoscopes using the principal of indirect ophthalmoscopy have shown significant promise, they are generally either difficult for the non-eye professional to use or significantly more expensive. Smartphone ophthalmoscopes using the principles of direct ophthalmoscopy offer to both provide ease-of-use and affordability (197).

D-Eye (D-Eye Srl, Padova Italy; Figure 15) re-directs the flash of a smartphone to a co-axial alignment with the camera optics by inserting a beamsplitter in the optical path (198). As the position and distance of both the camera and LED flash on the back face of the phone vary according to make and model, it is necessary for the position of the optics to be adjusted. D-Eye overcomes this problem by screwing a 'bumper' to the perimeter of the phone and attaching a unit containing the optics using magnets. By using a different bumper for differing phone models co-axial alignment of the camera and LED flash's optical path can be achieved. The drawback of this design is that a different bumper design needs to be manufactured for every handset for which compatibility is desired. As a result, the number of compatible smartphones is limited, with only Apple handsets being compatible at time of writing. Russo and colleagues compared D-eye mounted on an iPhone 5 (Apple Inc.) to biomicroscopy for the assessment of 240 eyes in 120 out-patients attending a diabetic eye centre in Ospedali Civili di Brescia, Italy (195). A

sensitivity of 0.90 (95% CI: 0.82-0.94) and specificity of 0.96 (95% CI: 0.90-0.98) was reported for a retinal specialist's detection of diabetic retinopathy. For the assignment of a particular grade of diabetic retinopathy by a retinal specialist a simple κ of 0.78 (CI: 95%: 0.71-0.84, $p<0.001$) was reported with 3.75% of eyes being ungradable with D-Eye compared to 1.7% with biomicroscopy. Regarding the detection of significant cystoid macular oedema sensitivity and specificity were 81 (95% CI: 0.54-0.94) and 0.98 (95% CI: 0.95-0.99) respectively with a simple κ of 0.79 (95% CI: 0.65-0.93).

As the images were acquired and graded by a retinal specialist it is difficult to assess from the results how D-Eye performs in the hands of general practitioners, nurses or non-clinical staff compares to biomicroscopy. Indeed, it would also be useful to understand how use by the non-clinician compares to standard retinal photography by a clinical photographer, which is the most common mode of retinal imaging in diabetic retinopathy screening programmes (145).

Giardini and colleagues also demonstrated a direct ophthalmoscope, based on a Galaxy S3 (Samsung) in 2013. Like the D-Eye, this involved redirecting the smartphone's LED flash using a custom optical component (199). As this design was further developed in this thesis, it is discussed in more detail in Chapter 5.

3.3.3 Visual Fields

3.3.3.1 Standard Visual Fields Testing

Many eye diseases and conditions result in specific blind spots, referred to as scotomas, or a loss of peripheral vision in advance of central vision loss. Visual acuity is therefore not the most appropriate measure of such vision loss as it primarily tests central vision. As was mentioned in the previous chapter, the two most common tests of visual fields are the Goldmann visual fields test and the Humphrey visual field analyser (HFA) (135). In each test the patient places their head on a chin rest inside a uniformly illuminated hemispherical dome, has one eye covered and is asked to fixate on a central point. The patient is then asked to respond when they perceive a visual stimulus by pressing a handheld button.

In the Goldmann test, the operator activates lights from the periphery inwards along a particular axis until the patient acknowledges that they can see the stimuli. By

repeating across a number of different angles, a map of the extent of the patient's peripheral vision can be produced.

The HFA instead automatically activates a series of visual stimuli throughout the entire visual field and thus is able to produce a full map of the patient's visual field.

In both tests, the contrast of the stimuli compared to the background is varied to give a measure of the retinal sensitivity throughout the visual field.

Both tests are reliant on equipment that is expensive and bulky. For this reason, assessing visual fields outside of eye clinics in well-resourced settings is rare. An inexpensive, mobile test that can be operated reliably by medical personnel with minimal optometry training is therefore highly sought after. Furthermore, the tests' requirements for the patient to fixate centrally and respond by pressing a button are problematic for non-compliant patients or those who have motor difficulties such as stroke patients. Thus, a visual fields analyser that is effective within such patient populations is also desirable.

3.3.3.2 Tablet-PC Visual Fields Testing

Tahir and colleagues tested the effect of viewing angle and screen reflections on the gamma function and screen uniformity of three tablet computer models (200). They found that a wide range of contrasts could be generated, although these were limited in number at the lowest contrasts. Particularly relevant to visual field testing was their finding that, although there is considerable non-uniformity in absolute luminance, there is minimal variance in contrast when the edges of the displays are viewed at an angle. However, the introduction of a light source above the tablets whilst the tablets were tilted at 45 degrees did have a significant impact on the measured contrast. This highlights the importance of controlling ambient lighting and tablet position during testing.

3.3.3.2.1 Visual Fields Easy

Visual Fields Easy (GLANCE Optical, Melbourne, Australia), an application for the iPad (Apple Inc.), uses a variable fixation point to test both the central and peripheral visual field without the need for bulky or expensive equipment. The central 30 degrees of vision is tested using a 64mm^2 (size V) fixation target on a 10 cd/m^2

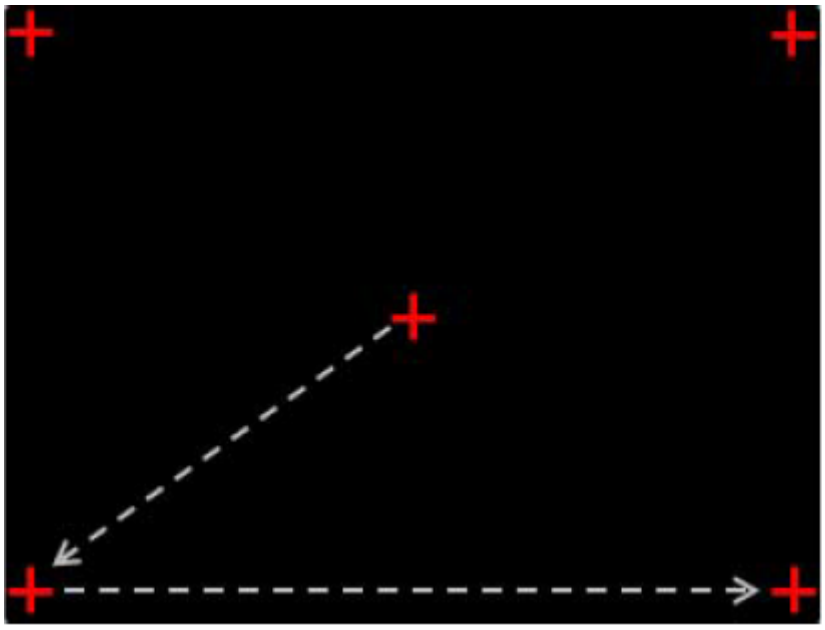

Figure 16 - Visual fields tests based on tablet PCs move the fixation target in order to increase the tested visual field beyond the angle subtended by the display (201). Reproduced under Creative Commons BY-NC-ND 4.0 license[11].

[11] License available at: https://creativecommons.org/licenses/by-nc-nd/4.0/legalcode

background. The test is capable of presenting a 16dB suprathreshold target for rapid screening or of testing 96 locations for more comprehensive testing of the visual field. The patient responds to these stimuli by touching the screen. Following the testing of the central field, the fixation target is moved to each corner of the display in turn in order to test each quadrant of the peripheral visual field, as shown in Figure 16. Thus, a full field of 34° horizontal and 25° vertical can be tested.

A comparison of the results recorded with Visual Fields Easy to those recorded with a HFA for 200 healthy, 200 glaucomatous and 50 diabetic eyes was reported by Johnson and colleagues (202). A correlation of missed targets of 0.75 ($p<0.0001$) and 0.60 ($p<0.0001$) was reported for the mean and pattern standard deviation respectively, as measured by the HFA.

3.3.3.2.2 Melbourne Rapid Fields

A subsequent version of the technology described in the previous sub-section, Melbourne Rapid Fields (MRF; GLANCE Optical) is a perimeter test based on an iPad (Apple Inc.) (203). The test also employs variable fixation, setting the fixation target to the centre of the tablet's display and then each one of the corners in sequence. In doing so the test can be used to test 66 locations through 30°, despite the iPad's display only subtending 17.4° x 12.9° at this distance. Stimuli were round and displayed for 300ms.

As the test uses a radial grid, additional test points are used to fill any gaps between peripheral points if the patient returns abnormal results.

Additionally, the test provides threshold estimates by using seven contrast steps between 0 and 30 dB (0, 6, 12, 17, 22, 26, 30dB) according to the Bayes methods (201). Thresholding begins at a single initial luminance with the following luminances being determined by a modified Zippy Estimation by Sequential Testing procedure (204).

Fixation is tested at the beginning of the test using a blind-spot monitor and throughout the central fixation test by presenting a stimulus in the location of the blind spot. As this technique cannot be implemented on the peripheral tests, a voice instruction is instead played at regular intervals during these tests. False-positives are also detected by including periods in which no stimulus is presented. Stimulus

size is increased with retinal eccentricity so to negate the eccentricity effect, a phenomenon whereby visual performance reduces towards the periphery of the retina (205). Therefore a constant threshold is expected across the field (205).
The patient registers by pressing the screen with a finger or by pressing the spacebar on a Bluetooth keyboard. The test takes 4-6 minutes in total depending on the field loss experienced by the patient. Goldmann and Humphrey's visual fields tests, by comparison, have been reported to both take approximately 14.5 minutes per an eye on average (135). As with the previous app, calibration using a radiometer is required.

Kong and colleagues compared outcomes obtained from ninety patients undergoing glaucoma investigation (age: range=18-91, mean=69.5, standard deviation=12.5) using the MRF hosted on an iPad 3 (Apple Inc.) to those attained using a HFA using the Swedish Interactive Thresholding Algorithm (SITA). All patients had prior experience of the HFA test and were excluded if they were not fluent in English. One eye having an acuity of 6/12 or better was selected at random for each patient and gave a reliable HFA-SITA result within 3 months of MRF testing. Testing was conducted by a clinician with the tablet and keyboard placed on a typing stand and the patients head unrestrained after being positioned at 33cm.

The authors found the mean defect recorded by MRF to have an overall strong correlation with those returned by HFA (ICC=0.93), however they also found that MRF returned a less negative mean defect than HFA, with a bias of 1.4dB. Good overall agreement was found between pattern deviation indices (ICC=0.86), however it was noted that this was weaker in eyes with more severe defects (ICC=0.53) although the sample size for this sub-group was relatively small (n=18).

Test-retest reliability was found to be comparable to HFA (ICC=0.93; 0.89 for mean defect and pattern deviation respectively with a bias of 0.1-0.5dB in each case).

The authors additionally found that although MRF was quicker (5.7±0.1 compared to 6.3±0.1 minutes) fixation losses occurred more often (36±4% compared to 6±4%) leading the authors to suggest that the blind-spot monitor is corrupted by free-space viewing. It

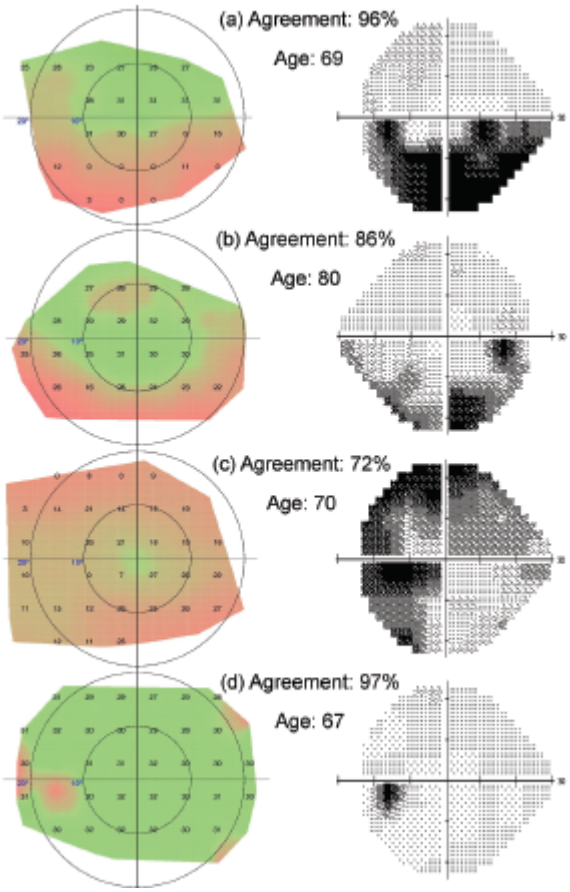

Figure 17 - Visual fields results acquired using 'Eyecatcher' for three glaucoma patients (a-c) and one health patient (d) (206). Green and red regions in the Eyecatcher output (left column) represent areas of the visual field where the stimuli were seen and not seen respectively. Superimposed numbers represent the Humphrey sensitivity values in decibels. Right column shows the corresponding Humphrey Visual Fields results in greyscale. Reproduced under Creative Commons BY-NC-ND 4.0 license[12].

[12] License available at: https://creativecommons.org/licenses/by-nc-nd/4.0/legalcode

was therefore suggested that future development include eye-tracking technology.

3.3.3.2.3 Eyecatcher

'Eyecatcher' is alternative tablet-based visual fields app that also makes use of a variable fixation target to map the visual field (206). However, instead of using static fixation and a screen or button press to register that the patient has observed a stimulus, the patient is instructed to look at a stimulus when they see it. The test then uses an infrared eye tracker (Tobii Eye Tracker, Stockholm, Sweden) to detect if the patient has moved their eyes from the original fixation point to the stimulus. This stimulus then becomes the fixation point for the next test and so on until a full map of the visual field is built. Smith and colleagues tested the app for the 20 degrees of central vision on a group of 12 glaucomatous and 6 healthy participants and compared the results against standard automated perimetry testing, as shown in Figure 17. A median suprathreshold defect concordance between Eyecatcher and standard automated perimetry was reported to be 83% (95%CI: 62-90%) and 96% (95% CI: 92-97%) for diseased and healthy eyes respectively. Whilst these only represent preliminary results, the prospect of an accurate visual fields test that is low-cost, mobile and only requires eye movements is a promising development with potential applications in remote locations, low-income settings and within low-mobility patient groups.

3.3.4 Anterior Segment Imaging

The gold-standard instrument for visualising the anterior segment is the clinical biomicroscope, more commonly referred to as the slit lamp (207). Standard slit lamps have a number of features, such as variable magnification and one or more light sources with variable intensity, intensities, colour and illumination angle. The operator also has a large degree of freedom over the positioning and focus of the slit lamp, while the patient remains stationary in an attached chin rest. This allows different depths of field to be achieved in order to visualise different components of the anterior segment in stereo including the cornea, iris and crystalline lens (207). These features allow the operator to identify a wide gamut of ocular pathologies such as cataract and corneal opacities (207). Anterior segment photography has classically been achieved with a slit lamp by introducing a beam splitter immediately

in front of the eyepieces in order to deflect the light towards a single-lens reflex camera. As was described in the section discussing smartphone ophthalmoscopy, it is straightforward to attach a smartphone camera optic to one of the eyepieces of a slit lamp and commercial adapters that do such are available (187). Doing so increases the ease with which anterior segment images can be shared with colleagues or stored in cloud-based storage. However, slit lamps themselves are bulky, relatively expensive and require a degree of skill to use (207, 208). Developing a mobile digital anterior segment imager that does not need to be attached to a standard slit lamp in order to operate, and whose operation is instead more akin to operating a smartphone camera, is therefore highly desirable as it would allow the task shifting of anterior segment imaging from doctors based in clinics to lower cadres, such as CEHWs in the community.

To this end, Myung and colleagues have demonstrated a means of eliminating the need for a slit lamp in the acquisition of digital anterior segment images (209). The authors first attempted to acquire images by attaching a commercially available smartphone camera macro lens and using the native flash of an iPhone 5 at a working distance of approximately 2.5cm from the subject's eye. However, it was found that, even when using Filmic Pro to control the illumination intensity, the brightness of the flash was too uncomfortable for study participants at the close working distance necessitated by the macro-lens' focal length. This prompted the authors to develop a simple adapter that combined the macro lens with an external LED light source with a brightness selected for patient comfort. The adapter is pocket-sized and can be easily attached and detached from any handset. There are a number of limitations to the adapter, notably that it does not have the ability to create a slit of light that can be used to estimate the depth of a corneal pathology or for capturing cells or flare. In addition, the relatively short working distance results in the necessity for disinfection between uses. Nevertheless, the authors were able to use this system to capture high quality anterior segment images of subjects displaying a number of different pathologies. This allowed them to claim that they had sufficient quality images with regards to the clarity of the cornea, quality of the epithelium, fluorescein uptake, state of the conjunctiva, shape of the pupil, health of the iris, presence or absence of a hyphaemia or hypopyon in the anterior chamber and the appearance of the eyelids

and lashes. Thus, given the low production cost, ease of use and reported quality of images this design offers the potential for a very useful anterior segment imaging tool, applicable to a variety of settings, included those in which resources are limited. However, a notable absence from the list of pathologies that could be detected was cataract. Given that this is the leading cause of global blindness, the ability to grade cataract is a key requirement of such a smartphone-based anterior segment imager.

Two notable, commercially available smartphone-compatible slit lamps are the PSL One and the PSL Classic (Keeler, Windsor, U.K.). Both these models have many of the features of a regular slit lamp with the added benefit of being lightweight and durable. The combination of these slit lamp models and Keeler's iPhone 4 adapter provides the user with the genuine ability to conduct mobile digital slit lamp photography. However, with the aforementioned portable slit lamps costing approximately £4000 and £5800 respectively (www.hce-uk.com) and the adapter costing an additional £95 (www.hce-uk.com) this remains an option that has a price beyond that which most non-specialists are able to afford. It has been reported that the slit lamp adapter is also compatible with the Haag-Streit 900 BM (Haag-Streit Holding, Köniz, Switzerland) and SL-3F (Topcon Corp., Tokyo, Japan) slit lamps if a varying degree of adaptation is applied (210).

3.3.5 Discussion

A number of research groups and start-up companies have contributed to the development of mHealth solutions for the delivery of eye care. These include four of the main tests and examinations used in ophthalmic diagnosis, namely, distance visual acuity, ophthalmoscopy, visual fields and anterior segment imaging.

Whilst there are many unverified vision apps available for download in popular app stores, a number of smartphone-based versions of the aforementioned tests and examinations with varying degrees of clinical evidence have begun to emerge. These include fully regulatorily approved devices in the cases of distance acuity and ophthalmoscopy (Peek Acuity and Paxos Scope, D-EYE and Peek Retina respectively).

Common advantages of the mHealth solutions discussed in this chapter include:

- Low manufacturing costs compared to standard equipment
- Suitability for field use
- Improved data fidelity owing to digitisation of the health data attained
- Possibility of integration with telemedicine systems
- Suitability for use by health workers with minimal clinical training.

These are in agreement with the goals extracted from the review of the global mHealth adoption literature featured in the previous chapter. The solutions were also ubiquitously described as having the potential to benefit eye care services in LMICs.

However, despite these advantages, none of the discussed technologies have yet been adopted at a scale that is likely to have a significant impact on public eye health. As such, an investigation of the barriers to at-scale adoption of these specific mHealth technologies is therefore warranted.

The proposal that the mHealth eye tests be used for case finding in the community or outreach clinics by personnel with little or no clinical training has particularly profound implications for the clinical workflow of the health system in which such devices are to be imbedded. Implemented at scale, this ought to result in the far greater engagement of lower cadres of health workers being engaged in the eye care workflow as well as higher numbers of patients being referred to treatment services.

Given that paucity of data on the health system impact was found to be the most commonly cited barrier to mHealth adoption in Chapter 2, it is therefore of upmost importance that such data is acquired if the discussed mHealth devices are to achieve adoption within eye care in LMICs.

4 An Introduction to Clinical Workflow Modelling

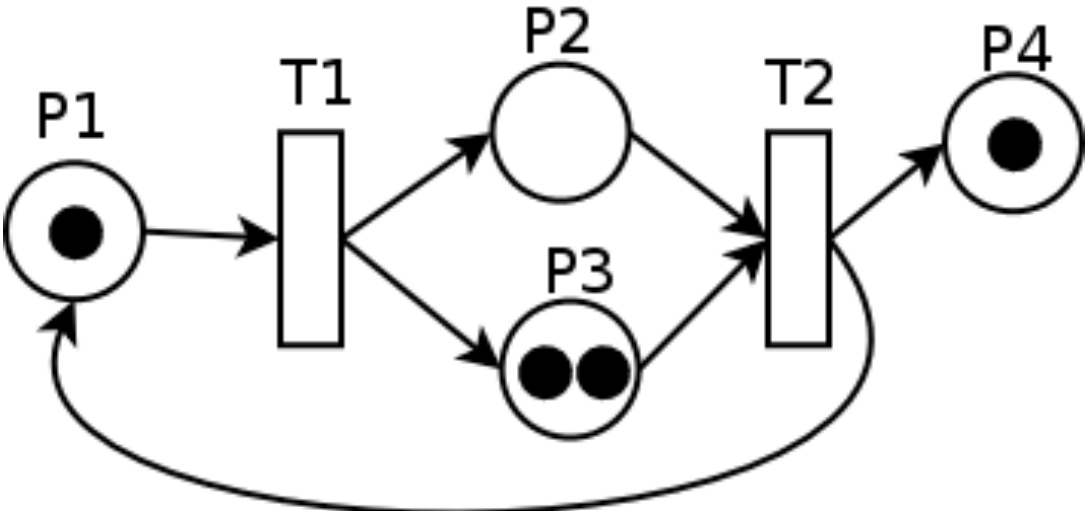

Image reproduced from wikipedia.org under CC BY-SA 3.0 license[13]

[13] https://creativecommons.org/licenses/by-sa/3.0/deed.en

4.1 Introduction

As issues relating to the clinical workflow have been frequently cited as being an implementation barrier for mHealth at scale, this chapter will investigate how consideration of the clinical workflow can be made earlier in mHealth development. In their 2009 review, Niazkhani and colleagues provided the following definition:

> "[The] clinical workflow [is] the flow of care-related tasks as seen in the management of a patient trajectory: the allocation of multiple tasks of a provider or of co-working providers in the processes of care and the way they collaborate." (211)]

In order to optimise such workflows, it is first necessary to produce a workflow specification which describes the clinical workflow. This requires a clinical workflow model, that is a set of concepts that are used to describe the processes, tasks, dependencies among tasks and the required roles that can perform these tasks (212).

The application of workflow modelling techniques, which have their origin in industry, to analysis of the clinical workflow is well established (213). This chapter will therefore begin with a systematic review of the scientific literature relating to the clinical workflow of mHealth designs and implementations in LMICs.

Following this, this chapter will examine workflow modelling techniques that may be of use in producing additional analyses of clinical workflows in LMICs which are pertinent to mHealth use. In particular, it will look at how consideration of the clinical workflow can be made during the design phase and in the design pilot studies attempting to validate mHealth hardware designs.

The final section of the chapter will then provide an overview of the specific workflow modelling language to be used in this thesis, that is timed Coloured Petri Nets.

<table>
<tr><td></td><td colspan="4">AND</td></tr>
<tr><td></td><td>Title Contains one of</td><td colspan="2">Title Contains one of</td><td>Title Contains one of</td></tr>
<tr><td rowspan="4">OR</td><td rowspan="4">workflow
careflow
system model
business model
process model
BPM</td><td colspan="2">LMIC
Africa</td><td colspan="2">mHealth
mobile health</td></tr>
<tr><td colspan="2">AND</td><td colspan="2">AND</td></tr>
<tr><td>low
middle
poor</td><td>country
countries
setting</td><td>health
disease
illness
injury
clinic
hospital</td><td>smartphone
mobile
phone
cellphone
SMS
app</td></tr>
<tr><td colspan="2">the name of any country listed as a low, lower middle or upper middle income country by the world bank in the 2018 fiscal year (214)[14]</td><td colspan="2"></td></tr>
</table>

Table 7 - Search criteria for the review of literature relating to the quantitative analysis of mHealth's impact on the clinical workflow within LMICs in the scientific literature.

[14] That is any one of: Afghanistan; Albania; Algeria; American Samoa; Angola; Argentina; Armenia; Azerbaijan; Bangladesh; Belarus; Belize; Benin; Bhutan; Bolivia; Bosnia and Herzegovina; Botswana; Brazil; Bulgaria; Burkina Faso; Burundi; Cabo Verde; Cambodia; Cameroon; Central African Republic; Chad; China; Colombia; Comoros; Dem. Rep. Congo; Rep. Congo; Costa Rica; Côte d'Ivoire; Croatia; Cuba; Djibouti; Dominica; Dominican Republic; Ecuador; Egypt; El Salvador; Equatorial Guinea; Eritrea; Ethiopia; Fiji; Gabon; The Gambia; Georgia; Ghana; Grenada; Guatemala; Guinea; Guinea-Bissau; Guyana; Haiti; Honduras; India; Indonesia; Iran; Iraq; Jamaica; Jordan; Kazakhstan; Kenya; Kiribati; Dem. People's Rep. Korea; Kosovo; Kyrgyz Republic; Lao PDR; Lebanon; Lesotho; Liberia; Libya; Macedonia; Madagascar; Malawi; Malaysia; Maldives; Mali; Marshall Islands; Mauritania; Mauritius; Mexico; Fed. Sts. Micronesia ; Moldova; Mongolia; Montenegro; Morocco; Mozambique; Myanmar; Namibia; Nauru; Nepal; Nicaragua; Niger; Nigeria; Pakistan; Panama; Papua New Guinea; Paraguay; Peru; Philippines; Romania; Russian Federation; Rwanda; Samoa; São Tomé and Principe; Senegal; Serbia; Sierra Leone; Solomon Islands; Somalia; South Africa; South Sudan; Sri Lanka; St. Lucia; St. Vincent and the Grenadines; Sudan; Suriname; Swaziland; Syrian Arab Republic; Tajikistan; Tanzania; Thailand; Timor-Leste; Togo; Tonga; Tunisia; Turkey; Turkmenistan; Tuvalu; Uganda; Ukraine; Uzbekistan; Vanuatu; Venezuela; Vietnam; West Bank and Gaza; Yemen; Zambia or Zimbabwe

4.2 Review of Clinical Workflow Modelling of mHealth in Low- and Middle-Income Settings

4.2.1 Aim

The aim of the review was to assess the current state of the scientific literature with respect to the quantitative analysis of mHealth's impact on the clinical workflow within LMICs.

4.2.2 Methods

The review was conducted and is presented in this thesis in accordance with the Preferred Reporting Items for Systematic Reviews and Meta-Analyses (PRISMA) guidelines for reporting systematic review (38).

4.2.2.1 Inclusion Criteria

It is clear from the review of global mHealth in Chapter 2 of this thesis that merely appropriating what is already in known about the effects of introducing mHealth into the clinical workflow in high-income settings is not sufficient for understanding the effects of the same in LMICs. Therefore, article inclusion was restricted to those specifically discussing the impact of mHealth on the clinical workflow of health systems in LMICs.

4.2.2.2 Exclusion Criteria

Articles qualitatively discussing the clinical workflow in such scenarios, whilst of interest, were considered out of the scope of this review. Other reasons for exclusion included the article not discussing the clinical workflow, not relating to mHealth, not concerning LMICs and using qualitative methods only.

4.2.2.3 Information Sources

The primary source of the information for this review was MIMAS Web of Knowledge.

4.2.2.4 Search Criteria

The search criteria used is shown in **Table 7**.

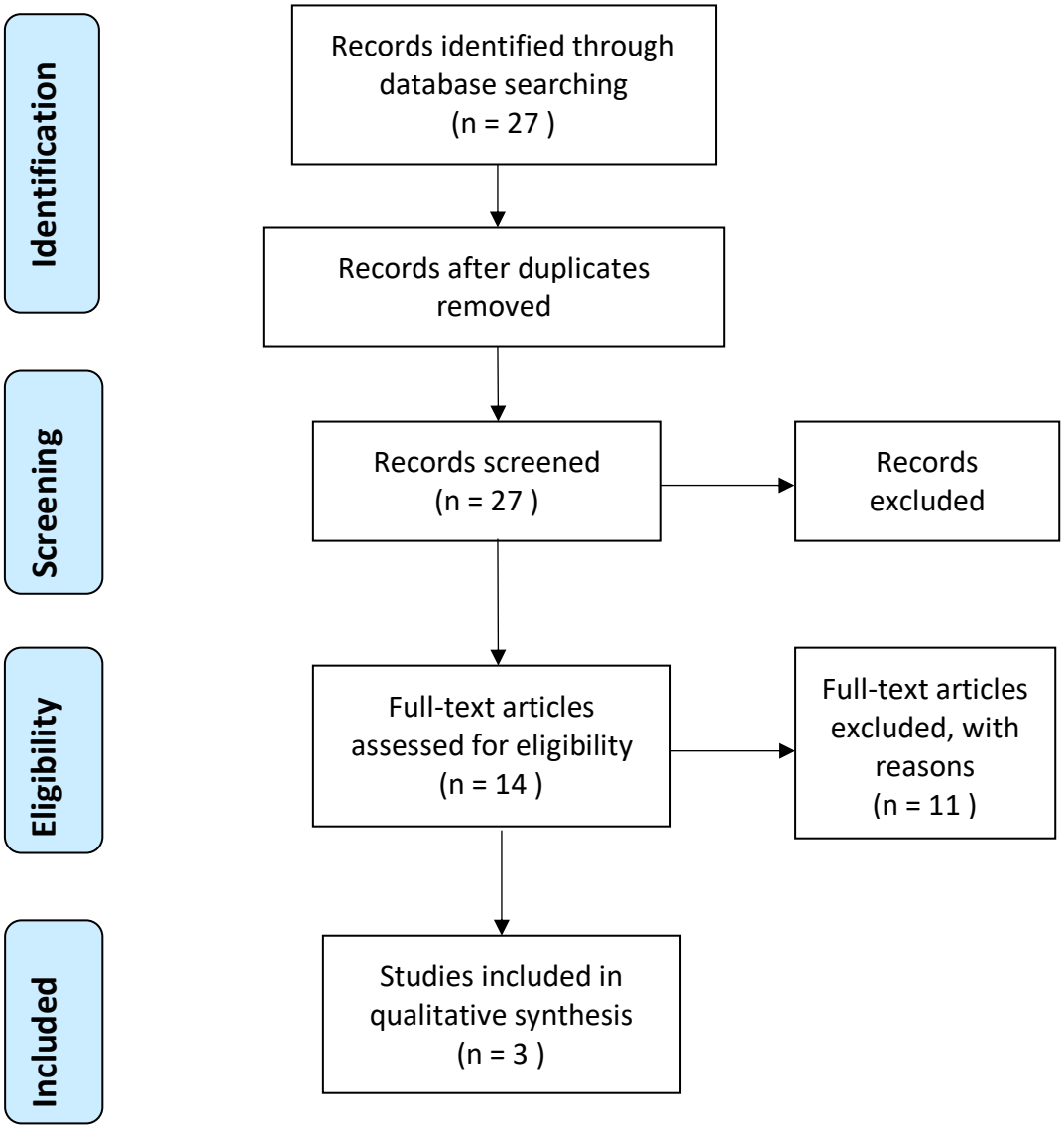

Figure 18 - PRISMA 2009 Flow Diagram for the review of clinical workflow modelling of mHealth in low- and middle-income settings. Adapted from (38) with permissions.

The clinical workflow is often referred to as simply “the workflow” or the “careflow” in the literature. Similarly, the workflow of a more general business system is commonly referred to as a “business process model” or by the acronym BPM. Hence, the search criteria used sought to capture use of any one of these terms within the article’s title.

As well as the more precise term “low- or middle- income country” used throughout this thesis, LMICs or part-there-of are variously referred to as low resource settings or poor countries. The search terms therefore sought to capture use of these terms within the title or reference to one or more of the nations defined as being a LMIC by the World Bank during the 2018 fiscal year (214).

Finally, other than explicit use of the terms “mHealth” or “mobile health”, reference to mHealth was sought by looking for reference to mobile devices (specifically any one of: “smartphone”, “mobile”, “phone”, “cellphone”, “SMS” or “app”) alongside mention of health, disease or a clinical setting (namely any one of: “health”, “disease”, “illness”, “injury”, “clinic” or “hospital”).

The indices searched were ‘Science Citation Index Expanded’, ‘Social Sciences Citation Index’, ‘Arts & Humanities Citation Index’, ‘Conference Proceedings Citation Index – Science’, ‘Conference Proceedings Citation Index – Social Science & Humanities’, ‘Book Citation Index – Science’, ‘Book Citation Index – Social Sciences & Humanities’ and ‘Emerging Sources Citation Index’.

4.2.2.5 Article Selection

Eligibility assessment was conducted in an unblinded manner by the author only. Articles were screened and reviewed according to the process represented graphically in Figure 18. Duplicates were removed using EndNote X7 (Thomson Reuters Corp.) leaving only unique articles whose titles were then screened for relevance. The articles that were considered eligible had their abstracts screened and those that were deemed to qualify underwent full-text assessment.

4.2.2.6 Data Collection and Synthesis

None of these records were duplicates and thus all of the records were considered eligible for abstract screening. Fourteen of the screened abstracts were deemed to qualify for full-text assessment of eligibility.

4.2.3 Results

4.2.3.1 Article Selection

27 records were returned from the database search detailed above. No duplicates were discovered using EndNote X7 leaving 27 unique articles whose titles were then screened for relevance. All 27 of these articles were then considered eligible for having their abstract screened of which 14 were deemed to qualify for full-text assessment of eligibility. The full-texts of each of these articles were available and eleven articles were deemed not to meet the eligibility criteria. Therefore, three articles were included in the qualitative synthesis in total.

4.2.3.2 Individual Article Characteristics and Results

In 2013 Chaiyachati and colleagues reported results concerning the tracking and reporting of adverse clinical events by healthcare workers using a feature phone application (215). A mixed-methods evaluation of five healthcare workers who were trained on the mobile application was conducted. Besides the primary outcome of number of adverse events recorded in comparison to a baseline, a number of other qualitative and quantitative outcomes were recorded. These included a quantitative analysis of phone usage patterns and a qualitative analysis of data collected through focus group interviews. The analysis of usage patterns was at a very gross level, and consisted of recording the proportion of available airtime, SMS and data bundles being refilled. This was reported to be 55%, 33% and 18% respectively. Other information recorded were login screen freezes (two reported), phone malfunctions (one reported) and phone losses and thefts (none reported). Whilst the reported data gives some insight into the impact on the clinical workflow of the healthcare workers, there was no attempt to quantify this impact further.

In 2015 Raghu and colleagues reported a study concerning how an mHealth system for assessing and managing cardiovascular disease risk fitted within the needs and environment of the Indian healthcare system (216). This tool was developed using the Agile development methodology (217). As well as collecting qualitative feedback through a survey using a four-point Likert scale, the authors also recorded timestamps for every click during the risk assessment (218). These were used to determine the median time taken for the assessment, the variation in this time

between the three assessors and the time taken for each of the four steps in the assessment process. The rate at which Bluetooth transmission was chosen over 'manual' transmission was also recorded. The authors suggested that the timing data acquired could be used to assess the maximum number of community participants that could be screened in a single day as well as the performance of individual healthcare assistants when combined with other performance data.

In 2016 Ali and colleagues reported results concerning the use of the 'Operational Data Kit (ODK) Scan' paper-to-digital system within the data management processes of the Tuberculosis Control Programme in Pakistan (219). ODK Scan is a mobile application that uses an Android smartphone's camera to capture images of specially designed paper forms that it then uses to populate a predefined template by using image analysis algorithms to understand the written data recorded within the form. Other tools within the ODK are then used to view, edit, verify, aggregate and synchronise the data. The study aimed to assess the quality of the data acquired by the system, the quantitative impact on the data management processes and collect user feedback. This was achieved through a mixed-methods approach involving the acquisition of quantitative and qualitative data. Firstly, the authors assessed the data quality compared to the standard digitisation process of transferring data manually into a spreadsheet. Secondly, the time spent filling in forms alongside the time spent on data transfer, aggregation and verification were recorded by observation and then compared to the same process using the ODK scan system. Finally, qualitative user feedback was acquired through a survey employing a Likert-scale assessment and semi-structured interviews (218). Analysis of the data quality showed this to be slightly degraded compared to the standard process (86% vs 94%). The speed at which some tasks were completed were observed to be slower with ODK (form filling and data verification) but quicker for data aggregation. The need for manual data transfer by courier, a process taking 1-2 days, was entirely eliminated. However, data collection, taking 3-4 days, was unaffected by the ODK Scan workflow. There was no quantitative analysis concerning the impact on the wider clinical workflow resulting from the increased time required to fill each form or verify each record. However, the qualitative analysis highlighted that field workers were unhappy with the length of time taken to fill in the new form.

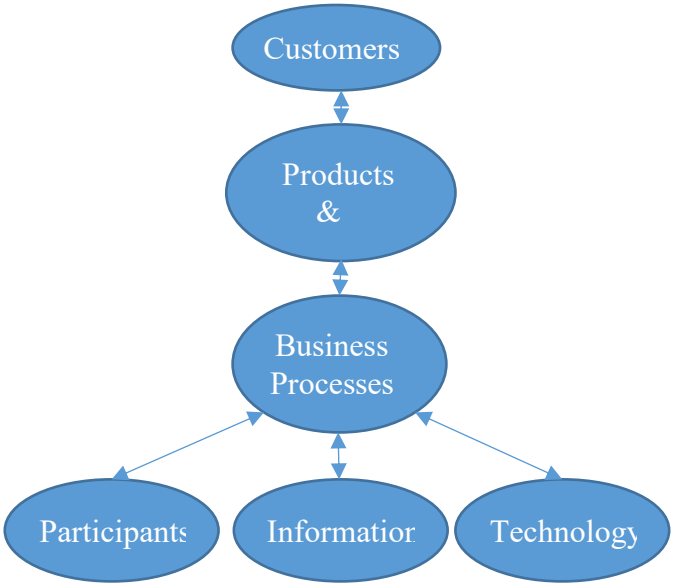

Figure 19 – Alter's work system framework (220)

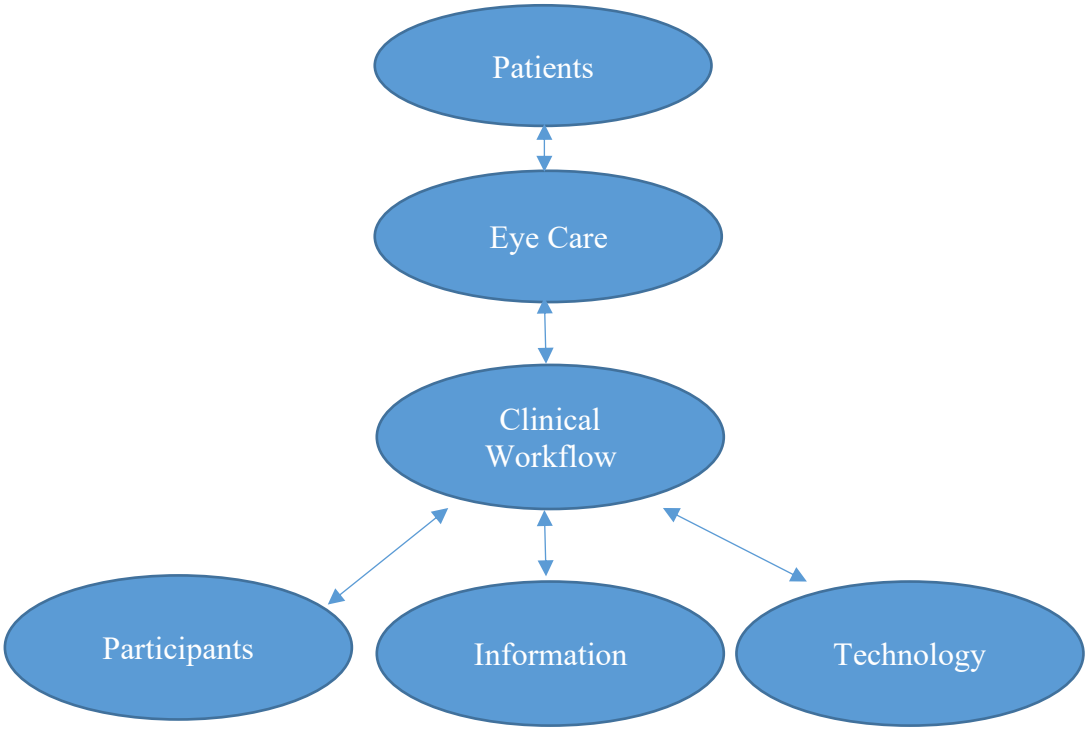

Figure 20 - An adaption of the Alter integrated view of an information system to the delivery of eye care (220).

4.2.4 Discussion

The literature search confirms the paucity of research focussing on quantitative analysis of the workflow impact caused by implementing mHealth in LMICs. Whilst all three studies that were included in the qualitative analysis recorded timings relating to the mHealth system in question, none used these data to simulate how the device design or its implementation at scale could be improved.

Robust quantitative analysis of the impact of mHealth on LMIC clinical workflows therefore represents a significant research gap. This thesis aims to narrow this gap by using workflow modelling to assess the impact of mHealth's implementation within a particular speciality in LMICs.

4.3 An Overview of Information Systems Development and Modelling

4.3.1 The Development Cycle

A useful sector to explore with regard to how analysis of the clinical workflow might improve mHealth design is that of enterprise information systems. Alter's framework for work systems, which is often used to understand enterprise information systems, defines a work system as "a view of work as occurring through a purposeful system" (220). The work system framework is represented graphically in Figure 19. Such work systems represent a general case that encompasses projects, supply chains, information systems amongst other cases. An information system is a software system that captures, transmits, retrieves, manipulates or stores information and exists to support one or more work system, in whole or in part (220, 221). An enterprise information system is such a system as applied to supporting an organisation.

Business processes describe the flow of work within an organisation (221). From Figure 19 the nature of business processes is clear. They consist of a set of activities that are coordinated to achieve an organisation's goal. It is intuitively assumed in this thesis that how an organisation delivers eye care can be represented using a similar framework, shown graphically in Figure 20. In this modified framework

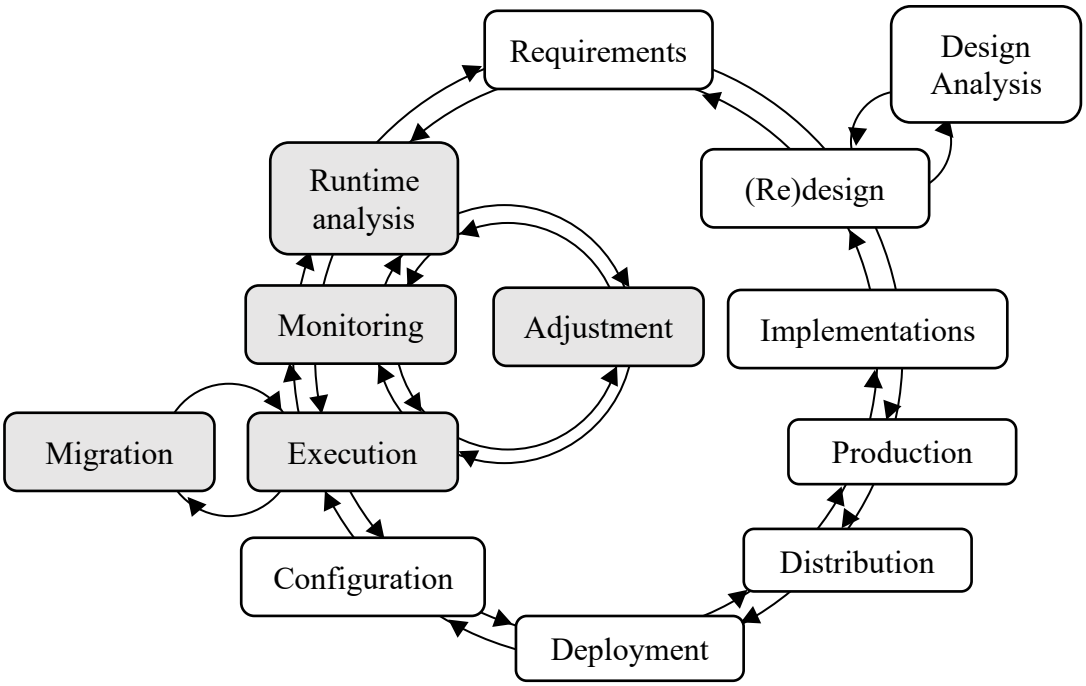

Figure 21 - The life cycle model of an enterprise information system. Each rectangle illustrates a phase in the life cycle and the arcs represent the order of the phases. The main cycle models the development process of a new information system. The shaded phases represent the development process of an existing information system. Adapted with permission from (223).

customers are considered patients (or clinical study participants). It then follows that the product and services being delivered are eye care via a clinical workflow rather than business processes. As with the original framework, the inputs to the clinical workflow are participants, information and technology. Whilst the exact nature of the participants, information and technology present in eye care are distinct from that of a typical business scenario, the differences are no greater than those found between, say, the construction industry and the IT industry.

Understanding the clinical workflow that a healthcare provider uses to deliver eye care is therefore crucial as it provides an insight into which staff, as a key participant type, and technology are required to deliver eye care to the patient and an understanding of which data are required to be transmitted processed and stored. A number of methods and tools exist to aid in the definition, automation and monitoring of business processes.

Workflow management systems (WfMSs), such as YAWL (Yet Another Workflow Language; YAWL Foundation, www.yawlfoundation.org), are information systems that seek to automate business processes, in whole or in part, by defining, managing and executing the process in software (222). The ultimate goal of doing so is to make sure the correct activities are undertaken by the correct people at the correct time (223).

Process mining is a collection of techniques that analyse the event logs that are typically generated by an enterprise information system. The aim of such analysis is the discovery of models of the business process behind the events generating the logs. The results of this analysis can be used to assess the system's adherence to the business process' design specification. Additionally, the generated business process model can be used for performance analysis and simulations testing hypothetical scenarios. ProM (Process Mining Group, Eindhoven University of Technology, Eindhoven, Netherlands) is an open-source project providing process mining capabilities (224).

To explore how such techniques can be used in the design of mHealth devices, it is useful to understand how they are used within the lifecycle of enterprise information systems. The life cycle model of an enterprise system, as defined by van der Aalst and Stahl is shown in Figure 21 (221).

The requirements, design and design analysis phases are the first three stages of development. These are therefore of specific interest in understanding how mHealth designs might be improved prior to implementation in a clinical setting, whether a large-scale roll-out or a pilot study with limited scope. Modelling plays an important part in each of these development stages. The aim of model use in this context is to describe the enterprise information system or the business processes supported by it in a way that abstracts away all aspects that are considered irrelevant to the design. Models can act either as an abstract description of an existing system or as a specification of a system yet to be developed.

In the requirements phase a coherent design specification is created by gathering the various requirements for the system. These requirements include those relating to the functionality of the system as well as non-functional requirements such as costs, maintenance and reliability.

It is often the case that there is already an existing enterprise information system that is not fully fit for purpose and that does not satisfy all of the requirements. In this case analysing the existing system can provide valuable inputs into the appropriate design for the new system by informing on which aspects of the old design function well and ought to be preserved in the new system. This is also of relevance when considering health systems, as digital systems within healthcare are most frequently designed to replace or enhance existing systems, even when these do not contain any electronic component. Analysis of existing clinical workflows therefore represents a useful first step and can provide the first set of model inputs.

Having begun by simply expressing the requirements in ordinary language, the requirements phase refines these and expresses them in specification languages and models cumulating in a domain model which is an object model that captures all of the concepts of the domain in question in terms of data and behaviour (225). However, even the most thoroughly executed requirements phase can result in an incomplete and ambiguously defined set of requirements. The construction of a model and experimentation with a prototype can help with the discovery of ambiguities and hidden requirements. In the context of enterprise information systems, such a prototype consists of an executable functional design model that is derived from the domain model. This provides both a formal description of the

information system and a prototype for simulation-based experimentation. These prototypes will not usually implement the entire functionality of the design. For example, user experience considerations will often not be included in this stage of development (226).

During the design analysis phase, validation of the design's conformance to the specifications is sought. As mathematical proof of such is rarely feasible given the complex nature of enterprise information systems, simulation is used to provide evidence regarding the design's conformance with the specifications. In order to do so, the models created in the previous development phases must be converted into executable models so that certain experiments (also known as runs or scenarios) may be run. It is important to note that only a finite number of experiments can be run. Therefore, due to computational limitations, it is not possible to analyse every possible value of the system's state, which is the vector containing all variables describing the system, in all but the most trivial of designs. As well as verifying the design, simulation also allows performance analysis to be conducted. This allows key performance metrics such as response times and flow times to be measured and for potential bottlenecks within the system to be identified. The process is conceptually similar to that which is used in mechanical, electronic and optical engineering, where a prototype is designed using a computer-aided drawing (CAD) software package and key performance metrics analysed using simulation software (227, 228).

Once the design has been finalised after a number of iterations resulting from design analysis, the information system goes through the implementation, production, distribution, deployment and configuration stages as is necessary. Upon completion of these, the system is then ready to be executed. During the execution phase, event logs are captured allowing information to be gathered regarding the activities that have been executed. These event logs can then be monitored by comparing real-time information extracted from the logs with the requirements and function design models. Further insights into the running system and its associated business processes can be extracted by more in-depth runtime analysis using techniques such as data and process mining.

It is important here to note a limitation of mHealth hardware compared to enterprise information systems. This is that hardware cannot be redeployed with design changes without manufacturing an entirely new device. It is therefore common for a number of prototypes to be produced prior to at-scale manufacture. These can typically be used to test certain key characteristics of the product without the costs associated with the tooling and materials required for mass-manufacture (229).

A further level of complexity is added to mHealth device design and design analysis, compared to products in other sectors, by the fact that it has the potential to impact upon patient outcomes. Scientifically robust, comparative randomised clinical trials are therefore required in order to establish the safety and clinical efficacy of the intervention and compare these to existing interventions (230). However, the time and resources required to conduct such trials are immense meaning that there is a strong incentive to ensure that the correct cohort sizes, eligibility criteria, trial centres, timelines and study protocols are established at the outset. For this reason, pilot studies are often conducted first to gain insight into the optimal trial design.

A pilot study is defined as a "small-scale investigation designed to test the feasibility of methods and procedures for later use on a large scale, or to search for possible effects and associations that may be worth following up in a subsequent larger study" (231). However, due to a misunderstanding of the primary purpose of pilot studies, their reporting often has a misplaced emphasis on statistical significance rather than its main focus, feasibility (232).

It should also be noted that pilot studies are distinct from proof-of-concept studies. These seek to determine whether an intervention is likely to work or not, usually in healthy participants by using surrogate markers as endpoints. Pilot studies, in contrast, are required to be conducted in a small sample taken from the intended patient population (232).

It is therefore important that, after conducting proof-of-concept analyses as necessary, pilot studies of mHealth pre-production prototypes be conducted by introducing these to workflows similar to those where they are perceived to have the greatest potential for impact. Process modelling and simulation based on these preliminary data then offers a means by which parameters relating to both the device's design and implementation can be optimised prior to construction of final designed-for-manufacture prototypes for use in Phase III clinical trials.

Finally, once mHealth hardware is deployed within the clinical workflow, whether as part of a trial or not, settings can still be adjusted, software updated and procedures changed. Process modelling therefore not only allows us to determine the impact on the effectiveness of medical hardware, but also what feasible action can be taken to continue to maximise effectiveness during clinical trialling (via use of adaptive trial designs (233)) and subsequent full health system implementation.

Thus, modelling the workflow of the system and its associated business processes not only helps with the specification and design of the system, but also allows the continued assessment of its fitness and improvement of its performance once implemented at scale. Such improved analysis of the performance of mHealth applications could provide a more accurate understanding as to why certain applications are not suitable for scale.

4.3.2 System Modelling

Dynamic systems, such as enterprise information systems, have a state that is subject to change. The state changes in such systems can be either continuous or discrete. It is a matter of conceptualisation as to whether a system is considered to have continuous or discrete state changes. In the modelling of most information systems it is most common for discrete state changes to modelled, with state changes occurring instantaneously (221).

It is assumed in this thesis that the core assumptions that apply to most information systems also apply to that of an eye care clinical workflow. This includes the assumption that clinical workflows participants, information, technology and patients can all combine to form a single state vector that changes only at a discrete set of points in time. It is intuitive that this ought to be with the case with patients arriving for appointments, technology being available for use and patients being provided with information at discrete moments in time, for example. Secondly, it is assumed that anything that can affect the state vector can be defined as an event which can be placed within an event list that is advanced by the simulation clock (234). Again, it is intuitively assumed that this applies in the case of the clinical workflow where, for example, a patient arriving at a clinic, an eye examination and staff clocking-off can all be described as events occurring in a defined sequence and at defined values of the system clock. It should be noted however that care is needed in conceptualising certain variables as discrete states that are acted upon by discrete events. For example, it could be argued that certain disease processes, such as open angle glaucoma, would be better conceptualised as continuous events, being a condition that progresses over time opposed to happening at an exact moment in time. It is therefore important to take care when modelling such variables in a discrete event system. In reality there is unlikely to be any significant difference between the condition progressing past a certain clinical threshold at 13:03:31 or 13:04:00 on the same day. However, whether this occurs in March or October of the same year might result in a significant difference. The implications of reducing a continuous variable to a discrete variable must therefore be thoroughly considered when designing a discrete event system.

Whilst intuitively appropriate, quantitative investigation of the above assumptions was not attempted as part of this PhD programme. As this is a limitation of this work, future research should seek to justify the assumptions more rigorously.

Given the aforementioned assumptions, we can define the state space as the set of possible states, with these states describing relevant information within the system which is subject to change (235).

A change from one state to another is called a state transition, or commonly just a transition (235). Transitions can be represented as an ordered pair, (x, y), where x

and y are states within the state space, that is x, y $\in$ S, where S is the state space. The transition relation, TR, is a set of all transitions possible within the system (221). It does not necessarily contain a transition for every pair of states as not all of these will be possible in a given system. Thus, TR $\subseteq$ S x S. States that are possible, through one or more transitions, given an initial state are referred to as reachable states. A state from which no further transitions are possible is called a terminal state (221).

A transition system can therefore be described by stating the state space, transition relation and initial state, (S, TR, S_0). A graphical representation, called a state-transition diagram, can also be produced by using notation such as the Unified Modelling Language (UML) (236). However, it is not feasible to produce a state-transition diagram for transition systems that have a large number of possible states without compromising the coverage of the state space. This is due to these models suffering from the state explosion problem, that is a situation where even a relatively simple system results in a state space of a size which a computer cannot feasibly verify (237). For example, nine parallel transition systems each consisting of ten states results in a state space containing 10^9 states, which is at the limit of feasibility with today's computing resources.

Markov models extend transition systems with probabilities and time (238). These also suffer from the state explosion problem and thus higher-level modelling and simulation techniques must be used to evaluate the level of complexity involved in information system modelling (239).

In addition, as the state space is of a size whereby capturing it within a mathematical set expression is implausible, it is instead captured within a data model. Examples of data modelling techniques include UML class diagrams, entity-relationship models and crow's foot diagrams (236, 240).

However, data models do not model behaviour. Thus, a process model is also required in order to model the transition relation. Process modelling techniques include Petri nets, UML activity diagrams, Business Process Model and Notation (BPMN) and Event-driven Process Chains (EPCs) (236, 241-243).

Process models are used for two main functions. Firstly, in the design phase, they force system designers and analysts to make explicit rules for business processes.

This exposes poor or inconsistent design decisions as well as allowing new design ideas to be formed. Secondly, they provide a starting point for business process analysis, including validation, verification and performance analysis.

Business process modelling tools use a graphical notation, opposed to an algebraic notation, to support the life cycle model. The reason for doing so is to make complex models easier to understand both for the designer and for those whom can give insight into the model's fitness for purpose, such as end-users. There is no standardised notation for business process modelling with there being many industrial business process languages in existence each with their own notation. In addition to the differing graphical notation and modelling constructs, most modelling techniques also initially lacked formal semantics. As simulation requires that such process models be converted into executable code, such formal semantics were added retrospectively to allow errors and ambiguities to be detected.

Software packages including business process modelling tools include ARIS Business Architect (Software AG, Darmstadt, Germany), BPM|one (Hyland, Westlake, OH, USA) and WebSphere Suite (IBM, North Castle, NY, USA).

Once a business process has been designed, it is then necessary to verify the model by examining properties of the model such as termination and hold states through exploring the reachable states. Many commercial languages do not support this and need to be transformed into Petri nets using software such as Woflan (swMATH, Berlin, Germany), LoLA (Humboldt University of Berlin, Berlin, Germany) and ProM.

Stochastic data concerning routing and timing is extracted from historical data and used to build the current state in a simulation model. Such a simulation can be useful for a variety of purposes. Firstly, it can be used to detect potential issues that may arise in the near future. Secondly, it can be used to discover business process through process mining (224).

The data model and process model are then combined to form a full system model.

4.4 Timed Coloured Petri Nets

Petri nets were devised by Carl Adam Petri in 1962 as a theoretical and conceptual means of describing information transmission and formation (244). Petri nets have a number of attributes that distinguish them from other system modelling techniques. Firstly, causal dependencies and independencies in a set of events can be represented explicitly. As a result, events that are independent of each other may occur concurrently, rather than sequentially. Secondly, Petri nets may be used to model a system at different levels of abstraction. For example, the transmission of individual operations within a microchip may be modelled as may high-level functions of entire business units (245, 246). Finally, given their formal semantics, it is possible to verify system properties that are modelled using Petri nets.

Coloured Petri Nets (CPNs) is a discrete-event modelling language that combines Petri nets with the functional programming language CPN ML, based on Standard ML of New Jersey (247, 248). It introduces two key concepts to standard Petri nets, data (referred to as colour) and time. CPN Tools (Eindhoven University of Technology, Eindhoven, The Netherlands) is a software suite that allows the editing, simulation, state space analysis and performance analysis of CPN models (249).

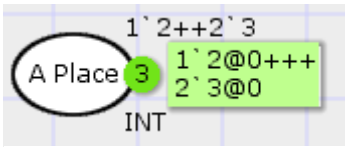

Figure 22 - A graphical representation of a place in CPN tools. The place shown contains tokens belonging to the timed integer colour set.

A CPN contains zero or more places. Each place has a unique identifier called a place label and may contain 'tokens' belonging to a single specified colour set. In CPN Tools, the colour set can either be assigned to one of a number of standard colour sets, such as integer, Boolean, character string or floating-point decimal, or to a user-defined colour set. Such user-defined colour sets can be lists or records of a defined structure, subsets of other colour sets or redefinitions of existing colour sets (such as a redefinition of the Boolean colour set having {yes|no} in place of {true|false}). Each place can be assigned an initial marking specifying the value and timestamp of one or more tokens that the place contains before a simulation is run. In CPN Tools, a place is represented by an oval and tokens by green circles with a number denoting how many tokens are inside a given place, as is shown in Figure 22. The value of each of a place's tokens is shown in a green square next to the place

with the timestamp shown on the right of an '@' symbol next to each token's data description. The initial marking is to the upper right of the place.

A Petri net also contains zero or more transitions. Transitions are connected to places via arcs. Arcs are unidirectional, either pointing from a place into a transition or from a transition into a place. When a transition 'fires' it consumes a token from each place connected by an arc pointing towards the transition. Likewise, it also produces a token in each place to which an arc points to from the transition. There is no limit on the number of arcs that can connect any transition and place. If there are insufficient tokens available for consumption by the transition then the transition cannot fire. The transition can also be ascribed a guard which provides a logical operation according to which the transition is allowed to fire, providing sufficient tokens are available for consumption. Which tokens the variables within the guard's logic refer to are determined by inscribing these variables on the transition's incoming arcs. Similarly, the value of the tokens generated by the transition can be set in the outgoing inscriptions. This can be set to a variable or combination of variables present on the incoming arcs, a constant or the result returned by a function. Finally, each transition may contain a time delay by which the timestamp of each generated token is incremented. Each generated token is then given a timestamp that equals the sum of the delay and the largest timestamp assigned to the consumed tokens. Where multiple transitions within a net can fire, the one whose token with the latest timestamp is earliest fires first. If multiple transitions' token with the latest timestamp have the same timestamp one of the transitions is selected at random. Transitions can also be assigned a priority, causing the higher priority transition to fire in the event where two or more transitions could otherwise fire. In CPN Tools, transitions are represented by rectangles and arcs by unidirectional arrows, as is

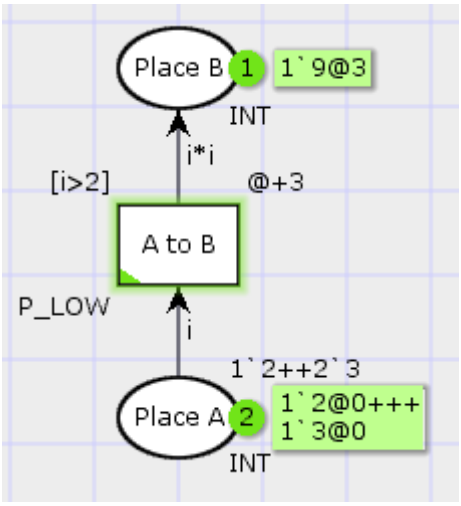

Figure 23 - A graphical representation of a transition connecting two places in CPN Tools. This example generates a token in Place B with a value that is the square of a token consumed from Place A if that token has a value greater than 2. The green outline signifies that the transition may fire in the next simulation step.

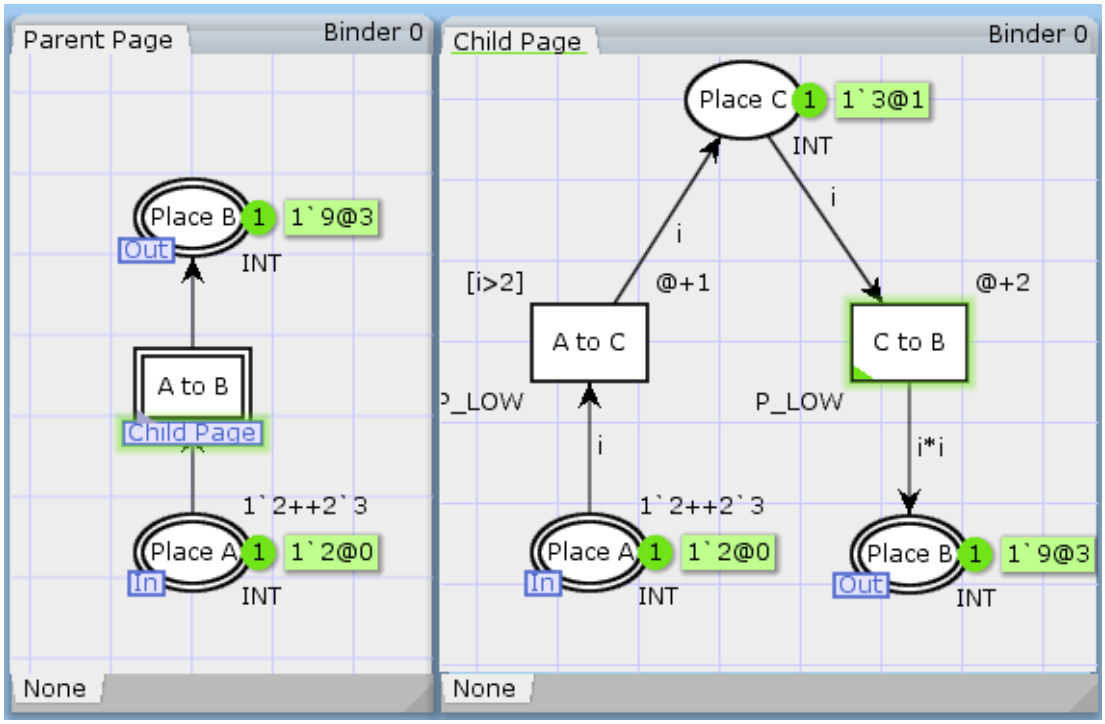

Figure 24 - A graphical representation of a hierarchical CPN, with two pages linked by a substitution transition, in CPN Tools.

shown in Figure 23. The full structure of a Petri net is known if the place, transitions and the ways in which they are connected to each other is known.

CPNs may also be hierarchical where an individual net is spread over a number of 'pages'. A page is connected to its sub-pages by 'substitution transitions'. These transitions essentially abstract the graphical representation of the sub-net contained in the sub-page into a single transition on the higher-order page. However, instead of immediately generating tokens at its output places, when a substitution transition fires the consumed tokens will cause a transition within the sub-page to fire. This transition has input places within the subpage that are demarked as input (or input and output) ports. These are linked to the input ports of the substitution transition on the high-order page and are essentially a replication of these within the subpage. Tokens only appear at the substitution transition's output places when tokens are generated at places within the sub-page that are demarked as output ports (or input and output ports). The process as represented in CPN Tools is shown in Figure 24. The application of CPNs to the clinical workflow is well-established (250-252). In this thesis, the aforementioned attributes of CPNs will be used in a similar manner to model the interactions between healthcare staff, mHealth technology and patients in an attempt to understand how mHealth can be better designed and implemented to deliver eye care in LMICs.

4.5 Conclusion

Modelling the impact of mHealth technologies on the entire clinical workflow via workflow modelling offers to provide evidence as to their effectiveness prior to design completion. Using such models to simulate the interaction between mHealth applications could also help to design and plan for better interoperability. Finally, testing the applicability of mHealth technologies to different settings by building workflow models that are generalizable, allowing them to be applied to different health systems, policy objectives, end-users, populations and communities will help to optimise designs capable of being deployed within sustainable business models.

SECTION 2

Chapter 5 - Design of a Smartphone Ophthalmoscope

5 Design of a Smartphone Ophthalmoscope

5.1 Introduction

This second section of this thesis now addresses Aims 1 and 2 of thesis as defined in Chapter 1. Namely, it concerns the designing of a novel mHealth eye-screening device, the modelling of a LMIC community-based eye clinic's workflow and the use of this model to demonstrate the interaction between the mHealth device and the clinic's workflow.

Before workflow modelling can be employed to demonstrate the interaction of an mHealth design with the clinical workflow of a LMIC community eye clinic, it is first necessary to choose a design problem. Having chosen a design problem, an mHealth design can be devised and prototypes produced in order to acquire the data necessary for delivering the workflow model via a clinical pilot study.

As was noted in Chapter 2, visualising the ocular fundus is an important step in identifying those suffering from several of the major causes of preventable blindness (253, 254). Conditions that can be identified include optic nerve abnormalities caused by glaucoma, microaneurysms stemming from DM, macular holes, retinal tears and even elevated blood pressure (143, 253, 255-259). As such, screening the ocular fundus for retinal disease is an important step that ought to be undertaken after identifying a person with low visual acuity or with other risk factors such as age and family medical history. Furthermore, it is recommended that certain high-risk groups, such as diabetes mellitus (DM) sufferers, be enrolled in regular retinal screening programmes (145).

Hence, it is highly desirable that the community eye health worker's kit includes an ophthalmoscope. However, standard, commercially available ophthalmoscopes are not entirely suitable for this purpose due to the proficiency that can be expected of community eye health workers (CEHWs). Indeed, medical doctors often lack proficiency in even the use of a direct ophthalmoscope, which is the easiest form standard ophthalmoscopy to perform (208, 260). As was highlighted in Chapter 3, no satisfactory solution exists that allows a CEHW to capture images of the ocular fundus and send these to a specialist grader for analysis. For this reason, a smartphone ophthalmoscope was designed for use in a portable eye examination kit for community health workers, by Giardini and colleagues, prior to the PhD

Figure 1

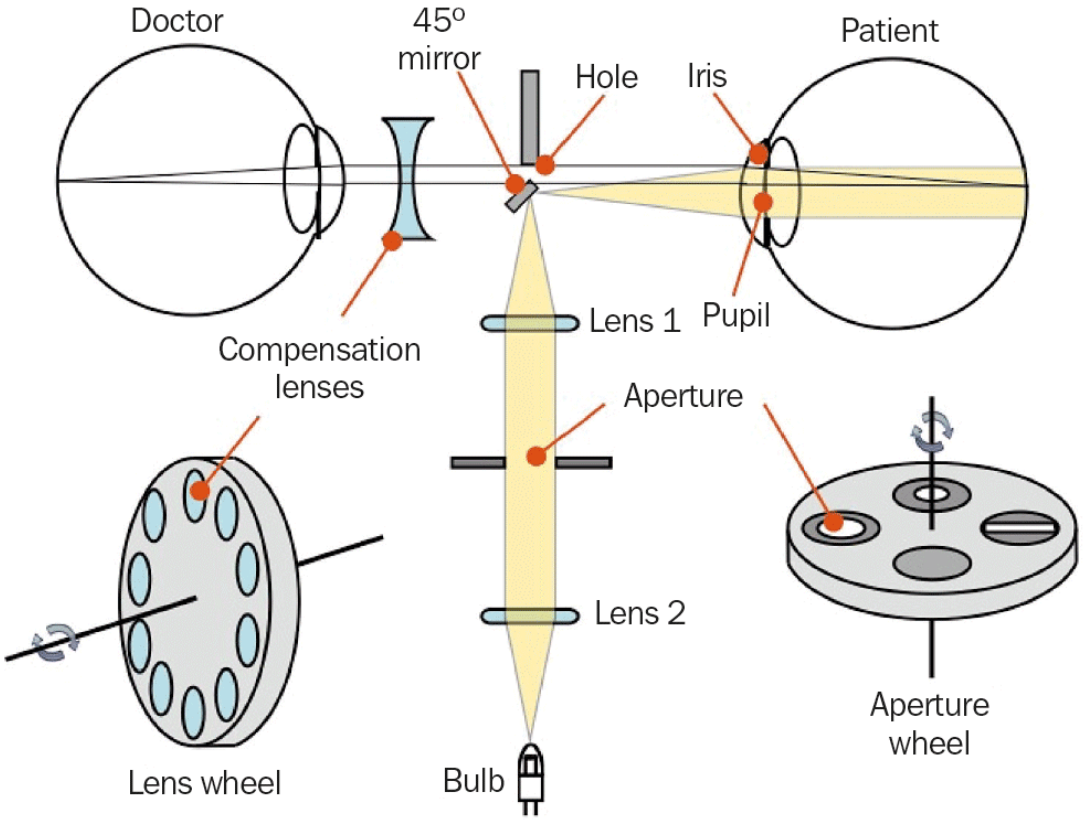

Figure 25 - The design of the classical direct ophthalmoscope. A light source is focussed onto a mirror close to the optical axis of the patient's eye and thus illuminates a spot in the centre of the ocular fundus. The observer then looks through a hole in the mirror allowing them to visualise the retina by inserting one of a set of compensation lenses that combines with optical systems of both patient and operator eye to form an image of the patient's ocular fundus on the observer's retina. Image reproduced from (263) under Creative Commons Attribution-NonCommercial 4.0 International License[15].

[15] License available from: https://creativecommons.org/licenses/by-nc/4.0/

programme described in this thesis (261). This device is described in detail in section 5.2.

However, as was highlighted in Chapter 2, designing a retinal imaging solution which is low-cost and easy-to-use is not enough to overcome the barriers to implementing such an mHealth solution at scale in LMICs. It is also key to understand the impact on the health system posed by introducing such a device. The prototypes described in this chapter therefore aim to be a means to stimulate the field and provide the preliminary data required to build workflow models that can begin to create an understanding of the potential impact on the clinical workflow. The results of simulations based on these models will then provide a quantitative model of the impact on the workflow of the design and implementation of smartphone-based retinal imaging solutions, so that they can be optimised for impact at scale.

5.2 Background

5.2.1 The direct ophthalmoscope

The direct ophthalmoscope is a handheld instrument that provides a non-stereoscopic, narrow field (approximately 5° subtended angle on the retina) of the ocular fundus (263).

Direct ophthalmoscopy requires a light source to be brought into co-axial alignment with the optical axis of the observer's eye, in the case of a classical ophthalmoscope, the design of which is shown in Figure 25, or the imaging optics in the case of a digital ophthalmoscope. This is typically achieved by focusing a collimated light source onto a mirror at a 45° tilt, thus projecting the light source towards the eye, through the pupil and illuminating the retina. The mirror has a small hole through which the user can visualise the retina owing to the close alignment between the illumination and imaging axes, meaning that no shadow is cast by the iris onto the retina from the user's perspective (263). The largest field-of-view, approximately 5° subtended angle, is achieved by getting as close as possible to the eye of the patient, as the iris acts as the aperture stop for the full optical system between the retina and the observer's eye (263).

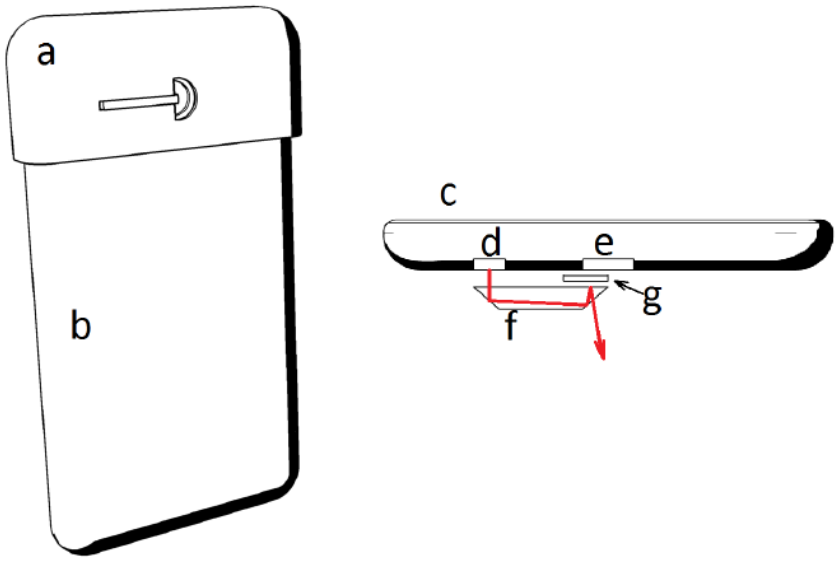

Figure 26 - The design of the original smartphone ophthalmoscope designed by Giardini and colleagues. Reprinted, with permission, from (261) © 2014 IEEE.

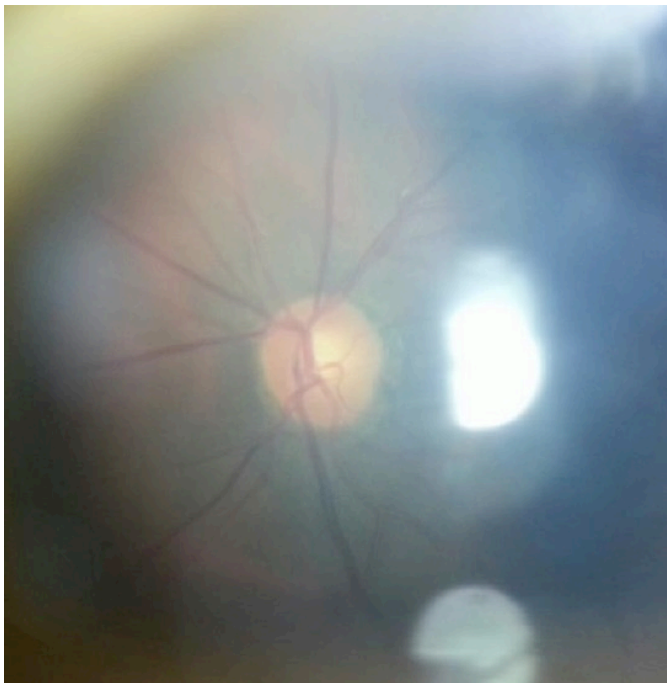

Figure 27 - An image acquired with the original smartphone ophthalmoscope designed by Giardini and colleagues. Reprinted, with permission, from (262) © 2014 IEEE.

Use of an ophthalmoscope for fundoscopy in a primary healthcare setting is useful for the diagnosis of a host of eye and non-eye related pathologies. However, those primary healthcare physicians who are entirely comfortable performing a patient examination using an ophthalmoscope are in the minority. For example, it has been reported that in Canada only 52.3% of resident family care doctors feel competent in performing fundoscopy, even though over 95% felt it was an important skill to have (208). Thus, owing to the difficulty of its use and interpreting any images attained, it is not a suitable tool for a community eye health worker with minimal clinical expertise.

5.2.2 Prior design of a smartphone ophthalmoscope

Giardini and colleagues' smartphone ophthalmoscope sought to overcome the difficulties presented in using a classical direct ophthalmoscope without losing the benefits of its low-cost and portability.

The key component of this smartphone ophthalmoscope, the design of which is shown in Figure 26, consisted of an adapter (a) that is secured onto the top of a smartphone (b). The adapter contains a hand-filed dove-prism (f) that diverts light from the phone's integrated LED flash (d) into near co-axial alignment with the phone's camera optics (e). The phone's display (c) can then be used to control any general photography camera app to take pictures of the ocular fundus. Dove prisms act as retroreflectors when a light source is incident on the longest face, thus the light from the LED flash was diverted onto a metallic reflective shield (g) which both achieved near co-axial alignment with the camera optics and prevented unwanted light scattered from the prism's edges from entering the camera lens. Thus, as shown in Figure 27, the illuminated part of the ocular fundus can be visualised by the camera for pupil sizes approximately greater than 4mm, a diameter that can typically be achieved under dilation by even those whose pupils dilate poorly (elderly DM sufferers for example) (264). As the pupil constricts when exposed to higher light levels, adequate dilation needs to be achieved pharmacologically, by instilling a 1% Tropicamide solution for example (265). The smartphone camera's autofocusing software removes the need for manual focussing

required when using a standard direct ophthalmoscope, greatly improving the ease of use.

However, as can be seen in Figure 27, a strong reflection from the cornea interferes with both the autofocus and auto-exposure. This can result in an image that is dark and focused on the cornea, making features on the fundus difficult to identify. The development of an improved design that is viable for use by eye health workers in the community was therefore required. The rest of this chapter describes the work undertaken as part of the PhD programme in order to achieve such a design.

5.3 Requirements

In order to realise the aim of producing a retinal imaging solution suitable for use by CEHWs in LMICs, a number of device requirements can immediately be specified from existing knowledge of fundoscopy. These requirements relate to the prototype's functionality, materials, operating environment, maintenance, conformance with relevant safety standards, aesthetics and ergonomics. Further requirements, relating to integration with the clinical workflow, also need to be fulfilled. Such requirements are defined in the next chapter based on workflow analysis seeded by data acquired using prototypes of the initial designs described in this chapter.

5.3.1 Functional Requirements

The device must be capable of imaging the retina through a dilated pupil. For a normal adult eye, a dilated pupil is typically 8mm in diameter (266). However, for those suffering from certain conditions, such as DM, pupil dilation can be restricted (264). Given the global prevalence of DR and the importance of retinal imaging in screening and monitoring this condition, it is important that the device is able to image eyes whose irises dilate as poorly as to have a maximum diameter of only 4mm.

The device must illuminate the retina so that the chosen camera system can image the retina with sufficient clarity, in terms of brightness, resolution and colour contrast. Image clarity is defined to be sufficient when a competent user can identify

any clinically relevant feature of the ocular fundus that would ordinarily be visible via classical fundoscopy. The smallest such features include retinal microaneurysms, which typically have a diameter of 15 to 85µm and small blood vessels, such as arteriole and venule with these having, when measure at the main retinal arcades near the optic nerve, a diameter of 160µm and 240µm respectively (267, 268).

Unwanted reflections, such as those from the cornea or the device itself, cannot be allowed to cause interference with the camera system's autofocus and white balance or have the potential to obscure clinically pertinent details.

The field-of-view must be such that it allows the entire posterior pole, that is the area between the superior and inferior temporal arcades and that most critical with respect to sight-threatening disease, to be visualised (253).

Finally, the adapter must not inhibit the operation of the smartphone on which it is hosted, allow its camera software to be operated as normal and not alter the appearance of the phone so that it appears as an unfamiliar device to both the operator and patient. It is hypothesised that perceived familiarity with the device ought to increase patient compliance with the test.

5.3.2 Material Requirements

The external casing of the device is required to be compatible with short-term contact with the skin and eyes of a patient. Furthermore, it is required that the device can be easily cleaned with a common disinfectant. Therefore, it should be chemically stable when exposed to disinfectant and not trap dirt or otherwise pose some other infection risk in a clinical setting.

5.3.3 Operating Environment

As the device is to be used in the community, it is important that it can be operated in environments where only basic attempts to darken the environment can be made, such as turning off room lighting, drawing curtains and stepping away from windows. As such, it should be able to visualise the retina in ambient lighting of up to 100 lux (269). In addition, it must be able to operate in temperatures ranging from 10 to 40°C in relative humidity <60% and withstand temperatures between 0 and

50°C and the same relative humidity when in storage.

5.3.4 Maintenance

Given that the device is intended for field use by a non-specialist it is important that it is easy for such a user to maintain and clean the device without the potential for them to cause damage to it in the process.

5.3.5 Safety Standards

The device must not pose any phototoxic risk when used as intended. Care must therefore be taken in limiting the light incident on the eye to safe limits with respect to its intensity and wavelength. An international standard, ISO 15004-2:2007, relating specifically to light hazard protection in ophthalmic instruments exists (270). It is therefore important that the device complies with this standard.

5.3.6 Ergonomics and Aesthetics

Attaching and detaching the device to its host smartphone must be an intuitive and simple process for the intended user. Once attached, the device must stay securely in-place without there being a risk of falling off. Furthermore, as even the slightest shift can cause misalignment of the camera and illumination source, the device must attach rigidly to the phone.

For maximal ease-of-use, the ergonomics of the device must be such that its operation is as close to using a smartphone camera for general photography as possible, thus making the retinal imaging task one that is intuitive and familiar to the non-specialist.

Further to this, the user must be able to both stabilise the phone and control the camera using two hands.

Finally, the mechanical design of the device must also be such that it does not pose a risk of injury to either the patient or the operator. Specifically, care must be taken so that the design minimises the risk of the device contacting a patient's cornea, even when used in very close proximity (at a 1mm working distance for example).

5.4 Design Iteration 1: First Samsung Galaxy S3-based Unit

5.4.1 Design

5.4.1.1 High-level design considerations

In order to create a design for a device that was, primarily, able to be effectively used with the lowest possible level of clinical skills and, secondly, had a low unit cost, it was elected to base the design on the principles of direct ophthalmoscopy, described in brief in Section 5.2.1.

Owing to the wide variety of smartphone camera and LED flash quality and positions, it was decided that an adapter for a specific handset be designed in order to demonstrate the concept of a smartphone ophthalmoscope of sufficient quality for ocular fundus screening. The Samsung Galaxy S3 (Samsung, Seoul, South Korea) was chosen as the host smartphone for the ophthalmoscope adapter given its reputation for having the highest quality smartphone camera at project inception in February 2013 (www.trustedreviews.com). Whilst the phone's end user cost was 500 GBP upon launch, it was considered more practical to demonstrate the concept and gather workflow data using a higher quality handset, and then make inferences about the lowest quality camera that is viable for the task as well as the hardware cost that offers best cost-effectiveness.

It was decided to use the smartphone's own LED flash as the light source for the adapter as this was deemed to be advantageous by removing the need for any additional electronic components.

5.4.1.2 Optical Design

5.4.1.2.1 Removal of corneal reflection

As was noted in Section 5.2.2, the strong reflection present in images captured using Giardini et al.'s design caused challenges with respect to focus and exposure. The reflection off the smooth surface of the cornea is specular whilst the reflection from the irregular surface of the ocular fundus is diffuse. The requirement to eliminate specular reflections without removing diffuse reflections is a common problem in imaging optics (271). A strategy frequently employed by designers is to use a linearly polarised light source. Light remains polarised under specular reflection

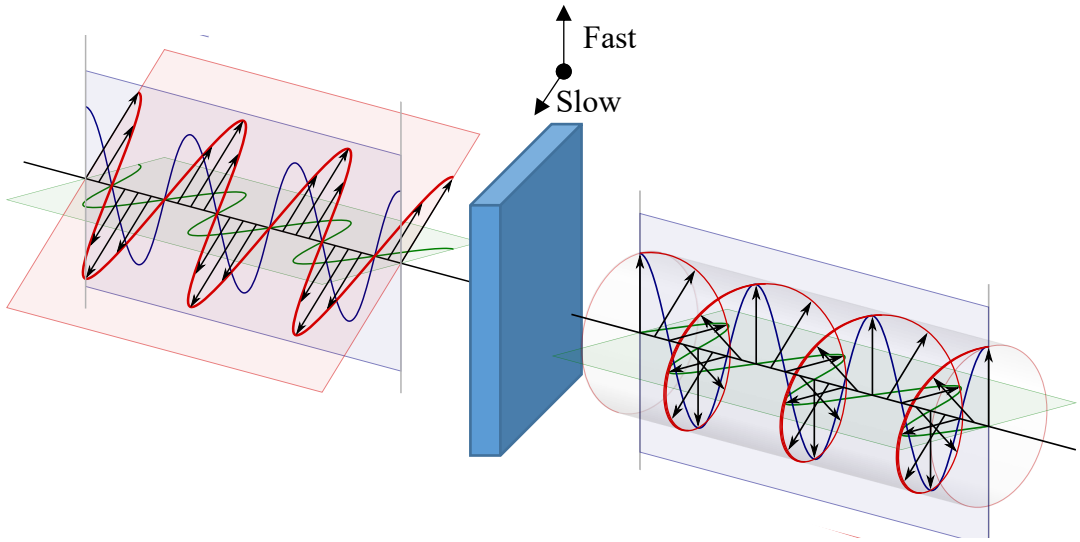

Figure 28 - The introduction of a π/2 phase shift between the two orthogonal components of 45° linearly polarised light (a) results in the two orthogonal components of polarisation adding as vectors to produce a rotating linear polarisation state (b) This is known as circularly polarised light. Image adapted from commons.wikimedia.org[16].

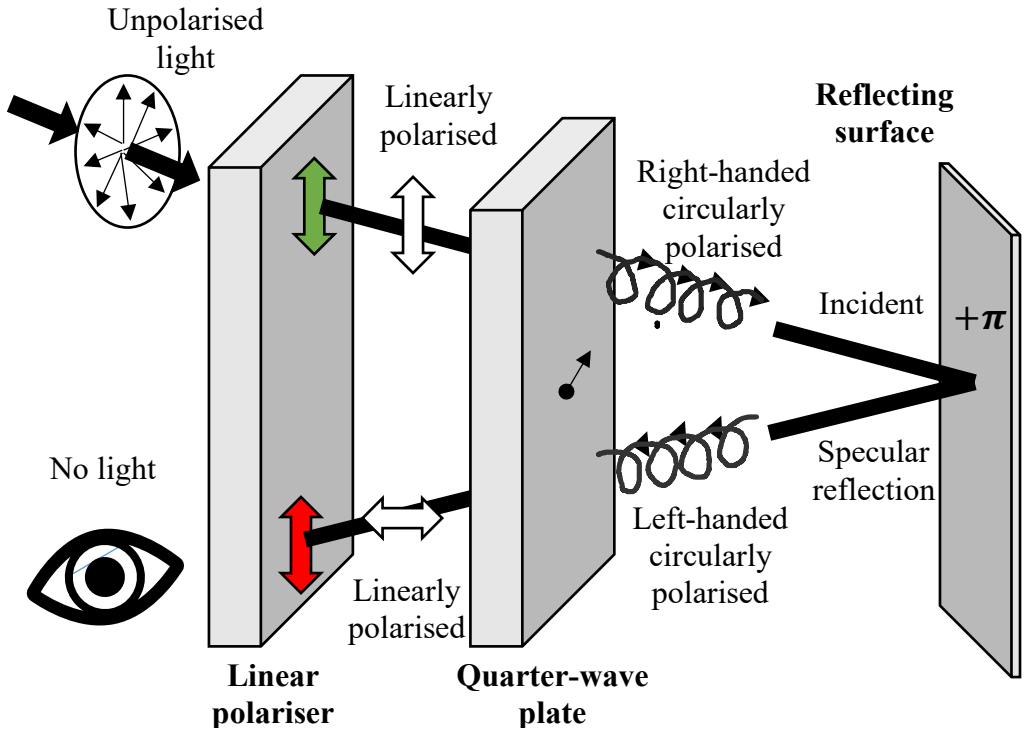

Figure 29 – A circular polariser, consisting of a linear polariser followed immediately by a quarter-wave plate (presented separated in this figure for clarity) does not allow transmitted light to be specularly reflected back through the polariser. The π radians phase shift experienced upon reflection the handedness of the light changes causing the linearly with a polarisation state which is at π/2 radians to that transmitted by the linear polariser. Hence the light is blocked.

[16] Released into the public domain by Dave3457. Full source URL: https://commons.wikimedia.org/wiki/File:Circular_Polarization_Linear_Polarized_Light_Entering_Quarter_Wave_Plate_Components.svg

whereas diffuse reflection results in complete depolarisation of the incident light (272). Hence, inserting a polarising filter in front of the imaging optics which is tuned to remove the polarisation angle of the light emitted by the light source, removes the specular reflection whilst allowing the diffuse reflection to pass. However, as the prototype was to be assembled by hand, it was believed that it may be too difficult to position polarising filters over the light source and camera optics so to be orientated at precisely 90° to one another. The use of circular polarising filters was identified as a solution to this problem. Circular polarising filters consist of a linear polarising filter attached to a quarter-wave plate with the angle of polarisation being at 45° to the fast and slow axes of the waveplate as shown in Figure 29 (273). The quarter-wave plate introduces a $\pi/2$ phase shift between the two orthogonal components of the polarised light emerging from the polarising filter (273). As a result of this relative phase difference the two polarisation states then add as vectors to produce a rotating linear polarisation state, as shown in Figure 28. Similarly, circularly polarised light incident on the quarter-wave plate will undergo a further $\pi/2$ phase shift converting it back to its linear polarisation state at 45° to the quarter-wave plates' fast and slow axes (273). However, as specular reflection off a higher refractive index medium causes a π phase shift, its handedness changes as shown in and thus will be at 90° to the original polarisation state if passed back through the same quarter-wave plate (273). Therefore, placing circular polarising filters of the same handedness in front of the light source and the camera optics ought to remove the corneal reflex from the image. As any misalignment between the orientation of the two waveplates' axes will simply result in a linear polarisation equal to 45° plus the difference in alignment, the configuration is not sensitive to the orientation of the circular polarising filters, so long as they are the same handedness and the polarisation axis of the linear polariser in each is at 45° to the axes of the quarter-wave plate to which it is attached.

5.4.1.2.2 Component choices

In order to create a light source in near-coaxial alignment with the smartphone's camera optics, as is required for direct ophthalmoscopy, the output of the LED flash needed to be directed laterally towards the camera lens and then, once close, redirected towards the participant's eye.

The adapter was also required to have a low profile in order to, firstly, allow the imaging optics to be positioned as close to the eye as possible and secondly to maintain an appearance and operation similar to that of a normal smartphone.

It was important that the polariser was the last component in the optical path before the participants eye to avoid any change in polarisation due to reflections off further optical components. Therefore, the polariser was required to be placed between the camera and the eye, contributing to the overall profile of the device. Hence, a thin circular polarising film was chosen as the polarising element. This offered the additional benefit of being suitable for being directly fixed to flat optical surfaces, reducing back-reflections by eliminating the air-polariser boundary. As the phase-shift caused by the quarter-wave plate is proportional to the optical path through the waveplate, it was necessary for the polarising film to be orientated so that the plane of the quarter-wave plate was in the plane perpendicular to the optic axis of the camera.

For the rest of the optical components required it was elected to use custom components as commercially available optical components of the required size could not be sourced. Furthermore, when the project was initiated in February 2014 only hand tools were available for the production of such custom optics.

Placing a right triangular prism in contact with the LED flash is one means by which the LED's output beam can be diverted so to be lateral to the optical axis. The square face in contact with the LED flash was chosen to have equal dimensions to the LED so to maximise the amount of light directed laterally. Another right triangular prism placed near the optical axis was chosen to direct the light beam towards the participants eye. Unlike the previous dove-prism design, this allowed the polarising film to be fixed directly to output face of the illumination optics whilst being within the plane perpendicular the camera's optic axis. In keeping with the design of a classical direct ophthalmoscope, the reflective face of this prism was at 45° to the normal. A rigid cylindrical light guide placed between the two prisms then channelled the light between the two prisms.

5.4.1.2.3 Optical modelling and simulation methods

The finer details of the optical design were determined using OpticStudio 14.2 (Zemax LLC, Kirkland, WA, USA) optical design software package. As the design comprises an illumination system, a non-sequential components model was created.

Detailed specifications for the Galaxy S3's flash could not be found within the publicly available literature. However, detailed specifications of the various LEDs produced by Samsung and marketed as suitable for use in smartphone camera flashes are publicly available. It was determined that the imbedded LED was like to be a 3432 1.4t (FH341B) reflector-integrated flash LED package (Samsung Group) or similar, given the closely aligning specifications (3.2mm by 3.5mm package and a typical luminous flux of 200 lm) (274). Hence the radiant power of the LED can be approximated to 293mW (i.e. the luminous flux divided by 683lm/W (275). The viewing angle of the LED is 124°.

As right triangular prisms with differing lateral dimensions are not standard components in OpticStudio, custom components were coded in order to match the lateral dimensions of the Galaxy S3's LED flash. The code for the variations of this component used in the model are shown in Appendix 5.1. The prisms were additionally surrounded by flat absorbing shapes to simulate an absorbent paint coating.

An aluminium coating (95% reflectivity) was chosen for the hypotenuse of each prism as this is the material typically used to coat the reflective surface of mirrored acrylic.

A silica cylinder was placed between the two prisms and within a 0.5mm thick absorbing pipe to simulate a cladded light guide.

The simulation of the adult eye developed by Tocci was used as a target for the illumination system with the retina comprising an absorbing detector surface on the anterior of the vitreous chamber (276). As visualisation peripheral retina much beyond the posterior pole is improbable via direct ophthalmoscopy the detection area was limited to a 30° angle subtended by the retina, that is the field-of-view typical for desktop retinal cameras.

Design #	Second Prism hypothenuse	Light guide diameter	Light guide length
M-6-3	6mm	3mm	6.4mm
M-6-2	6mm	2mm	6.4mm
M-6-1	6mm	1mm	6.4mm
M-3-2	3mm	2mm	8.4mm
M-3-1	3mm	1mm	8.4mm

Table 8 - The values for variable parameters in the five designs examined using non-sequential ray tracing.

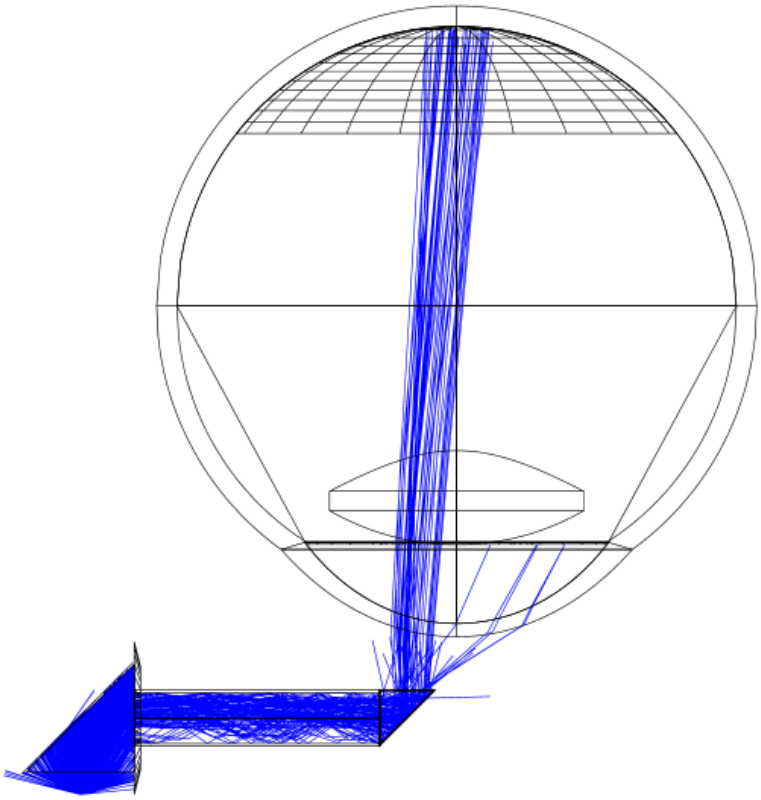

Figure 30 - Cross-section of the ray trace for design M-3-2 showing 1000 of the 100,000 rays in blue.

The working distance of the camera optic from the cornea when the phone was positioned as close as possible to the eye with the eye's and camera's optic axes in alignment was estimated to be approximately 7mm. Setting the eye simulation's pupil diameter to 8mm, that of a typical dilated adult eye, results in an entrance pupil of approximately 9mm diameter 3mm within the eye. Thus, according to simple trigonometry, any component entering a cone with an apex at the centre of the camera's aperture and of angle 48° will obscure part of the retina, as the camera has field-of-view well in excess of this.

The dimensions of the prism positioned closest to the camera, and consequently the length, diameter and positioning of the light pipe, were sought through simulation. As those samples of mirrored acrylic available had either 3mm or 6mm thickness, it was feasible to manufacture prisms with 3mm or 6mm hypothenuses respectively by hand. Additionally, the by-hand assembly of the components meant that positioning of the light guide on the prism surfaces was fairly course and as such fine adjustment of its positioning was not considered. Finally, the light guide diameter was restricted to those of commercially available components. A summary of the different variations of these parameters is shown in Table 8.

Four parameters were sought via ray tracing in order to determine the performance of the various illumination system configurations. The total luminous flux across the detector surface within a 30° subtended angle of the cornea informed on, overall, how well the area of the posterior pole likely to be visible via indirect ophthalmoscopy was illuminated by the system. The mean illuminance, as well standard deviation as of such, then provided a measure of the uniformity of this illumination. The difference in the mean luminous flux between the two vertically bisected hemispheres of the detector was also found to give an additional measure of illumination uniformity. Finally, the peak irradiance recorded on the detector was measured for comparison with regulatory standards (that is BS EN ISO 15004-2:2007 (270)) and to establish the safety of the illumination system with respect light hazard.

Design	Heatmap of retinal illuminance with 8mm pupil (lm/cm^2)	Heatmap of retinal illuminance with 8mm pupil (lm/cm^2)
M-6-3	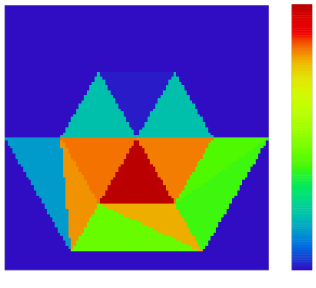	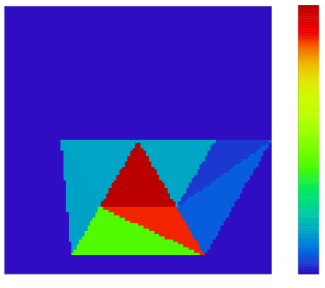
M-6-2	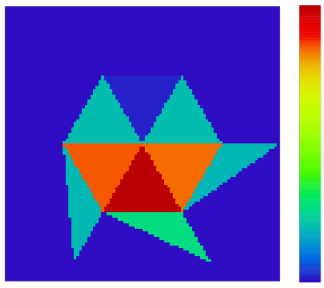	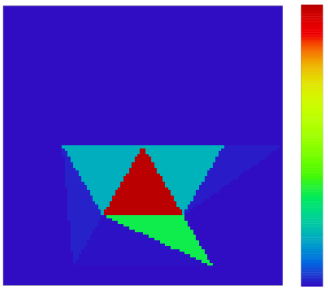
M-6-1	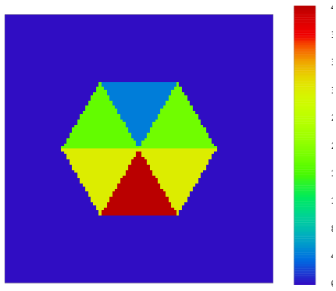	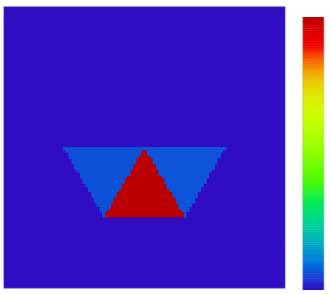
M-3-2	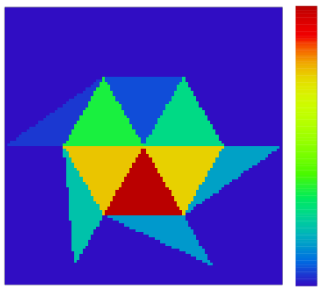	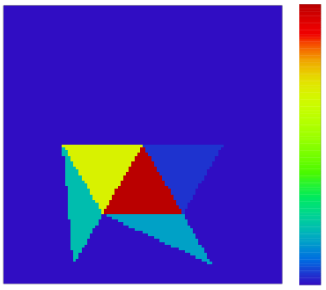
M-3-1	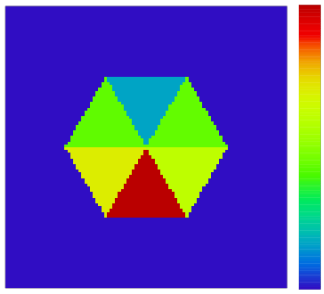	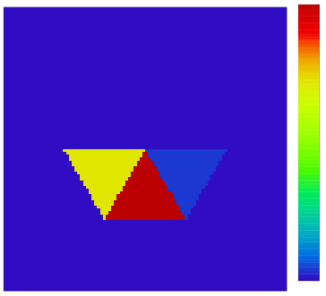

Table 9 – Heatmaps of the illuminance detected at the retina for the various designs after tracing 100,000 rays through an optical model of the design and a simulation of an adult eye.

100,000 rays were used in each simulation. Separate simulations were run for pupil diameters of 8mm and 4mm for each design, in order to account for the range of pupil diameters specified in Section 5.3.1.

5.4.1.2.4 Optical modelling and simulation results

The simulation results for each design are summarised in Table 10 and Table 11 (overleaf). Table 9 shows heatmaps of the luminous intensity calculated to be incident on the retina for each simulated design for 8 and 4mm pupil diameters.

The illumination provided by all five designs through an 8mm pupil was greater than 20 lm/m^2, below which the Samsung Galaxy S3 is known to acquire images of reduced texture and detail (www.dxomark.com/smartphones-beat-5-year-old-dscs/). Additionally, the peak irradiance was well below that which is likely to pose a thermal or photochemical hazard (0.7W/cm^2 and 220μW/cm^2 respectively). Designs M-6-3, M-6-2 and M-3-2 offered the strongest illumination of the posterior pole through an 8mm pupil (62.89, 66.72 and 66.05 lm/m^2 mean radiant flux respectively). However, the illumination was non-uniform, with one half of the posterior pole being poorly illuminated compared to the to the other, as is apparent from the designs' respective heatmaps shown in Table 9.

At a 4mm pupil diameter illumination was entirely constrained to the hemisphere opposite the illumination system. Design M-3-2 offered the highest mean radiant flux at 30.09 lm/m^2 across the posterior pole.

Optical design M-3-2 was therefore selected for prototyping.

Design #	Total luminous flux (lm)	Mean luminance ± SD (lm/m^2)	Difference in luminous flux between right and left retinal hemispheres (lm)	Peak irradiance (μW/cm^2)
M-6-3	4.239E-3	62.89±51.17	3.075E-3	17.8
M-6-2	4.497E-3	66.72±55.27	3.313E-3	19.4
M-6-1	1.715E-3	25.437±13.77	7.035E-4	6.5
M-3-2	4.452E-3	66.05±46.07	2.631E-3	18.8
M-3-1	1.678E-3	24.90 ± 12.96	6.408E-3	6.5

Table 10 – parameters describing the illumination of the retina of the Zemax adult eye model predicted by ray tracing optical models of the various designs when the eye's pupil was set to 8mm.

Design #	Total luminous flux (lm)	Mean luminance ± SD (lm/m^2)	Difference in luminous flux between right and left retinal hemispheres (lm)	Peak irradiance (W/m^2)
M-6-3	1.410E-3	20.92 ± 37.36	1.410E-3	14.0
M-6-2	1.564E-3	23.20 ± 40.29	1.563E-3	15.1
M-6-1	2.591E-3	3.84 ± 8.12	2.591E-3	3.0
M-3-2	2.028E-3	30.09 ± 46.88	2.028E-3	15.7
M-3-1	7.007E-3	10.40 ± 16.05	7.007E-4	5.3

Table 11 - parameters describing the illumination of the retina of the Zemax adult eye model predicted by ray tracing optical models of the various designs when the eye's pupil was set to 4mm.

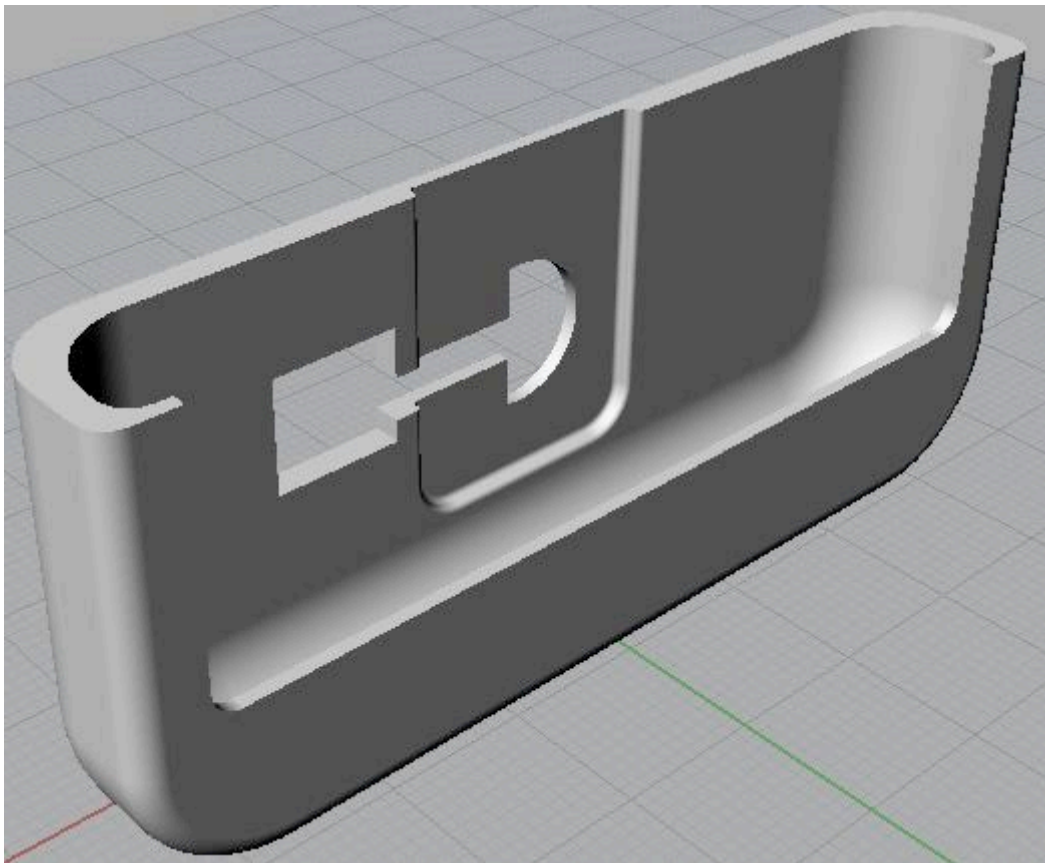

Figure 31 – CAD rendering of the 3D printed clip before any optical components are added.

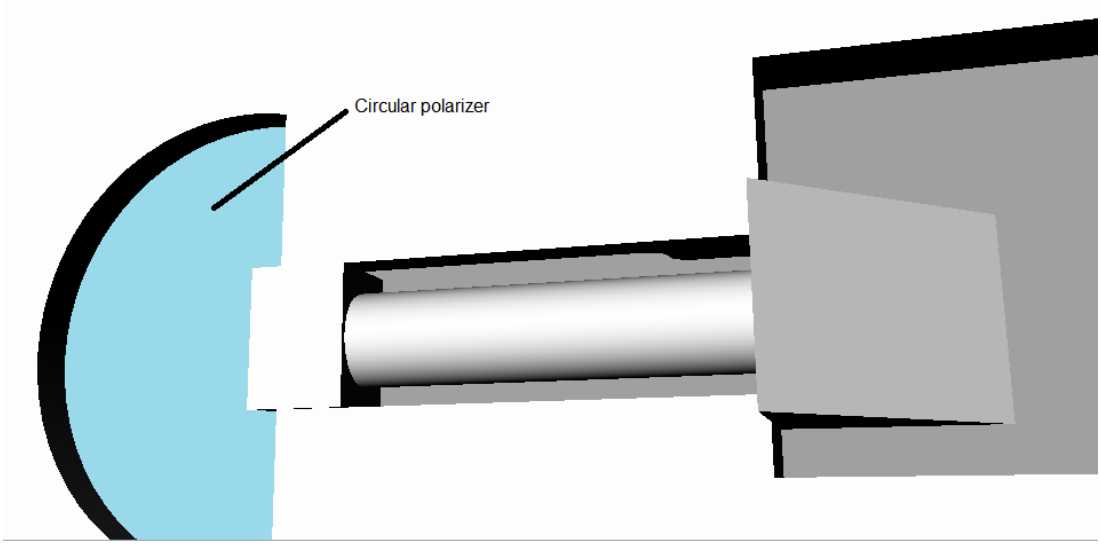

Figure 32 – CAD rendering of the adapter with optical components inserted but without the cap for shielding the LED flash being fixed.

5.4.1.3 Mechanical Design

Housing to contain the optical component and attach it in the correct position on the Samsung S3 was designed using the Rhinoceros 5 (Robert McNeel & Associates, Seattle, WA, USA) CAD software package. The design, shown in Figure 31, was such that it matched the phone's profile as close as possible. This aimed to allow for intuitive operation that is as close as possible to ordinary use of a smartphone for photography, as specified. The mechanical design aimed to be suitable for rapid prototyping using an UP2 3D printer(Tiertime, Beijing, China) as this was the only suitable 3D printer available to the author at the time. Thus the design's precision matched that of the UP2, namely a 0.4mm lateral print resolution with a 0.25mm layer height.

Additionally, owing to the 0.4mm lateral print resolution of the 3D printers available for use, the housing was designed so to be 1mm thick at its thinnest point. In the author's experience, a part that is two lines thick is thinnest possible without compromising its mechanical robustness, as it allows for the small omissions of printer extrusion, common when using low-cost 3D printers, without a hole through the entire part. Selecting the thinnest possible design allowed the phone camera to get as close to the eye as possible and therefore achieve maximal field-of-view.

The housing contained a window, allowing the phone's camera to operate unimpeded. This was surrounded by a recess on the interior of the housing to

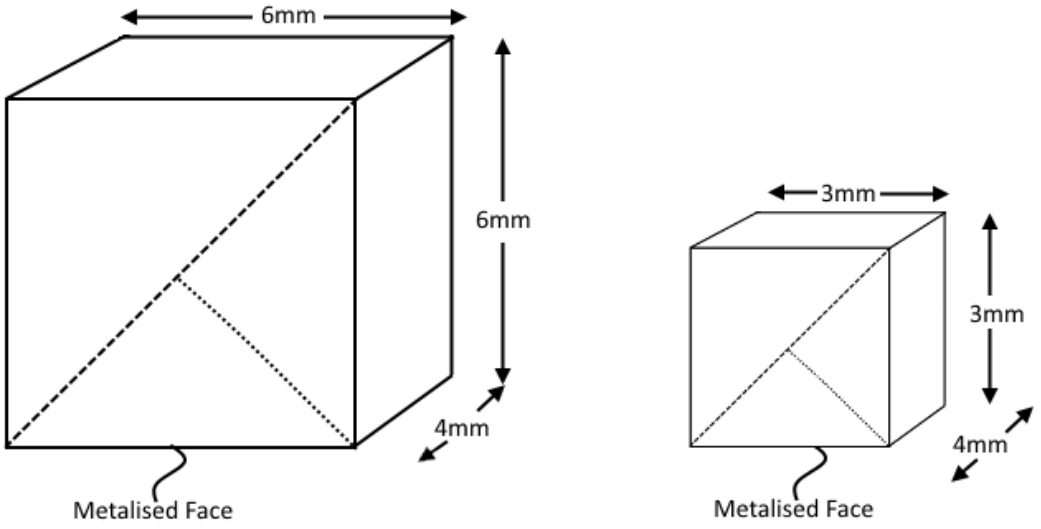

Figure 33 - The prism constructed for the adapter's optics were cut from cubes sawn from a PMMA mirror. In each case, the cuboids were filed down to the dashed line followed by filing down to the dotted line, creating a right-angled prism with the original metallised face intact and facing inwards.

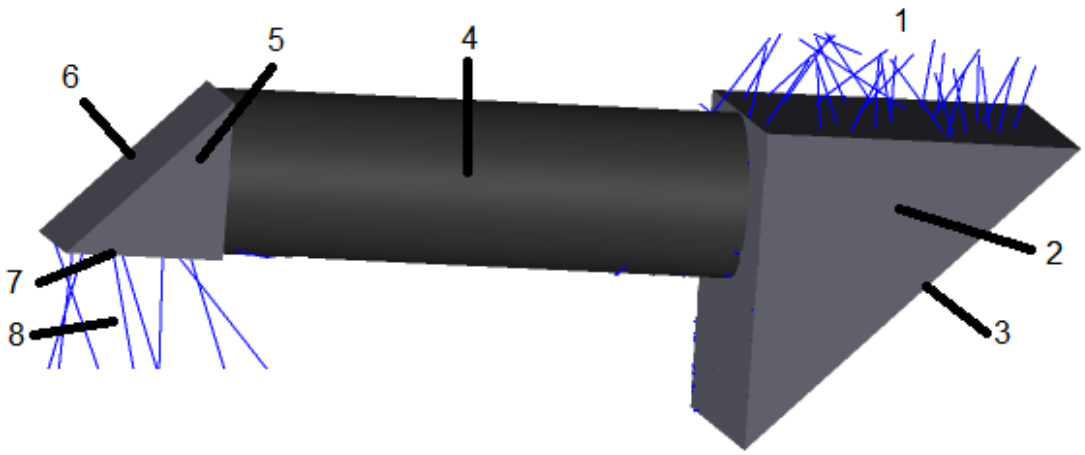

Figure 34 - Schematic of the optics housed in iteration one of the smartphone-based ophthalmoscope. Incoherent white light from LED source (1; example paths in blue) enters a PMMA right-angled prism of 4mm width (2) with a 6mm hypotenuse metallised hypotenuse (3). Light is guided along an 8.4mm length of cladded 2mm diameter silica optical fibre (4) to a PMMA prism with 4mm width and hypotenuse and 3mm length (5). This prism also has metallised hypotenuse (6) as well as having all but the face connected to the optical fibre and the output face (7) painted in near-UV and visible spectrum absorbing paint. The output face was fitted with a circular polarising filter causing incoherent, left-handed circular polarised light to emerge from the component (8; example paths in blue).

accommodate the Galaxy S3's protruding camera optic. This also allowed for easier placement of the polarising filter window that is shown in place alongside the rest of the optical components in Figure 32.

Finally, an occluding cap was separately designed to block any light from the LED flash that did not enter the prism, and thus prevent unnecessary specular reflections or discomfort to the patient. The cap was designed to be attached to the housing with cyanoacrylic glue (DIY Time Super Glue, Poundland Ltd., Willenhall, UK) as shown in Figure 35.

5.4.2 Prototyping

The prisms were manufactured by first sawing 3x4x3mm and 6x4x6mm cuboid sections from a 3mm and 6mm sheet of mirrored PMMA respectively (Silver Acrylic Mirror A4 Sheets 3mm/6mm thick, Gilbert Curry Industrial Plastics Co Ltd., Coventry, UK) with a fixed frame piercing saw (Axminster Tools and Machinery, Axminster, UK). A diamond file (RS Pro 160mm Diamond Square File, RS Components, Corby, UK) was then used to file the cubic sections, in the manner shown in Figure 33, in order to form right-angled prisms with a metallic hypotenuse facing into the prism. Having filed the prisms to the correct dimensions, each face was polished using a sequence of diamond papers of decreasing coarseness. An 8.4mm section of a 2mm diameter cladded light guide (OPMF 2000 polymer fibre, Farnell element14, Leeds, UK) was then cut with a scalpel and each end polished in the same fashion as the prisms. The prisms were then attached to the light guide in the orientation shown in Figure 34 an index-matching UV curing adhesive (Loctite 4305, Comar Optics, Linton, UK).

A 3x3mm square of left-handed circular polarising film (#88-089, Edmund Optics, Barrington, NJ, USA) was then cut using a scalpel and attached to the face of the second prism (6 in Figure 34) which was perpendicular to the optic axis using the aforementioned index-matching UV curing adhesive.

All areas where light was not intended to enter or leave the completed optical component were then painted using a UV curing paint (New Seduction Colour Gel, NSI Scotland, Glasgow, UK) and cured using the aforementioned UV torch. This

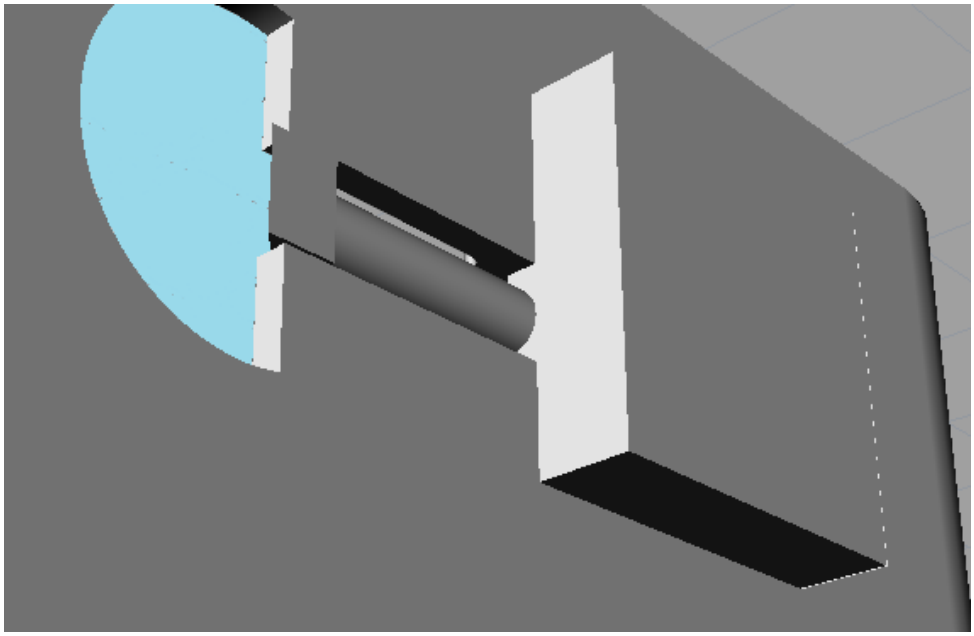

Figure 35 – CAD rendering of the assembled adapter included a cap to shield the LED light source.

Figure 36 - A completed prototype of the first design iteration in place on a Samsung Galaxy SIII.

prevented light reflecting directly from the component into the camera optics when attached to the phone.

The CAD was then exported as a stereolithography (STL) file, sliced for 3D printing using UP studio (Tiertime, Beijing, China) and printed in black polylactic acid (PLA; Tiertime) using an UP2 3D printer (Tiertime). The plastic housing was considered to be of sufficient build quality if the 3D printing process completed successfully and there were no obvious holes or gaps in the housing upon visual inspection in a well-lit environment. Any surface areas containing unwanted extrusions or roughness were hand-filed until smooth.

The components were then assembled as described above and shown in Figure 36. Appendix 5.2 contains a full list of components used in the manufacture of the prototype.

5.4.3 Performance Testing

5.4.3.1 Methods

5.4.3.1.1 Safety testing

Before the prototype can then be tested on real eyes, it is important to establish the safety of doing so. As the device is non-contact, the primary safety concern comes from shining light directly into the eye of the participant. BS EN ISO 15004-2:2007 specifies the emission limits for any ophthalmic device without its own bespoke standards for safety (270). As the demonstrator qualifies as a group 1 ophthalmic device the relevant test parameters are listed in 'Table 2 – Group 1 limit values for continuous wave instruments' of the standard (277). This includes three parameters for assessing the hazard in relation to the cornea and lens one of which takes account of the higher risk posed by shorter wavelength, higher energy illumination in ultraviolet part of the spectrum by applying a weighting factor. The retinal irradiance needs to be calculated according to Annex D of the standard to determine the value of the parameters describing the retinal photochemical, that is damage caused by visible light by a variety of biological mechanisms (278) and thermal light hazards. Both are weighted to account for the higher sensitivity to ultraviolet and infrared wavelengths respectively. The retinal photochemical hazard is calculated as for an aphakic eye, that is those without a lens, as the retinas of such

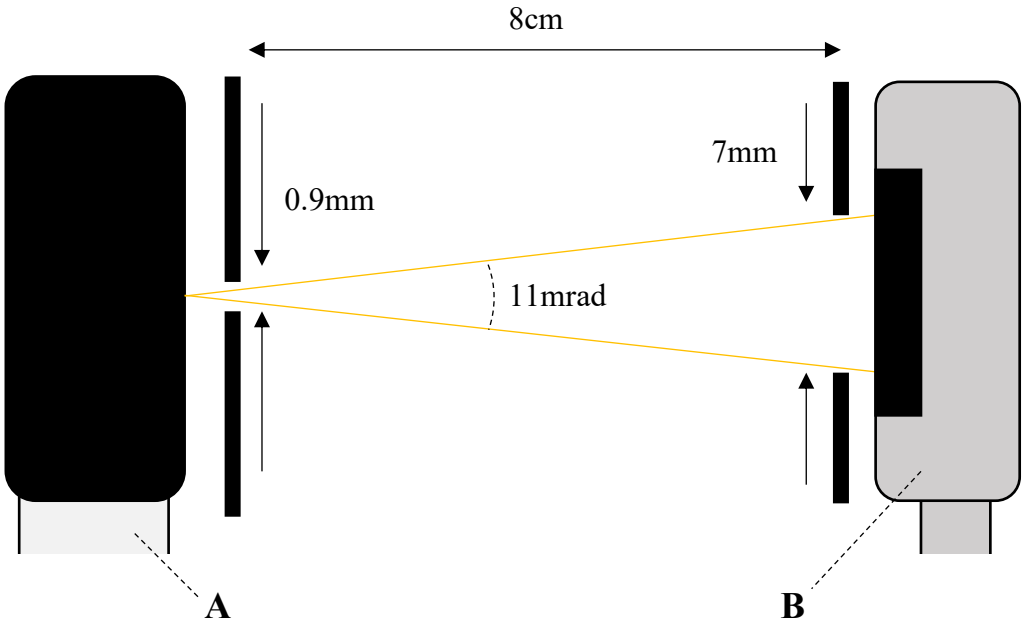

Figure 37 - Experimental setup for measuring the retinal photo hazard. A 0.9mm aperture was positioned over the brightest 'hotspot' on the illumination source of the ophthalmoscope adapter when fixed to the smartphone (A). The optical power sensor (B) was placed at 8mm from the illumination source. Placing a 7mm aperture over the sensor created the requisite 11mrad field of view as stipulated by BS EN ISO 15004-2 2007 (270)

eyes are not protected by the lens' absorption of ultraviolet light which therefore contributes strongly to this hazard in such cases (279).

$$E\ [\mathrm{mW\ cm^{-2}}] = \frac{\emptyset\ [\mathrm{mW}]}{A\ [\mathrm{cm^2}]} \quad \textbf{(2)}$$

Hence, values for the weighted corneal and lenticular ultraviolet radiation irradiance,

$$E_{S-CL}[\mu\mathrm{W\ cm^{-2}}] = \sum_{\lambda=250}^{400} E_\lambda[\mu\mathrm{W\ cm^{-2}}] \cdot S(\lambda) \cdot \Delta\lambda[\mathrm{nm}] \quad \textbf{(3)}$$

the unweighted corneal and lenticular ultraviolet radiation irradiance,

$$E_{UV-CL}\ [\mathrm{mW\ cm^{-2}}]\ = \sum_{\lambda=360}^{400} E_\lambda\ [\mathrm{mW\ cm^{-2}}] \cdot \Delta\lambda\ [\mathrm{nm}] \quad \textbf{(4)}$$

and the unweighted corneal and lenticular infrared radiation irradiance,

$$E_{IR-CL}\ [\mathrm{mW\ cm^{-2}}]\ = \sum_{\lambda=700}^{2500} E_\lambda\ [\mathrm{mW\ cm^{-2}}] \cdot \Delta\lambda\ [\mathrm{nm}] \quad \textbf{(5)}$$

could be calculated, where E_λ is the irradiance for the given spectral component, $\Delta\lambda$ is the size of the spectral component and $S(\lambda)$ is the UV radiation hazard weighting function which accounts for the cornea and lens' increased sensitivity to shorter wavelengths (see Appendix 5.6 for a table of values) (270).

For measurement of retinal radiance, an experimental setup was constructed as suggested in Annex D of ISO 15004-2 (270). As is shown in Figure 37, this involved placing a 0.9mm circular aperture over the brightest part of the illumination source and a 7mm aperture over the optical sensor. The 7mm aperture over the sensor is specified in the standard and ensures that only light that would pass through the pupil of a dilated eye contributes to the measurement. The size of the smaller aperture was determined by the standard's specification that only radiation that falls within a field-of-view of 11mrad be considered. As the pupil of the eye is the field stop, it therefore follows that the diameter of the smaller aperture,

$$d\ [\mathrm{m}] = 0.011 \times z\ [\mathrm{m}] \quad \textbf{(6)}$$

where z is the distance between the two apertures. If z is set to 8cm, d is therefore 0.9mm (270).

$$E_{A-R}\,[\mathrm{mW\,cm^{-2}}] = \sum_{\lambda=305}^{700} E_{\lambda}\,[\mathrm{mW\,cm^{-2}}] \cdot A(\lambda) \cdot \Delta\lambda\,[\mathrm{nm}] \quad \textbf{(7)}$$

and the weighted retinal visible and infrared radiation thermal irradiance,

$$E_{VIR-R}\,[\mathrm{mW\,cm^{-2}}] = \sum_{380}^{1400} E_{\lambda}\,[\mathrm{mW\,cm^{-2}}] \cdot R(\lambda) \cdot \Delta\lambda\,[\mathrm{nm}] \quad \textbf{(8)}$$

Measuring the radiant power transmitted through the second, 7mm diameter circular aperture, $\emptyset$, therefore allowed the irradiance, E, to be calculated according to the relationship shown in **(2)**, where A is the area of the 7mm diameter circular aperture. Hence, calculation of the retinal weighted photochemical aphakic irradiance, could be achieved, where $A(\lambda)$ is the aphakic photochemical hazard weighting function and $R(\lambda)$ is the thermal hazard weighting function which account for the differing sensitivity of the retina at different wavelengths (see Appendix 5.6 for a table containing values for both functions) (270).

5.4.3.1.2 Testing on healthy volunteers

Having visually assessed the resolution, colour and field-of-view by observing known features on the model eye's target the prototype was then tested on healthy adult eyes.

Ethical approval was sought and received from the University of Strathclyde Biomedical Engineering departmental research ethics committee before proceeding with human testing. As the objective of this test was simply to understand the design's performance in a small number of eyes and not produce a fully powered sample that is representative of a wider population, three participants were recruited from University of Strathclyde staff via direct correspondence with the author. The participant group was later augmented by including participants in other studies at different institutions who had the approval of their own ethical bodies to conduct imaging with the prototype.

After receiving informed consent from the participant, their dominant eye was established. The non-dominant eye was then dilated using 0.1% Tropicamide eye drops by a qualified clinical professional, who also made an assessment regarding the

health of the participant's eyes. After waiting approximately twenty minutes for the eye drops to take effect, retinal imaging was conducted in a similar fashion to that conducted on the model eye. That is, the optic nerve was located and imaged, followed by the macula and then the retinal arcades and periphery. The participant was instructed to fixate on a point in the distance throughout the imaging session.

The phone was held at the bottom by one hand whilst the other end, with the device attached, was held between the thumb and index finger of the other hand. The camera optic was then moved close to the anterior surface of the subject's eye. Approaching at approximately 45 degrees to the optical axis of the eye allowed the optic nerve to be quickly identified. The phone was steadied by resting the remaining three fingers of the hand holding the top of the phone on the subject's head.

The camera could be orientated in either portrait mode (vertical with the camera end of the phone at the top) or landscape mode (with the camera end of the phone closest to the subject's nose). Due to the geometry of the phone and adapter, it was not possible for the adapter to make contact with the eye when held in either of the positions.

The procedure was conducted in the presence of an ophthalmologist who dilated the participant's pupil and provided confirmation that the eye was healthy.

The still photographs and video captured during each of the session were then reviewed and the image quality assessed.

5.4.3.1.3 Assessment of image quality

In order to quantitatively analysis the prototype's performance, video extracts acquired from the healthy volunteers were identified where a visual assessment determined the recording to be in focus and at that correct working distance. Individual frames containing the optic nerve were then exported from these extracts as still images using the iMovie 10.1.10 video editing software package (Apple Inc.).

Image analysis was then conducted using the ImageJ 1.52i image processing software package (National Institutes of Health, Bethesda, MD, USA).

	Parameter	Safe Limit	Calculated Value
5.4.1.1	Weighted corneal and lenticular ultraviolet radiation irradiance	0.4 $\mu W/cm^2$	$(2.8\pm0.1)x10^{-5}$ $\mu W/cm^2$
5.4.1.2	Unweighted corneal and lenticular ultraviolet radiation irradiance	1 mW/cm^2	$(0.31\pm0.01)x10^{-3}$ mW/cm^2
5.4.1.3b	Weighted retinal radiance	2 $mW/(sr \cdot cm^2)$	$5.56x10^{-3}$ $mW/(sr\ cm^2)$
5.4.1.4	Unweighted corneal and lenticular infrared radiation irradiance	20 mW/cm^2	$(1.07\pm0.05)x10^{-3}$ $mW/(sr\ cm^2)$
5.4.1.5	Unweighted anterior segment visible and infrared radiation irradiance	4 W/cm^2	Exempt
5.4.1.6b	Weighted retinal visible and infrared radiation thermal radiance	6 $W/(sr \cdot cm^2)$	$2.60x10^{-5} W/(sr\ cm^2)$

Table 12 - Light hazard protection parameters, as defined by BS EN ISO 15004-2:2007, with the safe limits and the values calculated for the brightest prototype (270). The results showed that the prototype was safe for use in healthy adults.

Colour thresholding was used to isolate the optic nerve, background retina, shadow cast by the iris and corneal reflection. This was possible owing to the difference in colour profiles of these four features, with the optic nerve having a high pixel intensity high yellow component, the background retina having a high red component, the shadow having a low pixel intensity (i.e it is dark) and the corneal reflection having a high violet component. The number of pixels contained within the isolated areas and their mean pixel intensity were then recorded. The pixel intensity was weighted for photoptic perception given the interest in assessing the images' usefulness for assessment by a human operator (weighting factors: 0.30 for red, 0.59 for green and 0.11 for blue). Thus, the size and relative intensity of the corneal reflection as well as the size of the shadow could be quantified.

For consistency, comparisons were only made between images taken in the same eye. As working distance was not fixed and this affects the relative size of features on the ocular fundus as well as overall field-of-view, the area of each feature was normalised to the area of the optic disc. Indeed, it is common to measure distances on the ocular fundus in terms of 'disc diameters' in clinical tasks such as diabetic retinopathy screening (185). It should be noted that this means that the size of the corneal reflection, as recorded relative to disc, refers to the area of the ocular fundus that it obscures, as opposed to the area of the reflection itself on the cornea.

In total the analysis was conducted using three frames acquired using the prototype described in this section and compared to analysis of three frames acquired using a prototype of the previous design described in 5.2.2.

5.4.3.2 Results

5.4.3.2.1 Safety testing results

The total irradiance detected at a 1mm working distance from the optical power meter's sensor was 343 μW / cm2 ± 16 μW / cm^2. It therefore follows that that the demonstrator's illumination falls within the limits of parameters 5.4.1.2, 5.4.1.3 and 5.4.1.6, as can be seen in Table 12. A linear increase in optical power was detected after the sharp increase and decrease when the flash was activated or deactivated respectively. This was assumed to be the battery emitting in the mid-infrared as it heated or cooled due to the extra discharge required to power the LED. Such long

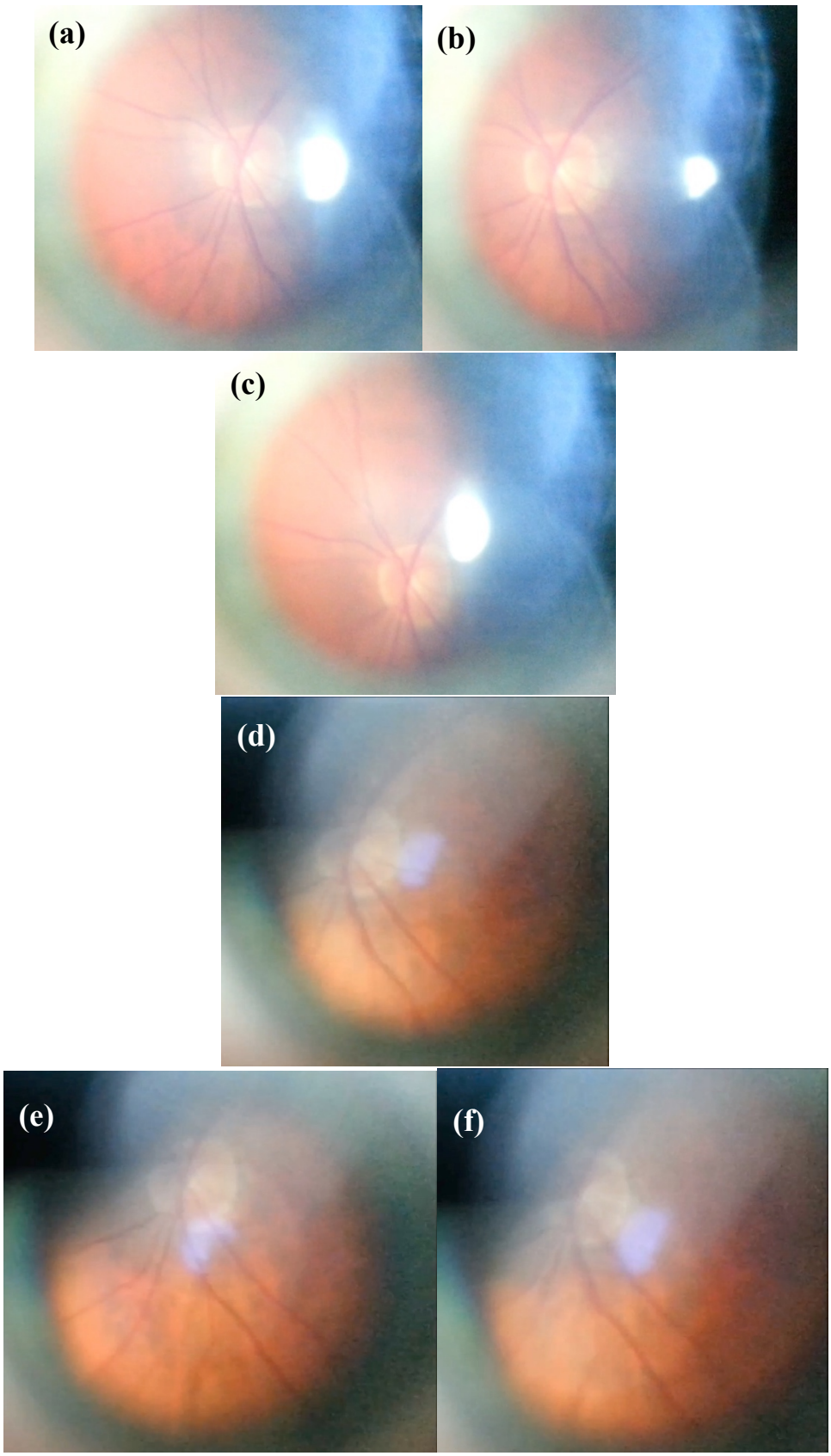

Figure 38 – The retinal images acquired using (a-c) a prototype of Giardini and colleagues design (199) and (d-f) the prototype of the first design iteration.

wavelength radiation is out of the band of interest for the optical power testing in question and was therefore discounted and only the sharp increase and decrease taken as a measure of the optical power.

For the retinal irradiance measurements, the power meter could not detect any change in radiant power when the LED flash was activated. An incident radiant power of 10μW, the minimum power that could be detected by the sensor, was therefore assumed.

It should be noted that the detection range in terms of wavelength did not encompass the entire range required for calculating the retinal visible and infrared radiation thermal hazard (Parameter 5.4.1.6). However, given the optical power had dropped to very low levels (<0.01 $\mu Wcm^{-2}nm^{-1}$) between 850 and 900nm it was deemed very unlikely that the prototype emitted significantly in the near-infrared.

5.4.3.2.2 Results of testing on a healthy volunteer

Videos of the same eye were acquired with each prototype with relative ease, however that conforming to Giardini and colleagues' design would frequently lose focus as the autofocus attempted to focus on the corneal reflection.

The images extracted for quantitative analysis are shown in Figure 38.

As is apparent visually in Figure 38 and quantitatively in Table 13, both prototypes allowed a substantial area around the optic nerve to be imaged, although over one third of the ocular fundus within the field-of-view of the camera was cast in shadow. According to basic geometry and assuming the optic disc is circular and subtended by a cone whose apex is in the centre of the cornea and apex angle is the typical 6° (280), the area of the ocular fundus visible was equivalent in size to an arc of the retina subtended by a cone with an apex angle of (23.4±3.4)° and (22.3±0.8)° for the previous and newer design respectively.

Two-sided, two sample t-tests found there to be no significant difference between the two prototypes with respect to the area of ocular fundus visible, proportion of ocular fundus under shadow and the area of ocular fundus obscured by the corneal reflection (p-values: 0.663, 0.776 and 0.777 respectively).

	Mean visible fundus (±S.E.)	Mean % fundus under shadow (±S.E.)	Mean corneal reflection size (±S.E.)	Mean corneal reflection weighted pixel intensity (±S.E.)
Previous design	(12.0±1.2)DA	(39.0±5.0)%	(0.38±0.09)DA	253.5±3.7
Design iteration 1	(10.8±0.3)DA	(37.0±4.4)%	(0.35±0.04)DA	187.8±11.6

Table 13 - Results of image analysis. DA = optic disc areas.

It was clear from visual inspection of the images that the corneal reflection created by the newer prototype was far dimmer than that of its predecessor. Indeed, the quantitative assessment of the reflection generated by the earlier prototype revealed that its modal pixel intensity was 255, the maximum possible value and thus implying that a large proportion of pixels within the reflection area were saturated. Moreover, a Mann-Whitney U test showed that the prototype of the newer design had a significantly less intense corneal reflection than that of the previous design ($W>10^6$; $p<10^{-15}$). As such it was possible to see certain features of the ocular fundus with the newer prototype even if these features were directly under the corneal features, such as large retinal vessels as can be seen in Figure 38e. This was not the case with the prototype of the previous design where retinal features were entirely obscured by the corneal reflection.

For the prototype of the previous design the mean pixel intensity of the visible parts of the retina (that is the ocular fundus excluding the optic nerve) was 161.0 and standard deviation 29.3. That of the later design was 107.9 and 49.9 respectively.

5.4.4 Discussion

The prototype of the design of a smartphone-based ophthalmoscope adapter described in this sub-section showed a marked reduction in the intensity of corneal reflection produced. The primary benefits of this improvement were more stable and consistent autofocussing during image acquisition and features of pathology being less likely to go unnoticed owing to being directly under the corneal reflection during image capture. However, a corneal reflection was still present in each of the images and therefore design improvements in this regard can be made. These include improvements that reduce the variance in the angle between the polarising film fixed to the prism and the polarising film in front of the camera. As was noted previously, the efficiency of the polarising filter reduces as this angle increases.

It was also found that the optical power produced by the prototype was considerably less than that modelled by optical simulation during the design process. This resulted in a dimmer retina in the images captured using the prototype compared to that of the previous design. A possible reason for this was that, owing to the prims

being hand filed, it was not possible to ensure the accuracy of prism angles. For the same reason, surface quality of the prism faces was also likely to have substantial variance.

Therefore, whilst the potential for quickly and easily imaging the retina when placed in the hands of a non-clinician was demonstrated by the testing described in this subsection, it was decided that a second iteration of the design was required in order to truly deliver a design suitable for providing a retinal imaging system to low skilled cadres within the eye health system, such as CEHWs. This second design iteration is described in the following subsection.

5.5 Design Iteration 2: Second Samsung Galaxy S3-based Unit

5.5.1 Design

5.5.1.1 High-level design changes

One means by which the optical efficiency of the previous design could be improved upon was to increase the proportion of light which was transmitted from the first mirrored face to the second mirrored face. To this end, the second design iteration replaced the assembled custom optic described above with a single rhomboid prism. In such a design total internal reflection can guide the light emitted by the smartphone's LED flash, proving the prism is appropriately sized. Thus, the light can, theoretically, be channelled between the two mirrored surfaces without loss, in contrast to the coupling loss experienced by design iteration 1 between the first prism and optic fibre.

Commercial sourcing of a rhomboid prism of the correct dimensions was not possible requiring that custom prototypes of the component be built. This was made possible by the installation of a TMX65 CO2 laser cutting machine (CTR Lasers, Northampton, U.K.) in the second half of 2014, after the first design iteration had been designed and prototyped. Furthermore, the use of such an instrument, which has a lateral precision of 0.1mm and an angle accuracy of 0.1°, could be manufactured with greater consistency, more quickly and thus at larger volumes.

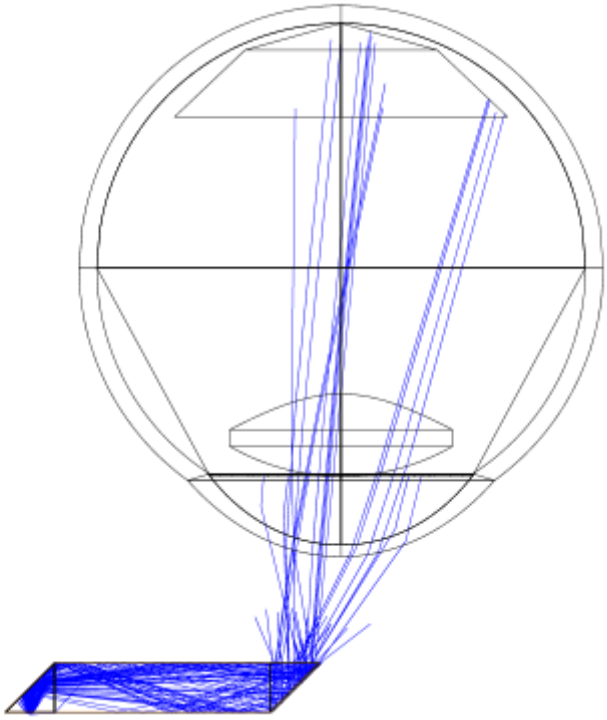

Figure 39 – Ray diagram of the rhomboid prism illuminating the Zemax model of an adult eye.

Design	Heatmap of retinal illuminance with 8mm pupil (lm/cm^2)	Heatmap of retinal illuminance with 8mm pupil (lm/cm^2)
Iteration 1	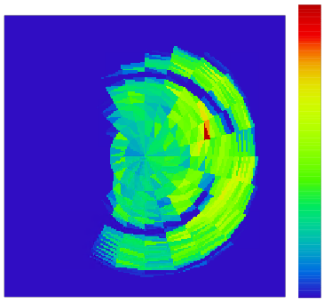	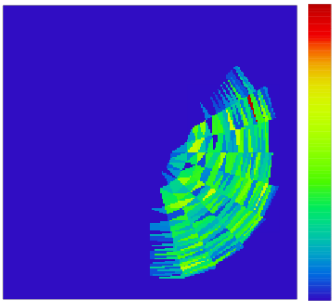
Iteration 2	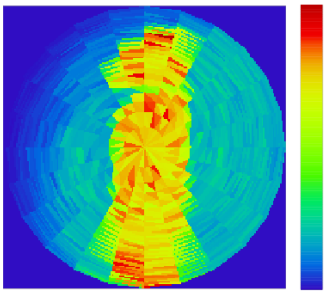	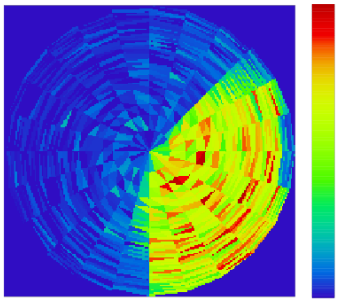

Table 14 - Heatmaps of the illuminance detected at the posterior pole of the retina for the first and second design iterations after tracing 100,000 rays through an optical model of the design and a simulation of an adult eye.

5.5.1.2 Optical Design

Given the application's sensitivity to thickness in the direction along the optical axis, the prism was sized so that its height matched the minimum thickness of the housing in which it was to be mounted. Emulating the design of a classical direct ophthalmoscope, the prism angles were set to 45° from the normal.

As in Section 5.4.1 it was assumed that optimal placement of the prism was so that, with the first angled face centred on the middle of the LED, the point of the prism closest to the camera's optical axis touched a cone whose apex, of angle 48° was centred on the camera aperture. As such the total length of the prism was calculated to be 14.4mm.

5.5.1.2.1 Optical modelling and simulation methods

The design was modelled as a non-sequential optical components model, shown in Figure 39, in Zemax OpticStudio with the smartphone LED and adult eye being modelled as outlined in Section 5.4.1.2.3.

The prism was modelled by coding a custom polygon object with the above dimensions. The prism material was set to acrylic, given its good optical properties and compatibility with the laser cutter, and the angled faces set to model an aluminium coating (95% reflectivity). The code for the variations of this component used in the model are shown in Appendix 5.3. Other than 2.2 by 3.0 mm gaps at the faces where the light beam was to enter and exit it, the prism was surrounded by flat absorbing shapes to simulate an absorbent paint coating.

A ray tracing simulation was then run according to the methods described in Section 5.4.1.2.3.

5.5.1.2.2 Optical modelling and simulation results

Table 14 shows heatmaps of the luminous intensity calculated to be incident on the retina for each simulated design for 8 and 4mm pupil diameters. The results show a more extensive illumination of the ocular fundus compared to the first iteration of the design. However, the results also suggest that the retina is exposed to light levels well in excess of that which is deemed to be safe. However, given the many

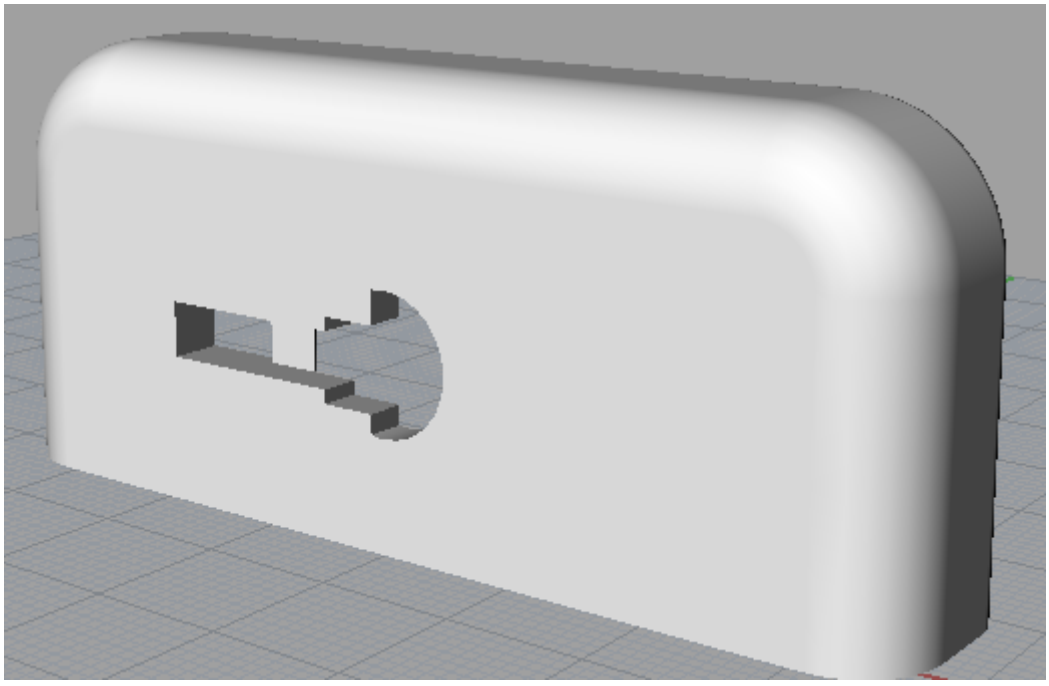

Figure 40 – The revised design of the 3D printed clip before any optical components were inserted.

Figure 41 – A schematic showing a cross-section of the rhomboid prism. Reflective metalic sheets were applied to the two angled faces of the prism whilst 9mm^2 squares of diffusing and polarising films were fixed to the output face.

Figure 42 - The prism was fixed so that there was an approximately 0.5mm lateral separation from the camera aperture.

inefficiencies that were not modelled, such as the surface quality of laser cut acrylic, it was decided to proceed with prototyping and optical power measurements to provide a real measure of the design's safety given the prototyping methods used.

5.5.1.3 Mechanical Design

The design and manufacture of the plastic housing remained largely similar to that of the previous design with the exception of a small rest bridging the channel for the optical component, as can be seen in Figure 40. This was to allow easier and more reliable alignment of the prism within the housing.

The purpose for this change related to the observation that the thickness of the prototype in the direction of the camera's optical axis was a critical parameter with respect to the viewing angle possible. Given that it was required for any cover to be at least 2mm thick in order to be mechanically robust, it was decided to use black tape instead and glue this in-place to ensure it did not fall off. Additionally, the cap which prevented light not entering the prism from escaping was replaced with a length of black tape. The reason for doing so was that, in the author's experience, any 3D printed wall was required to be at least 2mm thick in order to be mechanically robust. Thus, using tape, whose thickness is of the order of 100μm, offered significant potential to reduce the overall profile of the device, allowing the operator to get closer to the eye and thus increase the field-of-view.

5.5.2 Prototyping

The prism was manufactured by cutting the shape outline in Figure 41 into a 3mm thick PMMA sheet using the aforementioned laser cutter.

To increase the reflectivity of the 45-degree faces, a metallic sheet (Emergency Foil Space Blanket, Medisave, Weymouth, UK) was then fixed to each with UV curing adhesive (Loctite 4305) and cured using the aforementioned 1W UV torch. A $9mm^2$ square of diffusing film (Scotch Magic Tape 810, 3M, Maplewood, MN, USA) was also placed on the output face of the prism to provide a uniform illumination of the ocular fundus, using its own adhesive. Finally, a $9mm^2$ square of left-handed

Figure 43 - A length of black duct-tape was fixed over the prism channel to prevent light not entering the prism from causing unpolarised specular reflections and therefore image artefacts.

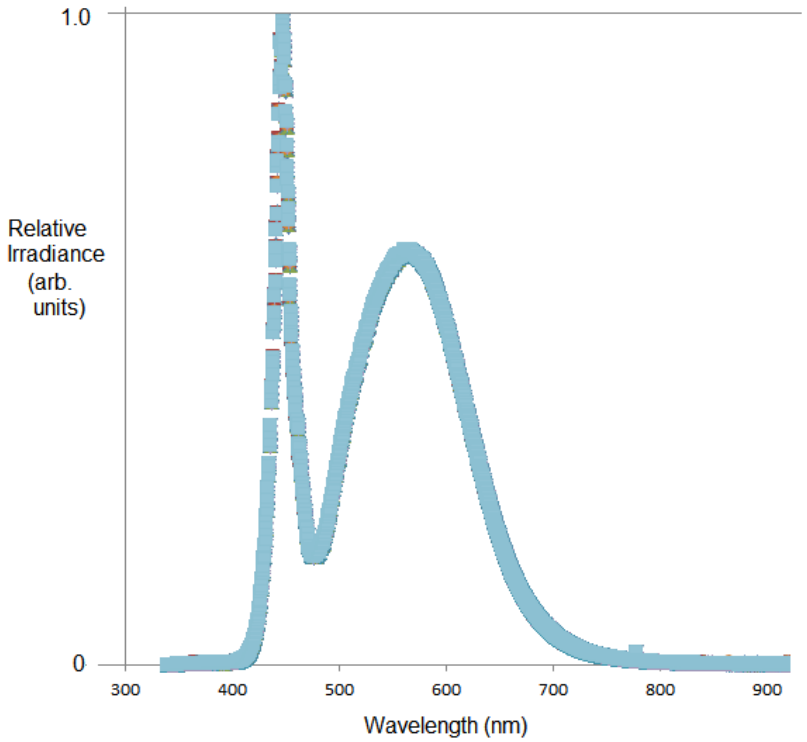

Figure 44 -Spectral distribution measured for the demonstrator's optical output.

circular polarising film (CP42HE circular polarizer, Edmund Optics) was fixed on top of the diffusing film to allow corneal reflections to be removed as with the previous design iteration. The prism was then inserted into the channel and positioned at approximately 0.5mm laterally from the camera aperture, as shown in Figure 42. It was held in place with the aforementioned adhesive that was again cured with a 1W UV torch.

A length of matte black duct tape (Advance Tapes AT160 Matt Black Cloth Tape, RS Components), was then placed over the prism channel, as shown in Figure 43, and fixed in place using the UV curing adhesive and 1W UV torch.

A full list of the components used in the manufacture of the prototype are shown in Appendix 5,4.

5.5.3 Performance Testing

5.5.3.1 Introduction and methods

As with the previous tests on healthy volunteers, before the prototype could be tested, it is important to establish the safety of doing so. The same safety tests as described in Section 5.4.3.2.2 were therefore conducted on the prototype of the second design iteration in order to establish conformance with BS EN ISO 15004-2:2007 and thus safety with respect to light hazard (270).

As per the methods described in 5.4.3.2.3, the performance of the second design iteration was assessed by imaging the same eye of a healthy volunteer with prototypes of both the first and second design iterations. Images from each imaging session were then extracted and analysed according to the methods described in 5.4.3.2.4.

5.5.3.2 Results

5.5.3.2.1 Safety testing results

The relative irradiance of the prototype's emissions between 300nm and 900nm are shown in Figure 44.

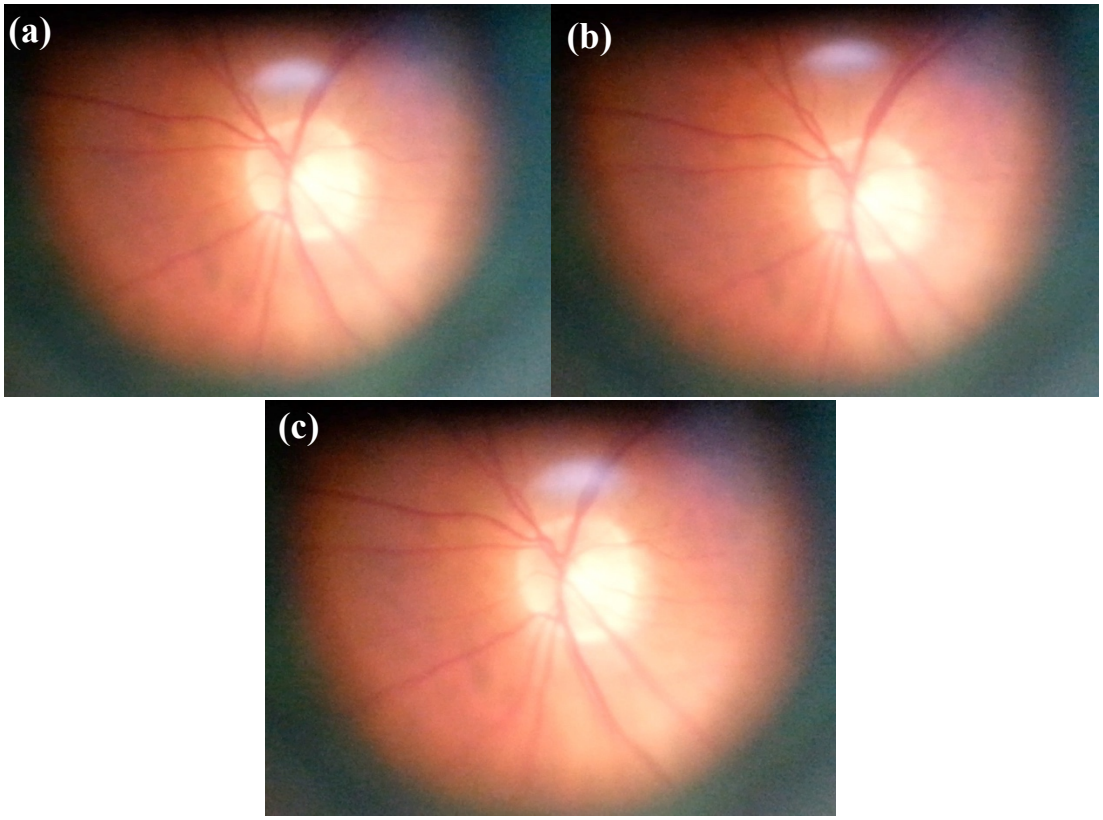

Figure 45 – The retinal images of a healthy participant acquired using a prototype of the second design

	Parameter	**Safe Limit**	**Calculated Value**
5.4.1.1	Weighted corneal and lenticular ultraviolet radiation irradiance	0.4 μW/cm^2	(6.93 ± 0.39) x 10-5 μW / cm2
5.4.1.2	Unweighted corneal and lenticular ultraviolet radiation irradiance	1 mW/cm^2	(7.51 ± 0.43) x 10-4 mW / cm2
5.4.1.3b	Weighted retinal radiance	2 mW/(sr·cm^2)	(3.98 ± 0.23) x 10-3 mW/(sr cm2)
5.4.1.4	Unweighted corneal and lenticular infrared radiation irradiance	20 mW/cm^2	(4.97 ± 0.28) x 10-3 mW/(sr cm^2)
5.4.1.5	Unweighted anterior segment visible and infrared radiation irradiance	4 W/cm^2	Exempt
5.4.1.6b	Weighted retinal visible and infrared radiation thermal radiance	6 W/(sr·cm^2)	(1.97 ± 0.11) x 10-5 W/(sr cm^2)

Table 15 - Light hazard protection parameters, as defined by BS EN ISO 15004-2:2007, with the safe limits and the values calculated for the brightest prototype (270).

iteration.

The total irradiance detected at a 1mm working distance from the optical power meter's sensor was 430 μW / cm2 ± 65 μW / cm2. It therefore follows that that the demonstrator's illumination falls within the limits of parameters 5.4.1.2, 5.4.1.3 and 5.4.1.6, as can be seen in Table 15. As with the previous prototype, a linear increase in optical power was detected after the sharp increase and decrease when the flash was activated or deactivated respectively. This was again assumed to be the battery emitting in the mid-infrared as it heated or cooled due to the extra discharge required to power the LED and was thus discounted from light hazard considerations.

For the retinal irradiance measurements, the power meter could not detect any change in radiant power when the LED flash was activated. An incident radiant power of 10μW, the minimum power that could be detected by the sensor, was therefore assumed.

5.5.3.2.2 Results of testing on a healthy volunteer

Videos of the same eye whose imaging was also described in 5.4.2 were acquired with the prototype of the second design iteration in the presence of an ophthalmologist who again confirmed that the eye was healthy.

The images extracted for quantitative analysis are shown in Figure 45.

As is apparent visually in Figure 45 and quantitatively in Table 16, as with the previous prototypes, a substantial area around the optic nerve to be imaged, although, a significant proportion of the field-of-view of the camera was again cast in shadow. According to basic geometry and assuming the optic disc is circular and subtended by a cone whose apex is in the centre of the cornea and apex angle is the typical 6° (280) the area of the ocular fundus visible was equivalent in size to an arc of the retina subtended by a cone with an apex angle of (24.8±2.4)°.

One-sided, two sample t-tests found the area of ocular fundus obscured by the corneal reflection to be significantly smaller with the prototype of the second design iteration compared to that of the first ($p=0.048$). The area of ocular fundus visible and proportion of ocular fundus under shadow were not significantly larger or smaller respectively ($p=0.229$ and $p=0.051$ respectively).

Design	Mean visible fundus (±S.E.)	Mean % fundus under shadow (±S.E.)	Mean corneal reflection size (±S.E.)	Mean corneal reflection weighted pixel intensity (±S.E.)
Design iteration 2	(13.4±0.9)DA	(32.6±3.2)%	(0.24±0.01)DA	127.5±51.6

Table 16 - Results of the image analysis on selected images of the ocular fundus of a healthy participant acquired with a prototype of the second design iteration. DA = optic disc areas.

A Mann-Whitney U test revealed that the prototype of the second design iteration had a significantly less intense corneal reflection than that of the first design iteration ($W>10^{6}$; $p<10^{-15}$). As such it was again possible to see certain features of the ocular fundus with the newer prototype even if these features were directly under the corneal features, such as large retinal vessels as can be seen in Figure 45c.

The mean pixel intensity of the visible parts of the retina (that is the ocular fundus excluding the optic nerve) was 127.5 and standard deviation 51.6.

5.5.3.3 Additional qualitative assessments of performance

In addition to the quantitative assessment of performance above, a number of images of different ocular fundi were acquired for qualitative assessment. Figure 47, an image acquired from a healthy 27-year-old white male, shows how it was possible to visualise the optic nerve, macula and much of the retinal arcades in a single image, as is typically desired in retinal photography with a desktop fundus camera (as opposed to a direct ophthalmoscope which has a much smaller field of view as noted previously).

Figure 48, an showing the ocular fundus of a healthy 34-year-old white British female, additionally shows how small details such as minor blood vessels could be visualise.

The prototype could also be used to visualise the retina in eyes that were less than fully dilated. For example, it was possible to image the optic nerve and the surrounding blood vessels in a 27-year-old white British male when not under mydriasis, as can be seen in Figure 46. It was not possible to visualise much of the peripheral retina at this pupil diameter as the shadow cast by the iris, which can be seen to be partly obscuring the image in Figure 46, would entirely cover the image at wider angles from the posterior pole.

Figure 46 - An image acquired through an undilated pupil (diameter, estimated to be between 3 and 4mm) belonging to a 27-year-old white British male using the re-designed prototype.

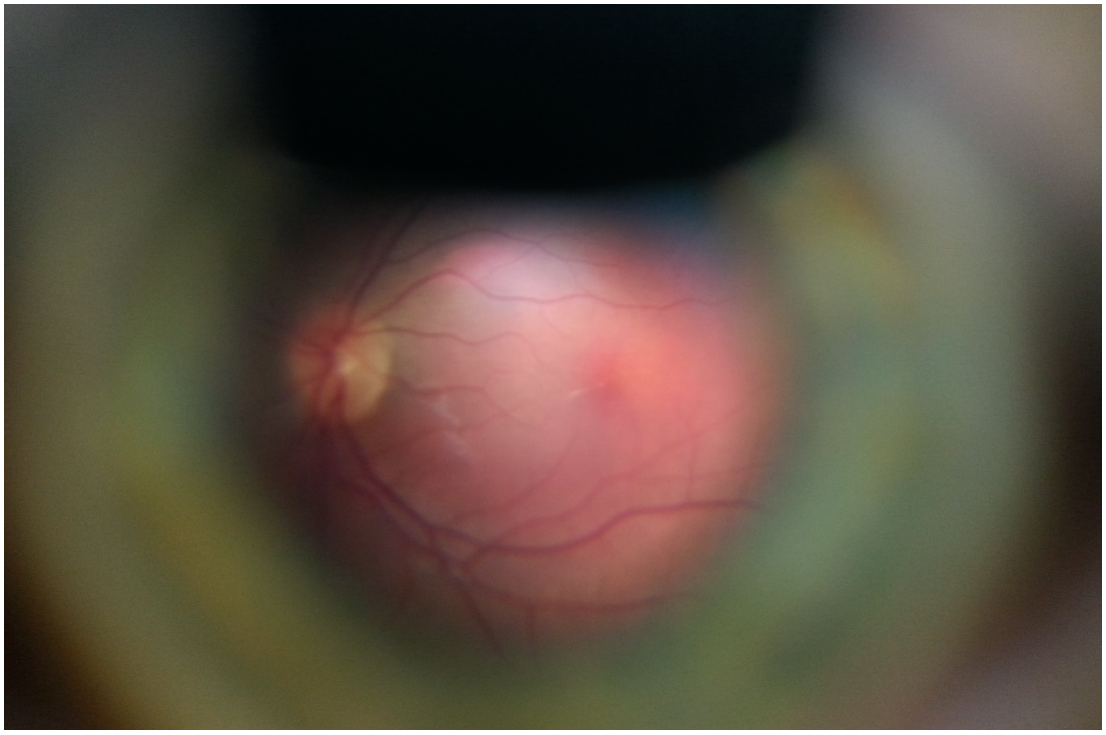

Figure 47 - An example of a fundus image acquired from the dilated eye of a 27 year-old white British male using the re-designed prototype. The field-of-view is far in excess of that of a standard ophthalmoscope with the optic nerve, macula and retinal arcades all being visible in this single image.

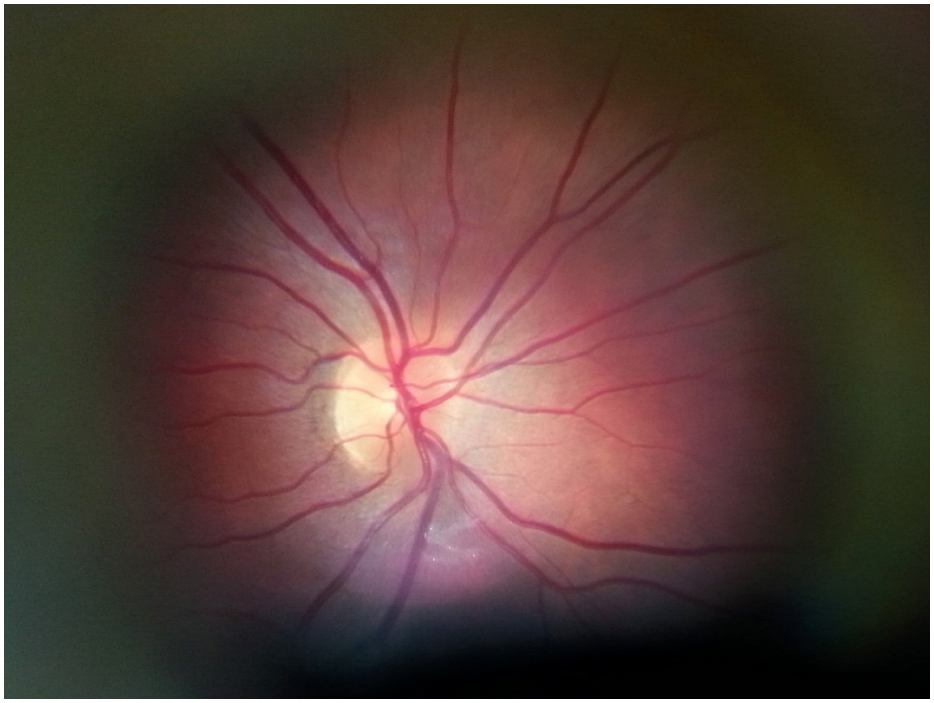

Figure 48 - An example of an ocular fundus image acquired through a dilated pupil belonging to a 34-year-old white British female using the re-designed prototype. The resolution of the image is such that minor blood vessels are clearly visible.

An image acquired from a black Tanzanian with advanced diabetic retionpathy is shown in Figure 49 overleaf. The quality of the image is somewhat reduced compared to those taken from healthy, white British eyes. The corneal reflection is much stronger, to the extent where it is not possible to the fundus directly underneath the artefact. There is also a much larger portion of the image which is obscured by shadowing and a weak, diffuse blue reflection originating from the lens. Nevertheless the advanced state of the retinopathy is clear from the image with numerous visible exudates.

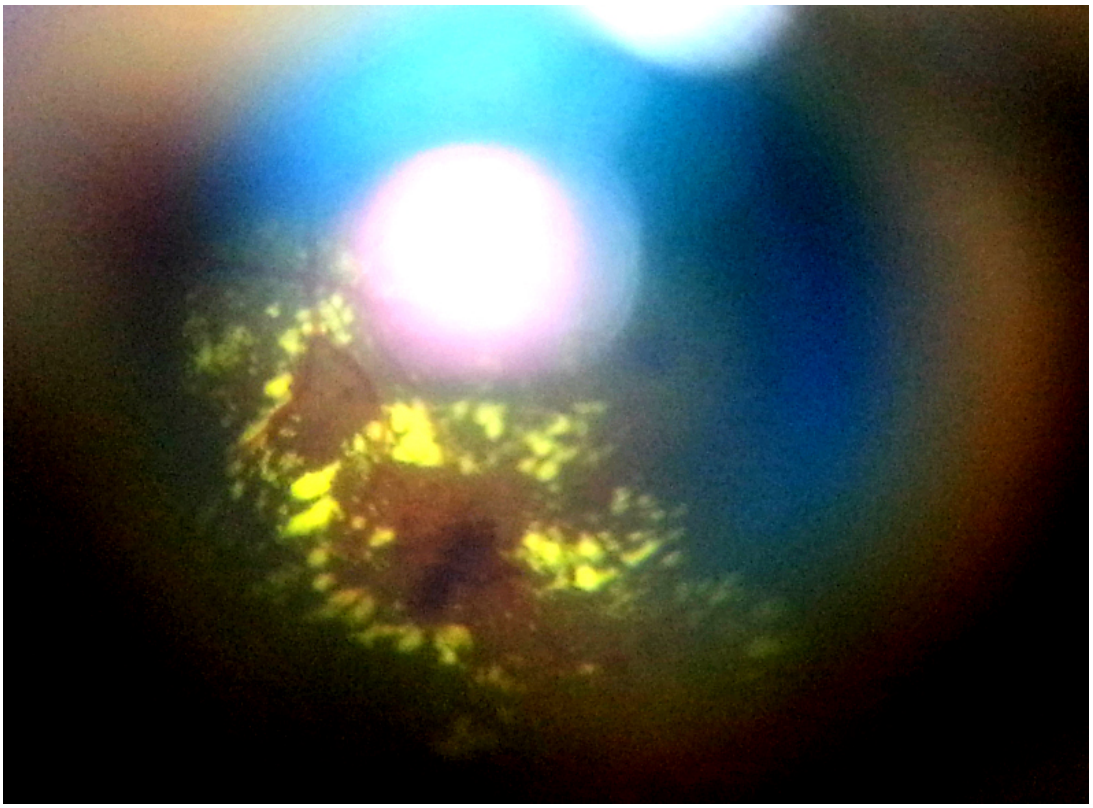

Figure 49 - An example image taken from the dilated eye of a Tanzanian black male with advanced diabetic retinopathy. Whist the retinopathy is clearly visible the image quality is notably reduced in comparison to the images of healthy eyes belonging to those with lighter retinal pigmentation. In particular, there is a strong purple corneal reflex and a greater degree of shadowing resulting from the smaller pupil diameter.

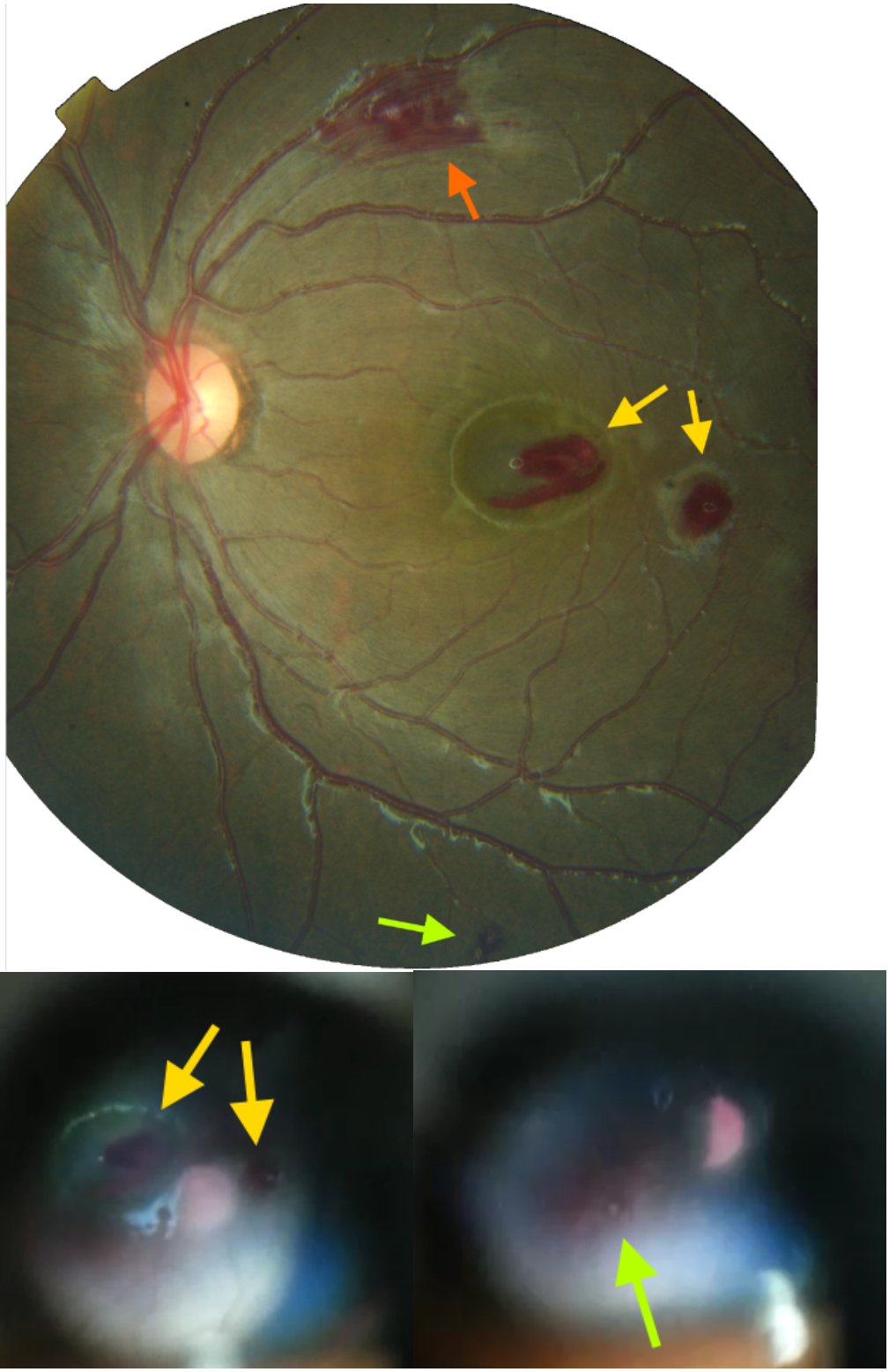

Figure 50 - Images of malarial retinopathy taken with a desktop retinal camera (top) and the Samsung Galaxy SIII based prototype (middle and bottom). Two large lesions near the macula (annotated with yellow arrows) were identified with both modalities, as was a small lesion below the lower arcade (annotated with a green arrow). A large lesion near the upper arcade (annotated with a red arrow) could be seen in the desktop retinal camera's image but was not identified with the prototype owing to the operator not sweeping the upper arcade.

Finally, images of a black Malian child suffering from malarial retinopathy (MR) are shown in Figure 50. This includes an image taken with a standard desktop retinal camera and two frames taken from a video acquired using the prototype. Two large lesions near the macula were visible with both modalities as was a small lesion below the lower retinal arcade. A large lesion near the upper retinal arcade was not seen during the prototype examination owing to the operator not imaging this area of the retina.

5.5.4 Discussion

The second version of the smartphone ophthalmoscope adapter was a marked improvement on the first with specular reflections being less apparent, in terms of intensity and size, in healthy white European eyes. However, it appears from qualitative assessment that in eyes with more darkly pigmented eyes and with greater degrees of corneal or lenticular opacity, corneal reflections were not only still visible but strong enough to obscure retinal details and interfere with the phone camera's autofocus and auto-exposure.

Imaging was possible with pupil diameters below 4mm, however there was a shadow cast on the retina by the pupil at all pupil diameters, similar to that of the previous design iteration. Whilst not preventing imaging, this did reduce the field-of-view that was possible to attain.

Nevertheless, the field-of-view achieved was well in excess of that which can be achieved with a classical direct ophthalmoscope. Indeed, it was possible to view the optic nerve, macula and much of the retinal arcades in a single image, as shown in Figure 47. This is approaching at the field of view required for DR screening, for example, which requires the entire optic nerve to be visible and the fovea to be at least two disc diameters from the edge of the image (281). By panning around the retina all of this area can be imaged.

However, as the testing in a MR clinic in Mali showed, features can be missed if the operator does not pan in every direction required to image every relevant part of the retina. Software to guide the user through the process of acquiring images of the disc, macula and peripheral retina in sequence could help to ensure that the entire

ocular fundus is imaged. However, developing such software is outside the scope of this project, instead detailed instruction about the processes was given to the operators of the device in further studies.

Therefore, a third iteration of the design was produced with the aim of further reducing corneal reflections and retinal shadowing and thus increasing the clarity of the image and attainable field of view in all eye types.

5.6 Design Iteration 3: Sony Xperia Z3 / Z3 Compact-based Unit

5.6.1 Introduction

As was mentioned in the above discussion, the need to reduce specular reflections and retinal shadowing drove the production of a third design iteration. To achieve this, two significant design changes were made. Firstly, a more efficient polarising filter was introduced and, secondly, two light sources at either side of the camera lens were used instead of one.

Furthermore, it was apparent at this stage that the Samsung Galaxy SIII had become obsolete. This attested to the swift development of the mobile device industry, highlighted in Chapter 2, and underlined the need to adapt to this rapid pace. As such, the design also aimed to allow the design to be more easily adapted to different phone models. Specifically, this involved no longer having to make accommodations for the integrated LED flash's optical power and position on the phone.

5.6.2 Design

5.6.2.1 High-level design changes

The first design change was to allow the device to be hosted on more recent smartphone models, namely the Sony Xperia Z3 and Sony Xperia Z3 Compact (Sony Corp., Tokyo, Japan). These models were chosen because a large number of the phones were gifted to the Commonwealth Eye Consortium for use in eye care mHealth research and because of the positive reviews their embedded camera had

received (www.trustedreviews.com). As was a similar cause with the Samsung Galaxy S3, it was noted that the end user costs of Xperia Z3 and Xperia Z3 Compact were 549 and 429 GBP respectively upon launch (www.techradar.com). However, it was again considered more practical to demonstrate the concept of a smartphone ophthalmoscope and gather workflow data using a higher quality handset, and then make inferences about the lowest quality camera that is viable for the task as well as the hardware cost that offers best cost-effectiveness.

The shadow cast on the retina in the previous iterations of the design was sought through the introduction of a second illumination source. As this would be impractical to achieve using the smartphone's embedded LED flash, this prototype instead incorporated its own LED light sources. It was therefore also required that custom electronics to be assembled within the prototype to drive the LEDs. It was elected to us the smartphone's own USB OTG 5v, 100mA output as a power source as this allowed the device to be driven from its host phone without having to rely on a battery or external power supply. The reasons for doing so were to reduce the complexity of the electronics, by eliminating the need for charging circuitry, and of the device's maintenance by not introducing an additional unit that needs to be charged regularly. It should be noted that frequently running a peripheral from a smartphone will drain its battery more quickly and thus the time spent imaging needs to form part of the workflow considerations (explored in Chapter 6).

5.6.2.2 Optical design

It was found to be impractical to use surface mount LEDs as mounting these close enough to the camera optic so to achieve sufficient alignment with the camera's optical axis proved challenging. Mounting through-hole LEDs laterally, however, allowed a light source to be placed very close to the camera optic. Selecting through-hole LEDs with a flat, cylindrical top of 2mm diameter (L-13PWC-Z, Kingbright, Taipei, Taiwan) then allowed for the easy mounting of a 45-degree metallised prism which in turn allowed the light sources to be brought into as close alignment as possible with the camera optics. The prism dimensions were sized so to allow the entire top face of the LED to be coupled to the prism.

To counter the corneal reflections still visible in the previous design iteration, higher efficiency linear polarising filters (Techspec High Contrast Plastic Linear Polarisers, Edmund Optics) were used in place of the circular polarising filters. This introduced the requirement that the filters be very careful positioned over the camera optics and on the device's prisms as even a slight misalignment dramatically reduced the efficiency of the filters.

5.6.2.3 Electronic design

A printed circuit board (PCB) design, a schematic diagram of which is shown in Figure 52 and its board layout shown in Figure 53, was created in KiCAD (KiCad Developers Team, http://kicad-pcb.org/). This had the purpose of hosting the 64Ω resistors necessary to drive the LEDs at 25mA when connected to a 5v supply, and to allow the correct positioning of the LED and prisms themselves. The design also involved a switch, allowing the light sources to be turned on and off, and pads that were large enough to connect the ground and 5v wires of an external supply.

Owing to the camera being placed in the top left (as viewed looking at the camera optic) of both of the handset models, it was necessary to design the PCB so that one LED was mounted along the x axis and the other along the y axis. If this were not the case, then the housing would have to extend well beyond the outline of the phone and likely inhibit the operator from positioning the camera as close to the participant's eye as possible.

Finally, a hole in the PCB allowed the camera to be exposed when the PCB was in place.

5.6.3 Prototyping

The prisms were cut from a 3mm thick metallised PMMA sheet by first cutting a 3mm wide strip of the sheet with the metal face turned down. This was then turned at 90

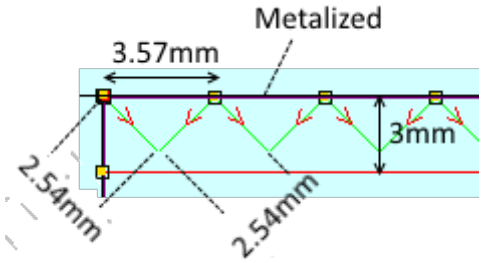

Figure 51 – Path of the laser cutter in cutting prisms for the prototype. Prior to this cut a 3x3x12mm cuboid was cut from a 3mm thick metalised acrylic sheet and flipped 90 degrees so the metalised phase was orthogonal to plane of the work bench and hence the prisms outline could be produced.

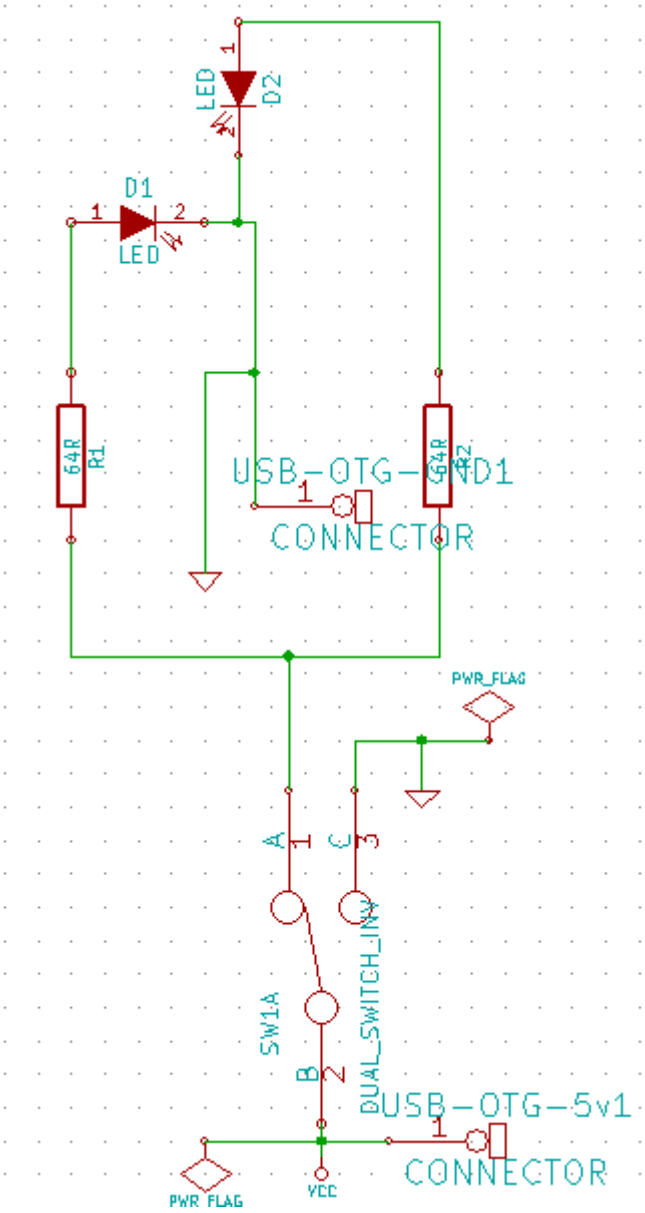

Figure 52 – Schematic diagram of the electronic design of the third design iteration.

degrees and re-inserted into the PMMA sheet, allowing a number of prisms with metallised hypotenuses to be cut as shown in Figure 51.

A prism was then attached to the top of each LED, using Loctite 4305 UV curing adhesive (Henkel); cured with the aforementioned 1W UV torch, so to reflect its light output at 90 degrees. As with the previous design, polarising filters were fitted to the output face of the prism. To attain optimal alignment, a sheet of polariser was held in a clamp stand above the prism with the polarisation axis at 90 degrees to that desired for the prism. The LED was then connected to a 25mA supply and a 9mm^2 square of the polariser positioned until the entire output face of the prism appeared black as viewed through the polarising sheet.

. The whole assembly was then painted with a number of coats of black UV curing paint (New Seduction Colour Gel, NSI Scotland), as was the edge of the output face of the prism. This, again, helped to avoid direct reflection of light into the camera optics and unpolarised light being reflected off the cornea.

.

The PCB design was engraved into a 0.8mm thick copper sheet (Modelcraft, Hobbycraft, Burton Upon Trent, UK) using an S63 PCB milling machine (LPKF Lasers & Electronics AG, Garbsen, Germany) and the components soldered by hand as shown in Figure 54. Care was taken to leave a gap of approximately 1mm between the two prisms.

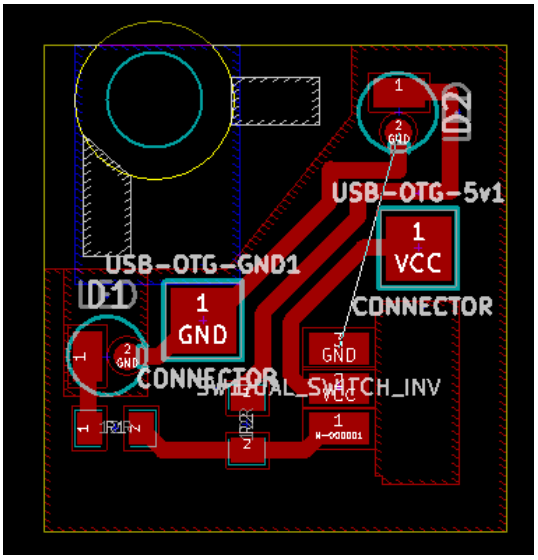

Figure 53 - Layout of the printed circuit board (PCB) designed to host the adapter's optics and electronics.

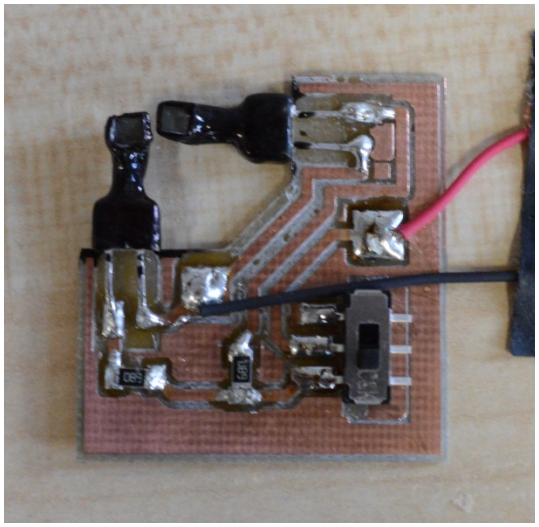

Figure 54 – Printed circuit board with assembled optics and electronics.

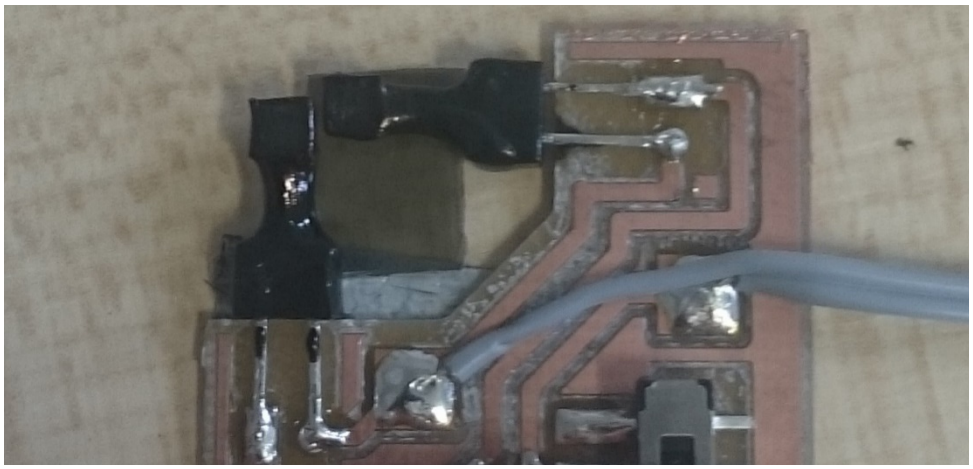

Figure 55 – Assembled PCB with linear polarising film attached.

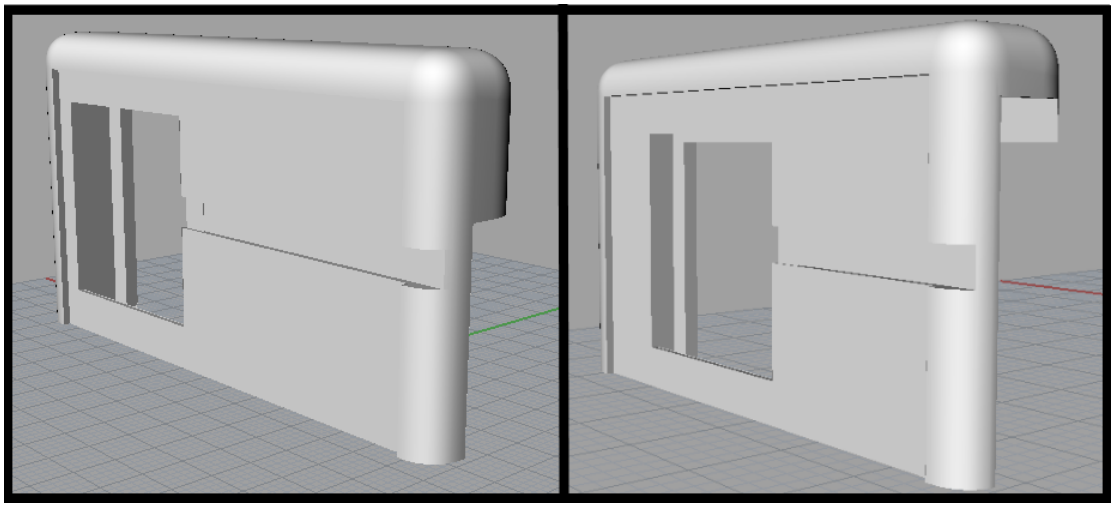

Figure 56 – CAD rendering of the clip designed to host the PCB and its USB OTG cable on a Sony Xperia Z3 (left) and Sony Xperia Z3 Compact (right).

To supply the necessary 5V, a USB on-the go (USB OTG) cable was attached to the ground and 5V pads.

A rectangle of the linear polariser was then cut and fixed to the PCB, as shown in Figure 55. The orientation of the polariser was such that it was crossed relative to the polarisers fixed to the prisms.

The completed PCB was then glued inside a 3D printed housing similar to that of the previous designs and which was designed in 3DS Max (Adobe, San Jose, CA, USA) by a technician. This design, shown in Figure 56, included a recess closely matching the dimensions of the PCB meaning that, once the PCB was in-place, further alignment of the optics was not required, as can be seen in Figure 57. As the dimensions of the Sony Xperia Z3 and Sony Xperia Z3 Compact differ, a separate CAD design for each was required. STL files of the CADs were then exported, sliced using Simplify3D (Simplify3d LLC, Blue Ash, O.H., U.S.A) and 3D printed in PLA using an Ultimaker 2 3D printer (Ultimaker B.V., Geldermalsen, The Netherlands).

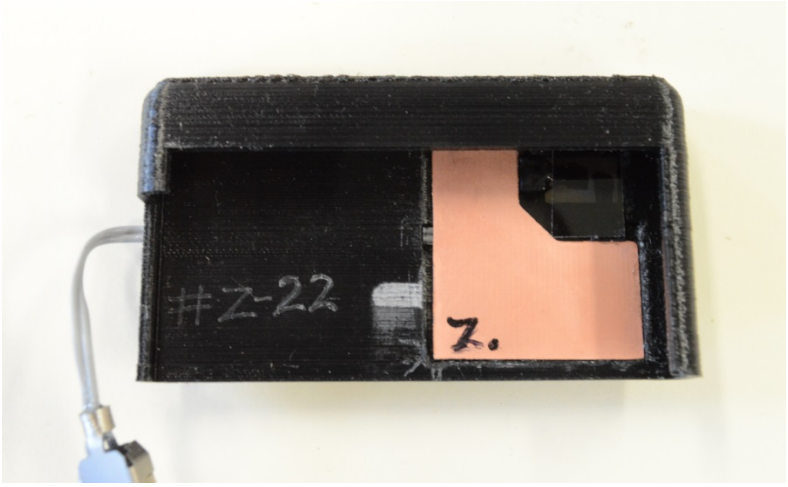

Figure 57 – The PCB was inserted into a recess in the back of the adapter and fixed in place with UV curing adhesive.

Finally, a cover cut from a 1mm thick high-impact polystyrene sheet (Hindley, St Austell, UK) using a TMX65 CO2 laser cutting machine (CTR Lasers) was fixed over the front face of the device, covering the electronics in order to protect them from damage. In addition, the portion of the USB OTG cable that ran along the front face of the device was also fixed in place with cyanoacrylic glue (DIY Time Super Glue, Poundland).

Figure 58 – The completed adapter in-place on a Sony Xperia Z3.

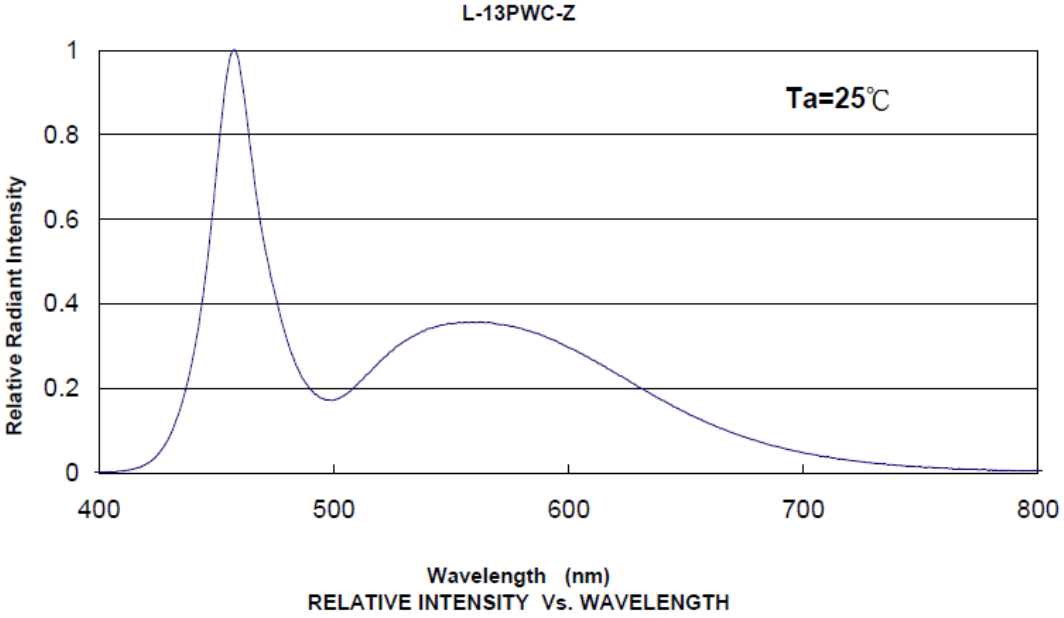

Figure 59 - Spectral distribution of the optical output of the LEDs used in the prototype (282).

A fully assembled prototype of the third design iteration is shown atop a Sony Xperia Z3 Compact in Figure 58. A full list of the materials used to construct the prototypes is shown in Appendix 5.5.

5.6.4 Performance Testing

5.6.4.1 Methods

5.6.4.1.1 Safety testing

As the device no longer relies on the phone flash, each of the components comprising the illumination sources in this iteration of the design were selected in the design stage, rather than being dictated by the smartphone's design. Thus, more was known about the spectral distribution of the light sources meaning that direct measurement of this was not necessary. However, to verify the optical safety of the device it was still necessary to measure the optical power entering the eye, as it was not possible to calculate this accurately owing to the bespoke nature of the prisms. As with the previous iteration, the design was deemed optically safe if it conformed to ISO 15004-2.2: 2007 (270).

Data pertaining to the spectral distribution of the LEDs used in the prototype, a graph of which is shown in Figure 59, was provided by the manufacturer upon request. The only other component having a significant impact on the spectral distribution was the linear polariser, the spectral transmission of which is shown in Figure 60. The spectral output of the assembled illumination system could therefore be determined by multiplying the relative radiant intensity for each spectral component of the LED by the transmission proportion of the polarising filter for the same spectral component.

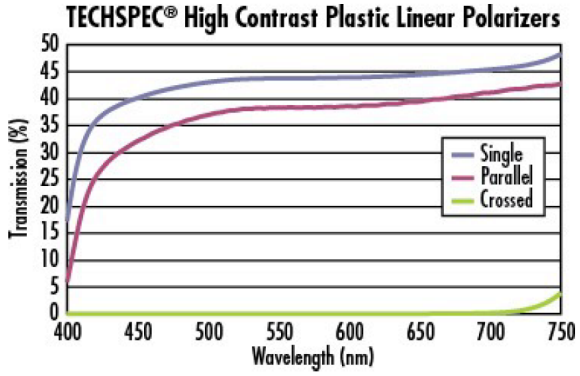

Figure 60 - Transmission spectrum of the linear polariser used in the prototype (283).

	Parameter	Safe Limit	Calculated Value
5.4.1.1	Weighted corneal and lenticular ultraviolet radiation irradiance	0.4 μW/cm^2	N/A
5.4.1.2	Unweighted corneal and lenticular ultraviolet radiation irradiance	1 mW/cm^2	N/A
5.4.1.3b	Weighted retinal radiance	2 mW/(sr·cm^2)	0.0710 mW/(sr cm^2)
5.4.1.4	Unweighted corneal and lenticular infrared radiation irradiance	20 mW/cm^2	0.124 μW/(sr cm^2)
5.4.1.5	Unweighted anterior segment visible and infrared radiation irradiance	4 W/cm^2	Exempt
5.4.1.6b	Weighted retinal visible and infrared radiation thermal radiance	6 W/(sr·cm^2)	0.113 mW/(sr cm^2)

Table 17 - Light hazard protection parameters, as defined by BS EN ISO 15004-2:2007, with the safe limits and the values calculated for the brightest prototype when used within the methods described for the performance testing below (270).

Optical power readings for each prototype were then acquired using the method as previously described for the prototype of the second design iteration. Likewise, these measurements were used in the same manner so to generate values for each of the relevant parameters detailed in BS EN ISO 15004-2:2007, namely 'weighted retinal radiance', 'unweighted corneal and lenticular infrared radiation irradiance' and 'weighted retinal visible and infrared radiation thermal radiance'. As the spectral distribution provided by the manufacturer specified that no light with a wavelength less than or equal to 400nm was produced, values for the 'weighted corneal and lenticular ultraviolet radiation irradiance' and 'unweighted corneal and lenticular ultraviolet radiation irradiance' were not calculated and assumed to be equal to zero.

5.6.4.1.2 Testing on a healthy volunteer

Performance testing was conducted on a healthy volunteer (27-year-old white British male) as per the methods described in 5.4.3.2.3. For comparison these methods were also repeated on the same eye using the prototype of the second design iteration.

5.6.5 Results

5.6.5.1 Safety testing results

The calculated values of each of the light hazard parameters, shown in Table 17, were found to be well within the safe limits.

As per the previous design, the prototype was exempt from the limit to the 'unweighted anterior segment visible and infrared radiation irradiance' owing to it having a diverging, rather than converging, illumination source.

5.6.5.2 Results of testing on a health volunteer

Videos of the white British 27-year-old male's eye were recorded using the prototype of the third design iteration and the prototype of the second design iteration for comparison.

The images extracted for quantitative analysis are shown in Figure 61.

As can be seen in Figure 61d-f and quantitatively in Table 18, a substantial area around the optic nerve was imaged. Shadowing was virtually non-existent, however the prisms did protrude into image obscuring the very periphery of the camera's

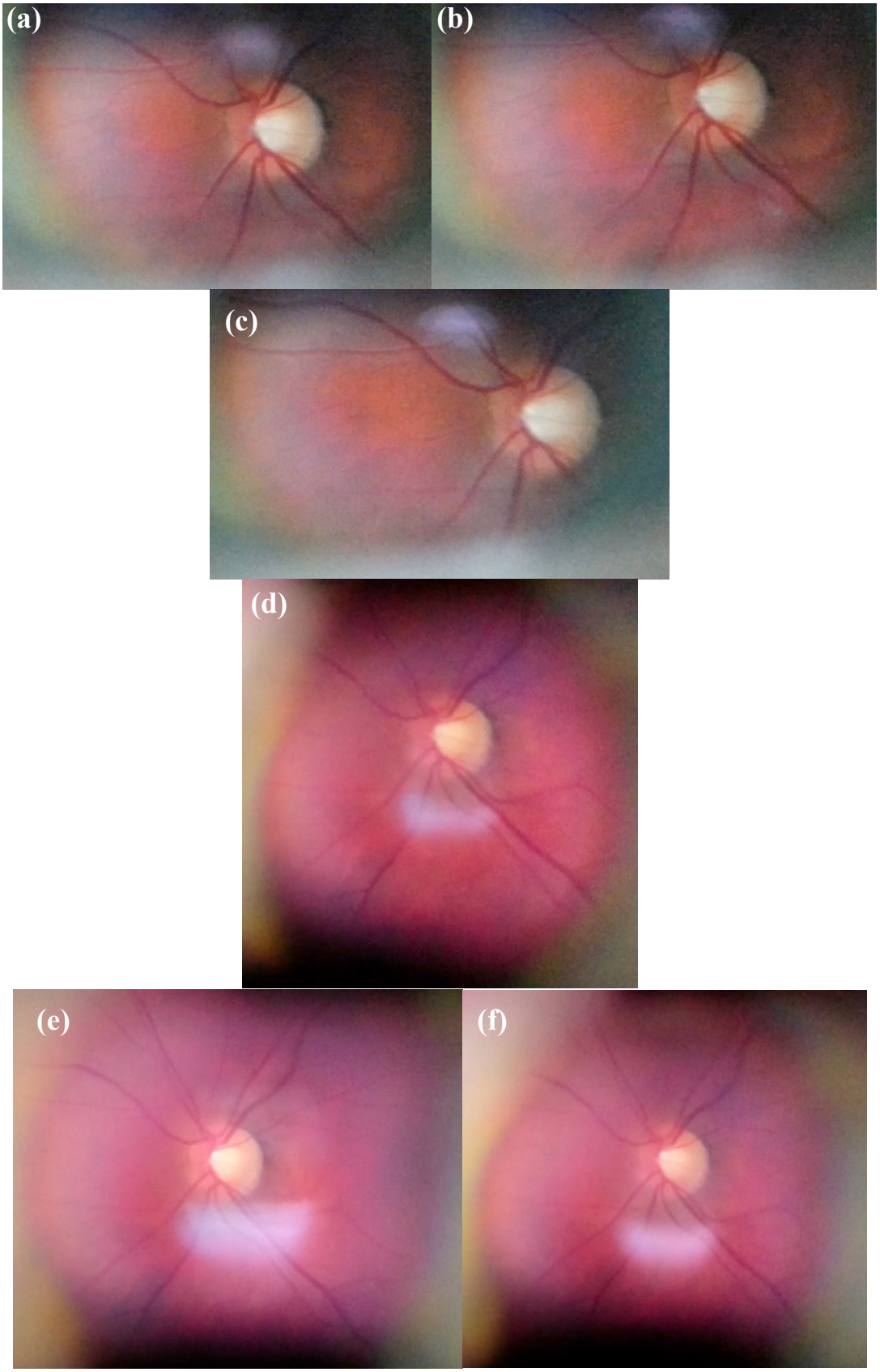

Figure 61 - Ocular fundus images of the same healthy volunteer (27-year-old white British male) acquired with (a-c) a prototype of the second design iteration and (d-f) a prototype of the third design iteration.

field-of-view of the ocular fundus. According to basic geometry and assuming the optic disc is circular and subtended by a cone whose apex is in the centre of the cornea and apex angle is the typical 6° (280), the area of the ocular fundus visible was equivalent in size to an arc of the retina subtended by a cone with an apex angle of (30.1±4.0)°. This compared to (21.7±2.4)° for the same estimate in the same eye when imaged with the prototype of the second design iteration.

Two-sided, two sample t-tests found that with the prototype of the third design iteration there was a significantly greater area of ocular fundus visible and a significantly smaller proportion of ocular fundus under shadow (p values: 0.0003 and 0.023 respectively). The area of ocular fundus obscured by the corneal reflection was not found to be significantly greater than in the images acquired using the prototype of the second design iteration (p = 0.305).

The two light sources in the prototype of the third design caused considerably different intensities of corneal reflection. The upper reflection was so faint that it was difficult to identify in the extracted frames and could not be quantified in terms of area or weighted pixel intensity. However, the lower reflection was found to be significantly more intense than that caused by the single prism of the second design iteration (Mann-Whitney U test; $W=5.3x10^{9}$; $p=2.2x10^{-16}$). Nevertheless, it was still possible to see certain features of the ocular fundus directly under the corneal reflection with both prototypes, such as large retinal vessels which can be seen identified in Figure 61d-f.

Design	Mean visible fundus (±S.E.)	Mean % fundus under shadow (±S.E.)	Mean corneal reflection size (±S.E.)	Mean corneal reflection weighted pixel intensity (±S.E.)
Design iteration 2	(10.2±0.8)DA	(45.6±1.6)%	(0.29±0.01)DA	88.5±16.4
Design iteration 3	(19.8±1.8)DA	(13.9±0.9)%	(0.664±0.277)DA	98.1±30.2

Table 18 - Results of the image analysis on selected images of the ocular fundus of the same healthy participant acquired with prototypes of the second and third design iteration. DA = optic disc areas.

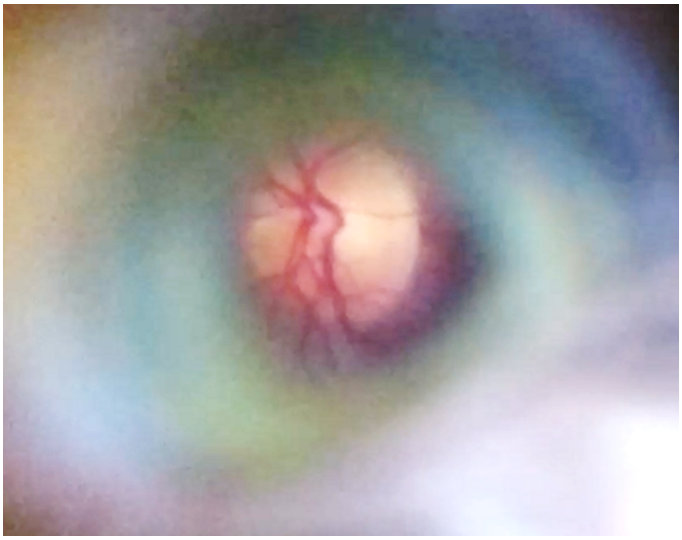

Figure 62 - An example image acquired from the undilated eye of a 22-year-old white-British female. No shadowing or specular reflections originating from the adapter optics are evident. The entire optic nerve is visible including fine details such as small blood vessels.

The performance of the prototype at smaller pupil diameters was also assessed by imaging the ocular fundus of a 22-year-old white-British female. As can be seen in Figure 62, the entire optic nerve could be visualised with several minor vessels being visible.

5.6.6 Discussion

The third iteration of the smartphone ophthalmoscope design was a notable improvement on the previous designs with regards to shadowing and the overall field of view. The corneal reflection caused by one of the illumination sources was essentially non-existent whilst the other was more intense than that of the prototype of the second design iteration. This highlights the need for very precise alignment when using linear polarisers to eliminate such reflections.

As both the optics and electronics were hosted on a single PCB, the design can be easily adapted to other phone models by redesigning the plastic housing. This redesign only requires that it fit the phone and position the PCB so that the optics are centred on the phone's camera, with a redesign of the optics or PCB layout themselves not being necessary.

5.7 Discussion

After undertaking three design iterations, a design was arrived at, prototypes of which demonstrated that it fulfilled the aim of providing a means to stimulate the field of CEHW accessible smartphone ophthalmoscopy.

The prototypes were able to capture images of very good quality, with details such as small blood vessels (Figure 62) and small lesions being visible, even with the second iteration of the prototype (Figure 50). The field-of-view, at up to 30° subtended angle on the retina, was far in excess of that of a classical direct ophthalmoscope and approaching that which is required for single image retinal screening (284). By taking a number of images centred on each of the optic nerve, macula and the retinal arcades this full area could be imaged.

Unwanted reflections were reduced in successive design iterations until these were no longer apparent in eyes without any lens or corneal opacities, provided that

Linear polarising filters could be installed with sufficient precision.

The prototypes were shown to be well within the safe limits for phototoxicity specified in ISO 15004-2.2: 2007 (270). Confirming conformance to this standard is something which is often overlooked in the scientific literature describing such devices, yet is a vital requirement in ensuring the device does not harm patients (285). Furthermore, the mechanical designs were such that this also posed minimal risk of harm, with it not being difficult to contact the participant's eye whilst using the prototypes as intended, and with no adverse events being reported.

The design was also robust enough for field use with few breakages being reported from field studies supplied with prototypes. This is an important factor given the challenges of working in the community in LMICs. For example, there are often no tarmacked roads in such locations resulting in the prototypes being exposed to extreme vibrations in transit and the CHW having to travel moderate distances on foot, exposing the prototypes to the elements.

Non-clinicians were capable of consistently capturing images whilst continuing to satisfy each of the above requirements in younger, healthy eyes. Poorly cooperating patients or patients with lens or corneal opacity present a problem however. Patients who find it difficult to fixate, for example, make it more difficult to ensure that every necessary area of the ocular fundus is adequately imaged. Careful training is therefore required and is suggested for subsequent studies. Ideally, a future version of the device would make use of software hosted on the phone that would guide the user through the process of capturing each view of the retina and even automatically capture an image when a new area of the retina is visualised.

Furthermore, it was generally perceived amongst users that, all else being equal, the Samsung Galaxy SIII allowed higher quality images of the fundus to be captured than the Sony Xperia Z3. This was despite the Z3 camera's superior resolution and performance in low-light conditions alongside its superior processing power and memory. It would therefore be highly beneficial to have a set of performance tests that could provide a better indication of a smartphone's suitability for ophthalmoscopy than can be derived from their specifications alone. An example of

such would be standardised quantitative evaluation of the resolution at which the retina is imaged by production of an eye model with an appropriate resolution target, such as an adapter version of the USAF 1951 target (183). Given the high pace of the mobile technology market, with updated iterations of specific smartphone models being released on an annual basis, this would allow both designers and end-users to select the most appropriate device for conducting fundoscopy without having regularly to test a selection of devices on a cohort of real eyes.

A universal adapter that has the flexibility to attach to phones of different dimensions would therefore be desirable as it would, to a degree, help to decouple the smartphone ophthalmoscope development process from the general smartphone market. Indeed, it was found that even within the same phone model slight differences in device dimensions exist meaning that adapters built to fit a certain handset precisely may not adequately fit those used in the field.

Having tested the above specifications in a lab environment, the next stage was to deliver prototypes to appropriately powered field studies to test these in real-life circumstances across a representative sample of eyes. To this end clinical validation of the prototypes was integrated into an ongoing study in SSA. 'The Nakuru Eye Disease Cohort Study', funded by the Medical Research Council and conducted by the International Centre for Eye Health at the London School of Hygiene and Tropical Medicine, involved the comparison of the vertical cup-to-disc ratio measured in images of 2000 eyes taken with a desktop retinal camera by a trained retinal photographer versus those taken with smartphone ophthalmoscope prototypes by a non-specialist eye worker (179). This study is described in more detail in section 6.1.

In addition to providing evidence of the repeatability in the field of the results found in the lab, the data from these studies were also to be used to seed analysis of the clinical workflow. The aim of this analysis was to gain insight into factors frequently cited as a barrier to mHealth adoption. Foremost of these, as highlighted in Figure 5 in Chapter 2, being a paucity of data on health system impact for which clinical workflow analysis is key. Furthermore, such analyses will also help gain understanding of other key barriers such as implementation costs, ongoing costs and the human resources and skills required. This in turn will provide further

specifications not only for a final design for mass adoption of the smartphone ophthalmoscope, but for the mass adoption of mHealth devices within eye care in general. In addition, the results ought to act as a useful resource for ensuring better strategic alignment of mHealth product and implementation design with the goals of health managers and health provider strategies.

To this end, the next chapter describes a retrospective clinical workflow analysis of The Nakuru Eye Disease Cohort Study and the placement of mHealth devices within this study. A validation study of a prospective modelling of the clinical workflow of DR screening with the smartphone ophthalmoscope in the Kilimanjaro region is also planned, details of which are given in the chapter discussing future works.

SECTION 3

Chapter 6 - Retrospective Analysis of the mHealth Devices in the Nakuru Eye Disease Study

6 Retrospective Analysis of the mHealth Devices in the Nakuru Eye Disease Study

"I'm deeply convinced that we need… different ways of approaching health, particularly in low income settings. Simply transposing systems from Europe, that are demonstrably failing, and trying to impose [these] on countries that are developing systems is not going to work and it's actually, I think, unethical." – Prof. Peter Piot, Director of London School of Hygiene and Tropical Medicine (The Peek social impact story: how technology and knowledge is increasing access to eye care, London, April 2017)

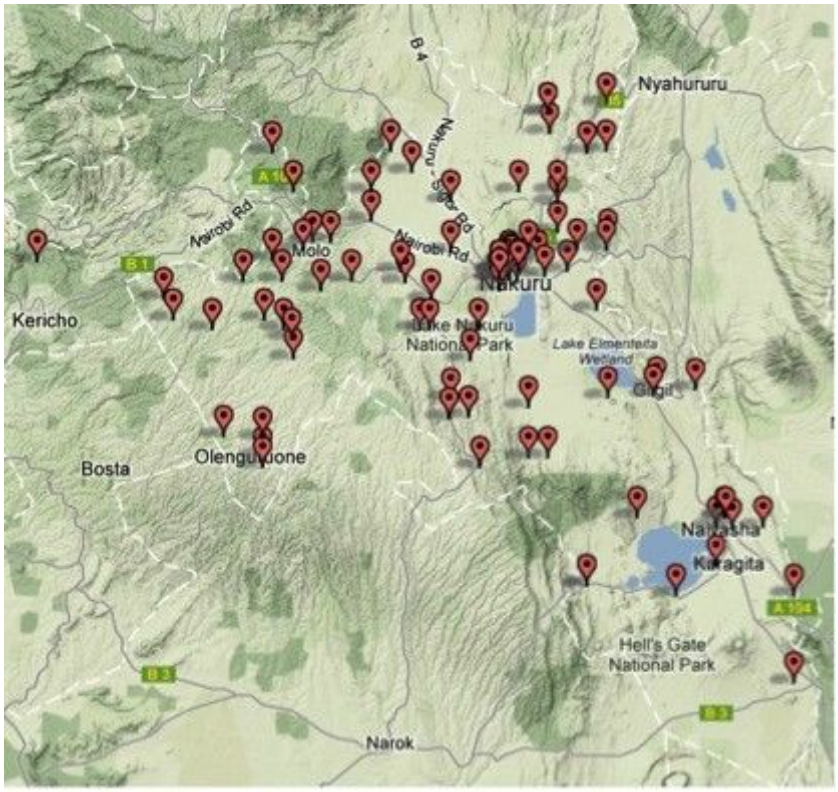

Figure 63 - Location of population clusters in Nakuru county (179). Image reproduced under Creative Commons CC BY 4.0 License[17].

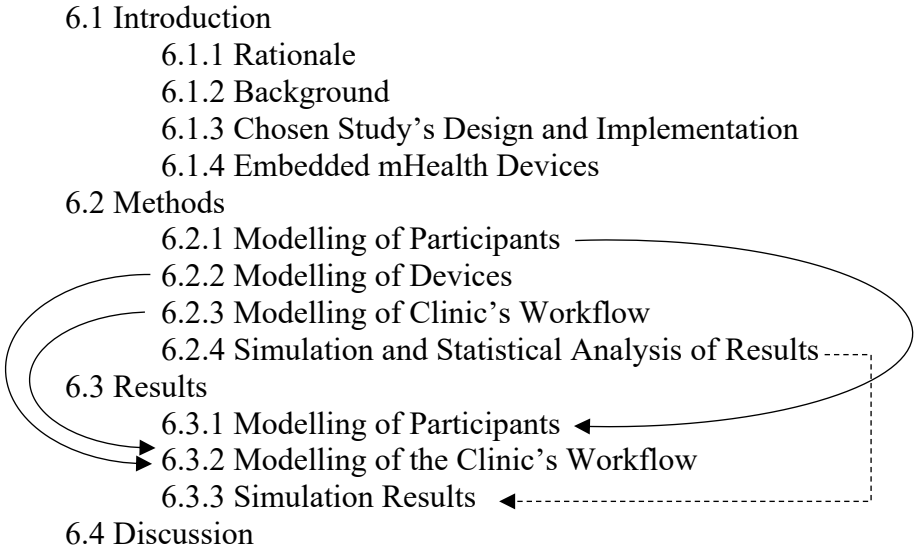

Figure 64 – Chapter organisational diagram. Arrows indicate the relationship between the methods used to build specific models or simulations and the results generated by applying these methods.

[17] License available at: https://creativecommons.org/licenses/by/4.0/legalcode

6.1 Introduction

6.1.1 Rationale

As was noted in Chapter 2, the most cited reason for successfully piloted mHealth devices failing to be adopted at scale is a paucity of data on health system impact. To assess this impact clinical workflow analysis is key. Furthermore, such analyses will also help gain understanding of other key barriers such as implementation costs, ongoing costs and the human resources and skills required.

The aim of this chapter is to conduct such a workflow analysis using the tools and techniques discussed in Chapter 4 in order to provide further specifications for a final design for mass adoption of the smartphone ophthalmoscope described in the previous chapter. Furthermore, it is expected that such analysis will also provide insights into requirements for the mass adoption of mHealth devices within eye care in general.

Additionally, the results ought to act as a useful resource for ensuring better strategic alignment of mHealth product and implementation design with the goals of health managers and health provider strategies.

Figure 64 contains a chart showing the structure of this chapter. The chapter begins with a description of the study chosen as the basis for the model (6.1.2 and 6.1.3), including the mHealth devices embedded within the study (6.1.4). This is followed by a description of the methods used to model the study population (6.2.1), devices (6.2.2) and the clinic workflow (6.2.3) involved in the study. Next, the methods used to run a series of simulations based on the models generated by the aforementioned modelling techniques is described (6.4). Finally, the results of applying all of the described methods are then detailed (6.3.1, 6.3.2 and 6.3.3) and discussed (6.4).

6.1.2 Background

The study chosen for the baseline workflow analysis was ‘The Nakuru Eye Disease Cohort Study’ (179). This recent study has provided a wealth of information regarding eye health in a low-income country (287-289). It involved the deployment of a temporary eye clinic with mHealth screening solutions being implemented both

in participants' homes and in the clinic alongside reference standard diagnostic equipment originally designed for hospital-based use. Furthermore, as is often the case in low-income countries, the clinic's workflow lacked complex interactions with other parts of the healthcare system, performing the screening, triage and referral functions in almost complete isolation.

6.1.3 Chosen Study's Design and Implementation

The study was a follow-up of fieldwork carried out during 2007 and 2008. During the baseline study 4414 participants aged 50 years and above and distributed across 100 population clusters, shown in Figure 63, underwent ophthalmic and general examinations (290). The follow-up involved the completion of ophthalmic examinations of 2185 of the baseline study's participants between 2012 and 2014.

The original study participants were retraced by contacting a local community leader, such as a church pastor or village elder, by phone and then deploying an advance team consisting of a local guide, a nurse and one field officer a day prior to the examination clinic.

At the examination clinic, participants were registered, following which they underwent anthropometry (height, weight, waist and hip circumference, bioimpedence, blood glucose and three blood pressure measurements), autorefraction, visual field, anterior segment, intraocular pressure and gonioscopy. The participants' pupils were then pharmacologically dilated, following which fundus photography and a dilated slit lamp examination, assessing the lens, optic disc and macula, were conducted. Data were recorded on paper records that were subsequently entered into a computer database. The only exceptions to this were the visual fields data as well as the fundus and anterior segment images which were sent securely to Moorfields Eye Hospital, London for grading and image quality assessment.

The clinic was staffed by an ophthalmologist, two ophthalmic nurses and a number of clinical officers.

6.1.4 Embedded mHealth Devices

Two prototype mHealth devices were embedded within the study's principal workflow. The Samsung Galaxy S3 based smartphone ophthalmoscope described in the previous chapter was inserted into the clinic in parallel to the desktop retinal camera. Fundus images from both the smartphone-based ophthalmoscope and retinal camera (CentreVue+ Digital Retinal System, Haag-Streit) were subsequently sent to Moorfields Eye Hospital, London for blind optic nerve grading.

Also deployed to the clinic was the 'Peek Acuity' tumbling E visual acuity test described in Chapter 3. This was used in the clinic in parallel to Snellen and ETDRS charts and in participants' homes in parallel with a Snellen chart.

Data from 2185 of the 4414 original study participants were acquired over the course of the Nakuru study. This included data from 300 participants concerning the efficacy of Peek Acuity and data from 2152 eyes concerning the efficacy of the smartphone ophthalmoscope with respect to optic nerve imaging.

Having received this data shortly after the completion of the study in March 2014, the clinical workflow analysis described in this chapter could then begin.

6.2 Methods

6.2.1 Modelling of Participants

The participant data were used to build a statistical model of patients of the same age range. The data collected included information relating to demographic, socio-economic and general health data as well as direct measures of eye health. For simplicity and simulation efficiency, those measures that were not directly related to the presence or absence of the conditions comprising at least one referral criterion were removed from the dataset used to construct the model, with the exception of age due to its strong correlation to eye health (17).

In order to make the data suitable for building a predictive model of a study participant, first any categorical values that were not part of an ordered set were removed and placed in a separate Boolean variable. For example, the VCDR would

ordinarily be recorded as a ratio between 0 and 1, however if an ocular opacity, such as a dense cataract, were to make grading of the disc impossible the VCDR was recorded as “cannot classify”. As such a new Boolean variable, ‘canFundus’, was created for each patient which was given the value 1 for every participant who had a ratio recorded and 0 for every participant whose VCDR was recorded as “cannot classify”. In addition, any variables that contained only a single value across all participants were noted and removed from the statistical analysis.

Boolean data types were converted to numerical equivalents by setting one value to 0 and the second to 1. Ordinal data types were converted to numerical equivalents by setting each value to the appropriate integer within a scale between 1 and the total number of values. Having converted all Boolean and ordinal data types to numerical equivalents, the data were then scaled, missing values replaced and suitable functions for each variable found using the R script shown in Appendix 6.1. Each data point was centred and scaled by subtracting the mean of the variable and dividing by the standard deviation.

As only 985 of 2185 participants had data recorded for every variable, it was necessary to replace missing data values within the dataset, rather than excluding those participants with missing data, in order to prevent potential bias and a substantial loss of precision and power. Data was known to be missing for a variety of reasons including corneal or lenticular opacity obscuring view of the retina and breakdown of the generator powering the clinic’s slitlamp, fundus camera and visual fields analyser. As visual acuity was available for the vast majority of participants, the data could be said to be missing at random and hence missing data could be replaced by multiple imputation. Multiple imputation is a general statistical approach which deals with the issue of missing data by creating multiple copies of the data with the missing values replaced by imputed values sampled from their predictive distribution based on multiple regressions of the observed data (291). Covariates in these multiple regressions include every other variable, whether observed or imputed (292). The regression model then forms the posterior predictive distribution with a non-informative prior distribution being used for the parameters in the regression model (292). The process of imputing missing values can be continued in a cyclical manner building interdependence and exploiting

correlation among the covariants (292). Multiple imputations can be generated by varying the random starting seed for a succession of imputation 'chains' (292). The 'Multiple Imputations with Diagnostics (mi)' package in R, which employs the bootstrap method to generate random imputations, was used to generate four imputation chains with 30 iterations on each chain (293).

A Spearman's correlation matrix for the dataset was then created across all of the remaining variables. Each of the statistically insignificant correlations ($p>0.05$) were removed from the matrix and the Cholesky decomposition of this matrix was found. Each variable was then investigated in isolation by using the method described by Gentle to remove the influence of the other co-variates on each variable (294). That is, by using the relationship described in **(9)** on the dataset,

$$\boldsymbol{P}_{norm} = \boldsymbol{P}_{uncorr}\boldsymbol{U} \qquad \textbf{(9)}$$

where $\boldsymbol{P}_{norm}$ and $\boldsymbol{P}_{uncorr}$ are the normalised, correlated and uncorrelated representations of one or more participants respectively and $\boldsymbol{U}$ is the Cholesky decomposition matrix of the correlation matrix.

For each of the variables in the cleaned, 'uncorrelated', dataset the goodness of fit for a number of common distributions were assessed using Minitab 17 (Minitab Inc., State College, PA, USA) using the 'individual distribution identification' function. These distributions included the normal, lognormal, exponential, Weibull, gamma, logistic and log-logistic. The function also applies the Johnson SU and Box-Cox transformations to the data and an attempt made to fit the distributions (295, 296). For each variable that could not be adequately described by at least one of the aforementioned common distributions (i.e. goodness of fit with $p<0.05$), an interpolated fit to the CDF was sought instead. To avoid overfitting as far as possible an interpolated fit using three points in the empirical cumulative distribution function (ECDF), at the beginning, middle and end, was first attempted. The appropriateness of the fit to the CDF was first assessed by comparing such to empirical cumulative distribution function (ECDF) using the Kolmogorov-Smirnov test (KS test) (297). If the test returned a p-value greater than 0.9 then the fitted curve was taken to be an adequate fit of the data. If the fitted curve was determined not to be a good fit then an interpolation using four equally spaced points from the

```
{Details=
        {ClusterId=1, StudyId=17, Age=58, blood_sugar=4.7,
        DM_diagnosis=false, DM_aware=false, will_travel_to_clinic=282},
LeftEye=
        {can_autorefract=true, visual_acuity=0.66, spherical_error=0.75,
        cylindrical_error=-1.25, VCDR=0.3, visual_field_loss=1, IOP=13, DR=1,
        DMac=false, AMD=1, needs_catarct_surgery=0,
        can_examine_fundus=true,
                DevMeasure=
                {DeviceVA=0.0, AutoSphere=0.0, AutoCylinder=0.0,
                DevCatSurg=0, DrGrade=1, DMacGrade=false, AmdGrade=1,
                VcdrGrade=0.1, TabVF=false, PuffTest=0}},
RightEye=
{can_autorefract=true, visual_acuity=1.06, spherical_error=-0.25,
        cylindrical_error=-0.75, VCDR=0.2, visual_field_loss=1, IOP=14, DR=1,
        DMac=false, AMD=1, needs_catarct_surgery=0,
        can_examine_fundus=true,
                DevMeasure=
                {DeviceVA=0.0, AutoSphere=0.0, AutoCylinder=0.0,
                DevCatSurg=0, DrGrade=1, DMacGrade=false, AmdGrade=1,
                VcdrGrade=0.1, TabVF=false, PuffTest=0}},
CompletedTests=
        {TumblingE=false, Autorefractor=false, FoV=false,
        UndilatedSlitlamp=false, DilatedSlitlamp=false, UndilatedDrs=false,
        DilatedDrs=false, GlassesFitting=false, BloodGlucose=false}}
```

Code Extract 1 - The CPN SML custom record modelling a participant. The record comprises four records holding data concerning: patient details ('Details'), actual and measured eye health parameters for each eye ('LeftEye' and 'RightEye') and the tests which the participant has undergone in a given simulation ('CompletedTests').

full range of the ECDF was assessed using the same method. This process was repeated until a good fit was found or until every point in the ECDF was included in the interpolation.

In order to allow individual representations of patients to pass through a CPN and interact with its simulation logic, it was necessary to represent individual patients as a vector containing values selected from each of the probability distributions calculated using the above method. The R script that achieved this is shown in Appendix 6.2. The appropriate correlation between each of the vector's variables was then assured by again using the relationship shown in equation (10) as per the method outlined by Gentle (293). For each participant, a vector containing meaningful values for each variable could then be found through equation (10),

$$\boldsymbol{P} = \left(\frac{\boldsymbol{P_{norm}}}{\boldsymbol{s_s}}\right) - \boldsymbol{s_c} \qquad \textbf{(10)}$$

where $\boldsymbol{P}$ is a matrix of all of the included variables which are appropriately correlated for one or more participants, $\boldsymbol{s_s}$ and $\boldsymbol{s_c}$ are matrices containing the scaling factors and the centring constant, originally applied to normalise the study data, repeated over a number of rows equal to the number found in $\boldsymbol{P}$ and $\boldsymbol{P}_{norm}$.
An example of a vector modelling an individual patient, as represented in CPN SML code, is shown in Code Extract 1. The patient vector comprises four records, describing general patient details, the left eye, right eye and which tests the patient has undergone. As describing the presence and severity of each of the eye conditions of interest[18], the eye records also contained a sub-record ("DevMeasure") for recording the results of the various examinations conducted throughout the clinical workflow.

[18] No, mild, moderate and severe visual field loss were represented numerically as 1, 2, 3 and 4 respectively

$$PPV = \frac{Sensitivity \cdot Prevalence}{Sensitivity \cdot Prevalence + (1 - Specificity) \cdot (1 - Prevalence)} \quad \textbf{(11)}$$

$$NPV = \frac{Specificity \cdot (1 - Prevalence)}{(1 - Sensitivity) \cdot Prevalence + Specificity \cdot (1 - Prevalence)} \quad \textbf{(12)}$$

Device	Variable	Accuracy	Variance	Mean Exam Time (minutes)	Exam Time Variance (minutes)
Peek Acuity	VA (logMAR)	-0.055 logMAR	0.0608 logMAR	1.283	0.176
Peek Retina	VCDR	-0.070	0.0240	0.875	0.263

Table 19 - Model parameters for the mHealth devices

6.2.2 Modelling of Devices

Medical devices were modelled in one of two different forms based on the type of data that they acquired.

For those instruments that collected continuous numeric data the results of a Bland-Altman analysis against the gold standard were used to determine the device's 'variance' and 'accuracy'. The variance was found from the standard deviation reported in the Bland-Altman analysis and the accuracy was taken to be the mean difference. The measurement recorded by the device, for a given participant, was then taken from a normal distribution centred on the actual value of the parameter in question plus the device accuracy and with a variance equal to that of the device. Where the device in question was the gold standard, both the accuracy and variance were taken to be zero.

For devices measuring ordinal variables, the reported positive predictive value (PPV) provided the probability of a device identifying each category correctly. In the case where a category was not correctly identified then the device was assumed to report an adjacent category to that which the participant actually had. Where there were two adjacent categories, the probability of arriving at either was taken from the ratio of the negative predictive value (NPV) of the two categories. For devices considered to be the gold standard all PPVs and NPVs were set to 1.0.

Where PPV or NPV were not reported in the literature for the device, the relationships in **(11)** and **(12)** respectively were used to determine the predictive values. In both these equations, prevalence is defined as the proportion of people in a sample with the characteristic of interest.

For each type of device, the total time spent on a given examination was taken from a normal distribution centred on the reported mean examination time with a variance equal to that reported in piloting the device. This was achieved using R's rnorm function.

Using the results from the embedded analysis of Peek Acuity and Peek Retina in the Nakuru study, these devices could therefore be modelled as shown in Table 19.

In each case, the results when the device was operated by a lay examiner were used.

6.2.3 Modelling of Clinic's Workflow

The clinic and outreach flow was discovered by a combination of discussion with the lead investigator of the 'The Nakuru Eye Disease Cohort Study', by observation of two of the temporary clinics (one rural, one urban) and by observation of outreach to one cluster by an advance team during a field visit to the study. The discovered clinical workflow was recorded and revised in a UML diagram.

The workflow diagram was then used to inform the construction of a timed CPN of the study's flow using CPN Tools 4.0.1 (Eindhoven University of Technology, Eindhoven, Netherlands). Patient data were coded into a custom colour set within the model using the offline R script shown in Appendix 6.2.

Simulations of the CPN were run using the ProM 6.7 process mining workbench (Eindhoven University of Technology, Eindhoven, Netherlands). The same software package was also used to conduct process mining on the generated log files.

The CPN was then adjusted to determine which instrumentation returns:

- the best value-add for the advance teams; how many advance teams are optimal;
- how many ophthalmologists are needed within the system;
- how efficient surgical procedures need to be to avoid being the bottleneck in the system;
- how often a clinic ought to be run for a given area;
- how the density of population clusters affects the conclusions.

The model considered the following causes of blindness: refractive error, cataract, glaucoma and diabetic retinopathy. Of the other major causes of blindness, trachoma was excluded due to their being no data showing that it is endemic in Nakuru county (298). Indeed, Narok county, immediately to the South of Nakuru is known to be non-endemic for trachoma and thus it was assumed that incidence of trachoma was likely to be low enough in Nakuru to exclude it from the model (298). With respect to onchocerciasis, extensive entomological work has shown that its only vector in Kenya is the *Simulium naevi* species of black fly and that the species' distribution is restricted to Nyanza province in the West of the country (299). Thus, the disease

	RE (300)	**Cataract** (120)	**DR** (301)	**Glaucoma** (302)	**AMD** (302)
Discharge	VA≤0.2 logMAR or cylinder ≤ 0.5 (with ready-mades)	PSC<2, NUC<3	No DM	VCDR < 0.5 and no peripheral vision loss	No AMD
Optometrist Referral	VA>0.2 logMAR and cylindrical error > 0.75D	PSC<2, NUC<3	<R2	VCDR < 0.5 and no peripheral vision loss	No AMD
Non-urgent ophthal-mologist referral	N/A	PSC≥2 or NUC=3	R2 or M1	0.5≤VCDR<0.7 or peripheral vision loss	Early or inter-mediate AMD
Urgent ophthal-mologist referral	N/A	N/A	R3	VCDR ≥ 0.7 and peripheral vision loss	Advan-ced AMD
DM Clinic Referral	N/A	N/A	DM and <R2	N/A	N/A

Table 20 – Diagnostic criteria used in the community eye screening programme.

was also excluded from the model. As data on rarer conditions and relatively minor ailments, such as conjunctivitis, dry eyes, etc., were not recorded in the original study, they were not modelled in the CPN.

A participant was considered to have refractive error that could benefit from treatment if he or she had an uncorrected visual acuity worse than 0.2 logMAR and no other eye condition other than background retinopathy (300). Such refractive errors were deemed to be suitable for rectification with ready-made spectacles with spherical lenses only if the participant had a cylindrical error of no greater in magnitude than 0.75D (301). Those with refractive errors unsuitable for correction with ready-made spectacles were considered to be in need of referral to an ophthalmologist for a full subjective refraction.

Any participants with DM were considered to require a referral to a diabetes clinic and routine eye examination. Participants with pre-proliferative DR were considered to be in need of a non-urgent referral to an ophthalmologist whilst those with proliferative DR were considered to require an urgent referral to an ophthalmologist for treatment (301).

Finally, participants with either a VCDR of 0.5 or greater or who were suffering from some form of peripheral vision loss were considered to have referable glaucoma (132). Those with both a VCDR of 0.7 or greater and some degree of peripheral vision loss were deemed to be in need of urgent referral to an ophthalmologist (132).

Thus, all variables included in the above referral criteria, variables relating to the observation of these criteria or variables with a significant correlation to any of the criteria were included in ultimate patient model, with the rest being excluded.
A summary of the various referral criteria is shown in Table 20.

Whilst a number of participants did have spectacles, the vast majority of these had poor vision even when aided. It was therefore considered unnecessary for the model to take account of participants who had low vision which was adequately corrected for with spectacles, as this constituted very few participants.

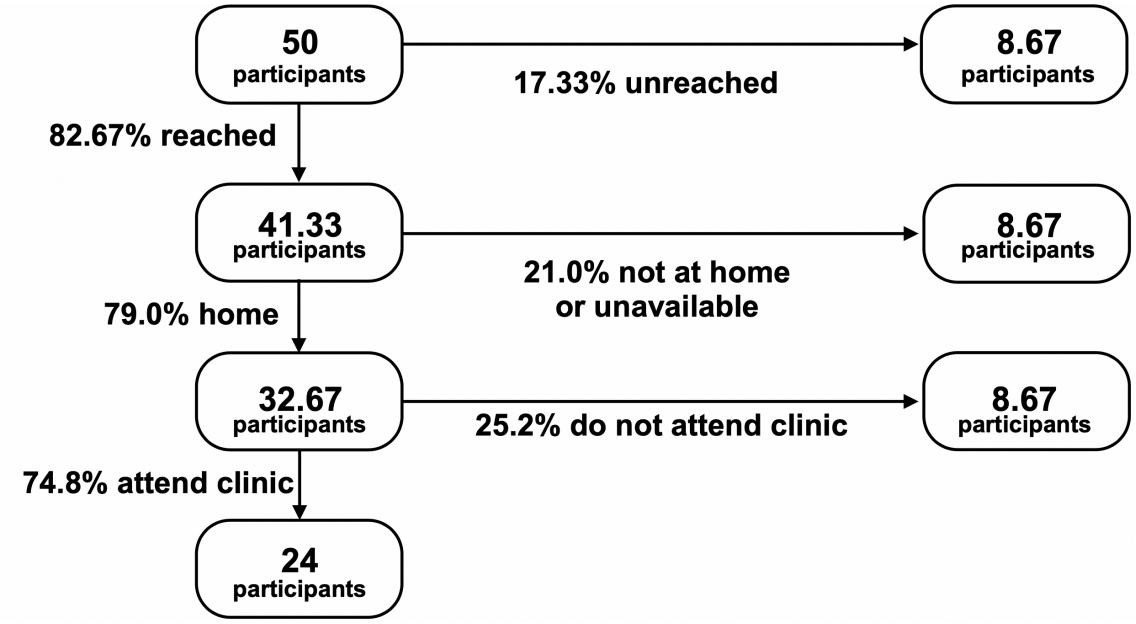

Figure 65 - Estimated probability of dropout at various stages in the flow of the participants in a population cluster of 50 participants.

In addition, none of the study participants was found to be taking anti-glaucoma medication and therefore the model assumes all participants found to have referable glaucoma are in need of referral.

It was estimated that of those patients who did not arrive at the clinic, one third could not be reached, one third were not reached due to time constraints, one third were reached but chose not to attend the clinic. As is shown graphically in Figure 63, it therefore follows that, as 52.0% of baseline participants did not present at clinic, 21.0% of those whose homes are reached cannot be contacted due to not being home or otherwise uncontactable. Thus, 25.2% of those who are contacted do not attend clinic. This is represented graphically in Figure 63.

Hence, the mean time spent traveling between houses could therefore be estimated to be 6.53 minutes if the time spent by the advance team at each cluster is approximated to eight hours and the time spent counselling each patient is five minutes. It was estimated that 95% of travel between houses fell within 5 minutes of the mean implying a standard deviation of 1.25 minutes.

6.2.4 Simulation and Statistical Analysis of Model

Simulations based on the CPNs were then run in ProM 6.7. As each simulation run consisted of over 100,000 steps and ProM saves logs to RAM until they are exported, a maximum of eight simulations were run in sequence. The resulting log file was separated by simulation run identifier (trace index) to allow analysis of each simulation run in turn. The log file was then filtered so to create one file with only outcome events and another with only the 'start clinic' and 'end clinic' events. For the outcome events, an HTML file containing a log summary was then exported for analysis in Microsoft Excel 2016 (Microsoft Corp., Redmond, WA, USA). A Petri net containing only the clinic start and end events was created using the inductive miner process in ProM. The file containing only the start and end events was then replayed on this Petri net, creating a comma-separated values file from which the clinic durations could be easily extracted in Excel.

The total number of simulation iterations required, R, was determined after the initial sixteen runs using the method adapted from that of Banks and colleagues as

Variable	D	p	Interpolation Points
Age	0.0332	0.0163	2185
RE: VA	0.0117	0.926	51
LE: VA	0.0116	0.931	97
RE: Can Autorefract	0.0120	0.912	89
RE: Sphere	0.0113	0.944	52
RE: Cylinder	0.0115	0.934	22
LE: Can Autorefract	0.0111	0.949	103
LE: Sphere	0.0120	0.913	45
LE: Cylinder	0.0122	0.902	45
RE: IOP	0.0119	0.919	90
LE: IOP	0.0116	0.933	99
RE: Cataract	0.0119	0.916	86
LE: Cataract	0.0115	0.933	130
Non-fasting Blood Glucose	0.0105	0.969	65
Taking Diabetes Medication	0.0122	0.902	97
RE: Visual Fields Loss	0.0118	0.919	97
LE: Visual Fields Loss	0.0120	0.912	95
RE: Can Examine Fundus	0.0118	0.920	35
LE: Can Examine Fundus	0.0121	0.908	31
RE: VCDR	0.0120	0.912	59
LE: VCDR	0.0112	0.947	26
RE: DR	0.00991	0.983	44
LE: DR	0.0120	0.912	26
RE: Diabetic Maculopathy	0.0120	0.911	52
LE: Diabetic Maculopathy	0.0112	0.947	41
RE: AMD	0.0120	0.911	41
LE: AMD	0.0116	0.931	45

Table 21 – Interpolation points used in chosen curves for each participant co-variant alongside the Anderson-Darling test statistic, D, and p-value for the curve's fit to the relevant study data.

described by Baudais and colleagues (303). This involves solving the inequality shown in **(13)** for each of the model's outputs.

$$R \geq \left(\frac{Z_{\alpha/2} S_0}{\varepsilon}\right)^2 \quad \textbf{(13)}$$

In this context, $Z_{\alpha/2}$ is the t-statistic for the student-t test at the chosen confidence limit of 0.05, S_0 is the sample standard deviation for the output parameter across the initial runs and ε is the specified error, which is the confidence limit multiplied by the mean of the output parameter across all the initial runs, x_0. The simulation was then run for an additional number of runs equal to the maximum R calculated across all output parameters, rounded up to the nearest integer.

The sensitivity and specificity of advance team screening and each clinic referral type were then calculated in Excel. In addition, the proportion of participants who were in need of a particular referral or treatment type and who went on to get this was calculated for screening and each referral type.

6.3 Results

6.3.1 Modelling of Participants

One patient who had aphakia in one eye was excluded from the analysis.

The results of the interpolated fits to the cleaned data are shown in Table 21. Other than for age, adequate fits, taken to be those returning $p > 0.9$ from a KS test, were found for each variable. For age the KS tests returned a maximum of $p = 0.0163$ even when all 2185 points were used to create an interpolation. It was therefore considered inappropriate to use an interpolated fit for this variable.

The parameters of the standard distributions that provided a reasonable approximation of all the variables are shown in Table 22.

Welch's Two Sample equivalence tests for unequal variances and sample sizes suggested that there was equivalence between the means of each of the generated populations and the test subset of the population data ($p<0.0001$ for each) (304). The only exception was age for which the null hypothesis of statistical difference was not rejected ($p=0.3067$).

Variable	Johnson SU Transformation	Distribution	Parameters	Anderson-Darling Statistic
Age	N/A	3-parameter Weibull	shape=1.6605 scale=1.7927 threshold=-1.5995	3.578 ($p<0.05$)
Right Sphere	γ=0.1802 η=1.3421;ε=0.1844 λ=1.0386	Normal	mean=-0.00948 SD=0.98448	0.481 (p=0.232)
Left Sphere	γ=0.02552 η=1.0913;ε=0.0171 λ=0.6804	Normal	mean=-0.00228 SD=1.01959	0.430 (p=0.308)
Left IOP	γ=-0.02148 η=0.901;ε=-0.0211 λ=0.4669	Normal	mean=-0.00228 SD=1.019	0.523 (p=0.183)
Can Exam Left Fundus	γ=0.07587 η=1.5190 ε=0.0049 λ=0.7304	Normal	mean=-0.01849 SD=0.9909	0.370 (p=0.424)
Left VCDR	γ=-0.9584 η=2.752;ε=-0.853 λ=2.267	Normal	mean=-0.02802 SD=1.007	0.524 (p=0.182)
Right DR Grade	γ=-0.09011 η=1.947 ε=-0.02790 λ=1.007	Normal	mean=-0.01228 SD=0.9858	0.414 (p=0.335)
Left DR Grade	γ=0.06817 η=1.845 ε=0.006322 λ=1.016	Normal	mean=0.00473 SD=1.014	0.224 (p=0.825)
Right Macular Oedema	γ=0.004723 η=1.204 ε=0.07729 λ=2.156	Normal	mean=-0.002 SD=0.9989	0.393 (p=0.376
Left Macular Oedema	γ=0.02413 η=1.720 ε=0.04269 λ=0.7877	Normal	mean=-0.00307 SD=0.9884	0.201 (p=0.882)
Right AMD	γ=0.5465 η=1.863 ε=-0.1923 λ=0.8190	Normal	mean=0.00347 SD=1.013	0.305 (p=0.569)
Left AMD	γ=0.2685 η=1.134 ε=0.1788 λ=0.5082	Normal	mean= -0.01224 SD= 0.99765	0.242 (p=0.771)

Table 22 – Distributions used to generate each co-variant describing a simulated participant.

6.3.2 Modelling of the Clinic's Workflow

The workflow diagram derived from discussion with the study lead investigator and direct observation of the clinic is shown in Figure 66.

All of the study participants are initially located within a population centre ((A) in Figure 66). As each of the clusters were sized so to contain fifty people matching the screening criteria of the original study (i.e. 50 years-of-age and above) the simulation program generates fifty participants per cluster. Upon generation, each patient record was populated with values for the each of the eye health parameters within the LeftEye and RightEye sub-records. These values were selected from the distributions listed in Table 22. In addition, willingness to travel to clinic independently selected from a value from 0 to 1000 according to a uniform distribution. Once contacted by the advance team, each participant would then progress to clinic registration ((C) in Figure 66) if their willingness to travel was above a certain threshold value (180, 0.18 being the proportion of study participants that were contacted during the NEDCS but did not subsequently travel to the clinic the following day). If their willingness to travel was below this threshold value then the participant's workflow would terminate with the record's final value being written to the log file.

Having registered, the participants would then progress to a station providing auto-refraction ((D) in Figure 66). As is the case with every device station described in this model, only one participant could occupy the station at one moment in time, forcing other participants to queue between the registration desk and auto-refraction. Next, the participants would progress to the waiting area where they would queue until either the VA station ((F) in Figure 66), visual fields station ((G) in Figure 66) or undilated slit lamp examination ((H) in Figure 66) became vacant. After completing this test, they would then be returned to the waiting area where they would queue until one of the remaining tests became vacant. They would repeat this process until they completed each of these tests after which they would progress to a station for the administering of dilating eye drops ((I) in Figure 66). Once fully dilated they would progress to a fundus camera station, once vacant, ((J) in Figure 66) before progressing for a dilated slit lamp examination ((K) in Figure 68). The

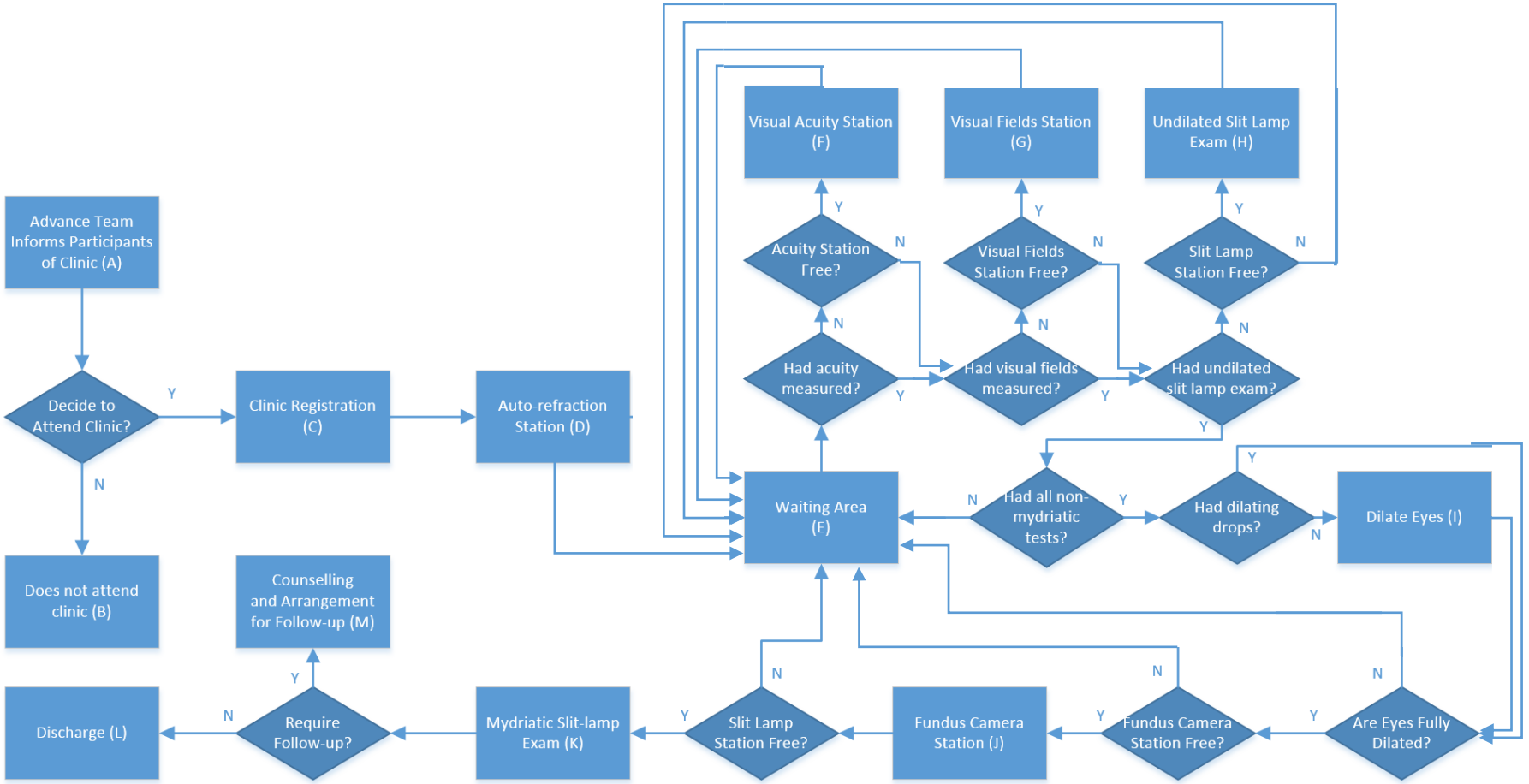

Figure 66 - Flow diagram of the clinic's workflow including advance team outreach.

undilated and dilated slit lamp examinations both involved the use of the same slit lamp and therefore only one of these stations could be occupied by a single participant at any given moment in time. Finally the patient would proceed for counselling and advice on necessary follow-up or treatment if required ((M) in Figure 66), with the participant's contact details being recorded for the arrangement of an appointment with and transportation to a specialist if follow-up or treatment was agreed upon.

This workflow was then translated into a timed, hierarchical CPN in CPN Tools. At the highest level, shown in Figure 67, the model involved loading the cluster data from file and then feeding each of these clusters, one at a time, to the 'Community Screening' subnet.

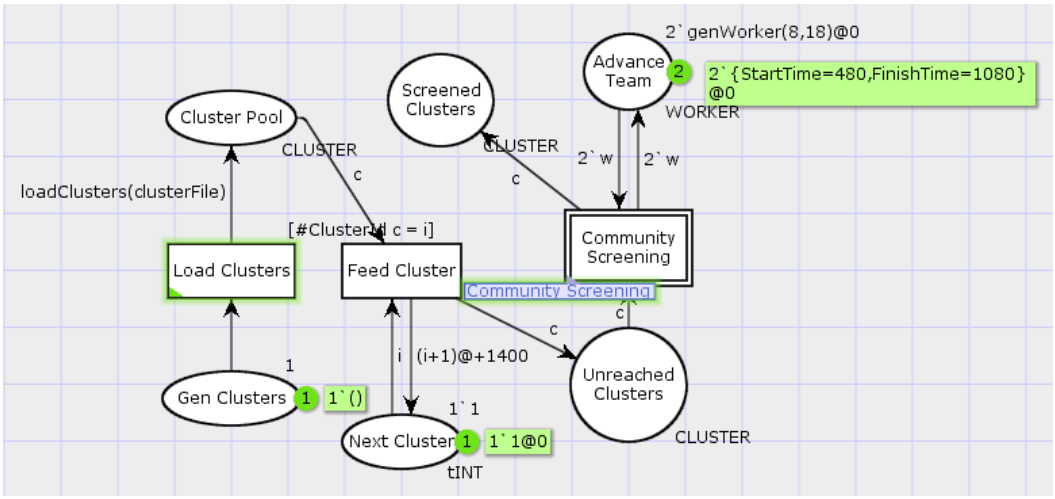

Figure 67 – The Coloured Petri net at the top of the model's hierarchy containing the logic for loading cluster details from file and feeding these into the community screening flow.

Within the Community Screening subnet, participants were loaded from file according to simulation run and current active cluster (A in Figure 68). The CPN was made aware of the current simulation number by reading this from a text file. Owing to the constraints of CPN Tools, each of the participant files created by the aforementioned R script concerned only ten participants from the same cluster. Giving the transition responsible for loading the participant tokens from file high priority ensured that all of a cluster's participants were loaded before screening of this cluster begun. After the simulation number had been read from the text file, the number contained in the file was then incremented, setting up the next simulation run (B in Figure 68).

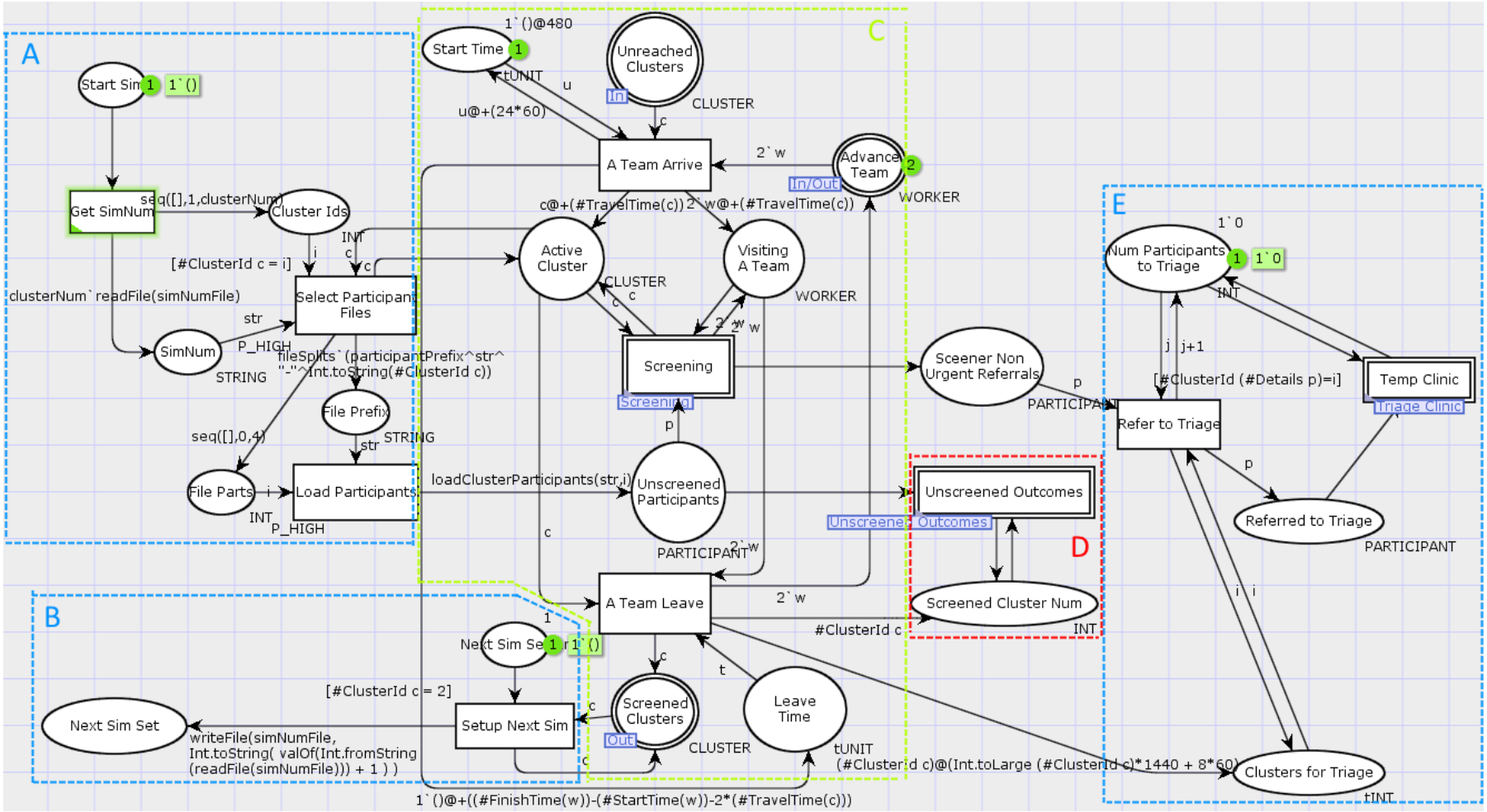

Figure 68 - The CPN created to describe the high-level flow of the Nakuru Eye Health Study.

Participant tokens would be then passed one at a time to the 'Screening' subnet until the advance team's 'home time' was reached, causing the 'A Team Leave' transition to fire and the advance team to return to the top level net (C in Figure 68). Any participant tokens left in the 'Unscreened Participants' place at this point were passed to the 'Unscreened Outcomes' subnet for determination of their outcomes (D in Figure 68).

The screening subnet, that for advance team screening using Peek Acuity and Peek Retina shown in Figure 69, first determined whether a participant could be reached once the advance team had arrived at their home. If not the participant token was passed to the 'Unreached Outcomes' to determine their outcome. Otherwise, the participant was subjected to the particular screening tests that were the subject of the simulation. The participant would then be informed about the clinic next day, or have their results explained if found to be not in need of referral to the clinic, and either passed to the 'Discharge' or back to the Community Screening net as a clinic referral as appropriate.

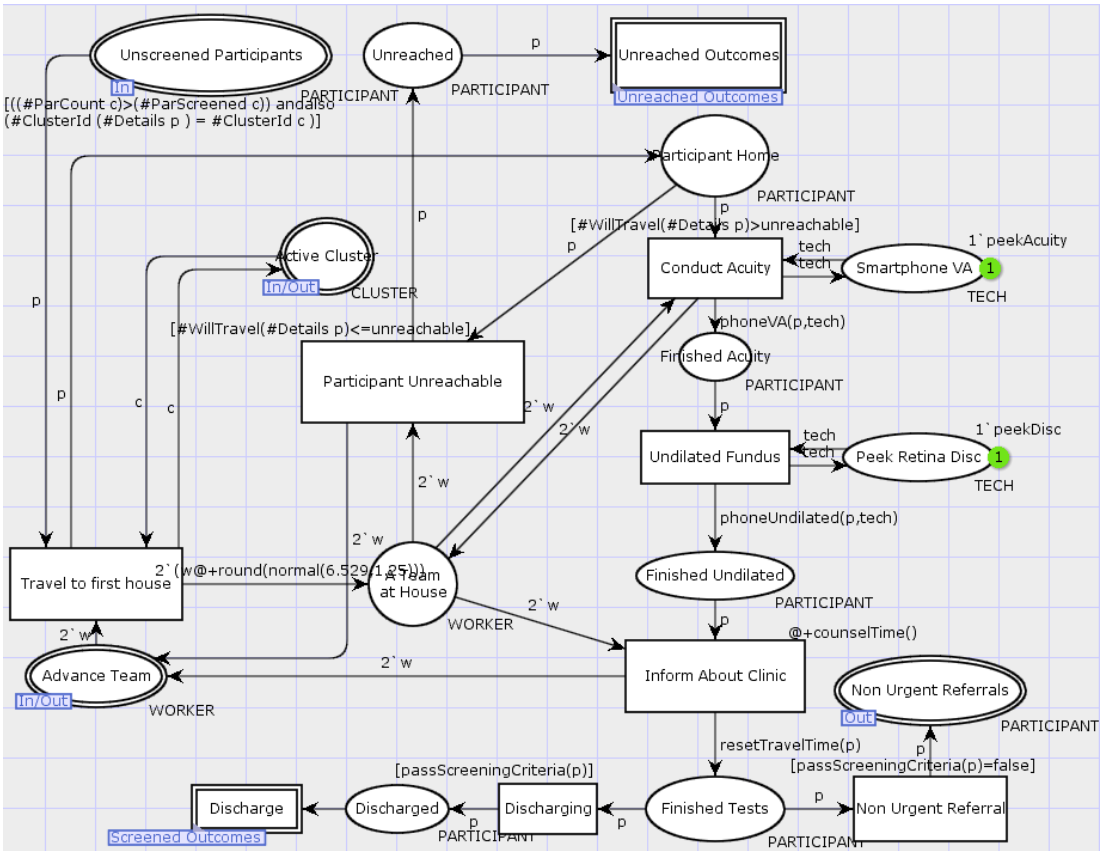

Figure 69 – Subnet for advance team screening using Peek Acuity and Peek Retina.

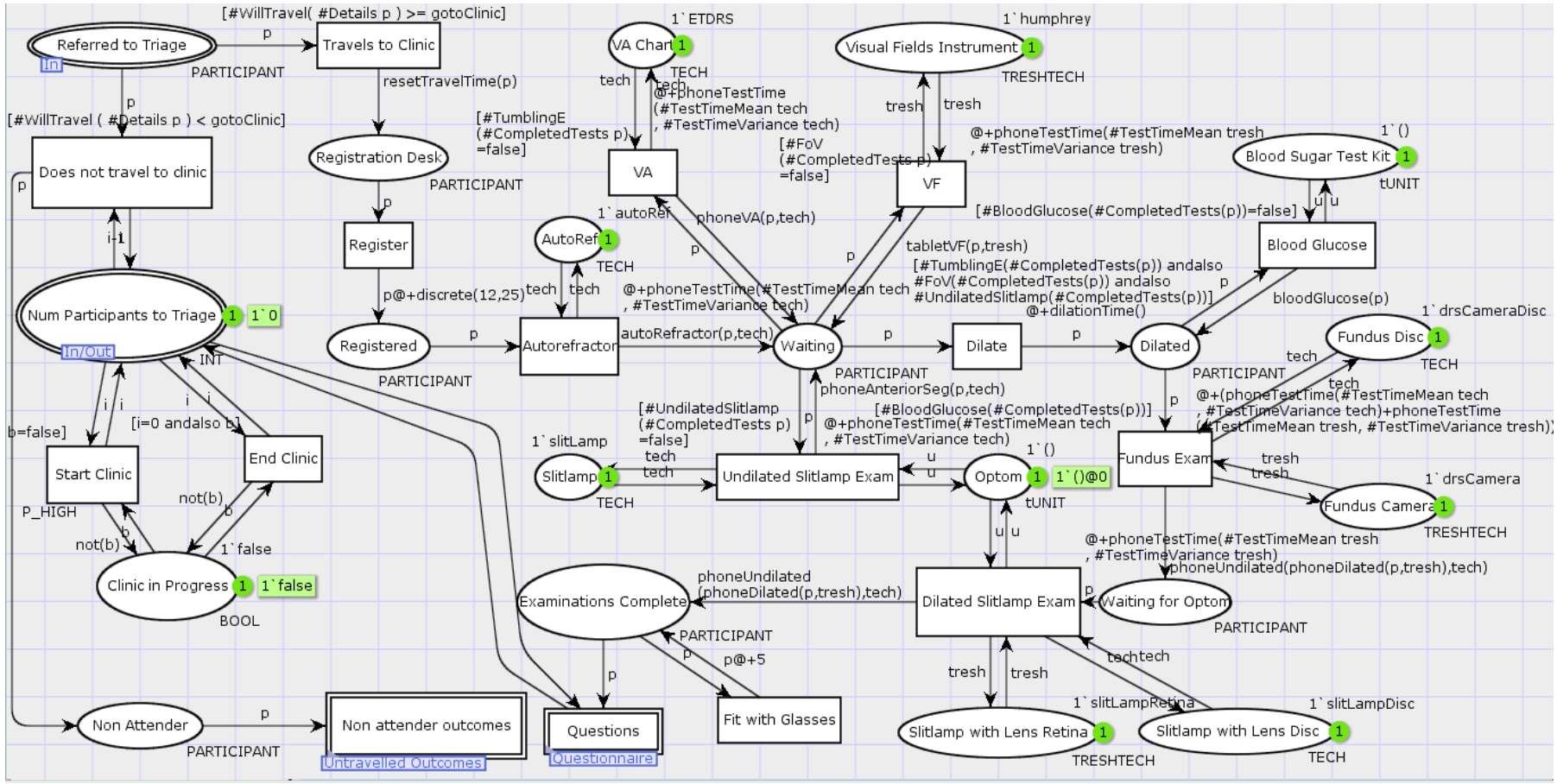

Figure 70 - The coloured Petri net (CPN) constructed to describe the high-level clinical workflow of the eye clinic. Participants enter the clinic via the 'Referred to Triage' place in the top-left of the net. Those participants who travel to the clinic progress through the clinic flow as per the workflow diagram shown in Figure 66 and then exit the net via the 'Questions' substitution transition which contains a counselling event plus the logic concerning referral criteria and ultimate patient outcomes. The place entitled 'Num Participants to Triage' contains a count of participants currently within the clinic's flow and is responsible for firing the transitions indicating the beginning and end of the clinic.

The following simulation day, the participant tokens gathered in the 'Screener Non Urgent Referrals' place in the study high-level flow, shown between C and E in Figure 68, were then fed one at a time into the temporary triage clinic subnet, shown in Figure 70. In this subnet, it was first determined whether the participant travels to the clinic or not. If not, then the participant token was passed to the 'Non attender outcomes' subnet for determination of the participant's outcome. Otherwise, the participant was subjected to test sequence described in Figure 66 and passed to the 'Questionnaire' subnet for determination of their referral type and eventual outcome. The 'Start Clinic' and 'End Clinic' transitions on the left of the subnet acted as markers within the simulation logs, firing only at the beginning and end of the end of the clinic's operations respectively for each cluster.

If consumed by any of the substitution transitions entitled 'Unscreened Outcomes', 'Unreached Outcomes', 'Discharge' or 'Non attender outcomes' a transition corresponding to the participant's outcome, that is the referral type they should have received, according to the criteria listed in Table 20 was fired.

When a participant was instead consumed by the 'Questions' substitution transition, within the triage clinic subnet, a transition was fired for both the referral type, based on values measured by the devices within the clinic, and the outcome, based on the participant's actual eye health.

6.3.3 Simulation Results

The estimates for the simulation iterations required for accurate results for each output of the models are shown in

Table 23. Of these, the largest was for proportion of DM sufferers receiving a referral to a DM clinic, which was estimated to provide accurate results after 222 iterations. Owing to time constraints, it was only possible to run 42 simulations per scenario. Urgent referrals and proportion of DR suffers who had their need met were therefore excluded from the analysis as more simulations were required to make analyses of these valid.

The results with respect to efficacy of advance team screening is shown in Table 24s.

Advance Team Screening Basis	Urgent Referral			Non-urgent Referral			Refractionist Referral		
	Sensitivity	Specificity	% Need Met	Sensitivity	Specificity	% Need Met	Sensitivity	Specificity	% Need Met
None	117	0	132	17	1	17	1	3	4
VA Only	129	0	112	18	1	18	1	3	4
VA and VCDR	147	0	137	16	3	16	1	3	8

Advance Team Screening Basis	DR Clinic Referral			Eye Specialist Refer Don't/Refer			Ready-mades Only		
	Sensitivity	Specificity	% Need Met	Sensitivity	Specificity	% Need Met	Sensitivity	Specificity	% Need Met
None	0	0	126	6	0	10	0	3	9
VA Only	15	0	190	3	31	4	1	3	15
VA and VCDR	10	0	222	3	41	3	1	3	8

Advance Team Screening Basis	Screening Refer / Don't Refer			Screening Times	
	Sensitivity	Specificity	% Need Met	Mean Time Per Clinic	Sample SD
None	0	0	1	1	17
VA Only	1	0	1	1	30
VA and VCDR	1	0	1	1	31

Table 23 - Estimates for the simulation iterations required for accurate results for each model outcome measure across the three simulation scenarios.

Given that all participants were referred when the advance team conducted no screening activities, the associated sensitivity and specificity were 1 and 0 respectively.

Advance Team Equipment	Sensitivity (±SE)	Specificity (±SE)	Proportion of participants with eye issue attending clinic (±SE)
None	1±0	0±0	0.4221±0.0028
Peek Acuity	0.9032±0.0025	0.9933±0.0050	0.3867±0.0027
Peek Acuity and Non-mydriatic Peek Retina	0.9216±0.0023	0.9931±0.0015	0.3921±0.0022

Table 24 - Screening efficacy of the advance team in each of the three simulation scenarios

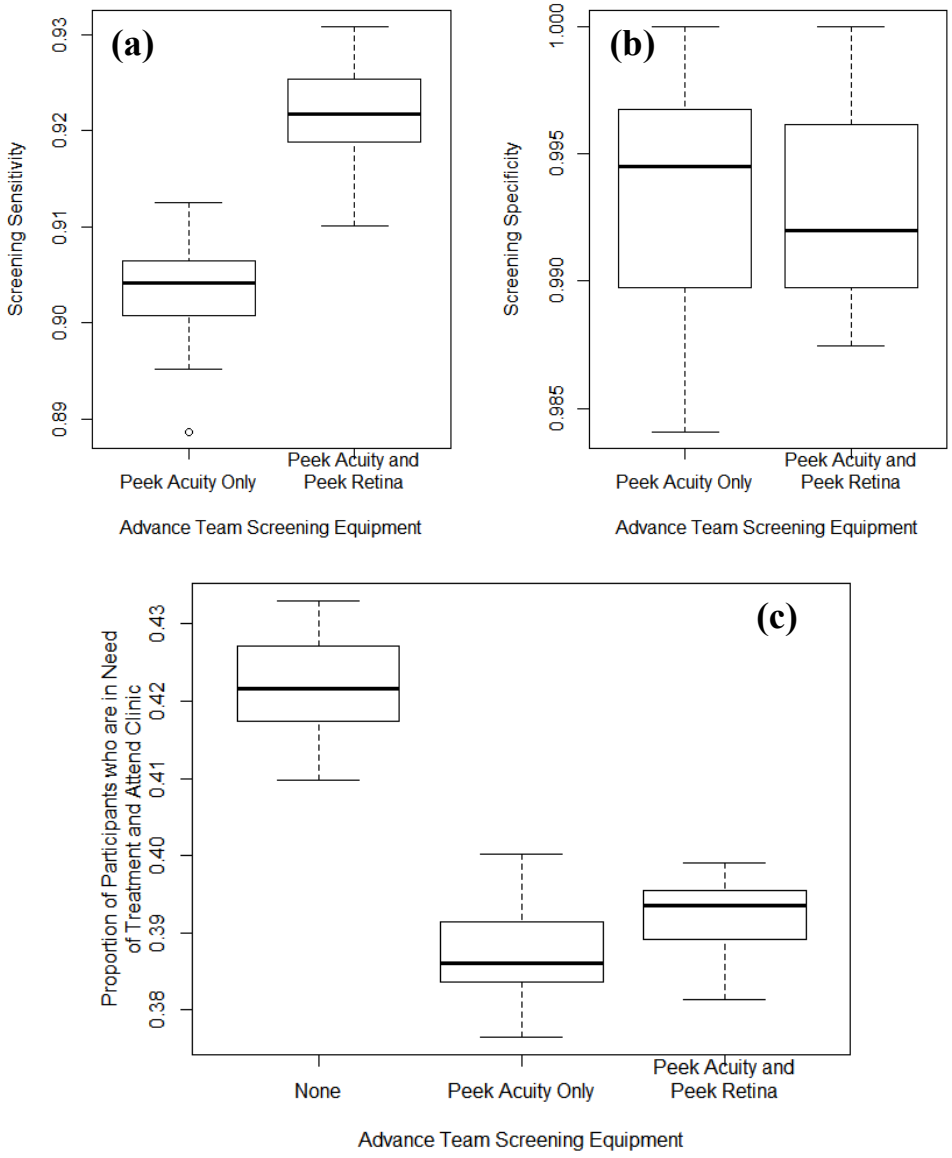

Figure 71 – Box plot of the community eye screening programme's sensitivity (a), specificity (b) and proportion of participants in need of treatment who attended clinic across all three simulation scenarios (c).

Advance Team Equipment	Referral Type	Sensitivity (±SE)	Specificity (±SE)	Proportion of participants needing care referred (±SE)
None	Urgent	0.4893±0.0474	1±0	0.2786±0.02880
	Non-urgent	0.8452±0.0313	0.9551±0.0060	0.4317±0.0159
	Refraction	0.4425±0.0029	0.9633±0.0127	0.2412±0.0041
	Needs Eye Specialist	0.8743±0.0147	1±0	0.4315±0.0076
	DR Clinic	1±0	0.9994±0.0003	0.1954±0.0197
	Ready-mades	1±0	0.8800±0.0129	0.4813±0.0124
Peek Acuity	Urgent	0.4868±0.0498	1±0	0.2519±0.0239
	Non-urgent	0.8372±0.0319	0.9487±0.0145	0.3811±0.0145
	Refraction	0.4414±0.0018	0.9563±0.0146	0.2351±0.0041
	Needs Eye Specialist	0.8713±0.0136	0.8243±0.0407	0.3883±0.0065
	DR Clinic	0.9584±0.0336	0.9993±0.0002	0.1123±0.0139
	Ready-mades	0.9940±0.0026	0.8708±0.0136	0.4506±0.0152
Peek Acuity and non-mydriatic Peek Retina	Urgent	0.5085±0.0555	1±0	0.2710±0.0285
	Non-urgent	0.8481±0.0300	0.9460±0.0123	0.3981±0.0142
	Refraction	0.4404±0.0034	0.9607±0.0139	0.2276±0.0056
	Needs Eye Specialist	0.8771±0.0129	0.8277±0.0475	0.3988±0.0057
	DR Clinic	0.9651±0.0270	0.9993±0.0003	0.1035±0.0139
	Ready-mades	0.9949±0.0023	0.8767±0.0130	0.4388±0.0111

Table 25 – Results for each of the screening programme's outcome measures for each of the three simulation scenarios.

Advance Team Equipment	None	Peek Acuity	Peek Acuity and non-mydriatic Peek Retina
Mean Clinic Time (minutes) (±SE)	414±1.6	370±2.0	377.3±1.7

Table 26 – Mean clinic times for each of the simulation scenarios

The equipment type given to the advance team had a significant impact on the sensitivity, specificity and proportion of participants in need of treatment attending a clinic ($F(2)=1359$, $p<0.001$; $F(2)=323468$, $p<0.001$; $F(2)= 110.3$, $p<0.001$ respectively) as can be seen in the box plot shown in Figure 71 overleaf. Post-hoc Tukey's HSD tests showed that providing the advance team with Peek Acuity and a non-mydriatic Peek Retina resulted in a statistically significant improvement in sensitivity with no significant difference in specificity ($p<0.001$ and $p=0.99$ respectively). However, there was not a significant difference in the proportion of participants in need of care who attended a clinic between these two screening scenarios ($p=0.0984$). Furthermore, both screening strategies resulted in a significantly smaller proportion of these participants presenting at clinic compared to the strategy whereby all participants were referred regardless of visual status ($p<0.001$ in each case).

The results with respect to each of the screening programme's outcome measures for each of the three simulation scenarios are shown in Table 25.

When comparing no screening by the advance team to both screening based on visual acuity only and visual acuity plus VCDR, there was a small (0.006, 95% CI:0.001-0.011 and 0.005, 95% CI:0.0002-0.0099 respectively) yet significant (Tukey HSD: $p=0.012$ and $p=0.040$ respectively) difference between the sensitivity in identifying those whose only necessary eye intervention was a pair of ready-made spectacles.

However, the proportion of all those whose only necessary eye intervention was a pair of ready-mades who went on to be identified as such was significantly lower when advance team screening was based on visual acuity and VCDR compared to referring all participants (Tukey HSD: $p=0.007$). There was not a significant difference between advance team screening based on visual acuity only and referring all participants (Tukey HSD: $p=0.060$) nor was there a significant difference between the two screening scenarios(Tukey HSD: $p=0.643$).

There was found to be a small (0.0136; 95% CI: 0.0022-0.0249) yet significant (Tukey HSD: $p=0.016$) difference between the number of participants that required a referral for specialist refraction receiving such between the scenario where participants were screened by visual acuity and VCDR.

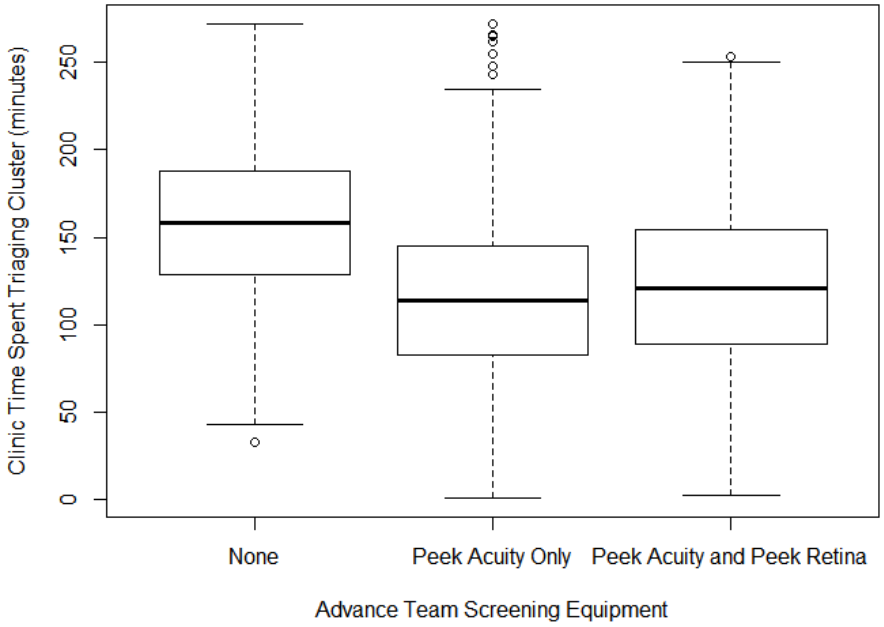

Figure 72 - Boxplot of the time spent conducting in-depth eye examinations in a temporary clinic per cluster.

When all participants were referred to the triage clinic all those needing referral to an eye specialist received such a referral. The specificity was significantly lower in both the other screening scenarios (Tukey HSD: p=0.003 in each case), however there was no significant difference in specificity between the two screening scenarios (Tukey HSD: p=0.998).

The proportion of the total number of participants in need of referral to any eye specialist who received such a referral was also significantly lower when screening based on visual acuity only was conducted by the advance team (Tukey HSD: p=0.003). However, there was not a significant difference between the two screen methods (Tukey HSD: p=0.432) nor screening based on visual acuity and VCDR and referring all participants to the triage clinic (Tukey HSD: p=0.069).

For all other measures, there was no significant difference between the three cases. The mean clinic time for each of the simulation scenarios is shown in Table 26. The equipment type given to the advance team had a significant impact on the clinic time required ($F(2)=356.9$, $p<0.001$) as can be seen in the box plot in Figure 72. Post-hoc Tukey's HSD tests showed that providing the advance team with Peek Acuity only resulted in a significantly shorter clinic time ($p<0.001$ for each) and that providing the advance team with both Peek Acuity and Peek Retina resulted in a significantly shorter clinic time compared to providing the advance team with no screening equipment ($p<0.001$).

6.4 Discussion

The results from the simulations described in this chapter give some useful insights into how to optimise the design and implementation of a smartphone-based ophthalmoscope for maximum impact.

6.4.1 Implications for an mHealth equipped advance team

There was a statistically significant difference in clinic time per cluster when the mHealth devices were introduced to the advance team without a drastic loss in sensitivity or proportion of participants with eye issues attending the triage clinic. The original study involved a nurse and clinical officer visiting the participants'

homes however, nothing in the models presented in this chapter requires more advanced skills than those of a community eye worker with minimal clinical training, providing that the mHealth devices themselves do not. Thus, the results suggest that it is worthwhile designing the mHealth screening devices for operation by CEHWs, rather than a higher cadre whose scarcity would necessitate the device being clinic-based.

Adding more advance teams would allow more participants to be reached within the day allocated for advance team outreach. Alternatively, the advance team could be allocated more than one day per a cluster, although it is unclear how having a clinic scheduled for more than one day after the initial advance team-participant encounter would affect referral uptake.

6.4.2 Referral adherence and pathway

The low sensitivity of urgent referrals and referrals to an optometrist is also noteworthy. The most likely cause of this was the frequent inability to conduct autorefraction or fundus imaging respectively. A potential solution to improving the sensitivity of referral for specialist refraction could be the inclusion of subjective refraction within the triage clinic itself, and offering this to all participants requiring spectacles. However, this would have major implications for the clinic's workflow as it is a time-consuming task requiring a specialist refractionist (119, 305). With regards to fundus imaging, there are few solutions that improve upon the diagnostic capability of a desktop fundus camera operated by a retinal photographer or biomicroscope indirect ophthalmoscopy (306). However, the development of new image analysis algorithms may aid in the identification of sight-threatening retinopathy, even in the presence of significant ocular opacities (306). In lieu of these, the programme could opt to refer those who cannot have their fundus adequately imaged for an urgent referral. Although, this would likely improve urgent referral sensitivity, it is likely to have a greater negative impact upon the specificity as many more participants are erroneously given an urgent referral.

The relatively low proportion of participants in need of any referral type who went on to receive the correct referral is a cause for concern and highlights that diagnostic

accuracy is not the most significant factor with respect to coverage of an eye care services.

The problem ought to be particularly acute if the rate of uptake of tertiary eye care appointments is considered. For example, Mtuya and colleagues found that 24.6% of DM patients who underwent eye examination at a DM clinic in the Kilimanjaro region of Tanzania, and who were deemed to have sight-threatening DR, then went on to attend the central eye hospital for expert examination and laser photocoagulation if required (307).

It is therefore important to consider what health education interventions and counselling techniques might better improve adherence to referrals. Simply giving CEHWs and clinic counsellors more time to converse with each person they encounter may improve report and thus likelihood of attending referral. Innovative health education technologies have also been developed to help address misunderstandings and knowledge gaps with respect to eye care. For example, Morjaria and colleagues recently conducted an RCT of a comprehensive eye health education package which was delivered alongside school vision screening with a smartphone-based visual acuity and data entry application, subjective refraction, spectacle fitting and delivery as required (305). The intervention included the provision of cards with vision simulations that explained the specific child's eye problem for him or her to take home to their parents or guardian. In addition, automated voice calls to communicate to parents and guardians regarding their child's vision. However, follow-up interviews with the study participants three months after receiving their spectacles showed that, whilst wearage rates were at a greater level than is usually found in such settings, there was little difference between wearage rates between the two study arms, thus underlining the difficulty in improving patient adherence with such interventions (308).

Improved communication with patients is another means by which adherence to referrals can be improved. A recent systematic review and meta-analysis of SMS reminder trials concluded that they were associated with a modest benefit with respect to referral attendance and should therefore be implemented (309).

Indeed, Rono and colleagues recently demonstrated the power of improved communication with respect to mHealth within eye care by linking a CEHW operated, smartphone-based visual acuity and data entry application to a SMS reminder system (310). In a randomised controlled trial (RCT) of the system versus a control arm of standard visual screening with Snellen charts by ophthalmic nurses, it was found that 2.5 times more schoolchildren attended a clinical referral with the mHealth-enabled system.

Finally, future work ought to investigate whether referring from advance team straight to an optometrist, ophthalmologist or DM clinic increases attendance to the extent that it provides better overall system outcomes in spite of reduced sensitivity and specificity compared to when participants are referred to a triage clinic.

6.4.3 Limitations and future work

There are a number of ways in which the simulations described in this chapter could be improved and enhanced. Firstly, it would be beneficial to conduct sensitivity analysis of the multiple imputations, parameters within the distributions used to generate participants, device parameters, workflow timings and probabilities. Such analyses would provide further information concerning the uncertainty of the simulation results (291, 311-313).

Secondly, an assumption was made that the measurement made by a given device ought to be taken from a normal distribution centred on the mean measurement. However, users may have a tendency to err on the side of caution and technical errors will not necessarily result in a normal or other common distribution of results around the actual value (314). Nevertheless, in the absence of better information concerning the devices involved in the workflow, the normal distribution is a reasonable approximation. More thorough quantitative analysis of the discrepancies between the data acquired with mHealth and reference standard devices during the Nakuru Community Eye Study may help to establish whether a normal distribution is indeed a valid approximation.

The model also assumes that there is one participant per a home. In reality, there are often two participants in a single home, reducing total travel and counselling time required by the CEHWs.

The model only considers those of 55 years and above, as is typical when conducting an eye health survey (315). Whilst approximately 80% of eye disease is indeed concentrated in this population, clinics will often receive people who have eye problems and have self-referred or have been referred by a family member (17). Furthermore, the total impact on quality of life can be far greater if a visual impairment is corrected at an earlier age and thus including younger age groups in the screening criteria ought to be considered. Extending the model to encompass the entire community would help to inform whether screening those of aged 55 years and above is justified or whether including a different age group would maximise impact.

Given that the GPS coordinates for each cluster are known, the model could be further improved by adding travel times to the model for both the advance team and triage clinic. Such times could be calculated based on estimations by mapping services such as Google Maps (Google Inc.) or GraphHopper Directions API (GraphHopper GmbH, Munich, Germany). Additionally, more accurate data concerning the time the advance team spent travelling between homes would be useful.

Future models ought also to consider other mHealth devices, such as dilated smartphone fundoscopy for identifying off-disc ocular fundus pathologies, tablet based visual fields tests and smartphone-based autorefraction (201, 203, 206, 316). The use of mobile data capture technologies for data capture and decision-making ought also to be explored. In addition, IOP measurements or gonioscopy were not included in the workflow for the sake of brevity. Adding these would provide an extra dimension to glaucoma diagnosis.

Subsequent versions of the model should also seek to extend the model so to include tertiary care. It is of vital importance when conducting any screening programme that adequate treatment is available for the conditions being screened. It is therefore important to know if existing services are already at capacity and, if not, if they are likely to be overwhelmed by a sudden influx of patients referred from a community

screening programme. A simple service analysis similar to those conducted as part of the Rapid Assessment of Avoidable Blindness is likely to provide enough information to model the minimum requirements of such an extension (315).

The model described in this chapter represents a somewhat high-level description of community screening and clinic triage operation. Discovering, a lower level workflow description would require more intensive analyses, such as time-and-motion (T&M) analyses similar to that discussed in Chapter 12 (317). The finer details provided by such would allow better definition of ergonomic requirements and a more extensive understanding of how the introduction of mHealth devices ought to impact upon other routine tasks within the clinical workflow.

Finally, connecting the simulation to health economic modelling would allow an estimation of implementation and ongoing costs to be made. Given that these were identified as two highly cited barriers in chapter two, an extension of the model towards providing financial projections ought to be a priority for future work.

6.5 Licensing Information

The dataset discussed in this chapter is available on license. Please contact University of Strathclyde Research and Knowledge Exchange Service to obtain a license (https://www.strath.ac.uk/rkes/; email: rkes@strath.ac.uk).

SECTION 4

Chapter 7 - Modelling of an ROP Screening Programme

7 Modelling of an ROP Screening Programme

Image reprinted from Seminars in Fetal and Neonatal Medicine, 20 / 5, Anand Vinekar,Chaitra Jayadev,Shwetha Mangalesh,Bhujang Shetty,Dharmapuri Vidyasagar, Role of tele-medicine in retinopathy of prematurity screening in rural outreach centers in India – a report of 20,214 imaging sessions in the KIDROP program, 335-345, Copyright (2015), with permission from Elsevier.

7.1 Introduction

Having discussed the use of mHealth to tackle visual impairment of adults in LMICs, the next four chapters move on to discussing the use of mHealth in case-finding for one of the greatest concerns with regards to childhood blindness, namely ROP. As was discussed in Chapter 3, ROP is a rising concern in LMICs who are on the cusp of the so-called 'third epidemic of ROP' if decisive action is not taken immediately, with ROP already accounting for up to 60% of childhood blindness in middle-income countries (318).

7.1.1 Aim

In the second chapter of this thesis it was found that, amongst the literature reflecting on global mHealth, the most commonly cited reason for the failure of mHealth programmes to progress beyond the pilot stage was a lack of data concerning the impact on the full healthcare system. Therefore, by making such considerations for a LMIC ROP screening solution during the design phase, a design that is more appropriate for implementation at scale in LMIC ought to be achieved. As discussed in Chapter 4, clinical workflow modelling with CPNs represents a practical and effective way of doing such.

In this chapter, four CPN models are considered. One of these closely models a current LMIC ROP programme, with the three others involving various alterations to the cadre responsible for retinal imaging and referral and discharge decisions. The results of simulations using these models are then presented in order to estimate what impact on the clinical workflow might be expected upon the introduction of such a low-cost screening solution for ROP in a LMIC.

The specific aim of this impact estimation is to identify the end user price-point, estimated maximum manufacture cost and how various tasks associated with the solution are best distributed amongst the different cadres involved with the patients' care. Therefore, of specific interest are the necessitated changes in:

- screening coverage
- treatment coverage
- task distribution amongst the relevant cadres
- ongoing costs
- setup costs.

The implications for the design for this solution are then discussed.

7.1.2 Model Basis

The Karnataka Internet Assisted Diagnosis of Retinopathy of Prematurity (KIDROP) programme is an initiative that has screened at-risk infants in Karnataka state, India since 2007 (319). The programme involves three screening teams visiting 81 rural and semi-urban neonatal clinics every week. Each team consists of a project manager, driver and an imaging technician who operates a RetCam Shuttle (Clarity MSI, CA, USA) widefield fundus camera. Patient management decisions are made by the technician onsite with the project manager counselling the patient's parents and arranging the appropriate next clinical step. Images are then uploaded to a web platform where an ROP specialist reviews the patient management decisions made based on the images via a smartphone app (320). ROP specialists involved in the programme then carry out treatment as required according to the appropriate clinical guidelines.

The KIDROP programme has been demonstrated to be highly effective in identifying those in need of laser treatment for ROP and ensuring that this treatment is delivered. For example, in 2014 it was reported that 41,237 imaging sessions had been performed since the programme's inception resulting in thousands receiving sight saving intervention. As such, although its setup and operational costs are likely to be prohibitive in lower resource settings, the programme represents a very good representation of best practice for ROP screening and treatment in a LMIC and thus a reasonable basis for the workflow models described in this chapter.

7.2 Methods

Conceptually, the workflow of any ROP programme can be described in four parts: **logistics** (i.e. movement of equipment and personnel between care centres), **screening**, **review of management decisions** and **treatment**. The workflows involved in these parts were each modelled in a different page in CPN Tools, with the exception of the treatment workflow, which was included with the logistics page. The reason for this being that the exact details of the treatment workflow were not of interest, given the models' aims, and thus would remain the same in each model. For the sake of simplicity of the model, all times were rounded to the nearest minute.

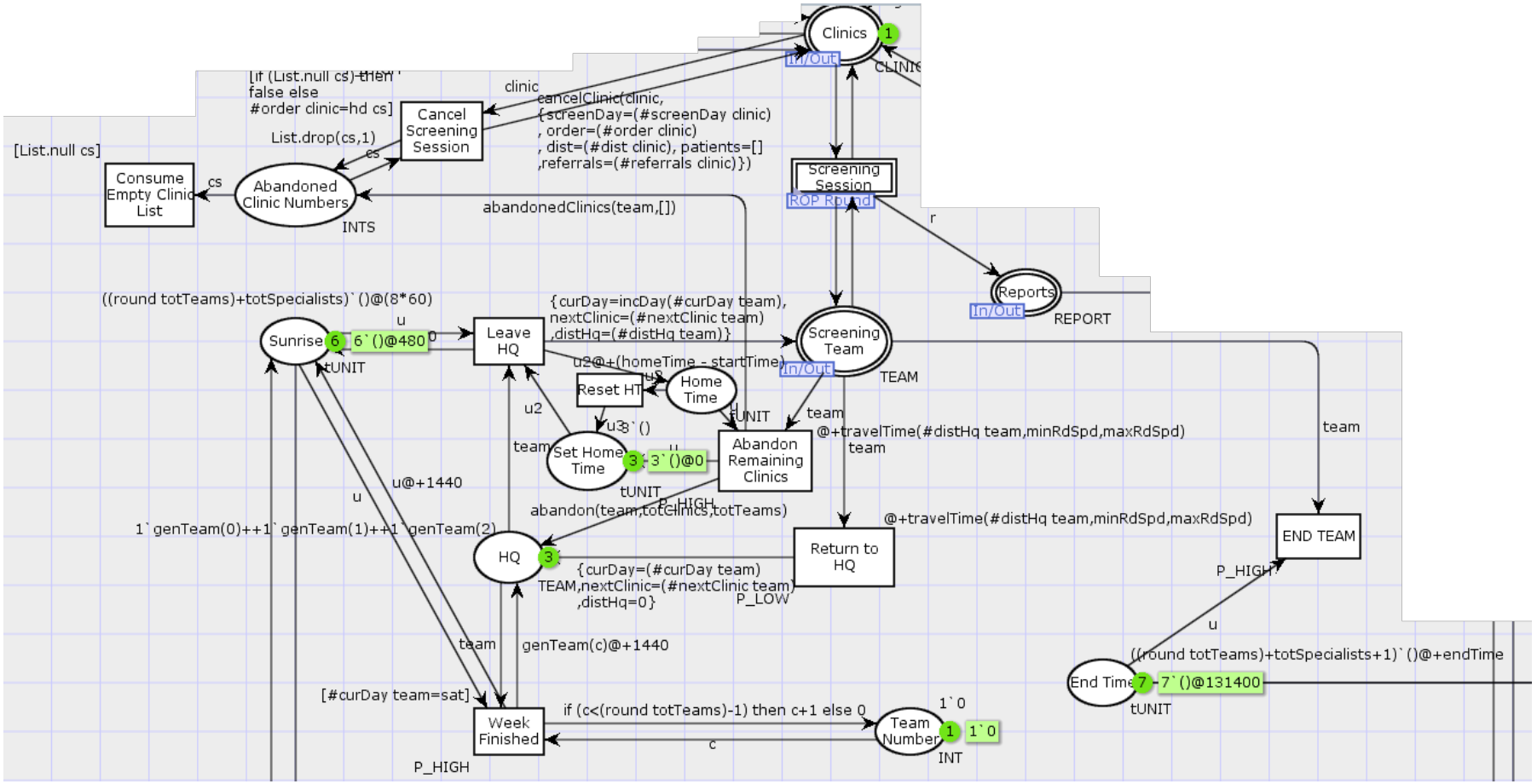

Figure 73 - CPN of the logistics workflow

7.2.1 Modelling of the Logistic Workflow

On average the screening teams in the KIDROP programme travelled 1200 to 1600 km a week each, visiting a total of 81 neonatal intensive care units (NICUs)in total (319). Because location data for each was not readily available, with few appearing in online maps for example, the 81 clinics were assumed to be divided equally between the three teams and the route taken by each team each day was assumed to be along the quickest route to the final NICU. That is to say that there were no 'short-cuts' from the final NICU back to the team's headquarters. Thus, it was estimated that the distance between each clinic was within a uniform distribution between 22 and 30 km with the distance from the last clinic back to the headquarters being the sum of these distances. A CPN describing the above logistic workflow is shown in Figure 71.

To determine the travel times involved in the logistic flow it was necessary to consider the speed of vehicles on Indian roads. It has been estimated the average road speed for trucks in India is between 30 and 40 km/h (320). The difference between the average speed of a typical vehicle and a truck can be estimated to be 20 km/h by comparing analyses of GPS data for each respectively (321, 322). The average travel speed in any given journey for the purpose of the model was therefore taken from a uniform distribution between 50 and 60 km/h. By way of comparison, this is still under the global average truck speed of between 60 and 80 km/h, emphasising the level of congestion on Indian roads. It should be noted that this average road speed ought to vary considerably depending on conditions such as the level of urbanisation and road surface, however these factors were considered too complex to model effectively given the publicly available data (320).

In the KIDROP programme, 22,596 imaging sessions were carried out during 2011 and 2012. The mean number of sessions per a child was 3.959 thus implying that 5708 were enrolled onto the programme during the period (319). In the models, it was assumed that the chance of an infant being enrolled in any one clinic is the same as the others and thus each day there is a probability of 0.097 of an infant being enrolled in any given clinic. The model does not account for multiple births per day,

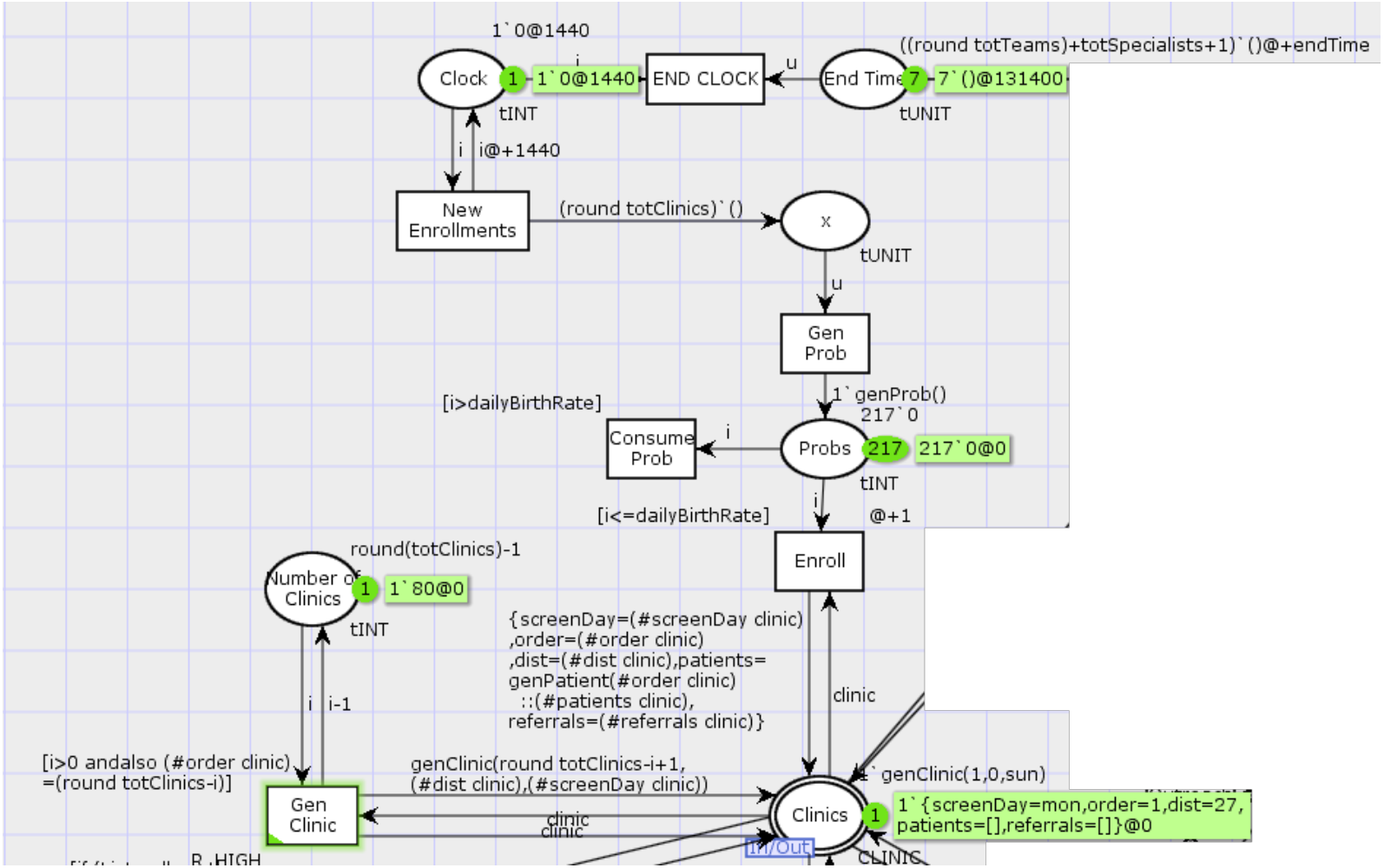

Figure 74 - CPN of the logic for clinic and patient generation

however ultimately what matters, in the context of this model, is the number of infants born between screening sessions and not how many infants are born on a given day.

The above also implies that a mean of 2.68 infants are enrolled for ROP screening in each clinic at any given time. To start with, 217 were therefore shared across the 81 NICUs with each NICU containing two or three infants. No referrals were loaded into the model at the start and all infants were assumed to be at the beginning of their screening course.

The CPN modelling patient generation is shown in Figure 74.

7.2.2 Modelling the Screening Workflow

The models' screening workflow was primarily based on The Royal Colleges of Ophthalmologists and Paediatrics and Child Health's guideline for the screening of ROP (159). Whilst these guidelines have the limitation of applying specifically to the UK context, the screening procedure undertaken varies little according to setting. The workflow involves the insertion of two or three dilating drops five minutes apart in each eye, followed by a fifty- to eighty-minute wait for full pupil dilation to occur. Comfort care techniques are then administered two minutes prior to the application of topical anaesthesia (323). After waiting thirty seconds for the eye to become anaesthetised, an ocular speculum is inserted to hold the infant's eyelids apart throughout the examination, and imaging begun. The process is then repeated for the second eye. Finally, the speculum is removed and the imaging team move onto the next infant or complete the round if no more infants remain to be screened.
A block diagram describing the workflow of the screening procedure for a single infant is shown in Figure 75 overleaf.
To achieve the most advanced level of competency in the KIDROP programme, a technician must image an infant's eye (measured as the time from speculum insertion to removal) in under two minutes (319). However this will not always be possible due to interruptions to administer patient care for example (159). Moral-Pumarega and colleagues reported the mean duration of an examination using wide-field digital retinal imaging, including such interruptions, as being 3.70 minutes with a standard

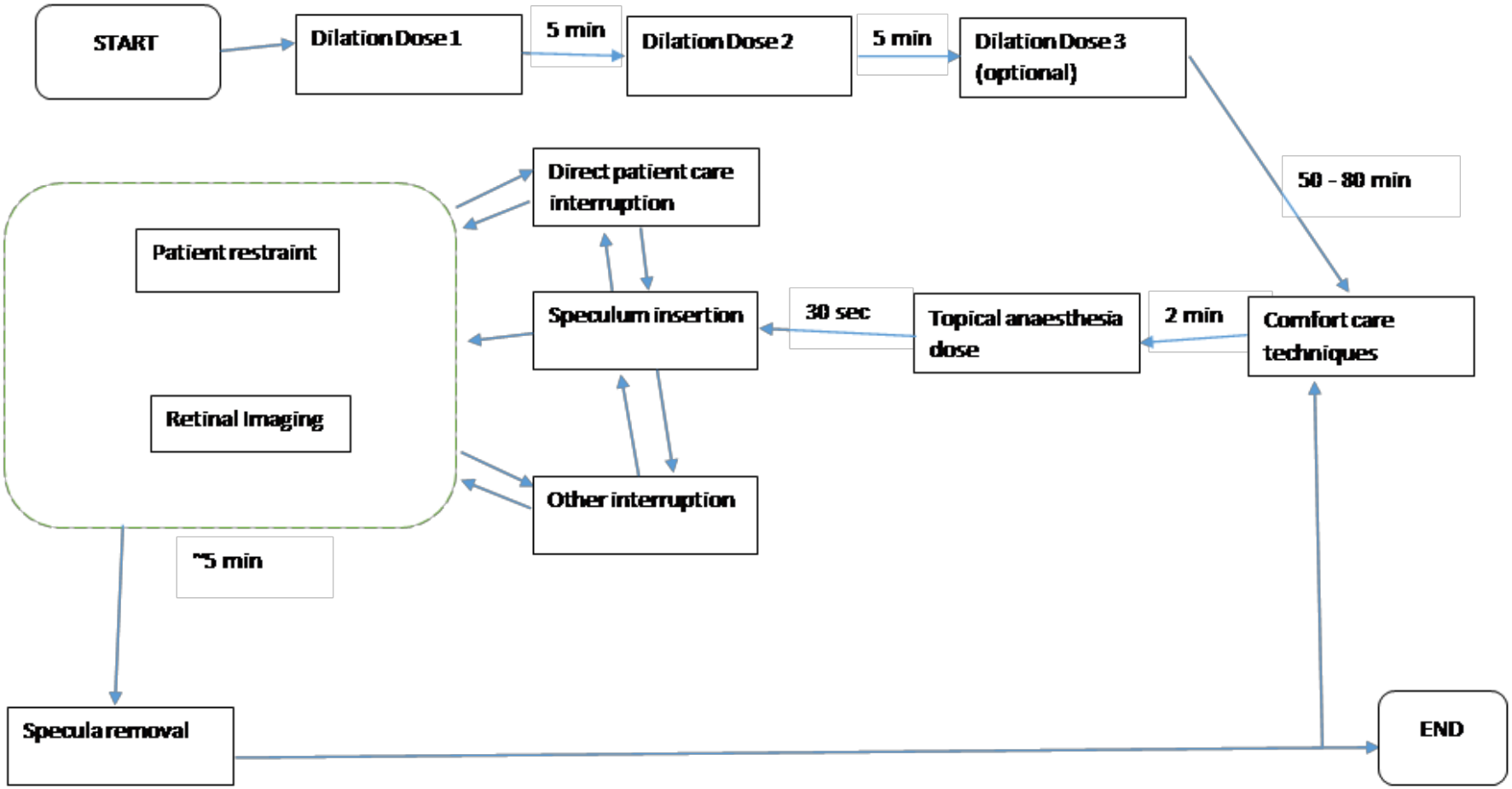

Figure 75 - A block diagram of the ROP imaging procedure for a single infant.

deviation 2.17 minutes and a range of 1 to 12 minutes (323). For the purposes of the model, this was assumed to fit a PERT distribution which is commonly used to estimate uncertainty in timing in project management (324). As CPN ML has no native PERT distribution, a user defined PERT function was defined using the fact that the PERT distribution is a special case of the beta distribution, namely

$$(max - min) \cdot B(\alpha, \beta) + min, \quad \textbf{(14)}$$

where max and min are the maximum and minimum possible values respectively, and $B(\alpha, \beta)$ is the beta distribution with the parameters α and β defined as per **(14)**,

$$\alpha = \left(\frac{4b+max-5min}{max-min}\right) \text{ and } \beta = \left(\frac{5max-min-4b}{max-min}\right) \quad \textbf{(15)}$$

where b is the expected value, which is calculated according to the below formula:

$$b = \frac{6\mu-min-max}{4}, \quad \textbf{(16)}$$

where μ is the mean. Thus, a 3-parameter PERT can be described by the following relationship which can be coded using CPN ML,

$$PERT(min, \mu, max) = (max - min) \cdot B\left(\frac{6(\mu-min)}{max-min}, \frac{6(max-\mu)}{max-min}\right) + min \quad \textbf{(17)}$$

As Moral-Pumarega and colleagues only recorded the time for imaging both eyes, the time was added only after the second eye was imaged in the model (323). Hence, the time taken to image both eyes, in minutes, was defined as,

$$t_{imaging} = 11 \cdot B(1.47, 4.54) + 1. \quad \textbf{(18)}$$

To simplify the CPN model, the screening team were not made to interact with every single step. Rather, for each infant, the team interacts with the first step, thus synchronising the infant with the team's timestamp at the beginning of the imaging workflow, and again at the end of imaging workflow, thus adding the time taken to image and grade each infant in sequence.

No data on the time taken to grade a retinal image for ROP could be found. However, it has been reported that the mean time taken for non-clinical graders to grade one of a set of 100 retinal images for DR is 2.1 minutes (interquartile range: 1.5-2.8 minutes) (281). Thus, the time taken to grade an image was calculated by approximating this range to a normal distribution centred on 2.1 minutes and with a standard deviation of 0.97 minutes.

In the case of the mobile screening team, it was assumed that dilation of infants is

Imaging Sessions	Likelihood
1	0.024
2	0.119
3	22.1
4	27.2
5	23.9
6	12.5

Table 27 - Likelihood of number of sessions as calculated from the data reported in Vinekar and colleagues (319). Infants requiring "five or more" sessions were split into five or six sessions.

timed so that all infants are fully dilated by the time that the screening team has arrived and unpacked.

Counselling was taken to take 10 minutes, the approximate length of a standard GP consultation (325).

7.2.3 Modelling of the Report Review and Management Decisions

The probabilities of the necessary number of weeks' that are required to elapse from enrolment, for a given infant, before a discharge or referral decision can be made is shown in Table 27.

The timing of retinal vascular events correlates more strongly with PMA than with postnatal age, and can occur at any point during the screening period mandated in the aforementioned guideline (326, 327). Therefore, the model assumes that there is equal probability of an infant requiring treatment once the determined time-period has passed whether this is one week or six weeks. In the KIDROP programme, 175 out of a subset of 1601 screened infants required referral for treatment at the end of their programme (i.e. 10.9%). This proportion is slightly higher than estimation of 5.1% reported by Blencowe and colleagues for all of India (328). This difference can be explained by local factors such as greater access to specialist neonatal care, given that Blencowe and colleagues' estimation was based off only 30% of at-risk infants having access to NICUs.

The PPV and NPV used for disagreement between the ROP specialist and screening team were taken from that found for 'treatment grade ROP' in the KIDROP programme, namely 81.5% and 98.6% respectively. It was not possible to understand how often there was disagreement between discharge and further follow-up, likewise nor was it possible to determine if any false positives subsequently went on to need treatment. As such, the model takes a simplified approach whereby true negatives and false positives have their initial decision for discharge or follow-up confirmed and false negatives and true positives were added to a surgical list.

The probability of referral after the final screening session was calculated by dividing the reported proportion of screened infants requiring treatment in the KIDROP programme, 10.2%, by the PPV giving 12.5%. The probability of discharge after the final screening session was therefore 87.5%.

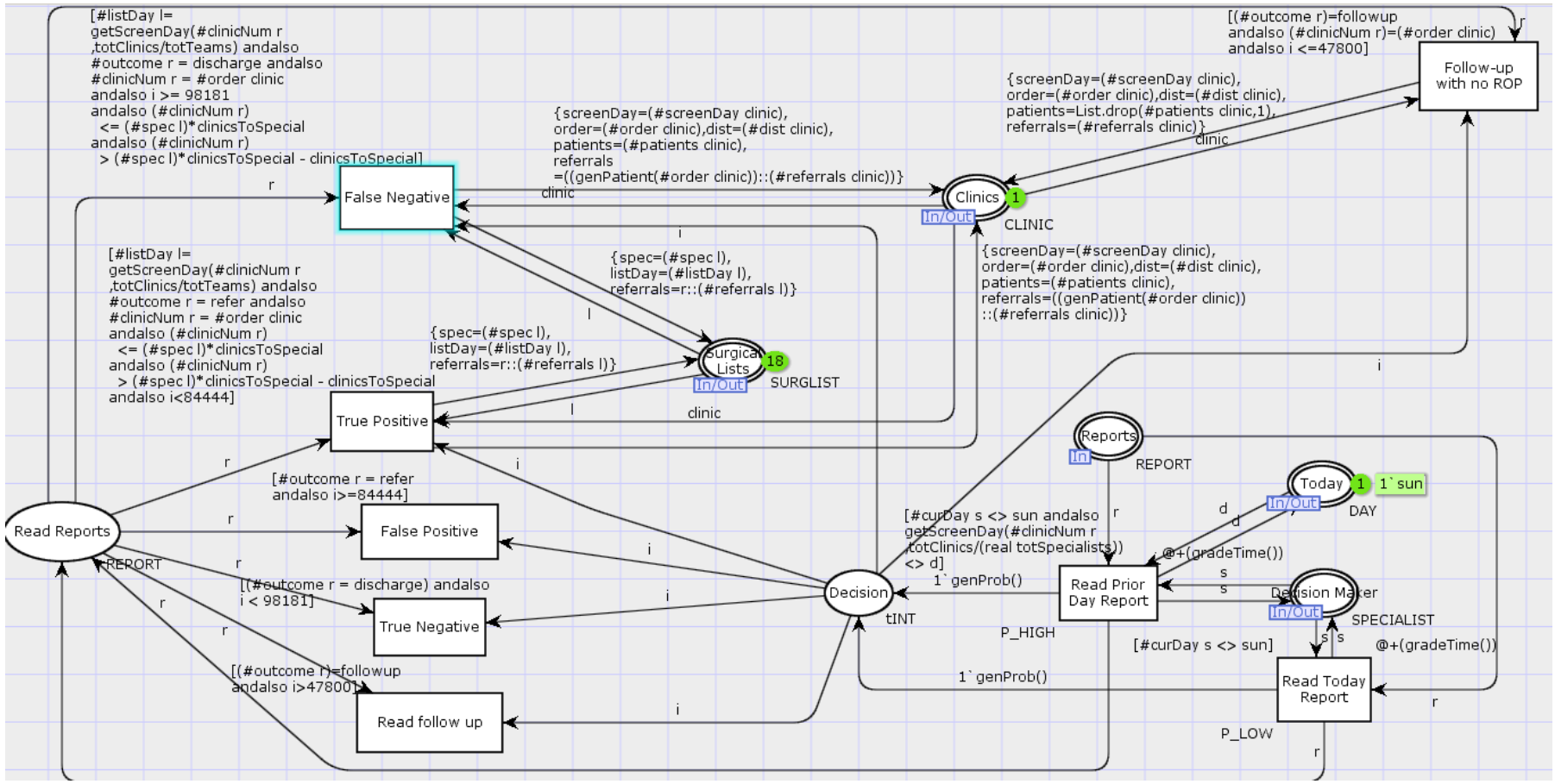

Figure 76 - CPN for screening report review.

The structure of the CPN representing review of management decisions is shown in Figure 76.

7.2.4 Modelling of the Treatment Outreach Workflow

There was taken to be one 'on-duty' specialist per HQ location. These specialists were only capable of providing treatment to NICUs that had been visited by the screening team based in their HQ. However, each specialist was allowed to review reports from any clinic.

When a report review resulted in a decision that surgery was necessary, the corresponding infant was added to a surgical list corresponding to the NICUs screening day. When every report from the previous day (or days) had been reviewed, the specialists would then embark on outreach to the NICUs where there was at least one infant in need of treatment. The specialists were only allowed to visit NICUs with the same screening day without returning to their HQ first. It was assumed that whilst the specialist is on outreach that he or she was not available to read reports.

The time for each laser treatment was taken from a uniform distribution between 15 and 20 minutes per eye (329). It was assumed that, in the case of a referral, both eyes required treatment. Successful versus unsuccessful surgical outcomes were considered out of the model's scope.

The structure of the CPN representing the specialists' workflow is shown in Figure 77.

7.2.5 Simulation and Statistical Analysis

For each model, five initial simulations of three months' of activity were run using ProM 6.7 (Eindhoven University, Eindhoven, The Netherlands). The event logs generated by these simulations were then process mined for analysis using ProM 6.7. The workflows for the screening team and ROP specialists were each extracted from the log files by filtering on the relevant events and then using an inductive miner to discover the Petri net for just these events.

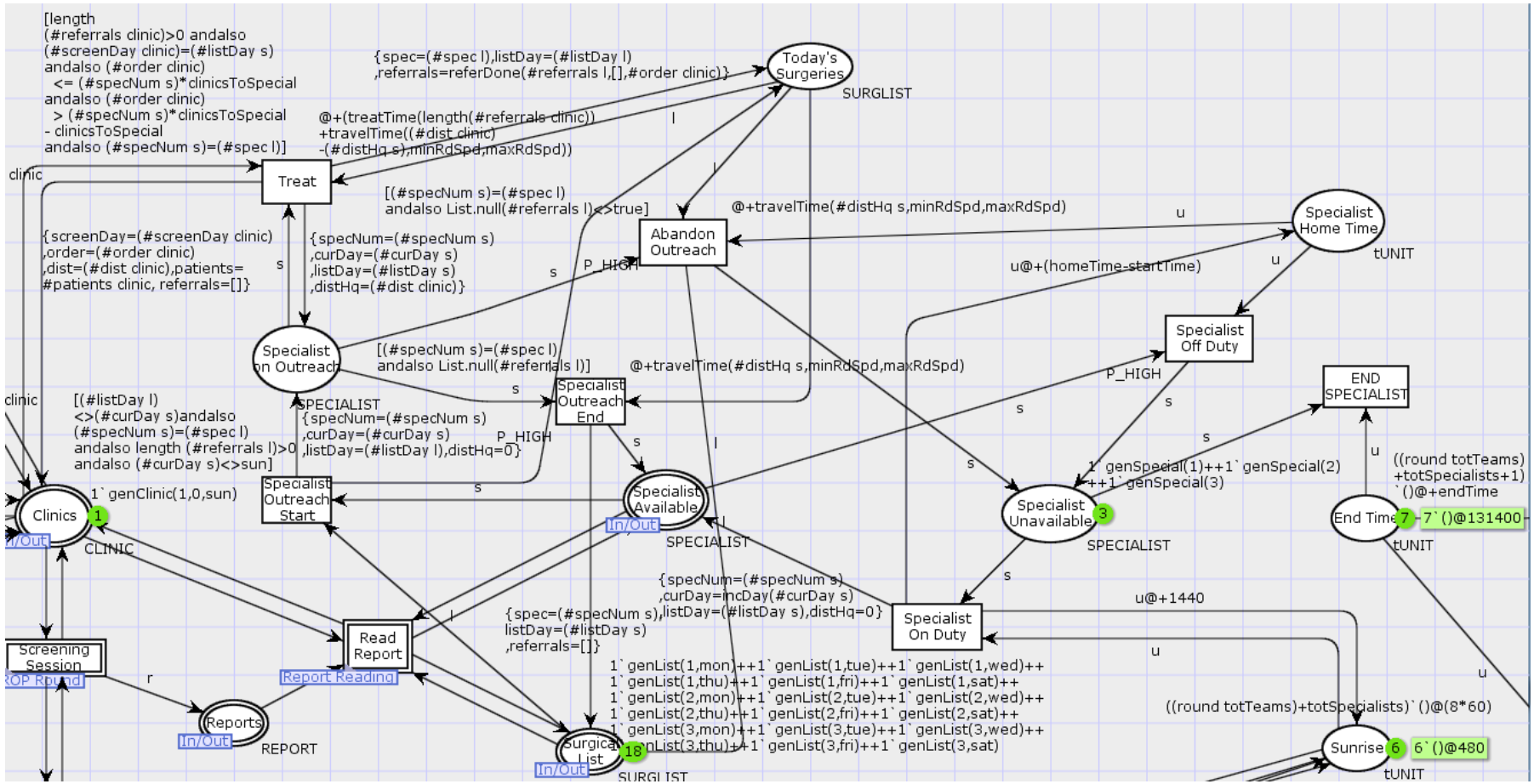

Figure 77 - CPN of the ophthalmologists' workflow, including linkage to screen report review.

The log file was filtered using the 'Filter events' action in ProM so that only the events indicating the start and completion of a screening session, as well as that for the final termination of the clinic after 3 months had elapsed. The PowerShell 2.0 (Microsoft Corp.) script shown in Appendix 7.1 was then used to separate these events into separate log files according to the clinic with which they were associated. A Petri net modelling only the remaining events was generated by arbitrarily choosing one of the 81 single clinic log files and using this as an input for the inductive miner in ProM. Each of the log files was then replayed on this Petri net to provide a sequence pattern manifest for each clinic. These were then exported as comma-separated data files and the start and end times of each screening session extracted using the PowerShell 2.0 script shown in Appendix 7.2.

To improve the reliability of results, the burn-in period required for the effects of the models' prior assumptions to be negated was calculated by plotting boxplots of the main quantitative prior assumption, namely infants enrolled in the programme, and visually assessing when this had achieved a steady value. This burn-in was then verified by excluding all enrolment data prior for the period and conducting a repeated-measures analysis of variance (ANOVA) for each model in R 3.2.1 to confirm convergence of this variable. Events prior to this point of convergence were then excluded from the subsequent analysis.

The total number of simulation iterations required (R) and summary statistics for the time spent screening infants in each clinic were calculated as was described for the community eye screening simulation in 6.2.4.

Due to computing resource restraints, a maximum of eleven simulations were run in sequence. Where more than eleven runs were required, multiple sequences were run and the relevant portions of the log files were concatenated into a single ProM-readable log file using TextPad (Helios Software Solutions, Preston, UK).

7.2.6 Estimation of Ongoing Programme Costs

Staff related programme costs were estimated by multiplying the reported median hourly rate for each role by the number of hours that the relevant model predicted they would be working on the programme over the simulation period. Hourly rates

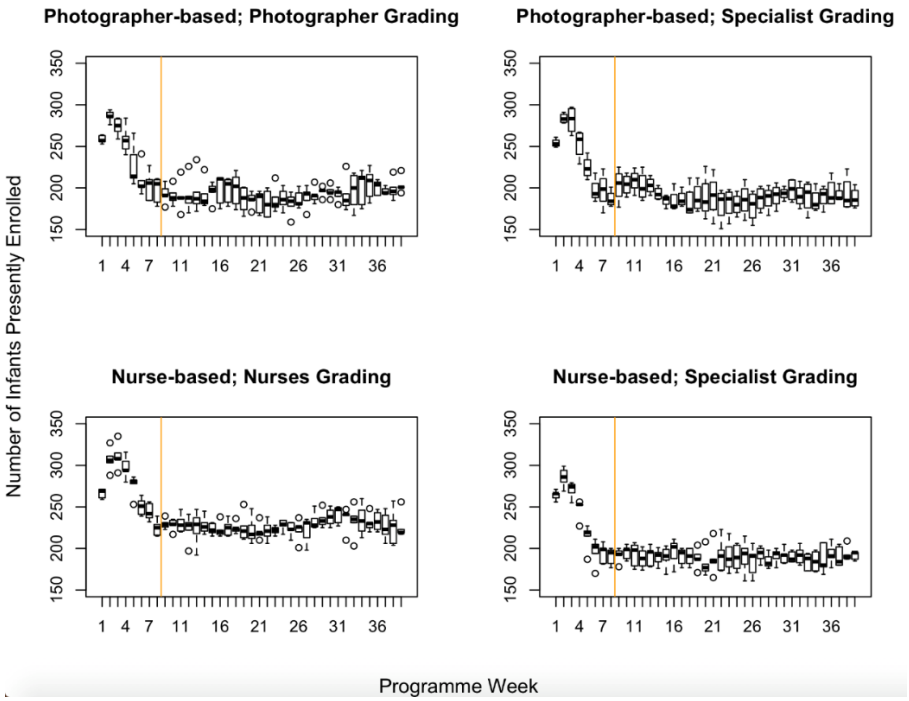

Figure 78 – Number of infants enrolled in the programme by programme week for each simulation scenario. The chosen burn-in is shown to the left of the orange line.

were taken to be 79.38, 83.64, 97.84 and 399.36 INR for the van driver, medical photographer, NICU nurse and ophthalmologist respectively (330). It was assumed that for each of the models, a full-time programme manager would be employed irrespective of time spent on individual tasks in the programme. Any overtime was priced at the same regular hourly rate.

For the retinal photographer-based models, it was assumed that the photographer and one NICU nurse, to restrain and provide care to the infant, were required for the duration of each screening session. For the nurse-based models, it was assumed that two NICU nurses were required for the duration of each screening session, with one performing the tasks relating to retinal imaging and the other, those relating to patient care. The driver was costed only for time spent on the road with the screening team as once the screening team was delivered he or she could then potentially be freed up for other tasks, albeit in the area local to screening time so that they can return to the clinic to take them to their next destination. Ophthalmologists were assumed to drive their own vehicles and therefore a driver was not required to be allocated to outreach related transport.

The other major ongoing cost incurred by such a programme is that of fuel. Fuel costs were estimated by multiplying the reported average diesel cost per kilometre in India, 2.42 INR/km, by the distances travelled by the screening team and ophthalmologist (331).

For all currency conversions the rate quoted by exchange rate website xe.com for the simulation start date, the 2nd January 2012, was used (xe.com/currencytables/).

7.3 Results

7.3.1 Simulations Summary

A provisional eight-week burn-in period was chosen based on visual assessment of the box plots shown in Figure 78. Repeated measures ANOVAs of the infants enrolled in the programme then verified that there was no significant difference in the number of infants enrolled in the programme after week 8 and thus that the burn-in period was appropriate (Nurse operated; specialist grade: $F(30,120) = 0.386$;

	Photographer-operated; specialist graded	Photographer-operated and graded	Nurse-operated; specialist graded	Nurse-operated and graded
$R_{Screening\ Time}$	2	3	1	1
$R_{Screening\ Team\ Travel\ Time}$	1	22	N/A	N/A
$R_{Outreach\ Time}$	5	1	7	3
$R_{Report\ Reading\ Time}$	6	N/A	3	N/A
$R_{Infants\ screened}$	3	4	2	1
$R_{Screening\ sessions}$	3	4	3	2
$R_{Sensitivity}$	2	3	1	1
$R_{Specificity}$	1	1	1	1
$R_{Screening\ Travel\ Dist.}$	1	1	N/A	N/A
$R_{Outreach\ Travel\ Dist.}$	9	22	6	7

Table 28 - The number of simulation runs estimated to be necessary so to arrive at results within 95% confidence.

Model	Infants Enrolled	Infants Completing Screening	Screening Sessions	Referral Sensitivity	Referral Specificity
Photographer-operated; specialist graded	2354 ±39	1690±48	6634±190	0.9392 ±0.0206	0.9420 ±0.0042
Photographer-operated and graded	2389 ±58	1723±56	6782±235	0.8743 ±0.0231	0.9748 ±0.0030
Nurse-operated; specialist graded	2335 ±46	1700±34	6751±197	0.9777 ±0.009	0.8012 ±0.0116
Nurse-operated and graded	2343 ±26	1689±21	7888±120	0.9308 ±0.0063	0.9549 ±0.0063

Table 29 - Infant enrolment and screening efficacy of the four different simulation scenarios

p=0.998, Nurse operated; non-specialist grade: F(30,120) = 0.919; p=0.591, Photographer operated, specialist graded: F(30,90) = 0.868; p=0.662 ,Photographer operated, non-specialist graded: F(30,120) = 1.002; p=0.474).

The estimates for the simulation iterations required for accurate results for each output of the models are shown in Table 28. Of these, the largest was for the time spent by the ophthalmologist on outreach in the photographer operated and graded model, which was estimated to provide accurate results after 22 iterations. For consistency, each model was therefore run 22 times in total.

7.3.2 Screening Coverage and Efficacy

Very few screening sessions were abandoned, with a mean of 1.80±1.48 and 1.80±1.10 sessions being missed screening activities being abandoned before every NICU had been reached for the photographer operated, specialist-graded and photographer operated, photographer graded respectively. In each case, only a single clinic was skipped every time a day's screening activities were abandoned. This equated to less than 0.1% of all scheduled sessions in each case. In the case of the photographer-graded model, this never resulted in a referral being missed. In the ophthalmologist-graded model, on average there were 0.5 referrals made a week that were after earliest diagnosis was possible due to screening sessions being cancelled.

Due to the nature of its design, no screening sessions were abandoned in the nurse-operated model.

The models' results relating to infant enrolment as well as screening efficacy are shown in Table 29. Significantly more screening sessions were conducted in the model where nurses' grading reports were not reviewed by an ophthalmologist (p=0.964, two-tailed Z-test). Grading sensitivity was found to be significantly lower in the photographer graded model compared to the nurse graded model (p=0.04253; Fisher's exact test; CI:95%) whilst the grading specificity was found to be significantly higher (p=0.0039; Fisher's exact test; CI:95%).

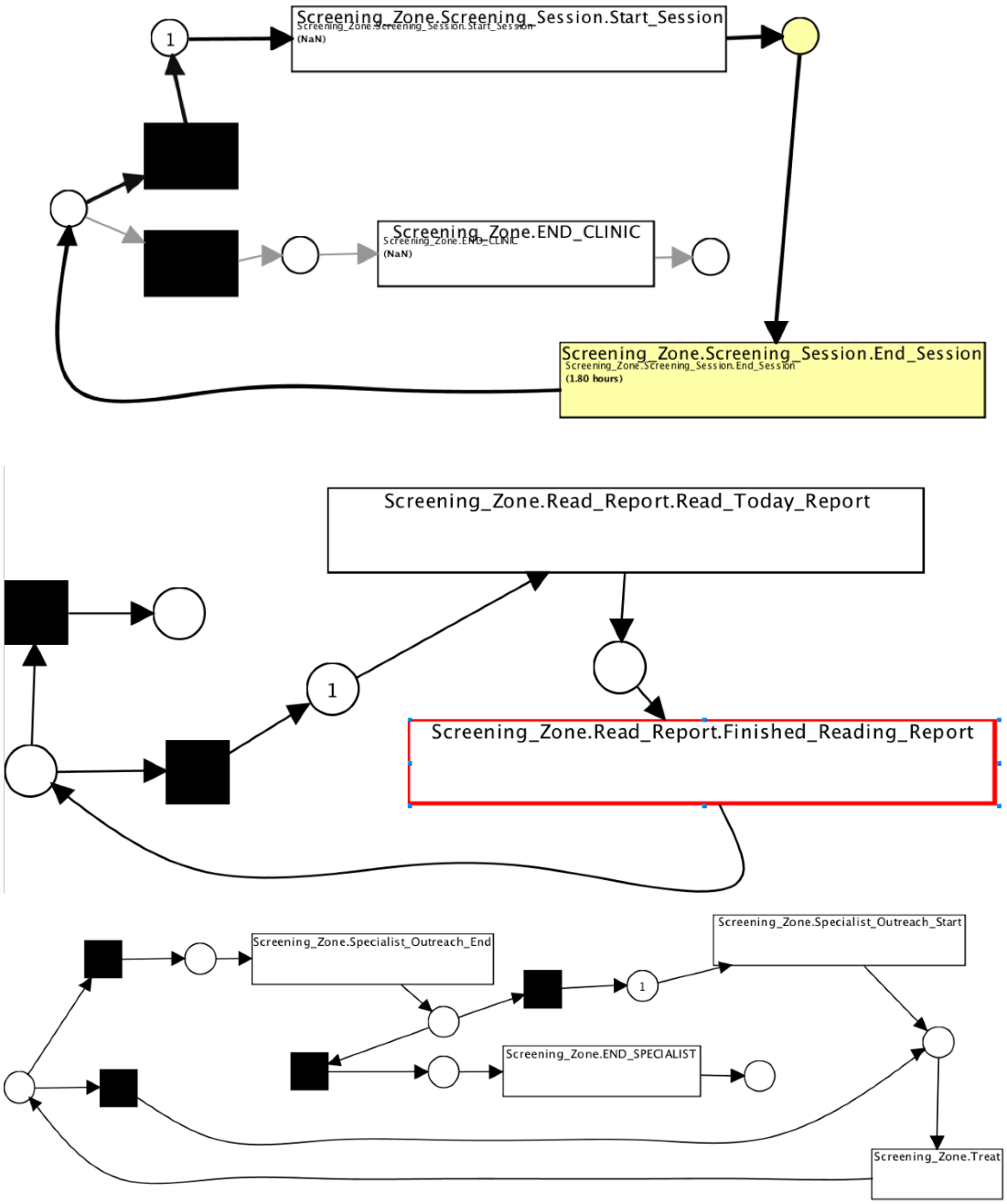

Figure 79 - The Petri nets generated by the inductive miner in ProM 6.7 to represent the high-level screening (top), report reading (middle) and treatment processes (bottom).

Model	Screening Team Travel (mins)	Screening (mins)	Outreach (mins)	Report Reading (mins)
Photographer-operated; specialist graded	68133±557	216620±4747	22499±904	10270±430
Photographer-operated and graded	67842±588	220619±5634	35529±2933	0
Nurse-operated; specialist graded	0	329023±4919	14866±708	12330±367
Nurse-operated and graded	0	355279±1923	51784±1886	0

Table 30 – The mean and standard error of the mean of the total time spent on each task across all simulation runs.

7.3.3 Treatment Coverage

No treatment outreach activities needed to be abandoned in any of the simulations of either model. This meant that all infants requiring treatment received this within 48 hours of referral, as per the treatment guidelines (159).

7.3.4 Task Distribution

The Petri net generated by the inductive miner in ProM 6.7 and used for extracting the total time taken for each screening clinic, screening report review and treatment clinic are shown in Figure 79.

The times allocated to each of the high-level tasks involved in the models are shown in Table 30. The time allocated to screening differed significantly across the models. The nurse graded model had more time allocated to screening than the other models owing to the additional time spent screening infants who would have been discharged had they been reviewed by an ophthalmologist (z=11.12; two sample z-test comparing to the sample with the next highest value). Significantly more time

	Staff Costs (INR) ± SD				Travel Costs (INR) ±SD		Total (INR) ±SD
Model	**Driver**	**Photo-grapher**	**NICU Nurse**	**Ophthal-mologist**	**Screening**	**Outreach**	
Photographer-operated; specialist graded	90144 ±737	396935 ±6663	353245 ±7742	283854 ±6015	312721 ±1894	40938 ±944	**1,436,034 ±22195**
Photographer-operated and graded	89760 ±778	402104 ±7897	359766 ±9188	236482 ±19525	314956 ±1905	62437 ±2305	**1,465,506 ±23,185**
Nurse-operated; specialist graded	0	0	1073082 ±16043	181018 ±5307	0	46199 ±844	**1,300,299 ±16919**
Nurse-operated and graded	0	0	1601244 ±14146	344672 ±12553	0	97856 ±1790	**1,601,244 ±8451**

Table 31 – The ongoing mean programme costs for each model. SD = standard deviation.

was also spent screening in the nurse operated, specialist graded model compared to its two photographer operated counterparts (z=36.76 and z=33.31 for comparisons with specialist graded and photographer graded respectively; two sample z-tests).

The amount of ophthalmologist time allocated to outreach also differed significantly across models. Both of the models where screening reports were not subject to ophthalmologist review had significantly more time allocated to outreach, owing to the likelihood of unnecessary referrals to the ophthalmologist (z=-9.494 and z=-40.98 for photographer-based and nurse-based respectively). Of these, the model where images were graded by nurses had a far greater time allocated to outreach due to the nurses having a higher propensity to err on the side of caution, resulting in more unnecessary outreach sessions. Furthermore, when the time spent reviewing screening reports was included, there was still a significant difference in the ophthalmologists' time required between non-specialist and specialist graded models (z=-1.991 and z=-22.85 for the difference between the two photographer and nurse operated models respectively.

7.3.5 Ongoing Costs

A breakdown of the various ongoing costs incurred in each programme are shown in Table 31. The nurse operated model with ophthalmologist screening reviews was found to have the significantly lower ongoing cost of 1,300,299±16919 INR (z=-16.58 compared to the next cheapest model). This model had significantly less cost being incurred on outreach travel and ophthalmologist time compared to its non-specialist graded counterparts (ophthalmologist time cost: z=-6.130 and z=-26.85 for comparison with photographer operated and graded and nurse operated and graded respectively; outreach travel cost: z=-14.79 and z=-58.377 for comparison with photographer operated and graded and nurse operated and graded respectively). It also had no cost associated with screening travel unlike the photographer-operated models. Of the other models, the nurse operated model that did not have ophthalmologist screening reviews was found to be significantly more expensive than the next most expensive model (z=12.30).

7.3.6 Setup Costs and Estimation of Camera Production Cost

The two main variables relating to the setup cost of the models considered are the price of the camera and the van required to transport it and the team. The retinal camera employed in the KIDROP programme is known to cost approximately 100,000 USD (332). The cost of purchasing a suitable vehicle per screening team and camera can be estimated to be approximately 1,542,310 INR (28,932 USD). The total setup cost when accounting for these two costs only can therefore be approximated to 386,796 USD.

If this setup cost were to be matched, the equivalent amount that is available to be spent on the retinal camera in the photographer operated and nurse operated models respectively would be 3704 and 4775 USD. As the nurse operated model with ophthalmologist screening reviews was shown to be the optimal model with respect to ophthalmologist time spent and ongoing costs, the latter setup cost was considered the upper limit for the end user cost of the ROP camera design.

It is reasonable to estimate that the medical device distributor involved in sale of the camera would require a 100% mark-up on the wholesale price and that the manufacturer would in turn require a 50% margin on the manufacture cost. Therefore, the target manufacture cost for the design was estimated to be 1400-1600 USD.

7.4 Discussion

The models presented in this chapter suggest that a nurse operated screening programme where screening reports are reviewed by ophthalmologists ought to provide significant improvements with respect to ongoing costs and burden on ophthalmologists. Both these factors are substantial barriers with respect to widespread implementation of ROP screening and treatment programmes in LMICs.

7.4.1 Design implications

Three main design implications can be extracted from the results detailed in this chapter. Firstly, as the nurse operated, specialist graded model was found to be advantageous in terms of ongoing costs, the device must be of an ease-of-use that allows operation with a

skill level that can be expected of a NICU nurse rather than a specialist retinal photographer. Therefore, the field-of-view ought to be as large as possible to minimise the need for scleral indention and the risk of key parts of the retina being missed out from an image set or video. Furthermore, the device should be as light and manoeuvrable as possible and not require a surgical-level of precision in the positioning of the camera, for example in the way that indirect ophthalmoscopy requires a lens to be placed at a very specific distance from the eye. Together, these conclusions suggest that a camera that employs direct ophthalmoscopy and that goes in contact or near-contact with the cornea, in order to attain the largest possible field of view, may be the most appropriate type of optical design.

Secondly, as the nurse-operated model reduces ongoing costs by not needing to move cameras between clinics, the end-user cost of the device must be such that one can be purchased for every clinic opposed to having a smaller number of more expensive 'roaming' cameras. Specifically, it was calculated that the end-user cost ought to be no more than 1600 USD, several orders of magnitude less than that of presently available wide-field fundus cameras. Thus, the design should seek to use stock components where possible, to reduce manufacturing costs, as opposed to incorporating custom lenses, for example.

Finally, given the significantly larger amount of time allocated to specialist outreach when specialists were not involved in grading, there is a requirement to send imaging reports to the main hospital for review by the ophthalmologist. The system must therefore be able to connect to the internet, either directly or via interfacing with a mobile device. Controlling the device and storing capturing images via a user interface deployed on a tablet PC capable of mobile internet connectivity would therefore be advantageous.

Future extensions of the ROP screening model could probe alternate screening protocols. Such protocols could include removing the use of ocular specula and scleral indention as well as the use of insulin-like growth factor 1 (IGF-1) in the prevention of ROP. The absence of ocular specula and scleral indention may reduce the quality of imaging but reduce more systemic impacts on infants. The use of IGF-1 is an interesting case to consider from a clinical workflow perspective given its considerable impact on screening duration, with infants needing to be monitored for longer before being discharged and the need for less laser photocoagulation treatments (156).

7.4.2 Limitations

There are a number of limitations of the models described. Foremost of these is the assumptions relating to travel distances. The inclusion of real data of the distances between clinics would improve the accuracy of the model. Similarly, no data concerning the length of time required to grade an ROP image could be sourced. Whilst grading of other retinal disease is not a dissimilar task, given the number of times this task was performed in the simulations, having ROP-specific estimates would yield more a reliable analysis. Additionally, the models also assume that each member of staff is constantly available for work within the programme during working hours, other than when engaged on another ROP related task. In reality, staff would be unavailable during various hours and even days throughout the week due to other commitments relating to their roles. Application of the model to a specific programme would need to consider this reality.

In future work a sensitivity analysis ought to be conducted in order to quantitatively determine the impact of variability in parameters, such as enrolment rate and travel distances. Such analysis would seek to understand how much the model coefficients can vary without changing the above conclusions and corresponding design choices they implicate (311). This would first require reasonable ranges and variability statistics for each parameter to be established as well as correlations between parameters, sensitivity indices and break-even values to be calculated (312, 333). After running an initial sensitivity analysis to exclude unresponsive parameters, a modelling experiment that allows an appropriate combination of parameter changes could then be run. A potential method for doing so would employ Mote Carlo approaches such as Latin hypercube sampling given that a complete factorial design is not likely to be computationally manageable owing to the number of possible scenarios (313).

Nevertheless, despite these limitations the results of the simulations are broadly in-line with the expectations of key-opinion leaders in the field of paediatric eye care in LMICs, and thus the design implications the simulations suggest have been incorporated into the designs discussed in the remaining chapters in this thesis.

7.5 Licensing Information

SECTION 5

Chapter 8 - Postmenstrual Age-dependent Statistical and Optical Models of the Preterm Eye

Chapter 9 - Design and Prototyping of a Preterm Infant Retinal Imaging Phantom

Chapter 10 - LMIC ROP Camera Technology Demonstrator

8 Postmenstrual Age-dependent Statistical and Optical Models of the Preterm Eye

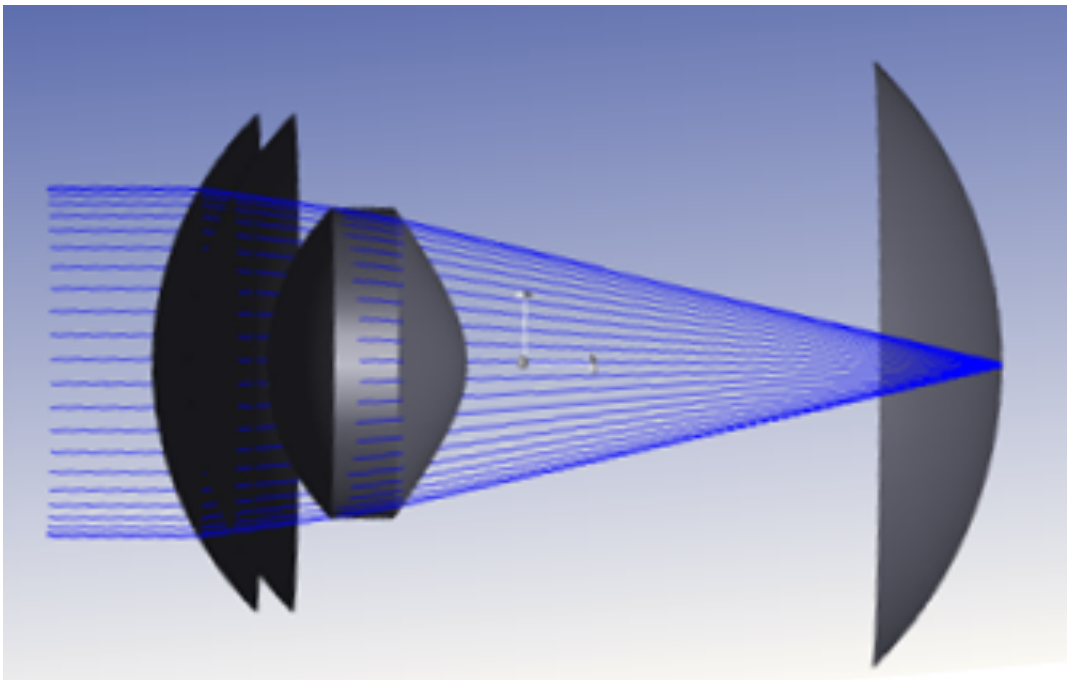

8.1 Introduction

The aim of this fifth section of the thesis is to design, prototype and lab-test a retinal imaging solution that offers an effective ROP programme in LMICs where screening for the disease is currently unfeasible. In order to achieve each of these objectives it is first necessary to understand how the eye develops during preterm.

The biometry of the eye during preterm is considerably different from that of the eye at term and later life (334). An optical model of the preterm eye is therefore useful in designing imaging equipment for the purpose of screening and diagnosing eye disease such as ROP during the preterm period (335). Additionally, such a model may have value with respect to other topics, such as understanding the eye's development during preterm, identifying abnormal biometries associated with certain diseases, simulating and planning surgeries and developing other types of diagnostic devices. However, to the author's knowledge, no such model has been described in the peer-reviewed literature. Furthermore, although there have been multiple studies investigating the anatomical characteristics of the preterm eye, it was not possible to find a study that has sought to measure all of the characteristics pertinent to a complete optical model nor a systematic review which sought to collate the disparate studies reported in the peer-reviewed literature.

This chapter therefore presents such an optical model of the preterm eye based on a meta-analysis of the peer-reviewed literature discussing preterm ocular biometry.

8.2 Methods

8.2.1 Protocol and registration

The literature review involved in this chapter was conducted and presented in accordance with the Preferred Reporting Items for Systematic Reviews and Meta-Analyses (PRISMA) guidelines (38). The completed PRISMA 2009 checklist used to track adherence to this protocol is included in Appendix 8.1.

	OR			
	AND		AND	
	Title Contains one of	**Title Contains one of**	**Title Contains one of**	**Title Contains one of**
OR	preterm premature neonatal prematurity	refractive error myopia hyperopia astigmatism keratometry refraction refractive status	Eye ocular cornea corneal pupil pupillary iris anterior chamber crystalline lens posterior chamber vitreous chamber retina anterior segment posterior segment	biometry dimensions size length width curvature diameter radius thickness depth conic refractive index index of refraction angle light reflex light reflexes

Table 32 - Search criteria for the review of the preterm ocular biometry scientific literature.

8.2.1 Inclusion criteria

Studies' eligibility for inclusion in the analysis was restricted to those investigating ocular biometry of the early life of prematurely born infants, which are those born at less than thirty-seven weeks' GA or 1500g and examined at or at less than fifty-two weeks' PMA.

8.2.2 Exclusion criteria

Whilst later development of the visual system of those born prematurely is certainly of academic and clinical interest (336), it was considered outside the scope for this thesis. Article selection was also restricted to those considering ocular biometry prior to any direct surgical interventions, cryotherapy or laser treatments.
Those articles discussing ocular features unrelated to the eye's optics, such as retinal features, were also excluded as were those investigating neuropathy, veterinary medicine or animal models.

Only articles in English, or for which an English translation of the abstract was available, have been included.

8.2.3 Information Sources

The U.S. National Library of Medicine's PubMed and MIMAS' Web of Knowledge databases were searched for studies to be included in the analysis.

8.2.4 Literature Search

The search criteria were constructed using the PICOS search strategy (patient population, intervention, comparison, outcomes and setting)[19].

The PubMed search terms were as specified in Table 32.

A similar set of search terms was used for searching Web of Knowledge. The exact code for both of these is included in Appendix 8.3.

[19] The PICOS worksheet used in constructing the search strategy is shown in Appendix 8.2.

Results from both searches were compiled using EndNote X7 (Clarivate Analytics, New York City, NY, USA). Supplementary searches were also conducted on both databases replacing the preterm, premature and neonatal terms with "foetal OR fetal".

8.2.5 Article Selection

Eligibility assessment was conducted in an unblinded manner firstly by the thesis' author and subsequently independently by his PhD programme supervisor. Articles were screened and reviewed according to the process represented graphically in Figure 81. After removing duplicates, the unique articles had their titles screened for relevance. Following this, articles deemed eligible had their abstract screened, with those qualifying then undergoing full-text assessment. Where disagreement arose between the reviewers as to the eligibility of an article for full-text assessment discussion was held until a consensus was reached.

8.2.6 Data Collection and Synthesis

Models of any data items relevant to an optical model were recorded in a bespoke server-based spreadsheet in Excel (Microsoft Corp.) which sorted by the data item modelled, co-variants and presence of disease.

8.2.7 Data items and Summary Measures

Each of the analysed studies were searched for data relating to any of the variables required to build an optical model of the eye. These include: the thickness, curvature, conic constant, diameter, refractive index and Abbe coefficient of the cornea or crystalline lens; the axial length of the anterior chamber, vitreous chamber or the eye as a whole; the refractive index and Abbe coefficient of the vitreous or aqueous humour; the curvature and conic constant of the ocular fundus; the thickness of the iris and diameter of the pupil.

8.2.8 Risk of bias in individual studies

Version 5.1.0 of 'The Cochrane Collaboration tool for assessing risk of bias' was used to assess the included studies risk of bias (337). An Excel worksheet based on the tables generated from RevMan 5.3 (The Cochrane Collaboration, London, UK) was used to compile the resulting risk assessments.

8.2.9 Synthesis of results

Where more than one study reported a given data item, a meta-regression was conducted using the 'metafor' package for R version 3.2.1 (The R Foundation for Statistical Computing, Wirtschaftsuniversität Wien, Vienna, Austria) (338). This involved creating a linear mixed-effects model using a restricted maximum-likelihood estimator for the given data item with post-menstrual age (PMA) as a moderator (339). For each model a Q_M-test was conducted to estimate the variation in the given data item explained by the model and to test the null hypothesis that the average effect of the moderators on the data item is zero (340). A Q_E-test was also conducted to calculate the I^2 statistic and provide an estimate of the proportion of the total variation across studies which is beyond chance, having accounted for the moderator or moderators (341).

The studies included in these meta-regressions were those that provided summary statistics for discrete PMAs. Where available, additional moderators, such as gestational age (GA) at birth, birth weight and inclusion of threshold ROP (t-ROP), were included in the analysis.

A comprehensive growth model of the preterm eye was then produced by applying the chosen individual growth models for each co-variant. For co-variants where no model of growth within the pre-term eye was available, a model for growth of the foetal eye was substituted if this was available from the supplementary literature searches. Where no model for either the preterm or foetal eye was available, reasonable assumptions were made based on what is known about the infant, child or adult eye.

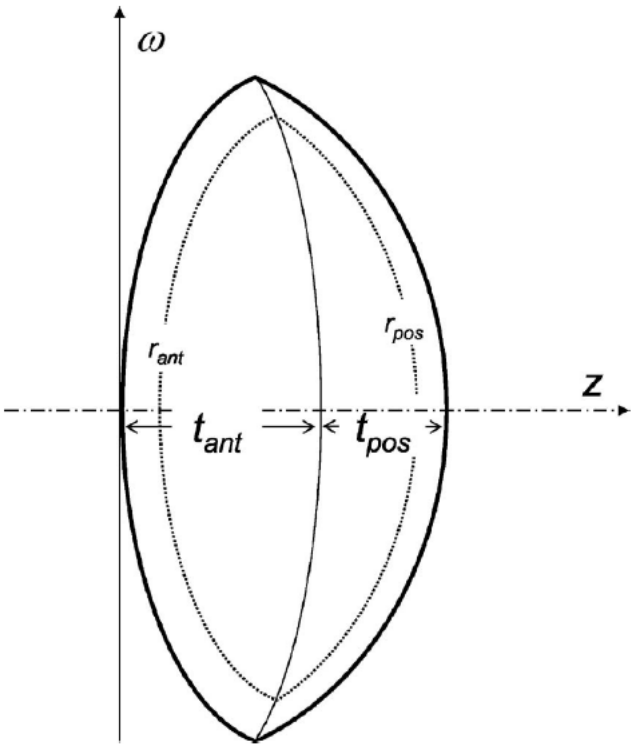

Figure 80 – The Navarro model of the crystalline lens comprising a cemented. r_{ant} and r_{pos} are anterior and posterior sides of a particular iso-indicial contour within the lens. t_{ant} and t_{pos} are the thicknesses of the anterior and posterior parts of the doublet respectively along the optical axis. Reproduced with permissions from (342).

As the vitreous chamber depth (VCD) was the least reported axial biometry, it was calculated as the axial length (AXL) reduced by the sum of the rest of the axial biometries. This avoided an inconsistency between the AXL and the axial lengths of its component parts.

8.2.10 Risk of bias across studies

For each study, funnel plots of the inverse of the co-variant's standard error were plotted. Symmetry was assessed both visually via funnel plots, and formally with the QE test for heterogeneity.

8.2.11 Optical modelling

The optical model was developed in Optic Studio 14.2 (Zemax LLC, 10230 NE Points Dr., Kirkland, WA, USA) and is available from the author's institutional repository (http://dx.doi.org/10.15129/fbe0b925-f28d-460c-b121-e3ada73a63cc).

The author is not aware of any existing model of the preterm crystalline lens. However, Navarro and colleagues have published an age-dependent gradient index lens model (342). This model overcomes the so-called 'Brown's Lens Paradox', that is the observation that the crystalline lens' radii of curvature decrease with age whilst the power of the lens increases (343). It does so by calculating the lens' index according to its external shape and an additional phenomenological parameter that varies with age. Initial testing of the optical model with a fixed refractive index showed that the Brown Lens Paradox holds, at least in part, for the preterm eye with the lens radii being required to take values which increase the lens power in order to achieve the refractive errors reported in the literature. Thus, it was considered a reasonable assumption that Navarro's model holds for preterm infants, however it should be noted that this has only been validated with child and adult lenses and not, to the author's knowledge, preterm lenses (344). Thus, it was possible to model a lens where the curvature and conic of the anterior and posterior surfaces differ. The model itself essentially comprises a cemented doublet as shown in Figure 80. Each part has a continuous refractive index distribution which increases monotonically from the surface to the centre. The two parts do not meet at the lens' equatorial

plane but rather, as has been observed experimentally, at a conicoidal surface (343). The position of this surface depends solely on the external dimensions of the lens and a single age-dependent parameter.

Using this model, it was further assumed that, as per the Zemax OpticStudio adult eye model, the anterior face of the lens is spherical and the posterior surface is hyperbolic in shape (276)

Given that both the anterior and posterior radii of curvatures of the crystalline lens as well as its posterior conic constant were unknown, it was not possible to solve these values algebraically despite having age-dependent values for the refractive error, as there are many possible solutions which could satisfy the problem. However, it is known that the crystalline lens' radii of curvature reduce as it develops during pre-term and early life, meaning that the "direction of travel" of both radii is defined. Similarly, the crystalline lens is known to become more aspherical as it develops, implying a conic constant that increases in magnitude with age. If it is then assumed that the shape of a pre-term infant's lens at 40-weeks' PMA are close to those of full-term infant at birth, the radii for each adjacent week (i.e. 39- and 41-weeks' PMA) can be found if it assumed that the correct solution is that which varies both radii of curvature by the smallest quantity possible along the direction of travel in order to satisfy the required refractive error.

The values from the Lotmar newborn eye model were used as starting values for the radii of curvature and, in absence of a value for an infant eye model, the posterior conic constant starting with that of the Zemax OpticStudio adult model (276, 345). As it is widely reported that the crystalline lens starts development as near-spherical and develops its aspherical shape as it grows, it was assumed that the conic constant of the preterm lens was less than that reported in the adult eye model. The mean spherical equivalent error was taken to comprise both the optical system's defocus and primary spherical error, combined using the method outlined by Rosenfield (346), that is,

$$M\ [\mathrm{D}] = -\frac{\left(4\sqrt{3}c_2^0 - 12\sqrt{5}c_4^0\right)}{R^2\ [\mathrm{m}]} \qquad \textbf{(19)}$$

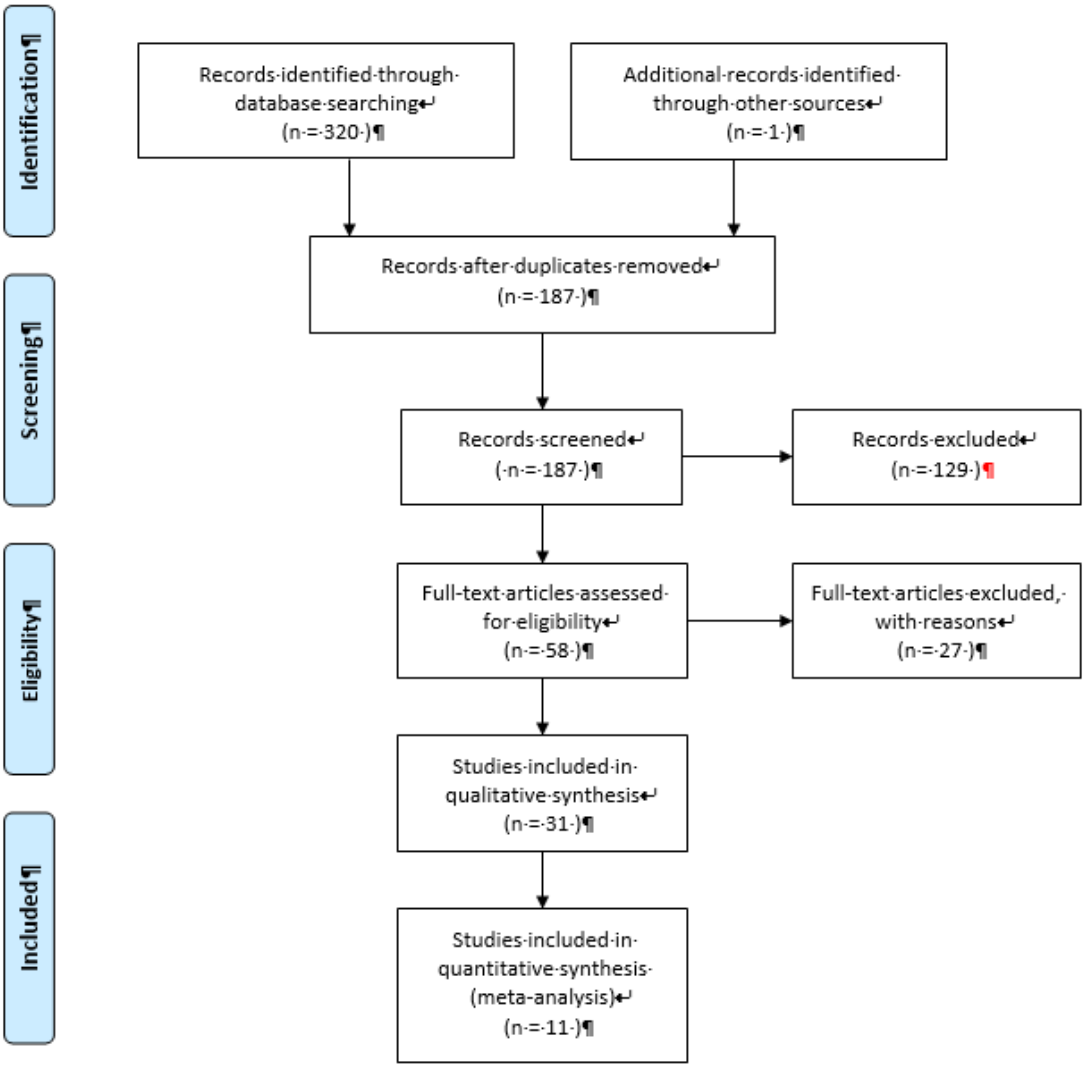

Figure 81 - PRISMA 2009 Flow Diagram describing the literature search conducted. Adapted from (38) with permissions.

where M is the MSE in dioptres, c_2^0 is the Zernike coefficient for defocus, c_4^0 is the Zernike coefficient for primary spherical error and R is the pupil radius. It was assumed that the primary spherical error only accounted for a total of 10% of the total mean spherical error as in the adult eye (346).

A damped least squares Monte Carlo simulation (referred to as 'Hammer Optimization' in Zemax Optic Studio (347)) was used to solve the model for the mean spherical error (MSE) of a 40-weeks' PMA preterm infant(348). A custom merit function was created to enforce the directions of travel and assumptions defined above and thus arrive at the solution that provided a lens shape closest to that of the Lotmar newborn eye model.

After calculating the remaining model parameters for 40-weeks' PMA, its lens curvatures and conic were used as starting values for similar simulations run for 39- and 41-weeks' PMA, whose results were used to seed simulations for one week younger and older respectively. This process was repeated until results were calculated for every week between 28- and 52-weeks' PMA.
Insufficient information regarding the axis and degree of astigmatism exists to allow the corneal deformation and retinal eccentricity to be modelled.
Statistical analysis of the simulation results was conducted using R version 3.2.1.

8.3 Results

8.3.1 Study selection

As is shown in Figure 81, 320 records were returned from the two database searches described in the methods section below, of which 134 were duplicates. One record identified outside of the searches by one of the thesis author's supervisor was added (317). As this record was later excluded during a full-text review, this was not taken to indicate a deficiency in the search criteria. 106 records were considered for abstract review after title screening. The principle reasons for article exclusion were a focus on long-term refractive status, retinal features, effects of specific treatments, neurology, veterinary medicine or animal models. Twenty-three articles were excluded due to their abstracts not being available or having no translation into

English. Additionally, ten records related to letters to the editor, editorials, case reports, reviews or meeting abstracts did not directly report the details of any clinical study. Beyond this, fifteen abstracts were found not to meet the inclusion criteria and thus fifty-eight articles were deemed to qualify for full-text assessment. The full-text of two of these studies was not accessible in English and twenty-five studies did not meet the inclusion criteria, leaving thirty-one studies for the qualitative synthesis. Eleven of the studies were found to report data that allowed their inclusion in the quantitative synthesis of results.

Lens diameter was the only ocular parameter not reported in the literature concerning preterm infants. Three sources concerning foetuses were considered eligible for review (349-351). One related to aborted foetuses, the others to live foetuses. The latter are a better model for preterm infants and thus were included in the quantitative analysis.

8.3.2 Study Characteristics and Findings

Of the thirty-one studies selected for qualitative analysis, ten investigated refractive error (352-359), three pupil diameter and light response (360-362), two corneal diameter (363, 364), seven axial length (354, 358, 365-369), six anterior chamber depth (354, 358, 366, 367, 369, 370), five corneal curvature (354, 355, 358, 371, 372), four lens thickness (354, 358, 367, 369), eleven central corneal thickness (364, 368, 373-381) and seven intra-ocular pressure (368, 373, 375, 376, 379-381). The characteristics and findings of these studies are summaries in Table 33 overleaf.

Study	Participants (n; inclusion criteria)	Control	Measurements Conducted	Findings / Comments	Reason(s) for exclusion from Quantitative Analysis
Graham & Gray (1963)	150 preterm infants < 1 wk old	98 infants born at full term	Cycloplegic refraction	Compares refractive error to hours of oxygen therapy.	Does not report GA, PCA, birth weight or ROP status.
Inagaki (1986)	7 preterm infants between 34 and 42 wks PCA	11 full term infants aged 2 wks	Cycloplegic keratometry	Report rapid growth of corneal curvature towards normal childhood range within 12 weeks.	Only 4 infants were premature and all were of GA ≥ 34
Robinson & Fielder (1990)	50 preterm infants <37 wks GA	None	Pupil diameter and light response	Light response never present at <27 wks PMA and always at >34 wks	Pupil diameter is not reported by PMA
Al-Umran & Pandolfi(1992)	127 preterm infants <36 wks GA	None	Horizontal corneal diameter	Corneal diameter ranged from 7.75 mm to 10mm.	Reports regression line versus GA in 1st week of life
Quinn et al. (1992)	2916 preterm infants at 3, 6, 12 months post-term with BW < 1251g	None	Cycloplegic refraction	Birthweight and ROP stage are strong predictors of myopic RE at 3 months post-term	Does not report mean MSE at 3 months corrected age.
Laws et al. (1994)	134 preterm infants with ROP stages 1-3, GA < 32wks or BW < 1500g; 32 < PCA < 41 wks	27 preterm infants without ROP selected randomly from O'Brien & Clark (1994)	Axial length	Stage 3 infants reaching the threshold for cryotherapy had shorter axial length than stage 3 infants not receiving treatment.	Included – assumed PMA was mislabelled as "post-conceptual age" and PCA as otherwise term would be defined as GA = 43wks
O'Brien & Clark (1994)	100 pre-term infants GA<32wks;BW≤1500g; no ROP	None	Axial length ACD LT	Found difference between sexes in axial length and that mean pre-term axial length was different from those reported for those born at term	Included
Kobayashi et al. (1997)	39 pre-term infants of 25-39wk GA	None	ACD; Trabecular-iris angle; Angle opening distance; Iris thickness	Measured internal ACD within two weeks of birth.	Included iris thickness. PMA was mislabelled as PCA (defined as GA + "actual age"). Univariate data could be extracted from graphs.

Study	Participants (n; inclusion criteria)	Control	Measurements Conducted	Findings / Comments	Reason(s) for exclusion from Quantitative Analysis
Cook et al. (2003)	68 preterm infants with GA<32wk or BW<1500g and 32<PMA<52wks with no ROP	None	CC; ACD; LT; AXL; RE	Reports linear models for growth of ACD, LT and AXL and quadratic models for growth of CC and RE each as functions of PCA.	Included
Friling et al. (2004)	99 preterm infants with GA of 22-40wks; BW of 570-4400g; ROP stage <2	None	Keratometry	Significant correlation between horizontal and vertical meridians. Found decrease in meridians and the difference between each with PCA	Included – PMA was mislabelled as PCA (defined as GA + ”actual age”)
Snir et al. (2004)	33 preterm infants of 40wks PCA and ROP stage < 2.	33 term infants of 40wks PCA	Refraction Keratometry	Found no correlation between refractive parameters and GA or BW.	Included data from right eye only. Assumed PMA was mislabelled as PCA (as mean GA + mean chronological age = “PCA” at examination)
Ton et al. (2004)	390 preterm infants measured at 2wks and 6 months PCA; GA<36wks; no ROP	None	Cycloplegic retinoscopy	High correlation between spherical equivalent of both eyes in same infant. No correlation found between mean RE and BW.	Postmenstrual ages are not reported
Kirwan et al. (2005)	35 preterm infants; 30<PCA<40wks	None	Corneal pachymetry Horizontal CD	Very strong inverse correlation between CT and horizontal CD.	Included – assumed GA = PMA and “GA at birth”= GA
Varghese et al. (2005)	327 preterm infants; 24 < GA < 36; 1wk old; no or pre-threshold ROP	276 1wk old infants born at 37 < GA < 43	Mydriatic streak retinoscopy		Data extracted from same cohort as Varghese et al. (2009)
Cook et al. (2008)	136 preterm infants with ROP stages 1-3+; GA<32wks or BW<1500g; 32<PMA<52wks	67 preterm infants that did not develop ROP	CC; ACD; LT; AXL; RE	Reports linear models for growth of CC, ACD, LT, AXL and RE for each stage or ROP. Cannot conclude whether ROP is causal of biometric changes opposed to GA or BW.	Included

Study	Participants (n; inclusion criteria)	Control	Measurements Conducted	Findings / Comments	Reason(s) for exclusion from Quantitative Analysis
Mactier et al. (2008)	33 preterm infants; GA<31wks; BW<1251g; 30<PMA<55wks	None	Axial Ultrasound (VCD) Pupil diameter	Pupil diameter increased to within adult limits by ~50wks PMA. Fits non-linear regression equations.	Pupil diameter included. VCD for specific PMAs cannot be discerned from article.
Osorio et al. (2009)	6 preterm infants < 30wks PMA	None	Pupil diameter and light response	No light responses	PMA is spread over four weeks.
Varghese et al.(2009)	299 preterm infants; GA < 37wks; PMA≈GA	256 infants born at term	Cycloplegic streak retinoscopy	Linear models for MSE as functions of GA, weight and length.	Included
Uva et al. (2011)	33 preterm infants; no ROP	33 full term infants	Corneal pachymetry Tonometry	IOP and CCT are moderately correlated. Weak correlation between CCT GA, BW and PMA.	CCT and IOP are not reported per GA or PMA.
Fledelius & Fledelius (2012)	28 preterm infants with threshold ROP; GA<31wks; BW<1600g	Previous "less immaturity-loaded study	Axial A-scan Ultrasound (ACD; AXL, LT)	T-ROP infants have slight eye elongation by increasing BW.	Included AXL. Breakdown of ACD and LT not given. Assumed PMA was mislabelled as PCA.
Gunay et al. (2014)	100 preterm infants; 25<GA≈PMA<34wks	None	Corneal pachymetry	Found decreasing CCT with GA.	Included
Muslubas et al. (2014)	45 preterm infants GA <35wks;	45 full-term infants	Corneal pachymetry Tonometry	At the mean gestational age of 36 weeks CCT is not different from that of full-term newborn.	Included – "age at exam" assumed to be PMA.
Ozdemir et al. (2014)	69 preterm infants; with ROP; GA<36wks BW<2500g	118 preterm infants without ROP	Corneal pachymetry Tonometry Axial A-scan Corneal diameter	BW and GA have an indisputable effect on ocular growth. Did not detect an effect of ROP on the CD, CCT or AXL	Results for different ROP stages are not reported; no significant difference between no and some ROP.
Acar et al. (2015)	470 preterm infants; GA<32wks; 26<PCA<45wks	None	Corneal pachymetry Tonometry	Linear relationship between PCA and both IOP and CCT. CCT declines dramatically up to 40wks PCA.	Included – assumed PMA mislabelled as PCA (discussion refers to the PMA in other studies as the PCA)

Study	Participants (n; inclusion criteria)	Control	Measurements Conducted	Findings / Comments	Reason(s) for exclusion from Quantitative Analysis
Hekimoglu et al. (2015)	50 preterm infants with corrected age = 0	Pachymetry on 28 of the same cohort	Corneal optical coherence tomography	No significant difference between methods. Reports thicknesses at several points of the cornea.	Results reported for too broad a range of PMAs for CCT analysis. Only source of anterior cornea shape information.
Jethani et al. (2015)	85 preterm infants; chronological age = 2 days, 8wks, 20wks, 1 year; ROP stage < 2	>260 PCA group	Corneal pachymetry	The CCT of preterm infants remained higher compared to term infants but was not statistically significant.	Included – assumed "PCA at birth" = GA as terms are used interchangeably
Karahan et al. (2015)	63 preterm infants; GA<34wks ROP stage≤2	55 infants with GA≥37wks	Corneal pachymetry Tonometry	IOP and CCT not related to age, BW, oxygenation time or ROP stage.	Insufficient detail is reported wrt. specific GAs or PMAs
Ozdemir et al. (2015)	159 preterm infants with ROP; GA≤36;	202 preterm infants without ROP	A-scan ultrasonic biometry: ACD, LT,VCD,AXL	LT, VCD, and AXL, but not ACD, are significantly correlated with birth weight and gestational age.	Insufficient detail is reported wrt. specific GAs or PMAs
Sekeroglu et al. (2015)	170 preterm infants; GA≤32wks	None	Corneal pachymetry Tonometry	CCT and IOP are positively correlated; GA, chronological age and BW are negatively correlated with CCT and IOP	Out of bounds of PMAs selected for analysis (>52 wks)
Acar et al. (2016)	110 preterm infants; GA=28wks; PMA = 32,34,36,38,40wks; BW ≥600g(boys);550g(girls)	None	Corneal pachymetry Tonometry	Strict selection criteria by gestational age and birth weight. Uses GA and PCA interchangeably, presumably in place of PMA.	Included – assumed "gestational age" of infants born at 28wks GA, referred to PMA.

Table 33 - Summary of the characteristics and findings of the studies included in the quantitative anlaysis. GA = gestational age; PCA = postconceptional age; PMA = postmenstrual age; BW = birth weight; AXL = axial length; CCT = corneal thickness; CD = corneal diameter; ACD = anterior chamber depth; LT = lens thickness; VCD = vitreous chamber depth; RE = refractive error (i.e. mean spherical equivalent)

KEY:	+	Low risk of bias	?	Unclear risk of bias	−	High risk of bias

Study	Selection	Performance	Detection	Attrition	Reporting	Other
Graham & Gray (1963)	+	?	+	+	?	+
Inagaki (1986)	+	?	+	−	?	+
Robinson & Fielder (1990)	+	−	+	−	?	+
Al-Umran & Pandolfi (1992)	+	−	+	+	?	+
Quinn et al. (1992)	+	+	+	+	?	+
Laws et al. (1994)	+	−	+	+	?	+
O'Brien & Clark (1994)	+	−	+	?	?	+
Kobayashi et al. (1997)	+	?	+	N/A	?	+
Cook et al. (2003)	+	+	+	?	?	+
Friling et al. (2004)	+	+	+	N/A	?	+
Snir et al. (2004)	+	+	+	?	?	+
Ton et al. (2004)	+	+	+	?	?	+
Kirwan et al. (2005)	+	+	+	+	?	+
Varghese et al. (2005)	+	+	+	+	?	+
Cook et al. (2008)	+	+	+	?	+	+
Mactier et al. (2008)	+	+	+	+	?	+
Osorio et al. (2009)	+	+	+	+	?	+
Varghese et al.(2009)	+	+	+	−	+	+
Uva et al. (2011)	+	+	+	+	?	+
Fledelius & Fledelius (2012)	+	+	+	+	?	+
Gunay et al. (2014)	+	+	+	+	?	+
Muslubas et al. (2014)	+	+	+	+	?	+
Ozdemir et al. (2014)	+	+	+	+	?	+
Acar et al. (2015)	+	+	+	+	?	+
Hekimoglu et al. (2015)	+	+	+	−	?	+
Jethani et al. (2015)	+	+	+	?	?	+
Karahan et al. (2015)	+	+	+	+	?	+
Ozdemir et al. (2015)	+	+	+	+	?	+
Sekeroglu et al. (2015)	+	+	+	+	?	+
Acar et al. (2016)	+	+	+	+	+	+

Table 34 - Summary of risk of bias within studies based on format developed by Higgins and colleagues (382).

8.3.3 Risk of Bias within Studies

Every study that was included in the analysis suffered from certain, mostly unavoidable, biases. These included a lack of personnel blinding due to the fact that all studies were conducted in coordination with ROP screening during which the investigator was either present or responsible for ROP grading and was therefore aware of the infants' birth weight, ROP stage, gestational and postmenstrual age. The use of control groups was sporadic throughout the included literature with fifteen having no control group, eight using infants born at full-term as controls and four comparing infants with ROP to preterm infants without ROP.

Whilst not entirely consistent across studies, the studies' exclusion criteria tended to remove infants with any abnormality that may have affected ocular biometries, except where the aim of the study was to investigate the influence of such an abnormality, like ROP. Consequently, it was considered that each study was at low risk of selection bias. The only study that gave rise to a particular cause for concern in this regard was that of Al-Umran and colleagues which included six measurements taken immediately after a participants' death (363). However, as this was a relatively small number of measurements given the scale of the study it was considered that their inclusion was unlikely to affect the overall outcome of the study.

Robinson and Fielder's study of pupil diameter was deemed to be at a high risk of performance bias owing to an eyelid speculum being used for very immature infants but not for more mature infants (360). Similarly, Al-Umran and Pandolfi reported using an eyelid speculum in some cases but not in others without specifying any criteria for how this decision was made (363). O'Brien and Clark, likewise, reported that they did not examine infants that were too "ill or fractious" without offering any criteria for the making of this assessment (366). Laws and colleagues also reported taking fewer measurements where "general medical conditions precluded prolonged examinations" (365). Insufficient information was provided on the methods used by Graham and Gray, Inagaki and Kobayashi and colleagues in order to make an informed assessment of the risk of performance bias (352, 370, 371). All other included studies were deemed to be at a low risk of performance bias.

In most of the cases, it was not possible to blind the researcher to the condition of the patient as measurements were taken alongside ROP screening. Nevertheless, given the objective measurements in question and the tools used to take these, none of the studies gave cause for concern in relation to detection bias.

The nature of dealing with such premature infants unavoidably gave rise to a number of indications of high risk of attrition bias in a number of studies. In Inagaki's study, half of the recruited participants were excluded for unknown reasons, in Robinson and Fielder's study twelve participants died before study completion and in Varghese and colleagues second study of refractive status 44 infants were excluded due to the absence of data for one of the reported measurements (359, 360, 371). Cook and colleagues stated that infants too unfit for examination were excluded from the study but it is unclear as to how many infants this effected meaning an assessment of the risk of attrition bias was not possible (354, 358). It was also unclear what happened to infants developing ROP in O'Brien and Clark's study (366). It was also unclear how many infants were excluded by Jethani and colleagues due to unavailability for one-year follow-up (378). Insufficient information on the number of infants excluded due to the development of threshold ROP in the studies conducted by Snir and colleagues and Ton and colleagues meant the risk of attrition bias was unclear (355, 356). The rest of the included studies either were deemed to have a low risk to this type of bias or did not collect longitudinal data.

For the vast majority of studies, it was unclear whether there was a reporting bias, as is generally the case (346, 382). Although the authors could not identify previously published protocols for any of the studies, three of studies were clearly built on previous studies with very similar methods and were therefore considered to be at low risk of a reporting bias (358, 359, 381).

No other sources of a bias risk were identified for any of the included studies.
A summary table of the risk of bias within studies is shown in Table 34. Whilst this highlights some concerns with the methods of certain studies, the authors did not consider any of the studies to be so flawed as to warrant exclusion from the final analysis.

Ocular Parameter	Model Terms ± S.E.
Corneal Central Thickness (CCT) [µm]	$(1494.7087 \pm 179.8967) - (250.7398 \pm 51.1467)Log(PMA)$
Corneal Diameter [mm]	$EXP([1.493626 \pm 0.066929] + [0.018796 \pm 0.001917]PMA)$
Corneal Anterior Radius of Curvature [mm]	$(6.87 \pm 0.027) + (0.0947 \pm 0.0039)(PMA - 40) - (0.0034 \pm 0.0005)(PMA - 40)^2$
Corneal Posterior Radius of Curvature [mm]	As anterior Radius of Curvature
Corneal refractive index	1.3770
Anterior chamber depth (ACD) [mm]	$(0.8060 \pm 0.1711) + (0.0363 \pm 0.0045)PMA$
Aqueous humour refractive index	1.3370
Iris thickness [µm]	$76.174 + 5.071PMA$
Pupil diameter [mm]	$\frac{9}{1 + (PMA/[28.8782 \pm 0.7939])^{(-3.8268 \pm 0.4382)}}$
Lens thickness (LT) [mm]	$(3.7336 \pm 0.0891) + (0.0053 \pm 0.0027)PMA$
Lens diameter [mm]	$(2.1934 \pm 0.2235) + (0.1013 \pm 0.0070)PMA$
Axial length (AXL) [mm]	$(9.914 \pm 0.4667) + (0.1674 \pm 0.0120)PMA$
Retinal radius [mm]	$-AXL/2$
Vitreous humour refractive index	1.3360
Mean Spherical Equivalent	$(-13.8665 \pm 2.7260) + (0.3024 \pm 0.0491)PMA + (0.0035 \pm 0.0014)BW$
Birth weight (BW) [g]	1088.8±29.4
Lens Anterior Radius of Curvature	$(86.2063 \pm 14.0876) + (0.8447 \pm 0.1359)PMA - (31.4242 \pm 5.3096)\log(PMA)$
Lens Posterior Radius of Curvature	$(3.9299 \pm 0.8389) - (1.6251 \pm 0.2282)\log(PMA)$
Lens Posterior Conic Constant	$(-11.8687 \pm 0.9673) + (2.4868 \pm 0.2631)\log(PMA)$

Table 35 - The terms for each of the optical modelled terms included in the optical model of the preterm eye. The terms are valid for 28 to 52 weeks' postmenstrual age.

8.3.4 Meta-analysis

Sufficient studies reported data on each of the ocular parameters growth with respect to postmenstrual age (PMA) with sufficient granularity to allow a meta-regression with respect to gestational age (GA) to be conducted for each. Mean BW and GA were included as additional moderators where this data was available. Graphical representations of the meta-regressions are shown in Figure 82 and Figure 83. The coefficients returned are shown in Table 35.

Birthweight was taken from Cook and colleagues' 2007 study as this study did not exclude infants suffering from ROP (369).

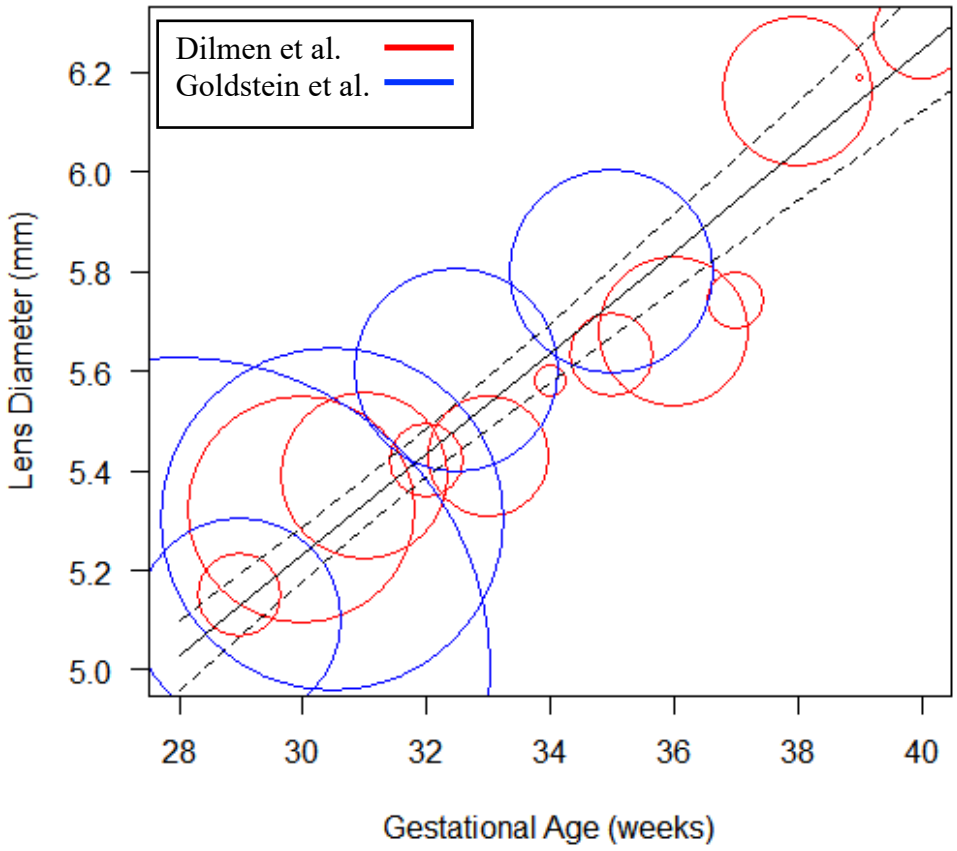

Figure 82 - Bubble chart of the meta-regression of studies reporting lens diameter of foetuses as a function of postmenstrual age with 95% confidence interval. Size of each bubble is proportional to the weighting factor applied to the data point in the regression.

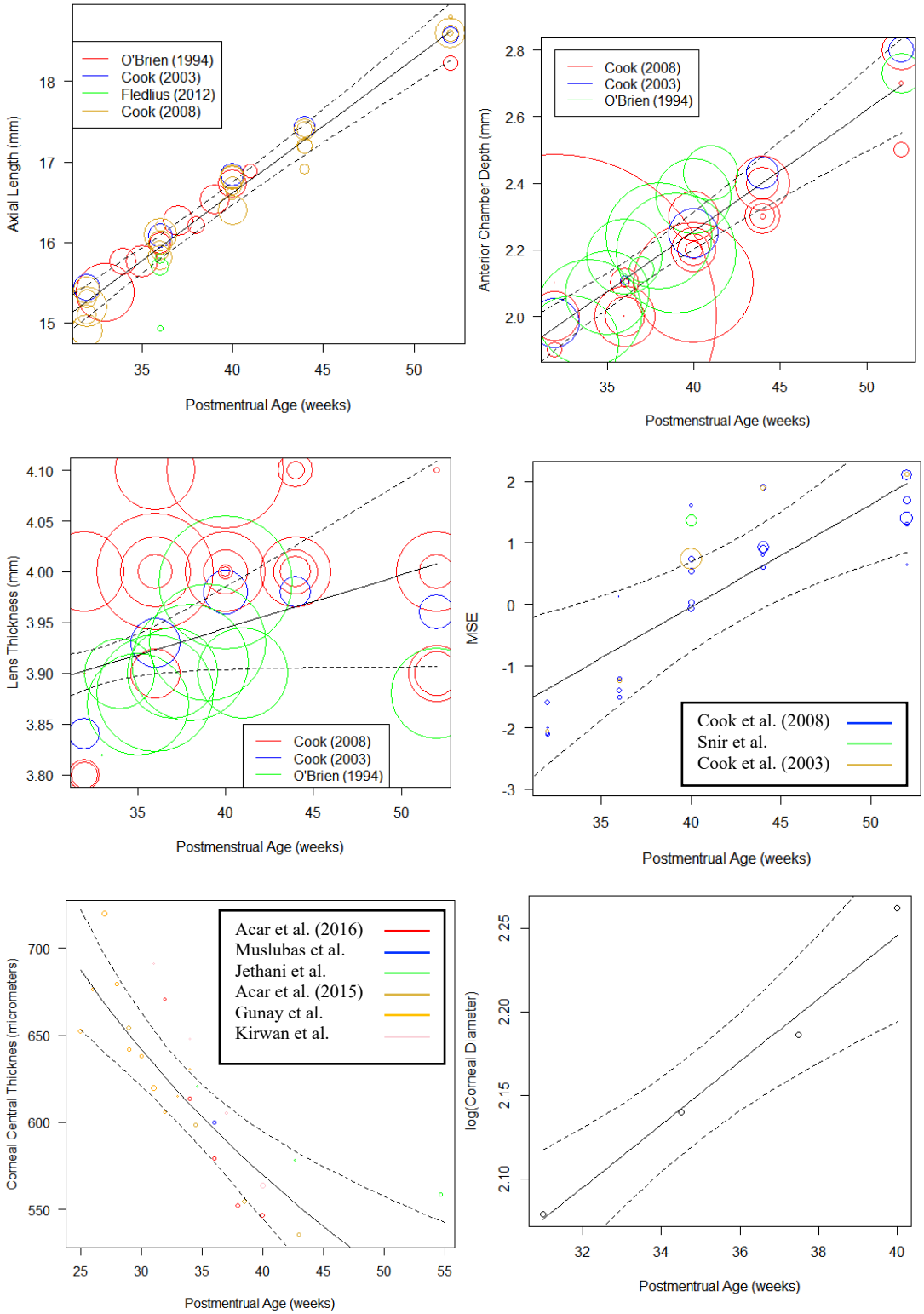

Figure 83 - Bubble charts of the meta-regression for axial length (top left), anterior chamber depth (top right), lens thickness (centre left), mean spherical error (centre right), corneal central thickness (bottom left) and log corneal diameter (bottom right) as a function of postmenstrual age with 95% confidence interval. Size of each bubble is proportional to the weighting factor applied to the data point in the regression.

8.3.5 Risk of Bias Across Studies

The results of the QE test for the ocular biometeries qualifying for meta-regression were as follows: axial length (AXL) = 6.7226 (p=1.0; degrees of freedom (df) = 41), Anterior chamber depth (ACD) = 7.5612 (p=1.0; df = 38), lens thickness (LT) = 9.3540 (p=1.0; df=38), mean spherical equivalent refractive error (MSE) = 17.5469 (p=0.9370; df=28), corneal central thickness (CCT) = 8.6218 (p=0.9990; df=25) and lens diameter (LD) = 9.7647 (p=0.8786; df=16). Graphical representations of the risk of bias across studies are shown in the funnel plots in Figure 84.

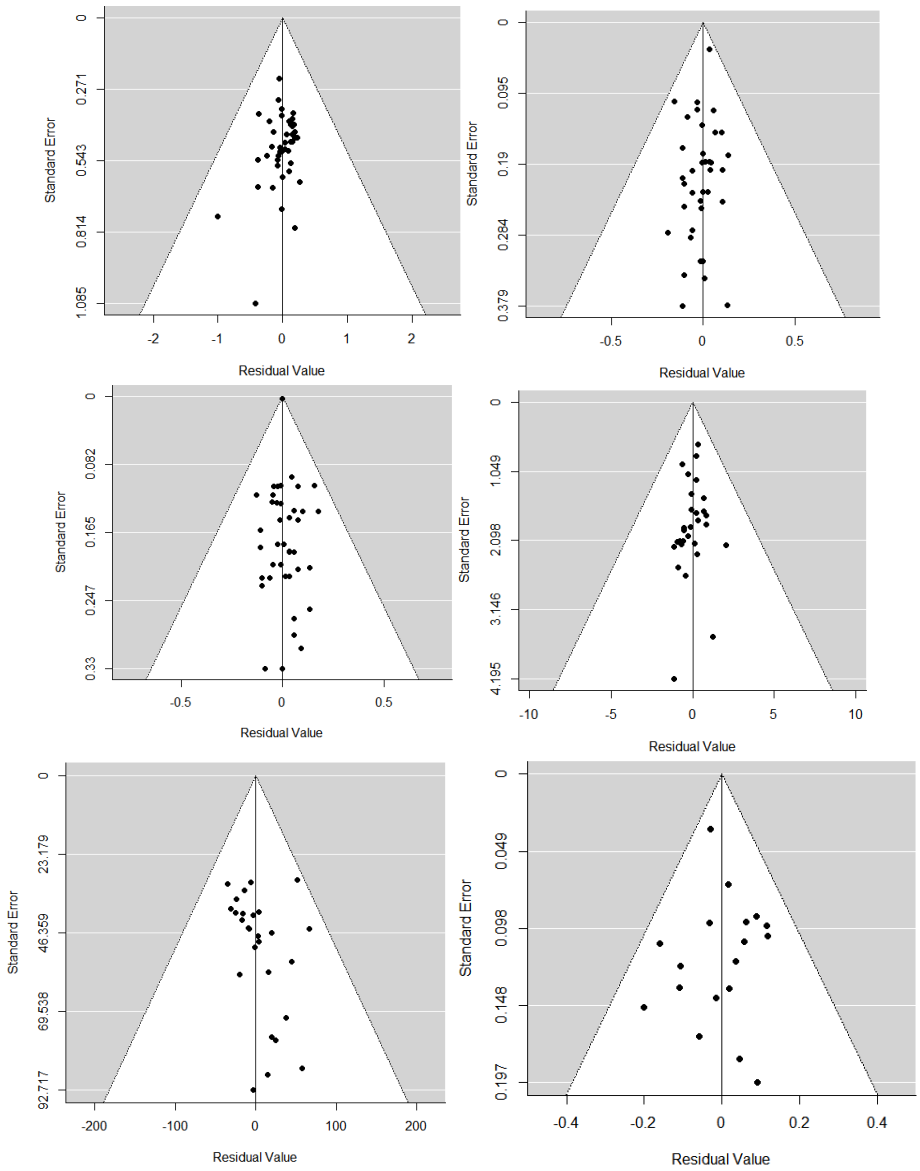

Figure 84 - Funnel plots for assessing bias between studies for meta-analyses of axial length (top left), anterior chamber depth (top right), lens thickness (centre left), mean spherical equivalent (centre right) and central corneal thickness (bottom left) in preterm infants and lens diameters in foetuses (bottom right). In each case, the charts suggest minimal bias between studies.

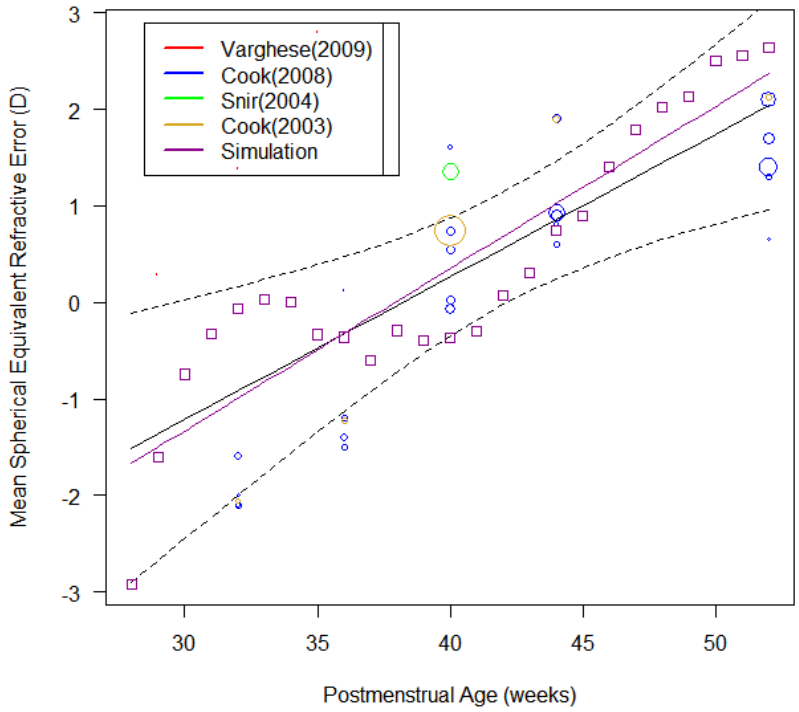

Figure 85 - 'Bubble chart' of the meta-regression for mean spherical equivalent refractive index as a function of postmenstrual age with 95% confidence interval and with simulation results and regression line superimposed in magenta. Size of each bubble is proportional to the weighting factor applied to the data point in the regression.

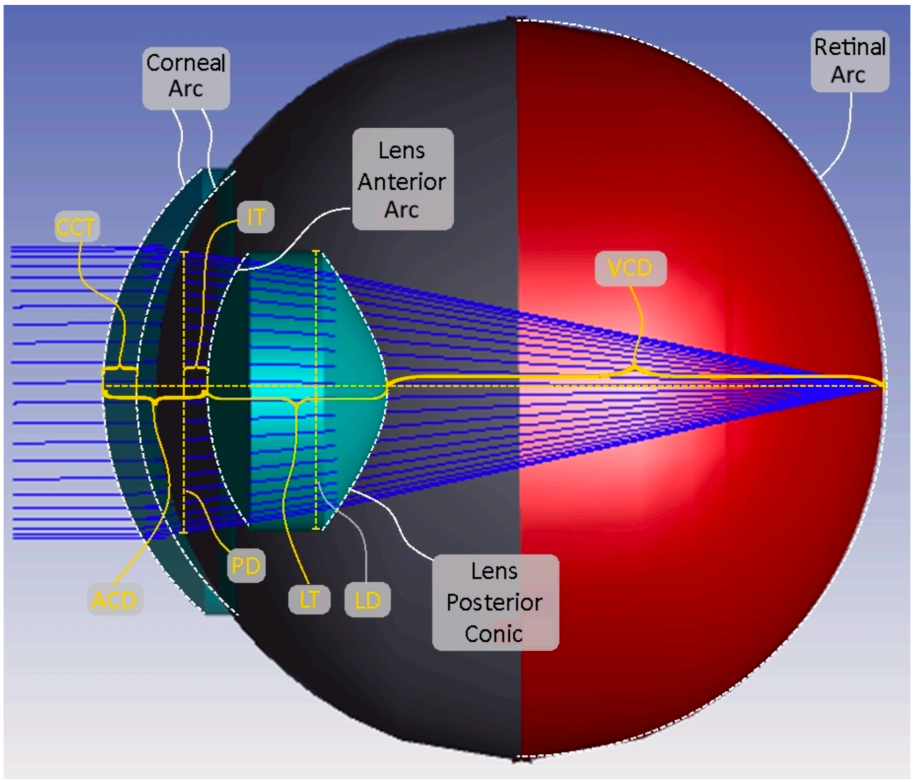

Figure 86 - A graphical representation of the optical model of the eye for 32 weeks' postmenstrual age. CCT=Corneal Centre Thickness; ACD=Anterior Chamber Depth; IT=Iris Thickness; PD=Pupil Diameter; LT=Lens Thickness; LD=Lens Diameter; VCD=Vitreous Chamber Depth; RoC=Radius of Curvature

8.3.6 Optical Model

Other than for 40 weeks' PMA no simulation converged to a solution that entirely satisfied the model requirements. In particular, there was a general tendency amongst the lower half of PMAs for convergence at a solution where all requirements other than the anterior curvature was satisfied, meaning that the anterior radius of curvature decreased with PMA. Such a solution was arrived at even when the requirement for higher anterior surface curvature at lower ages was heavily weighted compared to the other requirements.

The results of each simulation are shown in Figure 85 and the linear models fitted for the simulations' variables are shown in Table 35 alongside the other terms of the model. From the bubble-chart in Figure 85 it can be seen that the simulated results are largely within the confidence interval of the meta-regression, however having more information on the shape of the lens in preterm is likely to yield improvements to model and its alignment with measured values of the refractive index.

A rendering of the full modelled eye, including results of the meta-analysis and optical analysis, is shown in Figure 86. The optical model can also be downloaded via the DOI provided in Appendix 8.4.

8.4 Discussion

The above meta-analysis shows that, in the included studies, there is broad agreement in the growth in axial length, anterior chamber depth and corneal diameter during the first three months of a premature infant's life. It also shows a general agreement on the thinning of the cornea and a gradual shift from myopia to hyperopia over the same period. How the lens thickness changes during early development is less clear with some studies reporting no significant change and others reporting a slight increase in thickness with age. As such, there is a wide margin for error with respect to lens thickness in the statistically model, particularly in later weeks.

The subsequent optical analysis demonstrates that differences in corneal curvature and axial length alone cannot account for the refractive status of preterm infants.

The modelling demonstrates that changes in the lenticular curvature and conic may account for this discrepancy. Other potential contributors could include changes in the refractive properties of ocular media, which the model assumed to be constant with exception of the lens, and differences in the in the curvature of the posterior and anterior surfaces of the cornea. Furthermore, the lens shapes arrived in this model are only one of many potential solutions. Thus, further research and direct measurement of the preterm lens shape will be needed to confirm the accuracy of this model.

The model allows physical eye phantoms and retinal imaging designs to be simulated using optical design software and key optical parameters such as field-of-view, aberrations and resolution. The next chapter discusses a physical eye phantom based on the optical model presented in this chapter. The chapter following this then uses the optical model to simulate the performance within premature infants of a proposed optical design for a wide-field retinal camera.

The same is true of instrumentation for laser photocoagulation technology used to treat ROP, where the eye model is also a key element of the design toolchain, core to optical optimisation prior to animal and human testing.

Additionally, the model may provide a useful starting point for a nomogram[20] describing preterm eye growth in the first three months of life. Direct clinical applications of such a tool would be as a reference for identifying early indicators of ocular conditions in preterm infants that affect the biometry of the eye. For example, primary congenital glaucoma may be categorised by buphthalmos, an enlargement of the eye in all directions outside normal growth, or stretching of the cornea resulting in Haab striae, acute curvilinear breaks in Descemet's membrane (384).

More research with respect to the correlations between ocular biometries and other metrics of development, as opposed with PMA only, would allow the development of a nomogram that is more robust than the model presented. Nevertheless, the model provides clinicians with the most holistic reference for the average preterm eye to-date, and may therefore provide a means for identifying grossly abnormal

[20] A nomogram is "a graphic representation that consists of several lines marked off to scale and arranged in such a way that by using a straightedge to connect known values on two lines an unknown value can be read at the point of intersection with another line" (383)

biometries.

8.4.1 Limitations

The model has a number of limitations. Firstly, a lack of data describing the correlation between ocular parameters meant that it was only appropriate for this model to describe an "average" eye rather than providing tolerances for each parameter within the model. Further research allowing such tolerances to be included in the model would allow far more comprehensive testing of imaging systems designed specifically for preterm eyes, for example, as it would allow designs to be tested against non-average but nevertheless sufficiently common eye dimensions.

Secondly, the low number of included studies included in there is a substantial limitation of the meta-analysis. Specifically, there were four studies included for analysis of the axial length and means spherical equivalent; three for the anterior chamber depth, lens thickness and corneal central thickness; two for the lens diameter and only one for the iris thickness, corneal diameter and pupil diameter. The results must therefore be taken with a degree of caution. The low number of included studies may have, in particular, contributed to the large margins of error found with respect to lens thickness and mean spherical equivalent. However, in the case of the latter, it appears that the main cause of this large margin may simply be due to its wide range within the preterm population. Nevertheless, it should be noted that meta-analysis can still offer a better result than alternative forms of analysis, even when there are as few as two studies investigating a given measure (385).

Widespread use of the post-conceptional age is present throughout the literature despite the latest recommendations by the American Academy of Pediatrics stating that this term not be used in clinical paediatrics (386). In addition, it appears that a number of the reviewed publications have confused this term with the PMA which is not, strictly speaking, equivalent. More consistency in future studies would serve to improve subsequent versions of the model.

It should also be noted that, with the exception of the work of Mactier and colleagues, all of the studies included in the meta-analysis applied simple linear or quadratic models to their data. Without access to the raw data for each of the

included studies, it is impossible to apply more plausible growth models, trending towards known values in later life rather than infinity, and hence it was decided to maintain these models in the analysis. The model is therefore constrained to the limits of the data gathered within these studies and cannot be used to project into earlier or later life.

Finally, several studies involved the use of ocular specula to keep infants' eyes open (354, 358, 365, 367, 369, 372, 376, 377, 379, 381). It has been reported that use of an eyelid speculum increases IOP by an average of 4mm Hg which has the potential to significantly alter biometries (387). Friling and colleagues devised a novel technique in an attempt to reduced changes to ocular biometries due to the use of lid retractors and other studies reported taking care to avoid such changes (372). Topical anaesthesia was also used in a large number of the studies (354, 358, 365, 366, 369, 371, 376-38§) which it has been suggested may potentially cause temporary changes to the dimensions of the cornea (376).

8.5 Conclusion

This chapter has described an optical model of the preterm eye during its first weeks of development. This fills a gap in the scientific literature.

For the purpose of this thesis, the optical model allows an accurate preterm phantom of the preterm eye at 34 weeks' PMA to be designed and constructed, work that is described in Chapter 9. Chapter 10 then also uses the optical model to infer optical design parameters for a low-cost portable wide-field fundus camera for ROP screening.

9 Design and Prototyping of a Preterm Infant Retinal Imaging Phantom

9.1 Introduction

As was stated in the preceding chapter, no comprehensive optical simulation of the preterm eye currently exists. As a result, there are no optical phantoms described within the scientific literature or which are available for purchase commercially. Such a phantom is desirable for conducting reliable tests of the optical and ergonomic performance of prototype preterm retinal imaging devices as well as for training of clinical personnel involved in retinal imaging. This chapter describes the design and prototyping of such a phantom, based on the optical simulation described in the previous chapter.

9.2 Methods

9.2.1 Simulation of a Stock Lens Model

Having established a suitable optical model for the mean preterm eye during the period relevant to ROP screening, it is next necessary to design an optical system that is feasible for construction in the lab. Furthermore, the design must replicate, as far as possible, the dimensions and optical properties of the preterm model. Matching mechanical properties with that of the preterm eye was considered out of scope for this project given that the end goal was to demonstrate the feasibility of an ROP screener without distorting the eye.

A PMA of 34 weeks was chosen for the basis of the eye phantom as this the age at which it is recommended that a baby born at 30 weeks gestational age be first screened for ROP (159).

The process followed in designing the eye phantom was, firstly, where possible, to replace each component in the simulated 34-week PMA eye with a simulated representation of a stock optical component, either from Zemax OpticStudio's extensive component libraries or by modelling the component based on the datasheet provided by the manufacturer. If no stock component could be identified a custom component was introduced instead. Such custom components needed to be designed using a material that could be easily sourced and its dimensions and optical

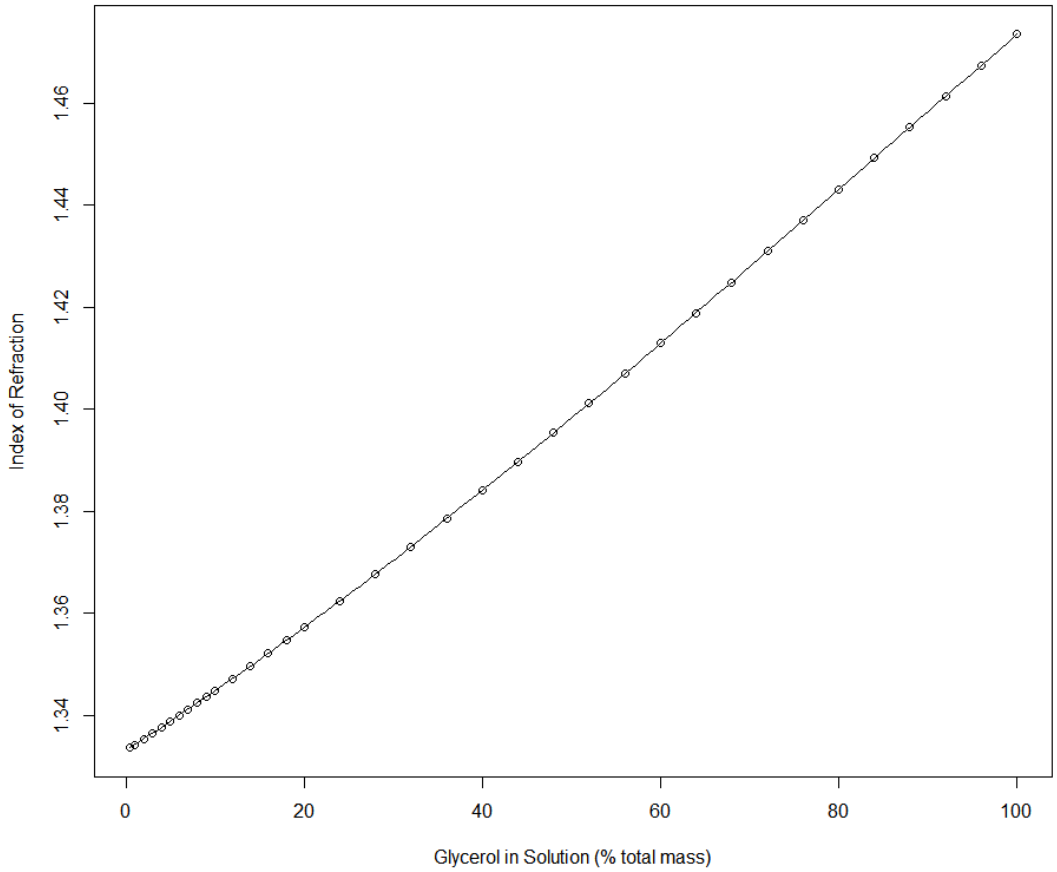

Figure 87 - index of refraction of glycerine as a function of percentage total mass of glycerol in the solution. Circles represent points reported in the 'CRC Handbook of Chemistry and Physics' and the connecting line represents a linear interpolation calculated in R using the approxfun function (338, 376).

properties needed to be designed to a magnitude and precision that could be realistically prototyped.

Of all of the necessary components, only the crystalline lens could be adequately modelled using a stock component, namely a biconvex fused-silica lens. For the cornea, a sufficiently thin or short diameter off-the-shelf meniscus lens could not be sourced and commissioning a custom lens was prohibit expensive. However, vacuum forming a component with dimensions similar to that of the modelled cornea is relatively straightforward and thus PMMA, being an optical suitable material that can be vacuum formed, was selected as an alternative and dimensions that were both as close as possible to the simulated cornea and realistic for manufacture were introduced in place of the simulated cornea.

The final optical components to be replaced within the simulation were the aqueous humour and the vitreous humour. Water is a reasonable model for each of these in terms of refractive index with a refractive index of 1.331 compared to 1.334 for both the aqueous and vitreous humours. Also, water exhibits very similar dispersion, that is the variance of refractive index by wavelength, as evidenced by their both having an Abbe number of 56, where the Abbe number,

$$V = \frac{n_{d-1}}{n_F - n_C}, \tag{20}$$

where n_d, n_F and n_C are the refractive indicies at the so-called Fraunhofer's lines, that is 587.6, 486.1 and 656.3nm respectively (388, 389). However, simply replacing each with water would result in a full optical system that has vastly different refractive properties to that of the simulated preterm eye. Thus, it was identified that a liquid with a higher refractive index was required to replace the aqueous and vitreous humours. Glycerine was selected as a good potential candidate given that the solution is transparent and has an Abbe number of 56, matching that of water. Thus the solution can be tuned to specific, relatively high refractive index, without adjusting the scattering properties, by altering the concentration of glycerol in an aqueous solution (390). For simplicity of construction, it was specified that the same solution be used to replace both the aqueous and vitreous humours. This was considered a reasonable simplification given the very similar optical properties of the two humours with respect to refractive index and dispersion as noted above.

Surface	Material	Anterior Radius	Posterior Radius	Thickness	Diameter	Notes
Cornea	PMMA	6.0mm	6.0mm	1.0mm	9.0mm	
Aqueous	25.23% Glycerine	-	-	1.0mm	-	
Iris	PLA Aperture	Infinite	Infinite	0.3mm	5.8mm	Stop
Lens	UV fused silica	4.8mm	-4.8mm	4.1mm	6.0mm	Edmund Optics ref: 49238
Vitreous	25.23% Glycerine	-	-	9.8mm	-	
Fundus	PLA	-7.8mm	-	-	15.6mm	

Table 36 - Optical properties of the components used in the eye phantom's optical design

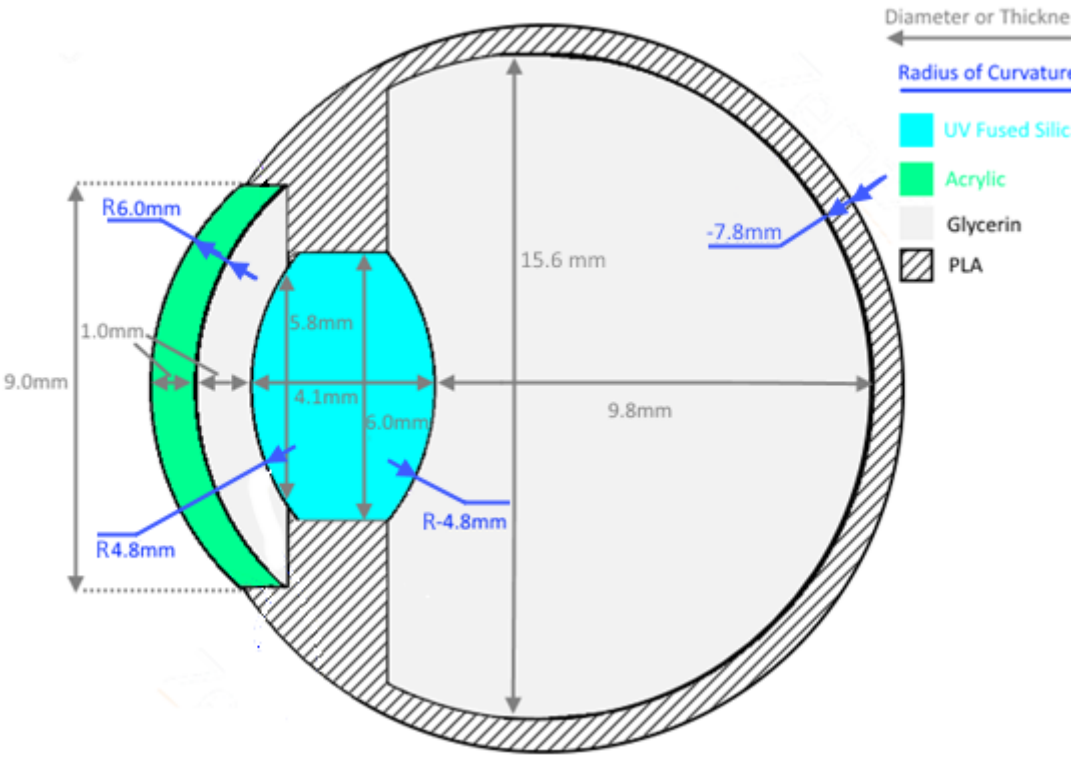

Figure 88 – An annotated schematic of the eye phantom's optical design

Zemax OpticStudio's damped least squares optimisation function was used to determine the required refractive index of the solution by setting the refractive index of both the aqueous and vitreous humours as variables and solving for the mean spherical error derived from the model described in the previous chapter. Owing to the constraint that both solutions have equal refractive indices, it was determined that a refractive index 1.364 was required to match the mean spherical error of the simulated preterm eye. Thus it was determined that a glycerine solution of 25.23 parts glycerol to 74.77 parts water was needed by interpolating between the points given in the 'CRC Handbook of Chemistry and Physics' (see Figure 87) (388).
A schematic of the full optical design of the eye phantom is show in Figure 88 and the component parameters that are pertinent to the optics of the system are shown in Table 27. A full list of the materials used is also provided in Appendix 9.1.

9.2.2 Construction of Preterm Infant Phantom, Eye and Enclosure

3D printing represented the most appropriate feasible manufacturing method for the eye phantom's exterior and optical components' housing. Rhinoceros 5 (Robert McNeel & Associates, Seattle, WA, USA) was used to draw the computer aided design.
Given the precision that could be achieved with a 3D printed component of this size it was possible to include three-dimensional features representing those found on the retina of an infant suffering from ROP in the design. This was achieved by tracing over a medical illustration of ROP on an infant's retina with appropriate three-dimensional shapes and then projecting this on the spherical surface representing the retina to create the necessary extrusions and grooves, as is shown in Figure 89 (390). Markers marking various subtended angles were also inserted as were markers marking the various retinal 'zones' (390).
A colour print of the design was originally considered by printing in coloured sandstone, however as the print was required to be waterproof, the coloured sandstone needed to be varnished which resulted in its surface being excessively reflective, as can be seen in Figure 90, and thus inappropriate for the application.

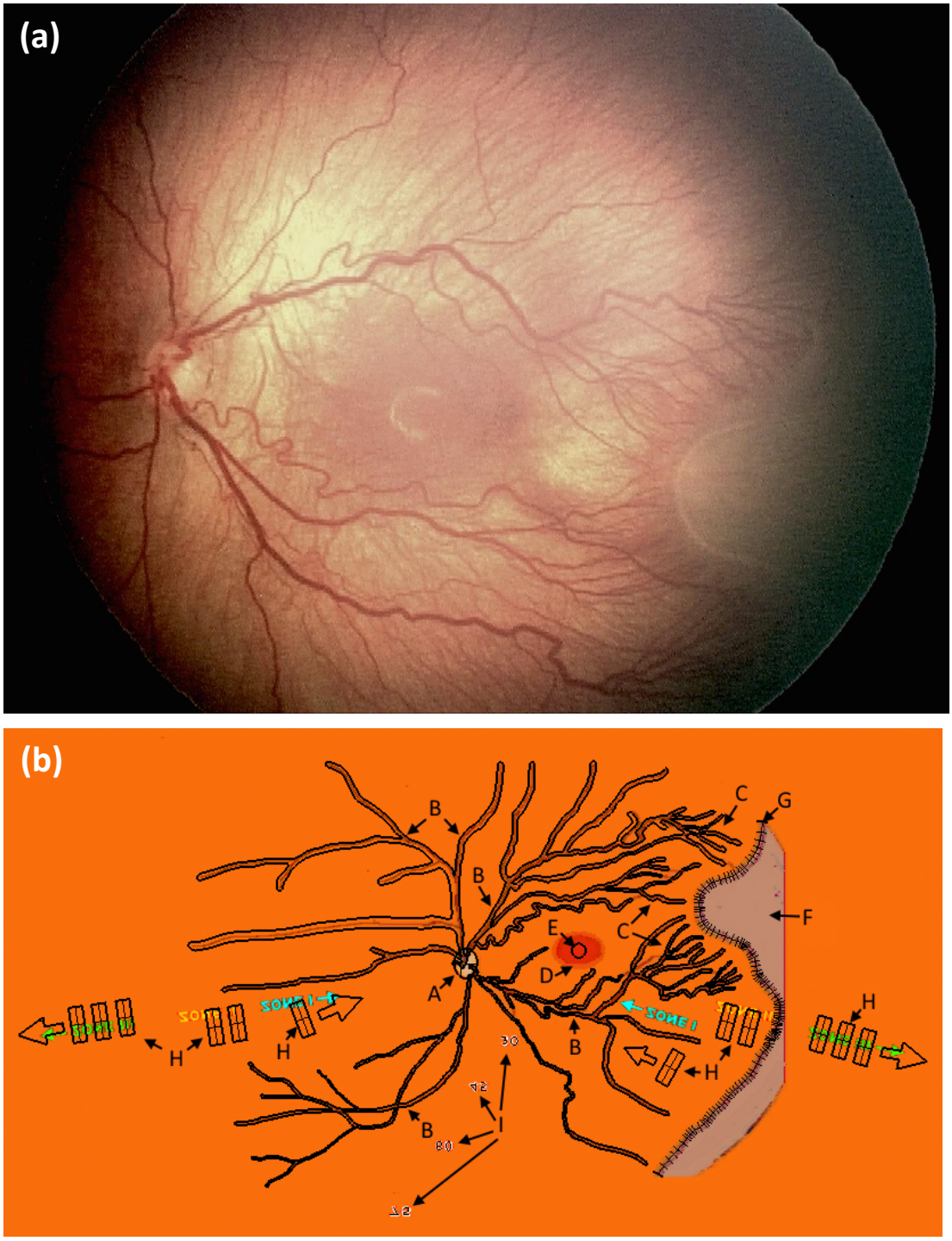

Figure 89 - A flat retinal target with 3 dimensional features (b) was created by tracing appropriate 3D shapes over a reference image taken from Gole et al. that is used as a reference for stage 2 ROP (a) (359). Certain features guided painting of the retina, such as an extrusion of the optic disc (A), and embossed features representing major blood vessels (B) and neovascularisation (C). Others sought to emulate three-dimensional features of a preterm ocular fundus such as the foveal pit (E) within the macula (D) and the retinal ridge (G) at the edge of a region of detaced retina (H). Finally, extrusions were also added to mark the various retinal zones (H) and subtended angles between 30° and 75° in 15° increments.

(a) reproduced with permission from (390).

).

Figure 90 - A rejected prototype of the eye phantom using coloured sandstone.

It was therefore decided to design for a single colour form and instead design in extra grooves and extrusions onto the retinal target to act as a guide for painting these by hand, as can be seen in the CAD rendering of the design shown in Figure 91. The housing itself consisted of two parts, shown in orange and white respectively in Figure 92, to allow the optical components to be inserted in the positions prescribed by the optical design and then held in place using index matching adhesive and two-part epoxy as appropriate (Loctite 4305, Henkel Technologies, Düsseldorf, Germany; Tommy Walsh Epoxy Resin Glue, Poundland). For the sake of practicality, the housing was somewhat thicker than that typical of an infant's sclera with this being of a thickness that would be too fragile for practical lab testing. Similarly, the rear half of the external surface was replaced with a cubic design rather than a hemispherical design to avoid the phantom rolling of a surface and to make it more stable for imaging (the need for the former having been learnt the hard way in a previous iteration of the design!).

The design was 3D printed using an E-Shell resin in an Perfactory Desktop XL 3D printer (both EnvisonTEC GmbH, Gladbeck, Germany) and post-cured in an Otoflash G171 flash curing UV source (EnvisionTEC GmbH).

To colour the retinal vessels and foveal pit on the eye phantom's retinal target, a carmine coloured etching ink (Intaglio Printmaker Ltd., London, United Kingdom) was mixed with a drying agent (Etching Ink Extender, Intaglio Printmaker Ltd.). This was applied to whole surface of the eye phantom's interior that was then wiped away using a Tarlatan gauze scrim (Intaglio Printmaker Ltd.) and, owing to high viscosity of the ink, resulted in the ink being left stuck in the grooves mapped onto the phantom's interior from the retinal vessels traced on the medical illustration of the retina. The ink was then left for approximately one week to dry.

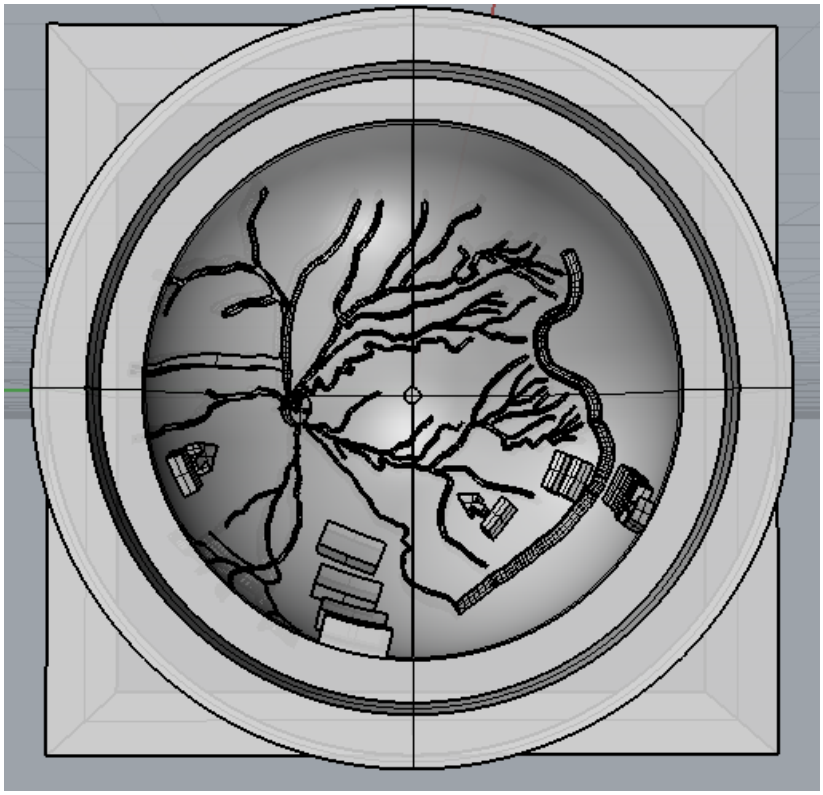

Figure 91 – CAD rendering of the second iteration of the preterm eye phantom's retinal design.

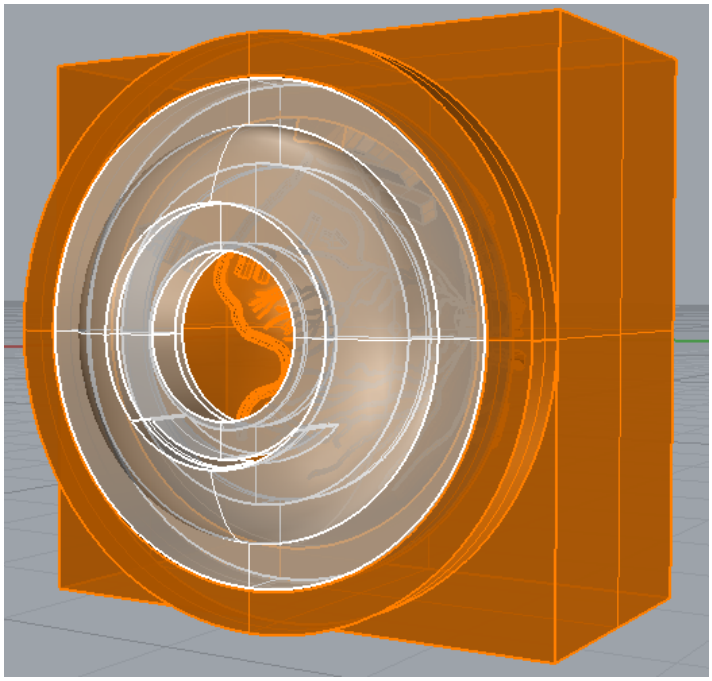

Figure 92 - The full eye phantom design consisted of two parts: the main cavity (orange) and the lens holder (white).

Acrylic paint was then used to paint the optic nerve and the retinal ridge by hand using a fine paintbrush. An image of the fully coloured retinal target, prior to final assembly of the eye phantom is shown in Figure 93.

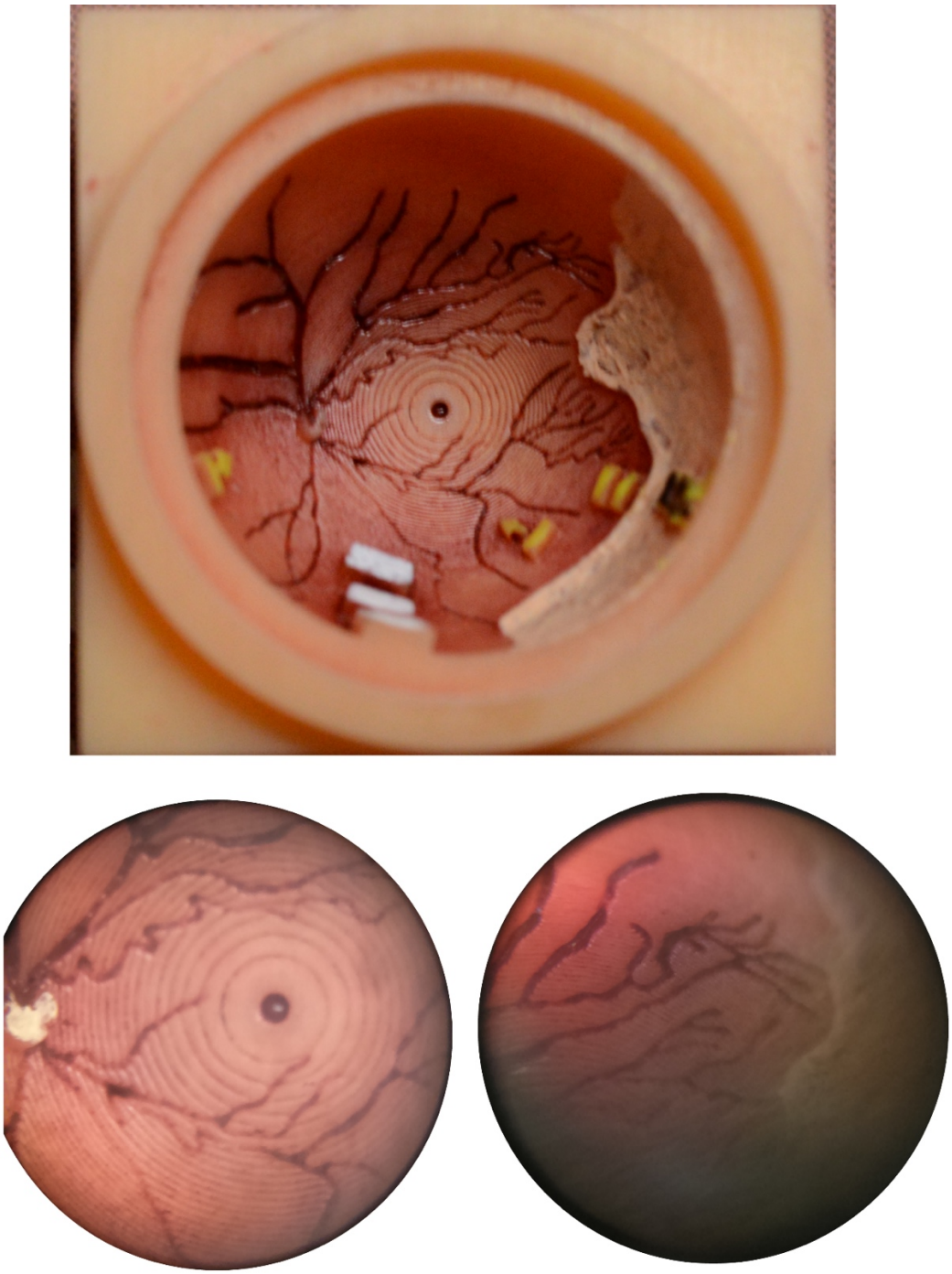

Figure 93 - The eye phantom's full retinal target (top) including optic disc, retinal vessels, retinal ridge, field of view markers (in white) and retinal zone markers (in yellow). The image in the bottom left show the optic disc, fovea and arcades under magnification. The image in the bottom right shows neovascularisation and the retinal ridge under magnification. The shadow in this image is caused by misalignment between the microscope eyepiece and camera optic.

Figure 94 – Left: A CAD rendering of the vacuum mould, consisting of a 3D printed part, in blue, and a 12mm diameter steel ball bearing in grey. Right: The PMMA meniscus lens representing the cornea in the eye phantom was formed by heating the PMMA sheet in an oven and then pulling over the mould that was sealed on top of a vacuum pipe.

Figure 95 - The fully assembled eye phantom

To vacuum form the optical component representing the cornea in the eye phantom it was first necessary to design an appropriate mould. This mould consisted of a 12mm diameter stainless steel ball bearing (Low Carbon Soft Steel Ball Bearings 12mm, Bearing Options, Saltash, UK) placed inside a cylindrical 3D print that allowed an 8mm diameter section of the ball bearing to protrude from the top. Thus, when a sheet of 1.0mm thickness was heated in an oven and pulled over the mould, once sealed to a vacuum pipe, as shown in Figure 94, an 8mm diameter meniscus lens with a 6mm radius of curvature was formed in the plastic. The lens was then cut from the rest of the PMMA using a hacksaw.

The biconvex UV-silica lens was fixed in place within the larger of the two 3D printed parts using UV curing adhesive. The two 3D printed parts and the PMMA meniscus lens were then joined using two-part epoxy. A 0.8mm syringe was then used to fill the eye phantom's internal cavity with a glycerine solution containing 25.23% glycerol by mass. The design of the phantom was such that inserting the syringe through a single hole in the top of the eye phantom caused glycerine to flow into cavities representing both the anterior and vitreous chambers. The fully assembled eye phantom is shown in Figure 95.

A phantom of the full preterm head was then designed by first taking a 3D scan of an existing silicone preterm phantom (Micro-Preemie Premature Baby Simulator, Simulaids Inc., Saugerties, NY, USA). In order to make a similarly sized preterm phantom that was also hollow, allowing the eye phantom to be inserted below the surface of the eyelid a 'skull' was designed underneath the CAD generated by the 3D scan using Rhinoceros 5 (McNeel & Associates). The purpose of this skull was not to be anatomically accurate but rather to allow insertion of the eye phantom in the correct location and to support a silicone skin with realistically placed external features relevant to use of an ophthalmic imaging device, such as the nose and brow.

The skull consisted of four separate parts: the main head and neck, a lid that could be placed or removed from the back of the skull to allow the eye phantom to be inserted or removed and two 'blanks' of the eye phantom. The eye phantom blanks aimed to represent the form of the actual eye phantom without the need for this to be used during the moulding purpose and to maintain the form of the preterm phantom when the eye phantom was not in place. A rendering of the CAD for the skull and eye

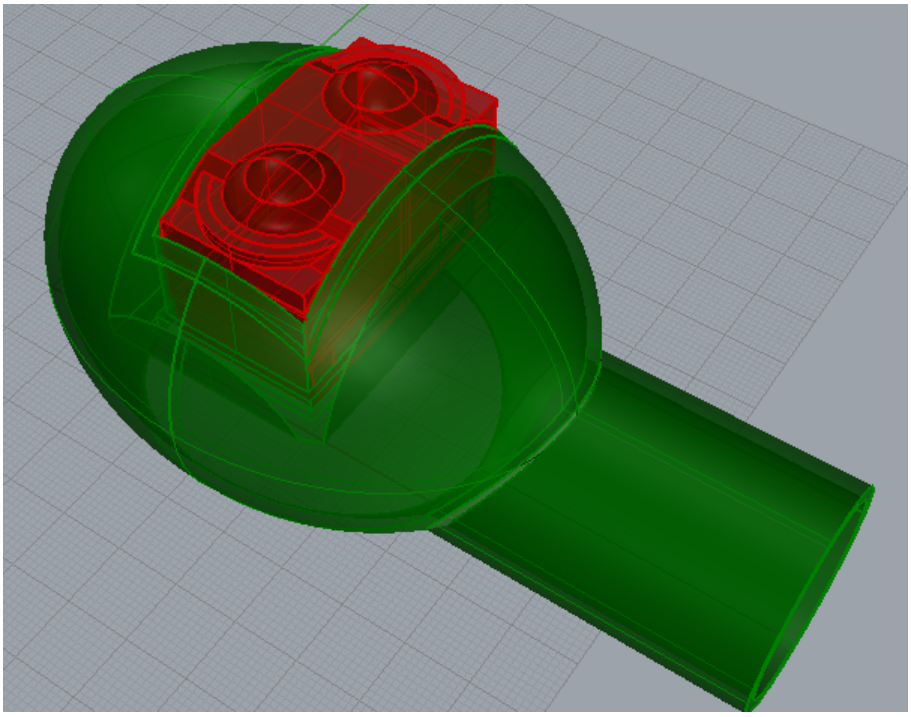

Figure 96 – A rendering of the CAD design for the preterm phantom's 'skull', around which the silicone skin was moulded. Two 'blanks' of the eye phantom are shown inserted into eye cavity in red.

Figure 97 - Skull phantom with eye phantom inserted in the position of the right eye and a blank inserted in the position of the left.

Figure 98 - Skull phantom prepared for insertion into the mould.

phantom blanks is shown in Figure 96.

The skull and blanks were printed in PLA (blue 2.85mm PLA, RS Components) using a Ultimaker 2 3D printer (Ultimaker B. V.). The skull with the eye phantom and a blank inserted is shown in Figure 97. A mould of the skin was created by mixing one part alginate to one part water by volume in a plastic container until approximately three quarters full. The skull phantom was prepared by inserting blanks in the position of both eyes and taping around the join with electrical tape, as shown in Figure 98.

The head of the preterm infant model was then covered in cling-film and held in the alginate, as shown in Figure 99, for 5 minutes.

The skull was then held in-place within the mould using a clamp stand at approximately 0.5mm away from the surface of the mould. 340g of each of the two parts of the silicone (platsil gel-10, Polytek Development Corp., Easton, PA, USA) were then mixed together with a fleshtone colourant. The mixture was then poured into the gap between the mould and skull until entirely filled. After waiting 35 minutes for the silicone to set, the mould was removed leaving the silicone-covered skull. The eyelids were slit with a scalpel and one of the eye phantom blanks replace with the optical eye phantom to complete the preterm phantom. The completed preterm phantom is shown in Figure 100.

Figure 99 – Creation of the preterm face mould.

Figure 100 - Fully assembled preterm infant phantom. Eye phantom is inserted in the position of the right eye with a 3D printed 'blank' being inserted in place of the left eye.

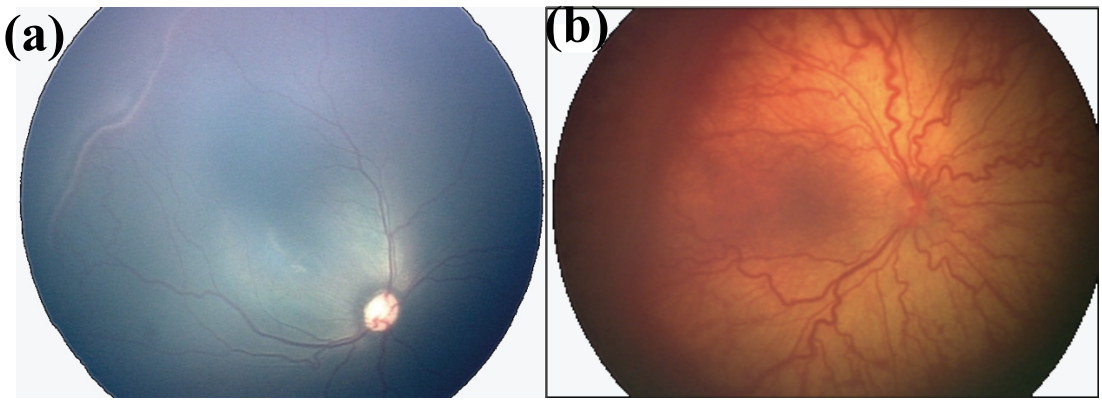

Figure 101 - Reference photographs used for making clinical decisions concerning ROP and selected for comparative image analysis versus the eye model. (a) is a darkly pigmented retina whilst (b) is moderately pigmented. Reproduced with permissions from (390).

9.2.3 Validation of Eye Phantom

Validation of preterm eye phantom was sought by acquiring photographs of the phantom's ocular fundus using the reference standard for widefield neonatal retinal photography, the RetCam 3 (Natus Medical Inc., Pleasanton, CA, USA). The imaging was performed by a consultant ophthalmologist proficient in the task at The Queen Elizabeth University Hospital, Glasgow, UK. Viscotears coupling gel (Bosch & Lomb UK, London, United Kingdom) was applied to the corneal surface of the lens in order to optically couple the eye with the camera optics. Image brightness and clarity were assessed visually and the illumination brightness and camera focus adjusted until the image was perceived to optimal. An image centred on the macula was then acquired and the image downloaded for analysis.

Three widely-used, and thus high-quality, ROP reference images were selected for comparison with the image of the eye phantom (390). The images, shown in Figure 101 and Figure 103b, were selected to provide a selection of different retinal pigmentations, with one being darkly pigmented, one moderately pigmented and one lightly pigmented. All three images were centred on the posterior pole to allow for easier and comparable estimations of the field-of-view.

Quantitative assessment of image contrast was conducted in ImageJ 1.51. The median, standard deviation, skewness and kurtosis were calculated for each image and the proportion of saturated pixels, if any, noted.

The field-of-view of the image of the eye phantom could be determined by measuring the distance between the centre of the fovea and the centre of the optic nerve. This distance does not equate to the actual distance between the two points across the curved surface of the retina but rather, if the eye is approximated to a sphere, the distance between the points on a plane connecting the points at the periphery of the digital image, as is shown in Figure 102. Application of the sine rule then gives

$$y = \frac{x_{FO} \cdot sin(90 - \theta_{FO})}{sin(\theta_{FO})} \quad \textbf{(21)}$$

where y is the distance between this virtual plane and the centre of the cornea in pixel units, x_{FO} is the distance between the fovea and optic nerve on the digital image

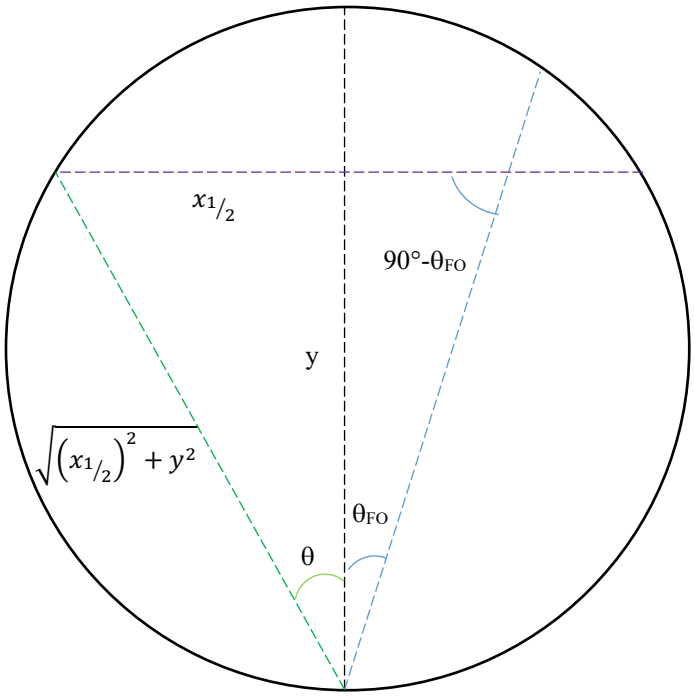

Figure 102 - Approximating the eye to a sphere allows the angle subtended by a digital fundus image to be calculated using simple geometry.

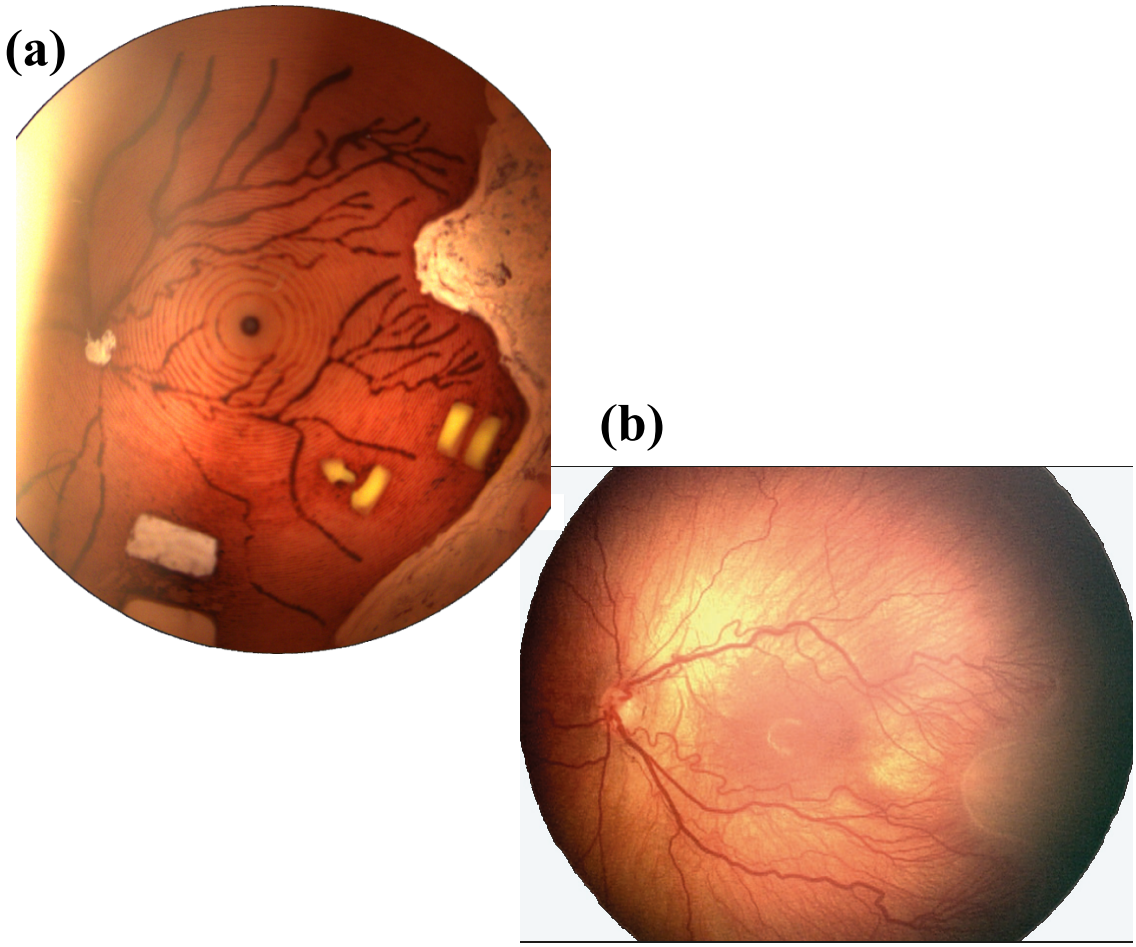

Figure 103 - Retinal image of the eye phantom (a) and a live preterm infant (b) acquired using a RetCam 3 (Natus Medical Inc., Pleasanton, CA, USA). (b) is reproduced with permissions from (390).

in pixel units and θ_{FO} is the angle subtended on the retina by the distance between the fovea and the optic nerve. θ_{FO} was measured to be 15.4 in the CAD design and was assumed to be 15 for the reference images, as is typical in real eyes (391, 392).

Applying Pythagoras theorem to determine the distance between the centre of the cornea and a point on the periphery of the image and the sine rule once more then gives,

$$\theta = sin^{-1}\left(\frac{x_{1/2}}{\sqrt{{x_{1/2}}^2 + \left(\frac{x_{FO} \cdot cos(\theta_{FO})}{sin(\theta_{FO})}\right)^2}}\right) \quad \textbf{(22)}$$

where θ is half the subtended angle of the image and $x_{1/2}$ is half the width of the image in pixel units.

9.3 Results

The ophthalmologist found imaging the eye to be very straight-forward and was able to acquire in excess of twenty images in under two minutes owing to the similarity of the task compared to imaging an infant under general anaesthetic.

The image selected for analysis is shown in Figure 103a. This image was selected owing to the fovea's alignment to the centre of the image being closer than any other image which was visually assessed to have reasonable clarity and illumination. This selection process was considered valid given that the reference images have also been selected owing to their high image quality in order to best communicate the main features of ROP.

The distance between the centre of the fovea and the optic nerve marker was measured to be 343 pixels. As the full width of the image was 1460 pixels, it could therefore be estimated that the field-of-view was 59.4°using equation **(22)**. By comparison, the subtended angle of the visible ocular fundus in the reference images were calculated to be 45.2°, 69.3° and 50.4° for the darkly, moderately and lightly pigmented eyes respectively. Therefore, it can be argued that field-of-view achieved

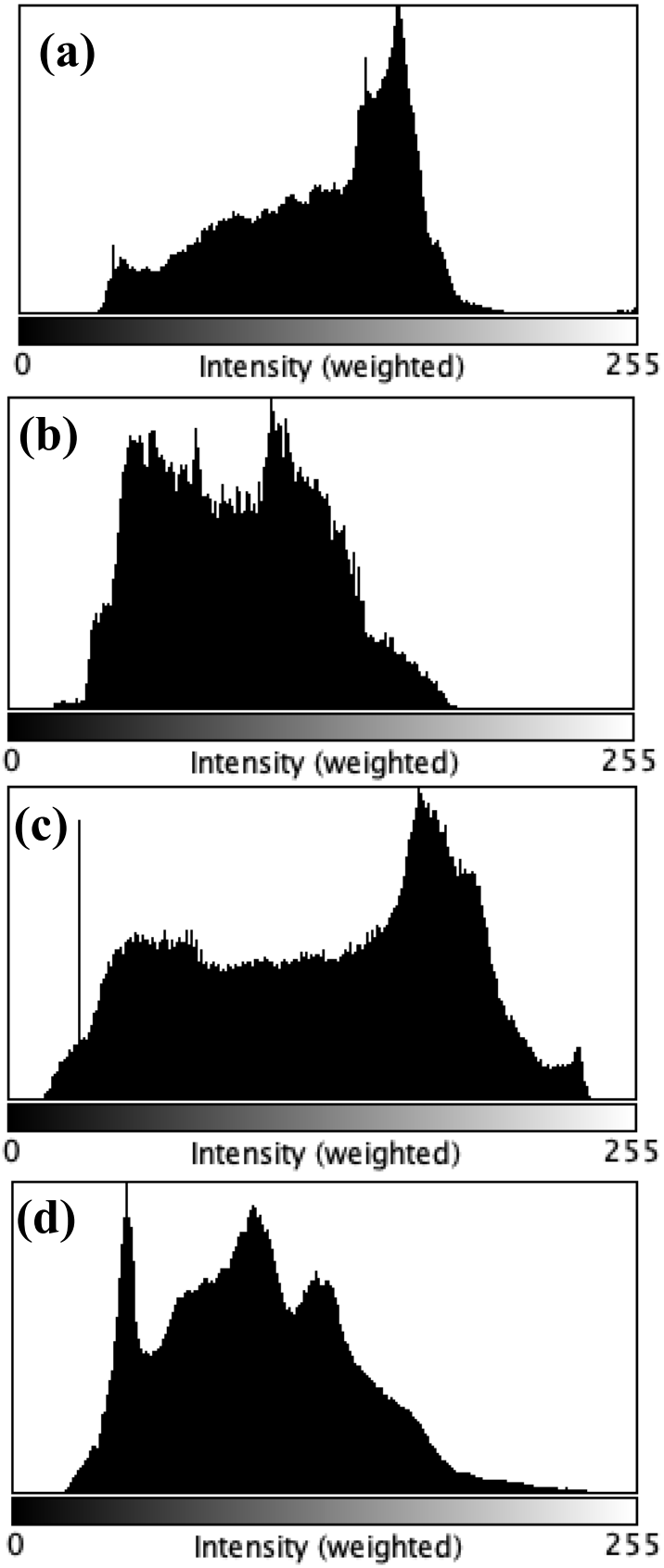

Figure 104 - Normalised histograms of weighted pixel intensity in the reference photographs shown in (a) Figure 101a, (b) Figure 101b and (c) Figure 103b as well as (d) that of the image acquired with the prototype . Each histogram is normalised to the number of pixels with the modal weighted pixel intensity.

when imaging the eye phantom with a widefield fundus camera falls within the range of values that would be expected for the same examination on a real preterm infant's eye.

Histograms of pixel intensity, weighted by perceived brightness (red: 0.30, green: 0.59, blue: 0.11) for each image are shown in Figure 104 and the shape parameters of each distribution in Table 39. The median and standard deviation of the eye model image's pixel intensity was within the range of those measured for the reference images. The image of the model eye also more skewed to the right than any of the reference images, implying that there were more tones present in the shadows of the image compared to the reference images. The mode eye image also had the least negative kurtosis of the four images meaning that it had more outliers in its pixel intensity distribution. Thus, it can be said with reasonable confidence that the image of the model eye was higher contrast than the images of the darkly and moderately pigmented eyes but not the lightly pigmented eye which had a substantially larger standard deviation of pixel intensity.

Finally, only the image of the darkly pigmented retina suffered from saturation of pixel intensity with 0.04% of pixels having the maximum possible pixel intensity (255). These were entirely located within the optic nerve.

Image	Median ± SD	Min	Max	Skew	Kurtosis
Dark reference	133 ± 37.4	20	255	-0.5	-0.4
Moderate reference	93±34.2	16	186	0.2	-0.8
Light reference	135±54.5	12	240	-0.2	-1.1
Eye phantom	98±38.9	15	246	0.4	-0.2

Table 37 - The shape parameters measured for the distribution of weighted pixel intensities for the reference photographs and the image of the eye phantom.

9.4 Discussion

To the author's knowledge, there is presently no description in the scientific literature of how to construct a preterm phantom for ocular imaging nor is there such a unit that is available commercially. The phantom described in this chapter was shown to be useful in testing the optical performance of retinal imaging technologies for use in preterm infants. Given the importance of such units in preventing a number of causes of childhood blindness, such a phantom represents a useful addition to the scientific literature. The phantom may also prove useful in providing a training aid for eye care personnel involved in retinal imaging workflows.

Further adaptations to the phantom upon the development of better simulations of the eye based on further understanding of the preterm eye's development and biometries, as discussed in the previous chapters, could result in more accurate eye phantom designs. In particular, a better understanding of the tolerances of the various parameters of the preterm eye would allow for a more robust, quantitative evaluation of the eye phantom. Furthermore, the development of an eye phantom that also simulates the mechanical properties of the preterm eye would be a welcome enhancement, as it would allow, for example, the testing of procedures involving scleral indentation. Similarly, it would be desirable to construct eye models with targets that provide more objective information regarding image quality, such as resolution and colour.

Moreover, it was necessary in the construction of a single eye phantom to select mean values for parameters which have fairly broad distributions within the preterm population. Therefore, the phantom does not replicate the difficulties with unusual geometries such as lower than average field-of-view. Additionally, the weighted pixel intensity distributions of the analysed images appear to show that the phantom allows for imaging with a contrast that is akin to an eye which is moderately to lightly pigmented. It therefore does not replicate the challenges associated with grading the lower contrast images that are acquired when imaging darkly pigmented eyes. This is notable limitation given that ROP poses the greatest challenge in the Indian subcontinent, where the population does have darkly pigmented eyes, and that Sub-Saharan Africa is also a region where ROP prevalence is increasing (148).

A final limitation of the eye phantom that should be noted is that it is static and therefore if used as a training aid does not accurately represent the movements made by a preterm infant who is not under general anaesthesia during a retinal imaging procedure.

10 LMIC ROP Camera Technology Demonstrator

10.1Introduction

As was discussed in Chapter 3, ROP is a leading cause of avoidable childhood blindness worldwide, with some 184,700 preterm infants estimated to develop the disease per year of which 20,000 are left severely visually impaired for the rest of their lives. Of those visually impaired by ROP 65% are born in middle-income regions (152). As timely laser treatment is known to preserve the sight of those suffering from ROP, screening programmes have been shown to be highly effective in high-income countries (152).

Such a programme requires an expert to grade the progression of ROP by viewing wide-field images of the retina. In the vast majority of ROP screening programmes, this achieved through indirect ophthalmoscopy by a specialist ophthalmologist. In such programmes, the ophthalmologist grades the image as he or she views the retina and then records what was seen in paper notes (159). Wide-field retinal photography offers the opportunity not only for the images to be recorded for future reference but for the task of imaging the retina to be undertaken by lower cadres within the infant's care team, such as specialist nurses (161). Furthermore, such imaging techniques have been shown to be less painful for the examined infant than binocular indirect ophthalmoscopy (332). Presently, only one retinal camera model that is capable of capturing a wide enough field for ROP screening has achieved widespread adoption for ROP screening, the RetCam 3 (393). However, the RetCam is expensive, costing in the region of 100,000 USD. As such, it is not a viable option for screening in most LMIC's NICUs. Furthermore, the camera is large, making it unfeasible to transport between units, and its imaging head is bulky and heavy affecting the ease-of-use.

This chapter describes the design, prototyping and testing of technology demonstrator for low-cost wide-field neonatal imaging. Such a design is only possible due to the preterm eye simulation described in Chapter 8. Testing such a prototype in a meaningful way without the use of human or animal models, is only possible due to the preterm optical phantom described in Chapter 9. Furthermore, the clinical workflow model described in Chapter 9 ensures that such a technology is appropriate for use within the context of an ROP screening programme.

10.2 Methods

10.2.1 Optical Design

It was concluded from the previous chapter's analysis that, from an ease-of-use perspective, a camera designed under the principles of direct ophthalmoscopy was more appropriate for it application than those of indirect ophthalmoscopy. As direct ophthalmoscopy tends to visualise a smaller retinal field-of-view than indirect ophthalmoscopy, before such a camera could be designed it was first necessary to establish whether direct ophthalmoscopy could achieve the wide field-of-view required for ROP screening. It is also necessary to miniaturise the camera as far as possible so to allow it to rotate around the eye, whilst remaining in near contact, and therefore visualise an extended field-of-view.

In addition, applying a coupling gel to the cornea between the camera optics and cornea is a means by which the area of visible retina can be increased by largely removing the refraction occurring at the air-cornea interface, which is the largest component of refractive power in the eye (266). Furthermore, reducing the difference in refractive index at this interface reduces the intensity of reflection from the anterior surface of the cornea back into the camera optics, this usually being the most significant artefact found to be present in direct ophthalmoscopy. In order for such a coupling gel to be used, the camera optics must be of a design whereby minimal distortion occurs when used in a fluid where the refractive index is greater than that of air. Moreover, the sensor array must be encapsulated in a way that allows the unit to be immersed in a liquid without damage being caused or the patient being put at risk of electric shock or mechanical trauma.

An imaging sensor initially identified as a candidate for use in the technology demonstrator was the Awaiba NanEye (NanEye2D RGB FOV160 F2.4, CMOSIS Germany GmbH, Nürnberg, Germany). This sensor had a number of attributes that made it appropriate for the application in question. These were: wide field of view (95 degrees in water), being waterproof, able to image in liquid owing to its flat anterior lens and the size of its front face being $1mm^2$, the smallest imaging sensor available commercially at time of purchase. Furthermore, its cost was within specification being for a single unit 350 EUR reducing by an order of magnitude in

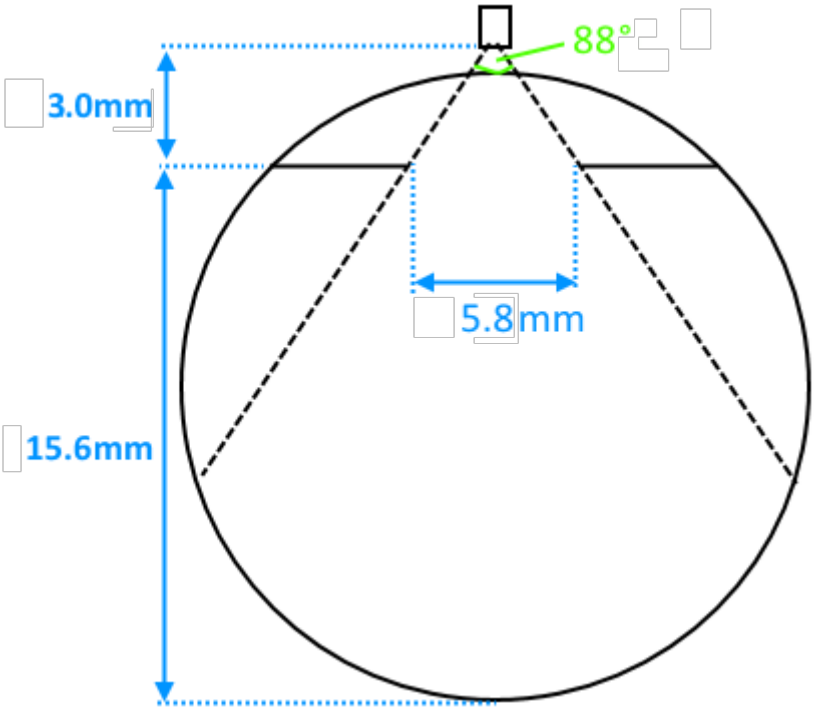

Figure 105 - A simplified optical model of the preterm eye at 34 weeks' PMA with micro-camera placed at a 1mm working distance.

bulk quantities. Its one potential drawback was its resolution; indeed, the image sensor has only 62.5k pixels (i.e. produces an image which is 250x250 pixels) suggesting the image resolution possible is limited.

The appropriateness of the camera's field of view was established by a simplified model of the eye shown in Figure 105 and based on the eye dimensions found for a 34-week PMA infant in Chapter 7. This approximated the eye to a sphere and does not account for refraction by the crystalline lens or the cornea-aqueous humour interface. Assuming a working distance of 1mm from the corneal surface and that an index matched fluid occupies the space between the camera optics and cornea, the maximum angle that can be imaged through a pinhole positioned on the optical axis is 88.°. This translates to a subtended angle of 110°, and whilst it should be noted that this simple model does not take into account the narrowing of the field-of-view by the crystalline lens, this is nevertheless comparable with other widefield fundus cameras. The Awaiba Naneye's field of view in water, at 95°, is therefore well matched for the application.

According to the same simple model, the number of pixels per a degree subtended angle is 2.35 pixels per degree. The minimum feature size that can be resolved on the retinal surface is therefore 58µm. The aforementioned limitations withstanding, this would suggest that the NanEye unit is able to resolve features pertinent to ROP diagnosis such as arteriole and venule which are typically 160µm and 240µm in diameter respectively (394).

The pinhole design of the Awaiba NanEye also has the advantage of providing a deep depth of focus, 3-50mm, which encompasses the full range of axial lengths for the ages explored by the preterm eye model established in Chapter 7. This means that its fixed focus optics are suitable for the application without the addition of any further optics enabling adjustable focal length.

10.2.2 System Design

A diagram of the high-level system design is shown in Figure 106. This consisted of three core parts: containing the illumination source, imaging sensor and optics and a camera grip housing both of the aforementioned parts, keeping them in close optical

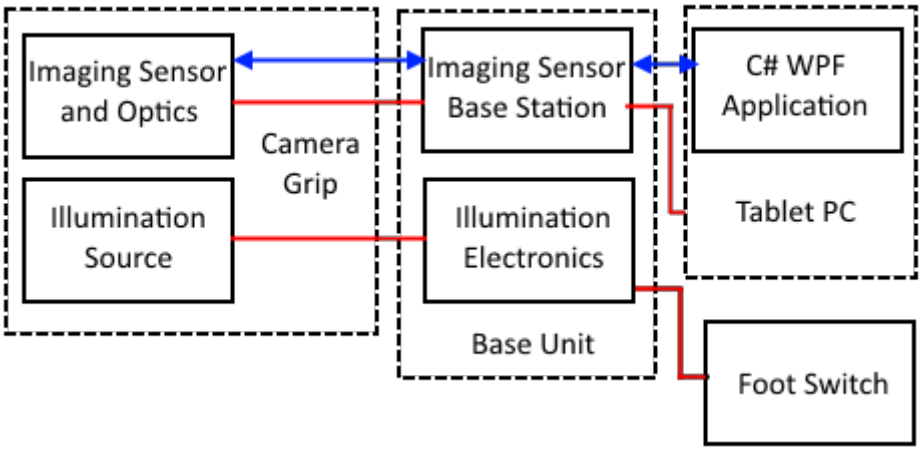

Figure 106 - System diagram for the ROP technology demonstrator. Red lines represent an electrical power connection and blue lines represent data flows.

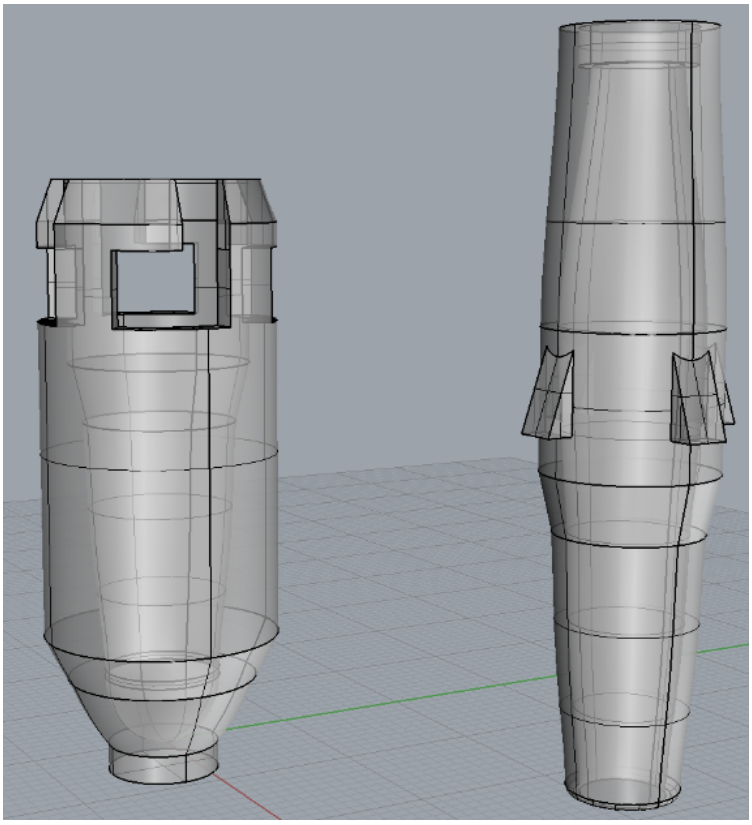

Figure 107 - CAD for the 3D printed camera grip (right) and its lockable cover (left).

alignment and, owing to their size and fragility, also allowing for their safe and ergonomic operation (particularly preventing the imaging cable from snagging); the base unit, containing the imaging sensor base station and illumination electronics and a tablet computer with custom software installed.

The mechanical design of the camera grip was derived from the conclusion of the analysis in the previous chapter, that is that the ergonomic design of the prototype be light and manoeuvrable as possible, allowing it to be operated by a neonatal nurse. A ballpoint pen has an ergonomic design that is both intuitive and allows for fine precision movements. The design was also required to be such that it could be operated in both hands by someone of either handedness in order to aid imaging of both eyes. The general form of the mechanical design was therefore based on that of a ballpoint pen with a high degree of rotational symmetry around its central axis, lacking any grips suited to a particular handedness (specifically, a University Silver/Blue Pen, University of Strathclyde, Glasgow, UK). A CAD for the camera grip was produced in Rhinoceros 5 (McNeel & Associates) and is shown in Figure 107. As the camera optics protruding from the grip had a larger diameter than a ballpoint the tip of the technology demonstrator was enlarged by comparison (Ø6mm ID; Ø8mm OD). An aperture (Ø6mm ID; Ø11mm OD) was also created at the other end of the grip to allow the wires connecting the light source and imaging sensor to reach a base unit housing the system's electronics.

A 3D print of the camera grip was produced by using Simplify3d (Simplify3d LLC) to slice the 3D print files and printing in PLA (RS 3D Printer Filament PLA 2.85mm, RS Components) using an Ultimaker 2 3D printer (Ultimaker B.V.).

The off-the-shelf camera sensor was glued (with Loctite 4305, Henkel Technologies) inside a hollowed-out ballpoint pen capsule (taken from aforementioned University Blue/Silver pen), this being rigid, protecting the sensor and its cables, and of appropriate dimensions for insertion into the camera grip. This capsule was then mounted on the end of a compressible spring that was cut to a length that meant when fixed to the capsule the combined assembly, when uncompressed, was approximately 1mm longer than the interior of the camera grip. This allowed the capsule to move in any direction in three-dimensional space once fixed inside the

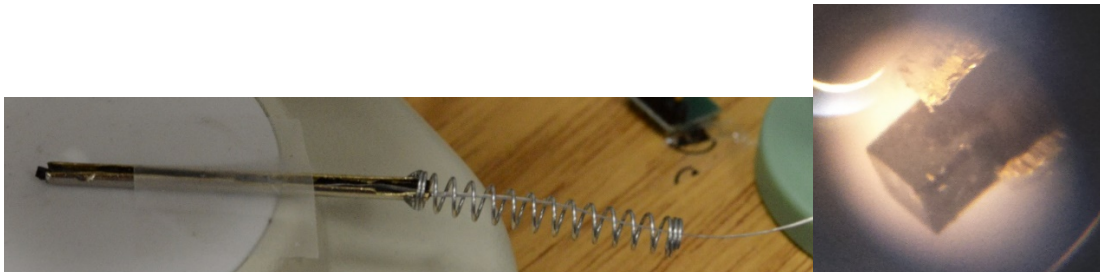

Figure 108 – The imaging sensor (shown magnified, right) was mounted within a spring-load capsule (left) to reduce the mechanical force on the cornea and sensor respectively during imaging.

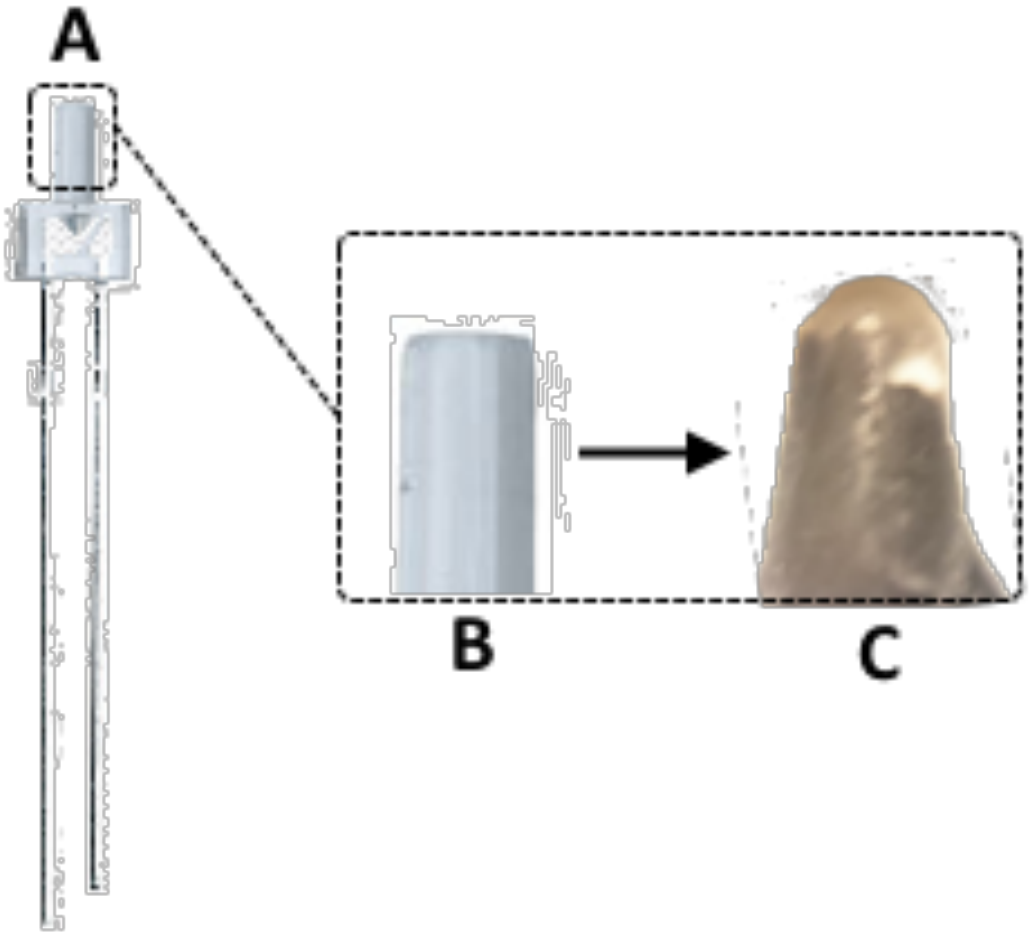

Figure 109 - The basis for the ROP Camera Technology Demonstrator was the Kingbright L-13PWC-Z White LED (A) the tip of which is shown magnified in B. The LED once a diffusing hemisphere had be placed on its top and its cylindrical face painted in black paint is shown in C.

camera grip and thus avoid excess pressure being exerted on the cornea during operation. The assembled capsule is shown in Figure 108. The imaging system was controlled by the electronics contained within the NanoUSB2 evaluation board (CMOSIS). The evaluation board consists of a miniaturised field programmable gate array (Spartan 3E, Xilinx Inc., San Jose, CA, USA) that deserialises and communicates with the NanEye imaging sensor and transfer this data via USB2 to a host computer (395). The computer used in the tests was an Iconia Tab 8 W (Acer Inc., New Taipei City, Taiwan). This was chosen for its touch-screen interface, low cost (100 GBP), ability to deliver a 5v supply over USB OTG, ability to connect to Wi-Fi and 4G networks and its portability, being light enough to be held in one hand or propped in a convenient position on a desk. Additionally, the evaluation board handles upstream configuration data for the sensor registers such as exposure time, offset and gain. The board is powered by the 5v line of the USB2 connection and creates a regulated power supply for the sensor. The custom-built illumination source, the tip of which is shown in Figure 109 and the full assembly within the camera grip in **Figure 110**, was constructed by mixing Barium Sulphate (OliverBrown, United Kingdom) powder with Loctite 4305 UV curing glue (Henkel Corp., Westlake, O.H., U.S.A.) with an approximately 1:1 ratio by weight. In order to produce a wide-angle, diffuse light source, a drop of this mixture was then placed on top of a 2mm flat top LED (L-13PWC-Z, Kingbright) and cured using a Lighte^2 E2 UV torch (Lumitorch). Next, those areas around the diffusing element were painted with black paint (Gel, NSI Scotland) to eliminate unwanted reflections. This unit was then mounted on a compressible spring fixed to a length of 3mm diameter PMMA rod (Round Plastic Rod Bar Acrylic 2mm diameter, Materials Testing and Technical Services Ltd, Kingston upon Thames, UK), in order to avoid electrical contact between the spring and the LED's electrodes. As with the imaging assembly, the compressible spring was cut to a length so that the combined length of the assembly was approximately 1mm longer than the internal cavity of the camera grip. After soldering 1m of multicore wire to each electrode, the assembly was then placed within the camera grip. The grip was then sealed with a circular cut of 0.5mm thick high-impact polystyrene sheet (HIPS, Hindley) that had two holes and a slit, cut

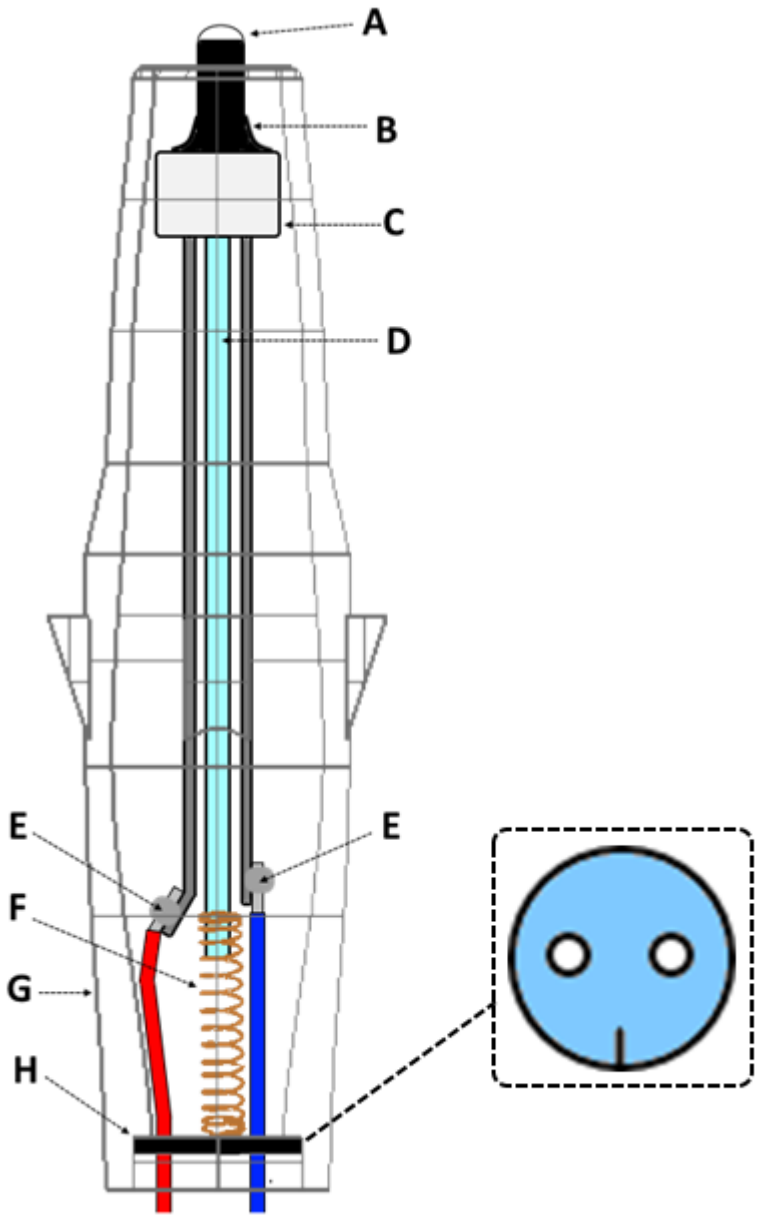

Figure 110 – Diagram of the assembled light source, consisting of a hemisphere of barium sulphate dispersed in UV curing adhesive.

using a TMX65 CO2 laser cutting machine (CTR Lasers), so that the multicore wire and imaging sensor's cable could connect with the backend unit. The assembled imaging and illumination system is shown in **Figure 110**. Here (A) hemispherical diffusing element fixed to a 2mm diameter cylindrical flat top white LED (C). The curved face of the LED's cylinder and face on which the cylinder is mounted were painted with UV curing black paint (B). A 2mm diameter PMMA rod (D) was fixed to the rear surface of the LED, allowing a compressible spring (F) to affixed in a position where it was not at risk of shorting the LED's electrodes. The illumination assembly was lowered through the rear of the unit's 3D printed housing (G) which was then sealed with a circular 0.5mm thick cap made of high-impact polystyrene sheet (HIPS) (H). Two holes were laser cut into the cap prior to insertion to allow the multicore wires, soldered to the cathode and anode respectively (E), to connect to the control electronics.

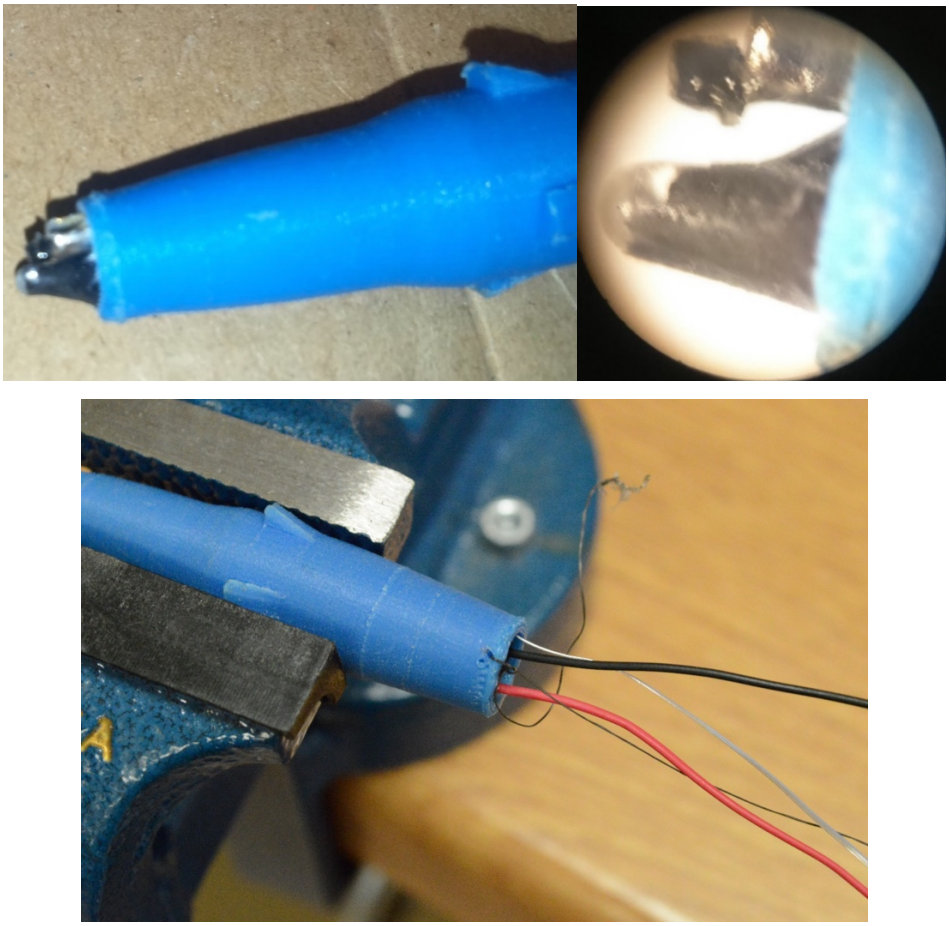

Figure 111 - The illumination source and custom optics as positioned within the camera grip (top-left; magnified top-right) and the rear of the camera grip after its full assembly but prior to wrapping the imaging sensor wires, illumination system wires and nylon thread in cable wrap.

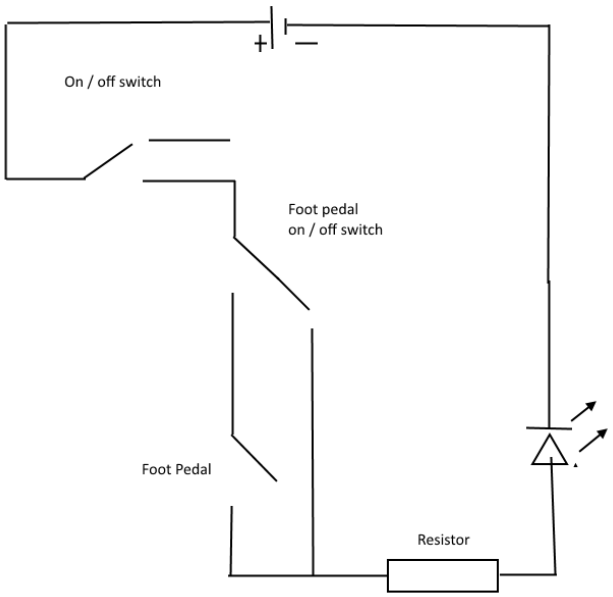

Figure 112 – Circuit diagram of the simple custom electronics that were used to control the illumination system.

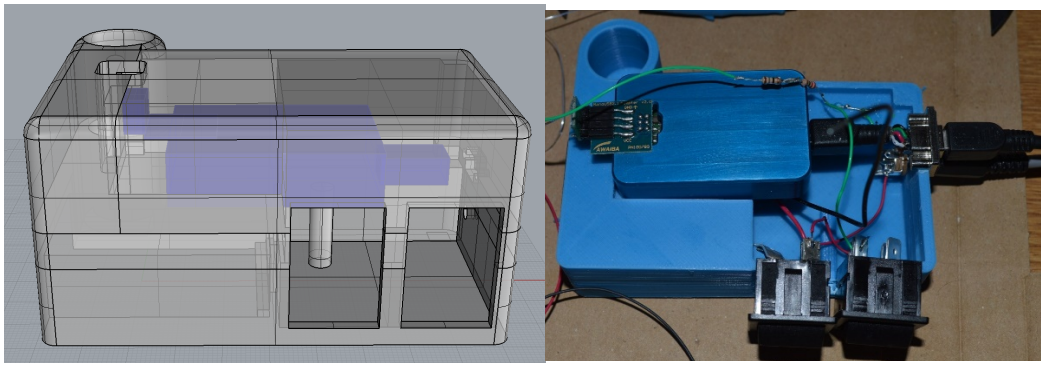

Figure 113 – CAD rendering of the back end unit (right) and the back end unit prior to final assembly (left) with electronic components in-place.

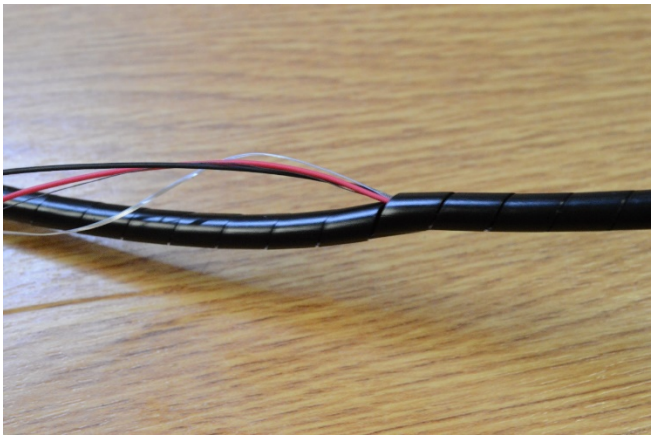

Figure 114 – The power and data wires connecting the imaging sensor and illumination system to the back-end unit were placed within a 4mm cable wrap to avoid damage.

The illumination system was powered via four 1.2v NiMH rechargeable batteries (Ansmann AG, Assamstadt, Germany) and was current limited by 18Ω and 200Ω resistors connected in series. Two rocker switches (On-Off Rocker Switch for Panel cut-out with width and height of 22mm and 30mm respectively, Arcolectric, Thousand Palms, CA, USA) allowed the illumination to be set to "off", "constant" or enabled only when a foot pedal was pressed. The foot pedal itself (Light Duty Momentary Polymer Foot Switch, RS Components) was connected with a 6.35mm diameter stereo jack (RS Pro 6.35 mm Cable Mount Jack Plug, RS Components) which can be disconnected if not in use. A circuit diagram for the illumination system's electronic design is shown Figure 112.

The base unit, shown in Figure 113, was designed using Rhinoceros 5 (McNeel & Associates) to hold the camera sensor's and illumination system's electronics, the four removable rechargeable batteries, two panel cutouts for the insertion of the rocker switches, a mini-USB B socket and a 6.35mm stereo jack socket (6.35mm Panel Mount Jack Socket, Switchcraft, Chicago, IL, USA). The base unit also contained a receptacle for placing the camera grip when not in use.

The power and data wires connecting the imaging sensor and illumination system to the back-end unit were place within 4mm internal diameter spiral wrap (RS Components) for protection, as can be seen in Figure 114. An ultra-high modulus polyethylene thread (Fireline 6LB break strength, 0.006" diameter Braided Beading Thread, Beadsmith, Carteret, NJ, USA), tied between the camera grip and back end unit, was also included in the cable assembly. This was given less slack than the wires so to take any mechanical strain that was unintentionally exerted on the cable assembly. The thread can be seen tied to the camera grip, next to the illumination source and camera sensor wires in Figure105.

The full system after assembly is shown in Figure 115. In the orientation shown in this figure, the rocker switch to the right of the front face, when enabled, requires a foot pedal, connected via the 3.5mm headphone jack socket on the lower right of the right face to be pressed for the illumination source to be enabled. The imaging sensor is connected to the tablet PC via the micro-USB B socket on the centre-right of right face. The full system is shown alongside the preterm infant phantom in Figure 116.

Figure 115 – The fully assembled base unit. The rocker switch to the left of the front face controls the illumination source. The camera grip is stored in the receptacle to the right and rear of the unit.

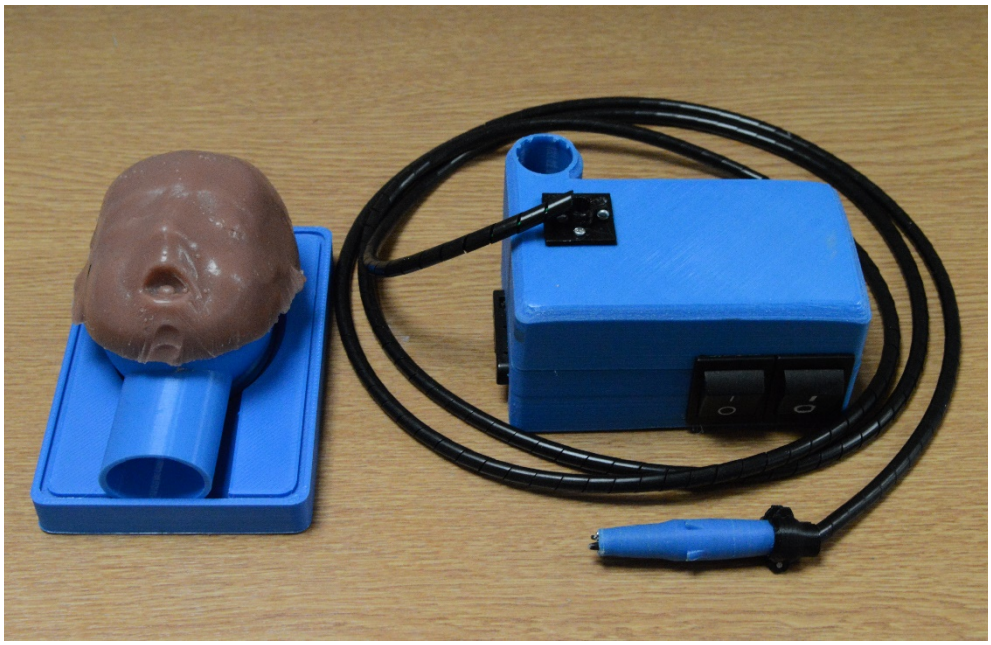

Figure 116 - The completed prototype of the ROP camera technology demonstrator (right) next to the preterm optical phantom described in Chapter 9 (left).

The full set of peripherals that are necessary to conduct lab-based assessment of the technology demonstrator are shown in Figure 117. The demonstrator (A) can be operate with continuous illumination or only turned on when a foot switch (B), connected to the demonstrator via a 6.35mm stereo jack (C), is pressed. The demonstrator connects to a mini-USB-B to USB-A assembly with USB-A to USB-A extension cable and finally a USB-A to micro-USB OTG adapter attached (D). This allows the demonstrator's image sensor to be controlled and its output acquired on an Iconia Tab 8 W tablet computer (E) running Windows 10 Home (Microsoft Corp.). The demonstrator's four AA batteries can be recharged using a standard mains battery charger (F). The demonstrator's imaging performance can be tested on the preterm infant phantom described in Chapter 8 (G) when Viscotears gel (H) is applied to the corneal lens surface to allow optical coupling with the camera optics. The solution inside the preterm eye phantom can be topped up from a vial of spare solution (I) using a syringe with 0.65mm needle attached (J).

A full list of the materials used to construct the technology demonstrator is provided in Appendix 10.1.

Figure 117 - The full set of equipment required for lab-based testing of the ROP Camera Technology Demonstrator.

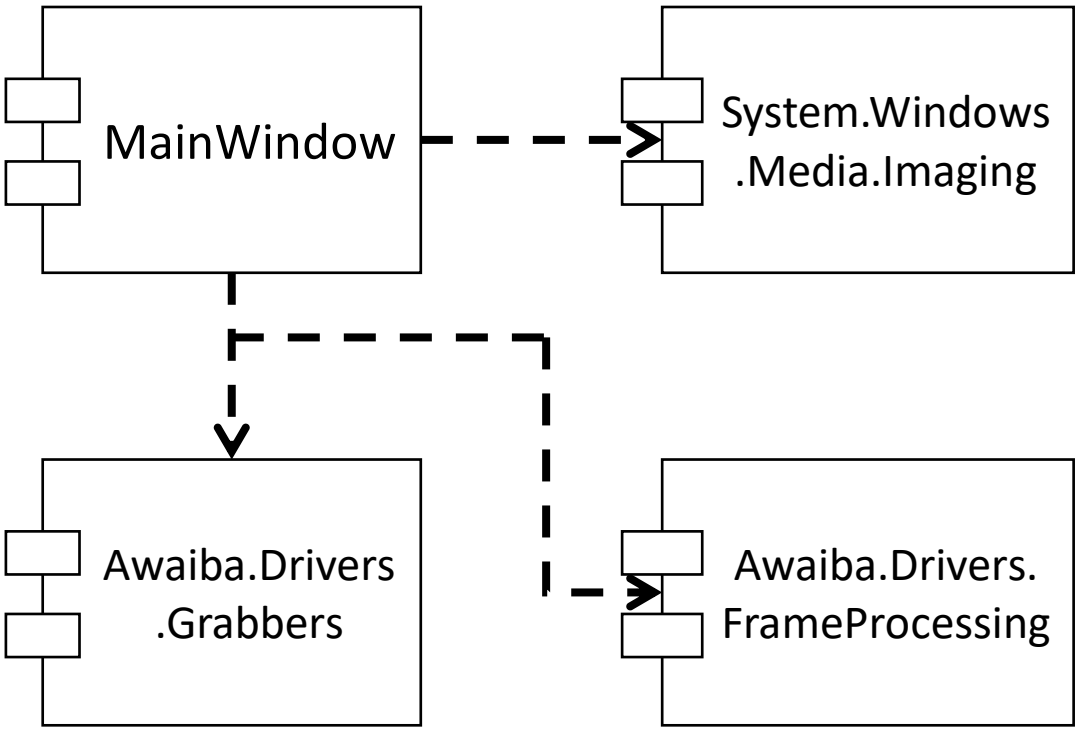

Figure 118 - A system architecture diagram for the ROP system's GUI.

Figure 119 - Screenshot of the system GUI. The GUI also allows control of the image sensor's exposure (top left) and the setting of the gain of each colour individually (bottom left). Every other image sensor setting is set automatically in software.

10.2.3 Graphical User Interface

A Graphical User Interface (GUI) was designed which allowed the prototype system to be tested on an optical preterm phantom using a mobile device. The scope of the software was restrained to allowing control of simple camera settings, namely exposure and colour, and allowing capture and export of images and video on a single tablet PC model. All other camera settings were set automatically in software to values determined by trial and error when testing the prototype system on the preterm phantom using a more powerful computer.

C# with Windows Presentation Foundation (WPF) was the technology used to build the system's software. This was chosen because C# is a modern software language for which supported Application Programming Interface (API) libraries exist for the imaging system used. Furthermore, C# with WPF is designed to allow quick development of GUIs, this representing a substantial part of the code, and was a language with which the author was already familiar.

A system architecture diagram of the GUI is shown in Figure 118. The GUI's class, MainWindow, used the Awaiba Drivers to capture and process the imaging sensor's output. The GUI then used Windows' (Microsoft Corp.) Media Imaging library to display the videos in real-time.
A screenshot of the GUI is shown in shown in Figure 119.

10.2.4 Performance Testing

The ROP system was tested against the model eye described in the previous chapter by an ophthalmologist with a sub-specialism in paediatrics. The ophthalmologist was not familiar with the design process of the system and was given only basic instruction in its operation. The imaging operation is shown in Figure 120. The model's eyelids were separated using the thumb and index finger of the operator's non-dominant hand. Optical coupling with the model eye was achieved by applying a liberal drop of Viscotears coupling gel and thus reflections from the cornea were essentially eliminated owing to their similar refractive index. The operator then inserted the tips of the imaging and illumination modules into the coupling gel, without coming in contact with the cornea, and attempted to identify the relevant retinal features, such as neovascularisation, the retinal ridge and the field-of-view markers. Video and still images were saved for subsequent analysis using the bespoke GUI.

Figure 120 - Acquiring retinal images from the preterm phantom described in Chapter 9.

A reference image of the eye phantom was taken using a RetCam 3 by a different ophthalmologist, thus ensuring operator blinding in each case.

Assessment of field-of-view and contrast were conducted as per the methods detailed in 9.2.3.

Image resolution was determined by observing the outermost concentric circular step caused by the increase of the layer height by one step during the 3D printing process. The Perfactory Desktop XL 3D printer prints in cubic voxels with sides of length 71µm (envisiontec.com), hence the phantom's retinal surface is not perfectly spherical but consists of steps whose height and width are each divisible by 71µm.

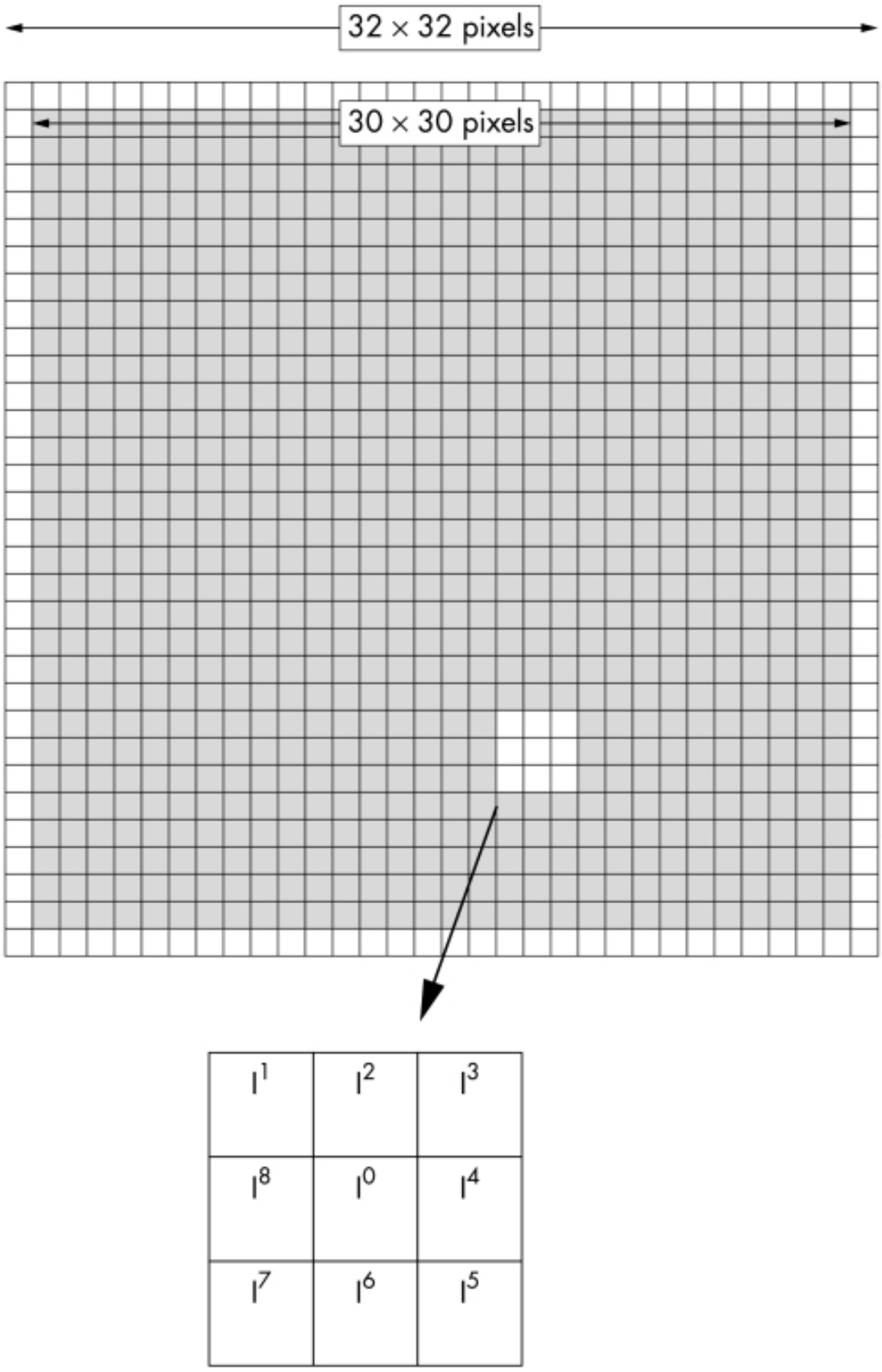

Figure 121 – Schematic diagram illustrating a 32x32 pixel region of interest and the notation used with respect to the weighted pixel intensities for the purposes of calculating the region's acutance. Reproduced with permissions from (396). Copyright © 2003, British Medical Journal.

Thus, the allowed values of the fundus, relative to the fundus' centre of curvature, are those solving,

$$z = R - 71n, \text{ [µm]} \quad \textbf{(23)}$$

where z is the height in the direction of the phantom's optical axis, R is the fundus' radius of curvature in microns and n is the 'step number' relative to the macula and is an integer between 0 and $2R/71$.

Therefore, the position of the corner of a given step can be found by solving the equation of a circle with radius R for z = n-0.5 and rounding x and z to the nearest integer divisible by 71. That is to say,

$$x = \left\lfloor \frac{\sqrt{R^2 - \left((R - 71(n-0.5)\right)^2}}{71} \right\rceil \cdot 71 \text{ [µm]}. \quad \textbf{(24)}$$

The distance between the two such adjacent corners which are both visible and have n closest to 2R/71 (i.e. are the closest to the equator) then gives the size of minimal resolvable object down to $\sqrt{2 \cdot 71^2} = 100\text{µm}$.

Acutance, that is how quickly image information transitions at an edge (397) was calculated according to the method described by Choong and colleagues (396), that is using the relationship,

$$G_{x^2} = \frac{\sum_{n=1}^{N} \left(\sum_{i=1}^{8} \left(\left(\Delta \mathrm{I}_n^i \right)^2 \right) \right)}{8N} \quad \textbf{(25)}$$

where G_x^2 is the unnormalized acutance, N is the total number of pixels and ΔI_{ni} is the difference in pixel intensity between the nth pixel and the adjacent pixel in position i according to the notation shown in Figure 121. The acutance is the normalised by dividing by I_0 the square of the mean intensity of a test image consisting of alternating pixels of minimum and maximum intensity (that is 0 and 255), and multiplying by 10000 giving the relationship,

$$Acutance = \frac{10000 \cdot G_{x^2}}{I_0}. \quad \textbf{(26)}$$

As the determination of acutance is computationally intensive, a region of interest is selected with all the pixels not on the periphery of this region being used as 'central' pixels in the analysis. For example, Choong and colleagues selected a 32x32 pixel

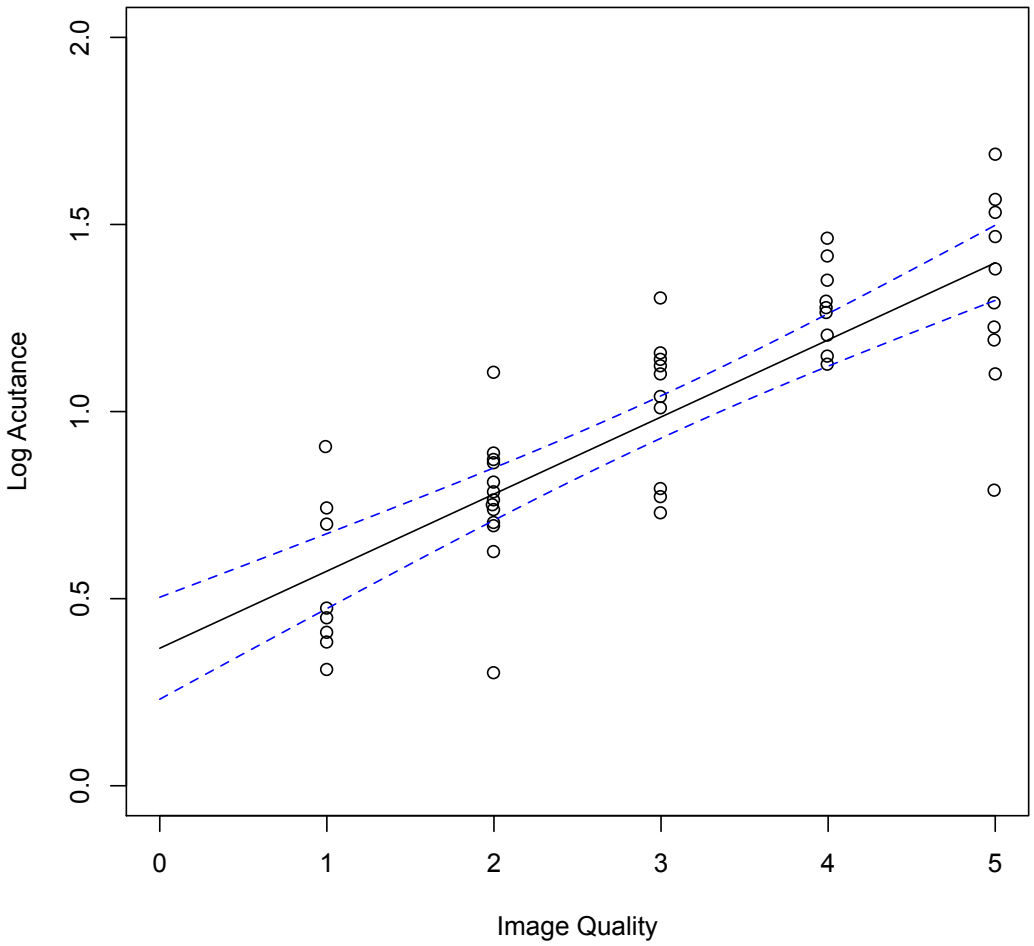

Figure 122 – Log base 10 acutance of 58 retinal images and subjective image quality, as graded by two experts, reported by Choong and colleagues (396). A linear fit has been added to the data (F=100; p<0.0001). Adapted with permissions from (396).

Quality	Grade
Poor	1
Moderately poor	2
Moderate	3
Moderately good	4
Good	5

Table 38 - The classification of image quality as devised by Choong and colleagues (396). Reproduced from (396) with permissions. Copyright © 2003, British Medical Journal.

region of interest containing a section of the retinal arcade (396).

Finally, Choong and colleagues also demonstrated a strong correlation between the base 10 logarithm of the acutance and the subjectively assessed quality of a fundus photograph. Thus a 'quality grade' can also be assigned where

$$Quality = \frac{\log_{10}(Actuance) - 0.368}{0.206} \quad \textbf{(27)}$$

according to the data presenting graphically by Choong and colleagues which is shown with a linear fit ($F=100$, $p<0.001$) in Figure 122 and where *Quality* corresponds to the classifications shown in Table 38.

10.3 Results

The ophthalmologist was able to obtain an in-focus image of retina over a wide field-of-view almost instantaneously with insertion of the imaging and illumination module tips into the coupling gel. Snapshots captured by the ophthalmologist are shown in Figure 125, Figure 124 and Figure 123. By rotating the imaging and illumination head around the cornea the ophthalmologist was able to image up to the equator, that is approximately 90° subtended

Figure 125 - - A snapshot with field of view snapshot approximately equal to 60 degrees subtended angle captured by an ophthalmologist.

Figure 123 - A frame taken from a video recorded using the imaging system. The temporal periphery can be seen up to approximately 90 degrees subtended angle.

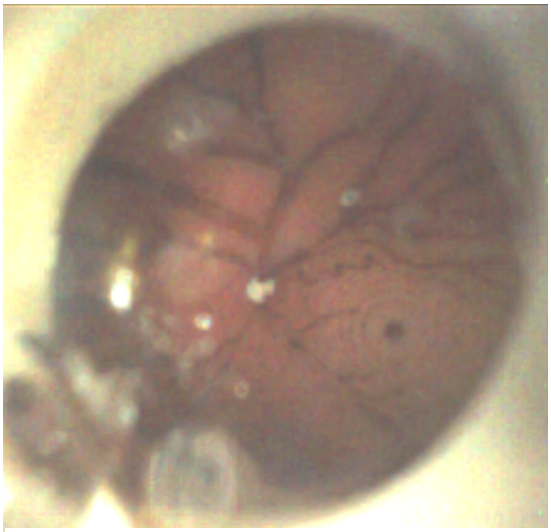

Figure 124 - A frame of the video captured by the ophthalmologist during her first imaging attempt. Almost all of Zone I is visible in this single image.

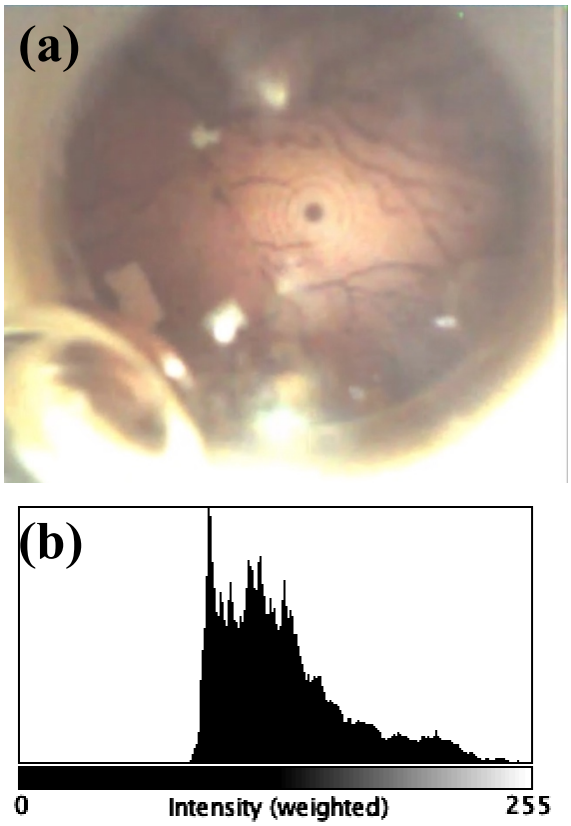

Figure 126 – The image acquired by a consultant ophthalmologist using the technology demonstrator which was selected for analysis (a) and a histogram of the weighted pixel intensity across the ocular fundus visible in the image (b).

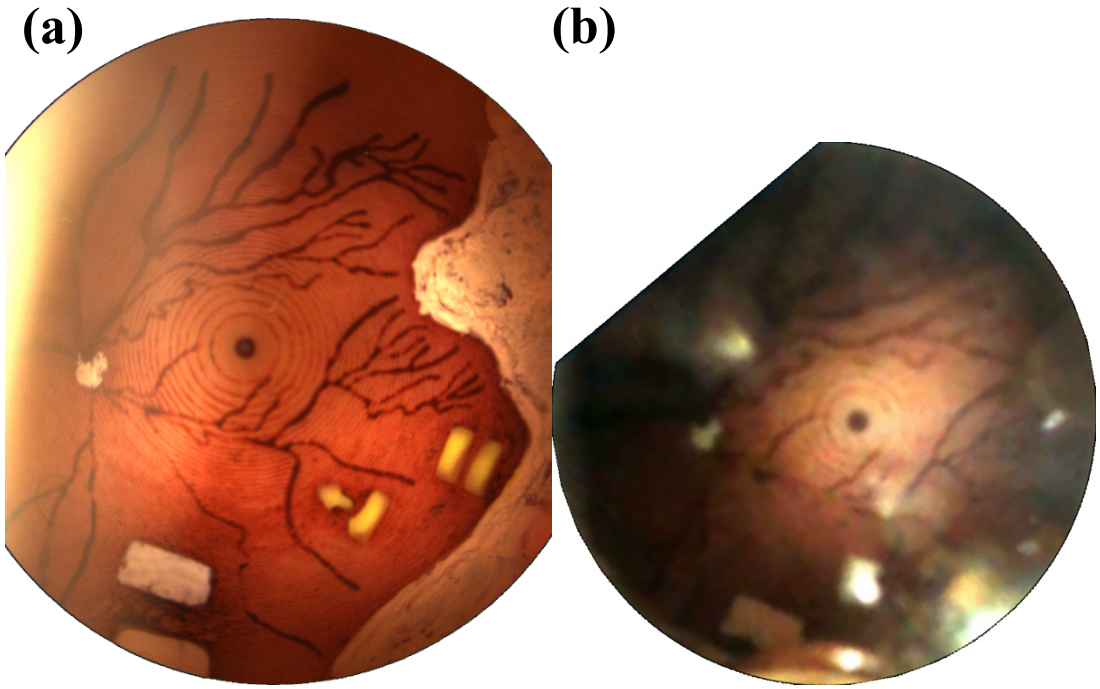

Figure 127- Images of the preterm eye phantom acquired with the RetCam 3 (a) and technology demonstrator after contrast enhancement (b).

angle, in every direction. Figure 123 shows an example image where the equator is visible.

An approximately 1mm diameter bubble was present in the anterior chamber of the ey phantom throughout the duration of the imaging session. Whilst this could not be removed, owing to the design not allowing trapped air to easily escape from the anterior chamber, the phantom could be orientated so that the bubble caused minimal obstruction of the fundus.

The image selected for analysis is shown in Figure 126a. A histogram of the weighted pixel intensity, shown in Figure 126b, suggested that the image was of low contrast but that the image's contrast could be enhanced by redistributing the pixels' range across the full range of pixel intensities to produce the image shown in Figure 127b. The histogram of weighted pixel intensities for the contrast enhance version of the image is shown in alongside that of the image acquired using the RetCam for reference. The shape parameters for the original image, contrast enhanced image and RetCam image discussed in Chapter 9 are shown in Table 39.

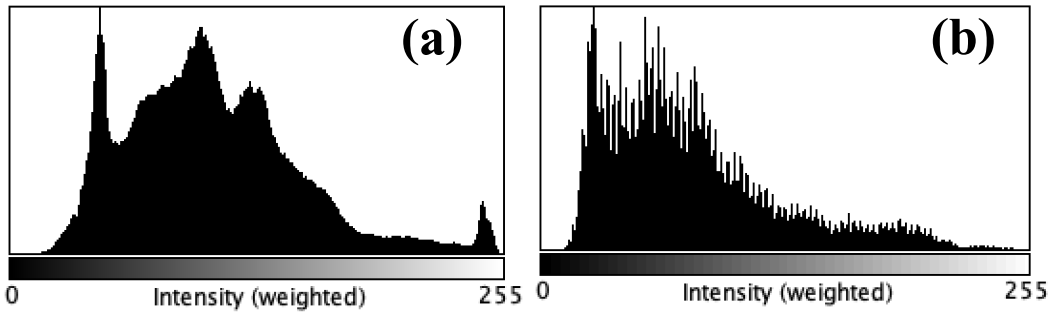

Figure 128 - Histograms of weighted pixel intensities within the image of the eye phantom acquired with the RetCam (a) and prototype after contrast enhancement (b).

Fort the image acquired using the prototype, the distance between the optic nerve and foveal pit was measured to be 235 pixels and thus, as the visible retina was 832 pixels across, the field-of-view of the image was calculated to subtend 52.2°.

The resolution and actuance was first assessed graphically but examining the weighted pixel intensity profile of the line shown in Figure 129. It is apparent both visually and from the graphs that the resolution and acutance is poorer in the image acquired from the prototype compared to that acquired by the RetCam. A significant

Image	Median (±SD)	Min	Max	Skew	Kurtosis
Recam	99.0±45.9	8	255	0.8	0.7
Prototype	126±32.0	85	252	1.0	0.6
Prototype contrast enhanced	63.0±50.0	0	255	1.2	1.1

Table 39 - Shape parameters for the distribution of weighted pixel intensities in the three analysed images.

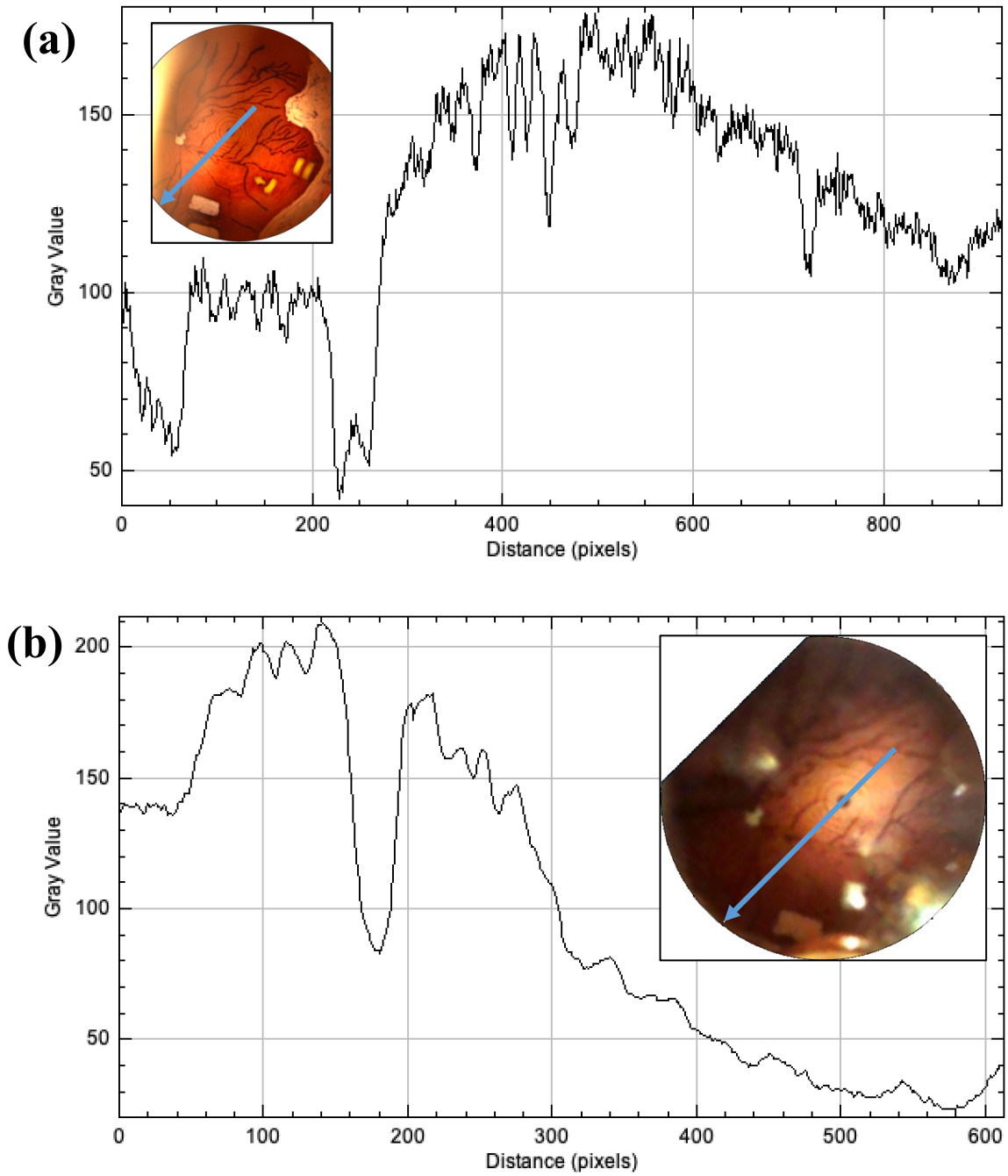

Figure 129 - The weight pixel intensity for the profiles shown inset for the image acquired by (a) the RetCam and (b) the prototype. The large minima at approximately 200 pixels distance correspond with the foveal pit whilst smaller minima occur where the profile crosses one of the radial steps resulting from the additive 3D printing process. The other large minima from approximately 0 to 50 pixels corresponds with a retinal vessel.

dropoff in intensity with distance from the image centre is also apparent in the prototypes' image.

The minimum step in the fundus' surface that was visible was three steps beyond the foveal pit. This corresponded to a resolution of 224.5µm.

A square region containing the foveal pit and three of the radial steps produced during the additative 3D print process, shown in Figure 131, was selected for analysis of image acutance. The acutance was calculated to be 1.84 for the prototype image compared to 23.94 for that acquired with the RetCam. These corresponed to image qualities of "poor" and "good" respectively.

Figure 130 - Comparison of the resolution of finer details on the preterm eye phantom as acquired by a RetCam 3 (a) and the technology demonstrator (b)

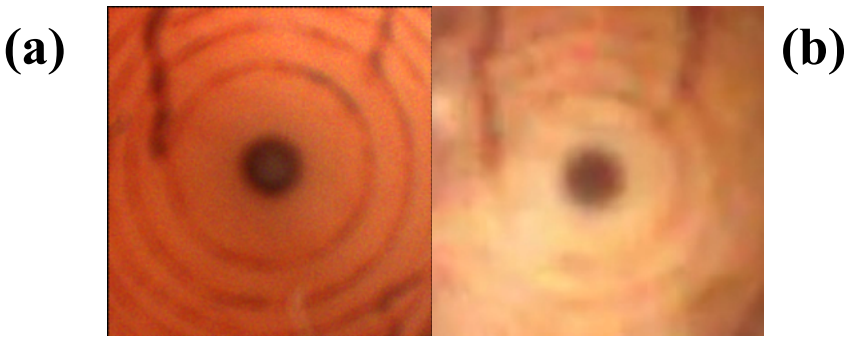

Figure 131 - Region of interest containing the foveal pit and three radial steps resulting from the additive 3D printing process acquired using (a) the RetCam (b) the prototype.

10.4 Discussion

The technology demonstrator described in this chapter is both smaller and lighter than the reference standard and has a component cost that suggests it could be made available for a fraction of the cost.

The field of view achieved on the eye phantom, whilst slightly less than that achieved with the RetCam 3, is within the range (45.2° to 69.3°) of those calculated in 9.3 for images acquired using the same camera model and presented as references for ROP clinical decision making (390). That is to say that the whole retina up to the equator can be imaged by rotating the imaging and illumination head around the cornea.

However, the acutance and image resolution are not of the same standard, as might be expected given the small image sensor resolution used in the technology demonstrator (250x250 pixels). Future iterations could therefore potentially afford to use slightly larger cameras in order to attain a higher image resolution. The acquisition of higher resolution images would not only improve the likelihood of diagnostic accuracy by a human grader, but would also allow for integration with automated or semi-automated retinal grading platforms such as VAMPIRE (University of Dundee, Dundee, UK) (398).

The contrast of the image acquired by the prototype was markedly poorer than that of the image acquired by the RetCam 3 and post-processing was required to correct this. Investigation of the optimal settings for the electronics' registers should therefore be included in future work in order to create high contrast images without the need for post-processing, as this would allow for better assessment of images in real time. It should be noted that it is unlikely for there to be a single set of optimal register settings for all eyes, given differences in retinal pigmentation between patients for example, and thus it is likely that the number of different settings be required for different eye types, as is the case when imaging adult eyes (399).

The illumination uniformity was also poorer than that of the RetCam 3 with a brightly lit central sport with substantial reduction in intensity towards the periphery. Further work should therefore include more detailed study of the optimal ratio of

barium sulfate to adhesive in creation of the custom optic.

Nevertheless, the technology demonstrator resolves key retinal features such as the retinal ridge and neovascularisation, although the latter is less obvious than in the RetCam's image. Finer details such as the radial lines formed during the 3D printing process and the paint texture on the ridge are not discernable. Coupled with the demonstrated field of view, the technology thus represents a viable solution for ROP screening but will do so with improved effectiveness if image quality is improved.

The ability of the ophthalmologist to pick up and use the system to this effect with minimal instruction and with relative ease suggests that training lower cadres to do so is feasible, as was identified as a key requirement during the workflow analysis conducted in the previous chapter. Further testing with neonatal nurses will be required to establish what a training module for users with little experience in eye care ought to consist of.

The system's ability to connect to a mobile device, a Windows tablet PC in this case, further suggests that the design adheres to the other key requirement identified in the previous chapter, namely that retinal images can be shared remotely with expert ROP graders. For the remote grading of these images to be feasible within a clinical context, the system will need to interface with a telemedicine service capable of image share and review. Such a service would allow graders to quickly view and annotate images as well as view other details about the patient. Importantly, they will also need to be easily able to compare the latest image set with previous images from the same eye, where these exist, allowing for disease progression to be monitored. Such a service ought to make use of image formats such as DICOM that allow the images to be combined with other patient data in a way that is interoperable with other healthcare information technology. The development of such software was clearly out of scope of this research programme, however future work should seek to establish if the system discussed in this chapter could be interfaced with existing IT systems used for the remote grading of ROP or in screening for other retinal pathologies such as DR. In this regard, it should be noted that although many such telemedicine platforms exist, most use propriety imaging formats and therefore it does not automatically follow that the system can be simply integrated with any of

these.

A fundamental limitation of this chapter is the use of a preterm eye phantom rather than a live preterm infant. Whilst, as discussed in Chapters 7 and 8, this phantom represents a likeness to the preterm eye beyond that found in any commercially available eye models, having similar dimensions and a two-lens design, there are certain aspects of the real preterm eye it does not attempt to imitate. For example, the mechanical properties of the eye, largely due to a lack of reliable data for preterm infants concerning this, are not emulated by the model. Thus, it is not possible to understand how scleral indention has on the visible retina. Additionally, the eye is in a fixed position and so does not test how the camera performs when the eye is not facing directly ahead or is moving during the process of imaging, it is therefore not possible to understand to what extent the eye is required to be immobilised during imaging.

Before the technology can be progressed to use in NICUs it will need to be designed within a product capable of clinical trialling on an appropriately powered cohort of real preterm infants. This will include consideration of infection control measures such as disposable tip or a reusable tip which can be quickly and easily disinfected (400). More robust consideration will also have to be given to designing a camera tip that is less likely to cause corneal abrasions, by the removal of sharp edges and corners. Doing so may necessitate placing a further component in front of the light source and camera optics. This may in turn have implications for the field of view that can be achieved, as the camera optics are not able to get as close to the cornea as is possible in the prototype described in this chapter.

Furthermore, as the prototype was only tested on a single phantom designed to imitate the average preterm eye at 34 weeks' PMA it does not account for any of the substantial variations that occur as the child ages during the screening period or that are present between infants of the same age. For the testing of future prototypes it may be beneficial to construct eye phantoms with the dimensions for different PMAs, as defined in Chapter 7, and at the limits of within age variation, again as defined in Chapter 7. The degree of a patient's retinal pigmentation is also known to have a significant impact on the illumination intensity and camera colour balance

required (399). Thus, it may also be beneficial to construct phantoms designed to emulate the range of retinal pigmentations found in preterm infants across ethnicities. Finally, although care has been taken to design a device that can be effectively used by a neonatal nurse, an analysis of its use by such a cadre has not yet been conducted. It is true that the author could, qualitatively, capture images and media as good as those acquired by a consultant ophthalmologist, however subsequent clinical evaluation of the device should seek to formally establish agreement between the ROP grade assigned when the same eye is imaged by a neonatal nurse and paediatric ophthalmologist in isolation.

10.5 Licensing Information

The technology intellectual property discussed in this chapter is protected by The University of Strathclyde. Please contact University of Strathclyde Research and Knowledge Exchange Service before any use of the information detailed in this chapter (www.strath.ac.uk/rkes; email: rkes@strath.ac.uk).

SECTION 6

Chapter 11 – Discussion and Conclusions

Chapter 12 – Proposals for Future Work

11 Discussion and Conclusions

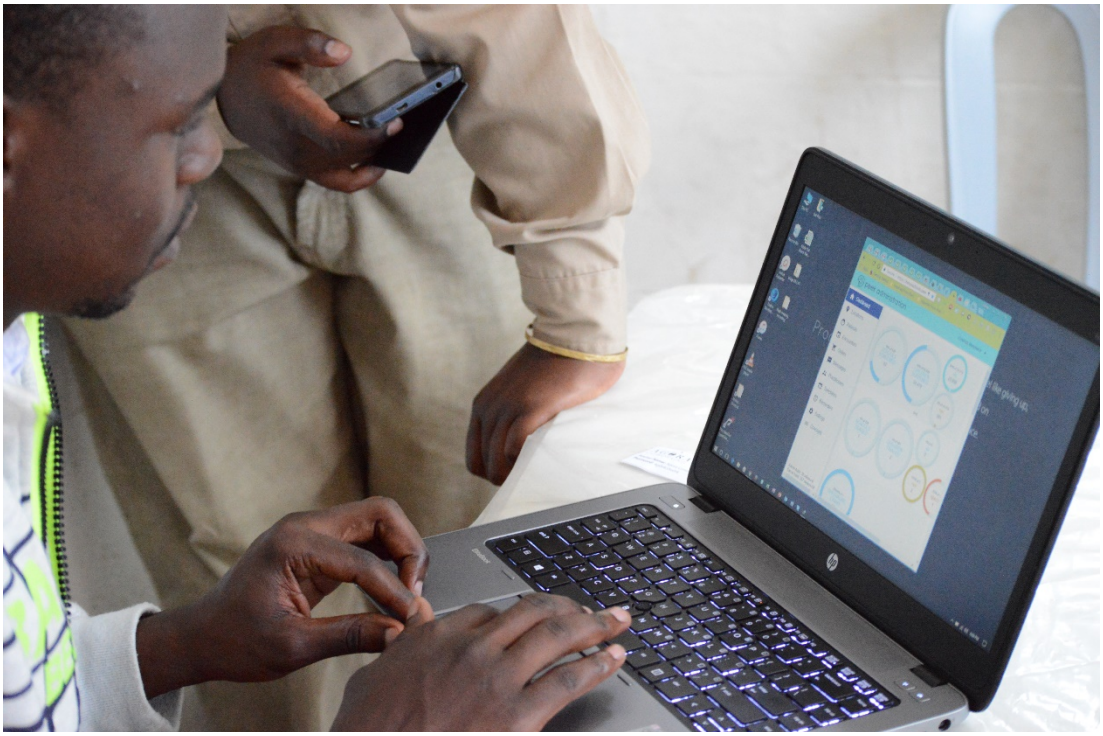

11.1 Contributions of this Thesis

During the course of this programme, the technical capability of mobile technology, such as computing power and imbedded camera quality, has continued to advance. Indeed, the power of mobile devices is now such that entire Hollywood feature films can been filmed using smartphones whilst technology companies, such as Google Inc. and Intel Movidius (San Mateo, CA, USA) are striving towards imbedding smartphones with specialist machine learning processors (401). Meanwhile, the cost of entry-level devices has continued to fall, with smartphone models being available for as little as 49 GBP (Vodafone Smart E8, Vodafone, London, UK). Hence, the proportion of people owning smartphones and tablet computers has steadily increased worldwide to the point of near-ubiquity (24). These recent developments have served to reinforce the understanding underpinning this thesis' hypothesis, namely that mobile technology is a powerful and widely available tool and will continue to be so for many years to come.

As a large number of reviews have already explored how this rise in connectivity could bring improvements within healthcare, it was sensible to compare the results and conclusions of these reviews rather than conducting yet another independent review. This review of reviews and critical analyses, described in Chapter 2, highlighted how advances in mobile technology present an unprecedented opportunity to connect those in need of healthcare to health services, particularly in LMICs.

However, the review also discovered that mHealth is still to achieve widespread adoption within healthcare in spite of the many successful 'pilot studies', where a device's effectiveness is tested in the context of a research study. A paucity of data concerning the impact of mHealth on the health system in which it is imbedded was found to be the most cited barrier to its adoption. In this sense, this thesis represents a contribution to lowering this barrier.

It is apparent from the review of mHealth devices developed for eye care in chapter 3, that, within eye care, the knowledge gap concerning mHealth's impact on the clinical workflow has been maintained by a misplaced emphasis on clinical statistical significance rather than feasibility of implementation. This is despite the fact, as

shown by the review of mHealth literature described in chapter 2, the top three most cited goals of mHealth, extended reach, improved resource efficiency and adherence and acceptance, relate to improvements within the clinician and patient workflows.

The work presented in this thesis has contributed to the narrowing of the aforementioned knowledge gap by navigating a development path involving design iterations based on proof-of-concept testing and workflow modelling and simulation based on pilot study data. The systematic review of the scientific literature relating to the clinical workflow of mHealth designs and implementations in LMICs returned very few results, none of which directly addressed the design of mHealth technologies. This reinforces the value of the work presented in this thesis, as it is one of a very small number of attempts to address the paucity of research in this field, which the review itself helps to highlight.

In the case of smartphone ophthalmoscopy, insufficient data was available in the literature to conduct reliable process modelling and simulation. For this reason, it was necessary to design and build the prototypes described in chapter 5 of this thesis. Lab-based and proof-of-concept testing on healthy participants allowed the iterative design of these prototypes so that they were appropriate for pilot testing within the clinical workflow of the target setting.

It was discovered in this process that a smartphone's quality with regards to general photography does not directly translate into its ability to capture fundus images with the appropriate attachment. As discussed in Chapter 5, it may therefore be beneficial to develop a 'universal adapter' that fits on a broad number of handsets as well as devising lab-based tests that are better predictors of fundus imaging performance compared to those designed for performance of general photography.

The results of both sets of simulations described in Chapters 6 and 9 suggest that the mHealth technologies that were analysed have the greatest potential for impact when placed in the hands of lower skilled cadres who are based closest to the patient population. This may partially explain why there has not yet been widespread adoption of smartphone ophthalmoscopy, as many designs rely on indirect ophthalmoscopy which requires a greater skill level than is typically possessed by either CEHWs or neonatal nurses (300). This also represents the least disruptive fit

for eye specialists in-so-much as the time required of staff at tertiary health centres to allocate to outreach activities is reduced and thus they are freed to concentrate on their specialist work at the tertiary care facility.

The models described in this thesis also suggest that amongst the most important factors for increasing effectiveness of eye care systems are health education, communication with patients and transportation of both the clinical staff and the patient to the next node of the pathway. The trialling of a number of interventions focusing on these areas within mHealth enabled eye programmes, such as those trialled by Morjaria and colleagues and Rono and colleagues as discussed in Chapter 6, have shown considerable promise but have also highlighted that these are difficult aspects requiring further research (308, 310).

A number of extensions to the model in the future would allow for deeper and more robust simulation of the LMIC community eye health clinical workflow. Inclusion of further mHealth enabled tests such as off-disc ophthalmoscopy, visual fields, smartphone-based autorefraction, tonometry anterior segment examination and test for other important co-morbidities such as DM would help to establish how the CEHW's eye examination kit could be further enhanced.

Furthermore, to understand the impact on health systems' workflow the models described in this thesis also provide a useful starting point understanding the implementation and ongoing costs, two other frequently cited barriers to adoption, of an mHealth enabled health programme. In particular, it would be interesting to understand the cost-benefit difference between programmes only offering treatment for those with visual impairment in both eyes, as is often the case in resource-constrained settings.

The results of the simulation of an Indian ROP screening programme gave particular insight with regards to the acceptable boundary on both types of cost. These represented clear insight into the engineering constraints that were incorporated into the design and prototype discussed in Chapter 10 of this thesis. Future work should seek to verify these engineering constraints through a clinical pilot study.

Whilst the stochastic timed CPNs used for these simulations were rather involved, it can be envisaged that simple estimations based on clinic data could likewise be used

to estimate cost-benefit metrics.

It is suggested that as many of the possible model extensions discussed in Chapters 5 and 9, as well as this chapter, be developed before progressing to clinical trialling of either of the mHealth technology discussed. Having made the models more closely aligned to the clinical reality, the simulation results and conclusions ought then to be validated against the trials' actually findings.

11.2 Limitations

As was initially posited, eye care did prove to be a suitable field for conducting the work describe in this thesis. The well-defined end-points for many of the eye disease discussed meant that the eye care workflow could be considered in relative isolation. For example, cataract surgery is treated by a single routine operation and refractive error is treated by prescribing a pair of spectacles.

However, other major causes of blindness, such as glaucoma require ongoing treatment and therefore do not have such a defined end-point. This means that the condition is not simply cured by referral to and one-off treatment by a specialist and halting progression of the disease is largely dependent on the patient's adherence to the treatment regime. The same is true of a DM or DR diagnosis during community screening. Such a diagnosis is only the beginning of lifelong management of DM and regular screening for DR. This is also of keen interest within global health, owing to it being the greatest cause of blindness in working age people. Its workflow also has interesting differences from other eye care workflows, as it involves close interactions with the other diabetic care pathways.

Similarly, whilst ROP is treated by a single round of laser photocoagulation and therefore has a defined endpoint, this falls within a complicated series of treatments that are required in very and extremely preterm births, some of which are in direct competition. Indeed, ROP itself arises from the need to provide preterm infants with more oxygen than they would naturally receive in utero. Future research should therefore consider the requirements of the other care pathways relevant to neonatal care and explore the interaction between these and that of ROP screening and treatment.

However, the clinical workflows selected do have limitations. Between them, these only considered lower cadre healthcare workers use of mHealth. Other powerful applications of mHealth include self-monitoring as well as use in treatment and rehabilitation. These involve use by patients and higher cadre healthcare professionals respectively. Future work could seek to use the techniques discussed in this thesis to ascertain their applicability to these different applications of mHealth.

The use of only those over 55 in the community eye health model is justifiable, given that approximately 80% of all eye disease occurs in this age group. Indeed it is typical for eye health surveys, and thus national eye care plans, to only consider this age group (301). It is important to recognise that this is a compromise between acquiring the best quality data possible and the time, financial and human resources required to conduct a full population eye study.

India represented a good basis for modelling a low-cost ROP screening solution, given that there are more births in India annually than in any other country. As noted above, exploring the requirements of other settings with high rates of ROP and comparing these to those extracted in the work presented in this thesis is therefore a logical next step.

A major limitation of both models is that they are each based on data from a single study. Applying the models to other similar scenarios in different LMICs would provide quantitative information concerning the generalisability of the conclusions drawn from the simulations' analysis. Examples could include any number of potential community eye programmes in SSA with respect to the community eye screening model. For ROP, other middle-income countries with less developed eye services than India but similarly high birth rates and rapidly improving maternal care, such as Nigeria or Indonesia, could be interesting candidates.

A further limitation of the work was that many of the modelled parameters, particularly timings were dependent on estimation or assumptions. Time and motion analysis would help to provide more objective, quantitative data regarding the workflow. Going into the finer details of conducting the relevant eye examinations may yield information that is pertinent to ergonomics and user interface design. For this finer level of detail, time and motion analysis would give the most accurate data.

However, this is a costly and time-consuming process and therefore process mining of application logs may be more appropriate where these exist, even if the data acquired is less reliable. Ideally, both would be acquired with the time and motion data giving robust insight into the full workflow and the software logs giving a breadth of information over longer periods of time and in larger variety of settings.

11.3 Conclusion

Given that, as a result of the clinical workflow modelling described in this thesis, a number of suggestions for enhancement of mHealth devices were identified, it is reasonable to conclude that clinical workflow modelling and simulation are useful tools for the design of mHealth devices. In particularly, their objective nature was beneficial in removing the effect of the mHealth designer's background and biases over the course of this work. This is particularly important given that designers are often based in high-income countries with the intention of developing a device for use in LMICs. Even when the designer is familiar with the target setting, whether through personal experience or by working closely with end-users and key opinion leaders, workflow modelling offers a means of removing biases and putting anecdotes to the test by forcing the quantification of estimates and assumptions and by considering these within the context of the full clinical workflow.

Of course, care must be taken for biases not to be incorporated into the design of the workflow model itself. In future work this risk could be mitigated by involving local health workers, programme managers and policy makers in the workflow model design process through techniques such as structured interviews and focus groups. To this end CPNs offer a useful framework owing to their visual nature (221).

That being said, and although workflow methods based on Petri nets are the industry standard, a thorough literature review of the modelling techniques available would perhaps give more insight into how more efficient, and thus more robust, models could be constructed.

Multi-chain Monte Carlo simulations (MCMCs), for example, would allow for optimisation of parameters. This could be used to identify reasonable boundaries for device variance, accuracy, examination time and cluster distance for example, as

well as sensitivity analyses. Nevertheless, such simulation techniques would still suffer from the state explosion problem as previously described. Thus, exploring how these techniques can be used to complement each other may be fertile ground for further research.

Moreover, when this programme was initiated, CPN Tools was an actively maintained application. However, whilst it is still listed as production software by its developer, no updates have been released since February 2015(cpntools.org). It therefore might be wise to conduct future workflow modelling using more actively developed software such as YAWL or BPM|One, although it should be noted that neither of these is open-source like CPN Tools.

Additionally, exploring alternative design and project management frameworks may also yield insight into how mHealth designs and design processes could be improved. Examples of such frameworks that could warrant investigation in this regard include Agile, Lean and Just-in-Time.

To conclude, it has become increasingly apparent that considering individual examination types in isolation is not sufficient for allowing mHealth technology to be designed and implemented in a way that empowers LMIC health systems. Indeed, the strategy of several mHealth companies has adapted from being simple manufacturers of mobile applications and device peripherals to providers of entire careflow solutions. If more mHealth developers do not adopt design and testing strategies that give due weight to clinical workflow analysis, such as those demonstrated in this thesis, it is likely that many more mHealth technologies will be developed to the proof-of-concept stage but not further.

Meanwhile, in their recent meta-analysis, The Vision Loss Expert Group estimated that in 2015 there were 36.0 million people who were blind (80% uncertainty interval (UI): 12.9-65.4 million) and 216.6 million with moderate-to-severe visual impairment (80% UI: 98.5-359.1 million) (17, 401). This represents an increase, in absolute terms, compared to the groups' 2010 estimate of people who were blind (32.4 million, 95% CI:29.4-36.5 million) and people who were moderately-to-severely visually impaired (191 million, 95% CI:174-230 million) (403). Moreover, it was also estimated that 1094.7 million people are estimated to have functional

presbyopia (80% UI: 581.1-1686.5) in 2015 (17, 402). Furthermore, the distribution of blindness and visual impairment continues to be disproportionally weighted toward LMICs (17, 402). Hence, it is as vital as ever to develop innovative means of tackling avoidable blindness and thus, it continues to be important not to squander the opportunity to improve health systems' reach, efficacy and cost-effectiveness, particularly in LMICs, using mHealth.

12 Proposals for Future Work

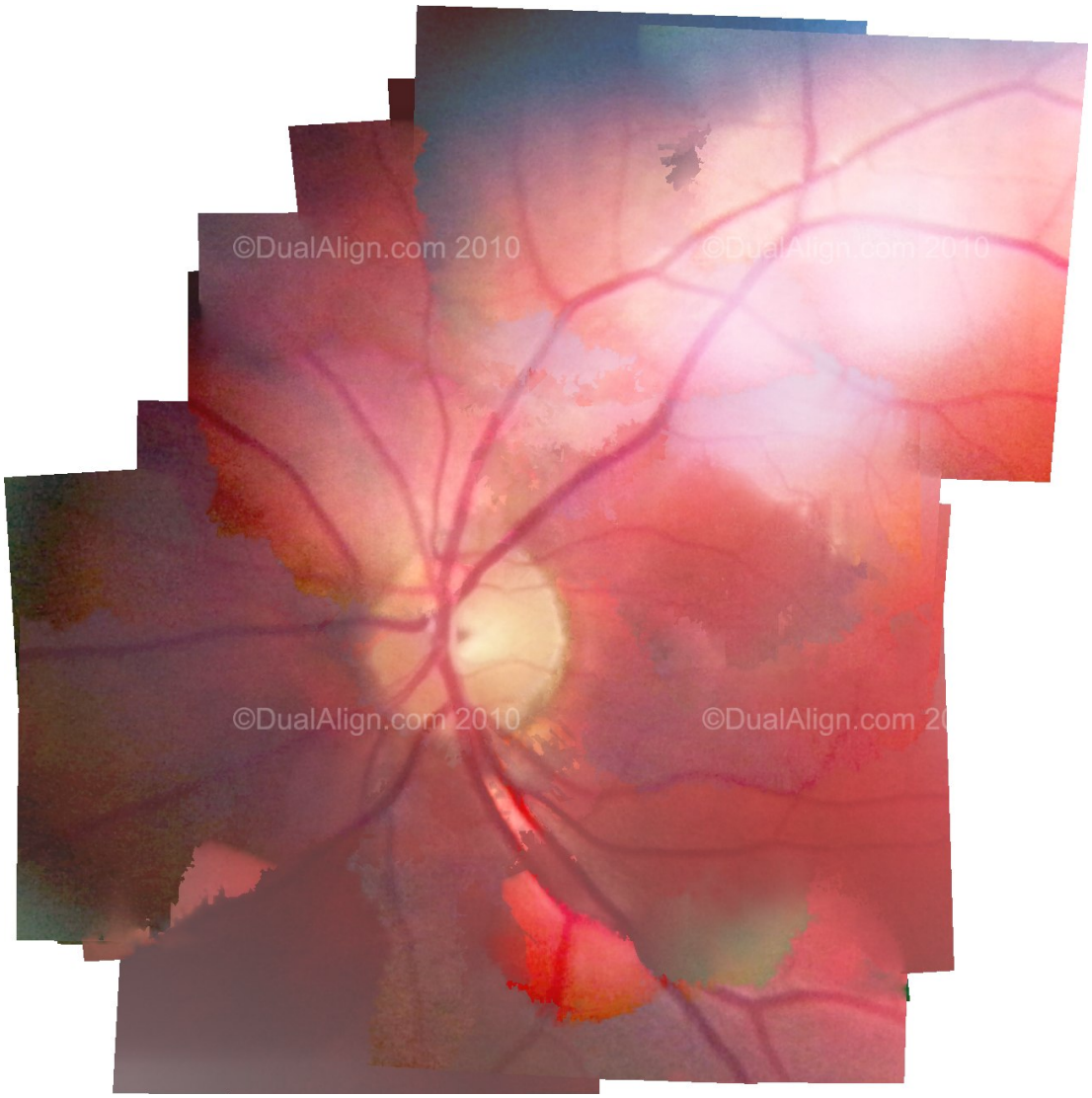

Figure 132 – A retinal mosaic produced from images acquired with one of the smartphone ophthalmoscope prototypes discussed in this thesis by i2k Retina (DualAlign LLC).

12.1 Smartphone Retinal Image Mosaicking

The retinal field-of-view that can be typically imaged by the smartphone ophthalmoscope prototypes discussed in this thesis, whilst larger than that of a standard direct ophthalmoscope, is far narrower than that acquired by a standard desktop retinal camera (typically 45°).

A technique that could increase the field of view visible in a single image is that of retinal mosaicking. This involves capturing multiple images of overlapping parts of the ocular fundus, identifying common features in the overlapping images and using these to align the images, creating a single image covering a larger area. Such software already exists for use with desktop retinal cameras that can be used to produce mosaics such as that shown in Figure 132. This involved manually removing non-retinal details captured in a set of images acquired using a smartphone ophthalmoscope prototype on a white male with dilated pupils.

It is clear from this image that directly using software designed for use with desktop fundus cameras with smartphone ophthalmoscopes is likely to introduce an unacceptable number of artefacts and result in the loss of clinically relevant information. Complications causing these issues include the variable distance and orientation of the smartphone's camera relative to the eye and the acquisition of non-retinal features such as the iris, sclera and face.

Viqueza and colleagues have demonstrated smartphone retinal mosaicking with more success with images acquired with a smartphone and Arclight direct ophthalmoscope (Arclight Medical, Liverpool, UK) (404). However, it is worth noting that the mosaics they report show a similar area of the retina to a single image acquired using one of the prototypes discussed in this thesis.

Further research is therefore required if single images approaching the field-of-view of a desktop retinal camera are to be attained. Furthermore, the development of real-time retinal mosaicking software would allow a smartphone ophthalmoscope operator to track which parts of the ocular fundus they have acquired images for, directly informing where to image next. This has great potential to improve drastically the competency of lower cadres when operating such smartphone ophthalmoscopes.

12.2 Diabetic Retinopathy Time and Motion Study

In the discussion of Chapter 6 it was noted that a number of major causes of blindness, such as DR, do not have the well-defined end-points that were assumed in this chapter. In particular, it was highlighted that a DM or DR diagnosis during community screening does not consist of a one-off treatment and thus represent an end-point in a patient's care pathway. Rather it represents the start of a life-long DM management and DR screening regime. Given the projected rise in prevalence of DM globally and the fact that DR is the main cause of blindness in working age people, it is important to better understand how DR screening programmes can be improved (167).

Owing to the importance of retinal photography in DR screening, as discussed in Chapter 2, and the lack of the equipment and expertise required to perform this in LMICs, there is substantial opportunity to improve access to DR screening for DM patients in LMICs by deploying a smartphone-based ophthalmoscope with the diabetic programmes of LMICs.

Analysis of the clinical workflow of a DR screening programme in a LMIC, similar to that reported for community eye health programme in Chapter 6, could therefore prove useful in improving understanding as to how smartphone ophthalmoscope adapters, similar to those reported in Chapter 5, might be adapted and implemented within the DR screening clinical workflow.

In the previous chapter, it was noted that a major limitation of the workflow analysis described in thesis was that many of the modelled parameters, particularly timings, were dependent on estimation or assumptions. Time and motion analysis is a business efficiency technique in which complex tasks are broken into smaller, simpler steps. The sequence of these steps is carefully observed in order to highlight redundant or wasteful motion and precise timings for each step recorded (405). Time and motion analysis could therefore help to provide more objective, quantitative data regarding the DR screening programme's clinical workflow. For example, going into the finer details of conducting the relevant eye examinations may yield information pertinent to the ergonomics and user interface design. Furthermore, conducting a time and motion study ought to help develop

understanding with regards to how appropriate analysis of mHealth application logs is for these contexts. Given the time and cost associated with time and motion studies is orders of magnitude greater than conducting data, process mining and other statistical analyses of application logs, understanding the boundaries of where the latter can provide useful and accurate information is of high importance.

No time and motion studies of diabetes clinics are known to the author. However, task categorisation based on previous studies of eHealth within the hospital setting, such as that by Overhage and colleagues, could represent a useful starting point (405). These could then be adapted for the DR screening clinical workflow by a combination of observation and interviews of key stakeholders. Following this, time and motion data could then be acquired before and after introduction of a smartphone-based ophthalmoscope into the clinical workflow. Typically, these two datasets would be acquired slightly before implementation and then a number of months after implementation, to negate learning effects (405). In addition, the development of a tablet computer-based application for recording the time and motion could represent an improvement on previous studies, which have tended to be paper-based.

12.3 ROP Camera Design for Manufacture

As was demonstrated by the clinical workflow modelling and lab-based testing described in Chapters 7 and 10 respectively, the portable retinal camera designed in the course of this research programme represents a promising solution for ROP screening in middle-income settings. The next stage in such a camera's development will be to create a design for manufacturing such a device at scale, and clinically validating such a device on real preterm infants versus the reference standard.

Such a design will need to tackle the limitations of this device as were noted in Chapters 10 and 11. These include accounting for infection control and avoidance of eye trauma. The design will also have to be such that mass manufacture is feasible and cost-effective.

Prototypes of this design then ought to be deployed to one or more NICUs and the grading of retinal images captured by a neonatal nurse using one of these prototypes

compared to those captured by a RetCam 3 (or equivalent) operated by a retinal photographer. The analysis of this data would then inform as to whether production and distribution of the camera at scale can by justified.

Indeed, the low-cost portable ROP camera technology developed in this thesis has recently been licensed to a third party with the purpose of achieving the above work and design for manufacture is expected to begin imminently.

12.4 Enhanced Clinical Workflow Modelling

In their 2015 review of the topic, Eckert and colleagues noted that integration of product models, such as mechanical, electronic and optical CAD, with process models, such as CPNs, is yet to achieve widespread adoption in industry (406). Yet they also advocated for its use, stating that with product and processes being modelled in separate tools leads to engineers having to make trade-offs between product design parameters and product development process efficiency "in their minds" (386). In contrast, integrating to the two model types makes the potential trade-offs explicitly and allows them to be discussed throughout an organisation (386). Similarly, in the development of medical devices the combination of product and process modelling into a single unified model could be hugely powerful, allowing for more robust simulations and the discovery of the optimal compromise where trade-offs between design parameters which are presently only discovered through modelling in either a CAD product model or clinical workflow model in insolation. For example, the variability of the preterm eye, as discovered in Chapter 7, is likely to impact upon the ease with which images of the full retina can be achieved which will in turn have consequences for the screening workflow. In future work it may therefore be interesting to consider how a Zemax OpticStudio extension might allow the Optical CAD to interface directly with the CPN describing the clinical workflow.

The models described in this thesis provide a basis for informing the configuration, monitoring and runtime analysis and adjustment stages of the life cycle. To this end, the life cycle model of an enterprise information system developed by Aalst and Stahl appears to represent a good high-level conceptualisation of the process of

designing, implementing and redesigning based on design analysis, and thus the technique deserves further investigation.

Future work should also look at combining the techniques discussed in this thesis with production implementations of mHealth systems. The results of both the community and ROP workflow simulations highlight that it is important that system logs capture data pertaining to the high-level screening flow, such as when a clinic begins and ends. Doing so will allow clinical leads and programme managers to better understand how long is spent performing clinical work versus non-clinical task such as travelling between patients or unpacking and packing equipment.

List of Publications

A number of articles relating to the work described in this thesis were published in peer-reviewed journals during the course of the PhD programme. References for these publications are cited below alongside a description of the author of this thesis's contribution to each.

Giardini, Mario E., et al. "A smartphone based ophthalmoscope." 2014 36th Annual International Conference of the IEEE Engineering in Medicine and Biology Society. IEEE, 2014.

> This article describes the original smartphone-based ophthalmoscope that was designed prior to the commencement of this research programme. The author assisted in reviewing and redrafting the manuscript.

Giardini, Mario E., et al. "Phone-based ophthalmoscopy for Peek, the Portable Eye Examination Kit." *Engineering in Medicine and Biology Society (EMBC), 2014 36th Annual International Conference of the IEEE*. 2014.

> This article describes the original smartphone-based ophthalmoscope that was designed prior to the commencement of this research programme. The author assisted in reviewing and redrafting the manuscript.

Bolster, Nigel M., et al. "How the smartphone is driving the eye-health imaging revolution." *Expert Review of Ophthalmology* 9.6 (2014): 475-485.

> The author conducted the literature review described in this article and drafted the original manuscript.

Bolster, Nigel M., Andrew Bastawrous, and Mario E. Giardini. "Towards a workflow driven design for mHealth devices within temporary eye clinics in low-income settings." *2015 37th Annual International Conference of the IEEE Engineering in Medicine and Biology Society (EMBC)*. IEEE, 2015.

> This article describes a preliminary clinical workflow model for a community eye-screening programme in a low-income country. It was a precursor to the work described in Chapter 6 of this thesis. The author built the models and ran the simulations described in the paper, drafted the manuscript and presented an oral presentation of the paper's contents at EMBC 2015.

Giardini ME, Bolster NM, Livingstone IAT inventors; London School of Hygiene & Tropical Medicine, University Of Strathclyde, Greater Glasgow And Clyde Health Board, assignees. Ophthalmoscope. World Intellectual Property Organisation application WO2016151288.

A patent application that sought to protect several of the innovations devised by the author, his supervisor and a collaborator during the work detailed in Chapter 5. The author and his supervisor equally shared 90% of the inventorship, reflecting their equal contribution to the invention of the intellectual property. The author also helped devise the claims detailed in the application.

Bolster, Nigel M., Mario E. Giardini, and Andrew Bastawrous. "The Diabetic Retinopathy Screening Workflow Potential for Smartphone Imaging." *Journal of diabetes science and technology* 10.2 (2016): 318-324.

The author conducted the literature review described in this article and drafted the original manuscript.

Bastawrous, Andrew, et al. "Clinical validation of a smartphone-based adapter for optic disc imaging in Kenya." *JAMA ophthalmology* 134.2 (2016): 151-158.

This article describes the clinical validation of the first and second iterations of the smartphone-based ophthalmoscope described in this thesis. The author designed the smartphone-based ophthalmoscopes used in this study as well as building the prototypes used.

Bolster NM, Giardini ME, Livingstone IAT, inventors; University of Strathclyde, assignee. Ophthalmoscope. World Intellectual Property Organisation application WO2017089817.

A patent application that sought to protect several of the innovations devised by the author, his supervisor and a collaborator during the work detailed in Chapters 9 and 10. The author and his supervisor shared the inventorship equally, reflecting their equal contribution to the invention of the intellectual property. The author also helped devise the claims detailed in the application.

Bolster NM, Bastawrous A. Examining the optic fundus and assessing visual acuity and visual fields using mobile technology. In: Atkinson A, Mabey D eds. Revolutionizing the delivery of health care in the developing world: rapid diagnostic tests, cheap imaging and other innovative technologies together with work force task-shifting at the primary point-of-care. Hoboke, NJ, USA: John Wiley & Sons, forthcoming.

The author conducted the literature review described in this article and drafted the original manuscript.

I certify that the above accurately represents previously published work included in this thesis for which I have been, in whole or in part, responsible for and clearly defines the extent of my contribution to this work.

Signed:

Date:

References

1. International Telecommunications Union. Key ICT indicators for developed and developing countries and the world (totals and penetration rates) [Data file]. International Telecommunications Union, ICT Statistics: Geneva, Switzerland; 2015. [cited 2016 Nov 16]. Available from: https://www.itu.int/en/ITU-D/Statistics/Documents/statistics/2014/ITU_Key_2005-2014_ICT_data.xls

2. The Nielsen Company. The Digital Consumer Report February 2014. New York (NY): The Nielsen Corporation; 2014.

3. Deglise C, Suggs LS, Odermatt P. SMS for disease control in developing countries: a systematic review of mobile health applications. Journal of Telemedicine and Telecare. 2012;18(5):273-81.

4. Iwaya LH, Gomes MAL, Simplicio MA, Carvalho T, Dominicini CK, Sakuragui RRM, et al. Mobile health in emerging countries: A survey of research initiatives in Brazil. International Journal of Medical Informatics. 2013;82(5):283-98.

5. Bloomfield GS, Vedanthan R, Vasudevan L, Kithei A, Were M, Velazquez EJ. Mobile health for non-communicable diseases in Sub-Saharan Africa: a systematic review of the literature and strategic framework for research. Globalization and health. 2014;10(1):1.

6. Aranda-Jan CB, Mohutsiwa-Dibe N, Loukanova S. Systematic review on what works, what does not work and why of implementation of mobile health (mHealth) projects in Africa. BMC Public Health. 2014;14(1):1-15.

7. Kallander K, Tibenderana JK, Akpogheneta OJ, Strachan DL, Hill Z, ten Asbroek AHA, et al. Mobile Health (mHealth) Approaches and Lessons for Increased Performance and Retention of Community Health Workers in Low- and Middle-Income Countries: A Review. Journal of Medical Internet Research. 2013;15(1).

8. Arie S. Can mobile phones transform healthcare in low and middle income countries? BMJ. 2015;350:h1975.

9. Kay M. mHealth: New horizons for health through mobile technologies: second global survey on eHealth. Geneva: WHO; 2011.

10. Agarwal S, LeFevre AE, Lee J, L'Engle K, Mehl G, Sinha C, et al. Guidelines for reporting of health interventions using mobile phones: mobile health (mHealth) evidence reporting and assessment (mERA) checklist. BMJ. 2016;352:i1174.

11. Tomlinson M, Rotheram-Borus MJ, Swartz L, Tsai AC. Scaling up mHealth: where is the evidence? PLoS medicine. 2013;10(2):e1001382.

12. Samhan B, Dadgar M, Joshi K. Mobile Health Information Technology and Patient Care: Methods, Themes, and Research Gaps. In: Lee H, Editor. Transactions of the international conference on health information technology advancement; 2013 Oct 17-18; Kalamazoo, MI, USA. Kalamazoo, MI, USA: Western Michigan University; 2013. p. 18-29.

13. Bastawrous MA, Hennig BD. The global inverse care law: a distorted map of blindness. The British journal of ophthalmology. 2012;96(10):1357-8.

14. Bastawrous A, Cheeseman RC, Kumar A. iPhones for eye surgeons. Eye. 2012;26(3):343-54.

15. Zurawski R, Zhou M. Petri nets and industrial applications: A tutorial. IEEE Transactions on industrial electronics. 1994;41(6):567-83.

16. Gehlot V, Matthew L, Sloane EB. From data to processes—Use of modeling and simulation in healthcare. In: Wong S, Wang, MD, Laine A, Editors. Proceedings of IEEE-EMBS International Conference on Biomedical and Health Informatics (BHI). 2016 Feb 16-19; Piscataway, NY, USA: IEEE; 2016.

17. Flaxman SR, Bourne RRA, Resnikoff S, Ackland P, Braithwaite T, Cicinelli MV, et al. Global causes of blindness and distance vision impairment 1990–2020: a systematic review and meta-analysis. The Lancet Global Health. 2017;5(12):e1221-e34.

18. Gilbert C. Retinopathy of prematurity: A global perspective of the epidemics, population of babies at risk and implications for control. Early Human Development. 2008;84(2):77-82.

19. DeGusta M. Are Smart Phones Spreading Faster than Any Technology in Human History? [Internet]. Cambridge, MA, USA: Massachusetts Institute of Technology; 2012 [cited 2018 Apr 18]. Available from: https://www.technologyreview.com/s/427787/are-smart-phones-spreading-faster-than-any-technology-in-human-history/

20. Voltornist, A. Mobile broadband reach expanding globally [Internet]. London, UK: GSM Intelligence; 2014 [cited 2018 Apr 18]. Available from: https://www.gsmaintelligence.com/research/2014/12/mobile-broadband-reach-expanding-globally/453/

21. Hughes N, Lonie S. M-PESA: mobile money for the “unbanked” turning cellphones into 24-hour tellers in Kenya. Innovations. 2007;2(1-2):63-81.

22. Hwang J-h, Yoe H, editors. Design and implementation of ubiquitous pig farm management system using iOS based smart phone. In: Kim T-h, Adeli H, Slezak D, Sandnes FE, Song X, Chung K-i, Arnett KP Editors. International Conference on Future Generation Information Technology. 2011 Dec 8-10; Berlin, Germany: Springer; 2011.

23. Pew Research Center. Device Ownership Over Time [Internet]. Washington, DC, USA: Pew Research Centre; 2015 [cited 2016 Sep 16]. Available from: http://www.pewinternet.org/data-trend/mobile/device-ownership/.

24. International Telecommunications Union. Global ICT Developments [Data file]. International Telecommunications Union, ICT Statistics: Geneva, Switzerland; 2016. [cited 16 Nov 2016]. Available from: https://www.itu.int/en/ITU-D/Statistics/Documents/statistics/2016/Stat_page_all_charts_2016.xls

25. GSM Intelligence. The Mobile Economy 2018. London, UK: GSM Intelligence; 2018 [cited 2018 Apr 18].

26. Palma MJ. Worldwide Tablet Semiconductor 2015-2019 Forecast. Framingham, MA, USA: International Data Corporation; 2015 May. 24 p. Report No.: 256259

27. McNair C, Chung J, Johnson M, Liu C. Worldwide Internet and Mobile Users. New York, NY, USA: eMarketer; 2017 Dec.

28. emarketer. Tablet Users to Surpass 1 Billion Worldwide in 2015 2015 [Available from: http://www.emarketer.com/Article/Tablet-Users-Surpass-1-Billion-Worldwide-2015/1011806.

29. Aker JC, Mbiti IM. Mobile phones and economic development in Africa. Journal of Economic Perspectives. 2010;24(3):207-32.

30. James J. Leapfrogging in mobile telephony: A measure for comparing country performance. Technological Forecasting and Social Change. 2009;76(7):991-8.

31. Statista. Number of apps available in leading app stores as of June 2016 [Internet]. Hamburg, Germany: Statista; 2016 [cited 2016 Nov 11] Available from: https://www.statista.com/statistics/276623/number-of-apps-available-in-leading-app-stores/

32. Mas I, Morawczynski O. Designing mobile money services lessons from M-PESA. Innovations. 2009;4(2):77-91.

33. Jacob F. The Role of M-Pesa in Kenya's Economic and Political Development. In: Koster MM, Kithinji MM, Rotich JP, editors. Kenya After 50: Reconfiguring Education, Gender, and Policy. New York: Palgrave Macmillan US; 2016. p. 89-100.

34. Istepanian RS, Jovanov E, Zhang Y. Introduction to the special section on m-health: Beyond seamless mobility and global wireless health-care connectivity. IEEE Transactions on information technology in biomedicine. 2004;8(4):405-14.

35. Qiang CZ, Yamamichi M, Hausman V, Altman D. Mobile applications for the health sector. Washington, DC: World Bank ICT Sector Unit. 2012 Apr. Report No.: 72604

36. Khazan O. In health technology, an enthusiasm gap between startups and doctors. The Washington Post [Internet]. 2011 Dec 6 [cited 2016 Nov 16]: On Small Business. Available from: https://www.washingtonpost.com/business/on-small-business/in-health-technology-an-enthusiasm-gap-between-startups-and-doctors/2011/12/06/gIQANFzXaO_story.html

37. Gagnon MP, Ngangue P, Payne-Gagnon J, Desmartis M. m-Health adoption by healthcare professionals: a systematic review. Journal of the American Medical Informatics Association. 2016;23(1):212-20.

38. Liberati A, Altman DG, Tetzlaff J, Mulrow C, Gøtzsche PC, Ioannidis JPA, et al. The PRISMA statement for reporting systematic reviews and meta-analyses of studies that evaluate healthcare interventions: explanation and elaboration. BMJ. 2009;339.

39. Subhi Y, Bube SH, Bojsen SR, Thomsen ASS, Konge L. Expert Involvement and Adherence to Medical Evidence in Medical Mobile Phone Apps: A Systematic Review. JMIR mHealth and uHealth. 2015;3(3).
40. Majeed-Ariss R, Baildam E, Campbell M, Chieng A, Fallon D, Hall A, et al. Apps and Adolescents: A Systematic Review of Adolescents' Use of Mobile Phone and Tablet Apps That Support Personal Management of Their Chronic or Long-Term Physical Conditions. Journal of Medical Internet Research. 2015;17(12).
41. de Jongh T, Gurol-Urganci I, Vodopivec-Jamsek V, Car J, Atun R. Mobile phone messaging for facilitating self-management of long-term illnesses. Cochrane Database of Systematic Reviews. 2012(12).
42. Gurol-Urganci I, de Jongh T, Vodopivec-Jamsek V, Car J, Atun R. Mobile phone messaging for communicating results of medical investigations. Cochrane Database of Systematic Reviews. 2012(6).
43. Kharrazi H, Chisholm R, VanNasdale D, Thompson B. Mobile personal health records: An evaluation of features and functionality. International Journal of Medical Informatics. 2012;81(9):579-93.
44. Ozdalga E, Ozdalga A, Ahuja N. The Smartphone in Medicine: A Review of Current and Potential Use Among Physicians and Students. Journal of Medical Internet Research. 2012;14(5).
45. Bastawrous A, Armstrong MJ. Mobile health use in low- and high-income countries: an overview of the peer-reviewed literature. Journal of the Royal Society of Medicine. 2013;106(4):130-42.
46. Bender JL, Yue RYK, To MJ, Deacken L, Jadad AR. A Lot of Action, But Not in the Right Direction: Systematic Review and Content Analysis of Smartphone Applications for the Prevention, Detection, and Management of Cancer. Journal of Medical Internet Research. 2013;15(12).
47. Fiordelli M, Diviani N, Schulz PJ. Mapping mHealth Research: A Decade of Evolution. Journal of Medical Internet Research. 2013;15(5).

48. Free C, Phillips G, Watson L, Galli L, Felix L, Edwards P, et al. The Effectiveness of Mobile-Health Technologies to Improve Health Care Service Delivery Processes: A Systematic Review and Meta-Analysis. PLOS Medicine. 2013;10(1).

49. Gurol-Urganci I, de Jongh T, Vodopivec-Jamsek V, Atun R, Car J. Mobile phone messaging reminders for attendance at healthcare appointments. Cochrane Database of Systematic Reviews. 2013(12).

50. Martinez-Perez B, de la Torre-Diez I, Lopez-Coronado M. Mobile Health Applications for the Most Prevalent Conditions by the World Health Organization: Review and Analysis. Journal of Medical Internet Research. 2013;15(6).

51. de la Torre-Diez I, Lopez-Coronado M, Vaca C, Aguado JS, de Castro C. Cost-Utility and Cost-Effectiveness Studies of Telemedicine, Electronic, and Mobile Health Systems in the Literature: A Systematic Review. Telemedicine and e-Health. 2015;21(2):81-5.

52. Mourcou Q, Fleury A, Diot B, Franco C, Vuillerme N. Mobile Phone-Based Joint Angle Measurement for Functional Assessment and Rehabilitation of Proprioception. BioMed Research International [Internet]. 2015 [cited 2016 Nov 12]. Available from: https://www.hindawi.com/journals/bmri/2015/328142/cta/. DOI: 10.1155/2015/328142

53. Anglada-Martinez H, Riu-Viladoms G, Martin-Conde M, Rovira-Illamola M, Sotoca-Momblona JM, Codina-Jane C. Does mHealth increase adherence to medication? Results of a systematic review. International Journal of Clinical Practice. 2015;69(1):9-32.

54. Ali EE, Chew L, Yap KY-L. Evolution and current status of mhealth research: a systematic review. BMJ Innovations. 2016:bmjinnov-2015-000096.

55. Al Dandah M, Du Lou AD, Meadel C. Mobile health and maternal care: A winning combination for healthcare in the developing world? Health Policy and Technology. 2015;4(3):225-31.

56. Steinhubl SR, Muse ED, Topol EJ. The emerging field of mobile health. Science Translational Medicine. 2015;7(283):283rv3.

57. Dehzad F, Hilhorst C, de Bie C, Claassen E. Adopting Health Apps, What's Hindering Doctors and Patients? Health. 2014;6:2204.
58. Baumgart DC. Smartphones in Clinical Practice, Medical Education, and Research. Archives of Internal Medicine. 2011;171(14):1294-6.
59. Swendeman D. Are mobile phones the key to HIV prevention for mobile populations in India? Indian Journal of Medical Research. 2013;137:1024-6.
60. Oreskovic NM, Huang TT, Moon J. Integrating mHealth and Systems Science: A Combination Approach to Prevent and Treat Chronic Health Conditions. JMIR mHealth and uHealth. 2015;3(2).
61. Schoenfeld AJ, Sehgal NJ, Auerbach A. The Challenges of Mobile Health Regulation. JAMA Internal Medicine. 2016;176(5):704-5.
62. Eysenbach G, Grp C-E. CONSORT-EHEALTH: Improving and Standardizing Evaluation Reports of Web-based and Mobile Health Interventions. Journal of Medical Internet Research. 2011;13(4).
63. Barton AJ. The regulation of mobile health applications. BMC Medicine. 2012;10.
64. Visser BJ, Buijink AWG. Need to peer-review medical applications for smart phones. Journal of Telemedicine and Telecare. 2012;18(2):124.
65. Editors TPM. A Reality Checkpoint for Mobile Health: Three Challenges to Overcome. PLOS Medicine. 2013;10(2).
66. Hawkes GA, Hawkes CP, Ryan CA, Dempsey EM. The demand for an educational smartphone app. Resuscitation. 2013;84(10):E139.
67. Kassamali RH, Ladak B. Smartphones make smarter students. Medical Teacher. 2013;35(5):425.
68. Labrique A, Vasudevan L, Chang LW, Mehl G. H_pe for mHealth: More "y" or "o" on the horizon? International Journal of Medical Informatics. 2013;82(5):467-9.
69. Richardson JE, Reid MC. The Promises and Pitfalls of Leveraging Mobile Health Technology for Pain Care. Pain Medicine. 2013;14(11):1621-6.
70. Steinhubl SR, Muse ED, Topol EJ. Can Mobile Health Technologies Transform Health Care? JAMA. 2013;310(22):2395-6.

71. Wang CJ, Huang DJ. The HIPAA Conundrum in the Era of Mobile Health and Communications. JAMA. 2013;310(11):1121-2.
72. Chan SR, Misra S. Certification of Mobile Apps for Health Care. JAMA. 2014;312(11):1155-6.
73. Powell AC, Landman AB, Bates D. Certification of Mobile Apps for Health Care Reply. JAMA. 2014;312(11):1156-7.
74. Charani E, Castro-Sanchez E, Moore LSP, Holmes A. Do smartphone applications in healthcare require a governance and legal framework? It depends on the application! BMC Medicine. 2014;12.
75. Ellaway R. The informal and hidden curricula of mobile device use in medical education. Medical Teacher. 2014;36(1):89-91.
76. Huckvale K, Car J. Implementation of Mobile Health Tools. Jama-Journal of the American Medical Association. 2014;311(14):1447-8.
77. Freeman WD. Implementation of Mobile Health Tools. JAMA. 2014;311(14):1448.
78. Steinhubl SR, Muse ED, Topol EJ. Implementation of Mobile Health Tools Reply. Jama-Journal of the American Medical Association. 2014;311(14):1448-9.
79. Gaglani SM, Topol EJ. iMedEd: The Role of Mobile Health Technologies in Medical Education. Academic Medicine. 2014;89(9):1207-9.
80. Kahol K. Mobile phone messaging to improve health. BMJ. 2014;349.
81. Merrell RC, Doarn CR. m-Health. Telemedicine and e-Health. 2014;20(2):99-101.
82. Ranney ML, Suffoletto B. Extending Our Reach: Use of mHealth to Support Patients After Emergency Care. Annals of Emergency Medicine. 2014;63(6):755-6.
83. Weinstein RS, Lopez AM, Joseph BA, Erps KA, Holcomb M, Barker GP, et al. Telemedicine, Telehealth, and Mobile Health Applications That Work: Opportunities and Barriers. American Journal of Medicine. 2014;127(3):183-7.
84. Angarita FA, Strickland M, Acuna SA. Incorporating smartphones into clinical practice. Annals of Medicine and Surgery. 2015;4(2):187-8.

85. Shaw RJ, Bonnet JP, Modarai F, George A, Shahsahebi M. Mobile Health Technology for Personalized Primary Care Medicine. American Journal of Medicine. 2015;128(6):555-7.

86. Khanna RR, Wachter RM, Blum M. Reimagining Electronic Clinical Communication in the Post-Pager, Smartphone Era. JAMA. 2016;315(1):21-2.

87. World Health Organization. The MAPS Toolkit: mHealth Assessment and Planning for Scale. Geneva: World Health Organization; 2015.

88. PriceWaterhouseCoopers. Emerging mHealth: paths for growth. New York, NY, USA: PriceWaterhouseCoopers; 2014.

89. Smith BM, Patty;. Sustainable Financing for mHealth. Palo Alto, CA, USA: Vital Wave Consulting; 2013.

90. Keisling K. Introduction to mHealth: How to Approach mHealth. Cape Town, South Africa: mHelp; 2014.

91. K4Health. The mHealth Planning Guide: Key Considerations for Integrating Mobile Technology into Health Programs [Internet]. Baltimore, MD, USA: K4Health; 2014 [updated 2014 August 26; cited 2016 Nov 16]. Available from: https://www.k4health.org/toolkits/mhealth-planning-guide.

92. Philippot A. Learn How to Budget for your Mobile Project. Boston, MA, USA: Dimagi; 2016. [cited 2016 Nov 16]. Available from: http://www.dimagi.com/blog/learn-budget-mobile-project/.

93. Sachs JD. From millennium development goals to sustainable development goals. The Lancet. 2012;379(9832):2206-11.

94. Bastawrous A, Rono HK, Livingstone IT, Weiss HA, Jordan S, Kuper H, et al. Development and validation of a smartphone-based visual acuity test (peek acuity) for clinical practice and community-based fieldwork. JAMA Ophthalmology 2015;133(8):930-7.

95. Bastawrous A, Giardini ME, Bolster NM, Peto T, Shah N, Livingstone I, et al. Clinical Validation of a Smartphone-Based Adapter for Optic Disc Imaging in Kenya. JAMA Ophthalmology 2015;134(2):151-8.

96. Manyika J, Chui M, Bughin J, Dobbs R, Bisson P, Marrs A. Disruptive technologies: Advances that will transform life, business, and the global economy: San Francisco, CA, USA: McKinsey Global Institute; 2013.

97. Barbour V, Clark J, Connell L, Ross A, Simpson P, Veitch E, et al. A Reality Checkpoint for Mobile Health: Three Challenges to Overcome. PLOS Medicine. 2013;10(2).

98. International Telecommunications Union. World Telecommunication/ICT Indicators Database. 20th edition. Geneva, Switzerland: Internation Telecommunications Union; 2016.

99. Falagas ME, Pitsouni EI, Malietzis GA, Pappas G. Comparison of PubMed, Scopus, web of science, and Google scholar: strengths and weaknesses. The FASEB journal. 2008 Feb;22(2):338-42.

100. Thylefors B, Negrel A, Pararajasegaram R, Dadzie K. Global data on blindness. Bulletin of the World Health Organization. 1995;73(1):115.

101. Pascolini D, Mariotti SP. Global estimates of visual impairment: 2010. British Journal of Ophthalmology. 2011;96(5): 614-18.

102. Resnikoff S, Pascolini D, Etya'ale D, Kocur I, Pararajasegaram R, Pokharel GP, et al. Global data on visual impairment in the year 2002. Bulletin of the world Health Organization. 2004;82(11):844-51.

103. Ackland P. The accomplishments of the global initiative VISION 2020: The Right to Sight and the focus for the next 8 years of the campaign. Indian Journal of Ophthalmology. 2012;60(5):380.

104. World Health Organization. Universal Eye Health: A Global Action Plan. Geneva, Switzerland: World Health Organization;2013.

105. Grimes CE, Bowman KG, Dodgion CM, Lavy CB. Systematic review of barriers to surgical care in low-income and middle-income countries. World Journal of Surgery. 2011;35(5):941-50.

106. Kaiser PK. Prospective Evaluation of Visual Acuity Assessment: A Comparison of Snellen Versus ETDRS Charts in Clinical Practice (An AOS Thesis). Transactions of the American Ophthalmological Society. 2009;107:311-24.

107. Taylor HR. Applying new design principles to the construction of an illiterate E chart. American Journal of Optometry and Physiological Optics. 1978;55(5):348-51.

108. Ferris FL, Kassoff A, Bresnick GH, Bailey I. New visual acuity charts for clinical research. American Journal of Ophthalmology. 1982;94(1):91-6.

109. World Health Organisation. Visual impairment including blindness (binocular or monocular). International Statistical Classification of Disease Related Health Problems 10th Revision (ICD-10). Geneva, Switzerland: World Health Organisation; 2016. Report No.: H54

110. Holden BA, Fricke TR, Wilson DA, Jong M, Naidoo KS, Sankaridurg P, et al. Global Prevalence of Myopia and High Myopia and Temporal Trends from 2000 through 2050. Ophthalmology. 2016;123(5):1036-42.

111. Blanco FG, Fernandez JCS, Sanz MAM. Axial length, corneal radius, and age of myopia onset. Optometry and vision science. 2008;85(2):89-96.

112. Wong TY, Ferreira A, Hughes R, Carter G, Mitchell P. Epidemiology and Disease Burden of Pathologic Myopia and Myopic Choroidal Neovascularization: An Evidence-Based Systematic Review. American Journal of Ophthalmology. 2014;157(1):9-25.e12.

113. Read SA, Collins MJ, Carney LG. A review of astigmatism and its possible genesis. Clinical and Experimental Optometry. 2007;90(1):5-19.

114. Rabinowitz YS. Keratoconus. Survey of ophthalmology. 1998;42(4):297-319.

115. Romín DM, Taboada JJE, Montés P, del Águila Carrasco AJ, Albert NM. Global prevalence of hyperopia. Journal of Emmetropia: Journal of Cataract, Refractive and Corneal Surgery. 2015;6(2):109-16.

116. Williams W, Latif A, Hannington L, Watkins D. Hyperopia and educational attainment in a primary school cohort. Archives of disease in childhood. 2005;90(2):150-3.

117. Moore B, Lyons SA, Walline J. A clinical review of hyperopia in young children. The Hyperopic Infants' Study Group, THIS Group. Journal of the American Optometric Association. 1999;70(4):215-24.

118. Leat SJ. Paediatric Assessment. In: Edwards KH, editor. Optometry: science, techniques and clinical management. London, UK: Elsevier Health Sciences; 2009.
119. Rosenfield M. Subjective Refraction. In: Edwards KH, editor. Optometry: science, techniques and clinical management. London, UK: Elsevier Health Sciences; 2009.
120. Thylefors B, Chylack Jr LT, Konyama K, Sasaki K, Sperduto R, Taylor HR, et al. A simplified cataract grading system The WHO Cataract Grading Group. Ophthalmic Epidemiology. 2002;9(2):83-95.
121. Jaafar MS, Robb RM. Congenital Anterior Polar Cataract: A Review of 63 Cases. Ophthalmology. 1984;91(3):249-54.
122. Chibuga E, Massae P, Geneau R, Mahande M, Lewallen S, Courtright P. Acceptance of cataract surgery in a cohort of Tanzanians with operable cataract. Eye. 2008;22(6):830.
123. Brusini P, Johnson CA. Staging functional damage in glaucoma: review of different classification methods. Survey of Ophthalmology. 2007;52(2):156-79.
124. King A, Migdal C. Clinical management of glaucoma. J R Soc Med. 2000;93(4):175-7.
125. Weinreb RN, Aung T, Medeiros FA. The pathophysiology and treatment of glaucoma: a review. JAMA. 2014;311(18):1901-11.
126. Spiegel D, Kobuch K. Trabecular meshwork bypass tube shunt: initial case series. British Journal of Ophthalmology. 2002;86(11):1228-31.
127. Haleem MS, Han L, Van Hemert J, Li B. Automatic extraction of retinal features from colour retinal images for glaucoma diagnosis: a review. Computerized medical imaging and graphics. 2013 Dec 31;37(7):581-96.
128. Bourne RR. The optic nerve head in glaucoma. Community eye health. 2006 Sep;19(59):44.
129. Kuehn MH, Fingert JH, Kwon YH. Retinal ganglion cell death in glaucoma: mechanisms and neuroprotective strategies. Ophthalmology Clinics. 2005;18(3):383-95.

130. National Institute for Health and Care Excellence. Glaucoma: diagnosis and management. London, UK: National Institute for Health and Care Excellence; 2017.
131. Leske M, Heijl A, Hussein M, et al. Factors for glaucoma progression and the effect of treatment: The early manifest glaucoma trial. Archives of Ophthalmology. 2003;121(1):48-56.
132. Wolffsohn JS, Cochrane AL. Low vision perspectives on glaucoma. Clinical and Experimental Optometry. 1998;81(6):280-9.
133. Huang D, Swanson EA, Lin CP, Schuman JS, Stinson WG, Chang W, et al. Optical Coherence Tomography. Science. 1991;254(5035):1178-81.
134. Kavitha S, Karthikeyan S, Duraiswamy K. Early detection of glaucoma in retinal images using cup to disc ratio. In: 2010 Second International conference on Computing, Communication and Networking Technologies; Karur, India. 2010 July 29-31; Piscataway, NY, USA: IEEE; 2010.
135. Beck RW, Bergstrom TJ, Lighter PR. A clinical comparison of visual field testing with a new automated perimeter, the Humphrey Field Analyzer, and the Goldmann perimeter. Ophthalmology. 1985;92(1):77-82.
136. Leasher JL, Bourne RR, Flaxman SR, Jonas JB, Keeffe J, Naidoo K, et al. Global estimates on the number of people blind or visually impaired by diabetic retinopathy: a meta-analysis from 1990 to 2010. Diabetes care. 2016;39(9):1643-9.
137. Ogurtsova K, da Rocha Fernandes JD, Huang Y, Linnenkamp U, Guariguata L, Cho N, et al. IDF Diabetes Atlas: Global estimates for the prevalence of diabetes for 2015 and 2040. Diabetes research and clinical practice. 2017;128:40-50.
138. Wilkinson C, Ferris FL, Klein RE, Lee PP, Agardh CD, Davis M, et al. Proposed international clinical diabetic retinopathy and diabetic macular edema disease severity scales. Ophthalmology. 2003;110(9):1677-82.
139. Hu FB. Globalization of Diabetes. The role of diet, lifestyle, and genes. Diabetes Care. 2011;34(6):1249-57.
140. Toussaint D, Cogan DG, Kuwabara T. Extravascular lesions of diabetic retinopathy. Archives of Ophthalmology. 1962;67(1):42-7.

141. Chew EY, Klein ML, Ferris FL, Remaley NA, Murphy RP, Chantry K, et al. Association of elevated serum lipid levels with retinal hard exudate in diabetic retinopathy: Early Treatment Diabetic Retinopathy Study (ETDRS) Report 22. Archives of Ophthalmology. 1996;114(9):1079-84.
142. Caldwell RB, Bartoli M, Behzadian MA, El-Remessy AE, Al-Shabrawey M, Platt DH, et al. Vascular endothelial growth factor and diabetic retinopathy: pathophysiological mechanisms and treatment perspectives. Diabetes/Metabolism Research and Reviews. 2003;19(6):442-55.
143. Fong DS, Aiello L, Gardner TW, King GL, Blankenship G, Cavallerano JD, et al. Retinopathy in diabetes. Diabetes Care. 2004;27(suppl 1):s84-s7.
144. Finkelstein D. Ischemic macular edema recognition and favorable natural history in branch vein occlusion. Archives of Ophthalmology. 1992;110(10):1427-34.
145. Peto T, Tadros C. Screening for diabetic retinopathy and diabetic macular edema in the United Kingdom. Current Diabetes Reports. 2012;12(4):338-45.
146. A Chandran; K K Nisha; S Vineetha, Computer aided approach for proliferative diabetic retinopathy detection in color retinal images, 2016 International Conference on Next Generation Intelligent Systems (ICNGIS), Sept. 2016.
147. El-Bab MF, Shawky N, Al-Sisi A, Akhtar M. Retinopathy and risk factors in diabetic patients from Al-Madinah Al-Munawarah in the Kingdom of Saudi Arabia. Clinical Ophthalmology (Auckland, NZ). 2012;6:269.
148. Hee MR, Puliafito CA, Duker JS, Reichel E, Coker JG, Wilkins JR, et al. Topography of Diabetic Macular Edema with Optical Coherence Tomography. Ophthalmology. 1998;105(2):360-70.
149. Control D, Group CTR. The relationship of glycemic exposure (HbA1c) to the risk of development and progression of retinopathy in the diabetes control and complications trial. Diabetes. 1995;44(8):968-83.
150. Nicholson BP, Schachat AP. A review of clinical trials of anti-VEGF agents for diabetic retinopathy. Graefe's Archive for Clinical and Experimental Ophthalmology. 2010;248(7):915-30.

151. Patz A, Fine S, Finkelstein D, Prout T, Aiello L, Bradley R, et al. Photocoagulation Treatment of Proliferative Diabetic Retinopathy: The Second Report of Diabetic Retinopathy Study Findings. Ophthalmology. 1978;85(1):82-106.
152. Blencowe H, Lawn JE, Vazquez T, Fielder A, Gilbert C. Preterm-associated visual impairment and estimates of retinopathy of prematurity at regional and global levels for 2010. Pediatr Res. 2013;74(S1):35-49.
153. Chow LC, Wright KW, Sola A. Can changes in clinical practice decrease the incidence of severe retinopathy of prematurity in very low birth weight infants? Pediatrics. 2003;111(2):339-45.
154. Pierce EA, Foley ED, Smith LE. Regulation of vascular endothelial growth factor by oxygen in a model of retinopathy of prematurity. Archives of ophthalmology. 1996;114(10):1219-28.
155. Sato T, Kusaka S, Shimojo H, Fujikado T. Vitreous levels of erythropoietin and vascular endothelial growth factor in eyes with retinopathy of prematurity. Ophthalmology. 2009;116(9):1599-603.
156. Hellström A, Ley D, Hallberg B, Löfqvist C, Hansen-Pupp I, Ramenghi LA, et al. IGF-1 as a Drug for Preterm Infants: A Step-Wise Clinical Development. Current Pharmaceutical Design. 2017;23(38):5964-70.
157. Hunter DG, Repka MX. Diode Laser Photocoagulation for Threshold Retinopathy of Prematurity. Ophthalmology. 1993;100(2):238-44.
158. Hellström A, Smith LE, Dammann O. Retinopathy of prematurity. Lancet. 1991 Jan 12;337(8733):83.
159. Royal College of Ophthalmology, Royal College of Paediatrics and Child Health, British Association of Perinatal Medicine, BLISS. Guideline for the Screening and Treatment of Retinopathy of Prematurity. London, UK: Royal College of Paediatrics and Child Health; 2008.
160. Solarte CE, Awad AH, Wilson CM, Ells A. Plus disease: Why is it important in retinopathy of prematurity?. Middle East African journal of ophthalmology. 2010 Apr;17(2):148.

161. Shah SP, Wu Z, Iverson S, Dai S. Specialist nurse screening for retinopathy of prematurity—a pilot study. The Asia-Pacific Journal of Ophthalmology. 2013;2(5):300-4.
162. Weaver DT, Murdock TJ. Telemedicine detection of type 1 ROP in a distant neonatal intensive care unit. Journal of American Association for Pediatric Ophthalmology and Strabismus. 2012;16(3):229-33.
163. Resnikoff S, Felch W, Gauthier T-M, Spivey B. The number of ophthalmologists in practice and training worldwide: a growing gap despite more than 200 000 practitioners. British Journal of Ophthalmology. 2012;96(6):783-7.
164. World Council of Optometry. Join the Celebration: 2017 Marks WCO's 90th Anniversary. World Focus. St. Louis, MO, USA: World Council of Optometry; 2017.
165. Palmer JJ, Chinanayi F, Gilbert A, Pillay D, Fox S, Jaggernath J, et al. Mapping human resources for eye health in 21 countries of sub-Saharan Africa: current progress towards VISION 2020. Human resources for health. 2014;12(1):44.
166. Cohen JE. Human population: the next half century. Science. 2003;302(5648):1172-5.
167. Whiting DR, Guariguata L, Weil C, Shaw J. IDF Diabetes Atlas: Global estimates of the prevalence of diabetes for 2011 and 2030. Diabetes Research and Clinical Practice. 2011;94(3):311-21.
168. Serrano-Pedraza I, Vancleef K, Read JC. Avoiding monocular artifacts in clinical stereotests presented on column-interleaved digital stereoscopic displays. Journal of Vision. 2016;16(14):13.
169. Sheedy JE, Bailey IL, Raasch TW. Visual acuity and chart luminance. Optometry and Vision Science. 1984;61(9):595-600.
170. Johnson CA, Casson EJ. Effects of luminance, contrast, and blur on visual acuity. Optometry & Vision Science. 1995;72(12):864-9.
171. Livingstone IAT, Tarbert CM, Giardini ME, Bastawrous A, Middleton D, Hamilton R. Photometric Compliance of Tablet Screens and Retro-Illuminated Acuity Charts As Visual Acuity Measurement Devices. PLoS ONE. 2016;11(3):e0150676.

172. Bristish Standards. BS 4274-1:2003 - Visual Acuity Test Types–Part 1: Test charts for clinical determination of distance visual acuity - Specification. 2003 [cited 2017 July 03].
173. Aslam TM, Murray IJ, Lai MY, Linton E, Tahir HJ, Parry NR. An assessment of a modern touch-screen tablet computer with reference to core physical characteristics necessary for clinical vision testing. Journal of The Royal Society Interface. 2013;10(84):20130239.
174. Brady CJ, Eghrari AO, Labrique AB. Smartphone-based visual acuity measurement for screening and clinical assessment. JAMA. 2015;314(24):2682-3.
175. Perera C, Chakrabarti R, Islam FMA, Crowston J. The Eye Phone Study: reliability and accuracy of assessing Snellen visual acuity using smartphone technology. Eye. 2015;29(7):888-94.
176. Tofigh S, Shortridge E, Elkeeb A, Godley BF. Effectiveness of a smartphone application for testing near visual acuity. Eye. 2015;29(11):1464-8.
177. Gounder PA, Cole E, Colley S, Hille DM. Validation of a portable electronic visual acuity system. Journal of Mobile Technology in Medicine. 2014;3(2):35-9.
178. Mahtani K, Spencer EA, Brassey J, Heneghan C. Catalogue of bias: observer bias. BMJ Evidence-Based Medicine. 2018 Feb 1;23(1):23-4.
179. Bastawrous A, Mathenge W, Peto T, Weiss HA, Rono H, Foster A, et al. The Nakuru eye disease cohort study: methodology & rationale. BMC ophthalmology. 2014;14(1):60.
180. Gupta R, Lam W-C. Medical students' self-confidence in performing direct ophthalmoscopy in clinical training. Canadian Journal of Ophthalmology/Journal Canadien d'Ophtalmologie. 2006;41(2):169-74.
181. Gerloff O. Über die Photographie des Augenhintergrundes. Zeitschrift für Psychologie und Physiologie der Sinnesorgane. 1891;29:397-403.
182. Langford M. Basic photography. Routledge; 2013 Mar 5.
183. Armed Forces Supply Support Centre. MIL-STD-150A - Military Standard Photograph Lenses. 1959 [cited 2017 July 03].

184. British Standards. BS EN ISO 10940:2009 - Ophthalmic Instruments: Fundus Cameras. British Standards; 2009 [cited 2017 July 03].

185. Fleming AD, Goatman KA, Philip S, Prescott GJ, Sharp PF, Olson JA. Automated grading for diabetic retinopathy: a large-scale audit using arbitration by clinical experts. British Journal of Ophthalmology. 2010;94(12):1060-10.

186. Gulshan V, Peng L, Coram M, Stumpe MC, Wu D, Narayanaswamy A, et al. Development and validation of a deep learning algorithm for detection of diabetic retinopathy in retinal fundus photographs. JAMA. 2016;316(22):2402-10.

187. Chan JB, Ho HC, Ngah NF, Hussein E. DIY-Smartphone Slit-Lamp adaptor. Journal of Mobile Technology in Medicine. 2014;3(1):16-22.

188. Blackenberg M, Worst C, Scheffer C. Development of a Mobile Phone Based Ophthalmoscope for Telemedicine. In: Lovell N, editor, 33rd Annual International Conference of the IEEE EMBS: 2011 Aug 30 - Sept 03; Boston, MA, USA; Piscataway, NY, USA: IEEE; 2011.

189. Coleman WT, inventor; Intuitive Medical Technology LLC, assignee. Smart-phone adapter for Opthalmoscope. United States patent US20120320340. 2012 Dec 20.

190. Welch Allyn. iExaminer - Eye Imaging on your Phone; 2016 [cited 2017 July 03]. Available from: https://www.welchallyn.com/content/welchallyn/americas/en/microsites/iexaminer.html.

191. Bastawrous A. Smartphone Fundoscopy. Ophthalmology. 2012.

192. Haddock LJ, Kim DY, Mukai S. Simple, inexpensive technique for high-quality smartphone fundus photography in human and animal eyes. Journal of Ophthalmology. 2013;2013:518479.

193. Lin S-J, Yang C-M, Yeh P-T, Ho T-C. Smartphone fundoscopy for retinopathy of prematurity. Taiwan Journal of Ophthalmology. 2014;4(2):82-5.

194. Myung D, Jais A, He L, Blumenkranz MS, Chang RT. 3D Printed Smartphone Indirect Lens Adapter for Rapid, High Quality Retinal Imaging. Journal of Mobile Technology in Medicine. 2014;3(1):9-15.

195. Russo A, Morescalchi F, Costagliola C, Delcassi L, Semeraro F. Comparison of smartphone ophthalmoscopy with slit-lamp biomicroscopy for grading diabetic retinopathy. American journal of ophthalmology. 2015;159(2):360-4. e1.

196. Maamari RN, Keenan JD, Fletcher DA, Margolis TP. A mobile phone-based retinal camera for portable wide field imaging. Br J Ophthalmol. 2014;98(4):438-41.

197. Timberlake GTT, Kennedy M. The Direct Ophthalmoscope: How it Works and How to Use It. Lawrence, KS, USA: University of Kansas; 2005.

198. Russo A, Civili PS. A Novel Device to Exploit the Smartphone Camera for Fundus Photography. Journal of Ophthalmology:823139; 2015.

199. Jordan S, Giardini ME, Livingstone IA, Bastawrous A, inventors; Greater Glasgow And Clyde Health Board University of Strathclyde London School of Hygiene and Tropical Medicine, assignees. Ophthalmoscope. United States patent application US20180042475. 2018 Feb 15.

200. Tahir HJ, Murray IJ, Parry NRA, Aslam TM. Optimisation and Assessment of Three Modern Touch Screen Tablet Computers for Clinical Vision Testing. PLoS ONE. 2014;9(4):e95074.

201. Vingrys AJ, Healey JK, Liew S, Saharinen V, Tran M, Wu W, et al. Validation of a Tablet as a Tangent Perimeter. Translational Vision Science & Technology. 2016;5(4):3-.

202. Johnson C, Thapa S, Robin A, editors. Visual field screening to detect glaucoma and diabetic retinopathy in Nepal using an iPad application program. . American Academy of Optometry; 2014.

203. Kong YXG, He M, Crowston JG, Vingrys AJ. A Comparison of Perimetric Results from a Tablet Perimeter and Humphrey Field Analyzer in Glaucoma Patients. Translational Vision Science & Technology. 2016;5(6):2-.

204. King-Smith PE, Grigsby SS, Vingrys AJ, Benes SC, Supowit A. Efficient and unbiased modifications of the QUEST threshold method: theory, simulations, experimental evaluation and practical implementation. Vision Research. 1994;34(7):885-912.

205. Sloan L. Area and luminance of test object as variables in examination of the visual field by projection perimetry. Vision Research. 1961;1(1):121-IN2.
206. Smith N, Bi W, Crabb D. Novel perimetry using eye tracking on a tablet computer–a feasibility study. Investigative Ophthalmology & Visual Science. 2016;57(12).
207. Mártonyi CL. Slit Lamp Imaging. Review of Ophthalmology. 2008.
208. Noble J, Somal K, Gill HS, Lam W-C. An analysis of undergraduate ophthalmology training in Canada. Canadian Journal of Ophthalmology / Journal Canadien d'Ophtalmologie. 2009;44(5):513-8.
209. Myung D, Jais A, He L, Chang RT. Simple, Low-Cost Smartphone Adapter for Rapid, High Quality Ocular Anterior Segment Imaging: A Photo Diary. Journal of Mobile Technology in Medicine. 2014;3(1):2-8.
210. Dragnev D, Mahmood U, Williams C, Kulshrestha M. Teleophthalmology: Eye Care in the Community In: Madhavan R, editor. Telemedicine. London, UK: IntechOpen Ltd. 2013.
211. Niazkhani Z, Pirnejad H, Berg M, Aarts J. The impact of computerized provider order entry systems on inpatient clinical workflow: a literature review. Journal of the American medical informatics Association. 2009 Jul 1;16(4):539-49.
212. Georgakopoulos D, Hornick M, Sheth A. An overview of workflow management: From process modeling to workflow automation infrastructure. Distributed and parallel Databases. 1995 Apr 1;3(2):119-53.
213. Georgakopoulos D, Hornick M, Sheth A. An overview of workflow management: From process modeling to workflow automation infrastructure. Distributed and parallel Databases. 1995 Apr 1;3(2):119-53.
214. The World Bank. World Bank Country and Lending Groups [Data file]. London, UK: The World Bank;2017.
215. Chaiyachati KH, Loveday M, Lorenz S, Lesh N, Larkan L-M, Cinti S, et al. A pilot study of an mHealth application for healthcare workers: poor uptake despite high reported acceptability at a rural South African community-based MDR-TB treatment program. PLoS One. 2013;8(5):e64662.

216. Raghu A, Praveen D, Peiris D, Tarassenko L, Clifford G. Engineering a mobile health tool for resource-poor settings to assess and manage cardiovascular disease risk: SMARThealth study. BMC medical informatics and decision making. 2015;15(1):36.

217. Beck K, Beedle M, Van Bennekum A, Cockburn A, Cunningham W, Fowler M, et al. Manifesto for agile software development [Internet]. 2001 [cited: 2017 Dec 03]. Available form: http://agilemanifesto.org/.

218. Likert R. A technique for the measurement of attitudes. Archives of Psychology. 1932.

219. Ali SM, Powers R, Beorse J, Noor A, Naureen F, Anjum N, et al. ODK Scan: Digitizing Data Collection and Impacting Data Management Processes in Pakistan's Tuberculosis Control Program. Future Internet. 2016;8(4):51.

220. Alter S. The work system method for understanding information systems and information systems research. Communications of the Association for Information Systems. 2002;9(1):6.

221. van der Aalst WM, Stahl C. Modeling business processes: a petri net-oriented approach. Cambridge, MA, USA: MIT press; 2011.

222. Van Der Aalst WM, Ter Hofstede AH. YAWL: yet another workflow language. Information Systems. 2005;30(4):245-75.

223. Van Der Aalst W, Van Hee KM. Workflow management: models, methods, and systems. Cambridge, MA, USA: MIT press; 2004.

224. van der Aalst WM, Reijers HA, Weijters AJ, van Dongen BF, De Medeiros AA, Song M, et al. Business process mining: An industrial application. Information Systems. 2007;32(5):713-32.

225. Fowler M. Patterns of enterprise application architecture. Boston, MA, USA: Addison-Wesley Longman Publishing Co., Inc.; 2002.

226. Blessing LT, Chakrabarti A. DRM, a design research methodology. Berlin, Germany: Springer Science & Business Media; 2009.

227. Aono K. Application note: Pcb design with eagle. East Lansing, MI, USA: Michigan State University. 2011.

228. Earle JH, Olsen D. Engineering Design Graphics: AutoCAD Release 14: Boston, MA, USA: Addison-Wesley Longman Publishing Co., Inc.; 1998.
229. Murata T. Product Design Review: A Methodology for Error-Free Product Development. Portland, OR, USA: Productivity Press; 1996.
230. Sibbald B, Roland M. Understanding controlled trials: Why are randomised controlled trials important? BMJ. 1998;316(7126):201.
231. Everitt BS. Medical statistics from A to Z: a guide for clinicians and medical students: Cambridge, UK: Cambridge University Press; 2006.
232. Thabane L, Ma J, Chu R, Cheng J, Ismaila A, Rios LP, et al. A tutorial on pilot studies: the what, why and how. BMC Medical Research Methodology. 2010;10(1):1.
233. Chow S-C, Chang M. Adaptive design methods in clinical trials–a review. Orphanet Journal of Rare Diseases. 2008;3(1):11.
234. Misra J. Distributed discrete-event simulation. ACM Computing Surveys (CSUR). 1986;18(1):39-65.
235. Laubenbacher R, Pareigis B. Equivalence relations on finite dynamical systems. Advances in Applied Mathematics. 2001;26(3):237-51.
236. Rumbaugh J, Jacobson I, Booch G. Unified modeling language reference manual, the: Pearson Higher Education; 2004.
237. Valmari A. The state explosion problem. Lectures on Petri nets I: Basic models. 1998:429-528.
238. Sonnenberg FA, Beck JR. Markov models in medical decision making a practical guide. Medical Decision Making. 1993;13(4):322-38.
239. British Standards. BS EN 62551:2012 – Analysis techniques for dependability — Petri net techniques. 2012 [cited: 2017 Dec 02].
240. Petersen JV. Absolute beginner's guide to databases: London, UK: Que Publishing; 2002.
241. Murata T. Petri nets: Properties, analysis and applications. Proceedings of the IEEE. 1989;77(4):541-80.

242. Dijkman R, Hofstetter J, Koehler J. Business Process Model and Notation. Berlin, Germany: Springer; 2011.
243. Scheer A-W, Thomas O, Adam O. Process modeling using event-driven process chains. Process-aware Information Systems. 2005:119-46.
244. Petri C. Kommunikation mit Automaten (Schriften des Rheinisch-Westfälischen Institutes für Instrumentelle Mathematik an der Universität Bonn, H. 2). Westfäl Inst f Instrumentelle Mathematik an der Univ Bonn. 1962.
245. Singh M, Theobald M. Generalized latency-insensitive systems for gals architectures. Proceedings FMGALS. 2003.
246. van der Aalst WMP. The Application Of Petri Nets To Workflow Management. Journal of Circuits, Systems and Computers. 1998;08(01):21-66.
247. Jensen K. Coloured petri nets. Petri nets: central models and their properties. Berlin, Germany: Springer; 1987. p. 248-99.
248. Ullman JD. Elements of ML Programming: ML97 Edition. Upper Saddle River, NJ, USA: Prentice Hall; 1998.
249. Westergaard M, Slaats T. CPN Tools 4: a process modeling tool combining declarative and imperative paradigms. Automatic Control and Computer Sciences. 2013;47(7):393-402.
250. Jansen-Vullers M, Reijers H, editors. Business process redesign at a mental healthcare institute: A coloured Petri net approach. In: Jensen K, editor. Proceedings of the Sixth Workshop and Tutorial on Practical Use of Coloured Petri Nets and the CPN Tools; 2005 Oct 24-26; Aarhus, Denmark; Aarhus, Denmark: University of Aarhus; 2005. p. 21-38.
251. Kuhr J-C, Pretzel J, Vagts DA, Aldred L, editors. Integrating humans, devices, and events in clinical workflow processes. International Conference on Business Process Management; 2008 Sep 1. Berlin, Germany: Springer; 2008. p. 408-15.
252. Jørgensen JB, Lassen KB, van der Aalst WM. From task descriptions via colored Petri nets towards an implementation of a new electronic patient record workflow system. International Journal on Software Tools for Technology Transfer (STTT). 2008;10(1):15-28.

253. Chatziralli IP, Kanonidou ED, Keryttopoulos P, Dimitriadis P, Papazisis LE. The value of fundoscopy in general practice. The Open Ophthalmology Journal. 2012;6:4.

254. Welch E. No fundoscopy, no defence. MPS Casebook. 2014;22(2).

255. Tarr JM, Kaul K, Wolanska K, Kohner EM, Chibber R. Retinopathy in diabetes. Diabetes: Springer; 2013. p. 88-106.

256. Lim SS, Vos T, Flaxman AD, Danaei G, Shibuya K, Adair-Rohani H, et al. A comparative risk assessment of burden of disease and injury attributable to 67 risk factors and risk factor clusters in 21 regions, 1990–2010: a systematic analysis for the Global Burden of Disease Study 2010. Lancet. 2012;2224-60.

257. Kwon YH, Fingert JH, Kuehn MH, Alward WLM. Primary Open-Angle Glaucoma. New England Journal of Medicine. 2009;360(11):1113-24.

258. Hovland KR. Vitreous Findings in Fellow Eyes of Aphakic Retinal Detachment. American Journal of Ophthalmology.86(3):350-3.

259. Siam A. Macular hole with central retinal detachment in high myopia with posterior staphyloma. The British Journal of Ophthalmology. 1969;53(1):62-3.

260. Benbassat J, Polak BCP, Javitt JC. Objectives of teaching direct ophthalmoscopy to medical students. Acta Ophthalmologica. 2012;90(6):503-7.

261. Giardini ME, Livingstone IA, Jordan S, Bolster NM, Peto T, Burton M, et al., editors. A smartphone based ophthalmoscope. In: Proceedings of The 36th Annual International Conference of the IEEE Engineering in Medicine and Biology Society. 2014 Aug 26-30; Boston, MA, USA; Piscataway, NY, USA: IEEE; 2014.

262. Giardini ME, Livingstone I, Bolster NM, Jordan S, Bastawrous A. Phone-Based Ophthalmoscopy for Peek, the Portable Eye Examination Kit. In: Proceedings of The 36th Annual International Conference of the IEEE Engineering in Medicine and Biology Society. 2014 Aug 26-30; Boston, MA, USA; Piscataway, NY, USA: IEEE; 2014.

263. Cordero I. Understanding and caring for the direct ophthalmoscope. Community eye health. 2016;29(93):17.

264. Smith S, Smith S. Reduced pupillary light reflexes in diabetic autonomic neuropathy. Diabetologia. 1983;24(5):330-2.

265. Steinmann WC, Millstein ME, Sinclair SH. Pupillary dilation with tropicamide 1% for funduscopic screening: a study of duration of action. Annals of Internal Medicine. 1987;107(2):181-4.

266. Gross H, Blechinger F, Achtner B. Human eye. Handbook of Optical Systems. 2008:1-87.

267. Ezra E, Keinan E, Mandel Y, Boulton ME, Nahmias Y. Non-dimensional analysis of retinal microaneurysms: critical threshold for treatment. Integrative Biology : Quantitative Biosciences from Nano to Macro. 2013;5(3):474-80.

268. Lee KE, Klein BEK, Klein R, Meuer SM. Association of Retinal Vessel Caliber to Optic Disc and Cup Diameters. Investigative Ophthalmology & Visual Science. 2007;48(1):63-7.

269. National Optical Astronomy Observatory. Recommended Light Levels. URL: https://www.noao.edu/education/QLTkit/ACTIVITY_Documents/Safety/LightLevels_outdoor+indoor.pdf.

270. International Standards Organisation, ISO 15004-2.2: Ophthalmic Instruments: Light Hazard protection. 2007.

271. Müller V. Elimination of specular surface-reflectance using polarized and unpolarized light. In: European Conference on Computer Vision 1996 Apr 14 (pp. 625-635). Springer, Berlin, Heidelberg.

272. Wolff LB, Boult TE. Constraining object features using a polarization reflectance model. IEEE Transactions on Pattern Analysis & Machine Intelligence. 1991 Jul 1(7):635-57.

273. Hecht E. Optics. Reading, MA, USA: Addison-Wesley, 2002.

274. Samsung Electronics Company Ltd. Flash LED. Datasheet: p22-23. URL:http://s1.dtsheet.com/store/data/001538187.pdf?key=629a92c144258250411be370cbf39895&r=1

275. Ashdown I, Eng P. Photometry and radiometry–a tour guide for computer graphics enthusiasts. In: Radiosity: A Programmer's Perspective. Haboke, NJ, USA: John Wiley & Sons; 1996.

276. Tocci M. Zemax OpticStudio Models of the Human Eye. Kirkland, WA, USA: Zemax LLC; 2007.
277. European Commission. 2017/745 - Medical Devices Regulation. 2017.
278. Wu J, Seregard S, Algvere PV. Photochemical damage of the retina. Survey of ophthalmology. 2006 Sep 1;51(5):461-81.
279. Miller S, James R, Landry R, Pfefer J. Optical characterization of cutaneous transilluminators for eye safety. Biomedical optics express. 2010 Oct 1;1(3):771-9.
280. Wanell BA. Contributed Numbers. URL: https://web.stanford.edu/group/vista/cgi-bin/wandell/contributed-numbers/
281. Goatman K, Philip S, Fleming A, Harvey R, Swa K, Styles C, et al. External quality assurance for image grading in the Scottish Diabetic Retinopathy Screening Programme. Diabetic Medicine. 2012;29(6):776-83.
282. Kingbright. 2mm Flat Top White LED Relative Intensity vs. Wavelength. L-13PWC-Z spectral data. 2009.
283. Edmund Opticcs Worldwide. High Contrast Linear Polarizing Film datasheet. 2015.
284. Bernardes R, Serranho P, Lobo C. Digital ocular fundus imaging: a review. Ophthalmologica Journal international d'ophtalmologie International journal of ophthalmology Zeitschrift fur Augenheilkunde. 2011;226(4):161-81.
285. Kim DY, Delori F, Mukai S. Smartphone photography safety. Ophthalmology. 2012;119(10):2200-1; author reply 1.
286. Bastawrous A, Mathenge W, Buchan J, Kyari F, Peto T, Rono H, et al. Glaucoma Features in an East African Population: A Six-year Cohort Study of Older Adults in Nakuru, Kenya. Journal of Glaucoma. 2018.
287. Bastawrous A, Mathenge W, Wing K, Bastawrous M, Rono H, Weiss HA, et al. The incidence of diabetes mellitus and diabetic retinopathy in a population-based cohort study of people age 50 years and over in Nakuru, Kenya. BMC endocrine disorders. 2017;17(1):19.

288. Bastawrous A, Mathenge W, Peto T, Shah N, Wing K, Rono H, et al. Six-Year Incidence and Progression of Age-Related Macular Degeneration in Kenya: Nakuru Eye Disease Cohort Study. JAMA Ophthalmol. 2017;135(6):631-8.

289. Bastawrous A, Mathenge W, Wing K, Rono H, Gichangi M, Weiss HA, et al. Six-Year Incidence of Blindness and Visual Impairment in Kenya: The Nakuru Eye Disease Cohort Study. Investigative ophthalmology & visual science. 2016;57(14):5974-83.

290. Mathenge W, Bastawrous A, Foster A, Kuper H. The Nakuru Posterior Segment Eye Disease Study. Ophthalmology. 2012;119(10):2033-9.

291. Sterne JA, White IR, Carlin JB, Spratt M, Royston P, Kenward MG, et al. Multiple imputation for missing data in epidemiological and clinical research: potential and pitfalls. BMJ. 2009;338:b2393.

292. Raghunathan TE, Lepkowski JM, Van Hoewyk J, Solenberger P. A multivariate technique for multiply imputing missing values using a sequence of regression models. Survey methodology. 2001 Jun;27(1):85-96.

293. Su YS, Gelman A, Hill J, Yajima M. Multiple imputation with diagnostics (mi) in R: Opening windows into the black box. Journal of Statistical Software. 2011 Dec 12;45(2):1-31.

294. Gentle JE. Computational statistics. Berlin, Germany: Springer Science & Business Media; 2009.

295. Johnson NL. Systems of Frequency Curves Generated by Methods of Translation. Biometrika. 1949;36(1/2):149-76.

296. Sakia R. The Box-Cox transformation technique: a review. The statistician. 1992:169-78.

297. Chakravarty IM, Roy J, Laha RG. Handbook of methods of applied statistics. Adbingdon-on-Thames, UK: Taylor and Francis; 1967.

298. Solomon AW, Kurylo E. The Global Trachoma Mapping Project. Community Eye Health. 2014;27(85):18-.

299. Noma M, Zouré HG, Tekle AH, Enyong PA, Nwoke BE, Remme JH. The geographic distribution of onchocerciasis in the 20 participating countries of the African Programme for Onchocerciasis Control:(1) priority areas for ivermectin treatment. Parasites & Vectors. 2014;7(1):325.

300. Gilbert C, Minto H, Morjaria P. Standard guidelines for comprehensive school eye health programs. London, UK: Sightsavers International, London School of Hygiene and Tropical Medicine, Brien Holden Vision Institute; 2017.

301. Ghanchi F, Bailey C, Chakravarthy U, Cohen S, Dodson P, Gibson J, et al. The Royal College of Ophthalmologists' clinical guidelines for diabetic retinopathy: a summary. Eye. 2013;27(2):285.

302. Amerasinghe N. Open Angle Glaucoma. BMJ Best Practice. 2016 [reviewed 2018 Mar; cited 2018 Apr 21]. Available from: http://bestpractice.bmj.com/topics/en-gb/373.

303. Baudais EB, K, Canty T, Custer A, Dassen R, Jody G, Guelzow A, et al. The Gnumeric Manual: GNOME Documentation Project; 2010 [cited 2017 Dec 06]. Available from: http://www.hep.by/gnu/gnumeric/gnumeric.shtml.

304. Welch BL. The significance of the difference between two means when the population variances are unequal. Biometrika. 1938 Feb 1;29(3/4):350-62.

305. Morjaria P, Bastawrous A, Murthy GVS, Evans J, Gilbert C. Effectiveness of a novel mobile health education intervention (Peek) on spectacle wear among children in India: study protocol for a randomized controlled trial. Trials. 2017;18(1):168.

306. Sudarsanam S, Mathew J, Panigrahi S, Fade J, Alouini M, Ramachandran H. Real-time imaging through strongly scattering media: seeing through turbid media, instantly. Scientific reports. 2016;6:25033.

307. Mtuya C, Cleland CR, Philippin H, Paulo K, Njau B, Makupa WU, et al. Reasons for poor follow-up of diabetic retinopathy patients after screening in Tanzania: a cross-sectional study. BMC ophthalmology. 2016;16(1):115.

308. Morjaria P. Spectacle Wear Among Children in a School-Based Program in India. PhD Thesis, London, UK: London School of Hygiene and Tropical Medicine; 2018.

309. Free C, Phillips G, Watson L, Galli L, Felix L, Edwards P, et al. The effectiveness of mobile-health technologies to improve health care service delivery processes: a systematic review and meta-analysis. PLoS medicine. 2013;10.

310. Rono HK, Bastawrous A, Wanjala E, DiTanna G, Macleod D, Weiss AH, et al. Smartphone-based visual impaitment screening in Kenyan school children: a cluster randomised trial. Lancet Global Health. 2018;6(8):e924-32.

311. Pannell DJ. Sensitivity analysis: strategies, methods, concepts, examples. Agric Econ. 1997;16:139-52.

312. Hamby DM. A comparison of sensitivity analysis techniques. Health physics. 1995;68(2):195-204.

313. Clemson B, Tang Y, Pyne J, Unal R. Efficient methods for sensitivity analysis. System Dynamics Review. 1995;11(1):31-49.

314. Ludwig CA, Murthy SI, Pappuru RR, Jais A, Myung DJ, Chang RT. A novel smartphone ophthalmic imaging adapter: User feasibility studies in Hyderabad, India. Indian Journal of Ophthalmology. 2016;64(3):191.

315. Kuper H, Polack S, Limburg H. Rapid assessment of avoidable blindness. Community Eye Health. 2006;19(60):68.

316. Bastawrous A, Leak C, Howard F, Kumar V. Validation of Near Eye Tool for Refractive Assessment (NETRA) – Pilot Study. Journal of Mobile Technology in Medicine. 2012;1(3):6-16.

317. Zheng K, Guo MH, Hanauer DA. Using the time and motion method to study clinical work processes and workflow: methodological inconsistencies and a call for standardized research. Journal of the American Medical Informatics Association : JAMIA. 2011;18(5):704-10.

318. Gilbert C. Changing challenges in the control of blindness in children. Eye. 2007;21(10):1338-43.

319. Vinekar A, Gilbert C, Dogra M, Kurian M, Shainesh G, Shetty B, et al. The KIDROP model of combining strategies for providing retinopathy of prematurity screening in underserved areas in India using wide-field imaging, tele-medicine, non-physician graders and smart phone reporting. Indian Journal of Ophthalmology. 2014;62(1):41.

320. KPMB Internation Cooperative. Logistics in India Part 1. Amstelveen, Netherlands: KPMB Internation Cooperative; 2010.

321. Bureau of Transportation Statistics. Freight Facts and Figures. Washington, DC, USA: United States Department of Transportation; 2010.

322. U.S. Drivers Not The Speed Demons You May Think [press release]. Concord, MA, USA: TomTom2010.

323. Moral-Pumarega MT, Caserío-Carbonero S, De-La-Cruz-Bértolo J, Tejada-Palacios P, Lora-Pablos D, Pallás-Alonso CR. Pain and stress assessment after retinopathy of prematurity screening examination: indirect ophthalmoscopy versus digital retinal imaging. BMC pediatrics. 2012;12(1):132.

324. Snyder CS, editor A Guide to the Project Management Body of Knowledge: PMBOK Guide. Philadelphia, PA, USA: Project Management Institute; 2014.

325. Cape J. Consultation length, patient-estimated consultation length, and satisfaction with the consultation. Br J Gen Pract. 2002;52(485):1004-6.

326. Palmer EA, Flynn JT, Hardy RJ, Phelps DL, Phillips CL, Schaffer DB, et al. Incidence and Early Course of Retlnonathy of Prematurity. Ophthalmology. 1991;98(11):1628-40.

327. Carden SM, Luu LN, Nguyen TX, Huynh T, Good WV. Retinopathy of prematurity: postmenstrual age at threshold in a transitional economy is similar to that in developed countries. Clinical & Experimental Ophthalmology. 2008;36(2):159-61.

328. Blencowe H, Moxon S, Gilbert C. Update on blindness due to retinopathy of prematurity globally and in India. Indian Pediatr. 2016;53(suppl 2):S89-S92.

329. The Royal Children's Hospital Melbourne. Treatment of ROP. Available from: https://www.rch.org.au/ophthal/patient_information/Treatment_of_ROP/ [cited 2017 May 06].
330. PayScale. Human Capital. 2017 [cited 2017 Dec 06]. Available from: https://www.payscale.com/.
331. Maruti Insurance. Fuel Cost Calculator. 2018 [cited 2017 Dec 06]. Available from: www.marutiinsurance.com/Fuel-Cost-Calculator.aspx.
332. Martinez C. Price for RetCan 3 & RetCam Shuttle 2017 [cited 2017 Dec 06]. Available from: https://www.freelists.org/post/optimal/Price-for-RetCam-3-RetCam-Shuttle,5.
333. Hoffman F, Gardner R. Evaluation of uncertainties in environmental radiological assessment models. Radiological assessments: a textbook on environmental dose assessment. Oak Ridge, TN, USA: Health and Saftey Research Division. 1983:11-1.
334. Birch EE, O'Connor AR. Preterm birth and visual development. Seminars in Neonatology. 2001;6(6):487-97.
335. Kaschke M, Donnerhacke K-H, Rill MS. Optical devices in ophthalmology and optometry: technology, design principles and clinical applications. New York, NY, USA: John Wiley & Sons; 2013.
336. O'Connor AR, Wilson CM, Fielder AR. Ophthalmological problems associated with preterm birth. Eye. 2007;21(10):1254-60.
337. Higgins JP, Altman DG, Gøtzsche PC, Jüni P, Moher D, Oxman AD, et al. The Cochrane Collaboration's tool for assessing risk of bias in randomised trials. BMJ. 2011;343:d5928.
338. Viechtbauer W. Conducting meta-analyses in R with the metafor package. Journal of statistical software. 2010 Aug 1;36(3).
339. Morrell CH. Likelihood ratio testing of variance components in the linear mixed-effects model using restricted maximum likelihood. Biometrics. 1998 Dec 1:1560-8.

340. Rosenberg MS, Garrett KA, Su Z, Bowden RL. Meta-analysis in plant pathology: synthesizing research results. Phytopathology. 2004 Sep;94(9):1013-7.
341. Ioannidis JP, Patsopoulos NA, Evangelou E. Uncertainty in heterogeneity estimates in meta-analyses. Bmj. 2007 Nov 1;335(7626):914-6.
342. Navarro R, Palos F, González L. Adaptive model of the gradient index of the human lens. I. Formulation and model of aging ex vivo lenses. J Opt Soc Am A. 2007;24(8):2175-85.
343. Brown N. The change in lens curvature with age. Experimental eye research. 1974 Aug 1;19(2):175-83.
344. Navarro R, Palos F, González LM. Adaptive model of the gradient index of the human lens. II. Optics of the accommodating aging lens. JOSA A. 2007 Sep 1;24(9):2911-20
345. Lotmar W. A theoretical model for the eye of new-born infants. Albrecht von Graefes Archiv für klinische und experimentelle Ophthalmologie. 1976;198(2):179-85.
346. Atchison DA. Objective Refraction. Rosenfield M, Logan N, Edwards KH, editors: Elsevier Health Sciences; 2009.
347. Radiant Zemax LLC. Zemax Optic Design Program User's Manual. Kirkland WA, USA: Radiant Zemax LLC; 2007.
348. Malacara-Hernández D, Malacara-Hernández Z. Handbook of optical design. CRC Press; 2016 Apr 19.
349. Gupta T, Kapoor K, Singh B, Huria A. Fetal orbital and ocular biometry at different gestational ages. Journal of the Anatomical Society of India. 2013;62(2):157-65.
350. Dilmen G, Köktener A, Turhan NÖ, Tez S. Growth of the fetal lens and orbit. International Journal of Gynecology & Obstetrics. 2002;76(3):267-71.
351. Goldstein I, Tamir A, Zimmer EZ, Itskovitz-Eldor J. Growth of the fetal orbit and lens in normal pregnancies. Ultrasound in Obstetrics & Gynecology. 1998;12(3):175-9.

352. Graham MV, Gray OP. Refraction of premature babies' eyes. British medical journal. 1963;1(5343):1452-4.
353. Quinn GE, Dobson V, Repka MX, Reynolds J, Kivlin J, Davis B, et al. Development of myopia in infants with birth weights less than 1251 grams. Ophthalmology. 1992;99(3):329-40.
354. Cook A, White S, Batterbury M, Clark D. Ocular Growth and Refractive Error Development in Premature Infants without Retinopathy of Prematurity. Investigative Ophthalmology & Visual Science. 2003;44(3):953-60.
355. Snir M, Friling R, Weinberger D, Sherf I, Axer-Siegel R. Refraction and keratometry in 40 week old premature (corrected age) and term infants. British Journal of Ophthalmology. 2004;88(7):900-4.
356. Ton Y, Wysenbeek YS, Spierer A. Refractive error in premature infants. J Aapos. 2004;8(6):534-8.
357. Varughese S, Varghese RM, Gupta N, Ojha R, Sreenivas V, Puliyel JM. Refractive error at birth and its relation to gestational age. Curr Eye Res. 2005;30(6):423-8.
358. Cook A, White S, Batterbury M, Clark D. Ocular Growth and Refractive Error Development in Premature Infants with or without Retinopathy of Prematurity. Investigative Ophthalmology & Visual Science. 2008;49(12):5199-207.
359. Varghese RM, Sreenivas V, Puliyel JM, Varughese S. Refractive Status at Birth: Its Relation to Newborn Physical Parameters at Birth and Gestational Age. PLoS ONE. 2009;4(2):e4469.
360. Robinson J, Fielder A. Pupillary diameter and reaction to light in preterm neonates. Archives of Disease in childhood. 1990;65(1 Spec No):35-8.
361. Mactier H, Maroo S, Bradnam M, Hamilton R. Ocular Biometry in Preterm Infants: Implications for Estimation of Retinal Illuminance. Investigative Ophthalmology & Visual Science. 2008;49(1):453-7.
362. Osorio MJ, Hertle RW, Painter M, Hinch K. Pupillary light reflexes in premature infants prior to 30 weeks postmenstrual age. Journal of American Association for Pediatric Ophthalmology and Strabismus. 2009;13(6):608-9.

363. Al-Umran KU, Pandolfi MF. Corneal diameter in premature infants. British journal of ophthalmology. 1992;76(5):292-3.
364. Kirwan C, O'Keefe M, Fitzsimon S. Central corneal thickness and corneal diameter in premature infants. Acta Ophthalmologica Scandinavica. 2005;83(6):751-3.
365. Laws DE, Haslett R, Ashby D, Obrien C, Clark D. Axial Length Biometry In Infants With Retinopathy Of Prematurity. Eye. 1994;8:427-30.
366. O'Brien C, Clark D. Ocular biometry in pre-term infants without retinopathy of prematurity. Eye. 1994;8 (Pt 6):662-5.
367. Fledelius HC, Fledelius C. Eye Size in Threshold Retinopathy of Prematurity, Based on a Danish Preterm Infant Series: Early Axial Eye Growth, Pre- and Postnatal Aspects. Investigative Ophthalmology & Visual Science. 2012;53(7):4177-84.
368. Ozdemir O, Tunay ZO, Petricli IS, Acar DE, Acar U, Erol MK. Analysis of the horizontal corneal diameter, central corneal thickness, and axial length in premature infants. Arquivos Brasileiros De Oftalmologia. 2014;77(4):225-7.
369. Ozdemir O, Tunay ZO, Acar DE, Erol MK, Sener E, Acar U. The relationship of birth weight, gestational age, and postmenstrual age with ocular biometry parameters in premature infants. Arquivos Brasileiros De Oftalmologia. 2015;78(3):146-9.
370. Kobayashi H, Kiryu J, Kobayashi K, Kondo T. Ultrasound biomicroscopic measurement of anterior chamber angle in premature infants. British Journal of Ophthalmology. 1997;81(6):460-4.
371. Inagaki Y. The rapid change of corneal curvature in the neonatal period and infancy. Archives of ophthalmology. 1986;104(7):1026-7.
372. Friling R, Weinberger D, Kremer I, Avisar R, Sirota L, Snir M. Keratometry measurements in preterm and full term newborn infants. British Journal of Ophthalmology. 2004;88(1):8-10.
373. Uva MG, Reibaldi M, Longo A, Avitabile T, Gagliano C, Scollo D, et al. Intraocular pressure and central corneal thickness in premature and full-term newborns. J Aapos. 2011;15(4):367-9.

374. Gunay M, Celik G, Gunay BO, Dogru M, Gursoy T, Ovali HF. Central corneal thickness measurements in premature infants. Int J Ophthalmol. 2014;7(3):496-500.
375. Muslubas IBS, Oral AYA, Cabi C, Caliskan S. Assessment of the central corneal thickness and intraocular pressure in premature and full-term newborns. Indian Journal of Ophthalmology. 2014;62(5):561-4.
376. Acar DE, Acar U, Tunay ZO, Ozdemir O, Dolgun A, Erdurmus M. The intraocular pressure and central corneal thickness in healthy premature infants. J Aapos. 2015;19(2):108-11.
377. Hekimoglu E, Erol MK, Toslak D, Coban DT, Dogan B, Yucel O. Comparison of Measurement of Central Corneal Thickness with Spectral Domain Optical Coherence Tomography and Standard Ultrasonic Pachymeter in Premature Infants. Journal of ophthalmology. 2015:6.
378. Jethani J, Shah K, Jethani M. Evaluating the change in central corneal thickness in neonates (term and preterm) in Indian population and the factors affecting it. Indian Journal of Ophthalmology. 2015;63(6):501-3.
379. Karahan E, Zengin MO, Tuncer I, Zengin N. Correlation of intraocular pressure with central corneal thickness in premature and full-term newborns. Eur J Ophthalmol. 2015;25(1):14-7.
380. Sekeroglu MA, Hekimoglu E, Petricli IS, Karakaya J, Ozcan B, Yucel H, et al. Central corneal thickness and intraocular pressure in premature infants. Int Ophthalmol. 2015;35(6):847-51.
381. Acar DE, Acar U, Ozdemir O, Tunay ZO. Determination of normal values of intraocular pressure and central corneal thickness in healthy premature infants-a prospective longitudinal study. Journal of AAPOS. 2016;20(3):239-42.
382. Higgins J, Altman DG. Assessing risk of bias in included studies. Cochrane handbook for systematic reviews of interventions: Cochrane book series. New York, NY, USA: John Wiley & Sons; 2008:187-241.
383. Merriam Webster [Internet]. 1st ed. Merriam Webster. 2019 [cited 5 January 2019]. Available from: http://www.merriam-webster.com/dictionary/nomogram.

384. Vislisel J. Haab striae in primary congenital glaucoma: The University of Iowa; 2015 [cited 2017 Oct 19] Available from: https://webeye.ophth.uiowa.edu/eyeforum/atlas/pages/Haab/index.htm.

385. Jeffrey CV, Therese DP, Hannah RR. How Many Studies Do You Need?: A Primer on Statistical Power for Meta-Analysis. Journal of Educational and Behavioral Statistics. 2010;35(2):215-47.

386. Newborn CoFa. Age Terminology During the Perinatal Period. Pediatrics. 2004;114(5):1362-4.

387. Axer-Siegel R, Bourla D, Friling R, Shalev B, Sirota L, Benjamini Y, et al. Intraocular pressure variations after diode laser photocoagulation for threshold retinopathy of prematurity. Ophthalmology. 2004;111(9):1734-8.

388. Haynes WM. CRC handbook of chemistry and physics. Boca Raon, FL, USA: CRC Press; 2014.

389. Millodot B. Dictionary of Optometry and Visual Science, 7th. edition. New York, NY, USA: John Wiley & Sons. 2009;92.

390. Gole GA, Ells AL, Katz X, Holmstrom G, Fielder AR, Capone Jr A, et al. The international classification of retinopathy of prematurity revisited. JAMA Ophthalmology 2005;123(7):991-9.

391. Rohrschneider K. Determination of the location of the fovea on the fundus. Investigative ophthalmology & visual science. 2004 Sep 1;45(9):3257-8.

392. De Silva DJ, Cocker KD, Lau G, Clay ST, Fielder AR, Moseley MJ. Optic disk size and optic disk-to-fovea distance in preterm and full-term infants. Investigative ophthalmology & visual science. 2006 Nov 1;47(11):4683-6.

393. Natus Medical Inc. RetCam 3 Pediatric Eye Imaging [brochure]. Pleasanton, CA, USA: Natus Medical Inc.; 2016.

394. Knudtson MD, Klein BEK, Klein R, Wong TY, Hubbard LD, Lee KE, et al. Variation associated with measurement of retinal vessel diameters at different points in the pulse cycle. British Journal of Ophthalmology. 2004;88(1):57-61.

395. CMOSIS. NanEye USB2 Evaluation Unit Documentation. Nürnberg, Germany: CMOSIS; 2015.

396. Choong YF, Rakebrandt F, North RV, Morgan JE. Acutance, an objective measure of retinal nerve fibre image clarity. British journal of ophthalmology. 2003 Mar 1;87(3):322-6.

397. Crane EM. Acutance and granulance. InImage Quality 1981 Dec 28 (Vol. 310, pp. 125-133). International Society for Optics and Photonics.

398. Trucco E, Ballerini L, Relan D, Giachetti A, MacGillivray T, Zutis K, et al., editors. Novel VAMPIRE algorithms for quantitative analysis of the retinal vasculature. In: Proceedings of the 2013 ISSNIP Biosignals and Biorobotics Conference. 2013 Feb 18-20; ; Boston, MA, USA; Piscataway, NY, USA: IEEE; 2013.

399. Tyler ME, Hubbard L, Boydston K, Pugliese A. Characteristics of digital fundus camera systems affecting tonal resolution in color retinal images. The Journal of Ophthalmic Photography. 2009;31(1):1-9.

400. European Commission. 2017/745 - Medical Devices Regulation. 2017.

401. 27 January 2016 Google and Movidius to Enhance Deep Learning Capabilities in Next-Gen Devices [press release]. Intel Movidius; 2016.

402. Bourne RRA, Flaxman SR, Braithwaite T, Cicinelli MV, Das A, Jonas JB, et al. Magnitude, temporal trends, and projections of the global prevalence of blindness and distance and near vision impairment: a systematic review and meta-analysis. The Lancet Global Health. 2017;5(9):e888-e97.

403. Stevens GA, White RA, Flaxman SR, Price H, Jonas JB, Keeffe J, et al. Global Prevalence of Vision Impairment and Blindness. Ophthalmology. 2013;120(12):2377-84.

404. Viqueza KDC, Arandjelovic O, Blaikieb A, Hwangb IA. Synthesising wider field images from narrow-field retinal video acquired using a low-cost direct ophthalmoscope (Arclight) attached to a smartphone. In: Proceedings of the 2017 IEEE International Conference on Computer Vision Workshops. 2017 Oct 22-29; Boston, MA, USA; Piscataway, NY, USA: IEEE; 2017.

405. Overhage JM, Perkins S, Tierney WM, McDonald CJ. Controlled trial of direct physician order entry: effects on physicians' time utilization in ambulatory primary care internal medicine practices. Journal of the American Medical Informatics Association. 2001;8(4):361-71.
406. Eckert C, Albers A, Bursac N, Chen HX, Clarkson J, Gericke K, et al. Integrated product and process models: towards an integrated framework and review. 2015.

Appendices

Appendix 2.1

PRISMA Checklist for Review of Reviews and Critical Analyses of Global mHealth Adoption

Section/topic	#	Checklist item	Reported on page #
TITLE			
Title	1	Identify the report as a systematic review, meta-analysis, or both.	12
ABSTRACT			
Structured summary	2	Provide a structured summary including, as applicable: background; objectives; data sources; study eligibility criteria, participants, and interventions; study appraisal and synthesis methods; results; limitations; conclusions and implications of key findings; systematic review registration number.	12,13
INTRODUCTION			
Rationale	3	Describe the rationale for the review in the context of what is already known.	12
Objectives	4	Provide an explicit statement of questions being addressed with reference to participants, interventions, comparisons, outcomes, and study design (PICOS).	12
METHODS			
Protocol and registration	5	Indicate if a review protocol exists, if and where it can be accessed (e.g., Web address), and, if available, provide registration information including registration number.	13
Eligibility criteria	6	Specify study characteristics (e.g., PICOS, length of follow-up) and report characteristics (e.g., years considered, language, publication status) used as criteria for eligibility, giving rationale.	13
Information sources	7	Describe all information sources (e.g., databases with dates of coverage, contact with study authors to identify additional studies) in the search and date last searched.	13
Search	8	Present full electronic search strategy for at least one database, including any limits used, such that it could be repeated.	13A, 13
Study selection	9	State the process for selecting studies (i.e., screening, eligibility, included in systematic review, and, if applicable, included in the meta-analysis).	14

Data collection process	10	Describe method of data extraction from reports (e.g., piloted forms, independently, in duplicate) and any processes for obtaining and confirming data from investigators.	14
Data items	11	List and define all variables for which data were sought (e.g., PICOS, funding sources) and any assumptions and simplifications made.	14
Risk of bias in individual studies	12	Describe methods used for assessing risk of bias of individual studies (including specification of whether this was done at the study or outcome level), and how this information is to be used in any data synthesis.	N/A
Summary measures	13	State the principal summary measures (e.g., risk ratio, difference in means).	N/A
Synthesis of results	14	Describe the methods of handling data and combining results of studies, if done, including measures of consistency (e.g., I^2) for each meta-analysis.	N/A

Section/topic	#	Checklist item	Reported on page #
Risk of bias across studies	15	Specify any assessment of risk of bias that may affect the cumulative evidence (e.g., publication bias, selective reporting within studies).	N/A
Additional analyses	16	Describe methods of additional analyses (e.g., sensitivity or subgroup analyses, meta-regression), if done, indicating which were pre-specified.	N/A
RESULTS			
Study selection	17	Give numbers of studies screened, assessed for eligibility, and included in the review, with reasons for exclusions at each stage, ideally with a flow diagram.	14
Study characteristics	18	For each study, present characteristics for which data were extracted (e.g., study size, PICOS, follow-up period) and provide the citations.	14-19
Risk of bias within studies	19	Present data on risk of bias of each study and, if available, any outcome level assessment (see item 12).	N/A
Results of individual studies	20	For all outcomes considered (benefits or harms), present, for each study: (a) simple summary data for each intervention group (b) effect estimates and confidence intervals, ideally with a forest plot.	14-19
Synthesis of results	21	Present results of each meta-analysis done, including confidence intervals and measures of consistency.	20A,20
Risk of bias across studies	22	Present results of any assessment of risk of bias across studies (see Item 15).	N/A
Additional analysis	23	Give results of additional analyses, if done (e.g., sensitivity or subgroup analyses, meta-regression [see Item 16]).	N/A

DISCUSSION			
Summary of evidence	24	Summarize the main findings including the strength of evidence for each main outcome; consider their relevance to key groups (e.g., healthcare providers, users, and policy makers).	21-26
Limitations	25	Discuss limitations at study and outcome level (e.g., risk of bias), and at review-level (e.g., incomplete retrieval of identified research, reporting bias).	27
Conclusions	26	Provide a general interpretation of the results in the context of other evidence, and implications for future research.	27
FUNDING			
Funding	27	Describe sources of funding for the systematic review and other support (e.g., supply of data); role of funders for the systematic review.	N/A

From: Moher D, Liberati A, Tetzlaff J, Altman DG, The PRISMA Group (2009). Preferred Reporting Items for Systematic Reviews and Meta-Analyses: The PRISMA Statement. PLoS Med 6(7): e1000097. doi:10.1371/journal.pmed1000097

Appendix 2.2

PICOS Worksheet and Search Strategy document for Review of Reviews and Critical Analyses of Global mHealth Adoption

PICOS Worksheet and Search Strategy

1. **Define your question using PICOS** by identifying: Patient Population or Problem, Intervention (treatment/test), Comparison (group or treatment), Outcomes, and Setting.

Your question should be used to help establish your search strategy.

Patient/Problem	Any human medical condition
Intervention	mHealth of any kind
Comparison	Standard practice
Outcome	Barriers and proposed solutions to integrating mHealth at scal
Setting	Any

Write out your question:
What are the barriers and proposed solutions to integrating mHealth of a kind at scale in replace of standard practice

2. Type of question/problem: **Circle one:** (Therapy/Prevention) Diagnosis, Etiology, Prognosis

3. Type of study (Publication Type) to include in the search: **Check all that apply:**

☑ Meta-Analysis	☑ Systematic Review	☐ Randomized Controlled Trial
☐ Cohort Study	☐ Case Control Study	☐ Case series or Case Report
☐ Animal Research	☐ In Vitro/Lab Research	☑ Editorials, Letters, Opinions

4. List main topics and alternate terms from your PICOS question that can be used for your search

List your inclusion criteria -gender, age, year of publication, language

Gender : either Age: any
Year : 2009 2011 – (last 5 years)
Language : English

List irrelevant terms that you may want to exclude in your search

5. List where you plan to search, i.e., CINAHL, MEDLINE, PubMed, PyscINFO, Dissertations/Thesis

Appendix 5.1

Code for non-sequential polygon object for Zemax OpticStudio modelling first design-iteration of the smartphone ophthalmoscope

```
! A 45-45-90 prism with mirrored hypothenuse and 4mm width
! Author: Nigel Bolster

C 1 "Splitter surface"

! front face vertices
V 1 -1 -1 0
V 2  1 -1 0
V 3  1  1 0
V 4 -1  1 0

! back face vertices
V 5 -1  1 2
V 6  1  1 2

! Define faces in following format:
! R vertex1 vertex2 vertex3 vertex4 isreflective face_group
! Where is reflective -1=absorb 0=refract 1=reflect
! Front face rectangle, reflective

! Front face rectangle
R 1 2 3 4 0 0

! Top face rectangle
R 4 3 6 5 0 0

! Bottom rectangle
R 1 2 6 5 0 1

! left side triangle
T 1 4 5 0 0

! right side triangle
T 3 2 6 0 0
```

Appendix 5.2

Bill of materials for prototyping the first design iteration of the smartphone-based ophthalmoscope

Quantity	Manufacturer	Item No/Manufacuturer No	Item Description
8.6g	3d Filaprint	PLA-BLA-1.75mm	Black 1.75mm PLA Filament
3x3 mm square	theplasticshop.co.uk	n/a	Acrylic Mirror Silver 3mm
6x4 mm square	theplasticshop.co.uk	n/a	Acrylic Mirror, Silver, 6mm thick, A4 sheet - Pack of 1
7mm	Farnell	1208905	OMPF2000 - FIBRE, POLYMER, 2MM BARE, 5M
<5g	Farnell	1676334	303389 - 4305 UV CURING, 28.3G
<5g	NSI Scotland	7838	New Seduction Colour Gel

Appendix 5.3

Code for non-sequential polygon object for Zemax OpticStudio modelling second design-iteration of the smartphone ophthalmoscope

```
! A rhomboid prism with 45 degree faces
! FSI Oct, 2014

! Define face groups:
C 0 "Bottom Face"
C 1 "Side Faces"
C 2 "Angled Faces"
C 3 "Top Face"

! front face vertices
V 1 -1.5 -1.1 0
V 2  1.5 -1.1 0
V 3  1.5  1.1 2.2
V 4 -1.5  1.1 2.2

! back face vertices
! back face vertices
V 5 -1.5 -1.1 12.4
V 6  1.5 -1.1 12.4
V 7  1.5  1.1 14.4
V 8 -1.5  1.1 14.4

! Define faces in following format:
! R vertex1 vertex2 vertex3 vertex4 isreflective face_group
```

```
! Where is reflective -1=absorb 0=refract 1=reflect
! Front face rectangle, reflective
R 1 2 3 4 0.9 2

! Back face rectangle, reflective
R 5 6 7 8 0.9 2

! Top rectangle, refractive
R 4 3 7 8 0 3

! Bottom rectangle, refractive
R 1 2 6 5 0 0

! left side rectangle, refractive
R 1 4 8 5 0 1

! right side rectangle, refractive
R 2 3 7 6 0 1
```

Appendix 5.4

Bill of materials for prototyping the second design iteration of the smartphone-based ophthalmoscope

Quantity	**Manufacturer**	**Item No / Manufacturer No**	**Item Description**
1275 mm	Ultimaker	Silver-Grey PLA 0.75kg	Grey 2.85mm PLA Filament
12 x 2.2 mm	theplasticshop.co.uk	n/a	Acrylic 3mm
<5g	Farnell	1676334	303389 - 4305 UV Curing, 28.3G
3 x 3 mm	Edmund Optics	#88-089	Left-Handed Circular Polarizing Film
3 x 3 mm	Sellotape	1766010	Matte Clever Tape
2 x (1.85 x 2.2 mm)	Safety Supply Company	SA-Q2023	Emergency Foil Blanket
<5g	NSI Scotland	7838	New Seduction Colour Gel

Appendix 5.5

Bill of materials for prototyping the third design iteration of the smartphone-based ophthalmoscope

Quantity	**Manufacturer**	**Item No / Manufacturer No**	**Item Description**
1275 mm	3dFilaprint, UK	Black PLA 0.75kg	Black 3mm PLA Filament
12 x 2.2 mm	theplasticshop.co.uk	n/a	Acrylic 3mm
66x37x0.5mm	Hindley	VAC0327	0.5mm thick HIPS sheet
<5g	Farnell	1676334	303389 - 4305 UV Curing, 28.3G
3 x 3 mm	Edmund Optics	#88-089	Left-Handed Circular Polarizing Film
<5g	NSI Scotland	7838	New Seduction Colour Gel
<5g		Barry M Cosmetics Ltd.	Black nitrocellulose-based paint (nail polish)
2	L-13PWC-Z	Rapid Electronics	2mm white flat-top LEDs
2	1840517	Farnell	68R resistors
20cm		Digikey	Wire
1	790-3647	RS Components	USB OTG micro-b cable
1	401-2002-1-ND	Digikey	Slide Switch
30 x 30 mm			0.8mm thick 2 layer FR4 insulated copper sheet

Appendix 5.6

Spectral weighting functions for light hazard protection calculations

Wavelength Band (nm)	Thermal Hazard, R(λ)	Aphakic Photochemical Hazard, A(λ)
305		6
335		6
340		5.88
345		5.71
350		5.46
355		5.22
360		4.62
365		4.29
370		3.75
375		3.56
380	0.00625	3.19
385	0.0125	2.31
390	0.025	1.88
395	0.05	1.58
400	0.1	1.43
405	0.2	1.3
410	0.4	1.25
415	0.8	1.2
420	0.9	1.15
425	0.98	1.11
430	0.98	1.07
435	1	1.03
440	1	1
445	1	0.97
450	1	0.94
455	1	0.9
460	1	0.8
465	1	0.7
470	1	0.62
475	1	0.55
480	1	0.45
485	1	0.4
490	1	0.22
495	1	0.16
500	1	0.1
505	1	0.079
510	1	0.06
515	1	0.05
520	1	0.0398
525	1	0.031

530	1	0.025
535	1	0.0199
540	1	0.0158
545	1	0.0126
550	1	0.01
555	1	0.0079
560	1	0.0063
565	1	0.005
570	1	0.004
575	1	0.0031
580	1	0.0025
585	1	0.002
590	1	0.0016
595	1	0.0013
600	1	0.001
700	1	0.001
705	0.98	
710	0.95	
715	0.93	
720	0.91	
725	0.89	
730	0.87	
735	0.85	
740	0.83	
745	0.81	
750	0.79	
755	0.78	
760	0.76	
765	0.74	
770	0.72	
775	0.71	
780	0.69	
785	0.68	
790	0.66	
795	0.65	
800	0.63	
805	0.62	
810	0.6	
815	0.59	
820	0.58	
825	0.56	
830	0.55	
835	0.54	
840	0.52	
845	0.51	
850	0.5	
855	0.49	
860	0.48	

865	0.47	
870	0.46	
875	0.45	
880	0.44	
885	0.43	
890	0.42	
895	0.41	
900	0.4	
905	0.39	
910	0.38	
915	0.37	
920	0.36	
925	0.35	
930	0.35	
935	0.34	
940	0.33	
945	0.33	
950	0.32	
955	0.31	
960	0.3	
965	0.3	
970	0.29	
975	0.28	
980	0.28	
985	0.27	
990	0.26	
995	0.26	
1000	0.25	
1005	0.25	
1010	0.24	
1015	0.23	
1020	0.23	
1025	0.22	
1030	0.22	
1035	0.21	
1040	0.21	
1045	0.2	
1050	0.2	
1400	0.2	

Table 40 - Spectral weighting functions for retinal hazard analysis.

Appendix 6.1

R-script for fitting curves to Nakuru Cohort Study Patient Data

```
# Script for fitting curves
# Last major edit 8th October 2015
library(pryr)

for (i in 2:ncol(sel_R))
{
	###############
	#Declarations#
	temp_y <- 0
	temp_x <- 0
	x <- vector()
	y <- vector()
	j <- 1
	# p_value threshold for ks.test:
	p_value <- 0.9
	test_results <- ""
	###############

	#Print column number heading:
	print(paste("--COLUMN ",i,"--", sep=""))

	# Build vectors for x and y values of ecdf:
	while (temp_y < 1)
	{
		if (ecdf(sel_R[,i])(temp_x) != temp_y)
		{
			temp_y <- ecdf(sel_R[,i])(temp_x)

			y[j] <- temp_y
			x[j] <- temp_x

			j <- j+1
		}

		temp_x <- temp_x + 0.0001

	}

	temp_x <- 0

	while (temp_y > 0)
	{
		if (ecdf(sel_R[,i])(temp_x) != temp_y)
		{
```

```
                temp_y <- ecdf(sel_R[,i])(temp_x)

                y[j] <- temp_y
                x[j] <- temp_x

                j <- j+1
        }

        temp_x <- temp_x - 0.0001

}

#Find the right order model:
model_form <- "x ~ y" #function(x) x
model <- lm(formula = as.formula(model_form))
ks_func <- "coef(model)[1] + coef(model)[2]*y"
#curve_func <- "coef(model)[1] + coef(model)[2]*x"

k <- 1
ks_test <- ks.test(x, eval(parse(text=ks_func)))

while(ks_test[2] < p_value & k < 12) # nrows = 2185
{
        k <- k+1
        #model
        model_form <- paste(model_form," + I(y^",k,")",sep="")
        model <- lm(formula=as.formula(model_form))

        #statistical tests
        ks_func <- paste(ks_func," + coef(model)[",k+1,"]*y^",k,sep="")
        ks_test <- ks.test(x, eval(parse(text=ks_func)))
}

#Print curve formula and statistical test results:
print(coef(model))
print(ks_test)

func_string <- coef(model)[1]

for (j in 2:length(coef(model)))
{
        func_string <- paste(func_string, " + ", coef(model)[j], "*x^", j-1,
sep="")
}
print(func_string)

#Present graphical analysis:
plot(y,x)
```

```
        #curve(eval(parse(func_string)), add=TRUE) #This doesn't work for some
reason

        print("---------")

        ##########
        #Clean-up#
        rm(temp_x)
        rm(temp_y)
        rm(j)
        rm(x)
        rm(y)
        rm(model)

        rm(model_form)
        rm(ks_func)
        #rm(curve_func)
        rm(k)
        rm(ks_test)
        ##########
}
# end of for loop cycling through sel_R columns
```

Appendix 6.2

R-script for generating participants for Nakuru community eye health workflow model

```
##########################################################################
#######
## Feb_18_Gen_Participant.R
          ##
## Participant Generation for Analysis in Excel and as Input for CPN Tools Model
                ##
## Author: Nigel M Bolster                                                ##
## Last Edit: 5th March 2018                                              ##
##########################################################################
#######
# Requires 18_Feb_Func_Generator.R to be run to populated list_ran_func2 function
list
# Note that the convention for boolean variables in the original data was true=1,
false=2
library(equivalence)
### SET THESE VARIABLES ###
n_participants = 5000
n_clusters = 100
n_files_per_cluster = 5
n_files = n_clusters * n_files_per_cluster
n_covariants = 27
scale_factors_dir = '/Users/nigel/Documents/PhD/Kenya Workflow/'
scale_factors_filename = 'Scaling-Factors.csv'
output_file_prefix = 'Routput/genParticipants'
n_runs = 50
############################
participants <- matrix(ncol=n_covariants,nrow=n_participants)
scaled_uncorr_participants <- matrix(ncol=n_covariants,nrow=n_participants)
scale_factors <-
read.csv(paste(scale_factors_dir,scale_factors_filename,sep=""),row.names=1)
all_runs_participants <- array(data=NA, dim=c(n_participants,n_covariants,n_runs))
NullDevMeasure = "{DeviceVA= 0.0, AutoSphere=0.0, AutoCylinder= 0.0,
DevCatSurg= 0, DrGrade= 1, DMacGrade= false, AmdGrade= 1, VcdrGrade = 0.1,
TabVF= false, PuffTest= 0}"
NullCompletedTests = "{TumblingE= false, Autorefractor= false, FoV= false,
UndilatedSlitlamp= false, DilatedSlitlamp= false, UndilatedDrs= false, DilatedDrs=
false, GlassesFitting= false}"
#All approximate functions that are preferable to interpolation curves:
#Age
list_ran_func2[[1]] <- function(v) {
   age <- rep(NA,length(v))
   for (i in c(1:length(age))) {
      age[i] <- rweibull3(1,shape=0.99441, scale=1.36827, thres=-1.35908) }
```

```
   return(age)
}
#Left Sphere
list_ran_func2[[8]] <- function(v) {
   sphere <- rep(NA,length(v))
   for (i in c(1:length(sphere))) {
      sphere[i] <- rnorm(1, 0.0679196 + 1.09652 * asinh((x-0.068132)/0.715053)) }
   return(sphere)
}
#Can Examine Left Fundus
list_ran_func2[[19]] <- function(v) {
   left.fundus <- rep(NA,length(v))
   for (i in c(1:length(left.fundus))) {
      left.fundus[i] <- rnorm(1, -0.0505754 + 1.43935 *
asinh((x+0.119294)/0.624592)) }
   return(left.fundus)
}
#Right DR Grade
list_ran_func2[[22]] <- function(v) {
   right.dr <- rep(NA,length(v))
   for (i in c(1:length(right.dr))) {
      right.dr[i] <- rnorm(1, -0.122822 + 1.80152 * asinh((x+0.0994509)/0.852853))
}
   return(right.dr)
}
#Left DR Grade
list_ran_func2[[23]] <- function(v) {
   left.dr <- rep(NA,length(v))
   for (i in c(1:length(left.dr))) {
      left.dr[i] <- rnorm(1, 0.0681699 + 1.84537 * asinh((x-0.00632200)/1.01631)) }
   return(left.dr)
}
#Right Macular Oedema
list_ran_func2[[24]] <- function(v) {
   right.mo <- rep(NA,length(v))
   for (i in c(1:length(right.mo))) {
      right.mo[i] <- rnorm(1, 0.00788016 + 2.30263 * asinh((x-
0.00665811)/1.33680)) }
   return(right.mo)
}
#Generate participant data for the specified number of simulation runs
for (run in c(1:n_runs)) {
         print(paste("Generating participants for Run", run, "..."))
         flush.console()
   for (col in c(1:n_covariants)) {
      scaled_uncorr_participants[,col] <-
list_ran_func2[[col]](runif(n_participants,0,1))
   }
```

```
# Multiply by the Chomelsky matrix to add correlations
scaled_participants <- scaled_uncorr_participants%*%clean_U
for (k in c(1:n_covariants)) {
   participants[,k] <- scaled_participants[,k] * scale_factors["SD",k]
   participants[,k] <- participants[,k] + scale_factors["Mean",k]
}
all_runs_participants[,,run] <- participants
#Round and convert variables from numerics:
p.age <- round(participants[,1],0)
p.bSugar <- round(participants[,14],1)
p.dmDiag <- participants[,15] < 1.5
p.dmAware <- participants[,16] < 1.5
p.willTravel <- round(runif(n_participants,0,1000),0)
le.canArefract <- participants[,7] < 1.5
le.va <- round(participants[,3],2)
le.sphere <- round(participants[,8]*4,0)/4
   le.sphere <- replace(le.sphere, le.sphere < -10, -10)
   le.sphere <- replace(le.sphere, le.sphere > 10, 10)
le.cylinder <- round(participants[,9]*4,0)/4
   le.cylinder <- replace(le.cylinder, le.cylinder < -10, -10)
   le.cylinder <- replace(le.cylinder, le.cylinder > 10, 10)
le.vcdr <- round(participants[,21],1)
   le.vcdr <- replace(le.vcdr, le.vcdr<0.1,0.1)
   le.vcdr <- replace(le.vcdr, le.vcdr>1,1)
le.vfLoss <- round(participants[,17],0)
   le.vfLoss <- replace(le.vfLoss, le.vfLoss<1,1)
   le.vfLoss <- replace(le.vfLoss, le.vfLoss>4,4)
le.iop <- round(participants[,11],0)
le.dr <- round(participants[,24],0)
   le.dr <- replace(le.dr, le.dr < 1, 1)
   le.dr <- replace(le.dr, le.dr > 4, 4)
le.dmac <- participants[,26] < 1.5
le.amd <- round(participants[,27],0)
   le.amd <- replace(le.amd, le.amd < 1, 1)
   le.amd <- replace(le.amd, le.amd > 4, 4)
le.catSurg <- round(participants[,13],0)
   le.catSurg <- replace(le.catSurg, le.catSurg < 0, 0)
   le.catSurg <- replace(le.catSurg, le.catSurg > 4, 4)
le.canFundus <- participants[,19] < 1.5
re.canArefract <- participants[,4] < 1.5
re.va <- round(participants[,2],2)
re.sphere <- round(participants[,5]*4,0)/4
   re.sphere <- replace(re.sphere, re.sphere < -10, -10)
   re.sphere <- replace(re.sphere, re.sphere > 10, 10)
re.cylinder <- round(participants[,6]*4,0)/4
   re.cylinder <- replace(re.cylinder, re.cylinder < -10, -10)
   re.cylinder <- replace(re.cylinder, re.cylinder > 10, 10)
re.vcdr <- round(participants[,20],1)
```

```
      re.vcdr <- replace(re.vcdr, re.vcdr<0.1,0.1)
      re.vcdr <- replace(re.vcdr, re.vcdr>1,1)
   re.vfLoss <- round(participants[,16],0)
      re.vfLoss <- replace(re.vfLoss, re.vfLoss<1,1)
      re.vfLoss <- replace(re.vfLoss, re.vfLoss>4,4)
   re.iop <- round(participants[,10],0)
   re.dr <- round(participants[,23],0)
      re.dr <- replace(re.dr, re.dr < 1, 1)
      re.dr <- replace(re.dr, re.dr > 4, 4)
   re.dmac <- participants[,25] < 1.5
   re.amd <- round(participants[,26],0)
      re.amd <- replace(re.amd, re.amd < 1, 1)
      re.amd <- replace(re.amd, re.amd > 4, 4)
   re.catSurg <- round(participants[,12],0)
      re.catSurg <- replace(re.catSurg, re.catSurg < 0, 0)
      re.catSurg <- replace(re.catSurg, re.catSurg > 4, 4)
   re.canFundus <- participants[,18] < 1.5
   print("Writing to CSV file...")
   flush.console()
   # Write matrix to csv file:
   write.csv(participants,paste0('Routput/raw_participants_',run,'.csv'))
   write.csv(data.frame(p.age,p.bSugar,p.dmDiag,p.willTravel
,le.canArefract,le.sphere,le.cylinder,le.vcdr,le.vfLoss,le.iop,le.dr,le.dmac,le.amd,le.ca
tSurg,le.canFundus
,re.canArefract,re.sphere,re.cylinder,re.vcdr,re.vfLoss,re.iop,re.dr,re.dmac,re.amd,re.
catSurg,re.canFundus)
      ,paste0('Routput/formatted_participants_',run,'.csv'))
   for (c.id in c(1:n_clusters))
   {
      if (c.id%%20==1) {
        print(paste("Writing participants ", (c.id-1)*n_participants/n_clusters+1, " to
",
         (c.id+19)*n_participants/n_clusters," to file..."))
             flush.console()
      }

      for (f.id in c(0:(n_files_per_cluster-1)))
      {
         output_filename <- paste0(output_file_prefix,run,"-",c.id,"-",f.id,".txt")
         cpn.string = ""
         write(cpn.string,file=output_filename)
         start.p.id = (n_participants/n_clusters)*(c.id-1) +
(f.id*n_participants/(n_clusters*n_files_per_cluster)) + 1
         end.p.id = start.p.id + n_participants/(n_clusters*n_files_per_cluster) - 1
         for (p.id in c(start.p.id:end.p.id))
         {
            # Construct participant record:
```

```
            cpn.string = paste0("1`{Details={ClusterId= ",c.id,", StudyId= ",p.id,",
Age= ",p.age[p.id],", bSugar= ",p.bSugar[p.id],", DmDiag= ",p.dmDiag[p.id],",
DmAware= ",p.dmAware[p.id],", WillTravel= ",p.willTravel[p.id],
            "},LeftEye={CanARefract= ",le.canArefract[p.id],", VA= ",le.va[p.id],",
Sphere= ",le.sphere[p.id],", Cylinder= ",le.cylinder[p.id],", Vcdr= ",le.vcdr[p.id],",
vfLoss= ",le.vfLoss[p.id],", iop= ",le.iop[p.id],", Dr= ",le.dr[p.id],", DMac=
",le.dmac[p.id],", Amd= ",le.amd[p.id],", NeedCatSurg= ",le.catSurg[p.id],",
CanFundusExam= ",le.canFundus[p.id],", DevMeasure= ",NullDevMeasure,"}",
              ",RightEye={CanARefract= ",re.canArefract[p.id],", VA=
",re.va[p.id],", Sphere= ",re.sphere[p.id],", Cylinder= ",re.cylinder[p.id],", Vcdr=
",re.vcdr[p.id],", vfLoss= ",re.vfLoss[p.id],", iop= ",re.iop[p.id],", Dr= ",re.dr[p.id],",
DMac= ",re.dmac[p.id],", Amd= ",re.amd[p.id],", NeedCatSurg= ",re.catSurg[p.id],",
CanFundusExam= ",re.canFundus[p.id],", DevMeasure= ",NullDevMeasure,"},
CompletedTests= "
              ,NullCompletedTests,"}")
            # Format string for CPN Tools:
            cpn.string = gsub("-","~",cpn.string)
            cpn.string = gsub("FALSE","false",cpn.string)
            cpn.string = gsub("TRUE","true",cpn.string)
            cpn.string = gsub("(?<= [0-9]), DmDiag|(?<= [1-9][0-9]), DmDiag",".0,
DmDiag",cpn.string,perl=T)
            cpn.string = gsub("(?<= [0-4]), Sphere|(?<= ~[0-4]), Sphere",".0,
Sphere",cpn.string,perl=T)
            cpn.string = gsub("(?<= [0-9]), Cylinder|(?<= ~[0-9]), Cylinder|(?<= 1[0-
9]), Cylinder|(?<= ~1[0-9]), Cylinder",".0, Cylinder",cpn.string,perl=T)
            cpn.string = gsub("(?<= [0-9]), Vcdr(?!Grade)|(?<= ~[0-9]),
Vcdr(?!Grade)|(?<= 1[0-9]), Vcdr(?!Grade)|(?<= ~1[0-9]), Vcdr(?!Grade)",".0,
Vcdr",cpn.string,perl=T)
            cpn.string = gsub("(?<= 1), vfLoss",".0, vfLoss,",cpn.string,perl=T)
            if (p.id!=end.p.id) {cpn.string<-paste0(cpn.string,"++")}
            # Write participant list to text file:
            write(cpn.string,file=output_filename,append=T)
          }
        }
    }
}
# Run and print statistical test for equivalence
for (i in c(1:n_covariants))
{
  print(cat(c("","--------------","Equivalence test for: ",colnames(unscaled)[i],"---------
----------"), sep="\n"))
  print(tost(unscaled[,i], all_runs_participants[,i,]))
}
```

Appendix 7.1

PowerShell 2.0 Script for Extracting Events by Clinic

```
#Log folder:
$dir_path = #directory containg files goes here
$input_prefix = #file prefix common across files goes here e.g. 'ROP-NewCam-1.33-non-special-grading-'
## CLINIC LOG EXTRACTION ##
$input_path = $dir_path + $input_prefix + 'clinic-screening.xes'
$fileContent = [io.file]::ReadAllText($input_path)
for ($i=1; $i -le 81; $i++){
  $output_file = $dir_path + 'Clinic-' + $i + '.xes'
  $fileHeader = "<?xml version=`"1.0`" encoding=`"UTF-8`" ?>`r`n<!-- This file has been generated with the OpenXES library. It conforms -->`r`n<!-- to the XML serialization of the XES standard for log storage and -->`r`n<!-- management. -->`r`n<!-- XES standard version: 1.0 -->`r`n<!-- OpenXES library version: 1.0RC7 -->`r`n<!-- OpenXES is available from http://www.openxes.org/ -->`r`n<log xes.version=`"1.0`" xes.features=`"nested-attributes`" openxes.version=`"1.0RC7`">`r`n`t<string key=`"concept:name`" value=`"Screening Clinic " + $i + "`"/>`r`n`t<trace>`n`r`t`t<string key=`"concept:name`" value=`"Run 1`"/>"
  "Writing to: " + $output_file
  $fileHeader > $output_file
  $regex = '\t\t<event>\n.*concept:instance.*,order=' + $i + ',.*\n.*org:role.*\n.*org:resource.*\n.*lifecycle:transition.*\n.*time:timestamp.*\n.*concept:name.*\n\t\t</event>\n\t\t<event>\n.*org:role.*\n.*concept:instance.*,order=' + $i + ',.*\n.*org:resource.*\n.*time:timestamp.*\n.*concept:name.*\n.*lifecycle:transition.*\n\t\t</event>\n|\t</trace>\n\t<trace>\n.*\n|\t</trace>\n</log>'
  $fileContent | select-string -Pattern $regex -AllMatches | % { $_.Matches } | % { $_.Value } >> $output_file
  (Get-Content $output_file) -replace '`n', '`r`n' | Set-Content $output_file
}
## SCREENING TEAM LOG EXTRACTION ##
# Extracts each specialist into a separate log file
$num_teams = 3
$input_file = $dir_path + $input_prefix + 'Screening.xes'
$get_team_regex = @('((?<=curDay=sat.*)28,|([1-9],|1.,|2[0-7],))' , '(((?<=curDay=sat,nextClinic=)55,)|((?<!curDay=sat,nextClinic=)28,)|(29,|3[0-9],|4[0-9],|5[0-4],))' , '(((?<!curDay=sat,nextClinic=)55),|(5[6-9],|6[0-9],|7[0-9],|8[0-2],))')
$fileContent = [io.file]::ReadAllText($input_file)
for ($i=1; $i -le $num_teams; $i++){
  $output_file = $dir_path + 'team-' + $i + '-screening.xes'
  $fileHeader = "<?xml version=`"1.0`" encoding=`"UTF-8`" ?>`r`n<!-- This file has been generated with the OpenXES library. It conforms -->`r`n<!-- to the XML serialization of the XES standard for log storage and -->`r`n<!-- management. --
```

>`r`n<!-- XES standard version: 1.0 -->`r`n<!-- OpenXES library version: 1.0RC7 -->`r`n<!-- OpenXES is available from http://www.openxes.org/ -->`r`n<log xes.version=`"1.0`" xes.features=`"nested-attributes`" openxes.version=`"1.0RC7`">`r`n`t<string key=`"concept:name`" value=`"ROP Screening Team " + $i + "`"/>`r`n`t<trace>`n`r`t`t<string key=`"concept:name`" value=`"Run 1`"/>"
  "Writing to: " + $output_file
  $fileHeader > $output_file
  #$regex = '\t\t<event>\r\n.*concept:instance.*nextClinic=' + $get_team_regex[$i-1] +
'.*\r\n.*org:role.*\r\n.*org:resource.*\r\n.*lifecycle:transition.*\r\n.*time:timestamp.*\r\n.*concept:name.*\r\n\t\t</event>\r\n\t\t<event>.*\r\n.*org:role.*\r\n.*concept:instance.*nextClinic=' + $get_team_regex[$i-1] +
'.*\r\n.*org:resource.*\r\n.*time:timestamp.*\r\n.*concept:name.*\r\n.*lifecycle:transition.*\r\n\t\t</event>\r\n|\t\t<event>\r\n.*concept:instance.*nextClinic=' +
$get_team_regex[$i-1] +
'.*\r\n.*org:role.*\r\n.*org:resource.*\r\n.*lifecycle:transition.*\r\n.*time:timestamp.*\r\n.*concept:name.*\r\n\t\t</event>\r\n\t\t<event>.*\r\n.*org:role.*\r\n.*concept:instance.*nextClinic=' + $get_team_regex[$i-1] +
'.*\r\n.*org:resource.*\r\n.*time:timestamp.*\r\n.*concept:name.*\r\n.*lifecycle:transition.*\r\n\t\t</event>\r\n|\t</trace>\r\n\t<trace>\r\n.*\r\n|\t</trace>\r\n</log>'
  #$regex =
'\t\t<event>\n.*org:resource.*\n.*org:role.*\n.*concept:instance.*nextClinic=' +
$get_team_regex[$i-1] +
'.*\n.*lifecycle:transition.*\n.*time:timestamp.*\n.*concept:name.*\n\t\t</event>\n\t\t<event>.*\n.*org:resource.*\n.*org:role.*\n.*concept:instance.*nextClinic=' +
$get_team_regex[$i-1] +
'.*\n.*time:timestamp.*\n.*lifecycle:transition.*\n.*concept:name.*\n\t\t</event>\n|\t\t<event>\n.*org:resource.*\n.*org:role.*\n.*concept:instance.*nextClinic=' +
$get_team_regex[$i-1] +
'.*\n.*lifecycle:transition.*\n.*time:timestamp.*\n.*concept:name.*\n\t\t</event>\n\t\t<event>.*\n.*org:resource.*\n.*org:role.*\n.*concept:instance.*nextClinic=' +
$get_team_regex[$i-1] +
'.*\n.*time:timestamp.*\n.*lifecycle:transition.*\n.*concept:name.*\n\t\t</event>\n'
  $regex = '\t\t<event>\n.*concept:instance.*nextClinic=' + $get_team_regex[$i-1] +
'.*\n.*org:role.*\n.*org:resource.*\n.*lifecycle:transition.*\n.*time:timestamp.*\n.*concept:name.*\n\t\t</event>\n\t\t<event>.*\n.*org:role.*\n.*concept:instance.*nextClinic=' + $get_team_regex[$i-1] +
'.*\n.*org:resource.*\n.*time:timestamp.*\n.*concept:name.*\n.*lifecycle:transition.*\n\t\t</event>\n|\t\t<event>\n.*concept:instance.*nextClinic=' +
$get_team_regex[$i-1] +
'.*\n.*org:role.*\n.*org:resource.*\n.*lifecycle:transition.*\n.*time:timestamp.*\n.*concept:name.*\n\t\t</event>\n\t\t<event>.*\n.*org:role.*\n.*concept:instance.*nextClinic=' + $get_team_regex[$i-1] +
'.*\n.*org:resource.*\n.*time:timestamp.*\n.*concept:name.*\n.*lifecycle:transition.*\n\t\t</event>\n|\t</trace>\n\t<trace>\n.*\n|\t</trace>\n</log>|\t\t<event>\n.*org:resource.*\n.*org:role.*\n.*concept:instance.*nextClinic=' + $get_team_regex[$i-1] +
'.*\n.*time:timestamp.*\n.*lifecycle:transition.*\n.*concept:name.*\n\t\t</event>\n\t\

```
t<event>.*\n.*org:resource.*\n.*org:role.*\n.*concept:instance.*nextClinic=' +
$get_team_regex[$i-1] +
'.*\n.*time:timestamp.*\n.*lifecycle:transition.*\n.*concept:name.*\n\t\t</event>\n|\t
\t<event>\n.*org:resource.*\n.*org:role.*\n.*concept:instance.*nextClinic=' +
$get_team_regex[$i-1] +
'.*\n.*time:timestamp.*\n.*lifecycle:transition.*\n.*concept:name.*\n\t\t</event>\n\t\
t<event>.*\n.*org:resource.*\n.*org:role.*\n.*concept:instance.*nextClinic=' +
$get_team_regex[$i-1] +
'.*\n.*time:timestamp.*\n.*lifecycle:transition.*\n.*concept:name.*\n\t\t</event>\n'
  #$regex = '\t\t<event>\n.*concept:instance.*nextClinic=' + $get_team_regex[$i-1]
+
'.*\n.*org:role.*\n.*org:resource.*\n.*lifecycle:transition.*\n.*time:timestamp.*\n.*c
oncept:name.*\n\t\t</event>\n\t\t<event>.*\n.*org:role.*\n.*concept:instance.*nextC
linic=' + $get_team_regex[$i-1] +
'.*\n.*org:resource.*\n.*time:timestamp.*\n.*concept:name.*\n.*lifecycle:transition.
*\n\t\t</event>\n|\t\t<event>\n.*concept:instance.*nextClinic=' +
$get_team_regex[$i-1] +
'.*\n.*org:role.*\n.*org:resource.*\n.*lifecycle:transition.*\n.*time:timestamp.*\n.*c
oncept:name.*\n\t\t</event>\n\t\t<event>.*\n.*org:role.*\n.*concept:instance.*nextC
linic=' + $get_team_regex[$i-1] +
'.*\n.*org:resource.*\n.*time:timestamp.*\n.*concept:name.*\n.*lifecycle:transition.
*\n\t\t</event>\n|\t</trace>\n\t<trace>\n.*\n|\t</trace>\n</log>'
  #$regex = '\t\t<event>\n.*concept:instance.*nextClinic=' + $get_team_regex[$i-1]
+
'.*\n.*org:role.*\n.*org:resource.*\n.*lifecycle:transition.*\n.*time:timestamp.*\n.*c
oncept:name.*\n\t\t</event>\n\t\t<event>.*\n.*org:role.*\n.*concept:instance.*nextC
linic=' + $get_team_regex[$i-1] +
'.*\n.*org:resource.*\n.*time:timestamp.*\n.*concept:name.*\n.*lifecycle:transition.
*\n\t\t</event>\n|\t\t<event>\n.*concept:instance.*nextClinic=' +
$get_team_regex[$i-1] +
'.*\n.*org:role.*\n.*org:resource.*\n.*lifecycle:transition.*\n.*time:timestamp.*\n.*c
oncept:name.*\n\t\t</event>\n\t\t<event>.*\n.*org:role.*\n.*concept:instance.*nextC
linic=' + $get_team_regex[$i-1] +
'.*\n.*org:resource.*\n.*time:timestamp.*\n.*concept:name.*\n.*lifecycle:transition.
*\n\t\t</event>\n|\t</trace>\n\t<trace>\n.*\n|\t</trace>\n</log>'
  $fileContent | select-string -Pattern $regex -AllMatches | % { $_.Matches } | % {
$_.Value } >> $output_file
  #$fileContent >> $output_file
  (Get-Content $output_file) -replace "`n", "`r`n" | Set-Content $output_file
}
## SPECIALIST OUTREACH LOG EXTRACTION ##
# Extracts each specialist into a separate log file
$input_file = $dir_path + $input_prefix + 'outreach.xes'
$num_specials = 3
$fileContent = [io.file]::ReadAllText($input_file)
for ($i=1; $i -le $num_specials; $i++){
  $output_file = $dir_path + 'specialist-' + $i + '-outreach.xes'
```

```
  $fileHeader = "<?xml version=`"1.0`" encoding=`"UTF-8`" ?>`r`n<!-- This file has
been generated with the OpenXES library. It conforms -->`r`n<!-- to the XML
serialization of the XES standard for log storage and -->`r`n<!-- management. --
>`r`n<!-- XES standard version: 1.0 -->`r`n<!-- OpenXES library version: 1.0RC7 --
>`r`n<!-- OpenXES is available from http://www.openxes.org/ -->`r`n<log
xes.version=`"1.0`" xes.features=`"nested-attributes`"
openxes.version=`"1.0RC7`">`r`n`t<string key=`"concept:name`" value=`"ROP
Specialist " + $i + " Outreach`"/>`r`n`t<trace>`n`r`t`t<string key=`"concept:name`"
value=`"Run 1`"/>"
  "Writing to: " + $output_file
  $fileHeader > $output_file
  $regex = '\t\t<event>\n.*concept:instance.*spec=' + $i +
',.*\n.*org:role.*\n.*org:resource.*\n.*lifecycle:transition.*\n.*time:timestamp.*\n.*c
oncept:name.*\n\t\t</event>\n\t\t<event>.*\n.*org:role.*\n.*concept:instance.*spec='
+ $i +
',.*\n.*org:resource.*\n.*time:timestamp.*\n.*concept:name.*\n.*lifecycle:transition.
*\n\t\t</event>\n|\t\t<event>\n.*concept:instance.*specNum=' + $i +
',.*\n.*org:role.*\n.*org:resource.*\n.*lifecycle:transition.*\n.*time:timestamp.*\n.*c
oncept:name.*\n\t\t</event>\n\t\t<event>.*\n.*org:role.*\n.*concept:instance.*specN
um=' + $i +
',.*\n.*org:resource.*\n.*time:timestamp.*\n.*concept:name.*\n.*lifecycle:transition.
*\n\t\t</event>\n|\t</trace>\n\t<trace>\n.*\n|\t</trace>\n</log>'
  $fileContent | select-string -Pattern $regex -AllMatches | % { $_.Matches } | % {
$_.Value } >> $output_file
  (Get-Content $output_file) -replace '`n', '`r`n' | Set-Content $output_file
}
## SPECIALIST GRADING LOG EXTRACTION ##
# Extracts each specialist into a separate log file
$input_file = $dir_path + $input_prefix + 'Specialist-Grading.xes'
$num_specials = 3
$fileContent = [io.file]::ReadAllText($input_file)
for ($i=1; $i -le $num_specials; $i++){
  $output_file = $dir_path + 'specialist-' + $i + '-grading.xes'
  $fileHeader = "<?xml version=`"1.0`" encoding=`"UTF-8`" ?>`r`n<!-- This file has
been generated with the OpenXES library. It conforms -->`r`n<!-- to the XML
serialization of the XES standard for log storage and -->`r`n<!-- management. --
>`r`n<!-- XES standard version: 1.0 -->`r`n<!-- OpenXES library version: 1.0RC7 --
>`r`n<!-- OpenXES is available from http://www.openxes.org/ -->`r`n<log
xes.version=`"1.0`" xes.features=`"nested-attributes`"
openxes.version=`"1.0RC7`">`r`n`t<string key=`"concept:name`" value=`"ROP
Specialist " + $i + " Grading`"/>`r`n`t<trace>`n`r`t`t<string key=`"concept:name`"
value=`"Run 1`"/>"
  "Writing to: " + $output_file
  $fileHeader > $output_file
  $regex =
'\t\t<event>\n.*org:resource.*\n.*org:role.*\n.*concept:instance.*specNum=' + $i +
',.*\n.*time:timestamp.*\n.*lifecycle:transition.*\n.*concept:name.*\n\t\t</event>\n\t
\t<event>\n.*org:resource.*\n.*org:role.*\n.*concept:instance.*specNum=' + $i +
```

```
',.*\n.*time:timestamp.*\n.*lifecycle:transition.*\n.*concept:name.*\n\t\t</event>\n|\
t\t<event>\n.*concept:instance.*specNum=' + $i +
',.*\n.*org:role.*\n.*org:resource.*\n.*lifecycle:transition.*\n.*time:timestamp.*\n.*c
oncept:name.*\n\t\t</event>\n\t\t<event>.*\n.*org:role.*\n.*concept:instance.*specN
um=' + $i +
',.*\n.*org:resource.*\n.*time:timestamp.*\n.*concept:name.*\n.*lifecycle:transition.
*\n\t\t</event>\n|\t</trace>\n\t<trace>\n.*\n|\t</trace>\n</log>'
  $fileContent | select-string -Pattern $regex -AllMatches | % { $_.Matches } | % {
$_.Value } >> $output_file
  (Get-Content $output_file) -replace '`n', '`r`n' | Set-Content $output_file
}
```

Appendix 7.2

PowerShell 2.0 Script for Extracting Event Timings

```
$dir_path = 'C:\Users\PC\ShareFile\Personal Folders\ROP\Workflow Model\Logs
and analysis\NewCam - India\1.33 9m All Runs\Sub-nets\'
## CLINIC SCREENING SESSION TIMINGS ##
# Extracts the the start and end times for each screening session
# from each clinic's individual subnet
$output_file = $dir_path + 'clinics-timings.csv’
$fileHeader = "Clinic,Start,Finish`r`n"
$fileHeader > $output_file
for ($i=1; $i -le 81; $i++){
  if ($i -lt 10)
  {
    $input_path = $dir_path + 'clinic-0' + $i + '.csv'
  }
  else
  {
    $input_path = $dir_path + 'clinic-' + $i + '.csv'
  }
  $fileContent = [io.file]::ReadAllText($input_path)
  "Writing from: " + $input_path
  $regex =
'Screening_Zone\.Screening_Session\.Start_Session\{.*,"complete",|Screening_Zone
\.Screening_Session\.End_Session\{.*,"start",'
  $fileContent | select-string -Pattern $regex -AllMatches | % { $_.Matches } | %
{"$i," + $_.Value } >> $output_file
}
$raw = [System.IO.File]::ReadAllText($output_file) #Get-Content $output_file -
Raw
$formatted = $raw -replace 'Screening_Zone\.Screening_Session\.Start.*d = ...
}","|\",\"start\",|\r\n..,Screening_Zone\.Screening_Session\.End_Session.*i = ..
}","|\r\n.,Screening_Zone\.Screening_Session\.End_Session.*i = . }","" ,"
$formatted = $formatted -replace '\",\"complete\",', ','
$formatted = $formatted -replace 'T', ' '
$formatted = $formatted -replace 'Z', "
#$formatted = $formatted -replace '"","', ','
$formatted = $formatted -replace 'S ar ', 'Start'
$formatted > $output_file

## SCREENING TEAM TIMINGS (direct from separated logs) ##
# Extracts the the start and end times for each screening session
# from each clinic's individual subnet
$output_file = $dir_path + 'Screening-Teams.csv’
$num_teams = 3
$fileHeader = "Team,Travel Start,Screening Start,Screening Finish,Start Return Trip,
Finished Return Trip"
```

```
$fileHeader > $output_file

for ($i=1; $i -le $num_teams; $i++){
  $input_file = $dir_path + 'team-' + $i + '-screening.xes'
  $fileContent = [io.file]::ReadAllText($input_file)
  "Writing from: " + $input_file
  $regex =
'Screening_Zone\.Screening_Session\.Travel_to_NICU\{.*\n.*\n.*\n.*start.*\n.*\"ti
me:timestamp\"
value=\".*(Z|\+01:00)|Screening_Zone.Screening_Session\.Unpack\{.*\n.*\n.*\n.*sta
rt.*\n.*\"time:timestamp\"
value=\".*(Z|\+01:00)|Screening_Zone.Screening_Session\.End_Session\{.*\n.*\n.*\
n.*start.*\n.*\"time:timestamp\"
value=\".*(Z|\+01:00)|Screening_Zone\.Return_to_HQ\{.*\n.*\n.*\n.*start.*\n.*\"tim
e:timestamp\"
value=\".*(Z|\+01:00)|Screening_Zone\.Arrived_at_HQ\{.*\n.*\n.*\n.*start.*\n.*\"ti
me:timestamp\"
value=\".*(Z|\+01:00)|Screening_Zone\.Screening_Session\.Travel_to_NICU\{.*\n.*
\"time:timestamp\"
value=\".*(Z|\+01:00)(?=.*\n.*start)|Screening_Zone.Screening_Session\.Unpack\{.*
\n.*\"time:timestamp\"
value=\".*(Z|\+01:00)(?=.*\n.*start)|Screening_Zone.Screening_Session\.End_Sessio
n\{.*\n.*\"time:timestamp\"
value=\".*(Z|\+01:00)(?=.*\n.*start)|Screening_Zone\.Return_to_HQ\{.*\n.*\"time:ti
mestamp\"
value=\".*(Z|\+01:00)(?=.*\n.*start)|Screening_Zone\.Arrived_at_HQ\{.*\n.*\"time:t
imestamp\" value=\".*(Z|\+01:00)(?=.*\n.*start)'
  $fileContent | select-string -Pattern $regex -AllMatches | % { $_.Matches } | %
{"$i," + $_.Value } >> $output_file
}
$raw = [System.IO.File]::ReadAllText($output_file) #Get-Content $output_file -
Raw
$formatted = ''
$formatted = $raw -replace '\"/>.*\n.*\n.*\n.*\n.*\"time:timestamp\" value=\"', ''
$formatted = $formatted -replace
'Screening_Zone\.Screening_Session\.Travel_to_NICU\{.*distHq=.*\} \}', ''
$formatted = $formatted -replace
'\r\n.,Screening_Zone\.Screening_Session\.Unpack\{.*distHq=.*\} \}', ','
$formatted = $formatted -replace
'\r\n.,Screening_Zone\.Screening_Session\.End_Session\{.*distHq=.*\} \}', ','
$formatted = $formatted -replace
'\r\n.,Screening_Zone\.Return_to_HQ\{.*distHq=.*\} \}', ','
$formatted = $formatted -replace
'\r\n.,Screening_Zone\.Abandon_Remianing_Clinics\{.* u = () }', ','
$formatted = $formatted -replace
'\r\n.,Screening_Zone\.Arrived_at_HQ\{.*distHq=.*\} \}', ','
$formatted = $formatted -replace '\r\n.,Screening_Zone\.Leave_HQ\{.* u2 = () }', ''
$formatted = $formatted -replace '\r\n.*<date key=\"time\:timestamp\" value=\"', ''
```

```
$formatted = $formatted -replace '\"/>', "
$formatted = $formatted -replace '\",\"complete\",|\",\"complete\"|\",\"start\",', "
$formatted = $formatted -replace '(?<=[0-9])T', ' '
$formatted = $formatted -replace '(?<=[0-9])Z', "
#$formatted = $formatted -replace '09:00:00.*09:00:00.*09:00:00(?=.*,.*,.*\n)',
'09:00:00'
$formatted > $output_file

## SPECIALIST OUTREACH TIMINGS ##
# Extracts the the start and end times for each screening session
# from each clinic's individual subnet
$output_file = $dir_path + 'Specialists.csv’
$num_specials = 3
$fileHeader = "Specialist,Start,Finish"
$fileHeader > $output_file

for ($i=1; $i -le $num_specials; $i++){
  $input_file = $dir_path + 'specialist-' + $i + '-outreach.csv'
  $fileContent = [io.file]::ReadAllText($input_file)
  "Writing from: " + $input_file
  $regex =
'Screening_Zone\.Treat\{.*,"complete",|Screening_Zone\.Specialist_Outreach_End\{
.*\"complete\"|Screening_Zone\.Arrived_at_hospital\{.*\"start\"'
  $fileContent | select-string -Pattern $regex -AllMatches | % { $_.Matches } | %
{"$i," + $_.Value } >> $output_file
}
$raw = [System.IO.File]::ReadAllText($output_file) #Get-Content $output_file -
Raw
$formatted = "
#$formatted = $raw -replace
'(Screening_Zone\.Treat.*\"Treat\",\")(?=(.*\r\n.*Treat))', "
$formatted = $raw -replace 'Screening_Zone\.Treat\{.*,distHq=.*\} \}\",\"', "
$formatted = $formatted -replace
'\r\n.,Screening_Zone\.Specialist_Outreach_End\{.*distHq=.*\} \}\",\"', ','
$formatted = $formatted -replace
'\r\n.,Screening_Zone\.Arrived_at_hospital\{.*distHq=.*\} \}\",\"', ','
$formatted = $formatted -replace '\",\"complete\"|\",\"start\"', "
$formatted = $formatted -replace '(?<=[0-9])T', ' '
$formatted = $formatted -replace '(?<=[0-9])Z', "
$formatted = $formatted -replace ',,', ','
$formatted > $output_file

## SPECIALIST GRADING TIMINGS ##
# Extracts the the start and end times for each screening session
# from each clinic's individual subnet
$output_file = $dir_path + 'Specialists-Grading.csv’
$num_specials = 3
$fileHeader = "Specialist,Start,Finish"
```

```
$fileHeader > $output_file

for ($i=1; $i -le $num_specials; $i++){
  $input_file = $dir_path + 'specialist-' + $i + '-grading.csv'
  $fileContent = [io.file]::ReadAllText($input_file)
  "Writing from: " + $input_file
  $regex =
'Screening_Zone\.Read_Report\..*Report\{.*\"Start|Screening_Zone\.Read_Report\..
*Report\{.*\n.*\"Start'
  $fileContent | select-string -Pattern $regex -AllMatches | % { $_.Matches } | %
{"$i," + $_.Value } >> $output_file
}
$raw = [System.IO.File]::ReadAllText($output_file) #Get-Content $output_file -
Raw
$formatted = ''
$formatted = $raw -replace 'Report\{.*,distHq=.*\} \}\",\"', 'Report'
$formatted = $formatted -replace
'Screening_Zone\.Read_Report\.Read_Today_Report', ''
$formatted = $formatted -replace
'\r\n.,Screening_Zone\.Read_Report\.Finished_Reading_Report', ''
$formatted = $formatted -replace '\",\"start', ','
$formatted = $formatted -replace
'Screening_Zone.Read_Report.Read_Today_Report', ''
$formatted = $formatted -replace ',`r`n', '`r`n'
$formatted = $formatted -replace '(?<=[0-9])T', ' '
$formatted = $formatted -replace '(?<=[0-9])Z', ''
$formatted = $formatted -replace 'Transition\",\"Read
Today\n|Transition\",\"Finished Reading Report\",\"', ''
$formatted = $formatted -replace 'Report\",\"', ''
$formatted = $formatted -replace ',`r`n', '`r`n'
$formatted = $formatted -replace '\n.*\.Finished_Reading_Report', ','
$formatted = $formatted -replace '.*,\"complete\",.*\n', ''
$formatted > $output_file

## GRADING OUTCOMES ##
# Tallies the outcomes recorded for each infant by simulation run
$input_file = $dir_path + $input_prefix + 'Outcomes.xes'
$output_prefix = $dir_path + $input_prefix  + 'outcomes'
$num_runs = 5
$fileHeader = "Run,Outcome,Timestamp"

"Reading: " + $input_file
$fileContent = [io.file]::ReadAllText($input_file)

for ($i=1; $i -le $num_runs; $i++){
  $output_file = $output_prefix + "-run" + $i + ".csv"
  $regex = '\t<trace>\n\t\t<string key=\"concept:name\" value="Run ' +$i +
'\"/>[\s\S]+?\t</trace>'
```

```
  "Writing from: " + $input_file + " to: " + $output_file
  $fileContent | select-string -Pattern $regex -AllMatches | % { $_.Matches } | % {
$_.Value } > $output_file
}
$output_file = $output_prefix + ".csv"
$fileHeader > $output_file

for ($i=1; $i -le $num_runs; $i++){
  $input_file = $output_prefix + "-run" + $i + ".csv"
  "Writing from: " + $input_file + " to: " + $output_file
  $regex =
'Screening_Zone\.Read_Report\..*\{.*\n.*org:role.*\n.*org:resource.*\n.*lifecycle:tr
ansition.*\n.*time:timestamp.*(Z|\+01:00)'
  $fileContent = [io.file]::ReadAllText($input_file)
  $fileContent | select-string -Pattern $regex -AllMatches | % { $_.Matches } | %
{"$i," + $_.Value } >> $output_file
}
$raw = [System.IO.File]::ReadAllText($output_file)
$formatted = ''
$formatted = $raw -replace 'Screening_Zone\.Read_Report\.|\{.*/>', ''
$formatted = $formatted -replace
'\r\n.,Screening_Zone\.Read_Report\.Finished_Reading_Report\{.*distHq=.*\}
\}\",\"', ','
$formatted = $formatted -replace
'\n.*org\:role.*\n.*org\:resource.*\n.*lifecycle\:transition.*\n.*time\:timestamp.*valu
e=\"', ','
$formatted = $formatted -replace '(?<=[0-9])T', ' '
$formatted = $formatted -replace '(?<=[0-9])Z', ''
$formatted > $output_file
## ENROLLED INFANTS ##
# Extracts timestamps for enrollment and referall / discharges
# for each run
$input_file = $dir_path + $input_prefix + 'enrolled.xes'
$output_prefix = $dir_path + 'enrolled'
$num_runs = 5
$fileHeader = "Run,Enroll//Discharge//Refer,Timestamp"

"Reading: " + $input_file
$fileContent = [io.file]::ReadAllText($input_file)

for ($i=1; $i -le $num_runs; $i++){
  $output_file = $output_prefix + "-run" + $i + ".csv"
  $regex = '\t<trace>\n\t\t<string key=\"concept:name\" value="Run ' +$i +
'\"/>[\s\S]+?\t</trace>'
  "Writing from: " + $input_file + " to: " + $output_file
  $fileContent | select-string -Pattern $regex -AllMatches | % { $_.Matches } | % {
$_.Value } > $output_file
}
```

```
$output_file = $output_prefix + ".csv"
$fileHeader > $output_file

for ($i=1; $i -le $num_runs; $i++){
  $input_file = $output_prefix + "-run" + $i + ".csv"
  "Writing from: " + $input_file + " to: " + $output_file
  $regex =
'Screening_Zone\..*\n.*time:timestamp.*(Z|\+01:00)\"/>\n.*lifecycle:transition.*start
.*\n|Screening_Zone\..*\n.*\n.*\n.*lifecycle:transition.*start.*\n.*time:timestamp.*(
Z|\+01:00)\"/>'
  $fileContent = [io.file]::ReadAllText($input_file)
  $fileContent | select-string -Pattern $regex -AllMatches | % { $_.Matches } | %
{"$i," + $_.Value } >> $output_file
}
$raw = [System.IO.File]::ReadAllText($output_file)
$formatted = ''
$formatted = $raw -replace
'Screening_Zone\.|Screening_session\.|(?<=(Enroll|Discharge|Refer|Followup_witho
ut_ROP))\{.*\}\"/>', ''
$formatted = $formatted -replace '.*org:role.*\n|.*org:resource.*\n', ''
$formatted = $formatted -replace '\n.*timestamp\" value=\"', ','
$formatted = $formatted -replace '\n.*lifecycle:transition|\" value=\"start\n', ''
$formatted = $formatted -replace '\" value=\"start', ''
$formatted = $formatted -replace '"/>', ''
$formatted = $formatted -replace '(?<=[0-9])T', ' '
$formatted = $formatted -replace '(?<=[0-9])Z', ''
$formatted > $output_file

## SCREENING TEAM TRAVEL DISTANCE ##
# Extracts the distance from Hq times upon termination of each screening day
# from each team's individual log

$output_file = $dir_path + 'Screening-Teams-Travel.csv’
$num_teams = 3
$fileHeader = "Team,Distance,Timestamp`r`n"

$fileHeader > $output_file

for ($i=1; $i -le $num_teams; $i++){
  $input_file = $dir_path + 'team-' + $i + '-screening.csv'
  $fileContent = [io.file]::ReadAllText($input_file)
  "Writing from: " + $input_file
  $regex =
'Screening_Zone\.Return_to_HQ\{.*\"start\"|Screening_Zone\.Return_to_HQ{.*\n.*\
"start\"'
  $fileContent | select-string -Pattern $regex -AllMatches | % { $_.Matches } | %
{"$i," + $_.Value } >> $output_file
}
```

```
$raw = [System.IO.File]::ReadAllText($output_file) #Get-Content $output_file -
Raw
$formatted = ''
$formatted = $raw -replace
'Screening_Zone\.Return_to_HQ\{.*distHq=|Screening_Zone\.Return_to_HQ{.*\n.*
distHq=|\",\"complete\",|\",\"complete\"|\",\"start\",', '
$formatted = $formatted -replace '\} \}\",\"', ','
$formatted = $formatted -replace '(?<=[0-9])T', ' '
$formatted = $formatted -replace '(?<=[0-9])Z', ''
$formatted = $formatted -replace '\",\"start\"|', ''
$formatted = $formatted -replace '\}, u = \(\) \}\",\"', ','
$formatted = $formatted -replace 'Transition\",\"Return to\nHQ\",\"', ''
$formatted > $output_file

## SPECIALIST TRAVEL DISTANCE ##
# Extracts the distance from Hq times upon termination of outreach
# from each specialist's individual subnet

$output_file = $dir_path + 'Specialists-Travel.csv’
$num_specials = 3
$fileHeader = "Specialist,Distance,Timestamp`r`n"

$fileHeader > $output_file

for ($i=1; $i -le $num_specials; $i++){
  $input_file = $dir_path + 'Specialist-' + $i + '-Outreach.csv'
  $fileContent = [io.file]::ReadAllText($input_file)
  "Writing from: " + $input_file
  $regex = 'Screening_Zone\.Specialist_Outreach_End\{.*\"complete\"'
  $fileContent | select-string -Pattern $regex -AllMatches | % { $_.Matches } | %
{"$i," + $_.Value } >> $output_file
}
$raw = [System.IO.File]::ReadAllText($output_file) #Get-Content $output_file -
Raw
$formatted = ''
$formatted = $raw -replace
'Screening_Zone\.Specialist_Outreach_End\{.*distHq=|\",\"complete\",|\",\"complete
\"|\",\"start\",', '
$formatted = $formatted -replace '\} \}\",\"', ','
$formatted = $formatted -replace '(?<=[0-9])T', ' '
$formatted = $formatted -replace '(?<=[0-9])Z', ''
$formatted > $output_file
```

Appendix 8.1

PRISMA 2009 Checklist

Section/topic	#	Checklist item	Reported on page #
TITLE			
Title	1	Identify the report as a systematic review, meta-analysis, or both.	144
ABSTRACT			
Structured summary	2	Provide a structured summary including, as applicable: background; objectives; data sources; study eligibility criteria, participants, and interventions; study appraisal and synthesis methods; results; limitations; conclusions and implications of key findings; systematic review registration number.	145
INTRODUCTION			
Rationale	3	Describe the rationale for the review in the context of what is already known.	145
Objectives	4	Provide an explicit statement of questions being addressed with reference to participants, interventions, comparisons, outcomes, and study design (PICOS).	145
METHODS			
Protocol and registration	5	Indicate if a review protocol exists, if and where it can be accessed (e.g., Web address), and, if available, provide registration information including registration number.	145
Eligibility criteria	6	Specify study characteristics (e.g., PICOS, length of follow-up) and report characteristics (e.g., years considered, language, publication status) used as criteria for eligibility, giving rationale.	145-6
Information sources	7	Describe all information sources (e.g., databases with dates of coverage, contact with study authors to identify additional studies) in the search and date last searched.	146
Search	8	Present full electronic search strategy for at least one database, including any limits used, such that it could be repeated.	146A,146
Study selection	9	State the process for selecting studies (i.e., screening, eligibility, included in systematic review, and, if applicable, included in the meta-analysis).	150-1

Section/topic	#	Checklist item	Reported on page #
Data collection process	10	Describe method of data extraction from reports (e.g., piloted forms, independently, in duplicate) and any processes for obtaining and confirming data from investigators.	146
Data items	11	List and define all variables for which data were sought (e.g., PICOS, funding sources) and any assumptions and simplifications made.	147
Risk of bias in individual studies	12	Describe methods used for assessing risk of bias of individual studies (including specification of whether this was done at the study or outcome level), and how this information is to be used in any data synthesis.	147
Summary measures	13	State the principal summary measures (e.g., risk ratio, difference in means).	N/A
Synthesis of results	14	Describe the methods of handling data and combining results of studies, if done, including measures of consistency (e.g., I^2) for each meta-analysis.	147
Risk of bias across studies	15	Specify any assessment of risk of bias that may affect the cumulative evidence (e.g., publication bias, selective reporting within studies).	148
Additional analyses (Optical modelling)	16	Describe methods of additional analyses (e.g., sensitivity or subgroup analyses, meta-regression), if done, indicating which were pre-specified.	148-9
RESULTS			
Study selection	17	Give numbers of studies screened, assessed for eligibility, and included in the review, with reasons for exclusions at each stage, ideally with a flow diagram.	149-50
Study characteristics	18	For each study, present characteristics for which data were extracted (e.g., study size, PICOS, follow-up period) and provide the citations.	150-3A
Risk of bias within studies	19	Present data on risk of bias of each study and, if available, any outcome level assessment (see item 12).	153-4
Results of individual studies	20	For all outcomes considered (benefits or harms), present, for each study: (a) simple summary data for each intervention group (b) effect estimates and confidence intervals, ideally with a forest plot.	154
Synthesis of results	21	Present results of each meta-analysis done, including confidence intervals and measures of consistency.	154A-6A
Risk of bias across studies	22	Present results of any assessment of risk of bias across studies (see Item 15).	156-7A
Additional analysis	23	Give results of additional analyses, if done (e.g., sensitivity or subgroup analyses, meta-regression [see Item 16]).	157-8

Section/topic	#	Checklist item	Reported on page #
DISCUSSION			
Summary of evidence	24	Summarize the main findings including the strength of evidence for each main outcome; consider their relevance to key groups (e.g., healthcare providers, users, and policy makers).	158-9
Limitations	25	Discuss limitations at study and outcome level (e.g., risk of bias), and at review-level (e.g., incomplete retrieval of identified research, reporting bias).	159-60
Conclusions	26	Provide a general interpretation of the results in the context of other evidence, and implications for future research.	160
FUNDING			
Funding	27	Describe sources of funding for the systematic review and other support (e.g., supply of data); role of funders for the systematic review.	N/A

From: Moher D, Liberati A, Tetzlaff J, Altman DG, The PRISMA Group (2009). Preferred Reporting Items for Systematic Reviews and Meta-Analyses: The PRISMA Statement. PLoS Med 6(7): e1000097. doi:10.1371/journal.pmed1000097

Appendix 8.2

PICOS Worksheet and Search Strategy document for review of preterm eye biometry literature

PICOS Worksheet and Search Strategy

1. **Define your question using PICOS** by identifying: Patient Population or Problem, Intervention (treatment/test), Comparison (group or treatment), Outcomes, and Setting.

Your question should be used to help establish your search strategy.

Patient/Problem	Preterm infants (Healthy or other)
Intervention	N/A
Comparison	N/A
Outcome	Eye biometries (see list)
Setting	NICU

Write out your question: pertinent to optical simulation
~~what/whether/if~~ How does the ocular biometries vary during preterm ~~infant~~

2. Type of question/problem: **Circle one:** Therapy/Prevention, Diagnosis, Etiology, Prognosis

3. Type of study (Publication Type) to include in the search: **Check all that apply:**

☑ Meta-Analysis	☑ Systematic Review	☐ Randomized Controlled Trial
☑ Cohort Study	☐ Case Control Study	☐ Case series or Case Report
☐ Animal Research	☑ In Vitro/Lab Research	☐ Editorials, Letters, Opinions

4. List main topics and alternate terms from your PICOS question that can be used for your search

Preterm OR premature OR neonatal AND
~~geometric dime~~ geometry of cornea, crystalline lens, ocular fundus, pupil, iris
OR refractive index of cornea, aqueous humour, lens, vitreous humour, ocular fundus, iris
OR refractive status

List your inclusion criteria -gender, age, year of publication, language

~~gestational age~~
prematurly born infants in NICU
will not consider data ≤60 wks GA
Languages = English or Italian
No restriction on pub. year

List irrelevant terms that you may want to exclude in your search

N/A

5. List where you plan to search, i.e., CINAHL, MEDLINE, PubMed, PyscINFO, Dissertations/Thesis

WoK and pubMed

Appendix 8.3

Full Preterm Biometry Meta-analysis Search Code

The full search terms can be run against PubMed by entering the following URL into an internet browser:
https://www.ncbi.nlm.nih.gov/pubmed/?term=(preterm%5BTitle%5D+OR+pre-term%5BTitle%5D+OR+premature%5BTitle%5D+OR+neonatal%5BTitle%5D+OR+%22gestational+age%22%5BTitle%5D+OR%22prematurity%22%5BTitle%5D)+AND+((%22refractive+error%22%5BTitle%5D+OR+myopia%5BTitle%5D+OR+hyperopia%5BTitle%5D+OR+astigmatism%5BTitle%5D+OR+keratometry%5BTitle%5D+OR+refraction%5BTitle%5D+OR+%22refractive+status%22%5BTitle%5D)+OR+((eye%5BTitle%5D+OR+ocular%5BTitle%5D+OR+cornea%5BTitle%5D+OR+corneal%5BTitle%5D+OR+pupil%5BTitle%5D+OR+pupillary%5BTitle%5D+OR+%22anterior+chamber%22%5BTitle%5D+OR+%22crystalline+lens%22%5BTitle%5D+OR+%22posterior+chamber%22%5BTitle%5D+OR+%22vitreous+chamber%22%5BTitle%5D+OR+retina%5BTitle%5D+OR+retinal%5BTitle%5D+OR+axial%5BTitle%5D)+AND+(biometry%5BTitle%5D+OR+dimensions%5BTitle%5D+OR+size%5BTitle%5D+OR+length%5BTitle%5D+OR+width%5BTitle%5D+OR+curvature%5BTitle%5D+OR+diameter%5BTitle%5D+OR+radius%5BTitle%5D+OR+thickness%5BTitle%5D+OR+depth%5BTitle%5D+OR+conic%5BTitle%5D+OR+%22refractive+index%22%5BTitle%5D+OR+%22index+of+refraction%22%5BTitle%5D+OR+angle%5BTitle%5D+OR+%22light+reflex%22%5BTitle%5D+OR+%22light+reflexes%22%5BTitle%5D)))
The full search query run against Web of Science Core Collection was as follows:
TI= (preterm OR pre-term OR premature OR neonatal OR "gestational age") AND ((TI= (eye OR ocular OR cornea OR corneal OR pupil OR pupillary OR "anterior chamber" OR "crystalline lens" OR "posterior chamber" OR "vitreous chamber" OR retina OR retinal OR axial) AND TI= (biometry OR dimensions OR size OR length OR width OR curvature OR diameter OR radius OR thickness OR depth OR conic OR "refractive index" OR "index of refraction" OR angle OR "light reflex" OR "light reflexes")) OR TI= ("refractive error" OR myopia OR hyperopia OR astigmatism OR keratometry OR refraction OR "refractive status"))

Appendix 8.4

Preterm Optical CAD Model

The files for constructing the optical model in Zemax OpticStudio are available from the following DOI: 10.15129/fbe0b925-f28d-460c-b121-e3ada73a63cc

Appendix 9.1

Bill of materials for prototyping preterm retinal eye phantom

Quantity	**Manufacturer**	**Item No / Manufacturer No**	**Item Description**
Various	EnvisionTech		EnvisonTech consumables
<5g	Intaglio		Carmine engraving ink
<1g	Intaglio		Manganese drier
	N/A	N/A	Acrylic paints (various colours)
	Edmund Optics		UV fused-silica lens
	RS Components		Blue 2.85mm PLA Filament
1	(Amazon)		12mm diameter ball bearing
1	Hurlbart	MAT_PET_075	0.75mm thick clear PETg A4 sheet
500 ml	Sigma-Aldrich	G7893	Glycerol
1			10ml syringe with 0.4mm needle
100ml	Bosch & Lomb		Viscotears

Appendix 10.1

Bill of materials for prototyping the low-cost portable widefield fundus camera

Quantity	Manufacturer	Item No / Manufacturer No	Item Description
1	CMOSIS	101438	NanEye2D with RGB sensor and 160° field-of-view optic with F# = 2.4
1	CMOSIS	101199	NanoUSB2.2 electronic base station.
<500g	RS Components		Blue 2.85mm PLA Filament
<50g	RS Components		Black 2.85mm PLA Filament
66x37x0.5mm	Hindley	VAC0327	0.5mm thick HIPS sheet
<5g	Farnell	1676334	303389 - 4305 UV Curing, 28.3G
5g	OliverBrown	111157963069	1000g Barium Sulphate
<5g	NSI Scotland	7838	New Seduction Colour Gel
<5g	Barry M Cosmetics Ltd.		Black nitrocellulose-based paint (nail polish)
2	Rapid Electronics	L-13PWC-Z	2mm white flat-top LEDs
20cm	Digikey		Wire
1	790-3647	RS Components	USB OTG micro-b cable
2	N/A	N/A	Compressible springs
1 of each	RS Components		18Ω and 200Ω resistor
2			Toggle switches
			Pedal switch
1	RS Components	2169886	
1m	RS Components		4mm internal diameter spiral wrap
1m	Farnell		4 core cable

[This page is intentionally blank]